

ice
Institution of Civil Engineers

publishing

Finite-element Design of Concrete Structures

Practical problems and their solutions

Second edition

G.A. Rombach



Finite-element Design of Concrete Structures

Practical problems and their solutions

Finite-element Design of Concrete Structures

**Practical problems and their
solutions**

Second edition

G.A. Rombach
University of Hamburg-Harburg

Published by ICE Publishing, 40 Marsh Wall, London E14 9TP.

Full details of ICE Publishing sales representatives and distributors can be found at: www.icevirtuallibrary.com/info/printbooksales

First published 2004

Second edition 2011

Also available from ICE Publishing

Structural Dynamics for Engineers, Second edition.

H.A. Buchholdt and S.E. Moossavi Nejad. ISBN 978-0-7277-4176-9

Structural Analysis with Finite Elements.

P. Rugarli. ISBN 978-0-7277-4093-9

Designers' Guide to EN 1992-1-1 Eurocode 2: Design of Concrete Structures (common rules for buildings and civil engineering structures).

A.W. Beeby. ISBN 978-0-7277-3105-0

Associate Commissioning Editor: Victoria Thompson

Production Editor: Imran Mirza

Market Development Executive: Catherine de Gatacre

www.icevirtuallibrary.com

A catalogue record for this book is available from the British Library

ISBN: 978-0-7277-4189-9

© Thomas Telford Limited 2011

ICE Publishing is a division of Thomas Telford Ltd, a wholly-owned subsidiary of the Institution of Civil Engineers (ICE).

All rights, including translation, reserved. Except as permitted by the Copyright, Designs and Patents Act 1988, no part of this publication may be reproduced, stored in a retrieval system or transmitted in any form or by any means, electronic, mechanical, photocopying or otherwise, without the prior written permission of the Publisher, ICE Publishing, 40 Marsh Wall, London E14 9TP.

This book is published on the understanding that the author is solely responsible for the statements made and opinions expressed in it and that its publication does not necessarily imply that such statements and/or opinions are or reflect the views or opinions of the publishers. Whilst every effort has been made to ensure that the statements made and the opinions expressed in this publication provide a safe and accurate guide, no liability or responsibility can be accepted in this respect by the author or publishers.

Whilst every reasonable effort has been undertaken by the author and the publisher to acknowledge copyright on material reproduced, if there has been an oversight please contact the publisher and we will endeavour to correct this upon a reprint.



Typeset by Academic + Technical, Bristol

Printed and bound in Great Britain by CPI Antony Rowe Limited, Chippenham and Eastbourne

Contents

	Preface	vii
	About the author	ix
	Notations	xi
01	General	1
	1.1. Introduction to FEM	5
	1.2. General problems of numerical analysis of concrete structures	7
	References	12
02	Truss and beam structures	13
	2.1. Corners in frame structures – rigid regions	14
	2.2. Beams with variable depth – inclined haunches	23
	2.3. Beams with halving joints and openings	29
	2.4. Soft supports – elastic bedding	37
	2.5. Shear walls with large openings	56
	2.6. Bracing of high-rise buildings	61
	2.7. Design of hollow box girder bridges	80
	2.8. Truss system – design of T-beam bridges	84
	2.9. Support conditions	105
	2.10. Dimensioning of reinforced beams	110
	2.11. Material nonlinear analysis of truss and beam systems	114
	References	136
03	Shear walls and deep beams	139
	3.1. Estimation of stress resultants of deep beams	141
	3.2. Modelling the support condition	145
	3.3. Dimensioning of deep beams	158
	3.4. Strut-and-tie models	166
	3.5. Singularities	169
	References	171
04	Slabs	173
	4.1. General	173
	4.2. Meshing – size of elements	180
	4.3. Material parameters – Poisson’s ratio	181
	4.4. Support conditions for slabs	183
	4.5. One-way slab	185
	4.6. Slabs that can lift from the supports	197
	4.7. Discontinuous line support	199
	4.8. Concrete joist floors	205
	4.9. Flat slabs	206
	4.10. Foundation slabs	228
	4.11. Skewed slabs	234
	4.12. Singularities	237
	4.13. Discretisation – generation of the element mesh	246
	4.14. Dimensioning of spatial structures	254
	4.15. Comparison with analytical methods and tables	261
	References	269
05	Shell structures	271
	5.1. Mesh generation	271
	5.2. T-beams	283

	5.3. Slab-on-beam structure	296
	5.4. Composite structures	310
	5.5. Singularities	310
	5.6. Material nonlinear analysis of shells and massive members	312
	References	318
06	Three-dimensional building models	321
	6.1. General problems	321
	6.2. FE modelling of a building	323
	6.3. Design of a building	329
	6.4. Portal frame bridge	335
	6.5. Checking and documentation of FE analyses	344
	6.6. The power of FE analysis	348
	6.7. Summary and conclusions	350
	References	350
	Index	351

Preface

Over the last few years, electronic data processing has changed the work of engineers throughout all fields of construction. This is particularly true for design of structures, doing which is impossible to imagine today without the help of computer software. Even simple structures such as, for example, a simply supported reinforced concrete beam under uniform loading, are designed using the help now easily available from computers. One must admire this. In many cases, these computer calculations are faster, less costly and thus more profitable than using manual calculations.

The developments over the last year or so have involved using yet more complex numerical models, as can be seen from the various contributions to conferences and journals on the subject. Today, it seems that modelling arbitrary complex reinforced structures with almost unlimited accuracy is only a question of adequate computer capacity, the size of the element mesh and the accurate modelling of the nonlinear material's behaviour. However, this involves the great danger that one only believes the results from the computer, and the engineer loses his or her feelings for the real behaviour of the structure. Thus, in this book, the author is critical of blind belief in computer-based results. The author advocates that one should not have totally blind confidence in the output of computer calculations, but rather take the numerical model used, and hence the results achieved, with a pinch of salt.

With the increasing complexity of numerical models, it becomes likely that important details may be overlooked, primarily due to the flood of information produced by computers. The collapse of the Sleipner platform (see Chapter 5), resulting from an erroneous finite-element (FE) calculation, impressively demonstrates this danger.

A complex numerical calculation should not be used to compensate for the engineer's lack of knowledge of the structural behaviour of a structure. An engineer should be able to simplify any real structure into well-defined, known, understandable and designable equivalent structural systems. Unimportant details should be neglected. It should always be kept in mind that even very complex structures, such as the chapel of St. Peters Church in Rome or the temples in Luxor and Karnak, have been built without the help of computers, and possibly even without knowledge of mechanics.

This book has been written for both the practicing structural engineer and for students who use computer software for designing concrete structures. The problems of FE calculations are illustrated, not just by theoretical systems, but also by relating to real structures, mostly those on which the author has actually worked. They concern systems from all fields of engineering. Furthermore, this book should help those people

who develop software for structural design to understand the difference between theory and the daily problems of designing reinforced concrete structures.

This book could not have been written without abundant help and support from friends and colleagues in practice and research. I am much indebted to Peter Whiting LL.B (Hons), BSc, FICE, for his thorough reviewing of the manuscript and for support of my work.

Guenter Axel Rombach
Hamburg
April 2011

About the author

Prof. Dr.-Ing. Guenter Rombach graduated in 1983 as a civil and structural engineer from the University of Karlsruhe, Germany, where he also obtained his doctorate in 1991 in the field of numerical simulations of granular flow in silos. In 1990, he joined a large construction company, where he worked as design and project manager for various projects, mainly big bridges, both in Europe and further afield. In 1995, he became technical manager in the construction project of one of the biggest segmental bridges in the world, the Second Stage Expressway System in Bangkok, Thailand. Since 1996, he has been full professor in the field of design of concrete structures at the University of Hamburg-Harburg, where he is in charge of undergraduate and graduate courses in the design of reinforced and prestressed concrete structures. In 1999, he became a certified checking engineer. Prof. Rombach is a member of several national and international professional committees that deal with design of concrete structures, for example, bridges. He has published several books about finite-element design of concrete structures and the design of prestressed structures.

Notations

In general, the symbols of Eurocode 2 are used. These are listed here, together with the additional abbreviations used in this book.

1 Latin upper case letter

A	Accidental action; cross-sectional area
A_c	Cross-sectional area of concrete
A_p	Area of a prestressing tendon or tendons
A_s	Cross-sectional area of reinforcement
$A_{s,min}$	Minimum cross-sectional area of reinforcement
$A_{s,prov}$	Area steel provided
$A_{s,req}$	Area steel required
A_{sw}	Cross-sectional area of shear reinforcement
b_c	Width of column
C	Symbol for grade of normal concrete
C_M	Wrapping torsional stiffness
D	Diameter of mandrel
E	Effect of action (member force)
E_c	Tangent modulus of elasticity of normal weight concrete at a stress of $\sigma_c = 0$ and at 28 days
$E_{c,eff}$	Effective modulus of elasticity of concrete
E_{cd}	Design value of modulus of elasticity of concrete
E_{cm}	Secant modulus of elasticity of concrete
E_s	Design value of modulus of elasticity of reinforcing steel
EI	Bending stiffness
F	Force; action
F_d	Design value of an action
FE	Finite element
G_k	Characteristic permanent action
H	Horizontal force
I	Second moment of area
L	Length
M	Bending moment
M_{Ed}	Design value of the applied internal bending moment
M_T	Torsional moment
N	Axial force
N_{Ed}	Design value of the applied axial force (tension or compression)
P	Prestressing force
P_0	Initial force at the active end of the tendon immediately after stressing
P_{mt}	Mean value of the prestressing force at time t , at any point distance x along the member
Q_k	Characteristic variable action
R	Resistance
R_d	Nominal value of resistance
S	Internal forces and moments
S	First moment of area
S_M	Centre of torsion of a cross-section
S_S	Centre of gravity of a cross-section
SLS	Serviceability limit state

T	Torsional moment
ULS	Ultimate limit state
V	Shear force
V_{Ed}	Design value of the applied shear force

2 Latin lower case letters

a	Distance; geometrical data
Δa	Deviation of geometrical data
a_1	Shift of moment curve
a_{sup}	Breadth of the support
b	Overall width of a cross-section, or actual flange width in a T- or L-beam
b_w	Width of web on T-, I- or L-beams
c	Concrete cover
d	Diameter; depth
d	Effective depth of a cross-section
d_g	Largest nominal maximum aggregate size
e	Eccentricity
f	Strength (of a material)
f_c	Compressive strength of concrete
f_{cd}	Design value of compressive strength of concrete
f_{ck}	Characteristic compressive cylinder strength of concrete at 28 days
f_t	Tensile strength of reinforcement
f_y	Yield strength of reinforcement
h	Height
h	Overall depth of a cross-section
i	Radius of gyration
k	Coefficient; factor
l	Length; span
l_b	Anchorage length
l_{col}	Height of a column
l_{eff}	Effective span of beams and slabs
l_n	Clear distance from the faces of the supports
m	Moment per unit length; mass
n	Number of vertical continuous members
r	Radius
$1/r$	Curvature at a particular section
s	Distance; spacing of stirrups
p	Mean transverse pressure over the anchorage length
t	Time being considered; thickness
t_0	The age of concrete at the time of loading
u	Perimeter of concrete cross-section, having area A_c
u, v, w	Components of the displacement of a point
v	shear force per unit length
v	Coefficient relating the average design compressive stress in struts to the design value of the concrete compressive strength (f_{cd})
v	Angle of inclination of a structure, assumed in assessing effects of imperfections

x	Neutral axis depth
x, y, z	Coordinates
z	Lever arm of internal forces

3 Greek lower letters

α	Angle; ratio
β	Angle; ratio; coefficient
γ	Partial safety factor
γ_C	Partial factor for concrete
γ_G	Partial factor for permanent action, G
γ_M	Partial factor for a material property
γ_Q	Partial factor for variable action, Q
δ	Increment; redistribution ratio
ζ	Reduction factor; distribution coefficient
ε	Strain
ε_c	Compressive strain in concrete
ε_{c1}	Compressive strain in the concrete at the peak stress f_c
ε_{cu}	Ultimate compressive strain in the concrete
ε_u	Strain of reinforcement or prestressing steel at maximum load
ε_u	Characteristic strain of reinforcement or prestressing steel at maximum load
θ	Angle; rotation
θ_F	Angle between the x-axis and the major principal stress in the concrete (measured in the anti-clockwise direction)
λ	Slenderness ratio
μ	Coefficient of friction between tendons and their ducts
μ	Moment coefficient
ν	Poisson's ratio
ν	Strength reduction factor for concrete cracked in shear
ν	Longitudinal force coefficient for an element
ξ	Ratio of bond strength of prestressing and reinforcing steel
ρ	Over-dry density of concrete in kg/m^3
ρ_l	Reinforcement ratio for longitudinal reinforcement
ρ_w	Reinforcement ratio for shear reinforcement
σ	Normal stress
σ_c	Compressive stress in the concrete
σ_s	Tensile stresses in reinforcement
τ	Torsional shear stress
\emptyset	Diameter of a reinforcing bar or of a prestressing duct
\emptyset_n	Equivalent diameter of a bundle of reinforcing bars
$\varphi(t, t_0)$	Creep coefficient, defining creep between times t and t_0 , related to elastic deformation at 28 days
$\varphi(\infty, t_0)$	Final value of creep coefficient
Ψ	Factors defining representative values of variable actions
	Ψ_0 for combination values
	Ψ_1 for frequent values
	Ψ_2 for quasi-permanent values

4 Subscripts

c	Concrete; compression; creep
b	Bond
d	Design
e	Eccentricity
eff	Effective
f	Flange
fat	Fatigue
fav	Favourable
freq	Frequent
g	Permanent action
i	Indices; notional
inf	Inferior; lower
j	Indices
k	Characteristic
l	Low; lower
m	Mean; material; bending
max	Maximum
min	Minimum
nom	Nominal
p	Prestressing force
perm	Permanent
pl	Plastic
q	Variable action
rep	Representative
s	Reinforcing steel; shrinkage
sup	Superior; upper
t	Torsion; time being considered; tension
unf	Unfavourable
w	Web
y	Yield

Chapter 1

General

Numerical calculations based on the finite-element method (FEM) are becoming a standard tool in the design of structures. Furthermore, the lower cost of computer hardware and improved performance of increasingly user-friendly software often obviate the necessity for manual calculations. This applies not only to complex 3D structures and slabs, shear walls and shells of complicated shape, but also to normal beams. It can be economical – since it is much faster – to design a simple supported reinforced concrete beam under uniform loading by using a computer. However, one saves working time only when the necessity for manually checking the numerical results is disregarded.

A few years ago, powerful computers were needed to conduct FE analyses, and only experts and big consulting offices were able to perform this analysis. Nowadays, the designing of an entire building can be handled by a simple PC. Graphical input makes it easy to generate 3D FE meshes with several thousand nodes. Computer programs can design concrete, steel or wooden structures that have linear or nonlinear material behaviour, under static or dynamic loading. There no longer seems to be any limitations. Nonetheless, this development has led to an increasing number of cases where FEM has been misused.

As daily experience shows, results from computer calculations are often trusted with blind faith. Users assume that expensive software for design of structures must be free from any error. A graphical pre-processor and a user-friendly input of systems and loadings may suggest that a computer program has a high degree of technical competence and reliability. Nevertheless, as practical experience shows, this confidence can only be justified to a very limited degree. Almost no software is free from errors. Therefore a critical approach is appropriate, as program errors may also occur in software that has been in use for a long time and which may not have been recognised to date.

It should always be kept in mind that FEM is only a numerical tool based on numerous assumptions and simplifications. This must be considered when using software for design of structures. Otherwise, the result of numerical calculations may turn out to be totally wrong. For explanation purposes, the following is a very simple example: a plate element only provides a numerical model of a real slab. It is assumed to have a linear strain distribution over its depth under pure bending. There are no stresses at the midplane. With such a plate element, one will never be able to estimate the normal forces of a

simple supported rectangular slab due to temperature changes or shrinkage, even if the supports are fully restrained in horizontal directions.

The modelling, the discretisation, of real reinforced concrete structures is the focal point of this book. The fundamental aspects are illustrated by practical examples of concrete structures. This book does not look into the fundamental basis of FEM, as numerous publications are already available (see, for example, Bathe, 1982; Hughes, 1987; Zienkiewicz and Taylor, 1989). The so-called state of the art of the FE techniques will not be discussed, as there seems to be a great gap between ongoing research and the day-to-day problems that a practicing structural engineer has to face. An engineer has neither the time to make highly sophisticated numerical models nor the experimental data to verify his analysis. He is not even interested in the 'correct' results. His goal is simply to estimate the required amount of reinforcement and its accurate arrangement (the 'dimensioning' of a structure), in order to build a safe and economical structure. The calculation of the member and internal forces and moments is only a required step to reach this goal.

The examples shown in this book are calculated using standard software, used in day-to-day practice, and not with one of the advanced general-purpose FE packages such as ABAQUS, ADINA or ANSYS, which offer a great variety of different elements and material models. Hence, the reader can easily verify the given examples using his or her own software. A further reason for the strong relation to practical design is that a user of a software package is not usually familiar with its theoretical background, and hence cannot modify it. It does not help the user to know, for example, that a reduced integrated three-noded shell element may give better results than a full integrated six-noded isoparametric element. He is just using the 'black box'. The user, however, is supposed to have sufficient knowledge to see and solve the problems that may occur in a FE analysis. This is where this book is intended to provide help.

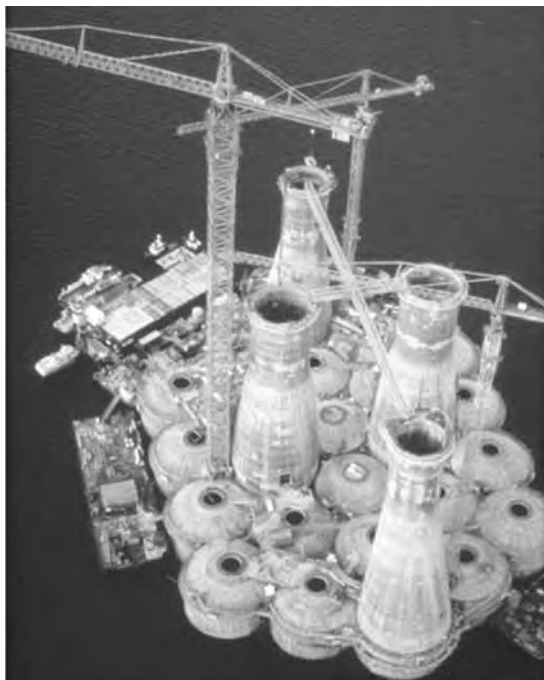
It is surprising that, in structural engineering, the use of FEM causes numerous problems, especially as this numerical method was first used by structural engineers. The world's first electronic programmable calculator was built by a structural engineer named Konrad Zuse (Zuse, 1984) in May 1941. He was tired of repeating calculation procedures when designing structures. Zuse also developed the first algorithmic programming language 'Plankalkuel'. In other fields of engineering, such as, for example, in the automobile or aircraft industries, the numerical FE analysis of highly complex problems, such as the crash behaviour of a car, the optimisation of aerodynamics or the processes in an engine, have become a day-to-day practice. The reason for this discrepancy is that these sorts of costly and complicated computer calculations are only economical for mass products. In contrast, a building is usually a unique structure whose costs depend on several factors, and not just the cost of building material. The numerical modelling of the complex behaviour of the composite material 'reinforced concrete' causes far greater problems than the elasto-plastic bi-linear behaviour of metals.

This book focuses on the numerical analysis of structures made of reinforced or prestressed concrete. FE calculations of concrete structures have the following different and exceptional features in comparison to other materials.

- Reinforced or prestressed concrete is a composite inhomogeneous material with a very complex nonlinear material behaviour, and thus an ‘exact’ model is far too costly for daily structural design. Therefore, the calculations of the member forces are mostly based on a linear elastic material model. Stiffness reductions, as a result of crack formations or the ‘yielding’ of concrete in regions with high compressive stresses, are ignored. The consequences of this very large simplification should be justified for each calculation.
- The required material parameters such as, for example, modulus of elasticity E_c , concrete compressive strength f_c or Poisson’s ratio ν , show a large scatter in comparison with other construction materials. Furthermore, they are often time-dependent. The actual quality of construction (workmanship, weather conditions, curing) is not known during the design phase; however, this can influence the material parameters.
- Concrete material is often used for massive members where, for example, the Bernoulli hypothesis of a linear strain distribution over the depth of the cross-section does not apply. Therefore, standard beam and plate elements should not be used for the design of the so-called discontinuity regions.
- Plane shell structures, such as slabs and shear walls, for example, are often made of reinforced concrete. For such members, a design based on an elastic material behaviour is not sufficient. The cracking of the concrete under tensile stresses has to be considered in the arrangement of the reinforcement of a deep beam. The pin supports of flat slabs may cause singularity problems.
- The actual arrangement of the reinforcement in a member is very important for the behaviour of a structure, and not just for the calculation of the forces and the amount of reinforcement required.
- There are numerous parts of a concrete structure where a fully detailed calculation of its load-bearing and deformation characteristics cannot be economically justified (such as for frame corners, corbels or footings).
- Most concrete construction components are unique, for which a major computer calculation is generally not economical.
- Concrete members can be produced with arbitrary shapes and cross-sections.
- The construction process, as well as the time-dependent behaviour of concrete, can be of considerable significance.
- For some load cases such as, for example, restraints or torsional moments, the forces are reduced by cracking and do not need to be considered in their full size in the calculations.

The uncritical or erroneous use of FE software can lead to serious damage, as the collapse of the Sleipner A platform (Figure 1.1) impressively demonstrates (Holand, 1997; Jakobsen and Rosendahl, 1994). This so-called Condeep-Platform had a total height of 110 m. The four towers rested on 24 cylindrical cells, each having a diameter of 24 m. On 23 August, 1991, the concrete platform collapsed completely during its lowering and sank down to the seabed. The actual financial damage was estimated at about US\$250 million. The cause of the total collapse was found to be the serious inaccuracies in the global FE analysis of the structure and faulty reinforcement arrangement in the connection area of the cell walls. The element mesh used for the calculations

Figure 1.1 Sleipner A platform (photo NC)



was too coarse to determine the actual forces in the members. This disaster raises a critical question, whether this sort of accident could still be allowed to happen nowadays. The essential causes of this case of damage and the consequences of the numerical analysis are discussed in detail in Section 5.1.1.

This accident significantly demonstrates an essential problem in complex numerical calculations: the insufficient control of the results due to the large amount of data output. The more complex the numerical models are, the more difficult it becomes to recognise the areas of possible mistakes and inaccuracies.

In this respect, it is the author's opinion that the modelling of a structure as a whole with the help of shell elements, for example, multi-storey buildings or bridges, is rarely meaningful, although this approach is often encouraged by software companies. A structural engineer must always be able to understand the behaviour of any complex structure and to idealise it, so that the flow of forces can easily be understood and calculated. Complex FE calculations can then be used to lower any excessive safety margins of simple models and produce a far more economical structure. However, complex FE models must never be used to replace either the design engineer or any of the engineer's missing expertise. Costly, sophisticated analyses do not always lead to more realistic results. Furthermore, the amount of a FE analysis should be considered with respect to the degree of accuracy that is actually needed. The results of any calculation can only be as accurate as the

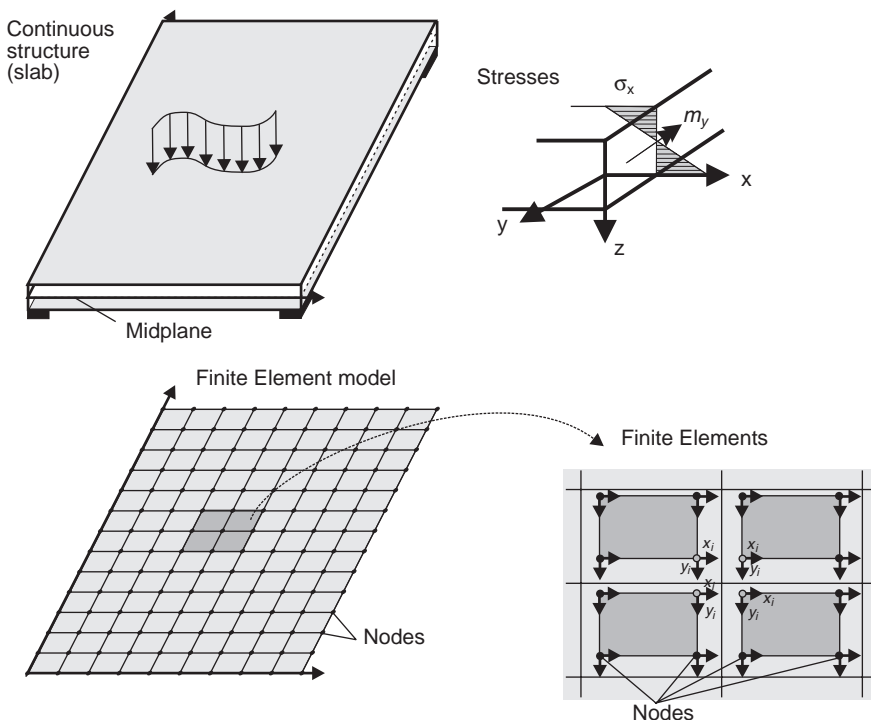
underlying assumptions of its numerical model. One should always keep in mind that there can always be considerable variation in the actual loading of a structure and in the properties of its materials.

1.1. Introduction to FEM

This very short introduction gives a brief précis of the basics of FEM. Further and more detailed information can be found in numerous other publications; for example, Bathe (1982), Hughes (1987) and Zienkiewicz and Taylor (1989).

In using FEM, a complex structure is subdivided into a finite number of individual components called ‘elements’ (discretisation) whose behaviour – the relation between their nodal displacements (static analysis) and their nodal reactions – can be specified by a limited number of parameters and analytical functions, the so-called shape or form functions (see Figure 1.2). All displacements, strains and stresses within an element, as well as the resulting nodal forces, can be calculated by means of the shape functions and their derivatives, respectively. The individual elements are only interconnected by their nodes. The solution of the complete system follows from the assembly of all of these elements. The stiffness matrices of all the elements $[K]^e$ are added to arrive at a

Figure 1.2 Numerical analysis of a continuous structure (slab)



global stiffness matrix $[K]$, from which the unknown nodal displacements $\{u\}$ can be calculated.

$$[K] \cdot \{u\} = \{F\}$$

where:

- $[K]$ is the global stiffness matrix $[K] = \Sigma [K]^e$
- $\{u\}$ is the vector of nodal displacements
- $\{F\}$ is the vector of nodal forces (loading).

The main task is to find form functions that can approximate the behaviour of a special structural element and satisfy the compatibility condition. For simple elements such as the two-noded truss element shown in Figure 1.3, the relation between the nodal

Figure 1.3 Two-noded plane truss element (without torsion)

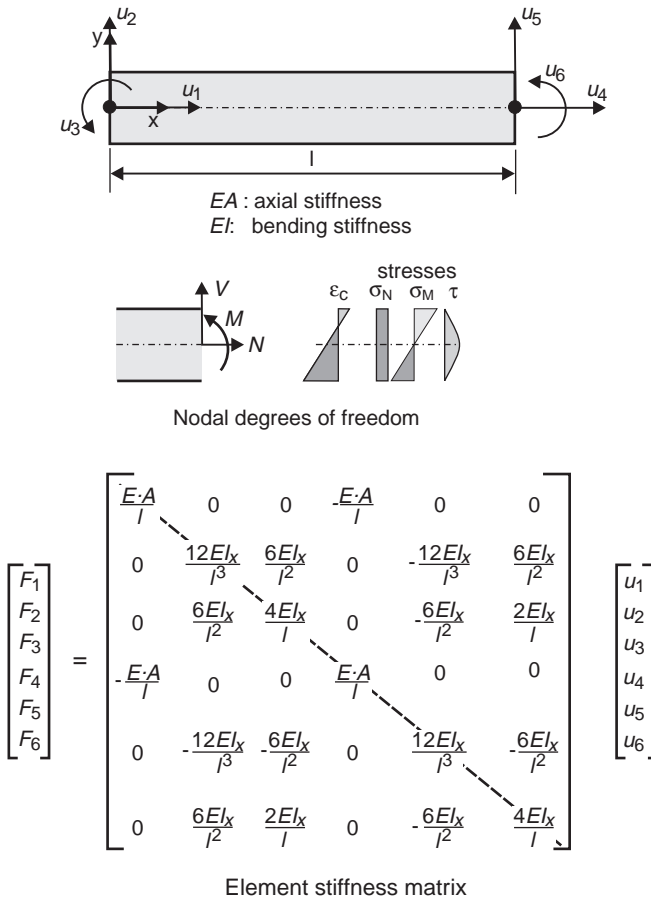
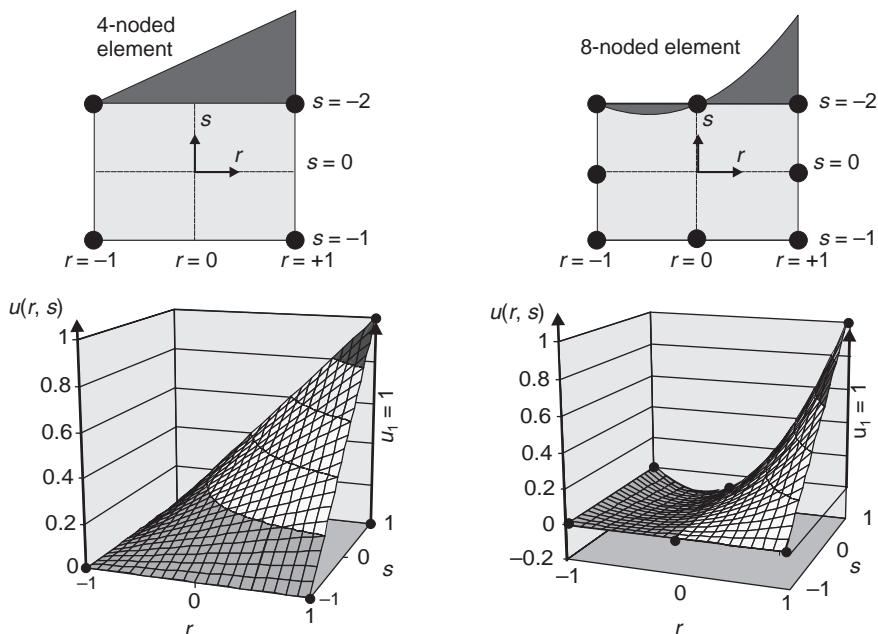


Figure 1.4 Displacements within a four-noded and eight-noded element for $u_1 = 1$



forces $\{F\}^e$ and the nodal displacements of each element $\{u\}^e$ can be found by means of equilibrium conditions. Shape functions are not needed for this simple approach.

For more complex elements such as, for example, plate or shell elements, virtual work or virtual displacement principles are used. Figure 1.4 shows the displacements within a four-noded and an eight-noded isoparametric element for a unit deflection of $u_1 = 1$ at node number 1. It can clearly be seen that both elements have different displacement distributions $w(x, y)$ and thus different strains ($\varepsilon \equiv w'(x, y)$), even if the nodal values are equal.

The basics of the FE technique set out in the preceding text therefore give the following important conclusions:

- An FE model is based on nodal forces and nodal displacements (static analysis).
- All values such as, for example, displacements, strains or stresses within an element, are calculated by means of shape functions.
- The nodal forces are calculated by shape functions and not by equilibrium conditions.

1.2. General problems of numerical analysis of concrete structures

The following is a summary of the significant problems in numerical analysis of reinforced concrete structures. A detailed discussion can be found in the chapters that follow.

1.2.1 Program errors

One should always keep in mind that computer software, in general, is not error-free. The more complex the software is, the sooner it becomes difficult for the software engineer to examine all of the possible eventualities in advance. This problem can be made worse for the user by the issue of updates to previously error-free software, which then suddenly produces incorrect results. This problem can only be resolved by independently checking calculations.

Next, a computer has limited accuracy; for example:

$$2^{45} - 0.8 - 2^{45} = -0.8008 \neq -0.8000$$

$$2^{50} - 0.8 - 2^{50} = 0.0 \neq -0.8000$$

1.2.2 Model errors

The majority of errors come from the modelling, that is, making an idealisation of a real structure (Figure 1.7).

1.2.2.1 Material model

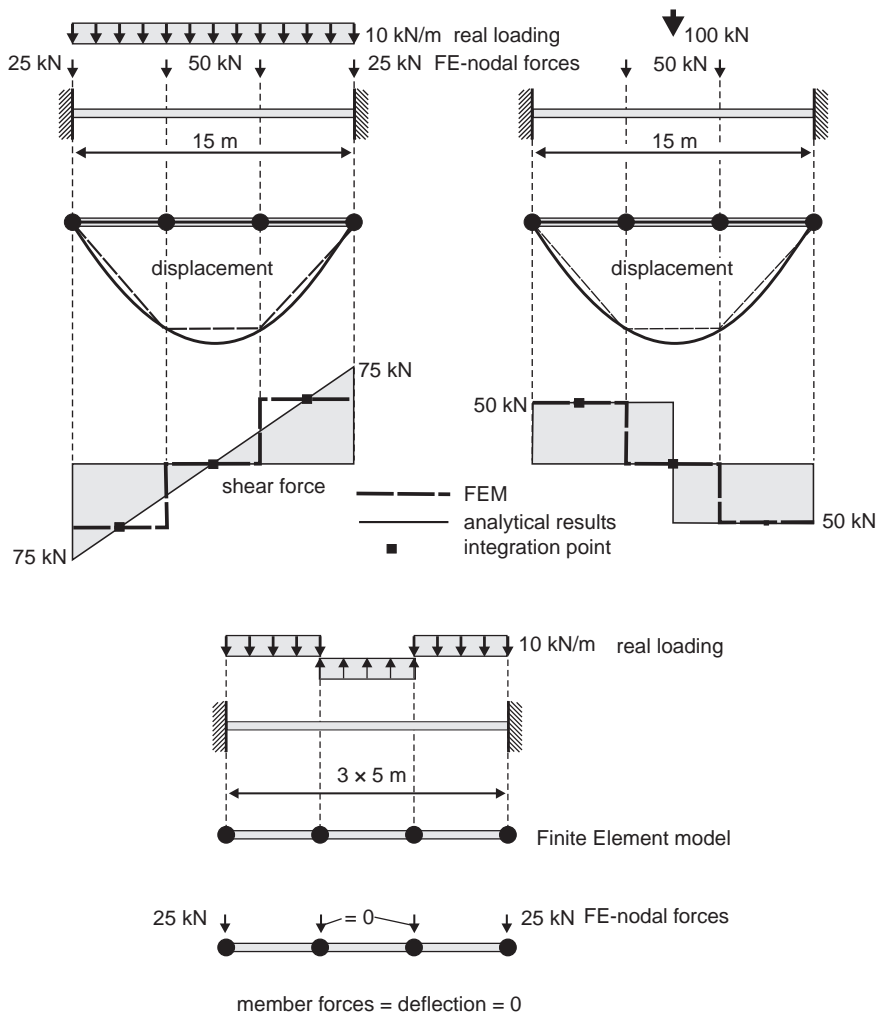
The calculation of the action effects (internal forces and moments) is usually based on linear elastic material behaviour, although it is well known that concrete is a highly nonlinear material. The Eurocode EC2, Part 1 (2004) allows for nonlinear or plastic analysis, but in design practice, such complex calculations are very seldom justified, due to the large amount of work needed and the difficulties in material descriptions. Furthermore, the combination of the results from various load cases is then no longer possible, which increases the work load substantially. Therefore, the design is usually based on a linear elastic material behaviour with limited redistribution of member forces. The accuracy of such simplified analysis is generally sufficient. In addition to slender columns or thin shell structures, there are other structures where the nonlinear behaviour may be significant. This aspect will be discussed in detail in Section 2.11.

1.2.2.2 Loading

An FE model is based on nodal forces and nodal displacements (Figure 1.3). This is still valid when the software allows for an arbitrary load arrangement to be possible. In this case, the computer program calculates the equivalent nodal forces. Depending on the size of the elements, this may lead to a considerable extension of the actual loaded area. This is important, for example, in the analysis of slabs under concentrated loads, such as wheel loads on bridge decks.

A single-span beam modelled by only three elements is used to demonstrate the problem of equivalent nodal forces (Figure 1.5). The beam on the left is loaded by a uniform load of $q = 10 \text{ kN/m}$. The software estimates the equivalent nodal forces to $F = 50 \text{ kN}$ for the inner nodes. Thus, the member forces for a beam loaded by two single forces instead of a uniform load are calculated. This results in incorrect shear forces. A beam with a single load in midspan (Figure 1.5 right) gives the same member forces. Thus, for this simple example, the FE analysis cannot distinguish between a uniform load and a concentrated load at midspan.

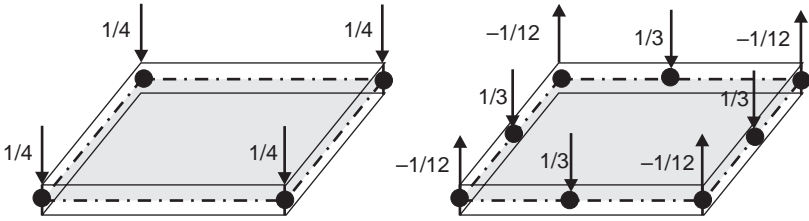
Figure 1.5 Difference between FE nodal loading and real loading



Furthermore, loads on fixed nodes are mostly neglected in the design and hence in the results. The total support force is only the sum of the loads on the unrestrained nodes. This has to be considered when support forces from FE analyses are used for the loading of other members. Loads on columns and walls, which may be fully restrained in the numerical model, are neglected by some structural software.

The nodal forces result from the chosen element with respect to its shape functions and not from 'engineering' experience. Figure 1.6 shows the nodal forces for a four-noded and an eight-noded plate element under constant vertical loading. For the four-noded element, the load is distributed equally to the nodes, whereas the eight-noded element shows uplifting forces at the edge nodes.

Figure 1.6 Nodal forces for a four-noded and eight-noded isoparametric plate element under uniform vertical loading



1.2.2.3 Determination of the required reinforcement

Nowadays, the estimation of the reinforcement required and its detailed arrangement in truss and plate structures is not a problem. However, this is not the case for deep beams and shell structures. Here, a software program in general is not able to make the best detailing of the reinforcement, as it is based on an element-wise analysis. Force redistribution, due to the cracking of the concrete, is not considered in a linear elastic analysis. In general, an FE model with shell elements will not be able to distinguish between a member in bending and one in compression, whereas their design must be different. Thus, the model can lead to incorrect results. The same is true for shear design.

1.2.2.4 Discretisation

The numerical modelling of a real structure, the ‘discretisation’ (subdividing a structure into a finite number of different elements), is where most of the errors are made (Figure 1.7). Here, among other matters, special note should be made of the following factors.

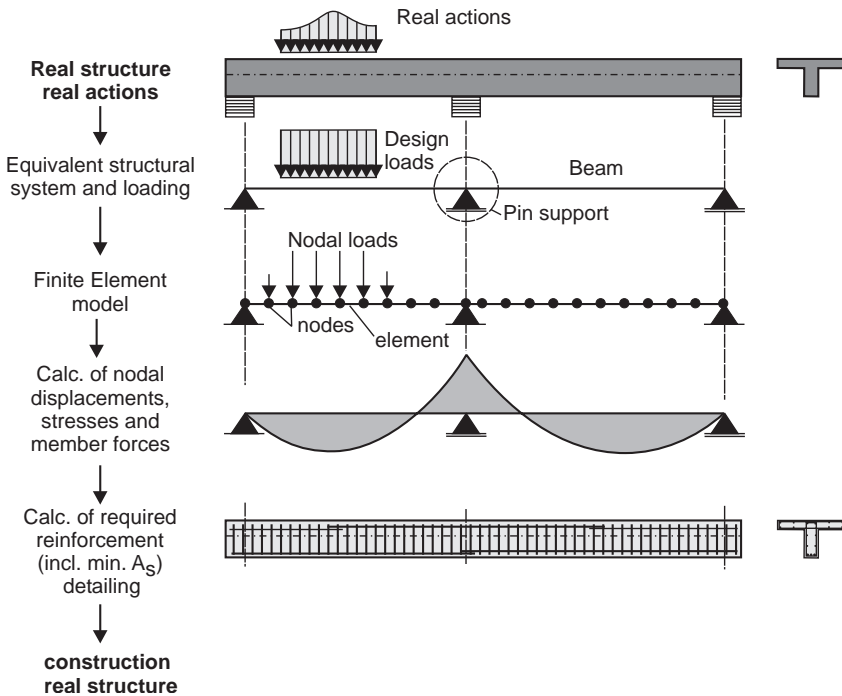
Size of elements

Some years ago, the number of elements was limited due to the capabilities of both computer hardware and software, whereas nowadays a sufficiently fine discretisation of an entire building can be done without any major difficulties. Furthermore, an element mesh can be produced very quickly by graphical pre-processors. Nevertheless, even automatic mesh generation should not be used in an uncaring or uncritical manner; engineering knowledge is still required. An inadequate modelling of apparently irrelevant details, such as, for example, small cantilever slabs of a bigger plate (Section 4.12.2) or openings in a flat slab near columns, can lead to faulty calculations and an unsafe design. A sufficiently fine element mesh should be used in regions of high deformation or stress gradients.

Element form functions, incompatible elements

In general, the user of a software program has no information of the numerical algorithms and the form functions for the elements on which the software is based. Nevertheless, the user should have the basic knowledge to understand at least the principal difference between a beam, a plate and a shell element, in order to understand

Figure 1.7 Numerical analysis of a real structure



that the various element types cannot be simply joined together, even if this is not hindered by the computer software (see Section 3.2.3).

Support

The numerical modelling of the supports of any structure should be carried out with great care, as this is where fundamental mistakes can be made. This aspect of a design will be explained for a beam in Section 2.9, for a deep beam in Section 3.2 and for a flat slab in Chapter 4.

Singularities

Singularities, or infinite stresses and internal forces, occur in slabs or shear walls under highly concentrated point-loads. It should be kept in mind that this problem only occurs in a numerical model caused by simplifications and assumptions of element behaviour. For example, the assumption of a linear strain distribution in a slab is not valid in the region of pin supports. A real structure does not show any infinite internal forces. In regions of high compression, the concrete may 'yield'. Tensile stresses may cause the formation of cracks. The high forces shown by an FE analysis in singularity regions do not happen in a real structure, and thus need not to be considered in the design, except by some additional reinforcement. Nevertheless, the user should know about these problems and how the results of the numerical analysis (e.g. bending moments and shear forces) should be interpreted.

Kinematic systems

In general, a software program gives out warnings or stops the analysis when a structure becomes kinematic. In these cases, the system of equations and thus the nodal displacements have no unique solution. These warnings can, however, be easily overlooked due to the great quantities of data produced, which can only be checked by graphical control. In addition, some software packages may automatically fix all kinematic degrees of freedom. If the distribution of forces is reasonable, these mistakes will not be noticed, and the structure will be designed for actions and erroneous member forces of a kinematic structure.

REFERENCES

- Bathe K-J (1982) *Finite Element Procedures in Engineering Analysis*. Prentice Hall, Englewood Cliffs.
- CEN (European Committee for Standardization) (2004) Eurocode 2, Part 1: Design of concrete structures – General rules and rules for buildings. December.
- Holand I (1997) *SINTEF Report No. 17: Sleipner A GBS Loss*. Main Report, Trondheim.
- Hughes TJR (1987) *The Finite Element Method*. Prentice Hall, Englewood Cliffs.
- Jakobsen B and Rosendahl F (1994) The Sleipner Accident. *Structural Engineering International* 3: 190–193.
- Zienkiewicz OC and Taylor RL (1989) *The Finite Element Method*. London.
- Zuse K (1984) *Der Computer – Mein Lebenswerk*. Springer, Heidelberg.

Chapter 2

Truss and beam structures

The internal forces and moments in trusses and beams can be determined by means of FEM as well as by load transfer methods. Either method produces the same model problems when considering actual structures.

Truss systems are not only used for analysing beams and columns. Nowadays, they are also used as an equivalent system for the structural analysis of flat shell structures such as shear walls (see Section 2.5) or T-beam bridges (see Section 2.8). The main reason for this simplification of spatial shell structures by simple beams is that the amount of calculations needed for beam or truss systems is considerably less than that needed for 3D shell design. This is especially true for the calculation of reinforcement requirements.

This chapter starts off by examining various detailed problems related to the correct modelling of the so-called ‘discontinuity regions’. *Discontinuity regions* are those where the essential assumption of truss elements – the Bernoulli hypothesis, which states that the section remains approximately plane before and after loading – is not valid. Examples considered are those of beam column intersections, frame corners, beams with abrupt or smooth change of cross-sections or openings, halving joints and inclined haunches.

Even if the action effects in these discontinuity regions cannot be calculated accurately, it is important to model the different stiffnesses of a structure. The main difference in the various models used for frame corners are shown using the examples of a frame bridge with shallow foundations and the transverse design of a hollow box girder bridge. The modelling of a foundation slab bedded on ground (Section 2.4.1) and a bridge column supported on piles (Section 2.4.3) will also be discussed.

Following the discussion of these detailed problems, we look at the design of whole structures. The calculation of coupled concrete shear walls with large openings, which are used as bracing elements in high-rise buildings, is shown in Section 2.5. Then, the modelling of a complex bracing system of a high-rise building, consisting of core elements of different shapes and shear walls, is discussed, followed by the analysis of a hollow box girder and a T-beam bridge by means of a grillage (plane grid) system. This chapter concludes by looking at some problems in the calculation of reinforcement requirements in beams and material nonlinear analysis.

2.1. Corners in frame structures – rigid regions

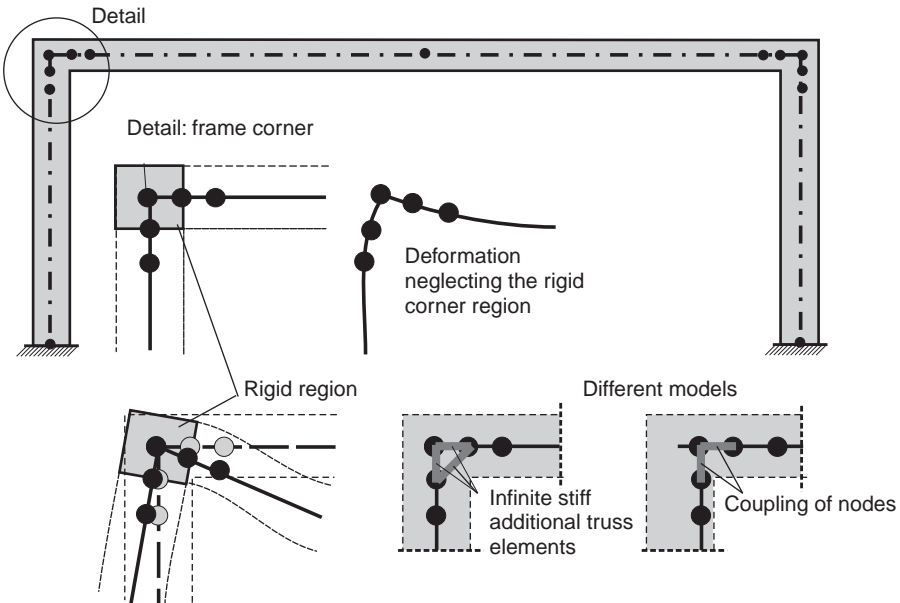
Beam column intersections are regions for which the assumption that a section remains approximately plane before and after loading (the Bernoulli hypothesis) does not apply. Here, truss analysis can only provide an approximate value for the member forces.

In design calculations, ‘exact’ values are often not needed. In general, the purpose of the structural analysis of a frame is not to calculate the maximum member forces at the beam column junction of the centrelines, but rather at the inner face of the corner for bending or at a distance of $0.5d$ to $1.0d$ for shear, depending on the design code (d = effective depth of a cross-section). However, the exact modelling of the stiffness of the frame corner is important, as these can have a large effect on both the internal forces and the deformation of a member or structure.

In a real structure, the frame corners generally behave like a stiff diaphragm. Therefore, in these areas, the nodes of the truss model cannot move independently of each other (see Figure 2.1). The simplest way of taking this condition into account is through a stiff coupling of the corner nodes. An alternative is to introduce an additional stiff inclined truss element. However, this may cause numerical problems because of the great stiffness differences of the system.

The following two examples will show the influence of the numerical modelling of beam column intersections. The first one is a portal frame bridge with shallow foundations,

Figure 2.1 Frame structure



which is widely used for road underpasses. The second example deals with the transverse design of a hollow box girder bridge.

2.1.1 Portal frame bridge

When modelling a truss system, the nodes must be in sections that are relevant to the design. Most computer programs determine the member forces and the reinforcement requirements only for the nodes at the beginning and the end of the element, or at the integration points.

The relevant sections for design are

- at a distance of $0.2d_{\text{beam}}$ from the inner face of the corner and at the inner face of the corner in the design procedure for bending moments
- at a distance of $0.5-1d_{\text{beam}}$ (depending on the design code) from the inner face of the corner in the design procedure for shear forces
- at midspan of the top beam for the estimation of the greatest bending moments and maximum deflections.

There are various loadings to be considered in the design of portal frame bridges (Figure 2.2). This means a considerable amount of work for the manual calculation of the member forces and the design. In addition to the dead and live loads acting on and adjacent to the frame, various earth pressure distributions have to be considered. In general, the structure should be designed for the following load cases

- dead load
- active earth pressure
- increased active earth pressure on both walls

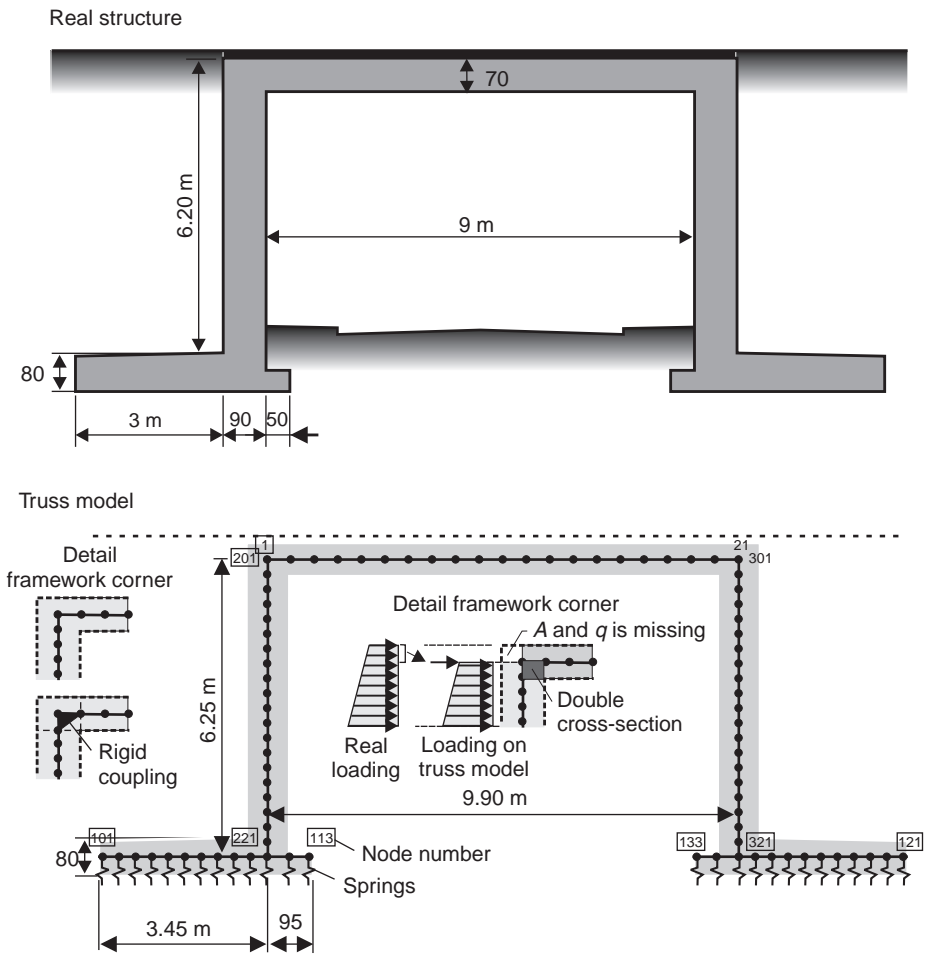
Figure 2.2 Portal frame bridge



- asymmetric earth pressure (increased active earth pressure on one wall and active earth pressure on the other)
- live load on the backfill (left/right)
- traffic loads on the bridge
- traction and braking forces of the traffic
- temperature variations, for example (for concrete bridges in Germany, see EC1), $\Delta T_{M,neg} = T_{e,min} - T_0 = -27\text{ K} - T_0$, $\Delta T_{M,pos} = T_{e,max} - T_0 = +37\text{ K} - T_0$
- differential temperature of the horizontal member $\Delta T_{M,pos} = +15\text{ K}$ and $\Delta T_{M,neg} = -8\text{ K}$ (for concrete bridges in Germany).

Furthermore, it must be remembered that, due to the short length of the foundation beam at the inner face of the frame (see Figure 2.3), member forces, as calculated by

Figure 2.3 Portal frame bridge – numerical model



the computer program, cannot be used for the purpose of design in this region. This is without doubt a discontinuity region to which the Bernoulli hypothesis does not apply. Nevertheless, the entire foundation should be modelled, since not only the member forces of the structure but also the soil pressure distribution and the settlements must be determined.

The truss elements will be located at the centreline of the beam and columns (Figure 2.3). But, in this case, the cross-section of the corner region will not be modelled correctly. However, the additional dead load can be neglected in general. The elastic bedding of the foundations can be modelled with individual springs or with special boundary elements. In this example, the bedding modulus is taken to be $k_s = 10 \text{ MN/m}^2$.

The walls are loaded by a trapezoidal earth pressure distribution. It should be kept in mind that the height of the truss model is smaller than the height of the real structure (i.e. the height of the column is 6.25 m, whereas the height of the real structure is $6.20 + 0.80 = 7 \text{ m}$; see Figure 2.3 for details). Therefore, additional horizontal loads must be applied on the corner nodes. The same applies to the vertical loads on the horizontal member.

Figure 2.4 shows the calculated bending moments, the shear forces and the displacement of the structure under dead load only. These were calculated both with and without coupling of the corner nodes to illustrate the effect of this measure.

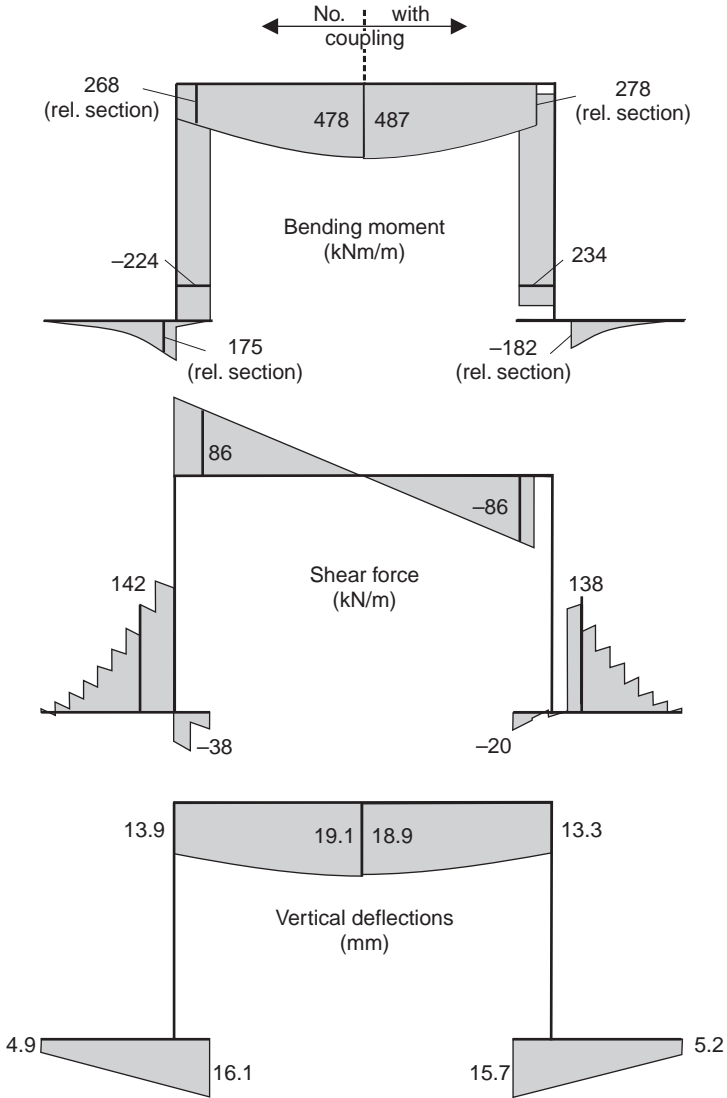
With this system, as expected, the influence of the nodal coupling is very small (see Figure 2.4). This further applies to the relevant design forces from an unfavourable combination of relevant actions. The differences are estimated at less than 3% for the bending moment in the critical sections, and approximately 6% for the vertical displacement at midspan.

2.1.2 Transverse design of a hollow box girder bridge

Figure 2.5 shows the cross-section of a hollow box girder bridge. In this particular case, these segments are the standard cross-section of one of the longest segmental hollow box girder bridges in the world, the Second Stage Expressway System (Figure 2.6) in Bangkok, Thailand (Rombach, 1997, 2003).

The design of a bridge is usually done separately for the transverse and longitudinal directions. In the following example, we are looking at only the transverse behaviour. To do this, a 1-m-wide section is taken of the bridge and modelled by truss elements. The variable depth of the beams and the inclination of the axis of gravity are taken into account (see Figure 2.7). There are pin supports under the webs, which are fully restrained in the vertical direction. This is a rough simplification of the real behaviour (see Figure 2.75). Distortions of the cross-section caused by unsymmetrical loads are neglected. The system is also a frame structure. Of further interest is the modelling of the corners, the junction between the inclined webs and the deck slab.

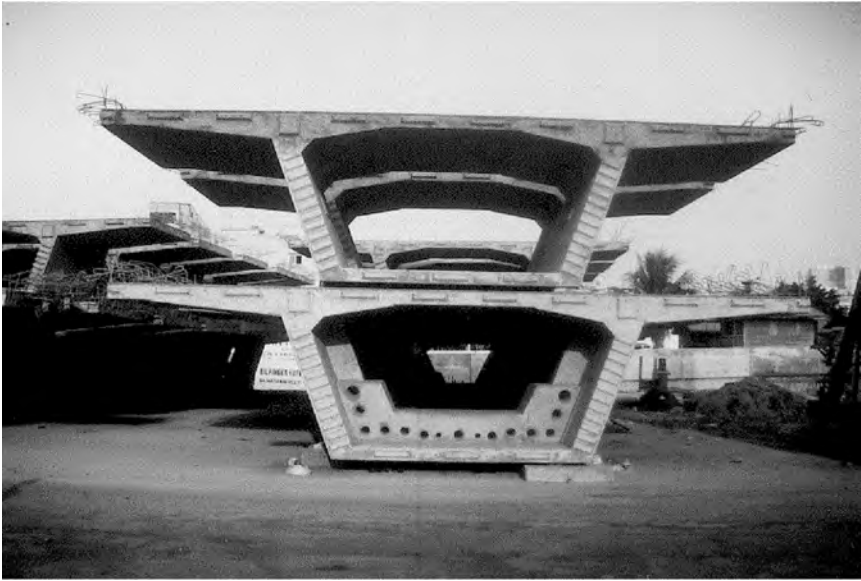
Figure 2.4 Shear forces, bending moments and deflections with and without coupling of the corner nodes for the load case 'dead load'



The behaviour of the structure will be examined under two different theoretical unit loadings, a linear loading of $q = 10 \text{ kN/m}$ at (a) the outer edge of the cantilever slab and (b) at midspan of the top slab.

For the load on the cantilever slab, the bending moments and displacements are only slightly (by 5%) influenced by the modelling of the corners (with/without coupling) (see Figure 2.9). For the line load acting at midspan of the top slab, the coupling of

Figure 2.5 Standard and deviator segment, Second Stage Expressway, Bangkok (Rombach, 1997)

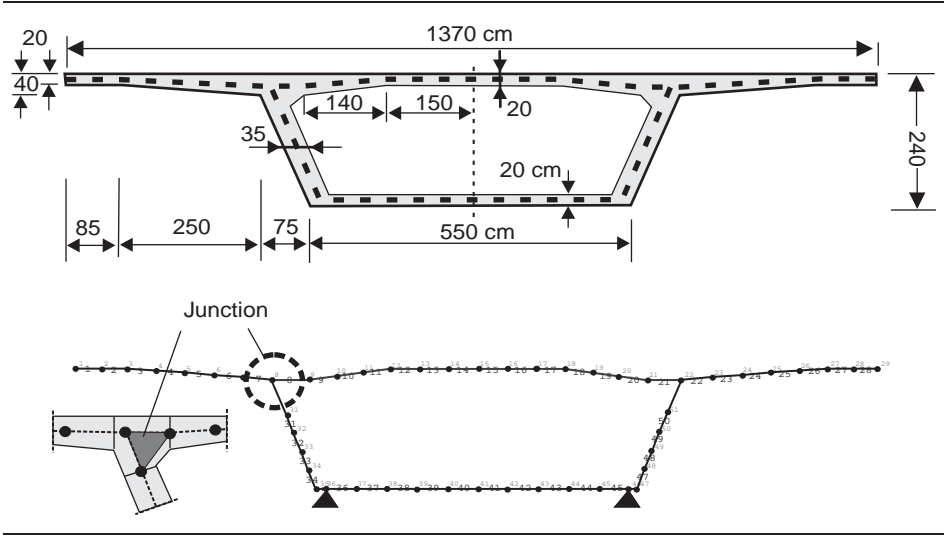


the corners causes the bending moments and the deflection at midspan to vary by approximately 10% and 50%, respectively. The latter value definitely cannot be neglected. The difference between the moment and displacement shows that the coupling of the corner nodes mainly reduces the span width. The increased restraint of the top slab does not have a significant effect on the member forces. The bending moment M_F of a fully restrained single-span beam under concentrated load at midspan is proportional

Figure 2.6 'Standard' span, Second Stage Expressway, Bangkok (Rombach, 1997)



Figure 2.7 Cross-section and resulting truss model of a hollow box girder bridge (standard segment, Second Stage Expressway, Bangkok)



to the span length to the power of 1 ($M_f = F_v l / 8$), whereas the deflection at midspan f is proportional to the span width to the power of 3 ($f = F_v l^3 / [192 \cdot E \cdot I]$). However, it must be pointed out here that the influence of the node coupling depends largely on the geometry of the system. The width of the webs of segmental hollow box girder bridges with external prestressing is very small in relation to in-situ constructions with bonded tendons. The latter usually has a web thickness of more than 50 cm due to the space required for the tendons and the couplers. Here, the influence of the coupling of the corner nodes on the shear forces and moments can be much larger.

With shell or membrane models (diaphragms), the behaviour of the ‘elastic’ structure can be analysed more precisely. This will be shown in the Chapters 3 and 4. However, the

Figure 2.8 Reinforcement layout

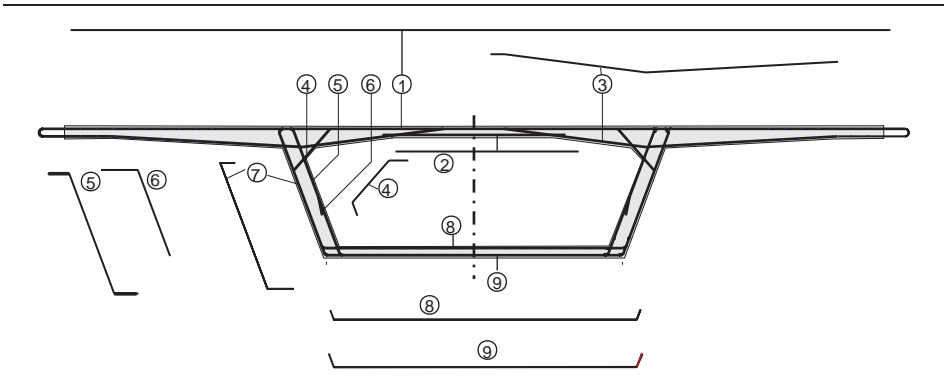
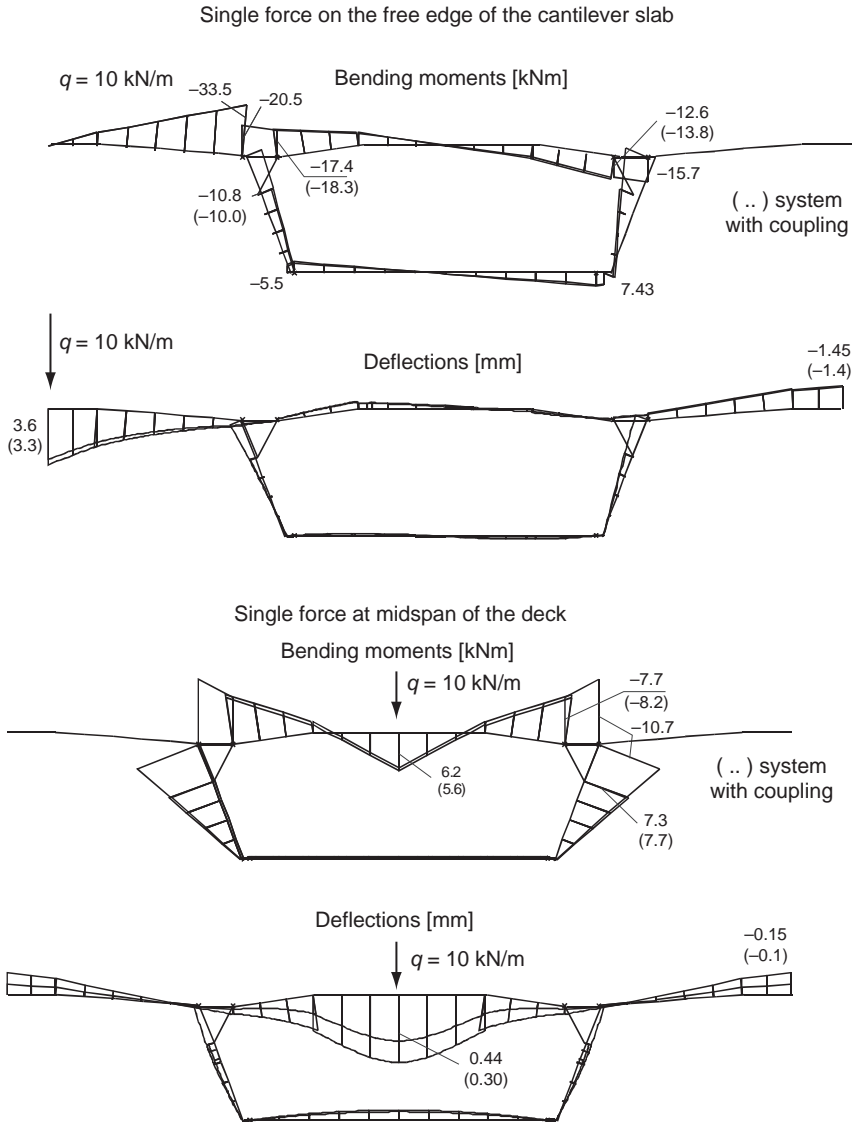


Figure 2.9 Bending moment distribution and deflections due to a single force at the free edge of the cantilever slab (top) and at midspan of the deck (bottom)



results of such calculations are presented here in order to show the complex stress distribution in corner regions.

Figure 2.11 shows the membrane forces in a web-deck slab-junction for a load of 10 kN/m acting at the free edge of the cantilever beam (FE mesh; see Figure 2.10).

Figure 2.10 FE mesh



One recognises a very complex force distribution, which certainly cannot be modelled by beam or truss elements based on the linear strain theory (the Bernoulli hypothesis). Outside this discontinuity region, the strains and stresses are linear over the depth of the section. The discontinuity region extends up to a distance $\approx h$ from the continuity.

In Table 2.1, the bending moments and the displacements in the relevant sections of the structure are compared with each other for both load cases. Good agreement can be seen in the bending moments. However, there are relatively big differences in the midspan displacements.

Besides the structural analysis, good detailing of the reinforcement in corner regions is very important with respect to both the load-bearing capacity and the serviceability of the structure (see Figures 2.8 and 2.12). Many experimental investigations were conducted and several theoretical design models have been evaluated to design such sections.

Figure 2.11 Main membrane forces and distribution of the horizontal resp. vertical membrane force n_x (flange) and n_y (web) over the section depth; loading: $q = 10 \text{ kN/m}$ at the free end of the cantilever slab

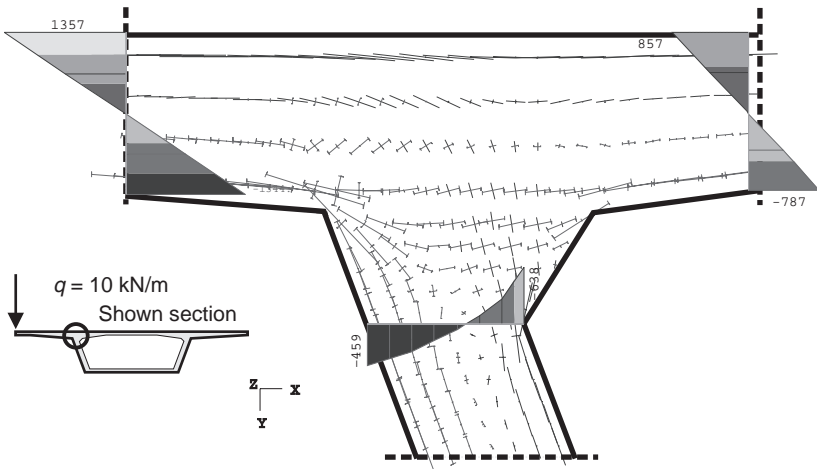
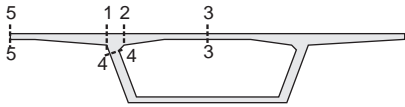
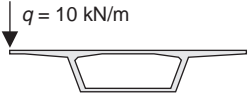
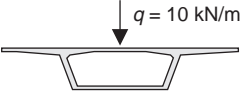


Table 2.1 Bending moments and displacements in the relevant sections

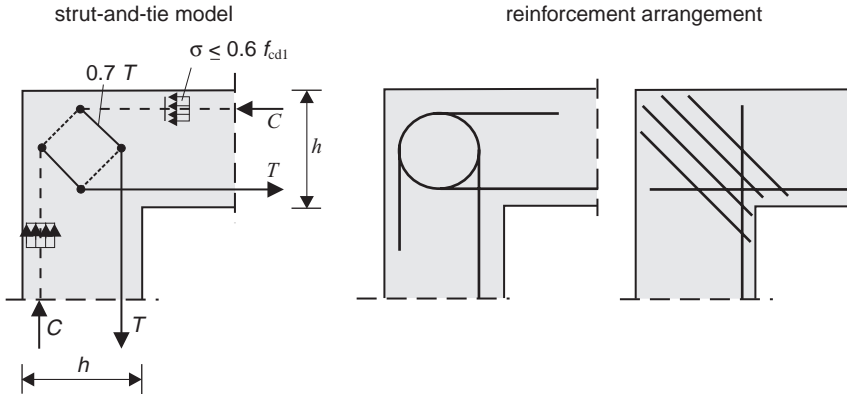
				
Bending moments: kNm/m	Section 1-1	Section 2-2	Section 3-3	Section 4-4
Load case 1: $q = 10$ kN/m at the free edge of the cantilever slab				
Truss model without coupling	-33.5	-17.4	≈ 0	-10.8
Truss model with coupling	-33.5	-18.3	≈ 0	-10.0
Shell analysis	-33.4	-18.3	≈ 0	-11.4
Load case 2: $q = 10$ kN/m at midspan of the deck				
Truss model without coupling	0	-7.7	6.2	7.3
Truss model with coupling	0	-8.2	5.6	7.7
Shell analysis	0	-7.7	5.3	8.0
Displacements: mm				
	Section 3-3	Section 5-5		
Load case 1: $q = 10$ kN/m at the free edge of the cantilever slab				
Truss model without coupling	≈ 0	3.6		
Truss model with coupling	≈ 0	3.3		
Shell analysis	≈ 0	3.7		
Load case 2: $q = 10$ kN/m at midspan of the deck				
Truss model without coupling	0.44	-0.15		
Truss model with coupling	0.30	-0.10		
Shell analysis	0.36	-0.17		

2.2. Beams with variable depth – inclined haunches

The depth of a beam may be increased to optimise the reinforcement arrangement at the intermediate supports (greater lever arm) and to reduce the midspan bending moment (Figures 2.13 and 2.14).

For frame structures with inclined haunches, the variable depth and the inclination of the axis of gravity should be modelled in addition to the coupling of the corner nodes.

Figure 2.12 Frame corner with high opening bending moment; strut-and-tie model and resulting arrangement of reinforcement (according to Schlaich *et al.*, 1987)



Furthermore, the inclined haunches should be discretised by a sufficient number of elements, as the cross-section is usually assumed to be constant within an FE.

As will be demonstrated later, the inclination of the axis of gravity generally only has a small influence on the action effects, where the system is not horizontally restrained. Nevertheless, this inclination should not be neglected, as it is very important with respect to the design for shear (Figures 2.15a–c). A straight beam axis with constant depth of elements will cause mistakes as the slope of the compression strut with respect to the tension chord is neglected. Therefore, the resulting change in the design shear resistance V_{Rd} is not considered (see Figure 2.15c).

$$V_{Rd} = V_{Rd,s} + V_{ccd} + V_{td} \quad (\text{Eurocode 2, 2004: Part 1, Equation 6.1}) \quad (2.1)$$

Figure 2.13 Frame corner with inclined haunch

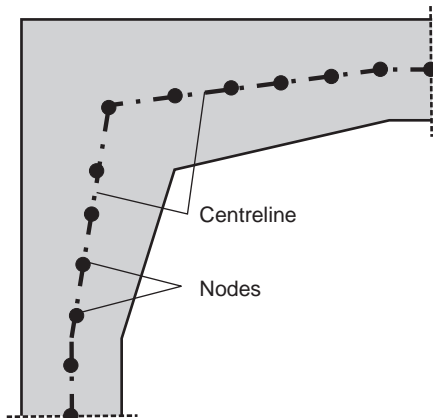


Figure 2.14 Haunched T-beam girder of a prefabricated industrial building

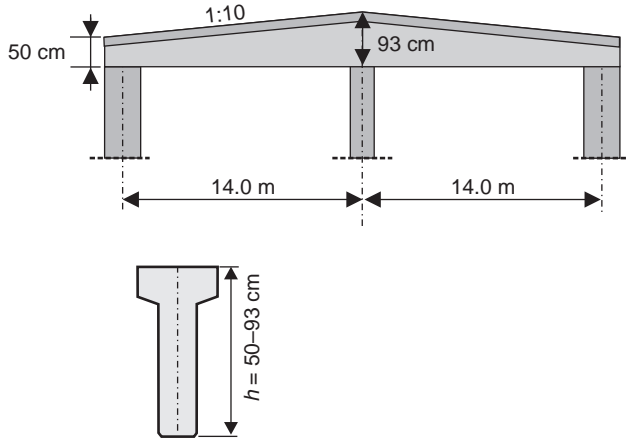
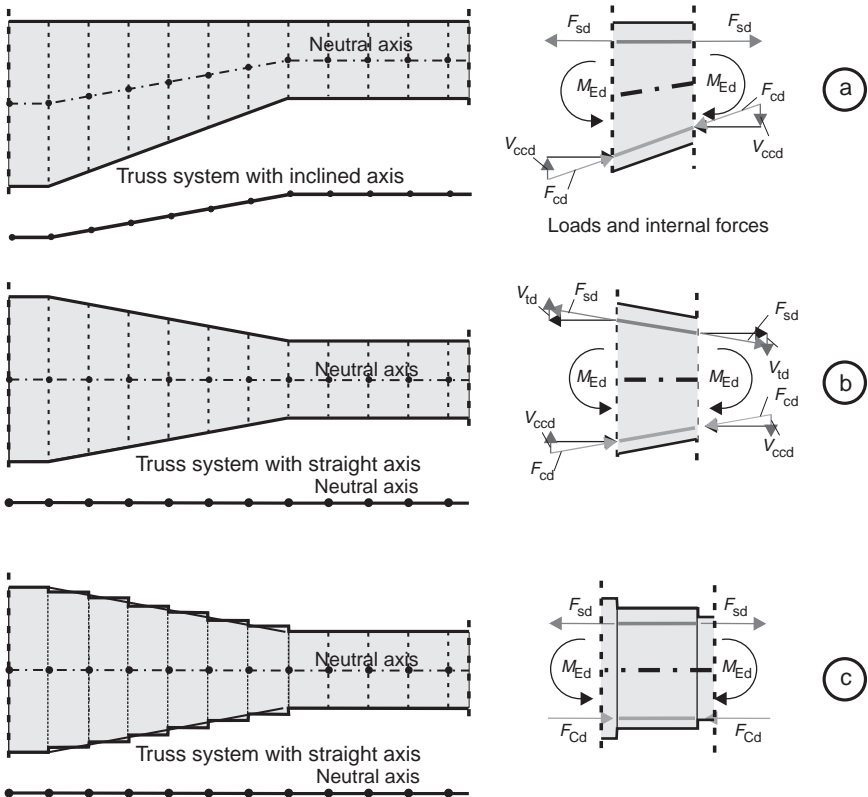


Figure 2.15 Various models for an inclined haunched beam and resulting internal forces and moments



where:

$V_{Rd,s}$ is the design value of the shear force that can be sustained by the yielding shear reinforcement.

V_{ccd} is the design value of the shear component of the force in the compression area, in the case of an inclined compression chord.

V_{td} is the design value of the shear component of the force in the tensile reinforcement, in the case of an inclined tensile chord.

The support conditions have to be checked when the inclination of the axis of gravity is considered in the FE model. For a straight single-span girder under uniformly distributed loads, a horizontal restraint of the supports does not change the member forces and moments in the structure. This is not true for inclined truss elements where the support nodes are fixed in the horizontal direction. The strutted frame system is modelled in the following example. Figure 2.16 shows the member forces and deflections for a fully restrained single-span beam of variable depth (inner span of a bridge). The span length is 50 m. In order to show the influence of the variable depth of cross-section, a relatively large depth of $h = 4.0$ m has been chosen at the supports, whereas in midspan the depth is only $h = 1.0$ m. Two different support conditions are considered:

Model (a): fully restrained supports

Model (b): no restraint in horizontal direction

As can be seen from the distribution of the member forces, a strutted frame system results if both supports are fully restrained. This causes high normal forces, even for the slender beam in the example. In Model (b), the support bending moment for the fully restrained system are reduced by 26%, the shear forces by 19% and the displacement at midspan by approximately 10% with respect to Model (a).

It should be noted that, per definition, normal forces are always in the direction of the beam axis and shear forces are perpendicular to it. That is why the shear forces at the supports are not equal to the vertical support force of 750 kN.

The manual calculation of the internal forces of a beam with variable depth can be made with the help of Figure 2.17. The diagram shows the relationship of the bending moment of a beam with constant depth to the one of linearly increasing depth, depending on the length of the inclined haunch and the depth of the beam h_a and h_h . For the previous system, the following bending moments are calculated manually:

Support bending moment $M_S = -8250$ kNm

Midspan bending moment $M_F = 1156$ kNm

Table 2.2 lists the member forces at the supports and midspan for the various models. The results of a shell analysis are also given for comparison.

The internal forces and the displacements of the truss model are confirmed by the shell model. There is also good agreement with the manually calculated results. As can be seen

Figure 2.16 Member forces and displacements of a single-span haunched beam for different support conditions

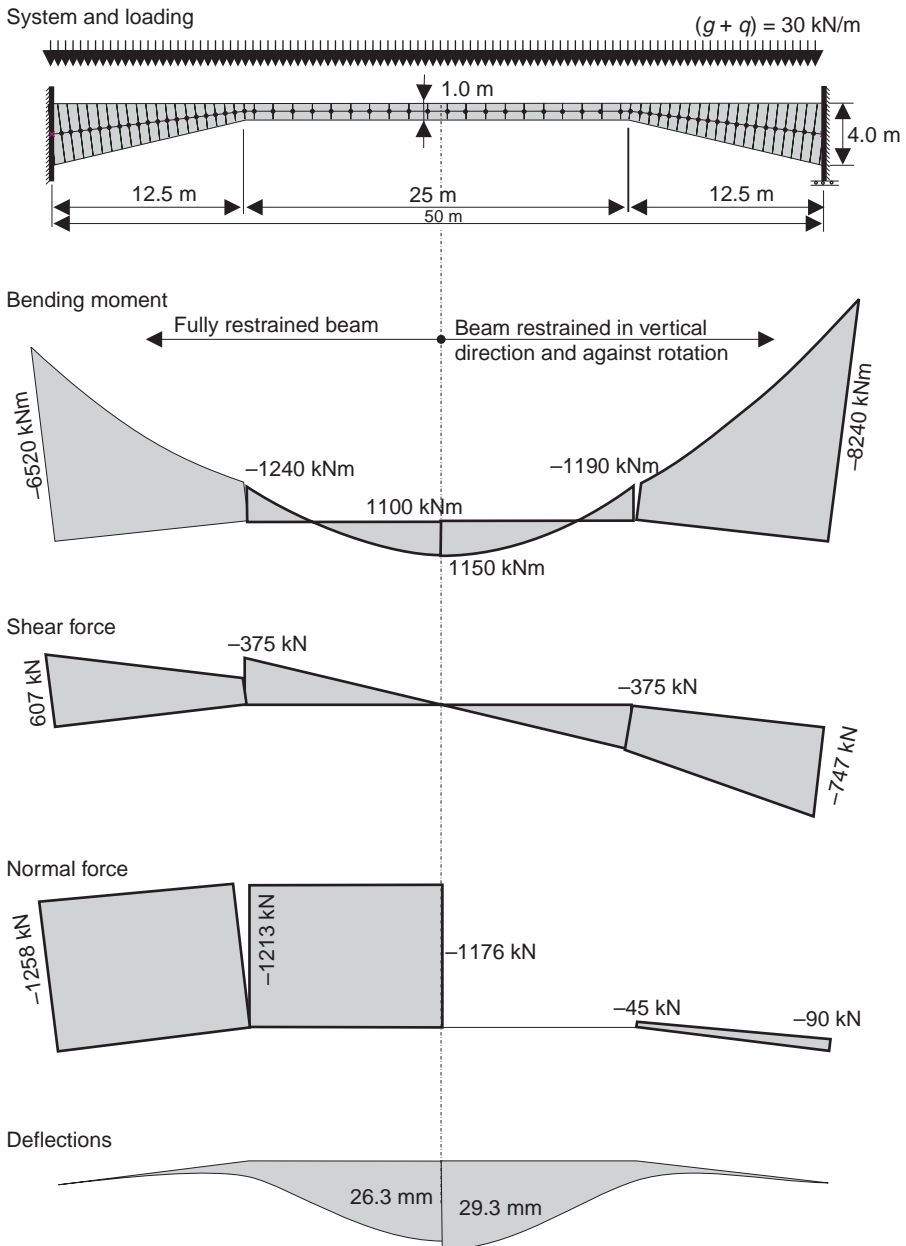


Figure 2.17 Factors for the calculation of the support and midspan bending moment of a haunched fully restrained beam (linear increase of depth)

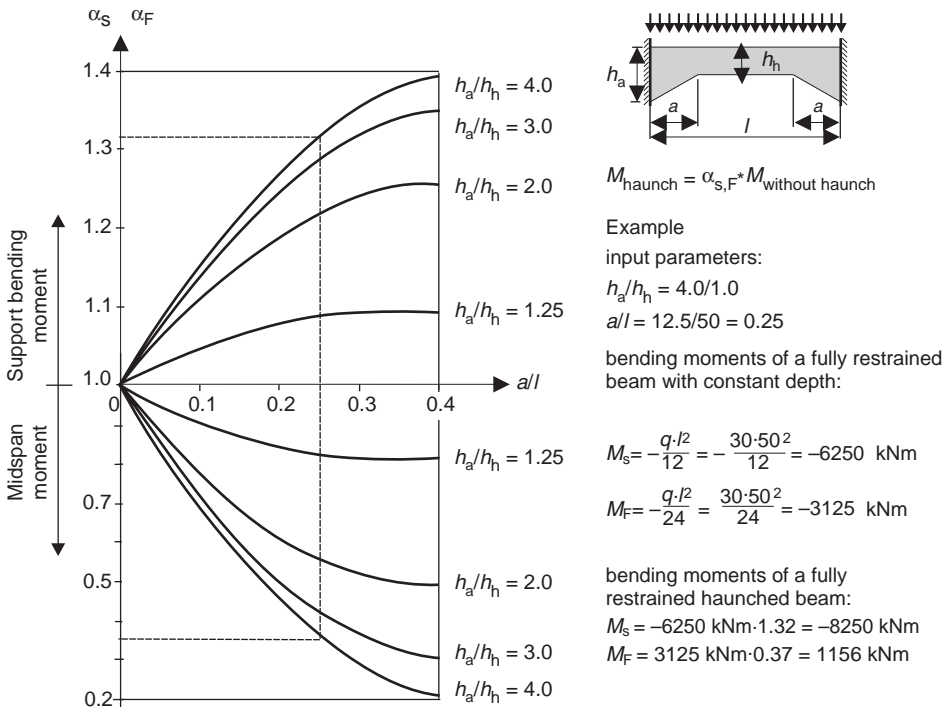


Table 2.2 Comparison of the member forces and displacements

	Analytical analysis (Figure 2.17)	Truss analysis straight axis	Truss analysis inclined axis beam fully restrained	Truss analysis inclined axis beam not restrained in horizontal direction	Shell analysis system fully restrained at the supports	Shell analysis system not restrained in horizontal direction at the supports	
Support							
N	0	0	-1258	-90	-1051	0	kN
V	750	750	607	747	750	750	kN
M	-8250	-8225	-6520	-8240	-6372	-8181	kNm
Midspan							
N	0	0	-1176	0	-1150	0	kN
V	0	0	0	0	0	0	kN
M	1156	1150	1100	1150	1150	1195	kNm
Displacement in midspan							
w	29.2	29.2	26.3	29.3	26.7	29.1	mm

from Figure 2.16, the horizontal restraint of the beam has a great influence on the internal forces.

To summarise: if the system is not restrained in the horizontal direction, and if there are no normal forces, the inclination of the axis of the truss elements can be neglected with regard to the member forces. However, for a shear design, the elements should be given a variable depth.

2.3. Beams with halving joints and openings

The Bernoulli hypothesis does not apply in beam–beam and beam–column intersections, regions of sudden change of cross-section or openings ('discontinuity regions'; see Figures 2.18 and 2.19). Therefore, one cannot analyse these areas precisely by using a truss system with FEs, which are based on a linear strain distribution over the depth of the cross-section. Nevertheless, the different stiffness values should be modelled, as the internal forces and deflections of a statically indeterminate system depend on it.

Figure 2.18 Discontinuity regions in truss structures

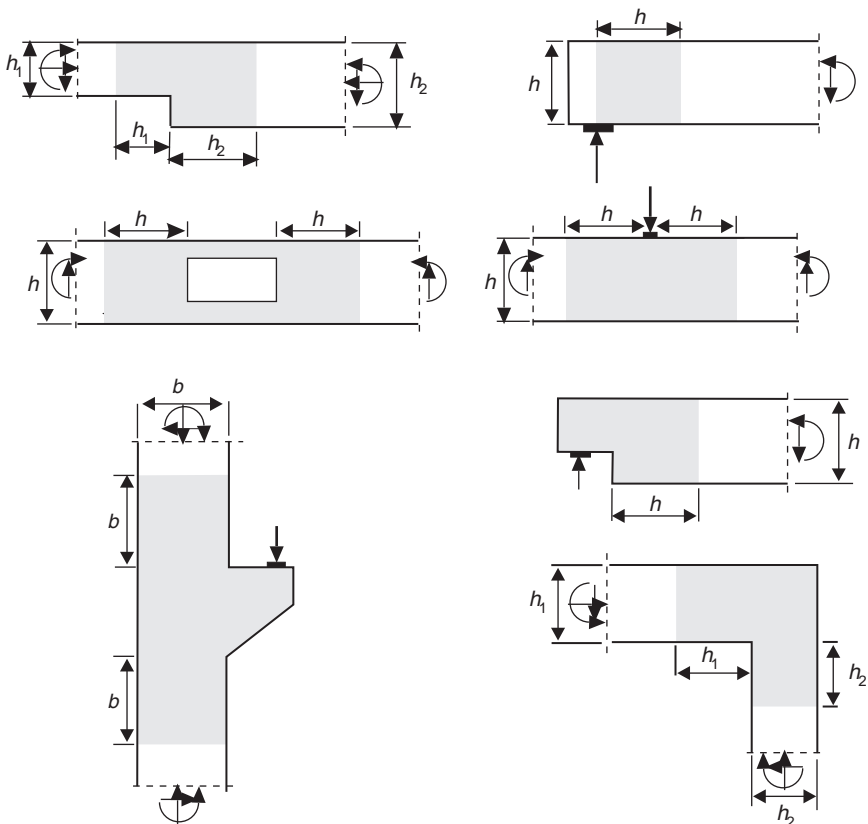
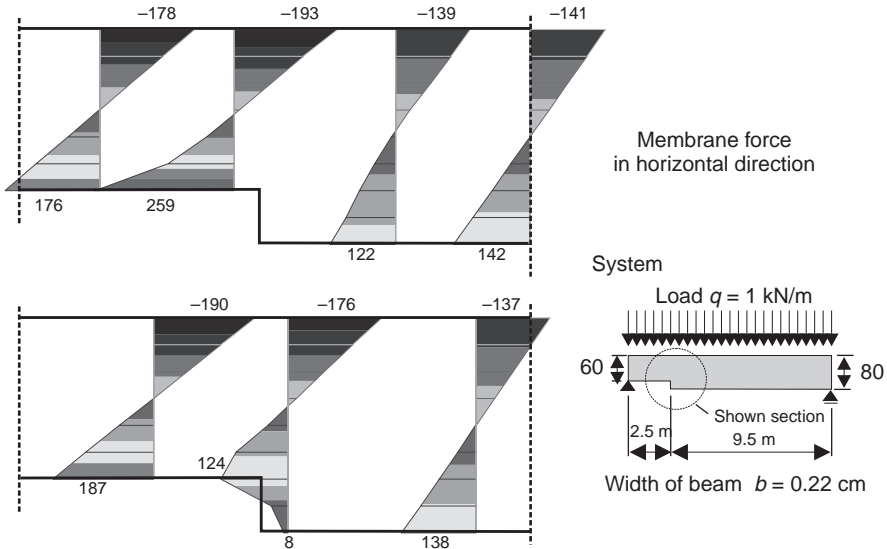


Figure 2.19 Horizontal membrane forces (= normal stress \times width of beam) in the region of a halving joint (shell analysis)



The location of the beam axis changes suddenly at a halving joint. This can easily be modelled by coupling the nodes in the joint similar to a frame corner. In the region of openings, two separate beams for the compression and tension chords should be used (Figure 2.20). The normal and bending stiffness of these elements should be fixed taking account of possible cracking in the tension zone or the ‘yielding’ in regions with high compressive stresses and the resulting reduction of stiffness.

Figure 2.20 Halving joint and opening in a beam

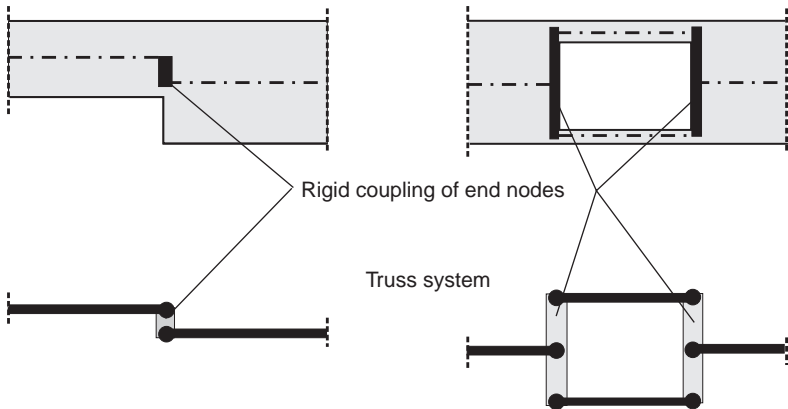
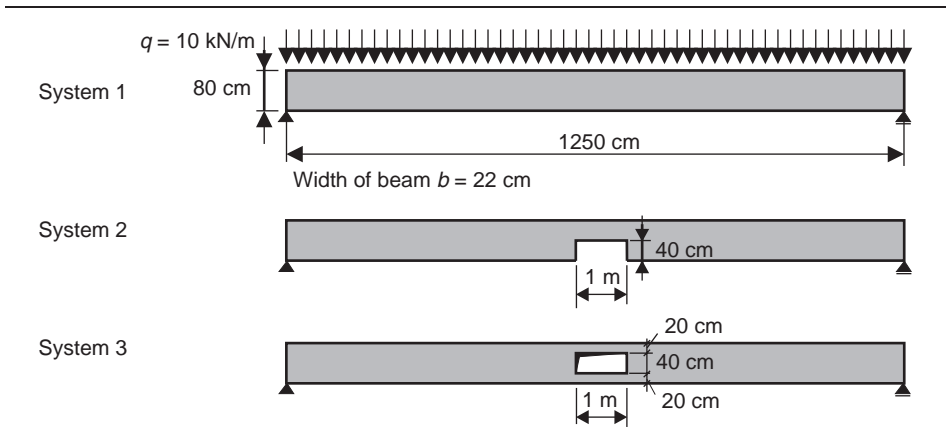


Figure 2.21 Different beams



In the following, the bending moment distribution of a single-span beam ($l = 12.5$ m) under a uniformly distributed load with an opening at midspan will be examined. This beam has been used as a girder for an existing industrial building. The results of the two different beam models and a shell model will be shown.

Only one half of the structure is shown, as the system and its loading is symmetric about the midspan. The following three systems have been analysed (Figure 2.21)

- System 1: beam without opening
- System 2: beam with an opening (1.0×0.4 m) at midspan at the lower side of the cross-section
- System 3: beam with an opening (1.0×0.4 m) at midspan on the centreline of the cross-section.

Figure 2.22 shows the bending moment distribution of the various models, both with and without considering such openings in the numerical model.

There is no change in the bending moment distribution of system number 2, as there are no normal forces acting on the beam. Therefore, the bending moment distribution does not depend on the opening with respect to the model. Nevertheless, a sudden change in strain can be observed near the opening (see Figure 2.23), which has a small influence on the deformation of the given structural system. Due to the assumption of the numerical analysis (elastic material behaviour, Bernoulli hypothesis), the strain in the concrete section is equal to:

$$\varepsilon_c = \frac{\sigma_c}{E_c} = \pm \frac{M}{E_c \cdot I} \cdot h/2$$

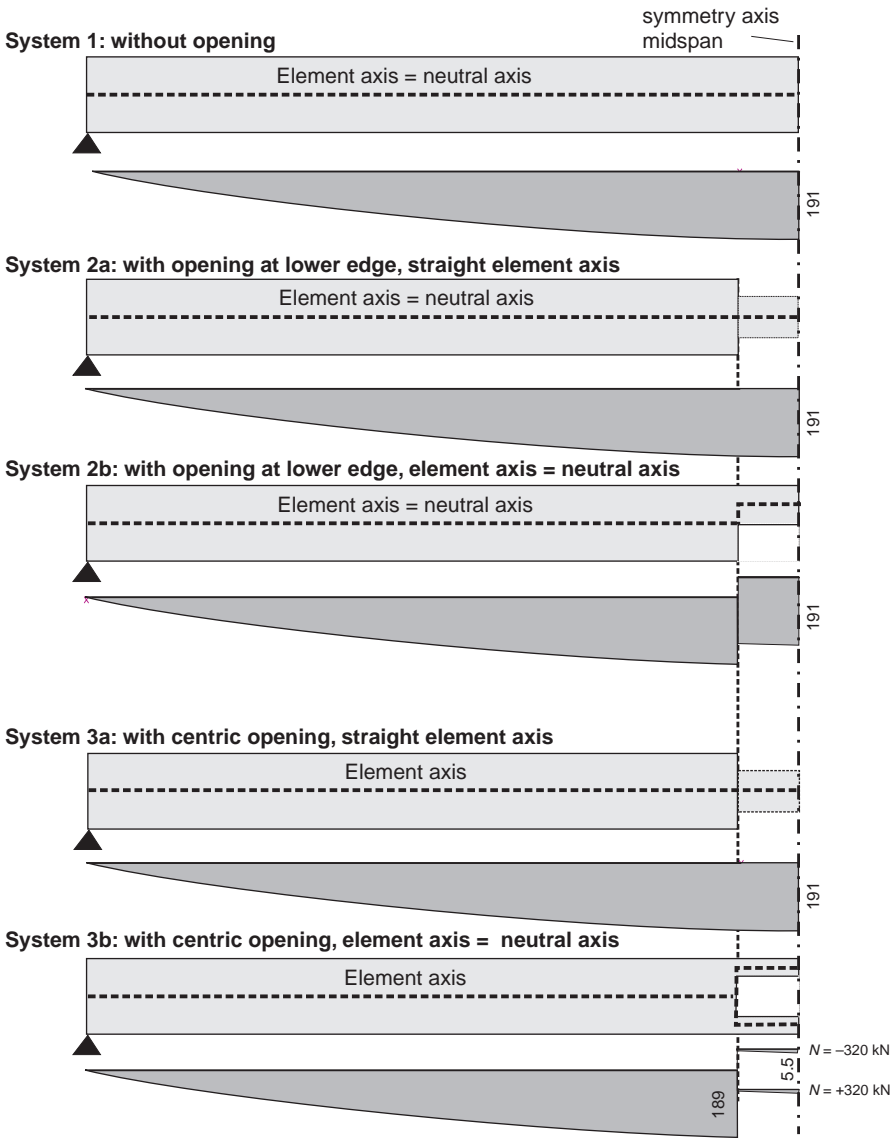
where:

M is the bending moment at the face of the opening

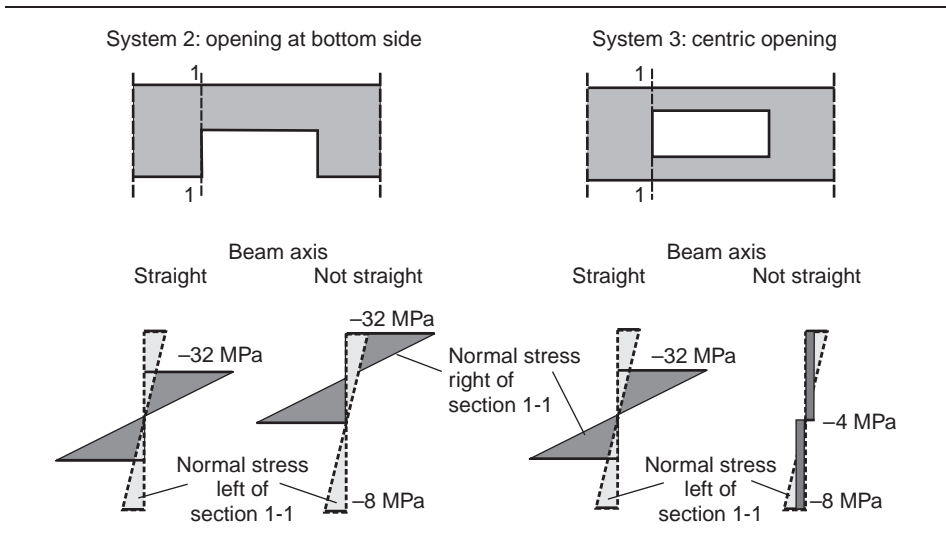
h is the overall depth of the cross-section left or right of the face of the opening

I is the second moment of area left or right of the face of the opening.

Figure 2.22 System and bending moments



In the case of a centric opening, the bending moment of the unweakened cross-section is replaced by a compression and a tension force. This different behaviour has to be modelled by two separate beams. No normal forces are calculated when this opening is neglected, and the beam axis is kept straight. This means that the stiffness is not modelled correctly, resulting in a doubling of the midspan displacement (Table 2.3).

Figure 2.23 Stress distribution near the edge of the opening – beam system


For comparison purposes, the internal forces and the deformations of the beam are calculated by a shell model. Figure 2.26 shows the membrane forces and the distribution over the depth of the beam in various sections. In most sections, a linear strain distribution can be seen. Here, the Bernoulli hypothesis is valid. Large differences are only obtained in the vicinity of the opening (see Figure 2.24). Thus, a beam system, which is based on a linear strain distribution, will always lead to incorrect results to a greater or lesser extent.

Design of the discontinuity regions can be done by strut-and-tie models (Figures 2.25 and 2.27). The results of a linear elastic shell model can be used to evaluate the load paths.

It must be noted that strut-and-tie models are only valid for the ultimate limit state design. A fully cracked structure is assumed. Therefore, these models cannot give any

Table 2.3 Deflection of the beam at midspan (in mm)




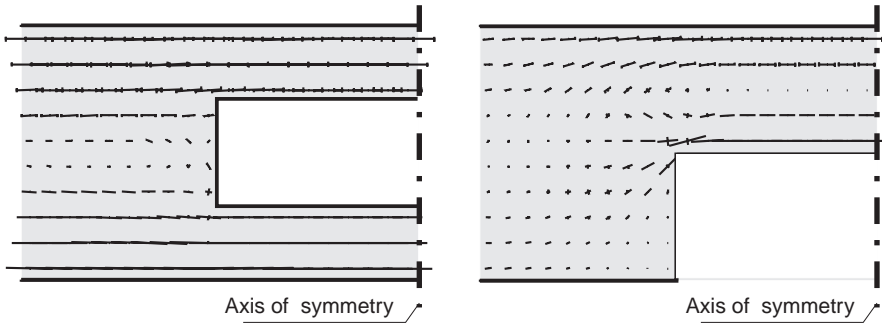
System	Beam axis	Truss model	Shell model
System 1 – no opening 	Straight	10.7	10.0
System 2 – opening at lower side 	(a) Straight	27.6	27.4
	(b) Jump	27.8	27.4
System 3 – centric opening 	(a) Straight	19.6	10.3
	(b) Jump	10.9	10.3

Figure 2.24 Membrane forces in the vicinity of the opening



information with regard to the serviceability of the structure (cracking). However, it can be useful to reduce the permissible stresses in the reinforcement in order to reduce the crack width in the D-region.

It should be noted that the shear force in the opening will be carried mainly by the compression member. This has to be considered in the design of the opening region.

The influence of the different FE models on the member forces in beams with openings was not significant in the earlier-mentioned example. However, this only results from the statically determinate structure and the assumption of a fully elastic material behaviour.

Figure 2.25 Strut-and-tie model for a halving joint (Schlaich and Schäfer, 1998)

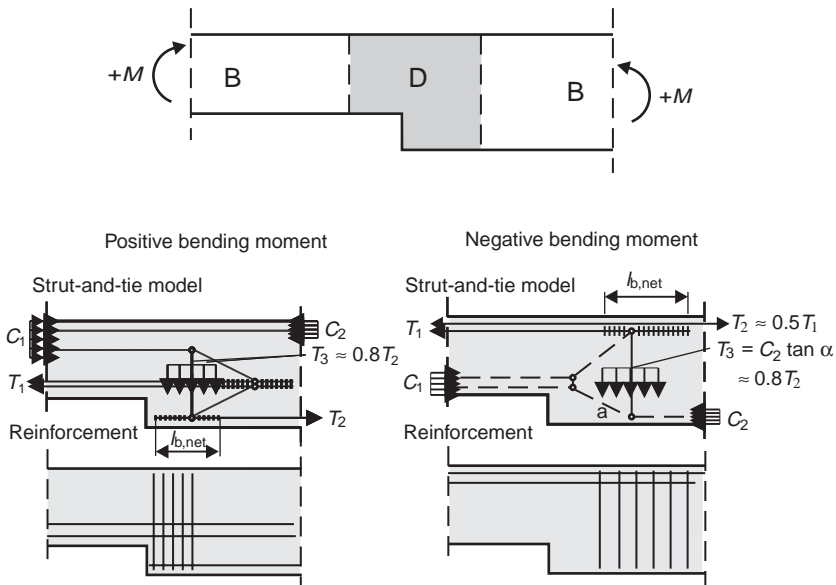
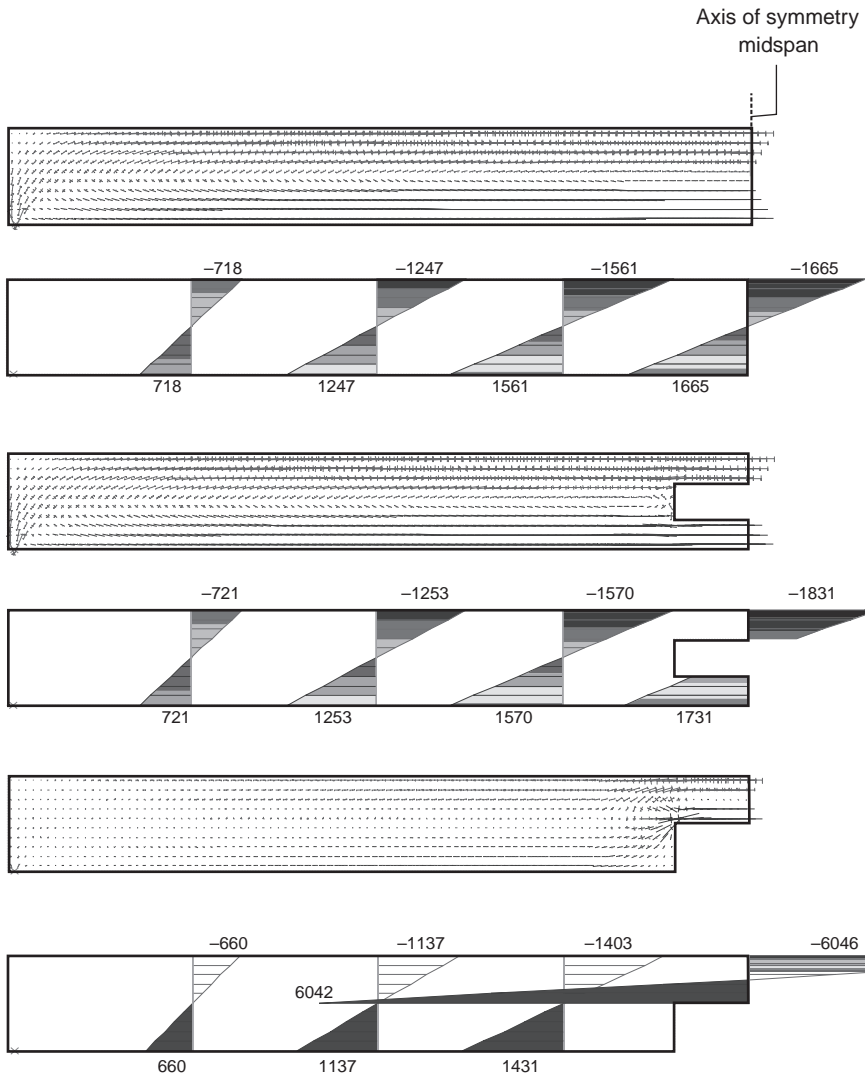


Figure 2.26 Main membrane forces in various sections (system and loading see Figure 2.21)

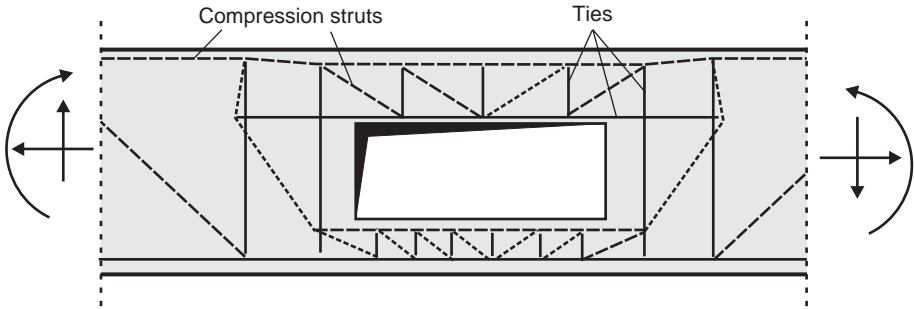


One of the main questions is the stiffness of the fully tensioned chord in the tension zone of the opening. Due to cracking of concrete, the stiffness is significantly reduced with regard to the elastic value.

This problem is clearly demonstrated in the following example for a fully restrained two-span beam under uniformly distributed loads (Figure 2.28). The beam has an opening of 20×50 cm close to the intermediate support. Three different models for the opening region are used. In the first system, the opening is neglected, whereas in the second, the tension and compression chord in the opening is modelled by two separate beams

Figure 2.27 Strut-and-tie model for a beam with an opening

Schlaich and Schäfer, 1998 © Wiley – VCH Verlag GmbH & Co. KGaA. Reproduced with permission.



that are rigid, coupled with the centre nodes of the undisturbed beam (Figure 2.20). In the third system, hinge couplings (no bending moments) are used to take account of the lack of bending stiffness in a fully tensioned member.

There are only very small differences for Models 1 and 2 (Figure 2.28). But, Model 3 results in totally different member forces. The left span tends to become a cantilever beam. The bending moment over the intermediate support becomes positive.

Figure 2.28 Member forces of a two-span beam for three different models used for the opening

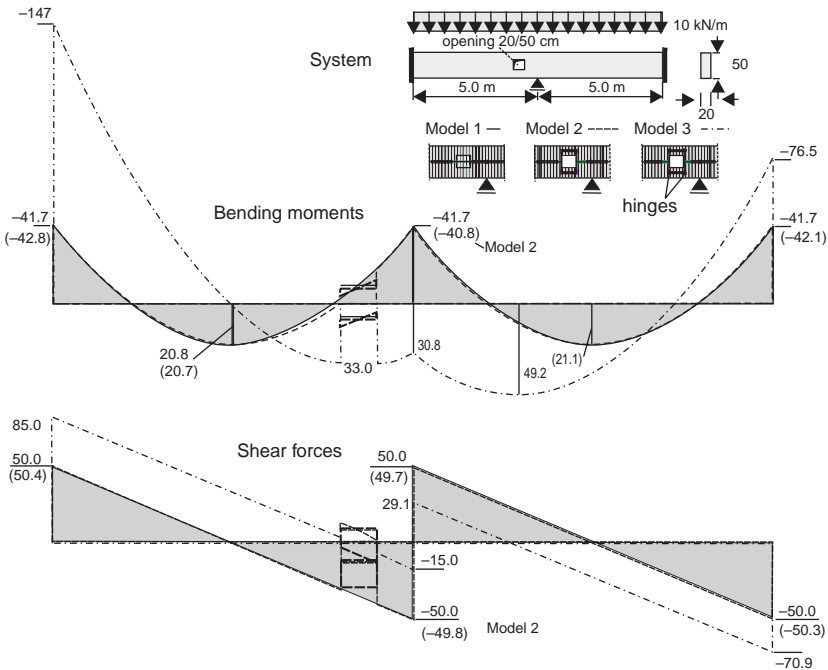
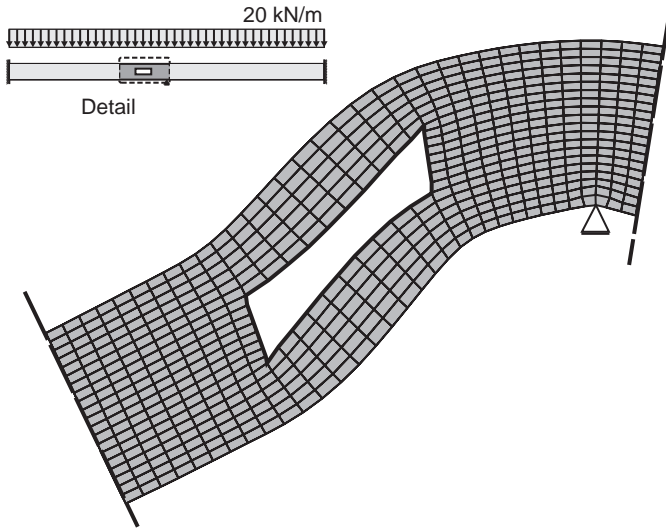


Figure 2.29 Deformation of girder in the opening region (plane shell analysis)



It should be pointed out, however, that Model 3 is an extreme case, presented just to demonstrate the importance of the correct manner of modelling the stiffness in the region of the opening. Parametric studies with different element stiffness have to be conducted to find the most realistic distribution of member forces for this system. Figure 2.29 shows the deformation of the girder in the opening region. Great shear deformations can be observed, which can hardly be modelled by beam elements. The horizontal stresses are almost linear in the opening region (Figure 2.30).

2.4. Soft supports – elastic bedding

2.4.1 Elastic bedded foundation beam

There are many structures where the supports are not fully or partly restrained and where the deflection of the supports cannot be neglected. For example, in the design of shallow foundations, the soil settlement, the interaction between the structure and the ground, must be considered. Also, the deformation of the support for structures on elastomeric bearings must not be neglected either. A soft support can be modelled by (Figure 2.31)

Figure 2.30 Horizontal stresses in MPa in the opening region (plane shell analysis)

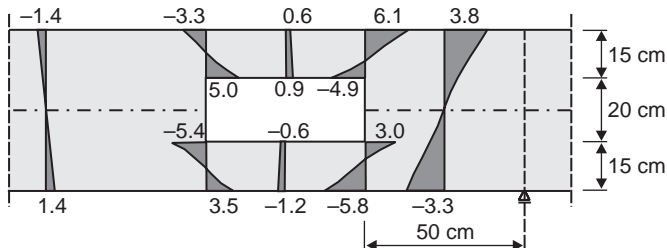
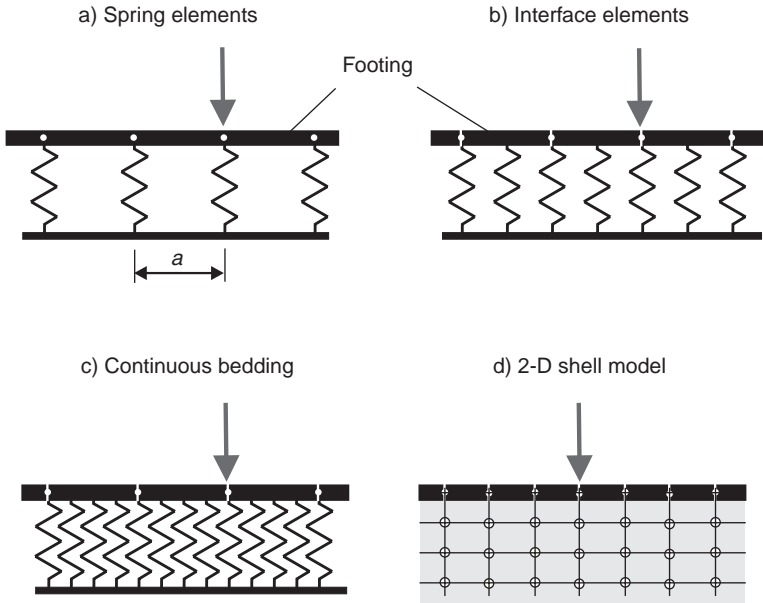


Figure 2.31 Different models for soft (elastic) support



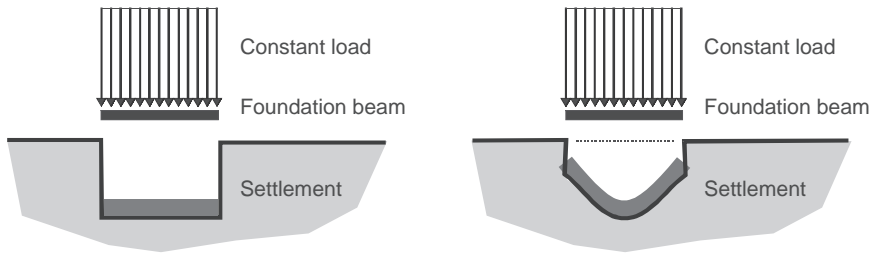
- (a) individual spring elements
- (b) special interface elements
- (c) continuous elastic supported elements
- (d) plane or 3D shell or volume elements.

The friction between the foundation and the ground can be modelled by horizontal springs. Linear as well as nonlinear spring characteristics can be used. A nonlinear analysis is required if certain load arrangements show tension stresses in the ground, which cannot occur in reality due to uplifting of the foundation beam.

The results of the model (a–c) are identical if the length or the spacing of the elements is sufficiently small. In practice, the advantage of using special interface elements instead of individual springs is that the normal stiffness does not depend on the length of the element for a given soil modulus. For individual springs, the stiffness depends on the spacing of the elements (Figure 2.31a). Continuous bedded elements are used in elastic supported foundation slabs, where the effects of the bedding can be directly introduced into the element stiffness matrices (see Section 4.10).

All of these methods, except the continuum model (d), are based on a linear relationship between the local force and the local deformation of the soil (foundation or stiffness modulus method). This method does not consider the shear stiffness of the soil. Therefore, in general, the displacements and associated reactions of the soil and the structure are not compatible (Figure 2.32). The error caused by this simplification can often be

Figure 2.32 Deformation of soil and structure – foundation modulus and constraint modulus method



neglected in practice. However, when designing a shallow foundation, one has to keep in mind that a uniformly distributed load on an elastic bedded beam or slab does not result in any member forces (see Figure 2.32). In such a case, it is recommended that studies with 2D or 3D continuum models are made (e.g. constrained modulus method). But, this usually requires a much greater effort. Please note that the considerable uncertainties of soil behaviour cannot be overcome by using more refined numerical models.

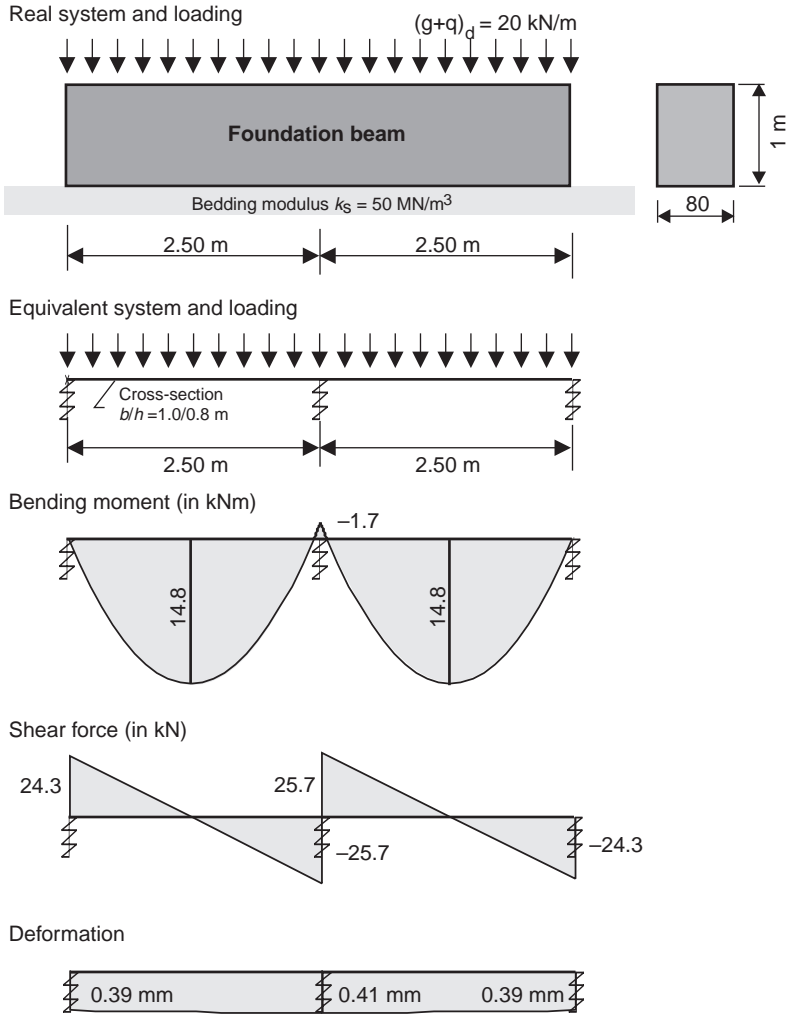
When using distinct spring elements, the reaction of the ground is introduced into the structures by single forces. Even at the free end of a foundation beam, a force is estimated, which results in a shear force at the end of the beam (Figure 2.33). Therefore, the calculated shear forces are only correct in the middle of each beam element. However, for design purposes, the distribution of the internal forces can be smoothed out.

The discretisation, the number of elements per length, has considerable influence on the member forces. This aspect will therefore be discussed in greater detail. As an example, an elastic supported beam with rectangular cross-section ($b/h = 1.0/0.8$ m) and a length of 5.0 m is analysed under a uniformly distributed load and a single load at midspan.

First, a very coarse element mesh is used, having only two beam and three spring elements (Figure 2.33). The spring stiffness is calculated for a constant influence width of $2.50\text{ m}/2 = 1.25$ m for the outer springs and 2.50 m for the inner springs. As demonstrated in Figure 2.33, even for a system under a uniformly distributed load, significant bending moments and shear forces are estimated. As mentioned previously, due to the assumption of the elastic modulus method, no bending moments and shear forces should be estimated under uniform loads. In principle, the calculated member forces correspond to a two-span continuous beam where the intermediate support has settled downwards. With a refined element mesh, the results are more reasonable (see Figure 2.34a). Here, the member forces and the displacement in midspan are plotted against the number of truss and spring elements.

At first, one would suppose that more elements are required for a beam with a concentrated load than for one under a continuous load. This is not the case, as the results of a parametric study demonstrate (see Figure 2.34b). Here, the member forces are plotted for

Figure 2.33 Beam supported on three elastic springs under uniformly distributed load

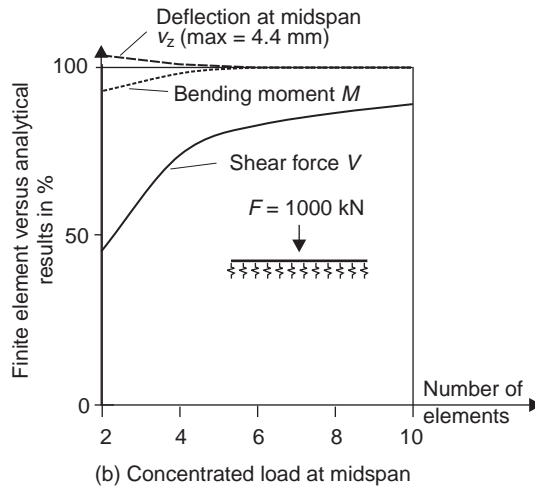
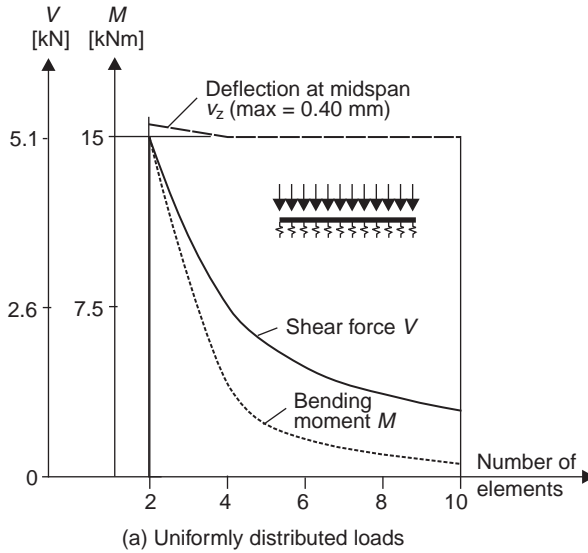


2–10 elements against the analytical values (see Figure 2.35). With regard to the bending moment and displacement at midspan, six elements are sufficient. For the shear forces, a more refined element mesh is required. The midspan deflection for both load cases is not very sensitive to the number of elements.

As the previous calculations have shown, the length of beam elements with respect to the distance of the springs is limited by the following requirements.

- *The deformation of the structure and the resulting soil reactions must be modelled with a sufficient degree of accuracy.* The element length is limited by the shape of

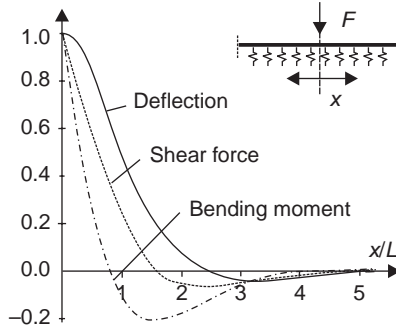
Figure 2.34 Midspan deflection, shear forces and bending moments of an elastic supported beam with increasing number of spring and beam elements



the structural deflection curve and the form functions of the used truss and interface elements. If the foundation has a small bending stiffness, as in the preceding example, the deflection curve can be described by using only a few elements.

It is generally recommended that the length of a beam element Δl depend on the so-called 'characteristic length' L . The following calculation provides the characteristic length for

Figure 2.35 Deformations and member forces of an infinite elastic bedded foundation beam under concentrated load



Deformation $y(x)$:

$$E_c \cdot I_c \cdot y(x) = \frac{F \cdot L^3}{8} \cdot e^{-x/L} \cdot [\cos(x/L) + \sin(x/L)]$$

Bending moment:

$$M(x) = -E_c \cdot I_c \cdot y''(x) = \frac{F \cdot L}{4} \cdot e^{-x/L} \cdot [\cos(x/L) - \sin(x/L)]$$

Shear force:

$$V(x) = -E_c \cdot I_c \cdot y'''(x) = -0.5 \cdot F \cdot e^{-x/L} \cdot \cos(x/L)$$

the preceding example

$$L = \sqrt[4]{\frac{4 \cdot E_c \cdot I_c}{k_s \cdot b}} = \sqrt[4]{\frac{4 \cdot 32000 \cdot 0.8^3 / 12}{50 \cdot 1.0}} = 3.23 \text{ m}$$

where:

EI is the bending stiffness of the foundation beam

b is the width of the beam

k_s is the bedding modulus of the soil.

This recommendation is based on the deflection curve of an infinite foundation beam. The displacement of such a structure under a single load is zero at a distance of $x/L = 3/4\pi, 7/4\pi, 10/4\pi, \dots$. The length of the element should be chosen to describe this deformation pattern with sufficient accuracy, depending on the form functions used (see Figure 2.35). In the case of a linear function, the length of the beam elements Δl should not be greater than approximately $1/4L$. For elements with quadratic and cubic functions, fewer elements are required.

- *The distribution of the member forces must be modelled with a sufficient degree of accuracy.* The correlation between the element length and the shear force

distribution results from the element type used in the numerical analysis. In the case of no internal element loads, they are based on the assumption of a linear shear force distribution within each individual element. Refinement of the element mesh results in a more accurate description of the actual maximum shear force under the concentrated load.

Elastic bedded beams have large bending moments under concentrated loads. These high values are usually not relevant for the design, as point-loads do not exist in reality. All forces act on a distinct load area. A load distribution with an angle of 45° can be assumed up to the centreline of the beam or slab (see Section 4.10). In the example, this results in a load area of greater than 0.80 m, which would reduce the maximum bending moment by 20%. The loaded area has to be modelled by at least two elements to describe the shear force distribution with a sufficient degree of accuracy.

In the case of a linear elastic analysis based on the bedding modulus method, one has to remember that tension forces cannot actually occur in the ground due to uplifting of the foundation beam. The bedding of the beam has to be neglected in those regions where the numerical calculation shows any uplifting of the foundation beam. In such a case, load case combinations are not permissible, and this will significantly increase the amount of calculation effort.

2.4.2 Influence of the nonlinear material behaviour of concrete

In the preceding examples, a linear elastic material behaviour has been assumed for the foundation beam and the ground. Not only the complex deformation characteristics of the soil, but also the change of stiffness of a concrete beam due to cracking may have a significant influence on the member forces and deflections, as will be shown in the following example.

A strip foundation having a thickness of $h = 60$ cm and a transverse width of $b = 5.0$ m is analysed (Figure 2.36). The calculations are carried out for a strip of 1-m width in the longitudinal direction. The system is loaded in the centreline by a wall. The geometry of the foundation beam and the bedding modulus have been chosen, so that for a central load of $q = 1000$ kN/m a reasonable amount of reinforcement and a realistic maximum settlement is calculated.

Figure 2.36 Elastic bedded foundation beam

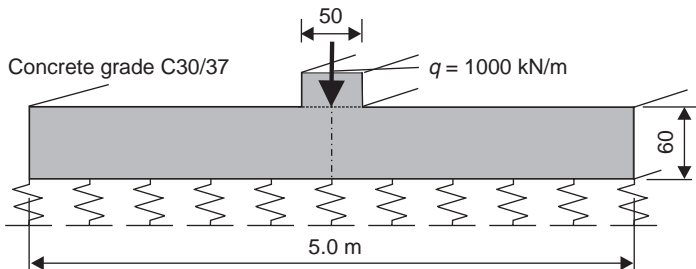
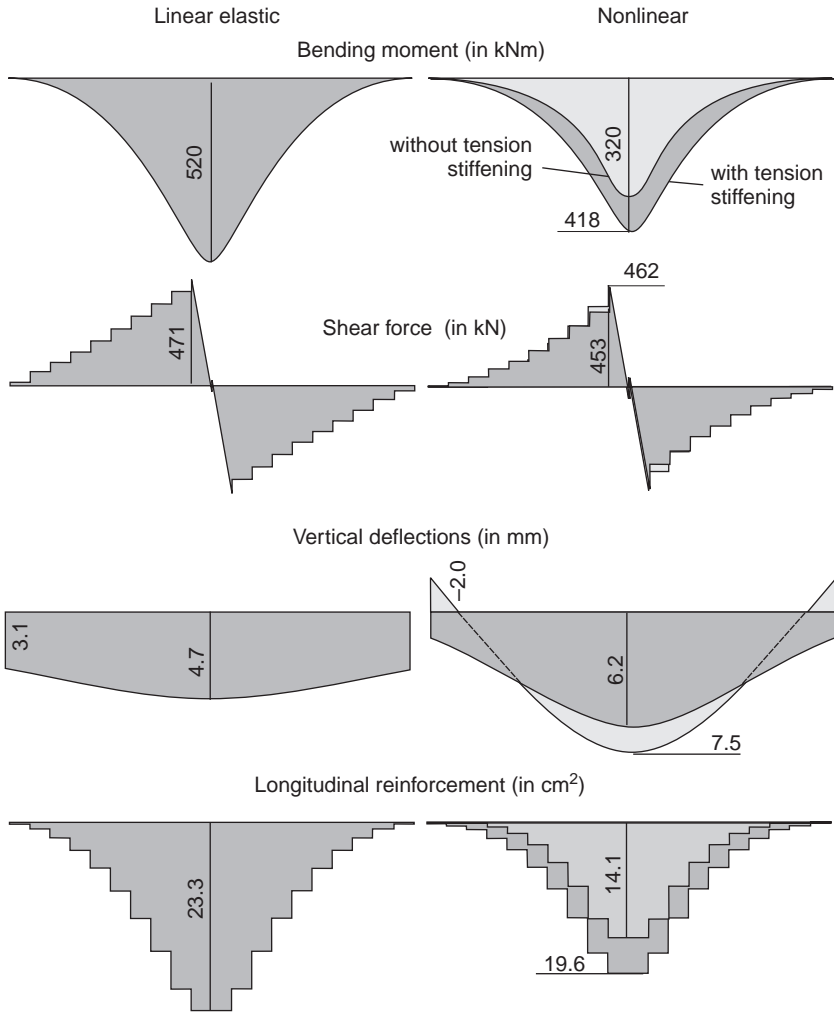
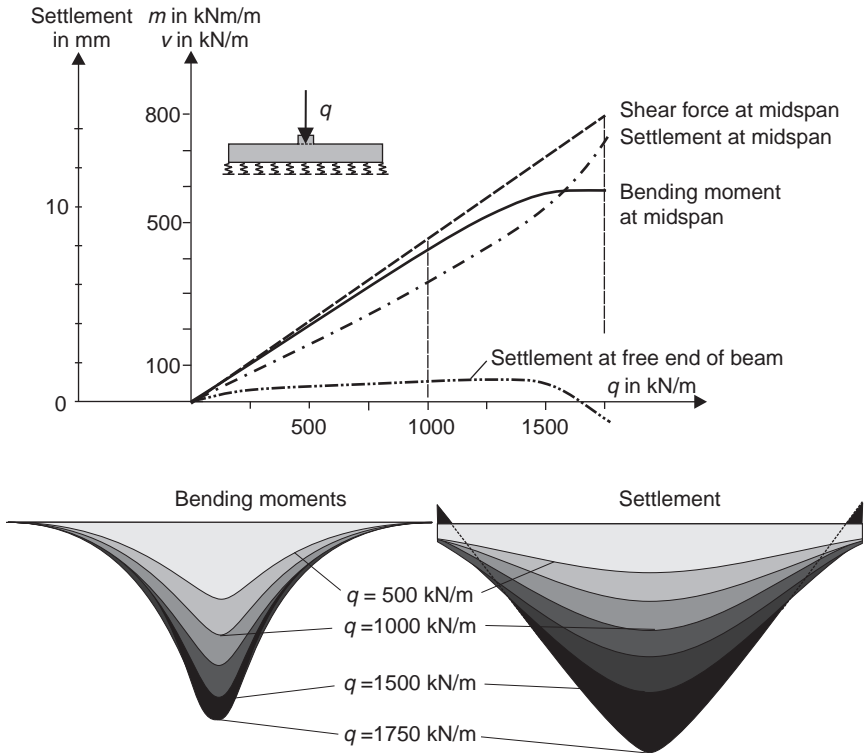


Figure 2.37 Member forces and settlements of a foundation beam with linear elastic and nonlinear behaviour of concrete (max load $q = 1000 \text{ kN/m}$)



The member forces, the settlements and the required reinforcement are shown in Figure 2.37 for a linear elastic as well as the nonlinear material behaviour of the reinforced concrete beam. For nonlinear calculations, the amount of reinforcement has been fixed by the results of the linear analysis. A linear elastic analysis results in a maximum bending moment under the wall of $m = 520 \text{ kNm/m}$ and a maximum displacement of $w = 4.7 \text{ mm}$. However, the maximum bending moment is reduced by 20–25%, and settlements are increased by 32%, when a nonlinear behaviour of the reinforced concrete beam and its resulting stiffness reduction in the region of the maximum bending moments are considered. Figure 2.37 (right) shows the results of the nonlinear analysis,

Figure 2.38 Bending moment and settlements with increasing load (nonlinear concrete material model)



both with and without taking the tension-stiffening effect (see Section 2.11.3) into account. It can be seen that neglecting the tension-stiffening effect, which gives the minimum stiffness, results in smaller bending moments. Therefore, this effect has to be considered in the design of foundation beams and slabs.

Figure 2.38 shows the distribution of the bending moment at midspan and the settlements of the strip foundation under an increasing load. At the beginning, there is a linear relation between the load and the vertical displacements and bending moment, respectively. The beam is uncracked, and its behaviour is fully elastic. At an approximate load of $q = 1400$ kN/m, the elastic load-bearing capacity of the critical section at the midspan is reached, starting the formation of cracks. A plastic hinge develops. In this area, the bending moment can only increase slightly. Any further increase in load-bearing capacity can only be possible for a load redistribution to the less stressed sections and a concentration of the soil pressure under the wall. This results in an excessive increase of the settlements of the beam. It should be considered in the design that a load increase with a safety factor γ does not affect the maximum bending moments but will lead to considerable increase in the settlements. The shear force at the relevant

section near to the wall does not depend on the stiffness of the system, but from the equilibrium condition.

2.4.3 Pile foundation – foundation of a bridge column

Pile foundations are used to transfer the loads from the structure to deeper and stiffer soil layers with a greater load-bearing capacity. They are required when the load-bearing capacity of a shallow foundation is insufficient or if the size of the foundation slab would be uneconomical.

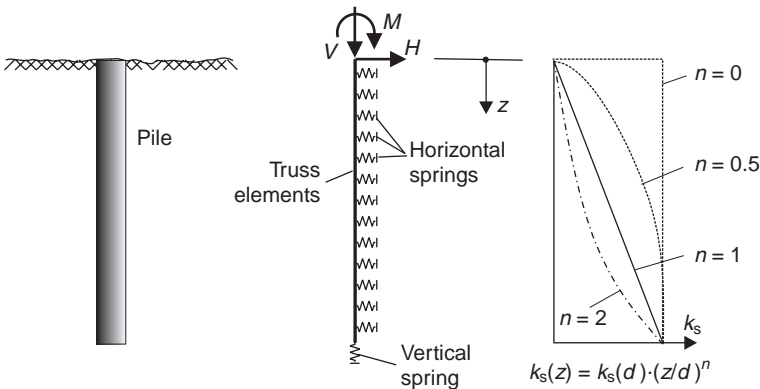
One must distinguish between bored and driven piles. Due to their great diameter and reinforcement, bored piles can carry normal forces and bending moments. Driven piles have small bending stiffness and, due to their slenderness, can only carry vertical loads.

In the following example, only bored piles will be discussed, as the vertical normal forces in driven piles can easily be estimated from the equilibrium conditions (see Figure 2.44).

Rigid piles can be modelled by linear elastic supported truss elements. The bedding modulus k_s and the stiffness of the horizontal springs may vary along the length of the pile and its circumference. According to Timm and Baldauf (1988), the distribution of k_s along the length of the pile respectively the exponent n should be chosen as follows (see Figure 2.39):

- $n = 0$ for cohesive soil under small to medium loads.
- $n = 0.5$ for medium cohesive soil and non-cohesive soil above the ground water level.
- $n = 1.0$ for non-cohesive soil below the ground water level or under greater loads.
- $n = 1.5-2.0$ for loose non-cohesive soil under very high loads.

Figure 2.39 Bored pile – numerical model and distribution of bedding modulus k_s for a horizontal force at the pile head



If there are no results available from actual pile tests, the bedding modulus k_s may be estimated by the following expression from DIN 4014 (1990):

$$k_s = E_s/d$$

where:

k_s is the bedding modulus

E_s is the stiffness modulus of the ground

d is the diameter of the pile $d \leq 1.0$ m.

The stiffness modulus for non-cohesive soils varies between $E_s = 100\text{--}200$ MN/m² for gravel and $E_s = 10\text{--}100$ MN/m² for sand. The horizontal support in the upper region of the pile by the ground should only be included in the design if it can always be guaranteed during the whole lifetime of the foundation.

It is rather difficult to choose the adequate soil properties. This problem will not be discussed further here. It should only be noted that, in every design, the distribution of the member forces and the displacements are considerably influenced by the behaviour of the soil.

The modelling problems will be further considered for a bridge column on a pile foundation (Schornbachtalbrücke; see Becker, 1994) (Figures 2.41–2.43). Figure 2.40 shows the dimensions of the structure. The bridge column is founded on 14 reinforced piles, each having a diameter of $d = 61$ cm. In order to simplify the numerical model, the pile inclination and the enlarged footing are neglected.

Loading

Only a horizontal braking force of $H = 870$ kN, acting at the top of the bridge column in the horizontal (y -) direction, is considered. This results in a bending moment at the bottom of the pile cap of:

$$M = 870 \text{ kN} \cdot 15.8 \text{ m} = 13\,750 \text{ kNm}$$

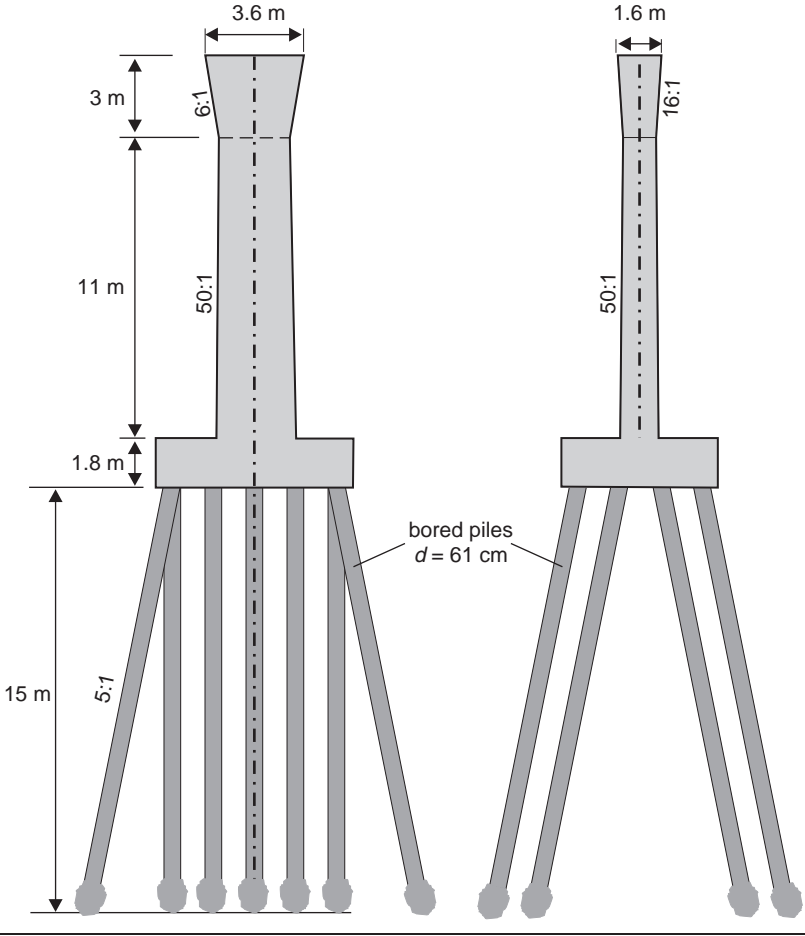
Manual analysis

The normal forces in the different piles can be calculated from equilibrium conditions if one neglects the deformation of the structure (rigid pile cap) and the bending stiffness of the piles. This results in normal pile forces of $F_2 = \pm 585$ kN for the outer row and $F_2 = \pm 195$ kN for the inner row (Figure 2.44). No bending moments are estimated in this approach.

Truss system

The piles are modelled with truss elements that are supported horizontally by spring elements (see Figure 2.46). A linear distribution of the bedding modulus along the length of the pile with $k_s = 0$ MN/m² at the head and $k_s = 100$ MN/m² at the pile toe is assumed. The interaction between the individual piles and the friction between the piles and the ground is neglected. The vertical settlement of the pile toe is modelled by linear elastic springs. For simplicity, a constant cross-section of the column is used in the following, since only the pile foundation is of interest in this example.

Figure 2.40 Pile foundation of a bridge column (Becker, 1994: Schornbachtalbrücke)



The pile cap cannot be modelled by truss elements, as this is a typical discontinuity region (see Figure 2.45). Therefore, the nodes of the pile’s heads are fixed to the lowest node of the column base. The pile cap is, therefore, modelled as an infinite rigid body. The disadvantage of this model is that the member forces of the pile cap are not calculated. Further investigations are required if the bending deformations of the pile cap cannot be neglected.

Variation of the vertical spring stiffness

The stiffness of the vertical spring at the pile toe can only be estimated by tests (e.g. DIN 4015; see Becker, 1994). The codes provide rough, approximate values only (Figure 2.47). As the stiffness of the vertical support of a pile may show a great scatter in practice, the results of a parametric study will be discussed in the following example. The stiffness of the vertical spring varies from $C = 400 \text{ MN/m}$ to infinity (pile toe fixed).

Figure 2.41 Bridge during construction



Figure 2.42 Bridge column



Figure 2.43 Pile boring rig



The stiffness of the vertical spring has a great influence on the bending moments (Figure 2.48) and the horizontal deformation (Figure 2.49) of the piles. A fixed vertical support reduces the greatest bending moment by a factor of 2 as compared with that from an elastic support with $C = 400 \text{ MN/m}$. The main reason for this big difference is the rotation of the pile cap. The greater the inclination of the infinite stiff pile cap due to settlements of the piles, the greater is the rotation of the pile heads and the resulting bending moments.

Figure 2.44 Manual calculation of the pile forces

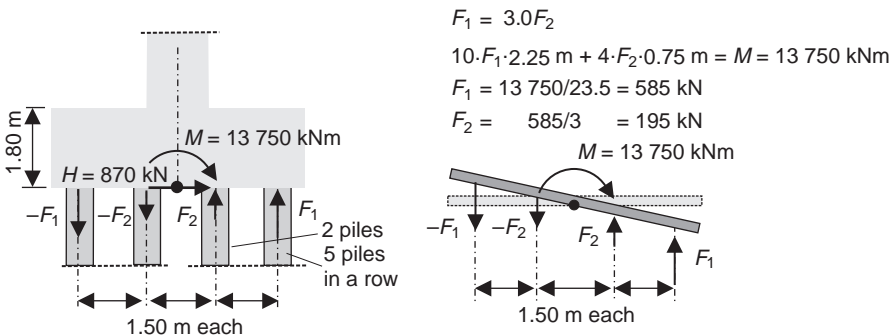


Figure 2.45 Flow of forces in a pile cap

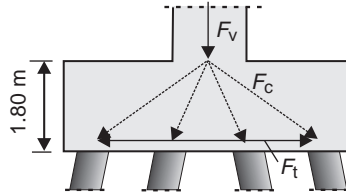


Figure 2.46 Truss model

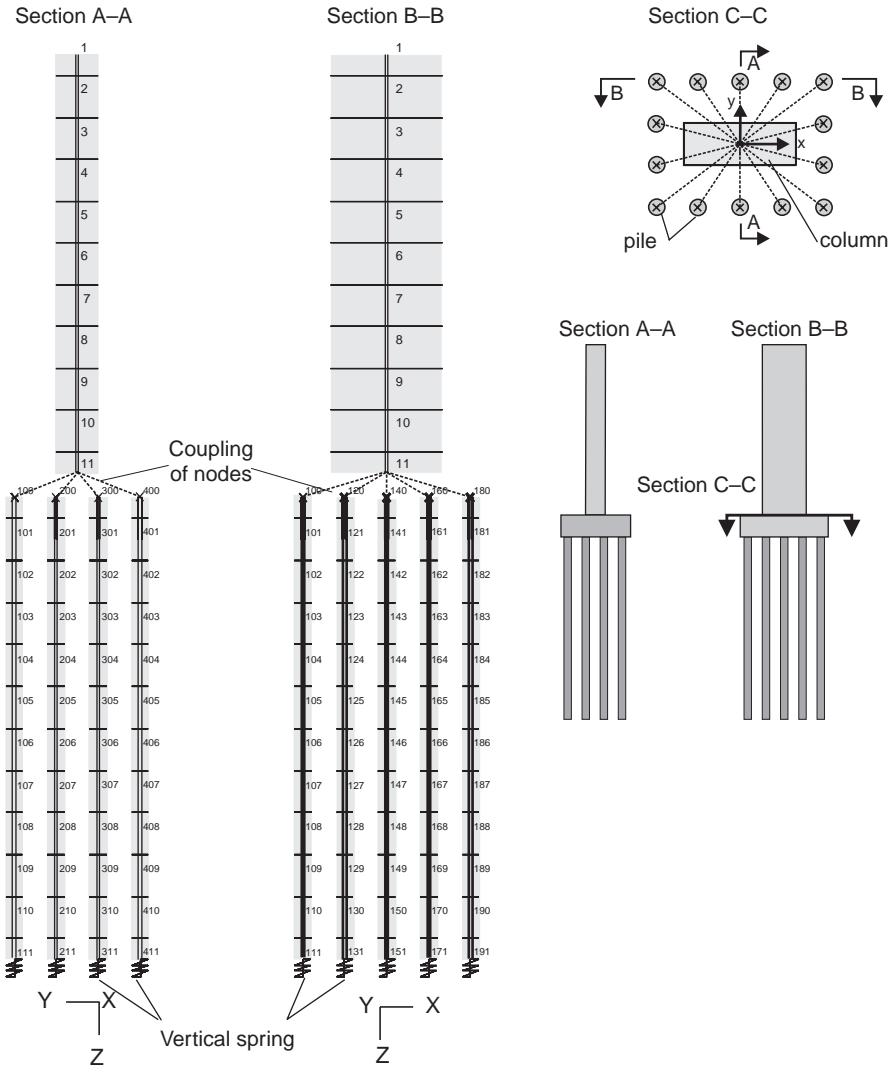


Figure 2.47 Load-settlement curves (according to DIN 4014, 1990)

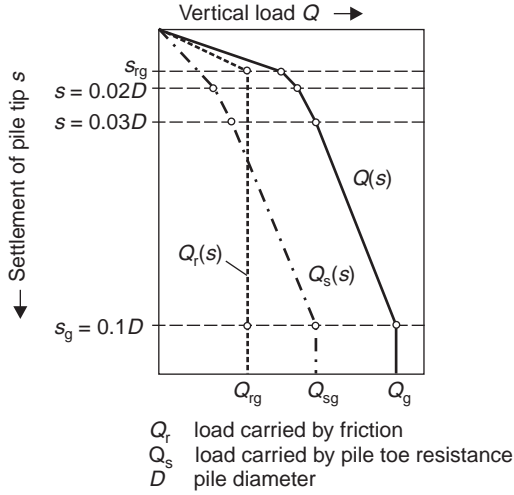


Figure 2.48 Bending moment distribution in the pile (load: $H_y = 870$ kN at column head)

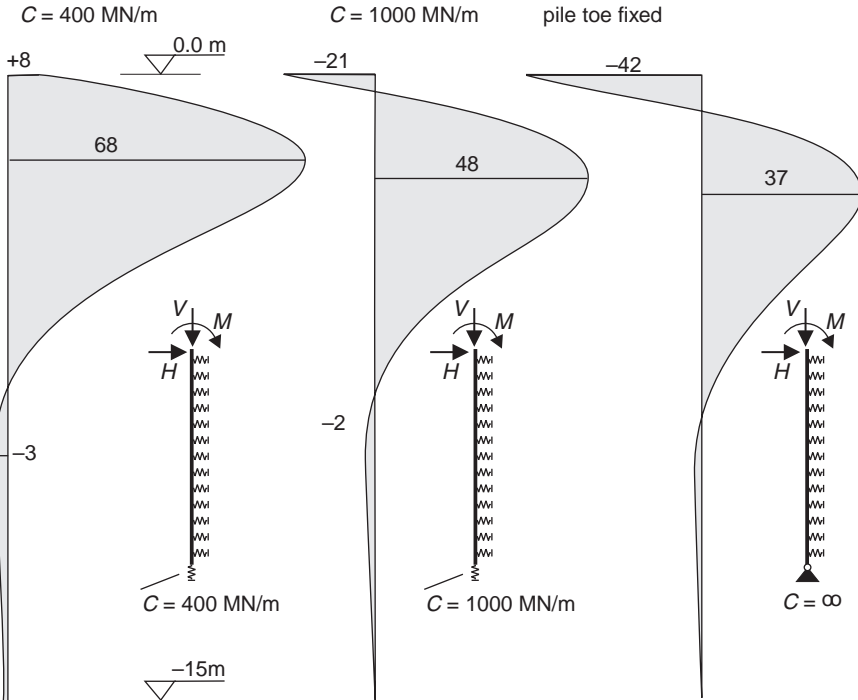
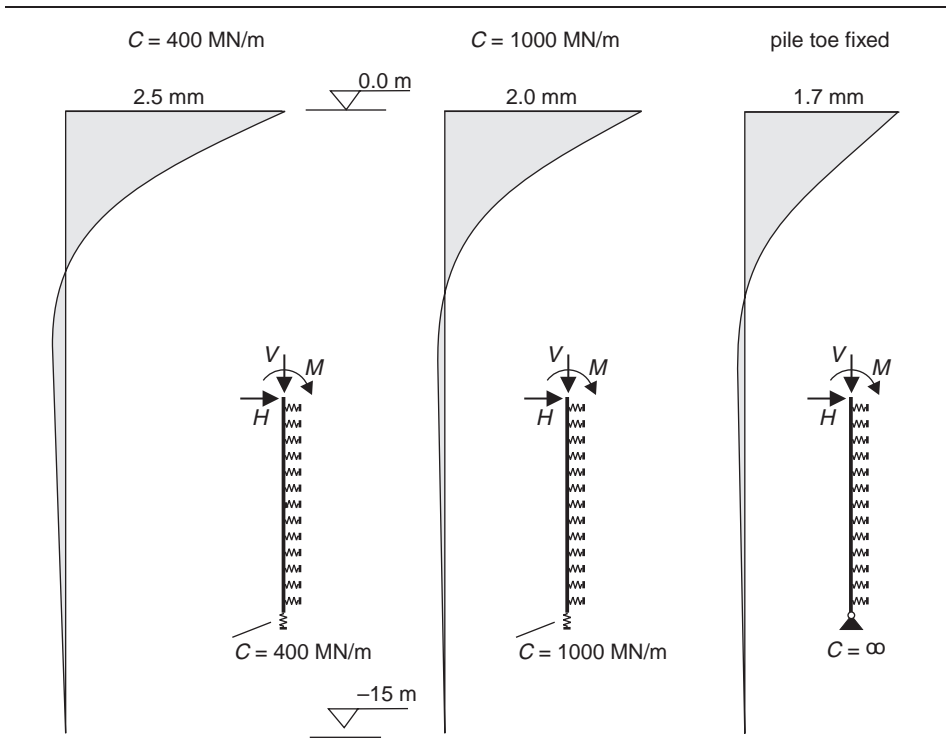


Figure 2.49 Horizontal deformation of the pile (load: $H_y = 870$ kN at column head)



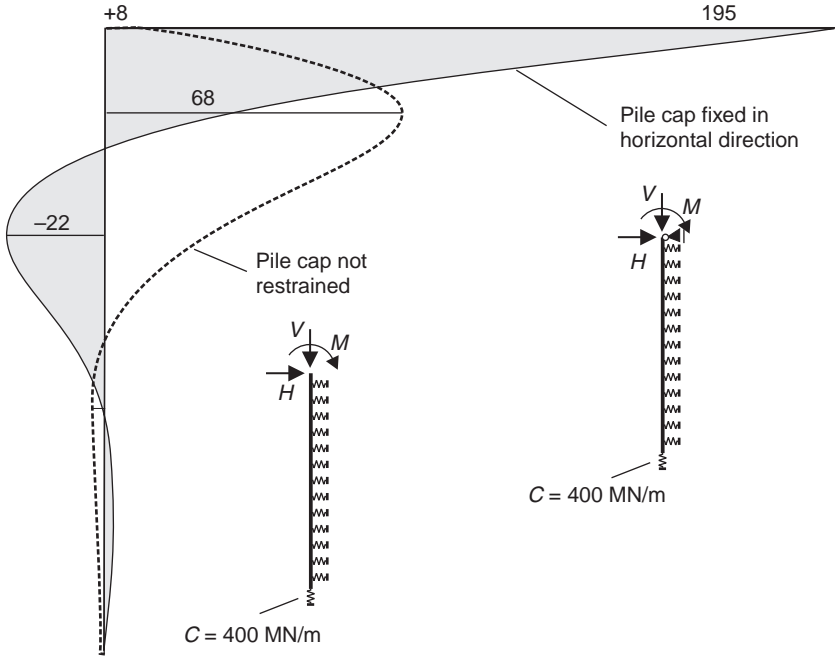
When comparing the bending moment distributions, one has to remember that a pile usually has a uniform reinforcement arrangement around its circumference. Therefore, the (\pm) sign of the bending moments does not matter.

The distribution of the normal forces is not shown in this example, as it is only slightly influenced by the stiffness of the vertical spring. The normal forces in the piles can easily be calculated manually from the bending moment at the base of the bridge column (Figure 2.44).

The main difference between a manual and a numerical analysis is that, in the latter, bending moments and normal forces are estimated. Bending moments may cause a high increase of the pile reinforcement due to the small lever arm of the internal forces.

In this example, the displacement and rotation of the pile cap does not significantly increase the member forces of the column. The horizontal deformation of the column head is less than 18 mm ($C = 400$ MN/m) or 8 mm (fully restrained), assuming an elastic material behaviour.

Figure 2.50 Bending moment distribution in the pile with resp. without horizontally fixed pile cap (load: $H_y = 870$ kN at column head)



Horizontal restraint of the pile cap

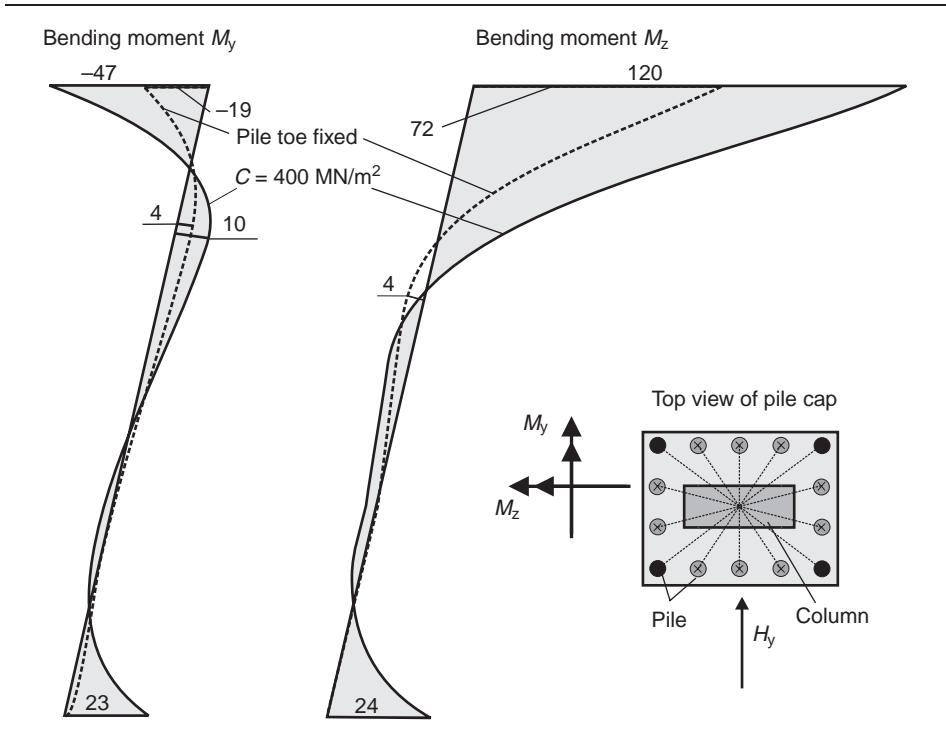
In the preceding analysis, it was assumed that the pile cap can move horizontally without any reacting forces of the ground. In reality, this displacement is partly restrained due to the friction between the pile cap and the ground, and the horizontal passive earth pressure. A horizontal fixation of the pile cap, as an extreme case, has a large influence on the bending moments of the piles (see Figure 2.50). The bending moment at the pile head increases from $M = 8$ kNm (no restraint) to $M = 195$ kNm ($C = 400$ MN/m).

Please note that long-term settlements of the soil underneath the pile cap may reduce the vertical and horizontal bedding of the pile cap. Thus, a bedding of the pile cap by the ground should be handled with great care.

Inclined piles

If the inclination of the outer row of piles is considered in the numerical model as in reality (Figure 2.40), the maximum bending moments are estimated at the pile heads (Figure 2.51). Again, there are large differences in bending moments between those of fully restrained and flexible supported pile toes.

Figure 2.51 Bending moment distribution in the edge piles (load: $H_y = 870$ kN at column head)



To summarise, the vertical restraint, the elastic bedding of the piles and their distribution along its length and any horizontal restraint of the pile cap have significant influences on the member forces in the structural system. All these parameters depend on the soil characteristics, which in reality scatter within a great range. Therefore, parametric studies may be required to estimate the correct relevant design forces.

As the restraint of the column due to the foundation shows less scatter, it may be useful to estimate the required design forces of the column by a separate model (i.e. a truss that is partially restrained at its lower end). The resulting forces can then be used as loads for the foundation.

A linear increase of the bedding modulus over the length of the piles has been assumed in the preceding example. In general, the restraint of the soil against horizontal deformation is not proportional to ground reactions. Therefore, such nonlinear behaviour has to be considered in case of large horizontal loads.

Please note that one must check that the calculated soil pressure is not positive (tension) or greater than permissible (passive earth pressure).

In the case of large bending moments, a nonlinear design of the piles (including the reduction of stiffness due to cracking) can result in a significant reduction of the maximum member forces. However, it is doubtful whether such a refined model is more accurate than a linear elastic one, as the basic input parameter, the soil stiffness, can show a great scatter in reality.

2.5. Shear walls with large openings

Shear walls are used in high-rise buildings as bracing elements (Figure 2.52). Modelling of such structures is a difficult task. At first, one may think of it as a 2D model with membrane (shell) elements (diaphragm). However, these calculations are generally too time-consuming for practical purposes. Furthermore, the estimation of the reinforcement requirements is difficult (see Chapter 3). With a truss model, one can only approximate the behaviour of a shear wall with large openings due to the considerable width of the structural elements and the non-uniform strain distribution in most parts of the structure. Nevertheless, its simplicity makes this model appealing to use. In such a case, one has to make sure that the stiffness of the whole structure is represented by the numerical model.

In a frame model, the structural system is modelled by straight truss elements that are located at the centreline of the cross-section of the individual members. Modifications are required for massive structural parts, such as the columns shown in Figure 2.53. In addition, it should be noted that truss models are only valid for slender shear walls (beam system) due to the underlying assumption of a linear strain distribution. Further investigations may be required for areas near the supports at the base of the structure.

The member forces of the horizontal ‘beams’ and vertical ‘columns’ are required for the design of the structure. In this case, one must consider the deformation behaviour of the whole structure. The different parts of the structure are modelled by straight truss elements. Special attention has to be given to the joints between the horizontal beams and the vertical ‘columns’. The horizontal beams are clamped at the inner face of the vertical ‘columns’ and not at their centrelines. If this is not considered, the span length would be much too large, and the calculated stiffness of the structure would be smaller than in reality. There are various possibilities to model the real behaviour of the structure (Figure 2.53).

- *Model a1 – special truss elements:* The horizontal beam is modelled by special beam elements that have infinite stiffness at both ends (Figure 2.53a).
- *Model a2 – beam with variable stiffness:* The horizontal beam is modelled by at least three elements, two very stiff elements at the ends and one with normal stiffness in between (see Figures 2.53a and 2.54). The considerable stiffness differences between the rigid and elastic beam elements may cause numerical problems.
- *Model b – modification of the stiffness:* Bending ($E \cdot I$) and normal stiffness ($E \cdot A$) of a fictitious member, having a constant cross-section, is increased in order to consider the real behaviour of the horizontal beam in the structure. The moment

Figure 2.52 Bracing elements of a high-rise building – frames and coupled shear walls

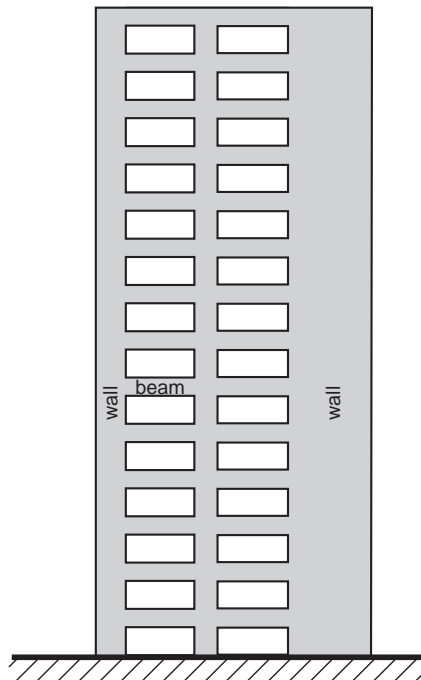
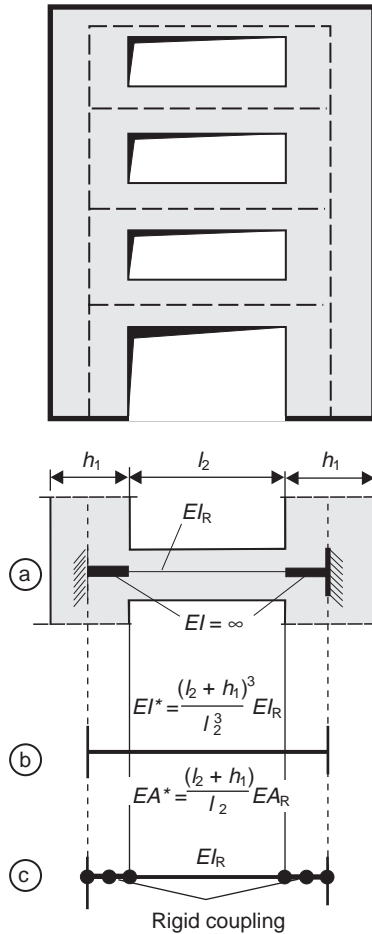


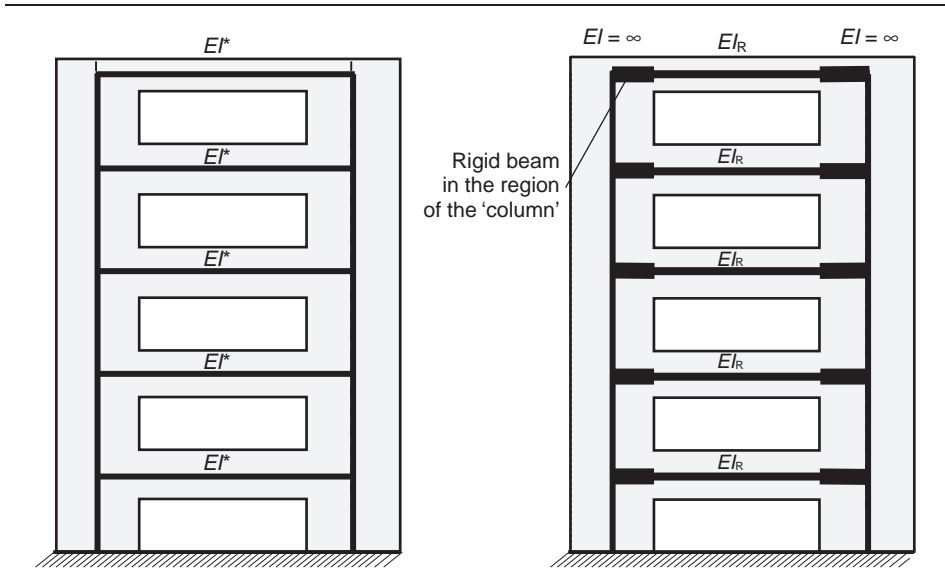
Figure 2.53 Models for a coupled shear wall system with large openings



of inertia of the new beam is calculated as though it has the same bending stiffness as the real beam, but with a shorter span length. It must be noted that the deformation of the horizontal beam is not calculated correctly.

- *Model c – coupling of the nodes at the joints:* Nodes in the joints are coupled together (see Figure 2.53c). This method has been previously explained in Section 2.1.
- *Model d – 2D shell model (diaphragm):* Shell models will be discussed in Chapter 3. Considerable effort is needed to evaluate such a model. It should be noted that the nonlinear material behaviour in different regions of the structure can hardly be modelled. Furthermore, the software cannot usually estimate reinforcement requirements. This is the reason why membrane models are not widely used in practice.

Figure 2.54 Models for a coupled shear wall with large openings



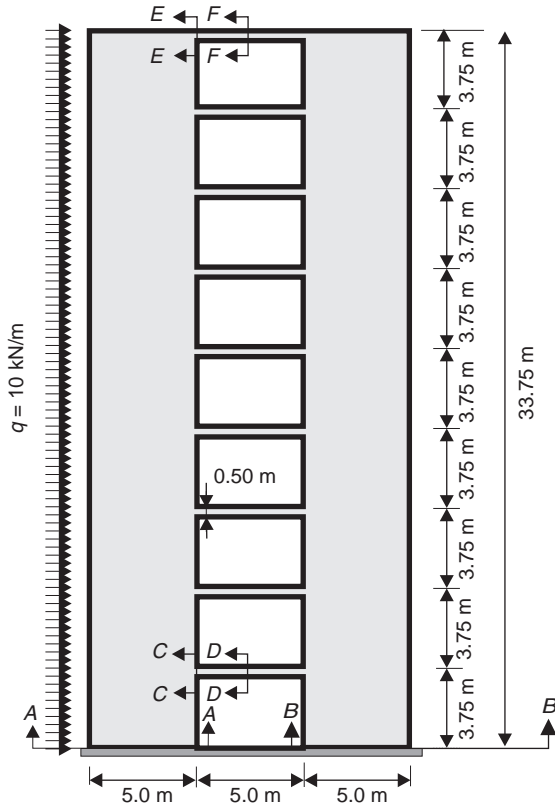
The major difference of these models will be examined for the system shown in Figure 2.55. The walls have a thickness of $t = 20$ cm. They are made of concrete-grade C35/45. The structure is loaded with a uniform horizontal load of $q = 10$ kN/m. The deflection pattern, which has been calculated with a shell model (diaphragm), is shown in Figure 2.56. A large shear and bending deformation in the upper horizontal beams can be observed.

Table 2.4 lists the member forces in a few sections of the various models. Figure 2.57 shows the member forces and the deformation of the shear wall calculated with a truss model and coupling of nodes at the joints. Models b and c give nearly the same results. Variations of the axial stiffness ($E \cdot A$) only slightly affect the member forces ($\approx 5\%$). As expected, the unmodified frame system results in much greater displacements, greater bending moments and less normal forces than the ones of a 2D shell system.

The resulting member forces of a shell model are provided in column 7 of Table 2.4. There is a good agreement in the results of the truss system. Therefore, the considerable effort required for a plane shell analysis does not seem to be justified for this particular structure.

The calculations shown earlier are based on a linear elastic material behaviour. The maximum tensile stresses in the horizontal beam are greater than the mean tensile strength of the concrete f_{ctm} (max $M = 41.2$ kNm, section E–E, $\sigma_{ct} = M/W = 41.2/8.33 = +4.9$ MPa), resulting in cracking of the horizontal girders and a reduced stiffness. This aspect must be considered in design if more precise data for the deformation of the structure is required. However, for the preceding example, the influence of the stiffness of the horizontal beams on the member forces is small.

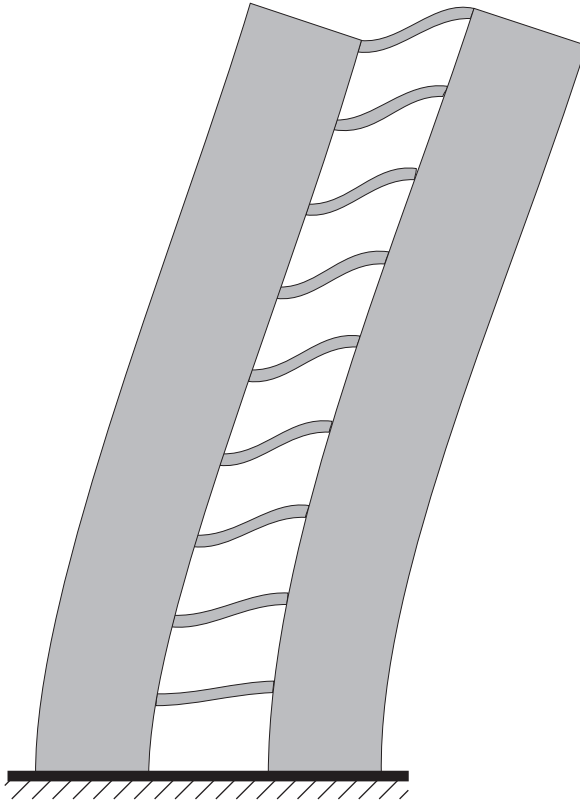
Figure 2.55 Shear wall with large openings



It should be noted here that the accuracy of a truss system in the lower region depends on the support conditions. A nonlinear strain distribution is likely to occur. If more precise information is needed, then a shell model (diaphragm) may be helpful.

In the preceding example, special beams are used to connect the two vertical elements ('columns') together. Considerable construction effort would be needed to build such beams. Therefore, they may be avoided where possible, and the existing slab may be used only as a coupling element. However, this results in a complicated 3D shell system that requires much calculation effort. To avoid this, a truss system may again be used. First of all, the cross-section properties of the equivalent, fictitious horizontal beams are needed. The effective width b_{eff} can be taken from diagrams provided by Wong and Coull (1980). The figures presented by them are only valid for simple regular systems, which are rarely built in practice. If more accurate values for the stiffness of the horizontal beams are required, then it is better to use a 3D shell model with a simplified equivalent structural system.

Figure 2.56 Deformation (shell model)



2.6. Bracing of high-rise buildings

The bracing elements of a building have (Figure 2.59) to be designed to resist the vertical loads and, more importantly, the horizontal actions (e.g. wind, earthquake and their resultant effects) on a structure. Furthermore, the stability of the structure must be ensured.

Nowadays, whole buildings can be modelled by 3D shell elements (see Chapter 6). However, this tremendous effort is not justified for ordinary structures. A truss system, where the whole structure is reduced to just the main load-bearing elements, the so-called ‘cores’, is sufficient for most cases in practice. In the real system, the bracing elements are connected together by slabs, which are assumed to be rigid in their midplane. Also, the bending stiffness of the slabs is neglected.

Simple regular systems with a congruent deformation pattern of the bracing elements can easily be designed with the so-called method of fictitious bars (equivalent beam method; see Figures 2.58, 2.60 and 2.61) (Beck and Schäfer, 1969). This simple method is often used to check numerical results, even for complex bracing systems. If

Table 2.4 Member forces of a shear wall with large openings (Figure 2.55 and Figure 2.56)

Sections (see Figure 2.53)	Without modifications	Model 3 with modified I^* (Figure 2.53b)	Model 3 with modified I^* , A^* (Figure 2.53b)	Model 4 coupling of nodes (Figure 2.53c)	Model 5 shell analysis		
Section A–A	N	25.6	133.2	133.2	133.2	117.8	kN
	V	200.1	187.7	195.2	195.2	191.9	kN
	M	-2818	-2216	-2251	-2251	-2316	kNm
Section B–B	N	-25.6	-133.2	-133.2	-133.2	117.9	kN
	V	137.4	149.8	142.3	142.3	145.5	kN
	M	-2621	-2146	-2112	2112	2199	kNm
Section C–C	N	-4.4	-9.2	-5.7	-5.7		kN
	V	-1.1	-6.6	-6.6	-6.6		kN
	M	2.7	16.5	16.6	16.4		kNm
Section D–D	N	-4.4	-9.2	-5.7	-5.7		kN
	V	-1.1	-6.6	-6.6	-6.6		kN
	M	0	0	0	0		kNm
Section E–E	N	-11.5	-17.5	-10.8	-10.8		kN
	V	-3.5	-18.5	-18.5	-16.5		kN
	M	8.7	41.2	41.2	41.3		kNm
Section F–F	N	-11.5	-17.5	-10.8	-10.8		kN
	V	-3.5	-18.5	-18.5	-16.5		kN
	M	0	0	0	0		kNm
Horizontal displacement	w_x	10.7	7.3	7.3	7.3	8.0	mm

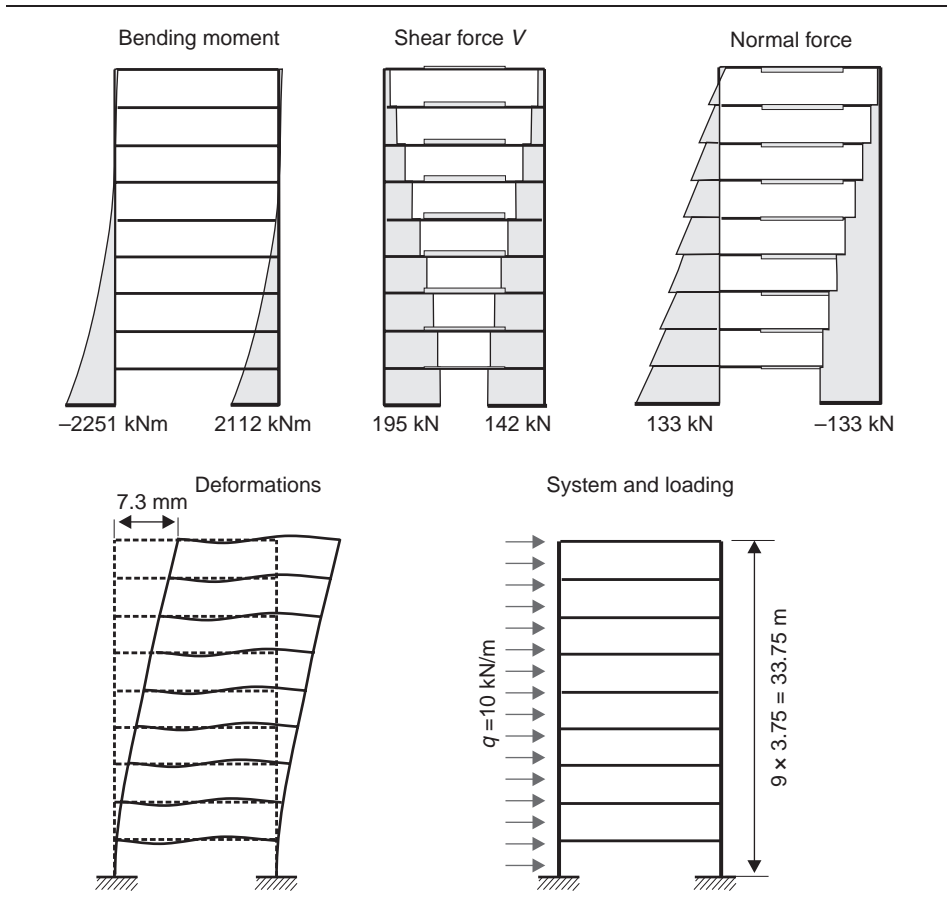
there are differences between the analytical and the numerical analysis, it is always a question of which are the correct member forces. Therefore, in the following text, the differences between manual and numerical models are discussed.

In reality, often complicated bracing systems are built like, for example, girders that have different cross-sections over their length or columns that are not continuous throughout the height of the building. In such cases, a manual calculation using the method of fictitious bars is not possible. A numerical analysis will then be required for a 3D truss model of the bracing system.

In addition, a numerical model can be useful where nonlinear material behaviour has to be considered, or when a dynamic analysis is required (i.e. earthquake effects).

Even in this day-to-day task, engineering knowledge is needed when using design software. There are several problems that may arise when using a truss model, such as

Figure 2.57 Member forces and deformation of a shear wall with large openings, nodes at the column/beam joints coupled (see Figure 2.53c)



- cross-sectional properties of the truss elements
- location of the axis of gravity of the trusses (axis of gravity – axis of torsion)
- modelling of the behaviour of the slabs – coupling of the truss nodes.

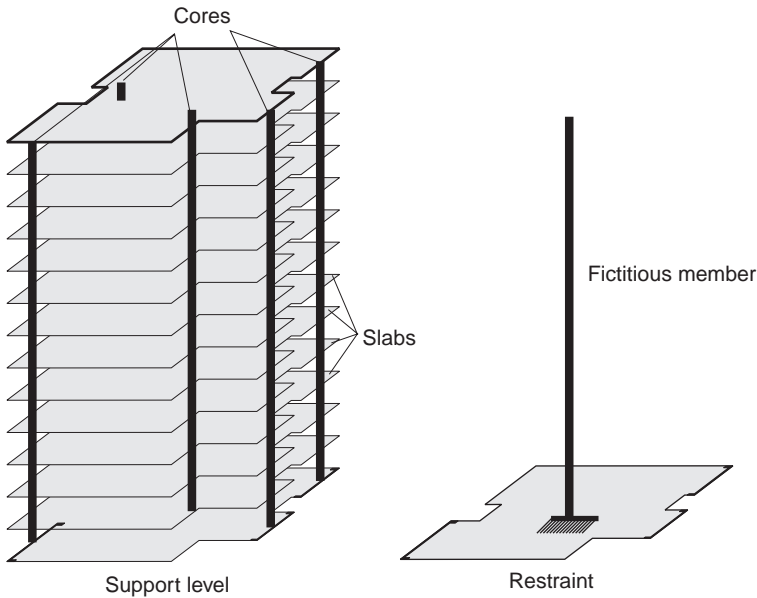
2.6.1 Equivalent cross-section of the trusses

The following stiffness parameters are needed for design purposes:

Normal stiffness	$E \cdot A$
Bending stiffness	$E \cdot I_x$ and $E \cdot I_y$
Shear stiffness	$G \cdot A_{sy}$ and $G \cdot A_{sz}$
Torsional stiffness (St. Venant)	$G \cdot I_T$
Torsional stiffness (warping torsion)	$G \cdot C_M$

For closed thin-walled sections, in which equilibrium is satisfied by a closed shear flow, these parameters can easily be calculated, for example, by means of software

Figure 2.58 Modelling of a bracing system – fictitious bar method



based on the linear elastic behaviour of the concrete material. However, the reduction of stiffness caused by crack formation in concrete (Stage II) has to be considered. It is well known that the torsional stiffness of a cracked member is significantly lower than the elastic value. Therefore, the torsional stiffness GI_T may be neglected for a concrete structure in Stage II condition. Rough data are given in ‘Heft 240’ of the German Association for Concrete Design (Grasser *et al.*, 1991). There, the following values are listed:

Beam uncracked (Stage I) $(G \cdot I_T)^I \cong 1/3 \cdot E_c \cdot I_T$

Beam cracked (Stage II) $(G \cdot I_T)^{II} \cong 0.1 \cdot E_c \cdot I_T$

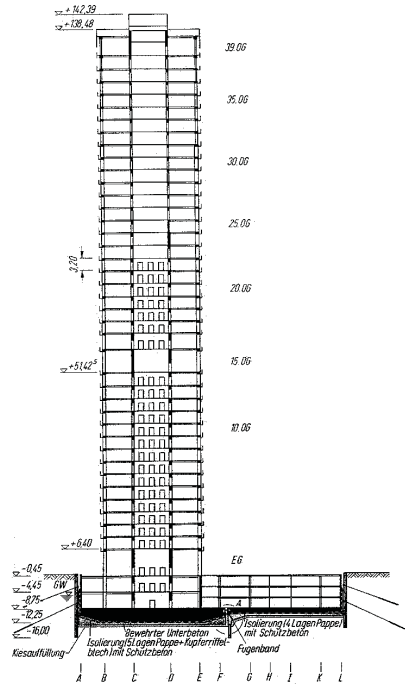
Shear modulus $G = \frac{E_c}{2 \cdot (1 - \nu)} \approx 0.6 \cdot E_c$ (Poisson’s ratio $\nu \approx 0.2$)

According to Eurocode 2, part 1 (2004) a structural member may be treated as uncracked if the greatest tensile stress σ_{ctd} under a certain load combination is less than the guaranteed tensile strength $f_{ct,0.05k}/\gamma_c$.

Very often, the bracing elements have large openings (e.g. for the doors to the elevator shaft), which may reduce the shear and torsional stiffness significantly. For beams with open cross-sections or for hollow box girders with openings, the influence of the floor slab has to be considered when calculating the stiffness parameters. An engineering judgement is required here.

Figure 2.59 High-rise building – bracing system (Mainzer Landstraße, Frankfurt)

Adapted from Schneider and Reeh, 1978 © Wiley – VCH Verlag GmbH & Co. KGaA. Reproduced with permission.

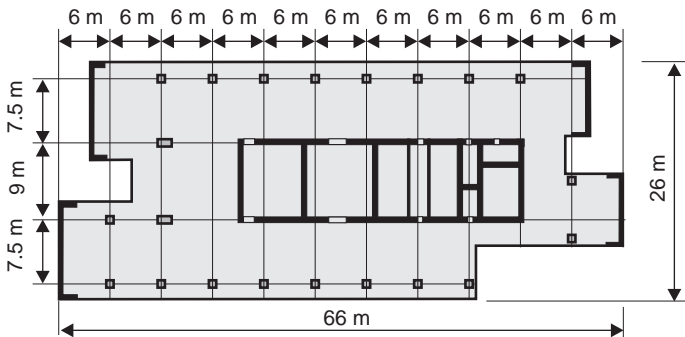


Construction period: 1972–1974

Height: 142 m over ground level

Foundation slab with 3.5 m thickness

Plan view



Further investigations are required if the bracing elements are located close to each other. In the fictitious truss model, it is assumed that the slab can only transfer normal forces and that it has no bending stiffness. This assumption is not valid if the distance between the individual bracing elements is small. In such a case, the cores may be modelled as one single stiff cross-section. An alternative is to introduce a stiff coupling of the nodes. This will be explained in Section 2.6.3.

Method of fictitious bars

Figure 2.60 Plan view with bracing elements

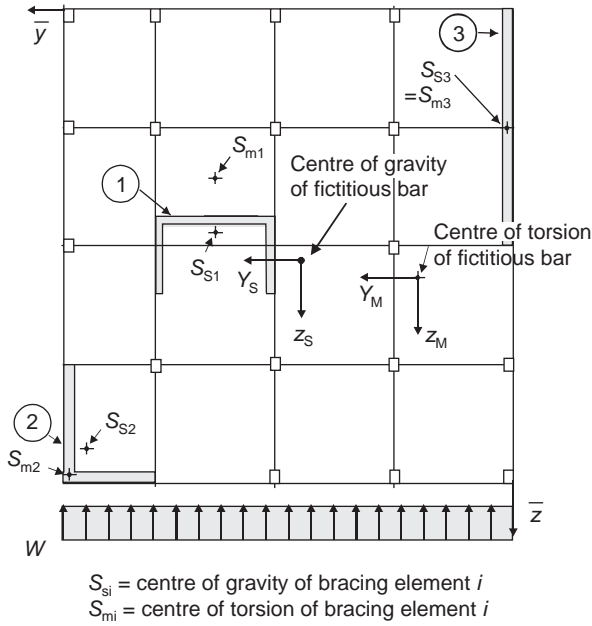
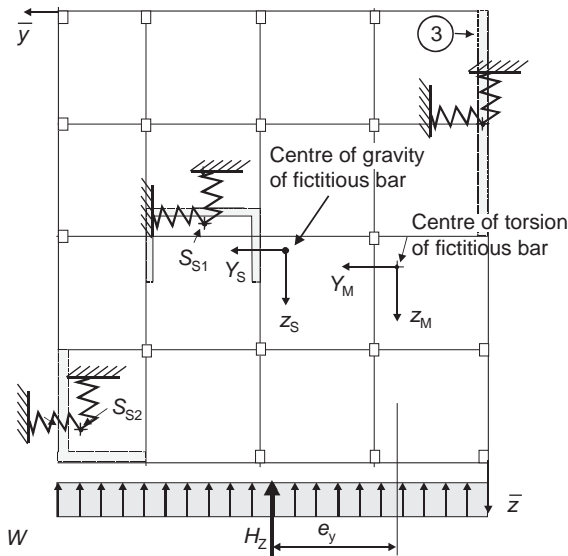


Figure 2.61 Simplified model with equivalent springs



The following items are neglected

- moment of inertia I_{yz} of the bracing elements
- wrapping torsional stiffness of the individual elements $G \cdot C_{M,i}$
- St. Venantsche torsion stiffness of individual elements $G \cdot I_{T,i}$
- shear deformations.

Forces due to translation:

$$H_{y,i} = \frac{H_{y,M} \cdot E \cdot I_{z,i}}{\sum_{i=1}^n E \cdot I_{z,i}}; \quad H_{z,i} = \frac{H_{z,M} \cdot E \cdot I_{y,i}}{\sum_{i=1}^n E \cdot I_{y,i}}$$

forces due to rotation:

$$H_{y,i} = -\frac{M_{x,M} \cdot E \cdot I_{z,i} \cdot z_{Mm,i}}{\sum_{i=1}^n E \cdot C_M}; \quad H_{z,i} = -\frac{M_{x,M} \cdot E \cdot I_{y,i} \cdot y_{Mm,i}}{\sum_{i=1}^n E \cdot C_M}$$

where:

$H_{y,M}$; $H_{z,M}$ are the resultant horizontal forces, related to the centre of torsion.

$M_{x,M}$ is the resultant torsional moment, related to the centre of torsion.

The member forces of the individual bracing elements are estimated on a cantilever beam loaded by horizontal forces H_y and H_z . Torsional effects of the individual elements are neglected.

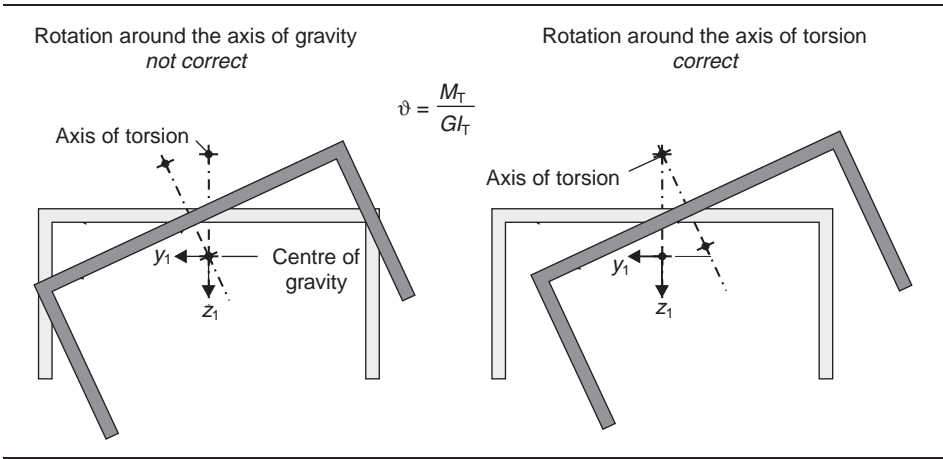
2.6.2 Location of the beam elements

In a numerical model, the beam axis coincides with the axis of gravity of its cross-section. All external loads and internal forces relate to this point. Special care should be taken for beams whose centre of gravity does not coincide with the centre of torsion. In such cases, torsional moments are calculated if a load does not act at the centre of torsion. Some software programs do not consider this effect. Also, some FE programs do not consider that the beam rotates around its axis of torsion and not around its axis of gravity (Figure 2.62). In such a case, the axis of the beam elements should be located in the axis of torsion. Otherwise, the stiffness of the global system is overestimated.

2.6.3 Coupling of nodes

The bracing elements are modelled by truss elements (see Figure 2.66). The axis of the elements coincides with the axis of gravity of the real system, as explained earlier. It is useful to introduce extra fictitious master nodes, to which all cores at one level are coupled (Figure 2.63). These nodes simplify the input of the external loading. They can be located at the centre of the load area. It should be noted that, in the numerical model, loads are usually only considered when the loaded node is connected to the truss system (see Figure 2.64).

Figure 2.62 Rotation of a beam with U-section under pure torsional moment



It is very time-consuming to model a slab by using shell elements. Therefore, the behaviour of the slab is simulated by special coupling of the truss nodes. The type of coupling – hinge, full or partially restrained – depends on the real system. The deck slab in normal buildings is usually relatively thin, and the distance of the bracing element and the columns is considerably large. In such cases, one may assume that the deck slab has no bending stiffness but an infinite normal stiffness. The slab may only transfer normal forces. The bending restraint of the bracing elements due to the slab is neglected.

Figure 2.63 Location of the bracing elements and master node

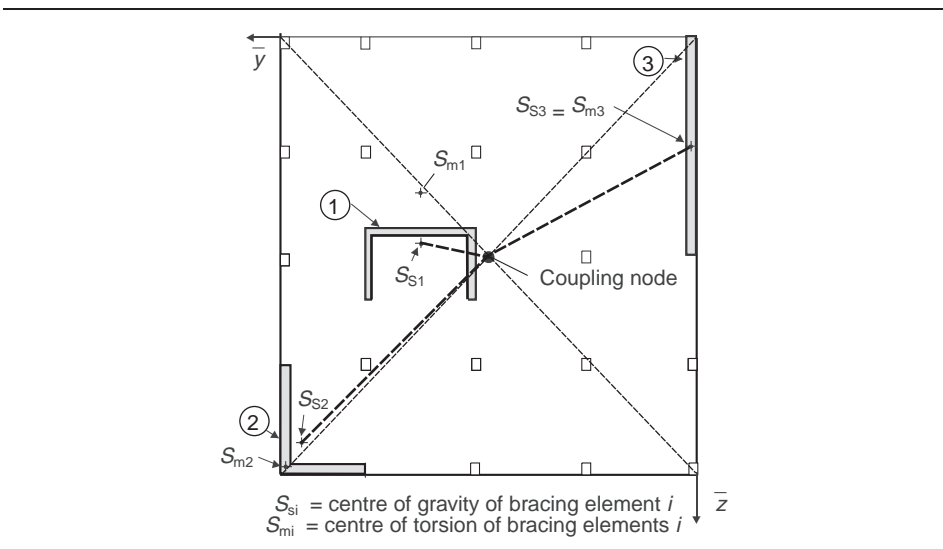
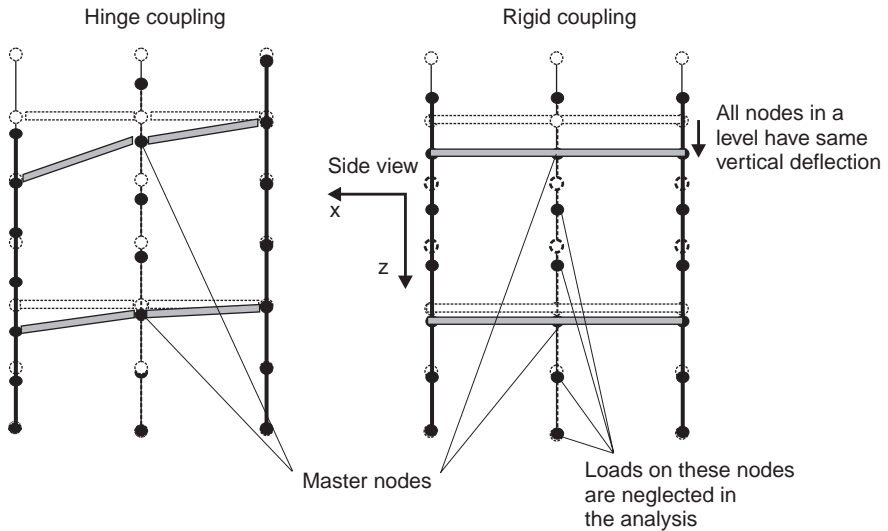


Figure 2.64 Coupling of nodes – elevation



The following different types of nodal coupling are used in practice (see Figure 2.65):

1. Bending stiff slab

$$v_x = v_{x0} + \varphi_{y0} \cdot (z - z_0) - \varphi_{z0} \cdot (y - y_0)$$

$$v_y = v_{y0} + \varphi_{x0} \cdot (z - z_0) + \varphi_{z0} \cdot (x - x_0)$$

$$v_z = v_{z0} + \varphi_{x0} \cdot (y - y_0) - \varphi_{y0} \cdot (x - x_0)$$

2. No bending stiffness, where the rotation of the nodes at the same level is not identical

$$v_x = v_{x0} + \varphi_{z0} \cdot (y - y_0)$$

$$v_y = v_{y0} + \varphi_{z0} \cdot (x - x_0)$$

3. No bending stiffness, where all nodes at the same level have the same rotation

$$v_x = v_{x0} + \varphi_{z0} \cdot (y - y_0)$$

$$v_y = v_{y0} + \varphi_{z0} \cdot (x - x_0)$$

$$\varphi_z = \varphi_{z0}$$

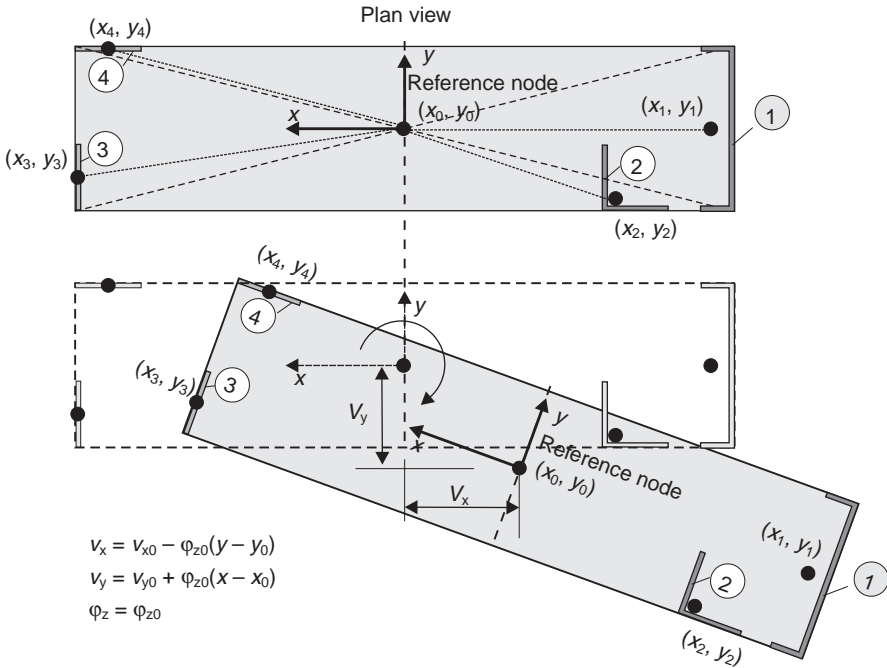
where:

v_{x0} , v_{y0} , v_{z0} is the displacement of the reference node

φ_{x0} , φ_{y0} , φ_{z0} is the rotation of the reference node.

Model 2 is used for comparison only. It does not reflect the real behaviour of the slab. Whether Model 1 or 3 should be used depends on the behaviour of the actual system with respect to the stiffness of the slab and the distance of the bracing elements. A stiff coupling (additional to coupling without bending stiffness: rotation $\varphi_x = \varphi_{x0}$, $\varphi_y = \varphi_{y0}$, $\varphi_z = \varphi_{z0}$) may cause restraints in the system, as can be seen from Figure 2.64.

Figure 2.65 Displacement and rotation of the bracing elements in case of a stiff slab



When the deformation and the rotation of all nodes in the same level are identical, vertical loads are distributed according to the normal stiffness of an individual bracing element. This does not reflect the actual behaviour of the structure. In reality, the vertical loads are carried by the bracing element, which is close to the load.

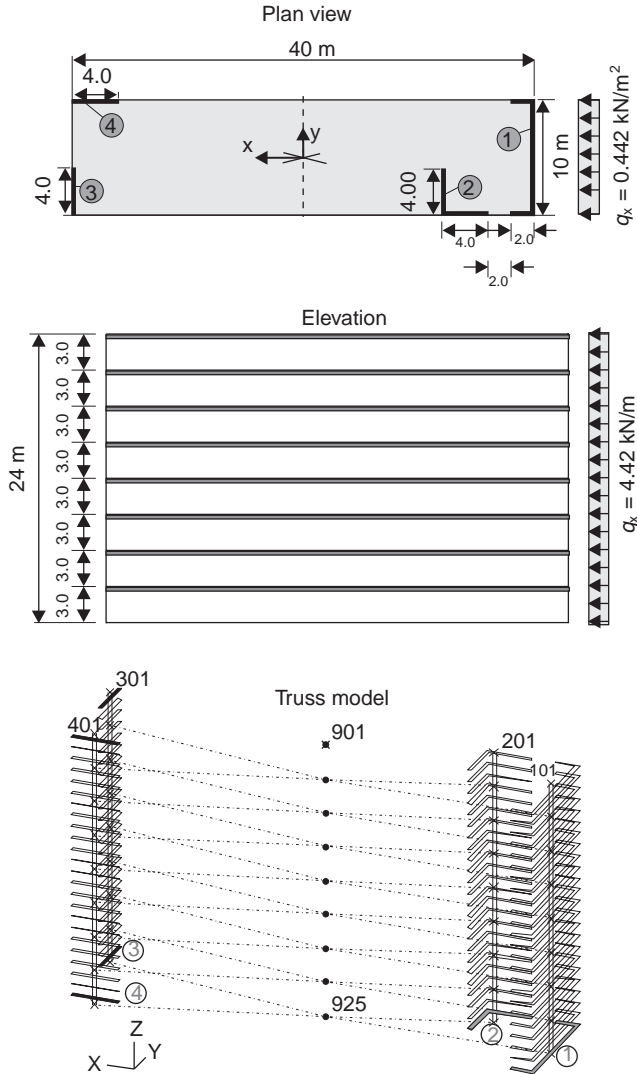
The actual deformation behaviour of a slab is generally similar to a slab without bending stiffness but which is infinitely stiff in its normal plane. In such a case, the rotation of all elements around the vertical axis φ_z must be identical at one level. Therefore, Model 3 should be used.

The axis of gravity of the different truss elements is coupled together, resulting in torsional moments where the axis of torsion does not coincide with the axis of gravity (e.g. cross-section with L- or U-shape). In this case, torsional moments and rotations are estimated.

2.6.4 Example – comparison of the various models

The following analysis will be done for the bracing system shown in Figure 2.66 (the height of the building is $h = 24$ m). This structure has been chosen as the member forces can be calculated by the equivalent beam (fictitious bar) method. Therefore, the manually calculated results can be used to verify the numerical models. There are four different bracing elements: two shear walls, a flanged member with L-shape, and a

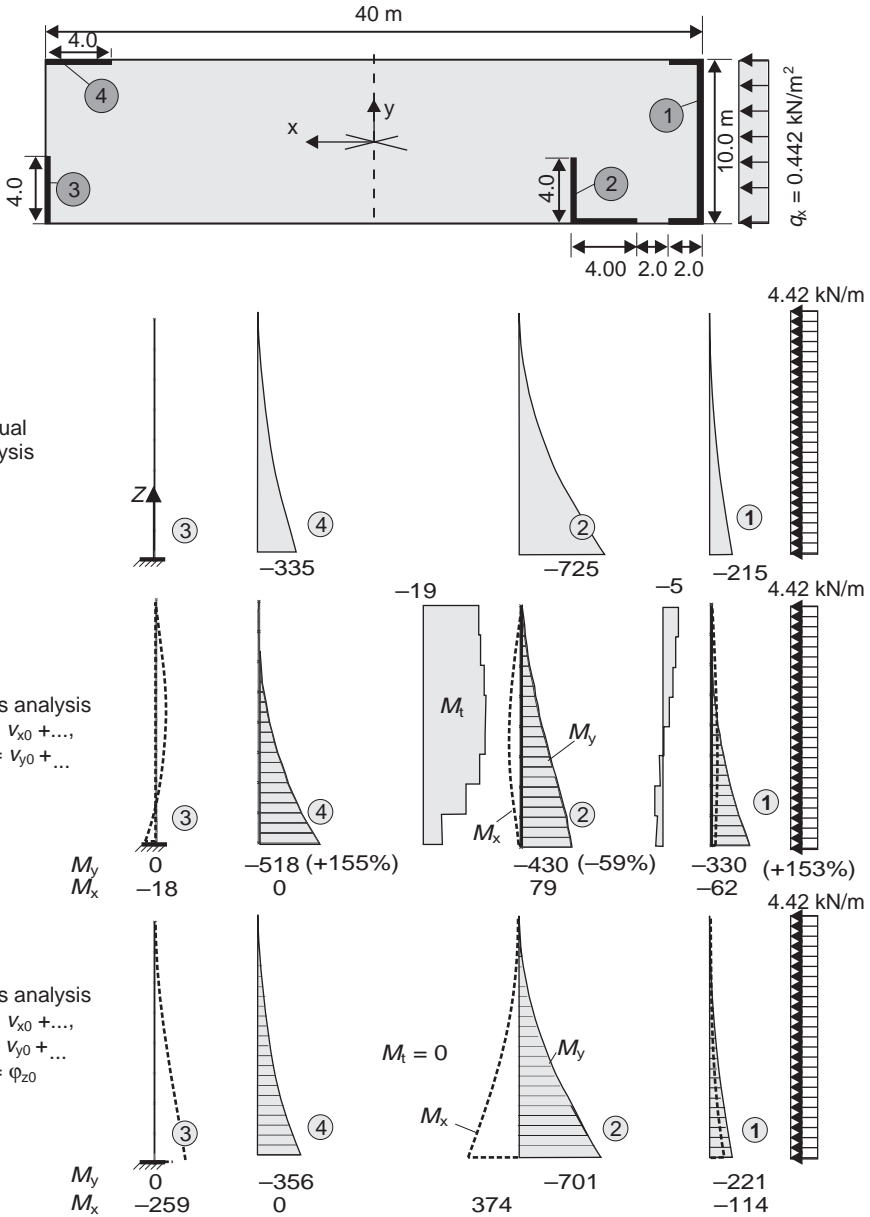
Figure 2.66 System, loading and truss model



member with U-shape. The slabs are modelled as mentioned before, using special restraints with and without coupling of the nodal rotation φ_z (φ_z is the rotation around the vertical axis).

For the sake of simplicity of further calculations, it is assumed that all bracing elements are fully fixed by the foundation slab. If the structure has a stiff box as a basement, it can be assumed that the trusses are fully restrained at ground level, thus resulting in smaller forces and displacements. A flexible foundation can be modelled by using spring elements at the base of the beams.

Figure 2.67 Bending and torsional moments of the bracing elements



The distribution of the bending moments, from the method of fictitious bars, are shown in Figure 2.67 for a uniformly distributed horizontal load of $q = 0.442 \text{ kN/m}^2$ (total horizontal force is $H = 106.1 \text{ kN}$) in the x-direction.

Table 2.5 Support reactions (horizontal force and restraint bending moment) of the bracing elements calculated with the method of fictitious bars

Element no.	1	2	3	4	Σ
Support force in x-direction: kN	18	60	≈ 0	28	106
Fixed end moment: kNm	-215	-725	≈ 0	-335	-12.75
Load distribution: %	17	57	≈ 0	26	100

The distribution of the total load between the different bracing elements is given in Table 2.5. The bending moments at the supports are listed in Table 2.6.

Figure 2.67 shows the bending moment distribution from manual analysis (fictitious bar method), and the values of the two different truss models. It can be seen that the coupling of the rotation around the vertical axis φ_z has a considerable effect on the member forces. The bending moments in the bracing elements numbers 1 and 3 are more than 1.5 times larger than for the system without coupling.

These large differences are caused by the torsional moments of element number 2, which results from the distance of the axis of gravity and the axis of torsion (Figure 2.68).

Figure 2.68 Deformation of bracing element number 2 for different locations of centre of torsion under uniform load

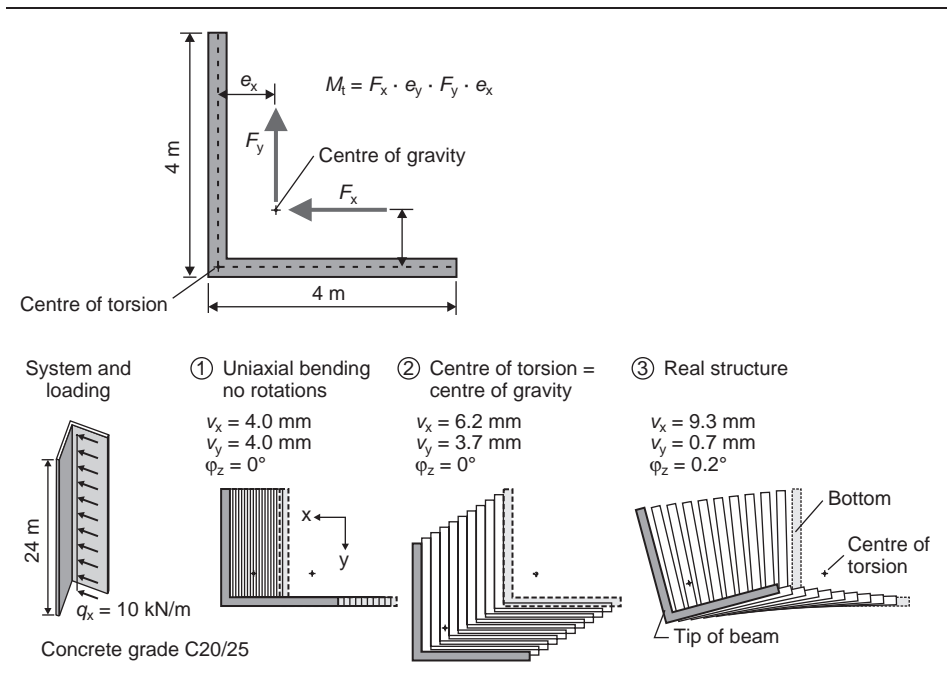


Table 2.6 Bending moment M_y at the supports of the bracing elements (in kNm)

Element no.	1	2	3	4
Method of fictitious bars	-215	-725	0	-335
Truss analysis ($v_{x,i} = v_{x0}$; $v_{y,i} = v_{y0}$)	-330	-430	0	-518
Truss analysis ($v_{x,i} = v_{x0}$; $v_{y,i} = v_{y0}$; $\varphi_{z,i} = \varphi_{z0}$)	-221	-701	0	-356
3D shell analysis	-267	-636	0	-334

Without coupling the rotation around the vertical axis, the transverse bending moments M_x are small. In the case of coupling of the rotation φ_z , the torsional moments of bracing element number 2 are nearly zero. On the other hand, the transverse bending moment M_x increases.

The small differences between the results of the equivalent beam method and the numerical truss model are caused by different assumptions for each model. Within the equivalent beam method, the bending stiffness of the bracing elements is considered, whereas the torsional stiffness of the individual members is neglected. This simplification is required in order to obtain a simple analytical solution. On the other hand, a numerical calculation will always be based on the linear elastic material behaviour. An elastic bending *and* a torsional stiffness are used in this example (Stage I – uncracked).

The assumption of linear elastic material behaviour should be checked in the case of large bending and torsion action effects. As already mentioned in Section 2.6.1, it may be necessary to neglect the torsional stiffness GI_T if any section of the beam is cracked.

The results of a 3D shell analysis are used to verify the truss models. The whole structure had been modelled with approximately 4410 shell elements (element size 1×1 m) (see Figure 2.69). The columns in the real building are neglected.

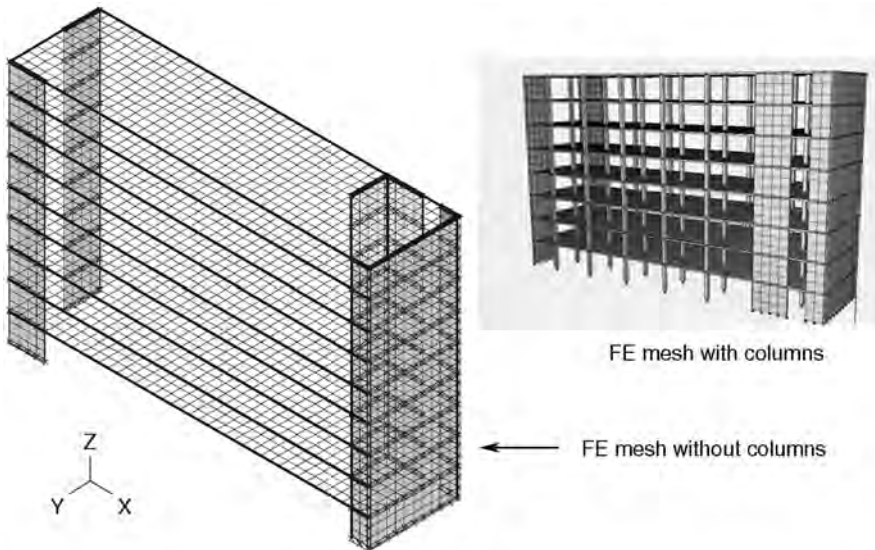
Table 2.7 summarises the main results of the shell analysis. The load on bracing element number 1 is increased by approximately 30%, and that of element number 2 is reduced by approximately 13% relative to the values from the equivalent beam method. Overall, there is a relatively good agreement with the results of the simple manual model.

In Figure 2.70, the deformation of the structure is plotted. The displacements are increased by a factor of 10 000 thus resulting in a big differential deformation between the bracing elements numbers 1 and 2.

In reality, the maximum displacements are approximately 1.1 mm in the x-direction and 0.2 mm in the y-direction only (concrete grade C35/40, linear elastic material behaviour).

The good agreement in the results of the three different models demonstrates that a considerable effort to calculate the ‘correct’ member forces, for example, with a 3D shell model, is generally not required. However, the time required for the 3D shell

Figure 2.69 3D shell model



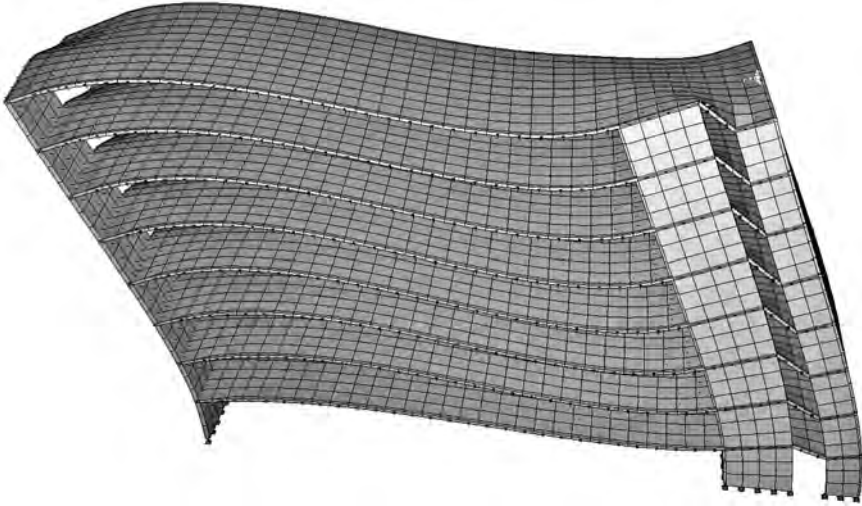
analysis is more than 100 times than that needed for the simple truss model. More time is needed for the discretisation, the verification of the results and for summarising the main output. In addition, a computer program can generally not calculate the correct arrangement of the reinforcement bars for a shell model, as will be demonstrated in Chapter 3. One advantage of a shell model is that, not only the bracing elements, but also the slabs can be modelled. Thus, the deformation and load-bearing behaviour of the structure is modelled with higher accuracy. However, the calculated member forces of the slabs cannot be used for the design, as the columns are neglected and the size of the plate elements is too big.

In Table 2.8, the bending and torsional moments, shear forces at the base of the columns and the deflection and rotation for a uniformly distributed load of $q = 0.442 \text{ kN/m}^2$ in the x-direction are listed for different numerical models.

Table 2.7 Support forces of the bracing elements (shell model)

Element no.	1	2	3	4	Σ
Support force in x-direction: kN	39	48	1	28	116
Support force in y-direction: kN	7	-12	5	0	0
Fixed end moment M_x : kNm	28	-2	-91	0	-65
Fixed end moment M_y : kNm	-267	-636	0	-334	-1237
Fixed end moment M_z : kNm	132	2	0	1	135

Figure 2.70 Deformed structure (increased by a factor of 10 000) loaded in the x-direction ($q = 0.442 \text{ kN/m}^2$)



The various analyses of the given bracing system can be summarised as follows.

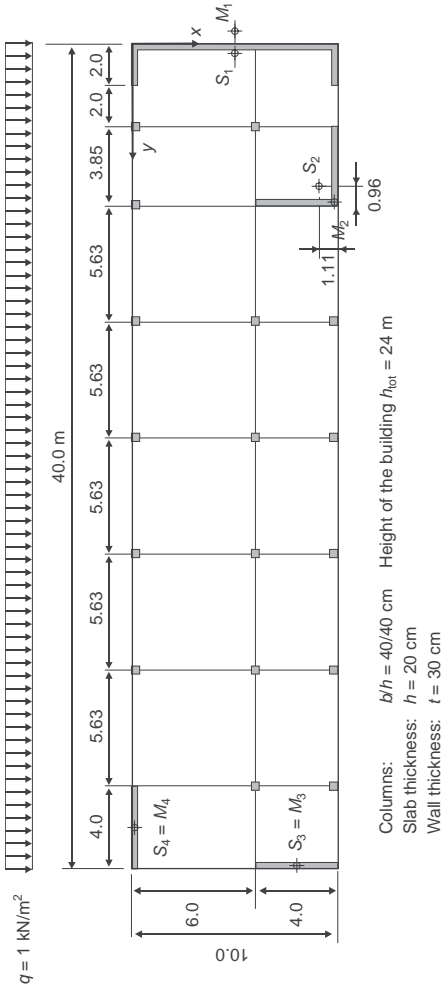
- The calculated bending moments of all truss models are greater than that of the 'real' structure (shell model number 6).
- There is a significant difference between the member forces of the various truss models and the more realistic shell model number 6.
- The results are very sensitive to the modelling of the slab. Rigid nodal coupling with $\varphi_{z,i} = \varphi_{z0}$ should be used.
- Wrapping torsion can be neglected with regard to the simplifications of the truss model.
- The support reactions are not very sensitive to the location of the beam axis as the global deformation behaviour dominates.

2.6.5 Checking for stability – stability parameter

In addition to the design of the structural elements of a building that can carry the relevant design loads, it is important to note whether the structure is classified as sway or non-sway. In case of a sway system, it is necessary to consider the deformation of the structure when calculating the member forces of all individual elements, including columns (second-order effect). In theory, this can easily be done with available software. It should be noted that the amount of calculations is increased significantly in such cases, as the combination of the various loadings may no longer be valid. Second-order effects may be ignored if they are less than 10% of the corresponding first-order effects (Eurocode 2, 2004: Part 1, Section 5.8.2).

In the case of manual analysis, the stability of the structure is checked with Equation 5.18 of Eurocode 2: Part 1 (2004), shown in the following text. Only if $F_{v,Ed}$ becomes bigger

Table 2.8 Support forces and deflections



Models

1. Fictitious bar method (manual analysis)
2. Truss model – without wrapping torsion – beam axis: centre of gravity
3. Truss model – with wrapping torsion – beam axis: centre of torsion
4. Truss model – with wrapping torsion – beam axis: centre of gravity
5. *Shell model without columns*
6. **Shell model with columns**

Core no. 1

Model	Shear force V_x : kN	Bending moment M_y : kNm	Torsional moment M_T : kNm	Deflection u_x : mm	Rotation φ_z
1. Fictitious bar method	322	-3869	230	-	-
Truss model					
2. No w.t. - centre of gravity*	318/265	-4069/-4357	7/197	0.8/1.9	-0.36/-1.8
3. With w.t. - centre of torsion*	346/404	-4083/-4864	42/302	0.8/1.0	-0.34/-0.57
4. With w.t. - centre of gravity*	352/412	-4233/-5025	42/308	0.8/1.1	-0.35/-0.60
Shell model					
5. <i>Shell model without columns</i>	273	-4102	154	0.7	-0.28
6. Shell model with columns	258	-3789	67	0.6	-0.21

Core no. 2

Model	Shear force V_x : kN	Bending moment M_y : kNm	Torsional moment M_T : kNm	Deflection u_x : mm	Rotation φ_z
1. Fictitious bar method	212	-2543	-204	-	-
Truss model					
2. No w.t. - centre of gravity*	182/194	-2447/-1741	3.6/-54	3.1/4.2	-0.36/1.8
3. With w.t. - centre of torsion*	140/46	-2490/-1171	3.0/-24	3.5/4.0	-0.34/1.8
4. With w.t. - centre of gravity*	134/44	-2251/-1029	3.0/-21	3.1/3.5	-0.35/1.5
Shell model					
5. <i>Shell model without columns</i>	246	-2217	5.8	2.6	-0.28
6. Shell model with columns	263	-2168	5.1	2.0	-0.21

Core no. 3

Model	Shear force V_x : kN	Bending moment M_y : kNm	Torsional moment M_T : kNm	Deflection u_x : mm	Rotation φ_z
1. Fictitious bar method	423	-5081	0	-	-
Truss model					
2. No w.t. - centre of gravity*	393/433	-4967/-5382	1.8/0	15/16	-0.36/0
3. With w.t. - centre of torsion*	412/448	-4921/-5456	1.4/0	14.3/15.7	-0.34/0
4. With w.t. - centre of gravity*	412/442	-5009/-5436	1.5/0	14.6/15.8	-0.35/0
Shell model					
5. <i>Shell model without columns</i>	386	-4184	1	11.5	-0.27
6. Shell model with columns	380	-3578	0.3	8.8	-0.21

Core no. 4

Model	Shear force V_x : kN	Bending moment M_y : kNm	Torsional moment M_T : kNm	Deflection u_x : mm	Rotation φ_z
1. Fictitious bar method	2.3	-27.3	0	-	-
Truss model					
2. No w.t. - centre of gravity*	6.3/7.3	-36/-40	1.8/0	14.4/15.5	-0.36/0
3. With w.t. - centre of torsion*	2.3/2.5	-27/-30	1.4/0	13.7/15.1	-0.34/0
4. With w.t. - centre of gravity*	2.3/2.5	-27/-29	1.5/0	14.0/15.1	-0.35/0
Shell model					
5. <i>Shell model without columns</i>	-4.7	0	-0.1	11	-0.26
6. Shell model with columns	-3.3	0	-0.7	8.4	-0.2

* Rigid coupling, $\varphi_{z,i} = \varphi_{z0}/\text{hinge coupling}$; w.t. = wrapping torsion

than the specific value, a more refined analysis, including second-order effects, is required. The same holds true in the case of an unsymmetrical arrangement of various bracing elements.

Stability parameter α

$$F_{v,Ed} \leq k_1 \cdot \frac{n_s}{n_s + 1.6} \cdot \frac{\sum E_{cd} \cdot I_c}{L^2} \quad (\text{Eurocode 2, 2004: Part 1, Equation 5.18})$$

where:

$F_{v,Ed}$ is the total vertical loads on braced and bracing members

n_s is the number of storeys

L is the total height of the building above the level of moment restraint

E_{cd} is the design value of the modulus of elasticity of concrete ($E_{cd} = E_{cm}/\gamma_{cE}$)

I_c is the second moment of area of uncracked bracing member(s).

The stability of a building depends on the bending stiffness of the bracing system $E_{cd}I_c$, the height of the building L and the total vertical load $F_{v,Ed}$. The latter value is the maximum load under serviceability conditions, including the reduction of the live loads allowed by Eurocode 2. The elastic modulus E_{cd} is given in the codes. Thus, only the moments of inertia I_{cy} and I_{cz} are unknown.

In the case of regular bracing systems, the required cross-section parameter is the total sum of the moment of inertia of the individual bracing elements in the relevant direction. In non-regular bracing systems, the equivalent moment of inertia I_c may be estimated by a comparison of the maximum horizontal deformation of a cantilever beam with the results from the truss model loaded by an arbitrary horizontal force (Figure 2.71).

The calculation can be based on linear elastic material behaviour, as long as the maximum tensile stress in the concrete is less than $f_{ctk;0.05}/\gamma_c$.

2.7. Design of hollow box girder bridges

The structural analysis of a hollow box girder bridge in the transverse direction has been provided in Section 2.1.2. Next, we consider its modelling in the longitudinal direction. In practice, the designs in the transverse and longitudinal directions are done separately (Figure 2.72). The bridge is modelled as an ordinary beam, having a rigid cross-section with no distortions due to either bending or shear (Figure 2.73) and linear strain distribution over the depth of the cross-sections. This model is used to estimate the longitudinal, shear and torsion reinforcements, the relevant support forces, the stresses, and the deflections of the bridge.

The torsional moments are estimated by assuming two bearings located at one support axis. In such a case, it is recommended that each bearing be considered separately in the numerical model, including the transverse spacing between them as well as their distance from the centre of gravity of the beam. This results in a 3D numerical model instead of a plane grillage system. The additional work is justified in this case, as the greatest

Figure 2.71 Estimation of the equivalent moment of inertia I_{equiv} of a bracing system

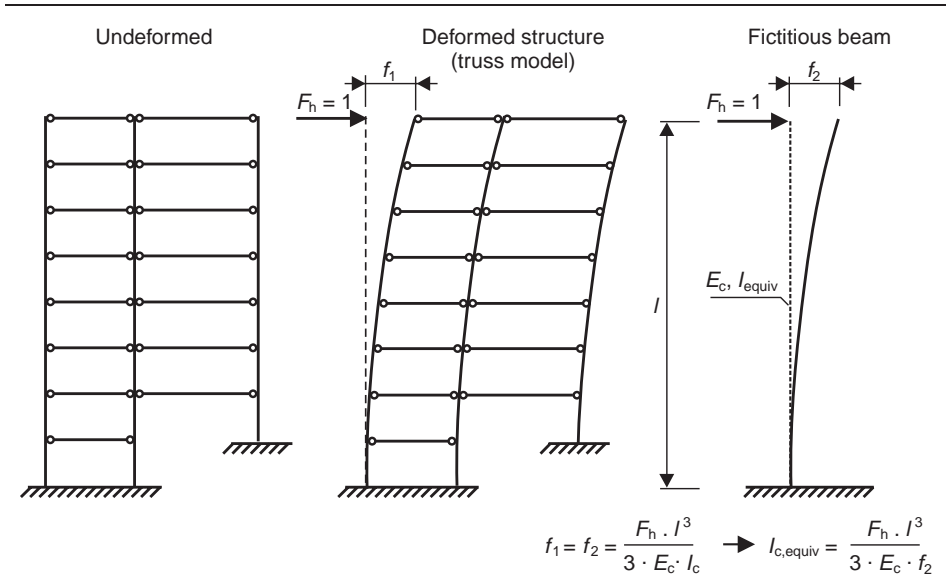


Figure 2.72 Structural models for design of a hollow box girder bridge

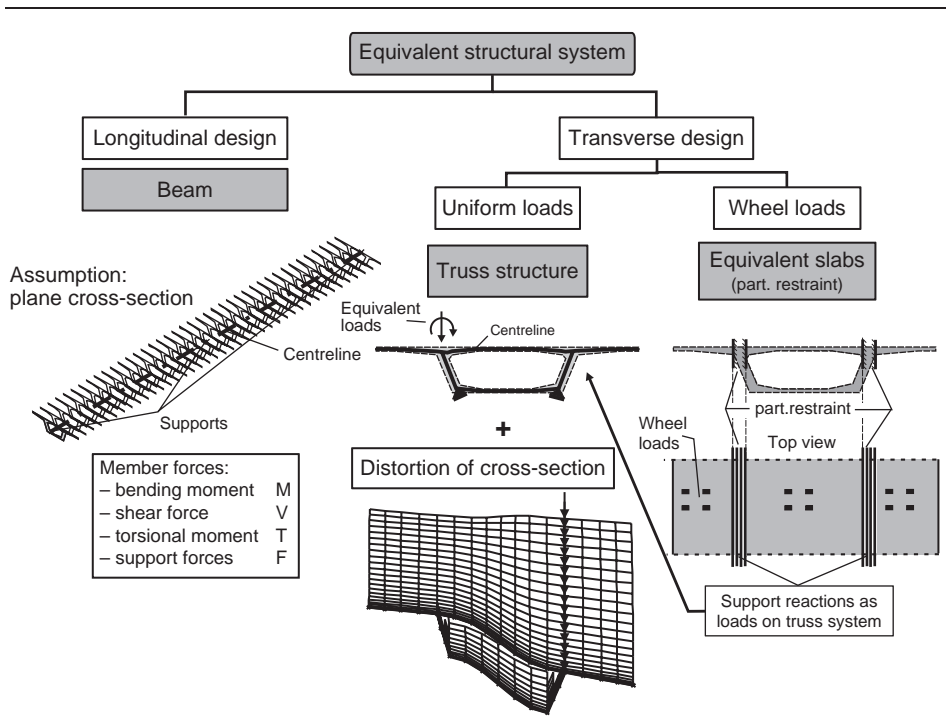
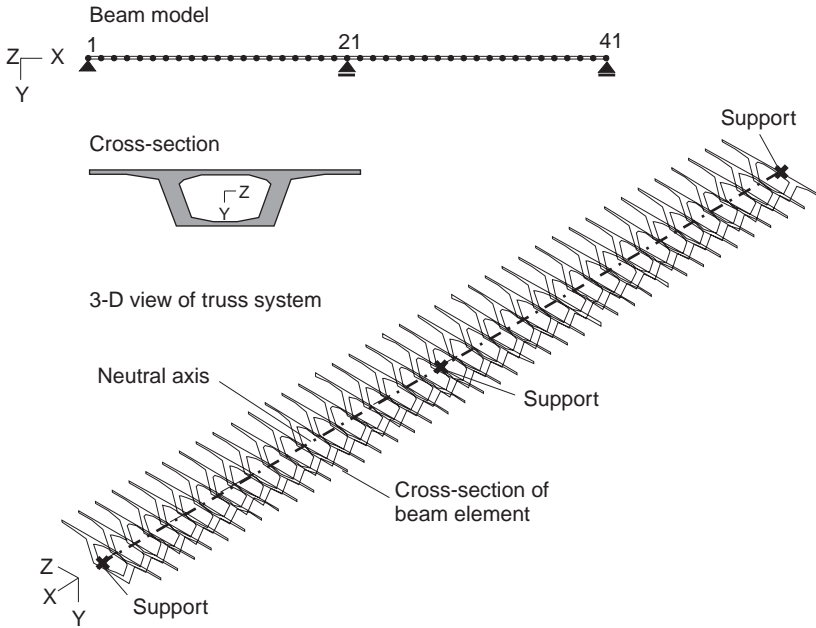


Figure 2.73 Numerical model of a two-span hollow box girder bridge



components of forces and deflections in each bearing are needed, and not only the maximum total support reactions. As an alternative, the rotation around the longitudinal axis may be restrained; however, this requires manual estimation of the relevant bearing forces from the vertical load and torsional moments. A 3D model is also required if a superstructure has an unsymmetrical cross-section.

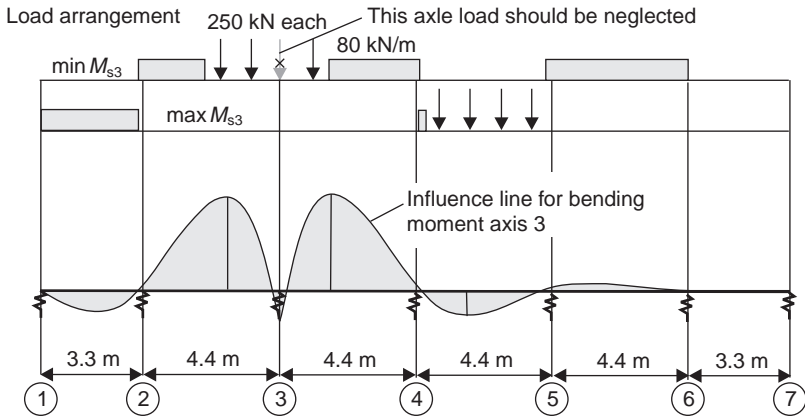
The diaphragms at the support axis are modelled by stiff beam elements, or more efficiently, by coupling of the nodes at the support. As an alternative, torsional restraints at the supports can be considered.

Various load cases have to be considered in the design of a bridge structure. They have to be combined in the most unfavourable manner. The relevant positioning of the traffic loads, for example, axle loads, can be considered in two different ways. The first one can ‘drive’ the traffic loads by the computer over the bridge in all different lanes. This results in an enormous number of load cases and a major computational effort. In addition, one has to know in advance which different parts of the structure should be loaded to get the greatest member forces (see Figure 2.74). Therefore, numerical integration of influence lines for each node and each force can be used as a reasonable alternative.

Influence line for

- bending moment – deflection curve caused by the rotation of $\Delta\varphi = 1$
- shear force – deflection curve caused by the deformation jump of $\Delta w = 1$.

Figure 2.74 Load arrangement by means of an influence line (train load UIC 71) max/min bending moment at axis 3



The beam model is based on a rigid cross-section (Figure 2.77). Distortions caused by unsymmetrical actions have to be considered separately by means of a frame system (Figure 2.75). This system may be supported either in the vertical direction or in the direction of the webs (see Section 2.1.2). For this model, the relevant member forces in the webs and in the transverse direction are estimated for a longitudinal uniformly distributed load.

Figure 2.75 3D shell model of a hollow box girder bridge (only one half of the structure is shown)

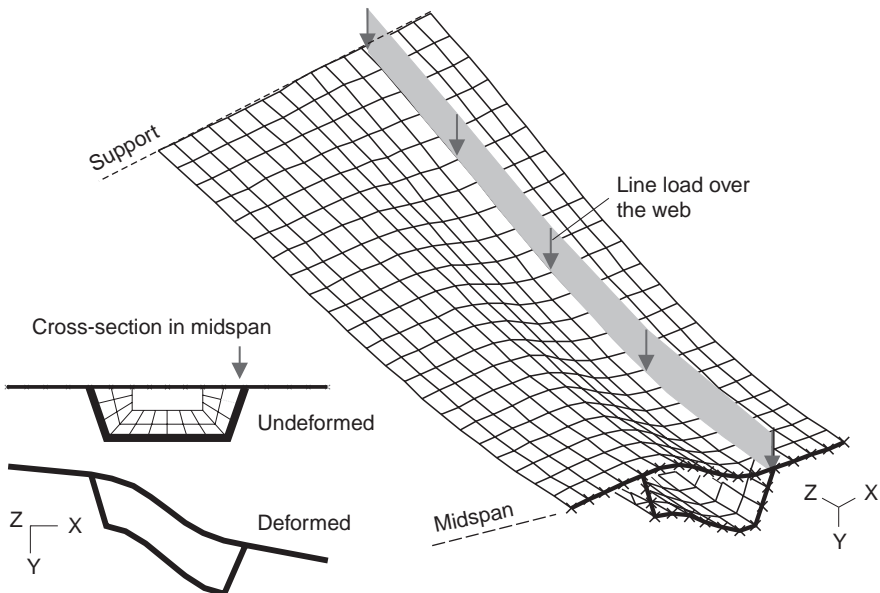
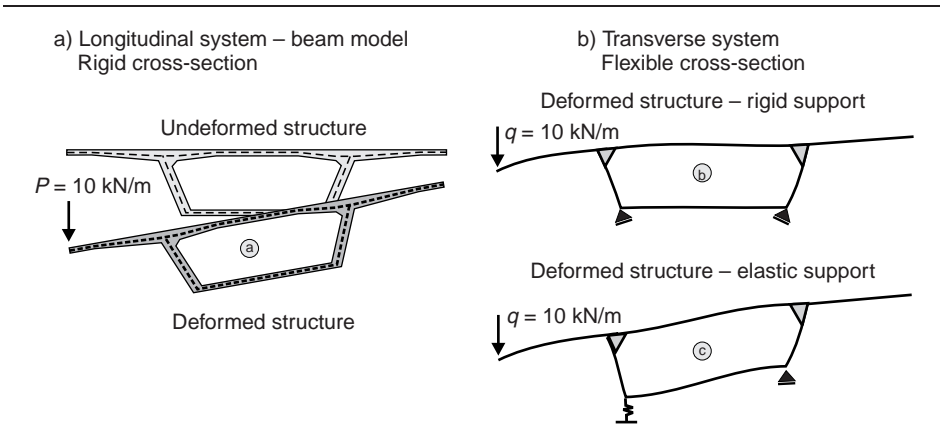


Figure 2.76 Distortion of a hollow box girder bridge at midspan; beam model (left) and real deformations (right, bottom)



The displacements may be considered approximately by analysing the equivalent forces in an elastically supported frame system (Figure 2.76).

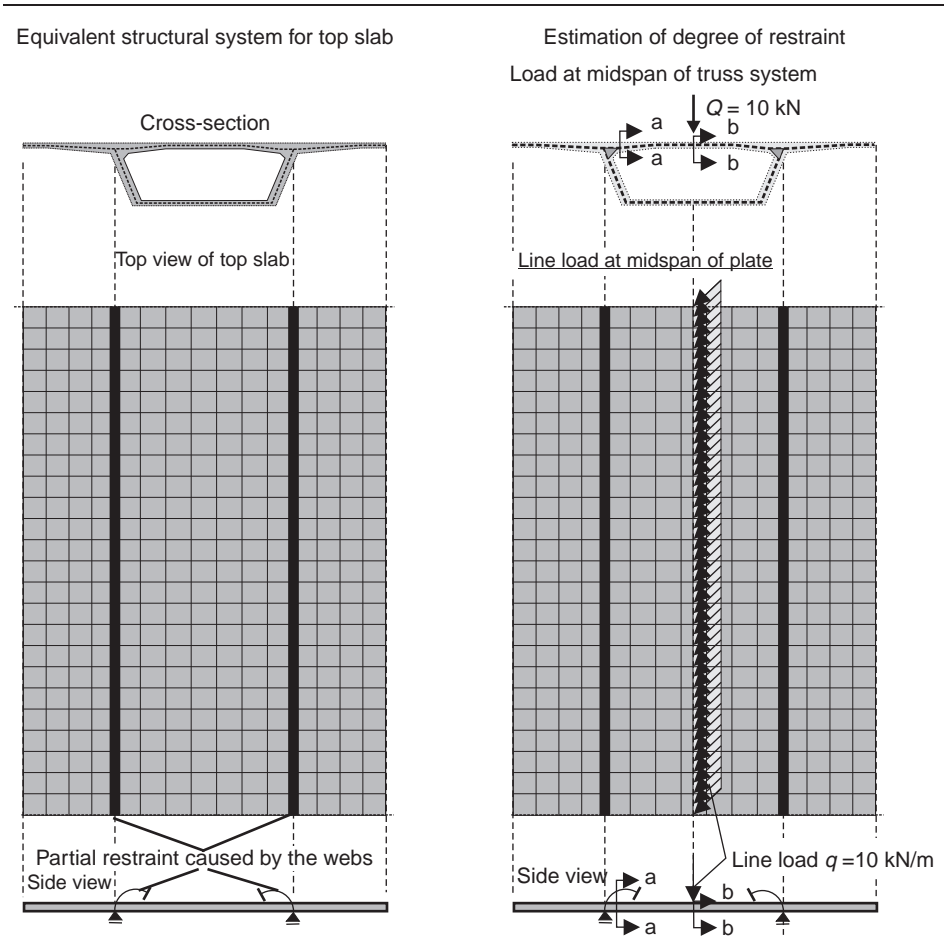
A slab system may be used to calculate the bending moments and shear forces caused by single forces (e.g. wheel loads) and non-symmetric loads on the top slab (see Section 4.11.3). This slab is partially restrained at the webs (see Figure 2.77). The stiffness of the equivalent bending springs can be estimated by comparison of the bending moment of a beam and a plate structure under a uniform line load. As an alternative, bending moments can be estimated from charts or influence lines, such as those of Homberg (Homberg, 1973; Homberg and Ropers, 1965). Sometimes, an interpolation of the values of different support conditions (fully or partially restrained at the web supports) and the location of the single loads is required. However, such an analysis may be more time consuming than an FE analysis. Further information on the analysis of plate structures is given in Chapter 4.

2.8. Truss system – design of T-beam bridges

Two decades ago, the capabilities of personal computers and the software available were not enough to compute a plate or a 3D shell system by means of FEM. Until then, 2D truss systems, for example, grillage, were used. One of the best-known examples for this idealisation of a 3D shell structure is the opera house in Sydney, Australia (Figure 6.26). At the time of construction, it was not possible to design the roof as a thin unstiffened shell. Therefore, a truss system was used instead of a more elegant spatial structure.

A grillage system is still widely used, for example, in prestressed T-beam bridges. For such structures, the results of a 2D plate or 3D shell analysis (see Figure 2.75) may be ‘nice looking’, but are generally of little use for a design where the resulting member forces are required rather than the accurate stresses and membrane forces. Also, a considerable amount of computation time is needed in order to consider all the relevant load cases.

Figure 2.77 Simplified equivalent system for a deck slab



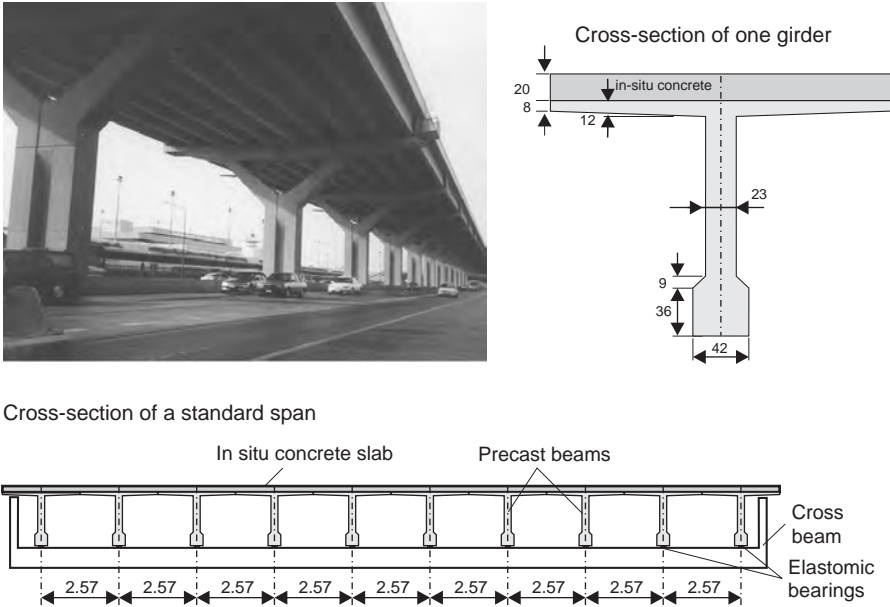
The example of a T-beam bridge is shown in Figure 2.78. This structure has been constructed by prefabricated T-beams with an additional cast-in-situ concrete top slab. However, before we consider the modelling of real structures, we will examine the essential special features of a grillage system for a simply supported rectangular slab.

2.8.1 Grillage models of rectangular solid slabs

The internal forces of a rectangular simple supported concrete slab can be determined from tables or by means of a spatial FE analysis. These methods can be used to check the results of a grillage system.

The solid two-way slab is represented by a 2D grillage system where the longitudinal and transverse beams are connected at the nodes. The loading is always perpendicular to the midplane of the slab. The following example only considers uniform loading.

Figure 2.78 Don Muang Tollway, Bangkok (Mühle and Kroppen, 1997)



After the discretisation of the structure, one has to determine the equivalent vertical line loads on the beams in both directions. This can be done by assuming that the displacement of the beams at the nodes, where they are connected together, should be the same (Figure 2.79). For midspan of a simply supported beam structure under uniformly distributed loading q ($q = q_1 + q_2 = \text{total load}$), this results in:

Maximum displacement of a simply supported beam under uniform loading:

$$w(x) = \frac{q \cdot l^4}{24 \cdot E_c \cdot I_c} \cdot \left(\frac{x}{l} - 2 \cdot \left[\frac{x}{l} \right]^3 + \left[\frac{x}{l} \right]^4 \right)$$

<p>System A ($x/l = 0.5$) – midspan (Figure 2.80 left)</p> $f_1 = \frac{5}{384} \cdot \frac{q_1 \cdot l_1^4}{E_c \cdot I_c}$ $f_2 = \frac{5}{384} \cdot \frac{q_2 \cdot l_2^4}{E_c \cdot I_c}$	<p>System B ($x/l = 0.1$) – near support (Figure 2.80 right)</p> $f_1 = \frac{5}{384} \cdot \frac{q_1 \cdot l_1^4}{E_c \cdot I_c}$ $f_2(x = 0.1l_2) \approx 0.0041 \cdot \frac{q_2 \cdot l_2^4}{E_c \cdot I_c}$
---	--

with $E_c I_c = \text{constant}$ and $f_1 = f_2$, this results in:

$$q_1 \cdot l_1^4 = q_2 \cdot l_2^4$$

$$q_1 \cdot l_1^4 = 0.3139 \cdot q_2 \cdot l_2^4$$

with $q = q_1 + q_2$, it follows:

$$q_1 = q \cdot \frac{l_2^4}{l_1^4 + l_2^4}$$

$$q_1 = q \cdot \frac{l_2^4}{3.186 \cdot l_1^4 + l_2^4}$$

$$q_2 = q \cdot \frac{l_1^4}{l_1^4 + l_2^4}$$

$$q_2 = q \cdot \frac{l_1^4}{l_1^4 + 0.3139 \cdot l_2^4}$$

with $l_1 = l_2$

$$q_1 = q_2 = 0.5 \cdot q$$

$$q_1 = 0.24 \cdot q; q_2 = 0.76 \cdot q$$

However, this load distribution only applies to one location. It follows from the deflected condition (see the right-hand side of Figure 2.79), as well as the previous calculations, that the equivalent load on the beams decreases from midspan to the supports, respectively, in the direction of the shorter span length. For simplicity, this non-uniformity is usually neglected in the analysis of a grillage system.

The accuracy of the analysis usually increases with the number of trusses in both directions. In the following example, the influence of the number of beams on the member forces and the displacements of a simply supported rectangular slab with an aspect ratio of $l_x/l_y = 1.5$ is examined (Figure 2.80). The structure is loaded by a uniformly distributed load of $q = 10 \text{ kN/m}^2$.

Figure 2.79 Load distribution for a grillage system

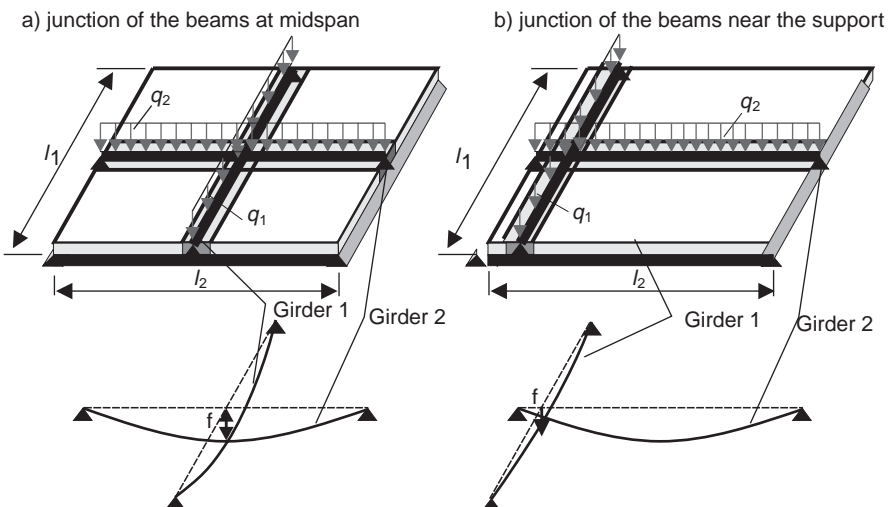
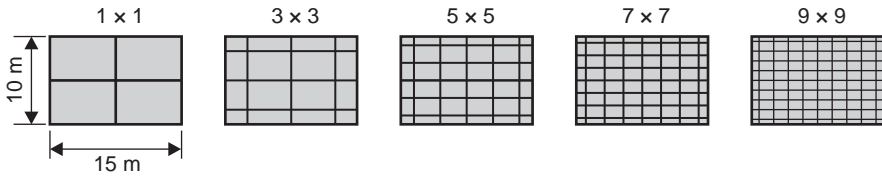


Figure 2.80 Grillage systems used in the analysis



For the purpose of comparison, the displacement at midspan and the relevant bending moments in both directions are calculated either by tables or by a 2D FE model (shell).

Czerny (1999) gives the following values (concrete grade C30/35, slab thickness $h = 30$ cm):

$$m_{x\text{m}} = 73.0 \text{ kNm/m}; m_{y \text{ max}} = 28.8 \text{ kNm/m}; f = 10.8 \text{ mm}$$

Figure 2.81 shows the bending moments, the shear force and the displacements of the grillage system with three girders in each direction. As would be expected, the load is mainly transferred in the direction of the shorter span width. The bending moment and shear force distribution show an unsteady distribution, which is caused by the discontinuous interconnection of the beam elements.

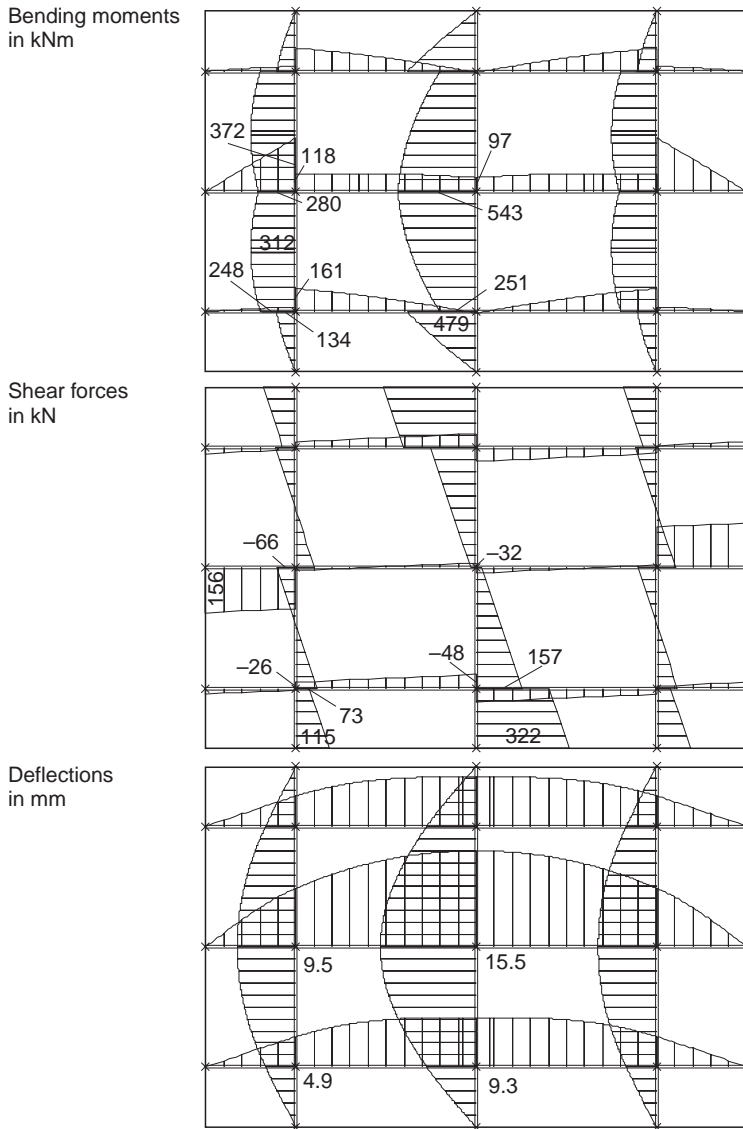
The convergence of the grillage model is shown in Figure 2.82. Here, the ratios of the results of the grillage system to that of the slab are given for an increasing number of beams in both directions.

A system with one beam in both directions results in 43% ($m_{x\text{m}}$) resp. 61% ($m_{y\text{m}}$) greater bending moments compared to the slab. This large error can be traced back to the fact that the 2D spatial load dispersion of a solid slab is not modelled by a girder grillage. Even for this simple system, at least 7×7 beams are required in order to achieve sufficient accuracy in the member forces. Figure 2.82 shows that, with more than 9×9 beams, the calculated results are lower than the correct values (factor < 1.0), which may lead to an unsafe design.

By means of a truss system, the forces in members can be calculated for slabs with reduced twisting stiffness or orthotropic slabs. Slabs that have a reduced twisting stiffness can only carry the loads in two orthogonal directions. The twisting bending moment m_{xy} cannot be sustained in the edges where two simple line supports meet. Some examples of systems with reduced twisting stiffness are

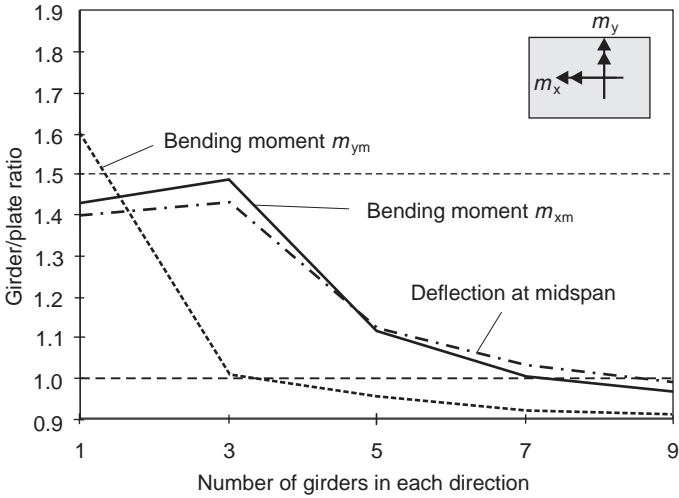
- precast concrete slabs without additional cast in situ concrete cover, if a joint is located closer than $0.3l$ from the corners (DIN 1045-1, 2008)
- slabs having large openings in the region of the edges
- slabs where the edges are not restrained against uplifting.

Figure 2.81 Bending moments, shear forces and displacements of the beams (3 × 3 division)



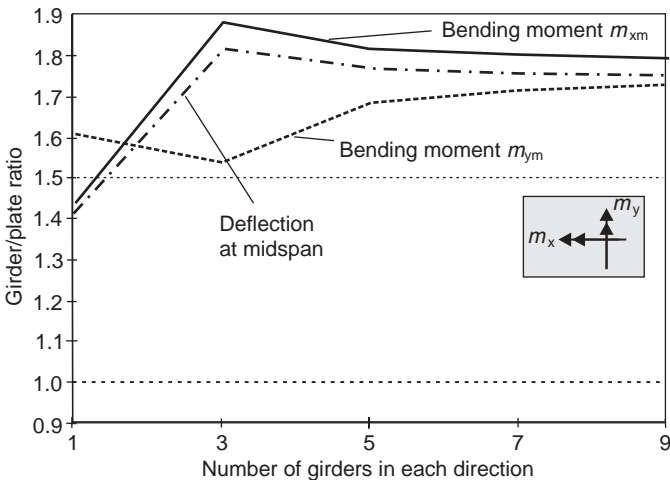
The reduction of twisting stiffness in the girder model is considered by reducing the torsional stiffness of the beam elements. Figure 2.83 shows the results for the extreme value $I_T=0$ in relation to that of the elastic value I_T for an increasing number of beams in each direction. The bending moments at midspan increase to more than 80%, if the torsional stiffness is neglected. This factor is significantly higher than the value given in 'Heft 240' of the German Concrete Association (Grasser *et al.*, 1991).

Figure 2.82 Bending moment and deflection at midspan of a grillage system against the correct plate values with increasing number of beams



According to this publication, the bending moments of an isotropic slab should be increased by only 26% (aspect ratio of the slab 1:1.5) if the real system has a reduced twisting stiffness. This big difference between the calculated values for $I_T=0$ and that of ‘Heft 240’ (Grasser *et al.*, 1991) can be traced back to the fact that the latter assumes a reduction and not a complete loss of the twisting stiffness.

Figure 2.83 Comparison of the bending moments and displacement at midspan with the plate values (stiffness against twisting moments) for an increasing number of beams in both directions with $I_T=0$



2.8.2 Double T-beam bridge

Different numerical models can be used for T-beams and ripped slabs. These will be discussed in detail in Chapter 5. In the following, only the modelling of a double T-beam by means of a grillage is demonstrated. As mentioned earlier, truss systems are still applicable, for example, as the dimensioning of prestressed beams is much more complicated if a shell model is used. Furthermore, the computational effort for truss systems is considerably less than that for folded slab analysis.

The procedure for a girder analysis is demonstrated for the double T-beam bridge shown in Figures 2.84 and 2.85. The numerical model is illustrated in Figure 2.87. The longitudinal girders are represented by straight beam elements. Their axis is located in the centre of gravity of the T-cross-section. Where the longitudinal girders have an unsymmetrical cross-section, which is very often the case for the outer girders (see Figure 2.85), the principal axis is not purely in the vertical or horizontal directions. This results in a two-axial bending for the beam, which can only be considered by a 3D numerical model. In order to avoid this additional effort, the inclination of the principal axes is generally neglected. This simplification is justified, since in most cases the effect of the inclination of the main axis on the member forces and moments is very small. Furthermore, the shear centre is placed in the centre of gravity of the cross-section. The effective width of the flanges has to be eventually taken into account. With these simplifications, the structural analysis of the bridge by using a flat truss system (grillage) is possible.

For simplicity, a pin support in the centre of gravity of the main girders and a restraint against torsion caused by the cross beams and the two separate bearings in each axis at the supports are assumed in the system shown in Figure 2.86. Therefore, the distance between the bearings and the distance of the support level to the centre of gravity has to be considered when estimating the relevant bearing forces.

Figure 2.84 Double T-beam bridge

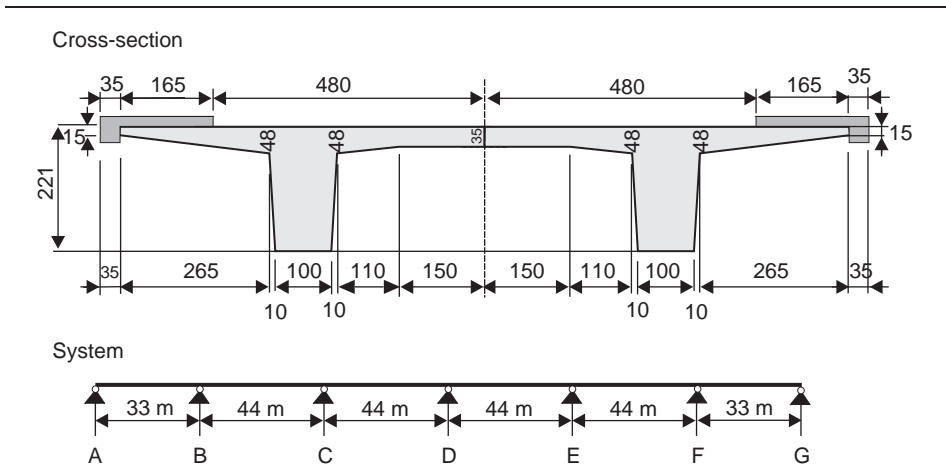


Figure 2.85 Cross-section of one girder

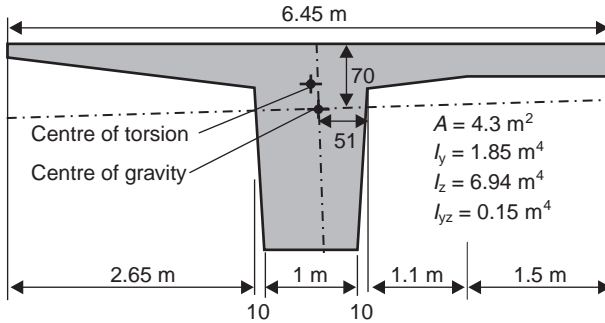
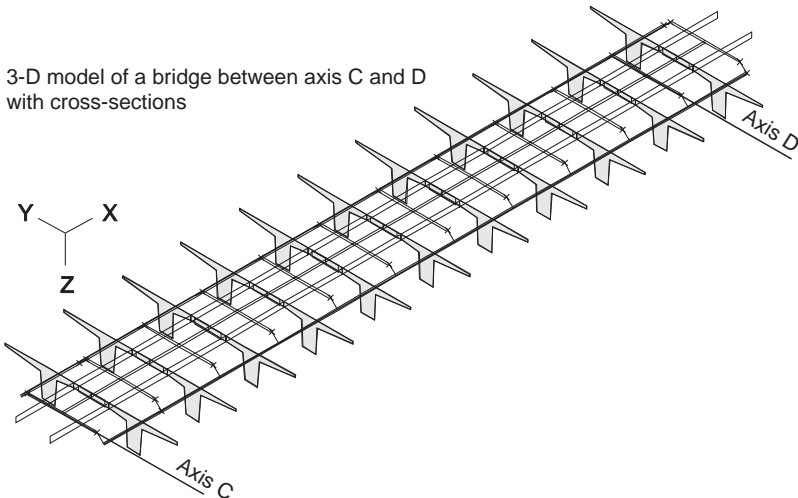
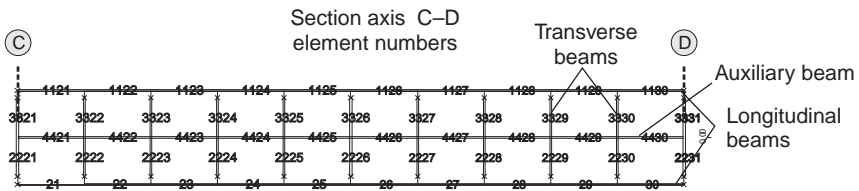
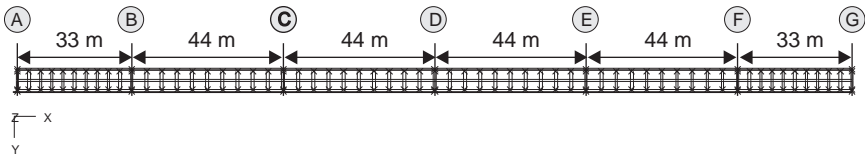


Figure 2.86 Numerical model of a double T-beam bridge



While the discretisation of the longitudinal girders creates no difficulties, detailed investigations are required for correct and realistic modelling of the transverse load-bearing behaviour of the bridge. This includes the vertical location of the equivalent ‘fictitious’ transverse beams, their connection with the longitudinal main girders and their bending stiffness.

2.8.2.1 Location of the beams in transverse direction

The transverse girders can either be arranged in the centre of gravity (model A) or at the height of the deck (model B) (Figures 2.87 and 2.88). The main difference between these alternatives is that model B requires a 3D truss model. The effect of the discretisation on the member forces will be discussed in Section 2.8.2.3 by a special example.

In case of torsion, the longitudinal girders rotate around their centre of torsion, which in case of a symmetric T-beam is located at the junction of the centreline of the flange and the web. It follows from this that a load on the flanges results in tension forces in model A and compression forces in model B in the transverse beams (Figure 2.89). However, since the torsional stiffness and thus the restraint against rotation of a T-beam are small, the difference between the two models can be usually neglected. It should be noted that, in case of model B, the end forces of the transverse beams are introduced into the T-beam eccentrically, which results in torsional moments in the longitudinal girder.

Figure 2.87 Location of the transverse beams

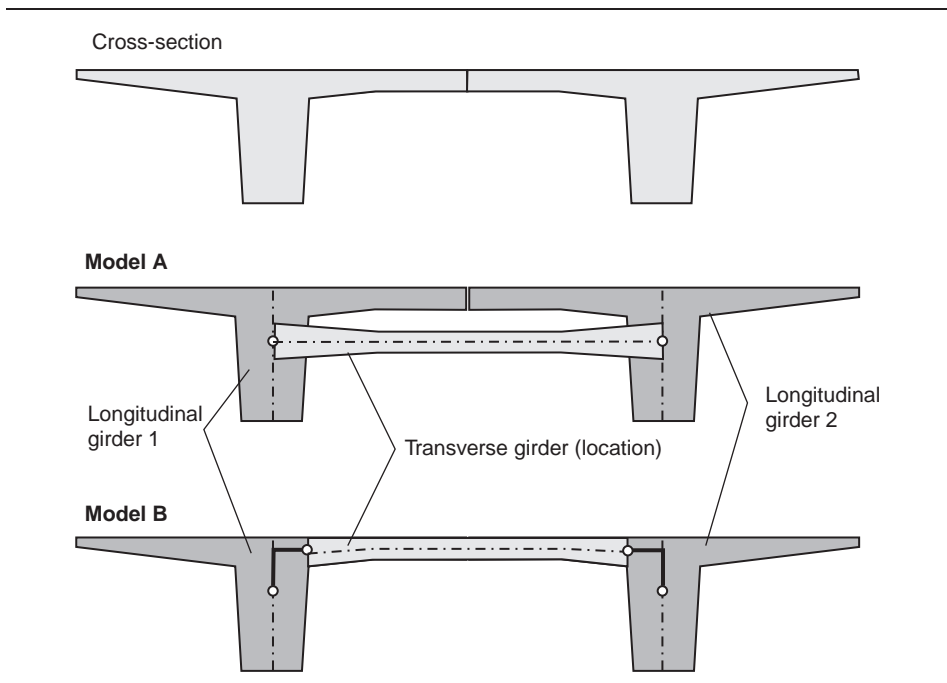
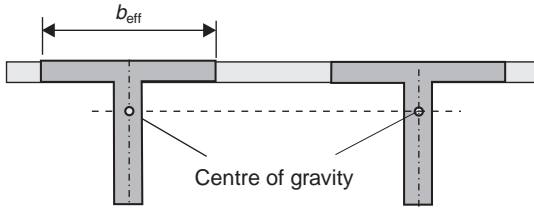


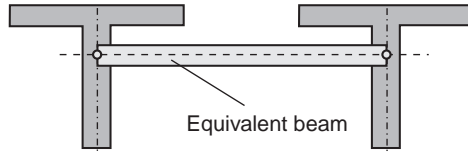
Figure 2.88 Two different models for a double T-beam bridge

Real system – cross-sections

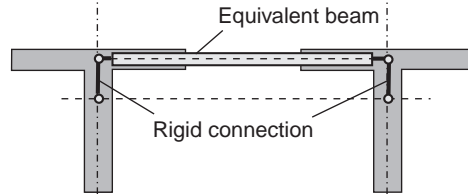


Truss system

a) Transverse beam in centre of gravity of longitudinal girder



b) Transverse beam in the centreline of the deck slab



Grillage – plan view

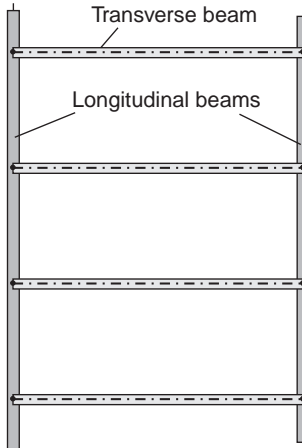
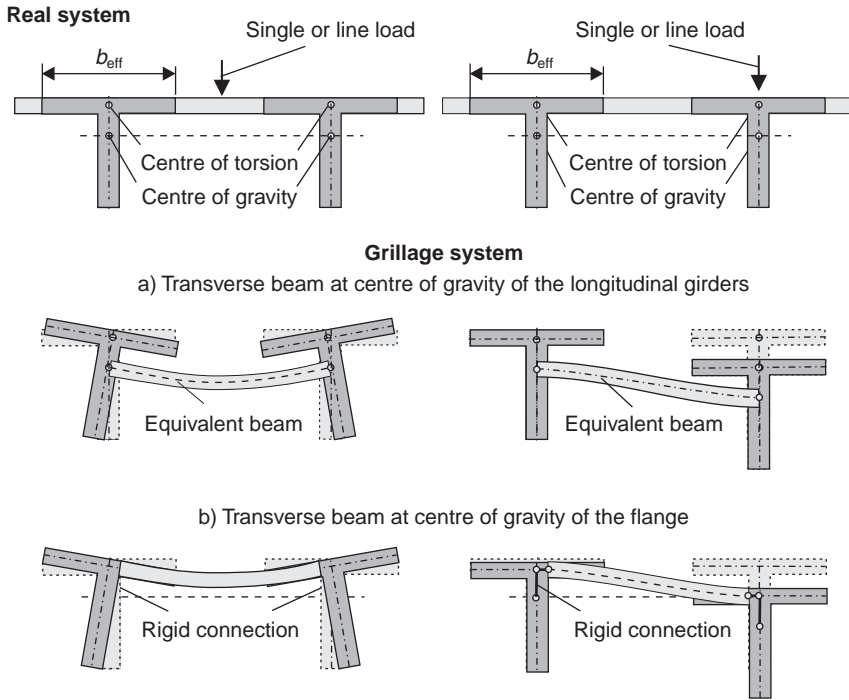


Figure 2.89 Deformation of the longitudinal and transverse beams under constant line loading



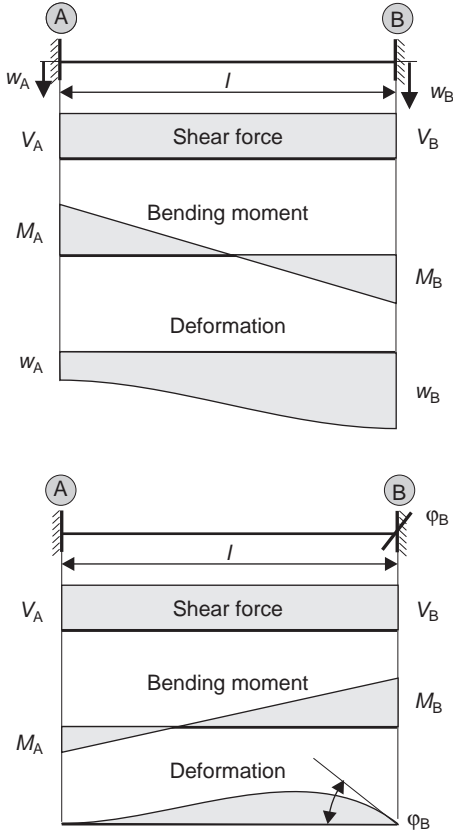
2.8.2.2 Number of transverse beams

The number of transverse beams, and hence their distance from each other, influences the load distribution in the transverse direction of the bridge deck. Therefore, the spacing of the transverse beams should not be too great. This is of special importance in case of concentrated loads (e.g. wheel loads on a deck). A point-load on a slab will always disperse in two directions, whereas a beam can only transfer the load in the direction of its longitudinal axis. In such a case, it is recommended to design the bridge in the transverse direction with another system, for example, a slab, modelled by 2D shell elements. This has already been explained for a hollow box girder bridge (see Figure 2.77). Thus, to improve the load transfer in the longitudinal direction, it may be useful to add additional (fictitious) beams in the longitudinal direction.

2.8.2.3 Section properties of the transverse beams

The stiffness of the transverse beams should be identical to that of the real slab. Due to the considerable stiffness of the longitudinal girders, it is assumed that the transverse beams are fully restrained by the longitudinal beams. If the transverse beam is located on the axis of gravity of the T-beams (model A), its span length is bigger than in reality ($l_{\text{beam}} = l_n + b_w$) (Figure 2.89). Therefore, the cross-section height has to be modified to get the same stiffness as the real slab. This can be done by comparing the angle

Figure 2.90 Member forces and deformation of a fully restrained beam due to vertical displacement or rotation of one support



Displacement of the support

$$V_A = V_B = \frac{12 \cdot E \cdot I}{l^3} \cdot (w_B - w_A)$$

$$V(x) = \frac{12 \cdot E \cdot I}{l^3} \cdot (w_B - w_A)$$

$$M_A = -M_B = -\frac{6 \cdot E \cdot I}{l^2} \cdot (w_B - w_A)$$

$$M(x) = -\frac{6 \cdot E \cdot I}{l^2} \cdot (w_B - w_A) \cdot (1 - 2 \cdot x/l)$$

$$w(x) = w_A + (w_A - w_B) \cdot \left[3 \cdot \left(\frac{x}{l}\right)^2 - 2 \cdot \left(\frac{x}{l}\right)^3 \right]$$

Rotation of the right support

$$V_A = V_B = \frac{6 \cdot E \cdot I}{l^2} \cdot \varphi_B$$

$$V(x) = -\frac{6 \cdot E \cdot I}{l^2} \cdot \varphi_B$$

$$M_A = -0.5 \cdot M_B = \frac{2 \cdot E \cdot I}{l^2} \cdot \varphi_B$$

$$M(x) = -\frac{2 \cdot E \cdot I}{l} \cdot \varphi_B \cdot (1 - 3 \cdot x/l)$$

$$f = -\frac{4}{24} \cdot l \cdot \varphi_B \text{ at } x = 2/3l$$

$$w(x) = -l \cdot \varphi_B \cdot \left[\left(\frac{x}{l}\right)^2 - \left(\frac{x}{l}\right)^3 \right]$$

of rotation or the vertical support force of a fully restrained single-span beam (Figure 2.91). The relevant deformation case depends on the stiffness of the whole system. If the longitudinal girders mainly deflect in the vertical direction under external loading, the support displacement Δw has to be used. In such a case, the shear force at the support is:

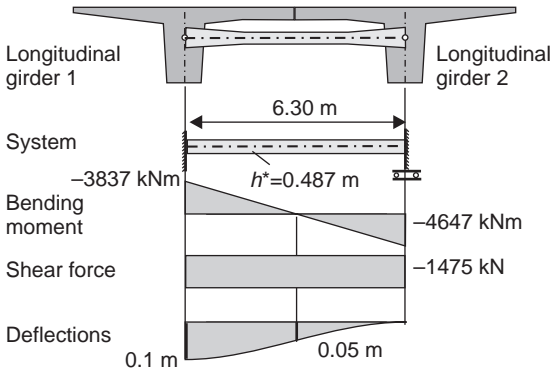
$$V_A = V_B = \frac{12 \cdot E_c \cdot I}{l^3} \Delta w$$

Thus, the equivalent moment of inertia is proportional to the span length powered by a factor of 3.

If the bending behaviour of the deck slab is the dominant feature, that is, the longitudinal girders rotate under external loading the unit rotation of the support $\Delta \varphi$ has to

Figure 2.91 Member forces and deformation of the equivalent structural systems due to a displacement of the supports of $w = 0.10$ m

Model A: transverse beams at the centre of gravity of the longitudinal girders



Estimation of the equivalent height of the transverse beam

$$V_A = -V_B = \frac{12 \cdot E \cdot I^*}{l^3} \cdot w_A \rightarrow I^* = \frac{V_A \cdot l^3}{12 \cdot E \cdot w_A} = \frac{b \cdot (h^*)^3}{12}$$

Model A: $l = 5.2 + 1.1$ m = 6.3 m

$$I^* = \frac{1.475 \cdot (5.2 + 1.1)^3}{12 \cdot 31939 \cdot 0.1} = 0.00962 \rightarrow h^* = 0.487$$

Model B: $l = 5.2$ m

$$I^* = \frac{1.475 \cdot 5.2^3}{12 \cdot 31939 \cdot 0.1} = 0.0054 \rightarrow h^* = 0.402$$

Model B: transverse beams in the centre of gravity of the flange

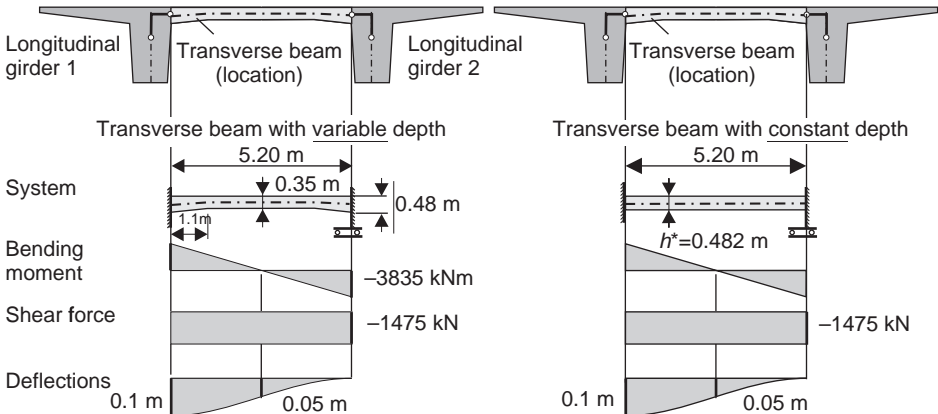
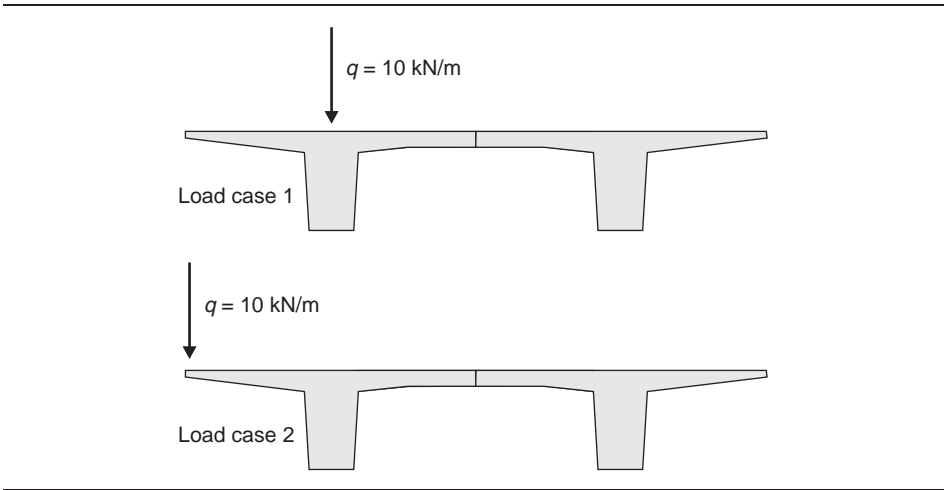


Figure 2.92 Load cases



apply. In this case, the equivalent moment of inertia is proportional to the span length powered by a factor of 2

$$V_A = V_B = \frac{12 \cdot E_c \cdot I}{l^2} \Delta w$$

In case of inclined haunches, as in the chosen example, the support forces due to the unit displacement $\Delta w = 1$ and the unit rotation $\Delta \varphi = 1$ may be estimated numerically by a plane truss system. As the bending moments are independent from the bending stiffness of the equivalent system (support bending moment of a fully restrained beam under uniformly distributed load $M = -q^2/12$), model A would result in correct shear forces but with incorrect bending moments (Figure 2.91). Therefore, in such cases, the model B is recommended, as the member forces in the longitudinal and transverse girders are needed for design.

2.8.2.4 Comparison of both models

Figures 2.93 and 2.94 show the member forces and deflection of the inner span of the double T-beam bridge shown in Figure 2.84 for both models of the transverse beams, namely a plane (grillage) and a 3D truss system. Two different unit loads are considered (Figure 2.92):

- load case 1: line load $q = 10 \text{ kN/m}$ in the centreline of longitudinal girder 1
- load case 2: eccentric line load $q = 10 \text{ kN/m}$
(is equivalent to $q = 10 \text{ kN/m} + m_T = 33.4 \text{ kNm/m}$).

From the figures in Table 2.9, it can be seen that the results of both models are quite similar except the transverse bending moment M_z , which is, from its definition, equal to zero in the case of a plane truss system.

Figure 2.93 Member forces and deflections between axis C and D – 3D truss system [mm, kNm]

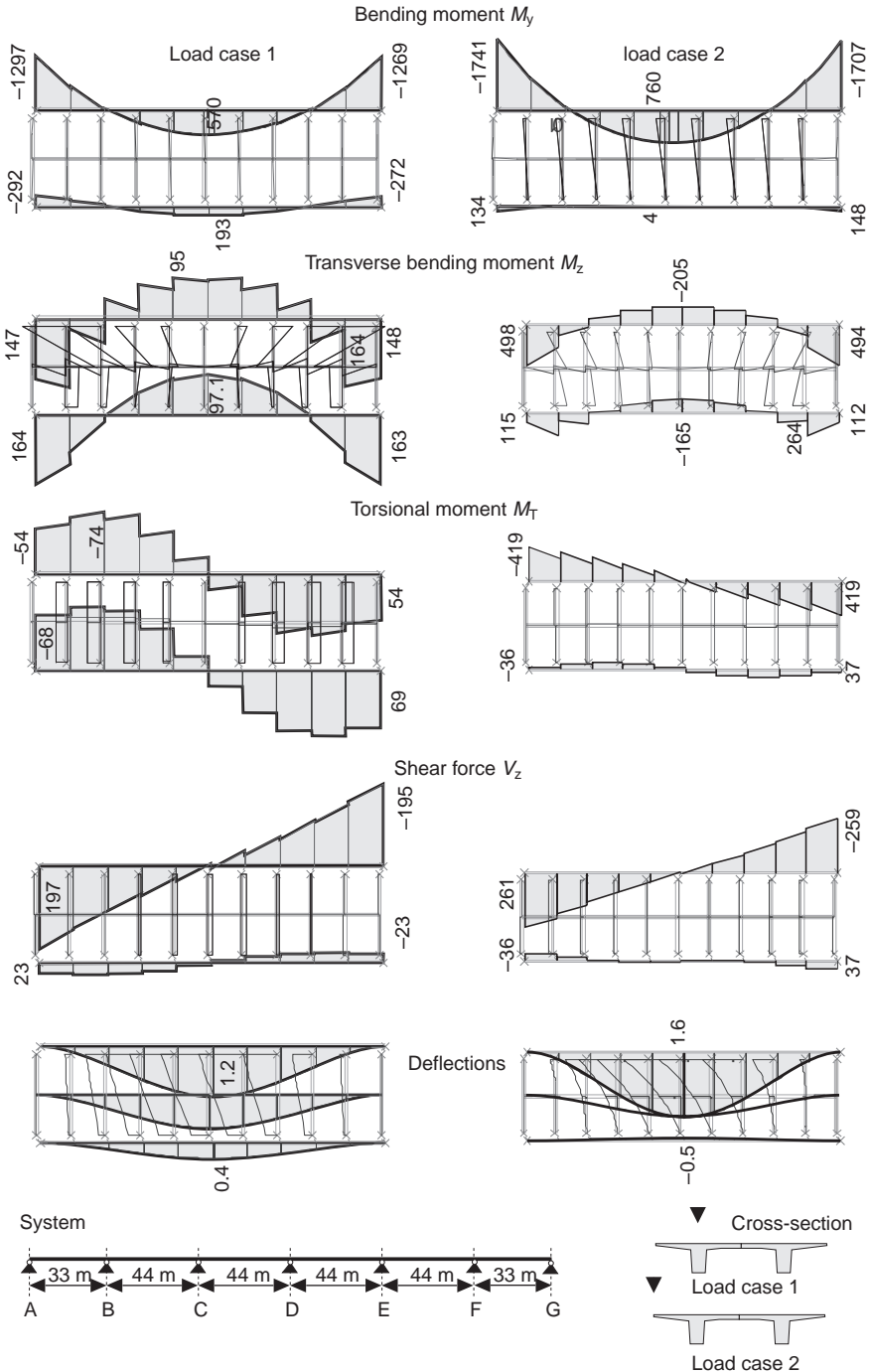


Figure 2.94 Member forces and deflections between axis C and D – 2D truss system [mm, kNm]

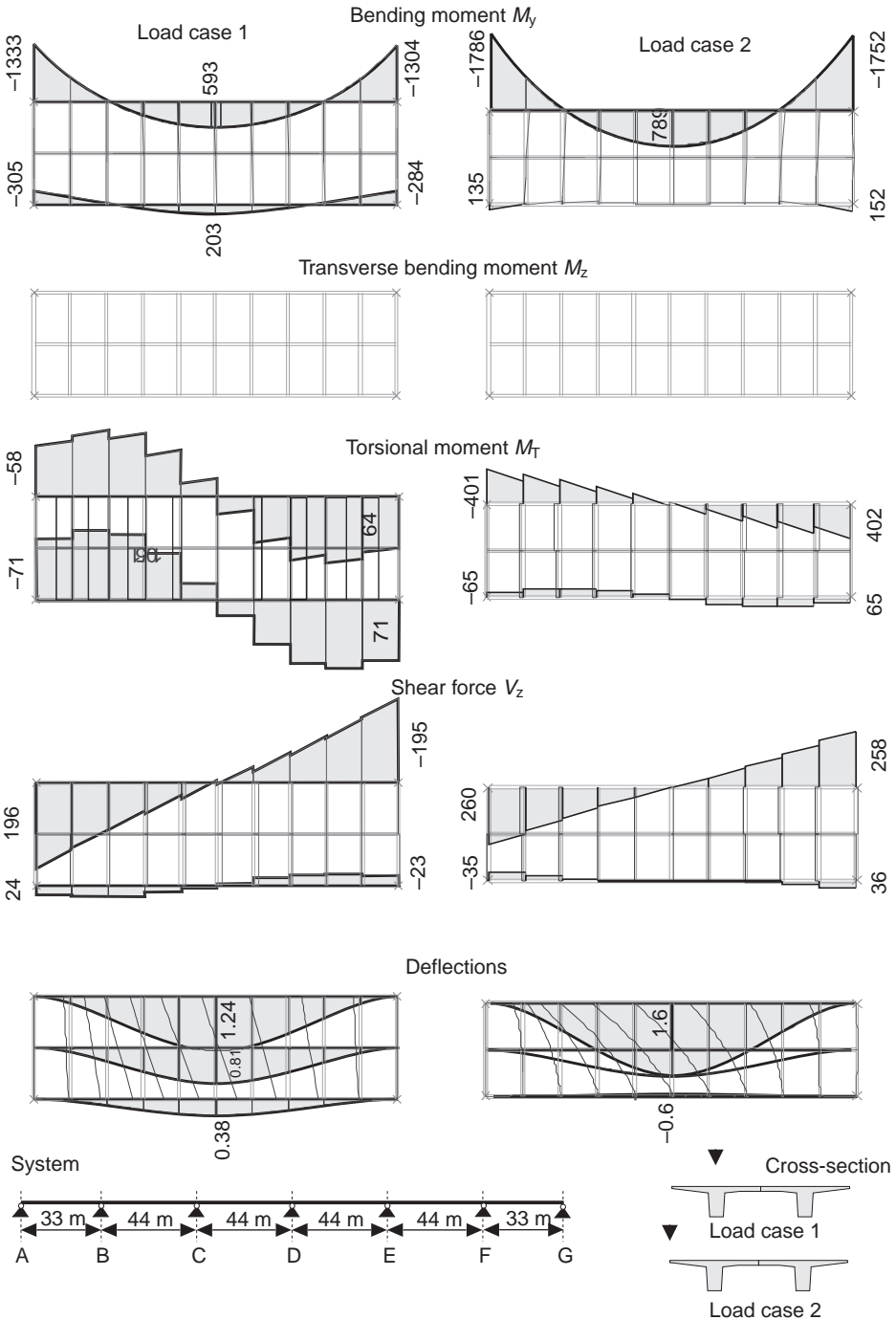


Table 2.9 Forces in members and displacements of the relevant sections [mm, kNm]

		Load case 1		Load case 2	
		Plane system	3D	Plane system	3D
Support axis	Bending moment (M_y)	-1333/-305	-1297/-292	-1786/135	-1741/134
	Bending moment (M_z)	0/0	147/164	0/0	498/115
	Torsional moment (M_T)	-58/-71	-54/-68	-401/-65	-419/-36
	Shear force (V_z)	196/24	197/23	260/-35	261/-36
Mid-span	Bending moment (M_y)	593/203	570/193	789/0	760/4
	Bending moment (M_z)	0/0	95/97	0/0	-205/-165
	Torsional moment (M_T)	≈ 0	≈ 0	≈ 0	≈ 0
	Shear force (V_z)	≈ 0	≈ 0	≈ 0	≈ 0
	Displacements	1.2/0.38	1.2/0.4	1.6/-0.6	1.6/-0.5

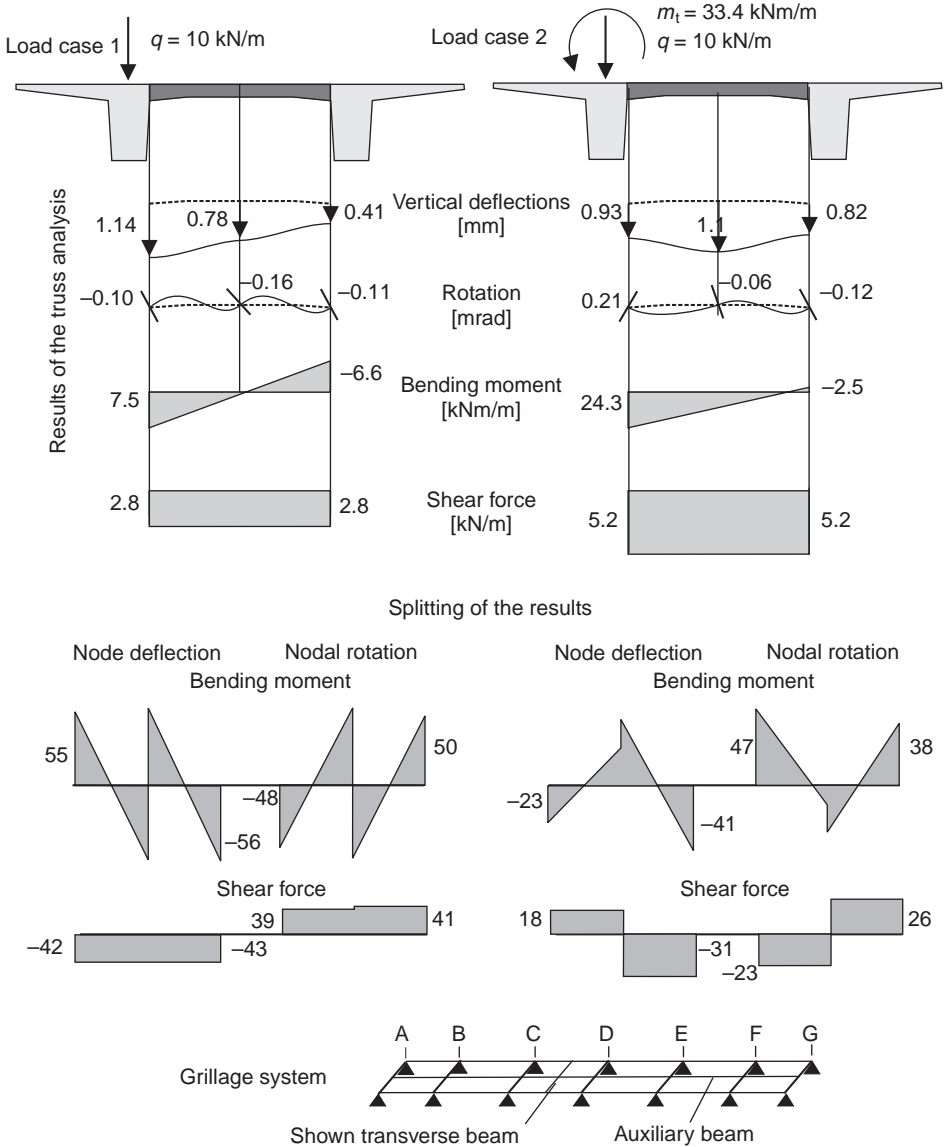
The sawtooth shape of the member forces (Figures 2.93 and 2.94) results from the local loading of the transverse beams. For dimensioning purposes, these values can be smoothed.

The different parts of the load transfer should be first analysed. This is done for the transverse beam in the middle of the span C–D. Figure 2.95 shows the member forces and displacements of this beam.

Using the numerically determined deformation pattern of the transverse beam, the two different parts of the shear force caused by either a vertical shift or a rotation of the supports can be calculated by means of the expressions provided in Figure 2.90. The resulting bending moment distributions are shown in Figure 2.95. For the two load cases, the shear forces due to vertical shift and those due to rotation have similar ranges and different signs. For this system, the equivalent stiffness of the transverse beam consists of both parts of equal size.

As noted in the preceding text, the equivalent stiffness of the transverse beams depends on different parameters and cannot be determined exactly. Therefore, the influence of the stiffness of the transverse beams should be examined in more detail. For this, the sectional height is varied from $h=0.0$ (no transverse beams) up to $h=0.60$ m. The study of parameters is made by a plane truss system (grillage). Figure 2.96 shows the bending moments at the supports M_s and at midspan of span C–D M_f of longitudinal girder number 1 for the different depths of the cross-sections. In Figure 2.97, the vertical support forces at axis C are plotted. This figure shows the significant influence of the loading. An increase in the section depth only results in minor changes in the bending moment, whereas its reduction causes considerable increase in the member forces of the loaded girder.

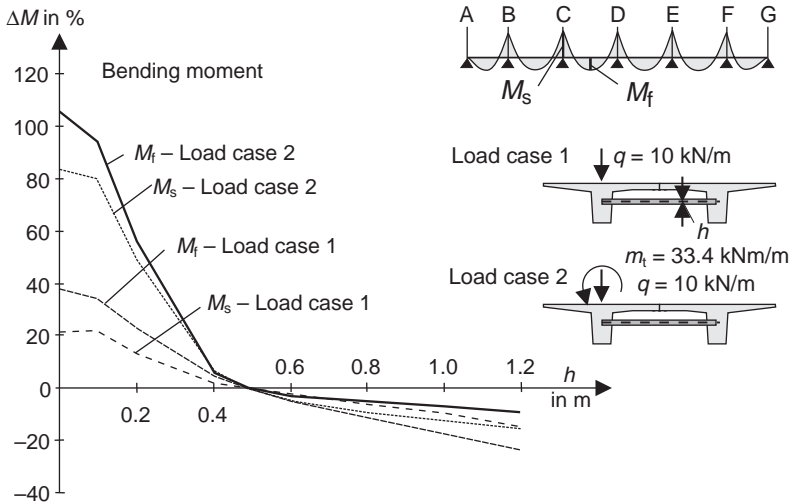
Figure 2.95 Member forces and deflection of the transverse beam at midspan of span C–D



2.8.3 T-beam bridge with several longitudinal girders

Eccentric loads, for example, loads on a cantilever slab, cause a sawtooth kind of pattern for the torsional moments in the longitudinal girders (see Figures 2.93 and 2.94). This pattern results from the local restraint of the longitudinal girders by the transverse beams, and vice versa. A design of the longitudinal girders for the peak torsional moments is, however, not required. This will be demonstrated in the following example.

Figure 2.96 Influence of the section depth h of the transverse beams on the bending moments of the loaded longitudinal girder



The peak values of the torsional moment decreases with the number and spacing of the transverse beams. This is demonstrated in the T-beam bridge shown in Figures 2.98 and 2.99. An eccentric constant line load of $q = 10$ kN/m at a distance of $a = 2.0$ m from the centreline of the outer girder (A) is applied. Figures 2.100 and 2.101 show the member forces and displacements of the longitudinal girders of an inner span between axes 3–4 for 10 and 5 transverse beams in each span. In the case of the 10 transverse

Figure 2.97 Influence of the section depth h of the transverse beams to the support forces at axis C

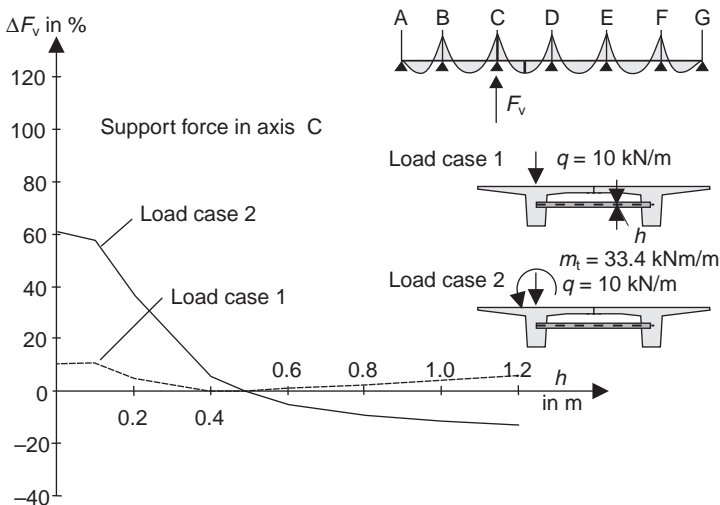
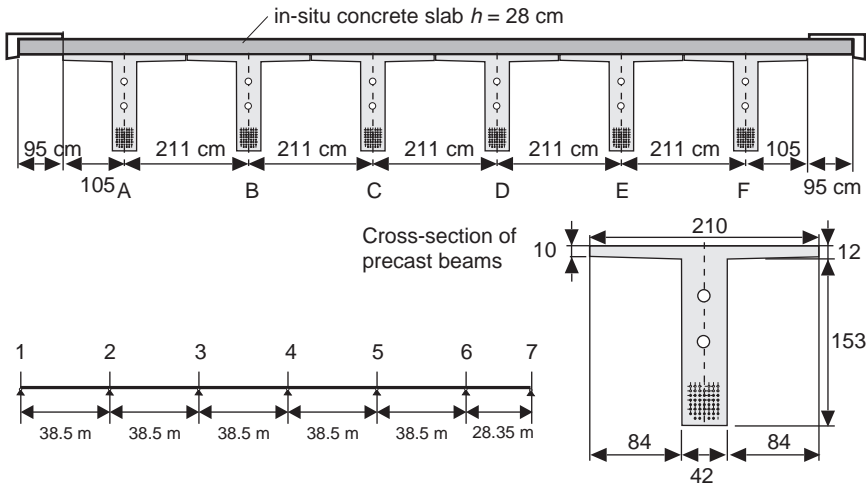


Figure 2.98 Theodor-Heuss-Bridge in Heidelberg (Becker, 1994)



Cross-section of superstructure



beams per span, the greatest torsional moment is $\max M_{T,10} = 51$ kNm, whereas half the number of transverse beams gives a value of almost double, that is, $\max M_{T,5} = 92$ kNm.

A further increase in the number of transverse beams would further reduce the calculated artificial torsional moments. Consequently, the calculated torsional moments are only the result of an inaccuracy of the numerical model. The considerable influence of the distance between the transverse beams can generally be traced back to the fact that the structure mainly carries the load on the cantilever slab by transverse bending of

Figure 2.99 Placing of the precast longitudinal girder



the slab and not by torsion of the longitudinal girders. Next, the torsional stiffness of a cracked member is very small.

It should be noted here that the design of the bridge not only has to consider its final condition but also its construction stages. The bridge shown in the earlier figures is a composite structure, consisting of precast T-beams and a cast-in-situ concrete slab. During construction, the precast beams have to carry the whole loads, whereas the cast-in-situ slab is nearly unstressed. Due to creep and shrinkage, load redistribution between the precast beams and the cast-in-situ slab takes place. In addition, the design in the transverse direction has to consider that the full height of the flange of the precast girders cannot be taken into account. The joint in the flanges between the precast longitudinal beams is not reinforced and is therefore not able to carry any tensile forces.

2.9. Support conditions

2.9.1 Vertical location of a support node

In the previous structural analysis, the support nodes are generally located in the centre axis of the beams for simplicity. However, in reality, the fixation is arranged in general in the lower side of a beam. The eccentric arrangement of the bearings results in additional horizontal deflections that must be considered in the design of the structure and the bearings (Figure 2.102).

A support on the lower side of a beam can be modelled by means of an additional node, which is fixed to the node above in the centreline (see Figure 2.103).

Figure 2.100 Forces in members of the longitudinal girder between axes 3 and 4 due to an eccentric line load of $q = 10 \text{ kN/m}$ – 10 transverse beams per span

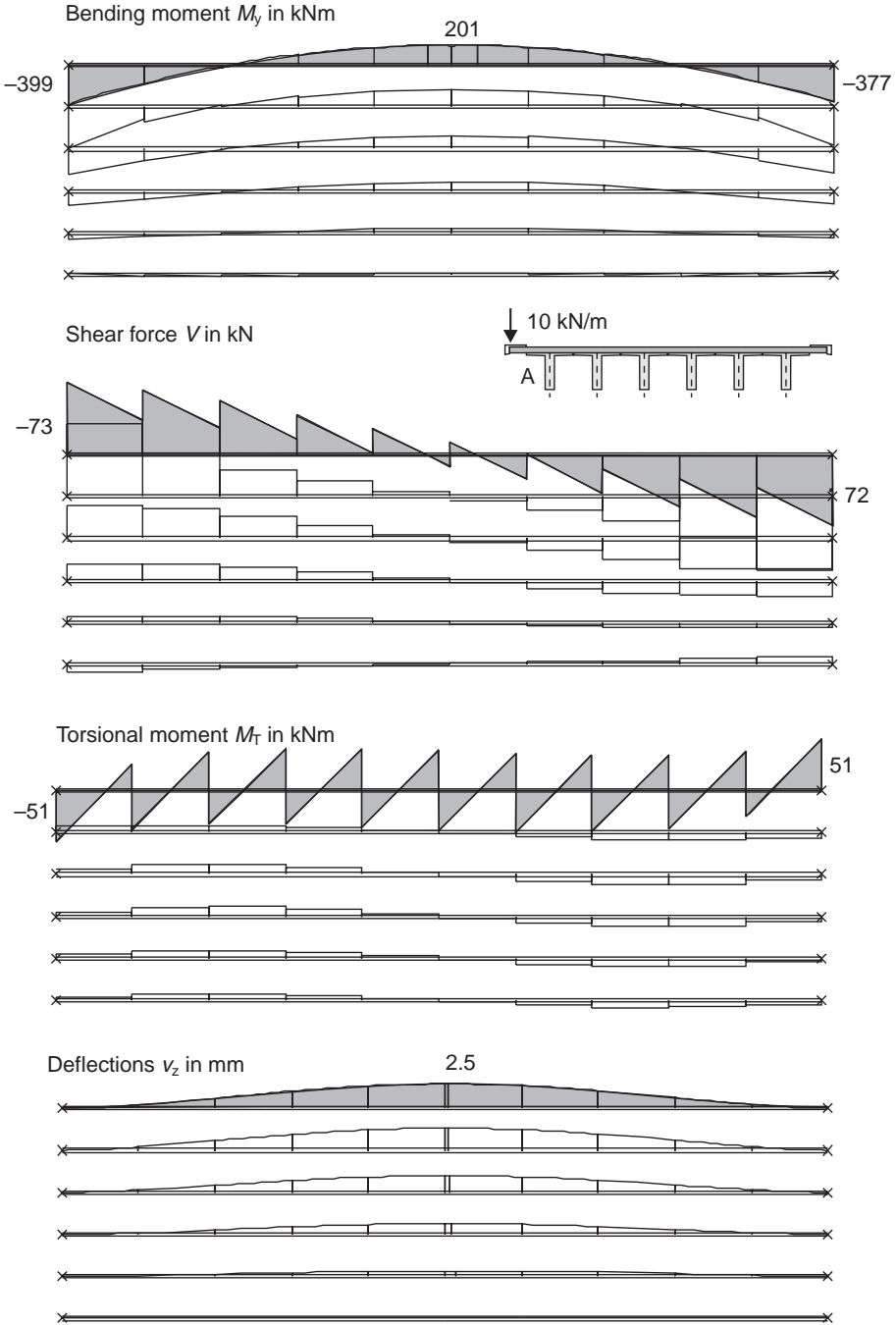


Figure 2.101 Forces in members of the longitudinal girder between axes 3 and 4 due to an eccentric line load of $q = 10 \text{ kN/m}$ – 5 transverse beams per span

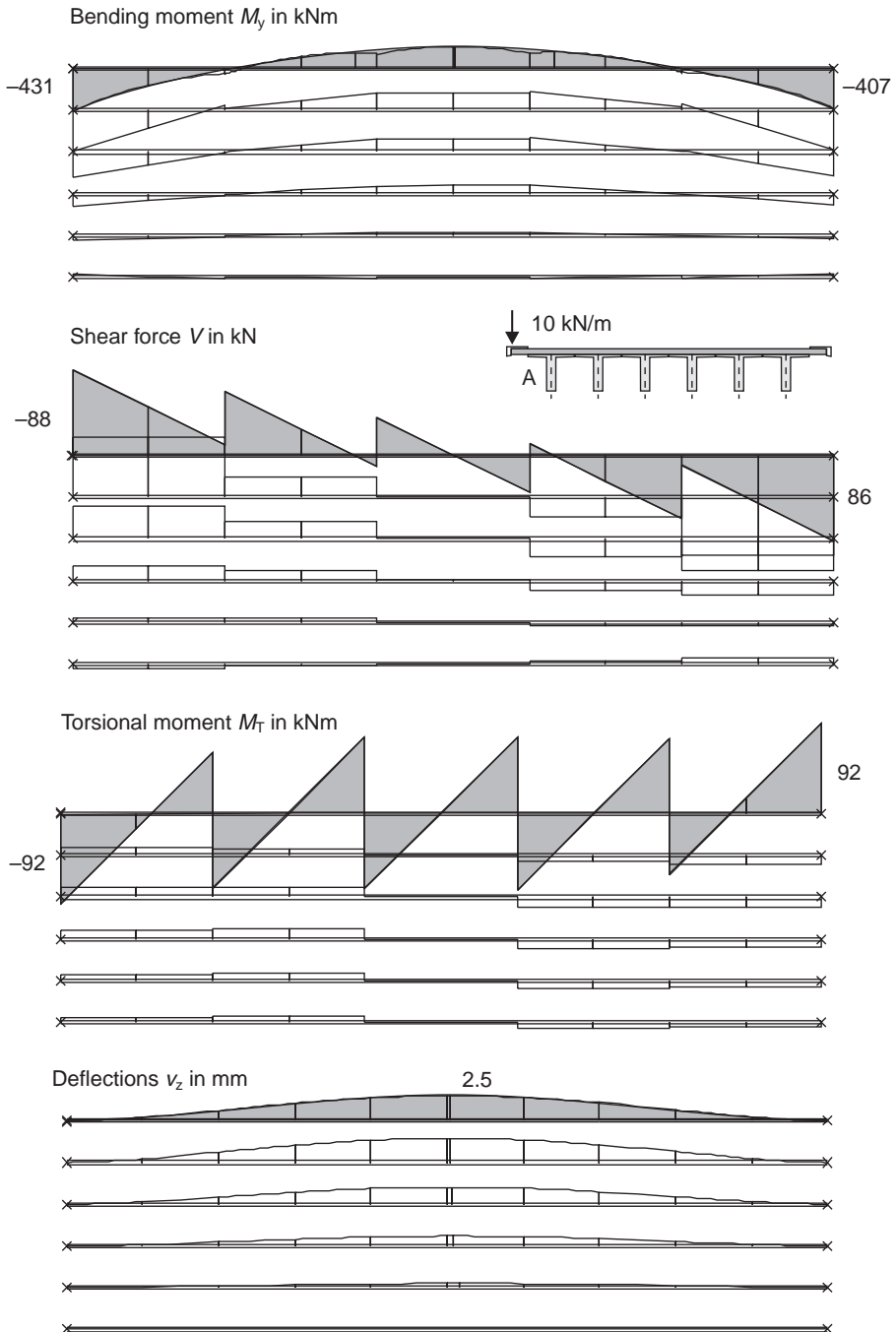
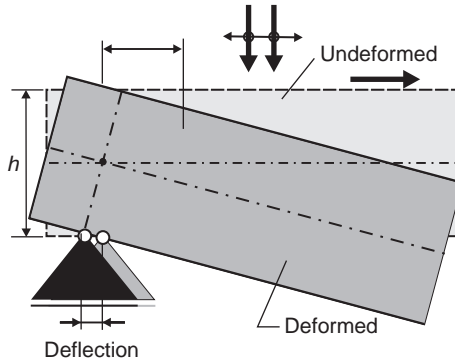


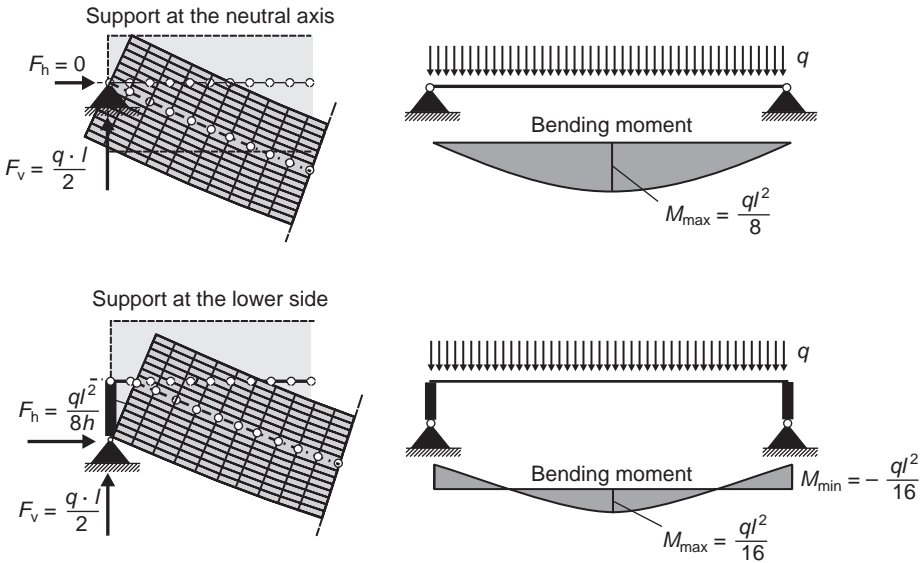
Figure 2.102 Horizontal deflection of the support



Small horizontal support forces occur due to pure bending if the fixations are located in the centre axis, as there are no stresses or strains in the neutral axis. However, significant horizontal forces F_h are obtained if the beam is fixed at the lower side in the horizontal and vertical directions. For a single-span beam with a rectangular cross-section under constant loading q , the restraint force F_h results in:

$$F_h = \frac{q \cdot l^2}{8 \cdot h} \quad (h = \text{depth of the beam})$$

Figure 2.103 Member forces of a beam with support in the centreline and at the lower side of the beam



The bending moment at the supports is equal to $M_s = -F_h \cdot h/2 = -q \cdot l^2/16$ and the midspan moment is reduced by 50% to $M_F = q \cdot l^2/16$ (see Figure 2.103).

However, the strong reduction of the midspan moment should be considered with great care. The horizontal restraint forces F_h and thus the significant changes of the bending moments of the beam can only happen in the case of an infinitely stiff support, which in reality does not exist. Furthermore, the restraint effect is reduced by the nonlinear strain distribution in the support region and the time-dependent deformations of concrete (creep and shrinkage).

The following example should serve as clarification. A single-span beam with a span length of $l = 40$ m under a uniform load of $q = 45$ kN/m is examined. The beam has a rectangular cross-section with $b/h = 0.42/1.9$ m.

The horizontal restraint force amounts to:

$$F_h = \frac{q \cdot l^2}{8 \cdot h} = \frac{45 \cdot 40^2}{8 \cdot 1.9} = 4740 \text{ kN}$$

The deformations at the lower side of the beams are as follows ($E_c = 30\,000$ MPa):

Cause	Horizontal deflection at the support	
Uniform load q	$u_q = \frac{q \cdot l^3}{4 \cdot E \cdot b \cdot h^2}$	= 15.8 mm
Bending moment due to F_h	$u_{F_h} = \frac{3 \cdot q \cdot l^3}{16 \cdot E \cdot b \cdot h^2}$	= -11.9 mm
Normal force F_h	$u_n = \frac{q \cdot l^3}{16 \cdot E \cdot b \cdot h^2}$	= -4.0 mm

The horizontal deflections of the beam due to shrinkage only is

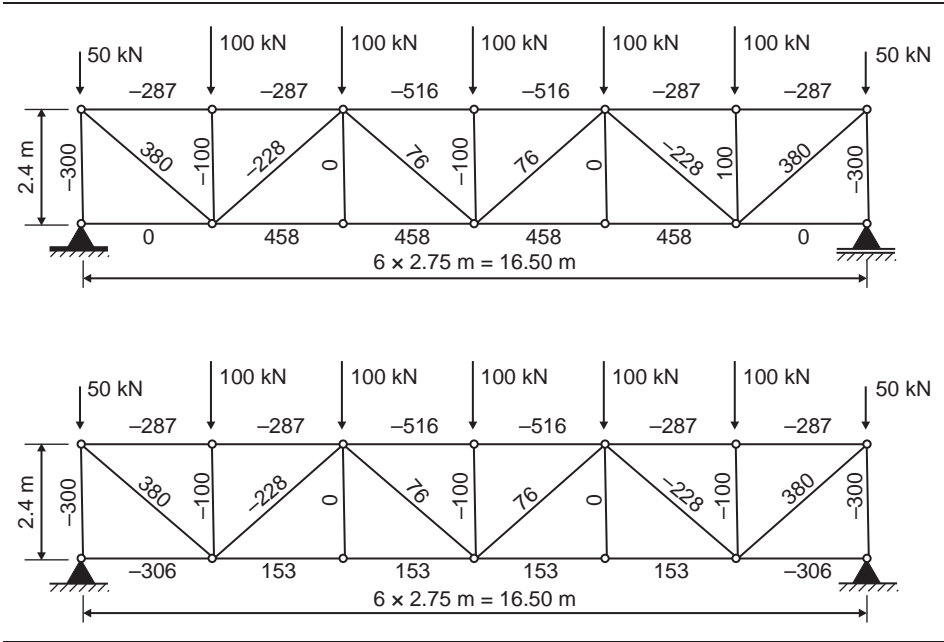
$$\Delta l = \varepsilon_{cs, \infty} \cdot l \simeq -5.0 \cdot 10^{-4} \cdot 40.000 = -20 \text{ mm.}$$

This reduces the restraint force F_h due to the uniform load q by 2/3.

2.9.2 Support of a truss

The modelling of the realistic support conditions must be treated with great care for truss structures. This will be demonstrated in the following simple example. Figure 2.104 shows the normal forces of a plane truss for two different support conditions. The upper system can move in the horizontal direction, whereas the deflections of the support nodes of the lower one are fully fixed. As can be seen from the normal forces plotted in Figure 2.104, the horizontal fixation has a big influence on the normal forces in the lower horizontal girders. The maximum tension force decreases by a factor of 2/3, from 458 kN to 153 kN, due to the horizontal restraint.

Figure 2.104 Normal forces of a truss for different support conditions



Please note that the horizontal fixation may be overlooked when the analysis is checked by a system plot only.

2.10. Dimensioning of reinforced beams

In the previous sections, the estimation of the member forces and deflections of truss and beam structures have been explained in detail. However, the goal of any design is not the calculation of the action effects in the members but the dimensioning of the system for the ultimate and serviceability limit state. Therefore, it is often not necessary to model the structure with a high degree of accuracy and to consider all possible actions and effects. The actual amount of structural analysis to be carried out should be adapted to the required accuracy.

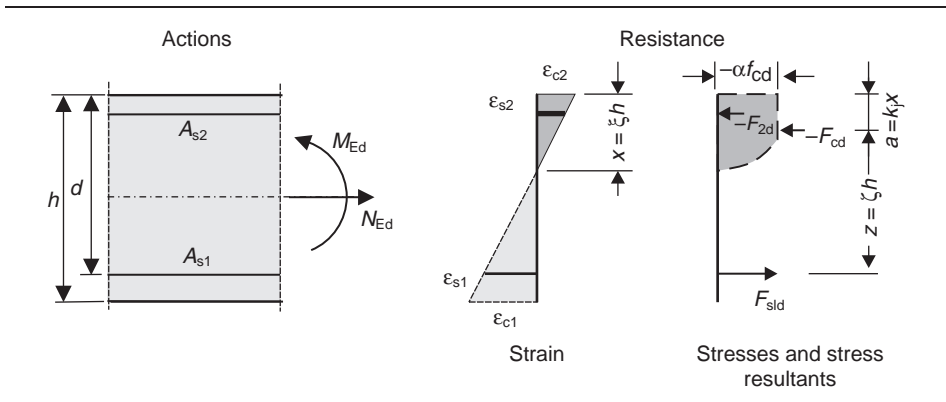
The following only refers to the ultimate limit state design (ULS), as the design for serviceability can be very different according to the requirements of the relevant codes.

2.10.1 Design for bending and normal forces

The computation and dimensioning of an arbitrary concrete cross-section under ultimate condition has been described in detail by Quast and Busjaeger in ‘Heft 415’ of the German Concrete Association (Busjaeger and Quast, 1990). Therefore, the following only provides some brief comments on this.

The design of a concrete cross-section requires the following items

Figure 2.105 Actions, strains and internal forces (resistance) of a reinforced concrete section



- checking of the structural safety: Balance between internal and external forces without exceeding the permissible stresses and strains of the materials
- estimation of the required reinforcement and its distribution in the beam under consideration of the ultimate and the serviceability limit state
- estimation of the strains and stresses.

The nonlinear behaviour of concrete and steel as building materials has to be considered in the design (Figure 2.106). In addition, concrete is not allowed to carry any tensile forces in the ultimate limit state design. The tensile strength of concrete is only used in the design of the serviceability limit state (crack width, restraint forces and displacements) if it results in an unfavourable effect.

The design is based on the straight strain distribution over the depth of the cross-section (Bernoulli's hypothesis) in Stage I (uncracked) as well as in Stage II (cracked) conditions.

Figure 2.106 Stress–strain diagram of concrete and steel according to EC2 part 1 Eurocode 2, 2004

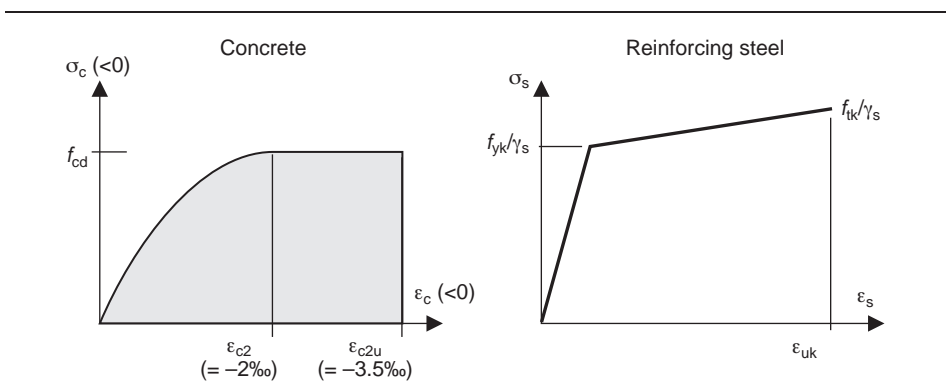
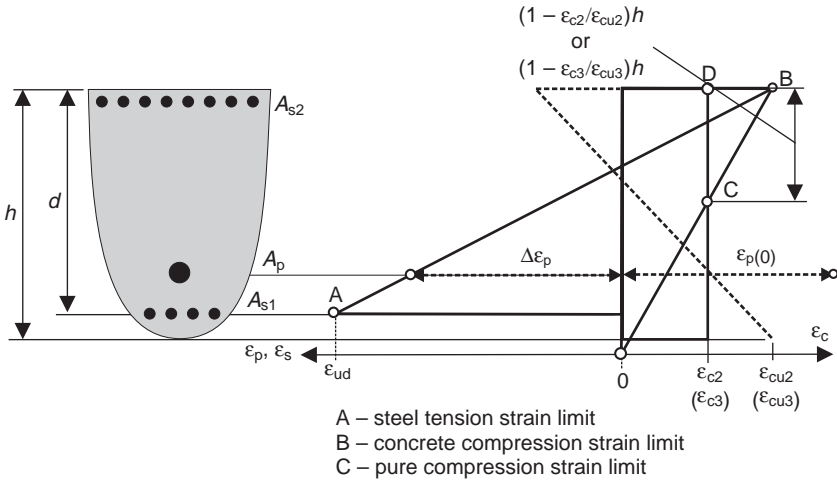


Figure 2.107 Possible strain distributions under ultimate limit state according to Eurocode 2 Eurocode 2, 2004



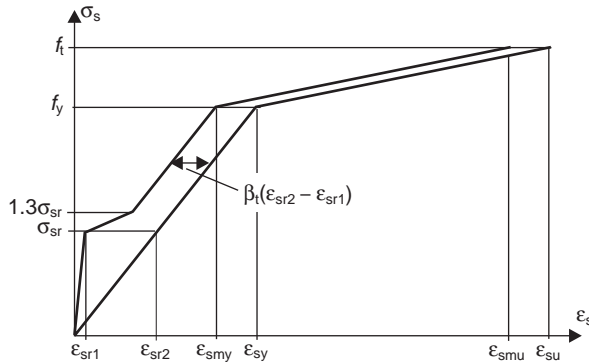
The nonlinear material behaviour with respect to the stress–strain relation is defined in the relevant codes (see Figure 2.106). It should always be kept in mind that these curves are only approximations of the real material behaviour for use in design. The parabola–rectangle stress–strain relation of concrete is only a simplification of the stress distribution in the concrete compression zone, and cannot be used for other design purposes. In reality, significant deviations may occur. The permissible strains in the concrete (Figure 2.107) have to be considered in the ultimate limit design in addition to the defined stress–strain relation of concrete.

For a more realistic estimation of the stiffness of a member, the tension-stiffening effect has to be taken into account (see Section 2.4.2). Otherwise, the stiffness of the member in the relevant section is underestimated. The tension-stiffening effect can be considered by modifying the stress–strain relation of reinforcing steel in Stage II, for example, according to Figure 2.108. From this figure, it can be seen that the tension-stiffening effect only has a significant influence on the stiffness of a member when the steel strain has not reached the point of yielding.

The dimensioning, that is, the estimation of the required reinforcement, can only be done by iteration. This is true even for simple rectangular cross-sections under uni-axial bending. For cross-sections of arbitrary shapes, such dimensioning is an optimisation problem. The designer must default a reasonable distribution of the reinforcing bars in the cross-section and give some information regarding the iteration process (i.e. how the calculated reinforcement in the different locations has to be increased or decreased).

In addition to the reinforcement required for the ultimate limit state, the minimum reinforcement and the ‘shift rule’ (horizontal displacement of the envelope line of the

Figure 2.108 Modified stress–strain diagram of steel with regard to the tension-stiffening effect
CEB-FIP Model Code 90



total tensile force) have to be considered. The latter is done by increasing the local normal force in the longitudinal tensile reinforcement by:

$$\Delta F_{sd} = V_{Ed} \cdot \frac{\cot \theta - \cot \alpha}{2}$$

where:

θ is the inclination of compression struts

α is the inclination of the shear reinforcement against the horizontal axis.

2.10.2 Design for shear and torsion

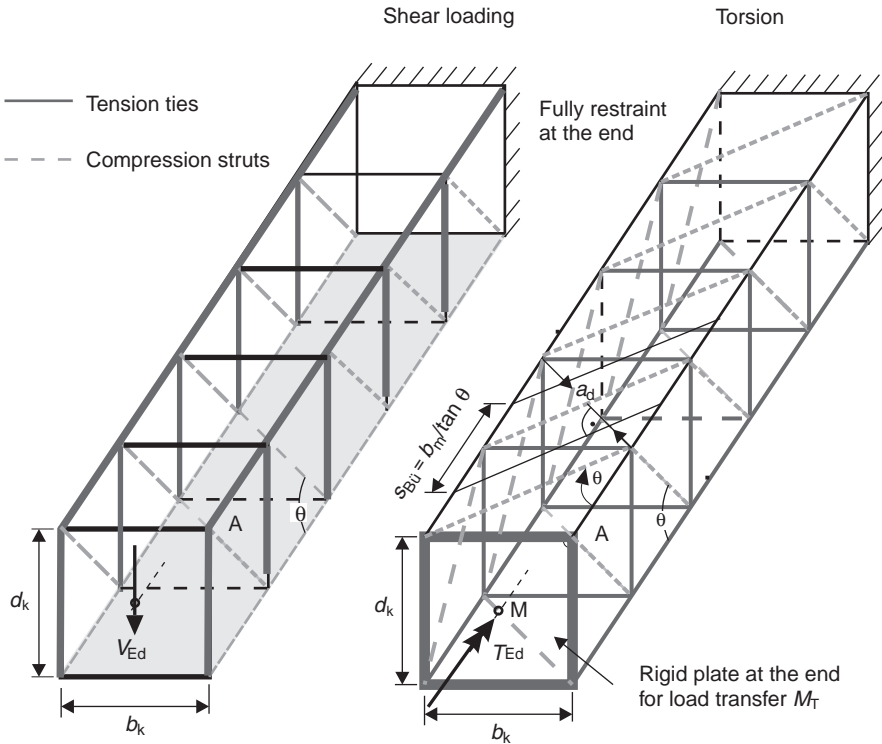
The design for shear and torsion for a cracked section is based on a strut-and-tie model (Figure 2.109). There are considerable differences between the various codes with regard to the permissible angle between the concrete compression struts and the main tension chord θ , the shear capacity due to the dowel effect, the shear friction in the cracks caused by aggregate interlock and the permissible stresses in the compression struts. Therefore, the results of the numerical calculation should always be verified by manual analysis of some critical sections of the beam.

The shear and compressive stresses depend on the minimum width of the beam in the tensile region. For polygonal cross-sections of an arbitrary shape, the relevant section for the shear design has to be defined by the user of the computer program.

In addition, the influence of point-loads close to the supports, the variation of the cross-section's depth (inclined haunches), and the influence of an indirect support has to be taken into account.

In case of torsion, a reduction in the resulting tensile force in the compression zone of the cross-section can be applied. It should be noted that torsion reinforcement is only required in case of equilibrium torsion, where the equilibrium of the structure depends on the torsional stiffness of the structural members. As the torsion stiffness of a concrete

Figure 2.109 Strut-and-tie model for shear and torsion design



member decreases significantly in case of cracking (Stage II), the minimum reinforcement is sufficient for compatibility torsion. The calculation of the internal forces is usually based on linear elastic material behaviour. Therefore, a computer program will always determine an amount of torsional reinforcement. This problem can be overcome by setting the torsional stiffness of the members to very small values.

2.11. Material nonlinear analysis of truss and beam systems

With the introduction of Eurocode 2 (2004), nonlinear analyses of concrete members were generally regulated for the first time. In most programs, the suitable algorithms are now implemented. Hence, it is supposed that the nonlinear analyses of concrete structures will increase in future, as structural engineers are always aiming to model a given structure with the best accuracy. Currently, the application of materially nonlinear calculations in practice is limited to slender columns, where the internal forces are significantly influenced by the deflection of the member. Hence, the deformation of the structure must be determined precisely.

Even if a nonlinear analysis can be easily done by means of the available software, it should be kept in mind that such a calculation is still very time consuming and needs

to be performed by an engineer with a lot of experience in the field of numerical analysis and design of concrete structures. The load combination is, in general, not allowed any more. Moreover, the size as well as the distribution of the reinforcement must be known before conducting the analysis. Nevertheless, the biggest problem is the modelling of the behaviour of the composite material reinforced concrete in the cracked state (Stage II). This aspect will be examined later. The stiffness of a cracked concrete section is influenced by numerous factors (e.g. amount and distribution of rebar, load transfer in cracks, orientation of cracks, etc.), and cannot be calculated unambiguously. Hence, parameter studies and the consideration of boundary values are often necessary with nonlinear analysis.

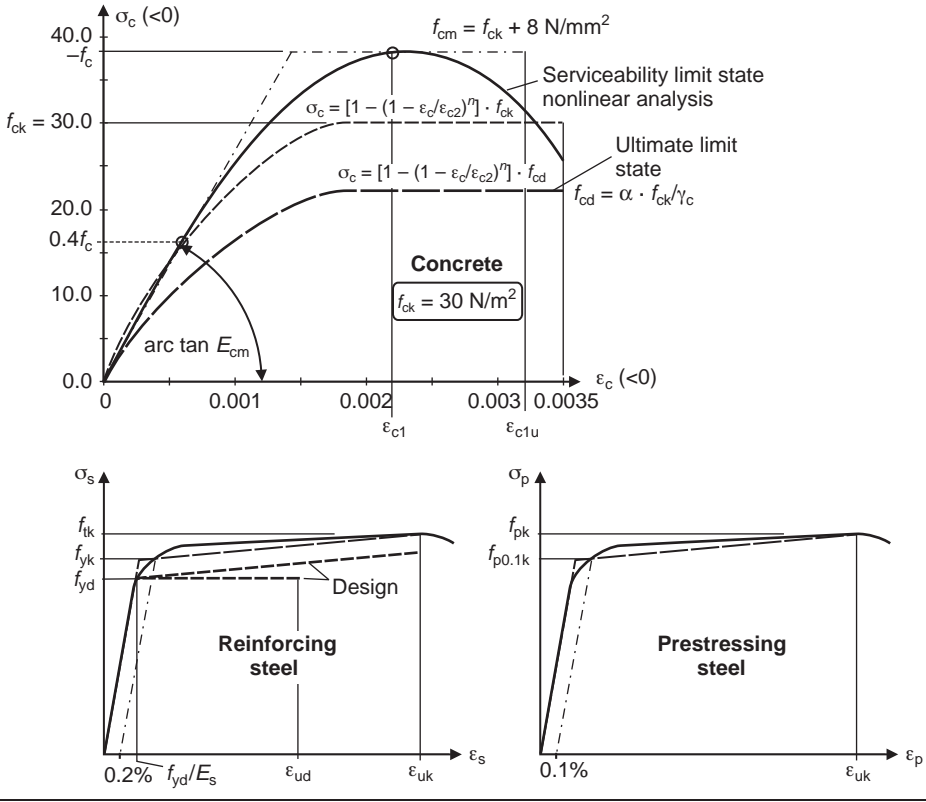
A material nonlinear structural analysis can be useful or necessary for the following reasons.

- To optimize a structure by consideration of load redistributions (e.g. for multi-span beams) – to exploit additional resistance.
- Reduction of member forces in case of restraints (e.g. temperature effects in monolithic bridges or in case of fire).
- In the ultimate limit state, if the member forces of a structure are significantly influenced by the deformations (e.g. by slender columns, second-order effects).
- Exact determination of the deformation of a structure (e.g. in case of flat slabs). Material linear analysis generally underestimates the deflections.
- Analyses of cases of structural failures and damages.
- Post-calculation of tests.

With material linear elastic analysis, it is supposed that a structure fails as soon as, in any cross-section, the load-carrying capacity is reached. This applies only for statically determined members. Statically undetermined structures for the most part show, by redistribution of forces, considerable additional load-bearing reserves that can only be considered in a materially nonlinear analysis. It should be pointed out that, in the materially nonlinear analysis of concrete structures, the estimation of the member forces and the design for the limit state is not sufficient proof of the safety of a structure. One has to check that a brittle failure of a member cannot occur. This is done by limiting the plastic rotation of a section. A brittle failure may happen when the concrete reaches its limit strains before the reinforcement yields. The limited rotation of a concrete section limits the theoretical value of force redistribution of an elastic member. The verification for the rotation capacity of a concrete section is given in the codes.

The algorithms used in the calculation of the load-carrying capacity, based on the nonlinear stiffness of any massive concrete beam or column under biaxial bending with normal forces, have been known for a long time and are implemented in numerous programs (Busjaeger and Quast, 1990). The required stress–strain relations for concrete and steel can be taken from the codes (Figure 2.110). The simple parabola–rectangle diagram for concrete should be used only for calculations in the ultimate limit state. For the estimation of realistic deflections, as well as for nonlinear analysis, a more realistic stress–strain relation, as given in Figure 2.110, is needed.

Figure 2.110 Stress–strain-curves according to EC2 (Eurocode 2, 2004) for concrete, cold-worked reinforcing steel and prestressing steel



The stress–strain diagram of concrete can be estimated from the following equation.

$$\frac{\sigma_c}{f_{cm}} = \frac{k \cdot \eta - \eta^2}{1 + (k - 2) \cdot \eta} \quad (\text{Eurocode 2, 2004; Part 1-1, Equation 3.14})$$

where:

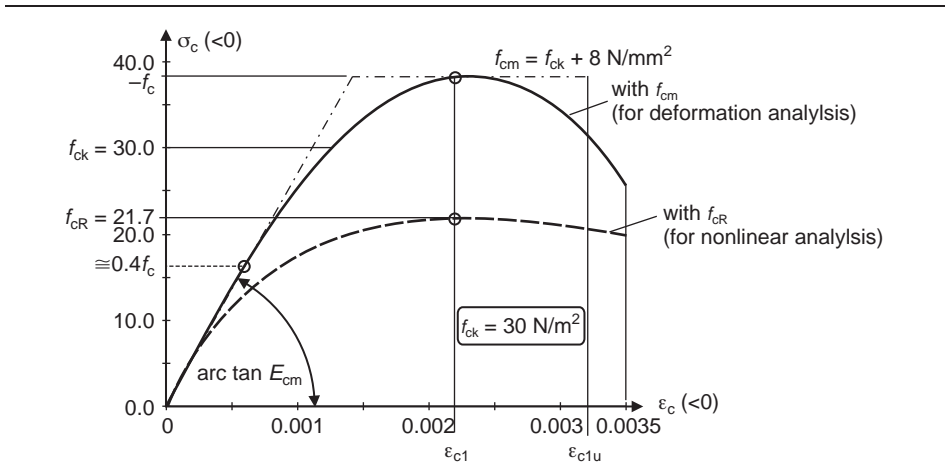
$$\eta = \epsilon_c / \epsilon_{c1}$$

$$k = 1.05 \cdot E_{cm} \cdot |\epsilon_{c1}| / f_{cm}$$

Figure 2.111 shows the σ – ϵ curve for a concrete-grade C30/37 for deformation and nonlinear analysis. The meaning of the various compressive concrete strengths f_{cm} , f_{cR} and f_{cm} / γ_c is explained later.

Most programs can handle any polygonal stress–strain relation. The problem of a material nonlinear analysis for beams and columns, therefore, does not exist in the more-or-less complicated material description of the concrete.

Figure 2.111 Stress–strain-curves for concrete C30/37
According to Eurocode 2, 2004



In the ultimate limit state, the concrete tensile strength may not be considered. This assumption considerably underestimates the stiffness of a beam. Hence, a realistic estimation of the load-deflection behaviour of a structure is not possible with this simplification. Realistic values can be obtained only if the tension-stiffening effect, the stiffness of the concrete in tension, is considered. There is no generally accepted procedure on how this should be done. In the following, two very different approaches that lead to partially different results will be discussed.

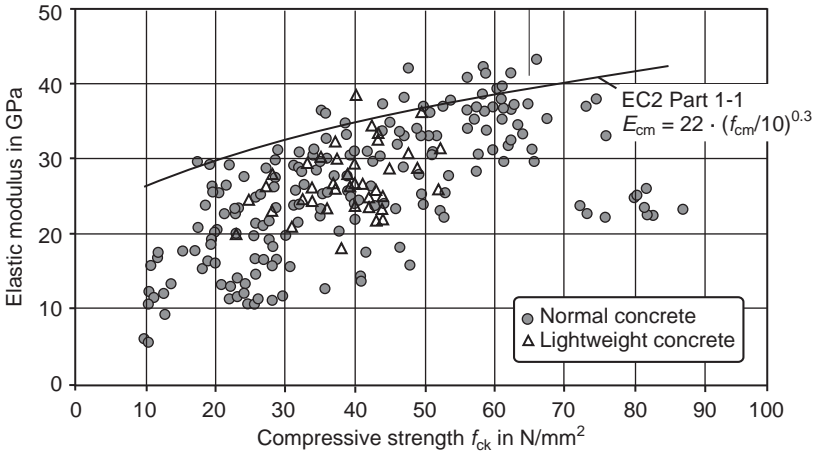
According to Eurocode 2-1 (2004), the steel strains can be reduced by a certain level (Figure 2.108). Another attempt considers a concrete tensile strength dependent on the concrete strain at the level of rebar (Quast, 1981). It is not yet clear which attempt gives more realistic results. It seems dependent on the structure and the loading.

In the following, the main problems of a material nonlinear analysis of a reinforced concrete member will be discussed. Some simple approximation methods will be mentioned, which are necessary for checking the numerical results. A cantilever beam should serve to explain the interactions.

2.11.1 Deflections in the uncracked state (state I)

The estimation of the member forces is mainly based on the simplification of the elastic material behaviour of concrete. This simplification is justified in spite of the known nonlinearity of the composite material concrete, because the distribution of member forces in a statically undetermined structure is dependent not on the absolute value of the flexural stiffness in a section but only on the distribution of the stiffness in the structure. The cracking in a multi-span beam in the ultimate limit state, in the field and support cross-sections, mostly leads to roughly the same reduction of the flexural stiffness of the member.

Figure 2.112 Modulus of elasticity E_c of concrete specimens in relation to the characteristic compressive strength f_{ck} . Adapted from Rühl (2000) with permission



With a linear analysis of beams and trusses, there becomes only one material constant, the modulus of elasticity of concrete E_c , which is needed. Nevertheless, this value in reality is not fixed. It depends on numerous factors, such as the amount of cement or the hardness of the gravel.

Figure 2.112 shows the measured modulus of elasticity E_c for concrete specimens in relation to the characteristic compressive strength f_{ck} . The big scatter even in the elastic state can be seen clearly.

Furthermore, E_c is not constant due to the nonlinear material behaviour of the concrete even in uncracked conditions. Therefore, even a complex nonlinear analysis of a concrete member can only give an approximation of the real deformations.

The modulus of elasticity E_c can be determined from the various stress–strain curves of concrete. To avoid this effort, which involves high inaccuracy (see Figure 2.112), mean values of E_{cm} are given in Eurocode 2 (2004) for different concrete grades. E_{cm} is the secant modulus of elasticity between $\sigma_c = 0$ and $\sigma_c \approx 0.4f_{cm}$ (Figure 2.111).

$$E_{cm} = 22 \cdot (f_{cm}/10)^{0.3} \quad (f_{cm} \text{ in MPa, } E_{cm} \text{ in GPa})$$

(Eurocode 2, 2004: Part 1-1, Table 3.1)

Nevertheless, the secant modulus E_{cm} is often needed to estimate the deformation of a member, because with an existing concrete stress σ_c , the accompanying strain ε_c is needed. The tangent elastic modulus E_{c0m} is to be used if the strain increment $\Delta\varepsilon_c$ is needed for a given stress increment $\Delta\sigma_c$.

The differences between the tangent and the secant moduli are smaller than 15% for normal concrete (Table 2.10). With regard to the scatter of material parameters, in

Table 2.10 Secant modulus of elasticity of concrete in GPa#Data taken from Eurocode 2, 2004

f_{ck}	20	25	30	35	40	45	50	55
f_{cm}	28	33	38	43	48	53	58	63
E_{cm}	29.962	31.476	32.837	34.077	35.220	36.283	37.278	38.214
E_{cm} from σ - ε curve	24.191	26.186	28.019	29.726	31.386	33.087	34.769	36.344

reality (Figure 2.112), these differences and any ‘accurate’ analysis for E_c seem to be more or less of a theoretical nature.

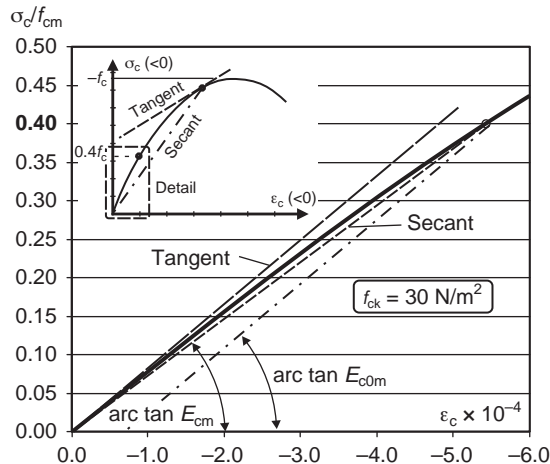
The stress–strain curve of concrete is linear for compressive stresses smaller than $0.4f_c$, as can be seen from Figure 2.113. Hence, it is possible in the serviceability state to attach a triangular-shaped compression zone. With this simplification, the deflections of a structure in the cracked state can be easily determined manually (see Section 2.11.2).

The deformation of a concrete structure increases with time due to the time-dependent behaviour of concrete (creep and shrinkage). Creep deflections can easily be estimated by means of a modified modulus of elasticity.

$$E_{c,\text{eff}} = \frac{E_{cm}}{1.0 + \varphi(t)}$$

Nevertheless, this simplification is only valid if the distribution of the member forces does not change. Shrinkage leads to curvature and deflections due to the bond between reinforcing bars and concrete.

Creep parameters and shrinkage strains can be taken from Eurocode 2 (2004) or from DAfStb 525 of the German committee on concrete structures (DAfStb, 2003).

Figure 2.113 Stress–strain diagram of concrete grade C30/37 – secant and tangent modulus of elasticity

Nevertheless, the big scatter of the creep factor should be kept in mind, with the coefficient of variation lying at approximately 30%. Hence, the arithmetic values can considerably deviate from the deflections appearing in a real structure.

The preceding explanations should merely make clear the difficulties with the definition of the modulus of elasticity E_c , even in the uncracked, linear elastic state. In view of the large variations in the material parameters in the construction practice, and in particular of the creep factors as well as the very large influence of the cracking of concrete (State II) on the stiffness of a member, complex or ‘exact’ analysis seems to be rarely required. For the exact estimation of the real deflections, all influencing factors must be known. However, this is only the case for the post-calculation of existing structures and if these structures were examined before thoroughly.

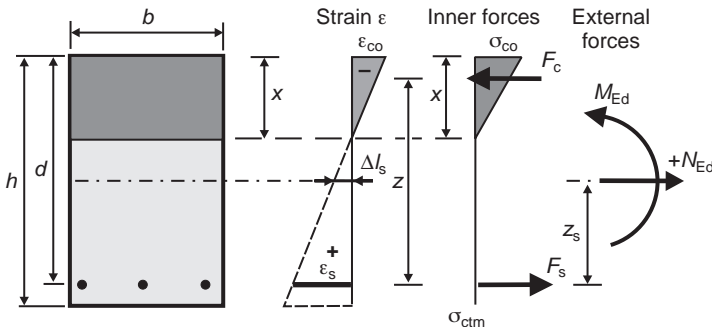
2.11.2 Deflection analysis in the cracked state – without tension-stiffening

The minimum structural stiffness and the maximum deflections are estimated if the tensile strength or the tension-stiffening effect of the concrete is neglected. Nevertheless, this does not result in safe design and maximum reinforcement, respectively. For the effects that depend significantly on structural stiffness, such as restraint effects, for example, too much of a reduction in stiffness arises and, consequently, the member forces are underestimated.

The advantage in disregarding the tension-stiffening effect particularly lies in the fact that the deflections of a reinforced concrete beam or column with rectangular cross-section can be estimated in the cracked state rather easily by hand. Therefore, it is possible to control the results of a numerical analysis. Furthermore, the calculated deflections are upper bound values.

For the following calculations, a triangular-shaped concrete pressure zone (see Figure 2.114) is assumed, and the tension-stiffening of the concrete is neglected. Furthermore, only beams under pure bending are treated. The external normal force N_{Ed} is positive for tension.

Figure 2.114 Concrete cross-section in the cracked state



From the force, balance follows:

$$\sum F_h = 0 \quad F_s = |F_c| \implies \varepsilon_s \cdot E_s \cdot A_s = -\varepsilon_{co} \cdot E_c \cdot b \cdot \frac{x}{2}$$

$$\varepsilon_s \cdot E_s \cdot A_s = -\varepsilon_{co} \cdot E_c \cdot b \cdot \frac{x}{2}$$

Geometrical condition (Figure 2.114):

$$\frac{\varepsilon_s}{d-x} = \frac{-\varepsilon_{co}}{x} \implies \varepsilon_s = \frac{-\varepsilon_{co}}{x} \cdot (d-x)$$

$$\frac{-\varepsilon_{co}}{x} \cdot (d-x) \cdot E_s \cdot A_s = -\varepsilon_{co} \cdot E_c \cdot b \cdot \frac{x}{2} \implies (d-x) \cdot E_s \cdot A_s = E_c \cdot b \cdot \frac{x^2}{2}$$

$$2 \cdot (d-x) \cdot \frac{E_s}{E_c} \cdot \frac{A_s}{b} = x^2 \implies 2 \cdot (d-x) \cdot \alpha_e \cdot \rho_1 \cdot d = x^2$$

where:

$$\rho_1 = \frac{A_s}{b \cdot d}; \quad \alpha_e = \frac{E_s}{E_c}$$

Solution of the second-order equation:

$$x = -\frac{2 \cdot \alpha_e \cdot \rho_1 \cdot d}{2} \pm \sqrt{(\alpha_e \cdot \rho_1 \cdot d)^2 + 2 \cdot \alpha_e \cdot \rho_1 \cdot d^2}$$

$$x = d \cdot \sqrt{(\alpha_e \cdot \rho_1)^2 + 2 \cdot \alpha_e \cdot \rho_1} - \alpha_e \cdot \rho_1 \cdot d$$

$$x = d \left(\sqrt{[2 + \alpha_e \cdot \rho_1] \cdot \alpha_e \cdot \rho_1} - \alpha_e \cdot \rho_1 \right)$$

The height of the compression zone is independent of the loading. The lever arm of the internal forces in the cracked state is: $z_{II} = d - x/3$.

Remark: The equation $z_{II} = (1 - 0.6 \cdot \mu_{Eds}) \cdot d$ is valid only for $\varepsilon_s = 5\%$ and for the parabola–rectangle stress–strain curve, that is, in the ultimate limit state.

For pure bending (Figure 2.114):

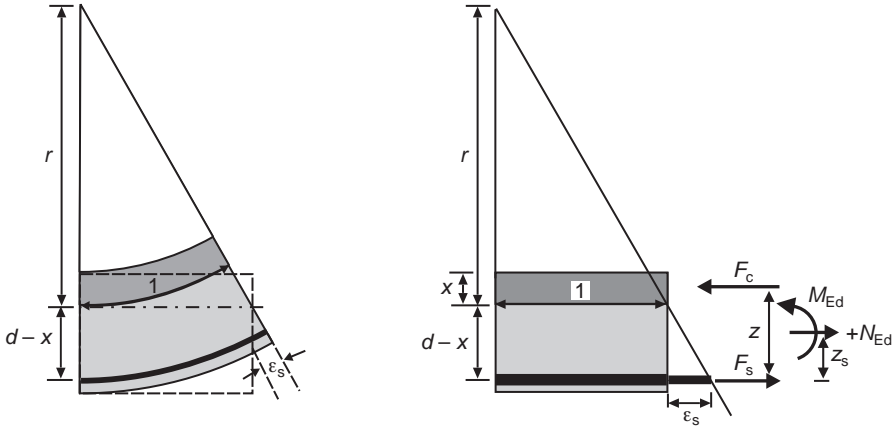
$$M_{Ed} = F_s \cdot z_{II} = A_s \cdot E_s \cdot \varepsilon_{sd} \cdot z_{II} \implies \frac{M_{Ed}}{A_s \cdot E_s \cdot z_{II}} = \varepsilon_{sd}$$

For the deflection calculation, the second derivation of the deformation $w''(x)$ of a member is needed. This value is also called curvature $1/r$.

From a geometrical consideration (Figure 2.115), it follows that:

$$\frac{1}{r_{II}} = \frac{\varepsilon_s}{(d-x)}$$

Figure 2.115 Curvature $1/r_{II}$ in the cracked state



Therefore, the curvature $1/r_{II}$ results in:

$$\frac{1}{r_{II}} = \frac{\epsilon_s}{(d-x)} = \frac{M_{Ed}}{z_{II} \cdot A_s \cdot E_s \cdot (d-x)}$$

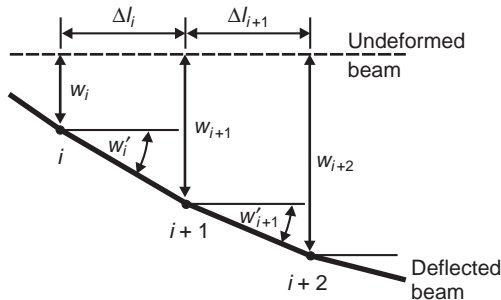
where: $z_{II} = d - x/3$

The height of the compression zone x and also the lever arm of the internal forces z only depend on the constant factor $(\alpha_c \rho)$. Thus, the distribution of the curvature is similar to the distribution of the external bending moment if the height of the cross-section as well as the reinforcement is constant through the whole member.

Now, the deformation of a member can be determined easily by double integration of the curvature (Figure 2.116). Further details are available in Section 2.11.3.1.

$$w = \iint w'' dx = \iint \frac{1}{r} dx = \int \bar{M} \cdot \frac{1}{r} dx = \int \bar{M} \cdot \frac{M}{E \cdot I} dx$$

Figure 2.116 Deflections of a beam



$$w_i'' = \frac{w'_{i+1} - w'_i}{\Delta l_i} = \frac{1}{r_i} \implies w'_{i+1} = \frac{1}{r_i} \cdot \Delta l_i + w'_i$$

$$w'_{i+1} = \frac{w_{i+1} - w_i}{\Delta l_i} \implies w_{i+1} = w'_{i+1} \cdot \Delta l_i + w_i$$

If the deflections in a few sections are needed, it is easier to determine the required values by means of the moment–area method (principle of conservation of energy). More details are given in Section 2.11.3.1.

The length of the neutral axis is enlarged when the section cracks (Figure 2.114). This effect must be considered in case of restrained forces.

2.11.3 Deflections in the cracked state with consideration of the tension-stiffening effect

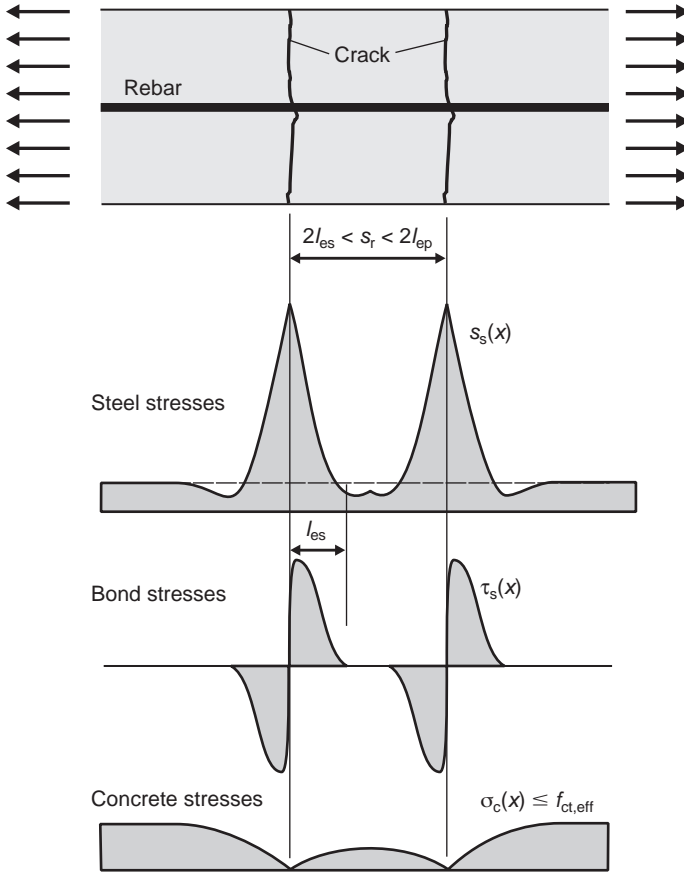
To get realistic values for the deformation of a structure, the cracked state and the tensile strength of concrete between the cracks, the so-called *tension-stiffening effect*, have to be considered.

The basics of such an analysis will be explained on a simple tensile member shown in Figure 2.117. In the elastic, uncracked State I, the reinforcing bars show the same (small) strain like the concrete if one neglects creep effects. Due to the different elastic moduli of concrete and steel, the tensile stresses in the reinforcement gives: $\sigma_s = \alpha_e \cdot \sigma_c$ (where $\alpha_e = E_s/E_c$).

If one increases the tensile stresses, the first crack will open in the cross-section that shows the smallest concrete tensile strength $f_{ct,av}$. In the crack, the whole of the external force is carried only by the reinforcing bars. This results in the maximum steel strain and stress. By contrast, the concrete tension is zero. Due to the bond between rebars and concrete, shear forces are transferred from the reinforcement to the concrete on both sides of the crack. Consequently, the tensile stresses increase in the concrete until they reach the local concrete tensile strength $f_{ct,av}$ again, and a new crack opens. This process goes on with increase in the external normal force until so many cracks have opened that the concrete tensile stresses cannot reach the tensile strength, due to the small bond or transition length. This state is called the final cracking state. The concrete carries a part of the external tensile force between the cracks and increases the stiffness of the member with regard to the pure State II.

This process can be modelled theoretically by means of a 3D nonlinear FE model if, in addition to the concrete and the reinforcement, the bond is considered by contact elements and suitable bond models. Besides the large effort required for such a complex numerical analysis, the realistic modelling of the inhomogeneous composite material (reinforced concrete) causes significant problems. The crack pattern in a reinforced concrete member also depends, in addition to the loading, on the wide-ranging material parameters, the various restraint effects that can hardly be considered in reality and the arrangement of stirrups in the beam or the arrangement of the reinforcing bars. Hence, such complex 3D FE analysis should be carried out for research purposes only, where the

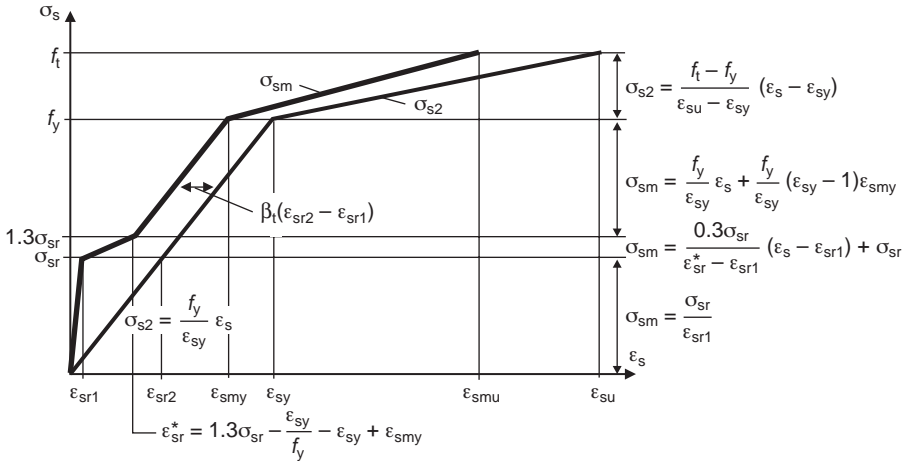
Figure 2.117 Distribution of tensile and bond stresses between two cracks



results can be verified by tests. Nonlinear calculations are useful for failure analysis where all input parameters (loads, real material parameters, etc.) as well as the crack pattern are known.

Hence, in practice, for nonlinear analysis, easy calculation models are required. Two very different methods are available and in use. According to Eurocode 2 (2004), the steel strain in the rebars for the pure State II can be reduced to consider the tension-stiffening effect. This results in an increase of the stiffness of the structure. The size of the reduction depends on the strain difference in the reinforcement $\Delta\varepsilon_s = \varepsilon_{sr2} - \varepsilon_{sr1}$ shortly before and immediately after the cracking, and is fixed in the code (CEB-FIB Model Code, 1990) (Figure 2.118). The strain difference $\Delta\varepsilon_s$ is big for slightly reinforced cross-sections, because the tensile force in the concrete before cracking must be carried by the small amount of reinforcement after the crack opens. This results in big steel strains ε_{sr2} . In contrast to the procedure described in the following, the strain change $\Delta\varepsilon_s$ is nearly independent of the steel strain in the final cracked state (Figure 2.118).

Figure 2.118 Modified stress–strain curve for concrete steel to consider the tension-stiffening effect
CEB-FIB Model Code, 1990



The equations to estimate the modified steel strains from DAfStb (2003) are listed in the following text.

Uncracked: ($0 \leq \sigma_s \leq \sigma_{sr}$): $\epsilon_{sm} = \epsilon_{s1}$

Cracked: ($\sigma_{sr} < \sigma_s \leq 1.3 \cdot \sigma_{sr}$): $\epsilon_{sm} = \epsilon_{s2} \cdot \frac{\beta_1 \cdot (\sigma_s - \sigma_{sr}) + (1.3 \cdot \sigma_{sr} - \sigma_s)}{0.3\sigma_{sr}} \cdot (\epsilon_{sr2} - \epsilon_{sr1})$

Final cracking: ($1.3 \cdot \sigma_{sr} < \sigma_s \leq f_y$): $\epsilon_{sm} = \epsilon_{s2} - \beta_1 \cdot (\epsilon_{sr2} - \epsilon_{sr1})$

Yielding of the steel:

($f_y < \sigma_s \leq f_t$): $\epsilon_{sm} = \epsilon_{sy} - \beta_t \cdot (\epsilon_{sr2} - \epsilon_{sr1}) + \delta_d \cdot (1 - \sigma_{sr}/f_y) \cdot (\epsilon_{s2} - \epsilon_{sy})$

where:

ϵ_{sm} is the mean steel strain.

ϵ_{uk} is the ultimate steel strain.

ϵ_{s1} is the steel strain in the uncracked state.

ϵ_{s2} is the steel strain in the crack in the fully cracked state.

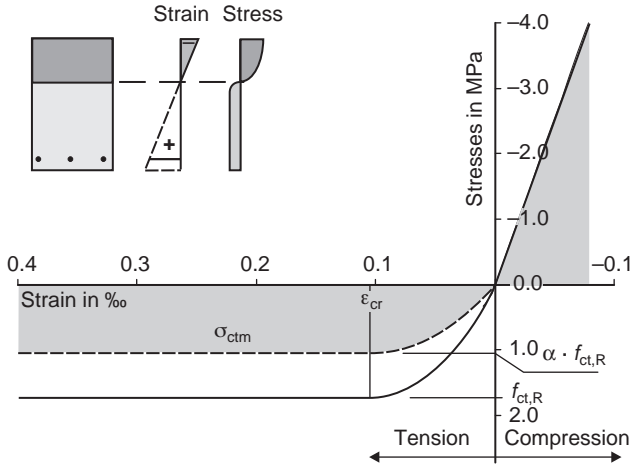
ϵ_{sr1} is the steel strain in the uncracked state under the loads, where f_{ctm} is reached.

ϵ_{sr2} is the steel strain in the crack under the loads, where f_{ctm} is reached.

β_t is the parameter to consider the influence of the load duration or a repeated load on the mean strain ($= 0.40$ for a short duration; $= 0.25$ for a constant load or for frequent load changes).

σ_s is the tension stress in the tension reinforcement that is calculated on the basis of a cracked cross-section (tension in the crack).

Figure 2.119 Tensile stress–strain curve in concrete according to Quast (1981)

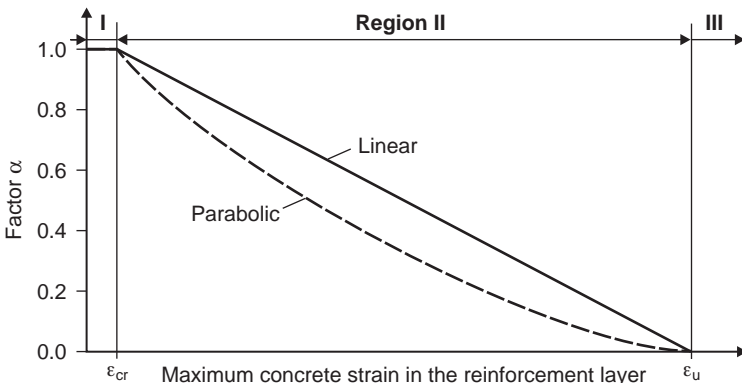


σ_{sr} is the tension stress in the tension reinforcement that is calculated on the basis of a cracked cross-section for the loads that lead to the first cracking.

δ_d is the factor for the consideration of the ductility of the reinforcement ($= 0.8$ for high-ductile steel; $= 0.6$ for normal-ductile steel).

Quast (1981) suggests considering the tension-stiffening effect by a tensile strength of the concrete f_{ct} in the tensile region of a member (Figure 2.119). The actual value of f_{ct} depends either linearly or squarely on the maximum concrete strain in the level of the reinforcement (Figure 2.120). If the member is uncracked, the full tensile strength $f_{ct,R}$ should be applied. If the reinforcing bars reach the yield strength, the bond

Figure 2.120 Reduction of the concrete tensile strength as a function of the concrete strain in the most strained steel fibre



between the concrete and the reinforcement is strongly disturbed and, therefore, according to Quast (1981), the concrete stiffening effect should be neglected. In the region between these limit values, the maximum concrete tensile stress σ_{ctm} is reduced as a function of the concrete strain of the most stretched steel fibre with the value α (Figure 2.120).

This procedure shows a better correspondence with test results than a reduction of the steel strain, as the calculation of 38 tests of concrete members (Quast, 1981) has shown.

In the calculation, the mean concrete tensile strength f_{ctm} will not be used but a tensile strength $f_{ct,R}$. Quast (1981) suggests using the following values:

$$\begin{aligned} \text{arithmetic tensile strength: } f_{ct,R} &= |f_{cm}|/20 \approx 0.6f_{ctm} \\ \text{strain when the concrete tensile strength is reached: } \varepsilon_{cR} &= |\varepsilon_{c1}|/20 \\ \text{ultimate strain of the concrete (see Figure 2.120): } \varepsilon_u &= 0.002. \end{aligned}$$

The deflections can be calculated by hand with the help of the curvatures of a member if one assumes a constant modulus of elasticity E_c in the compression region and the parabolic-shaped curve of the concrete stresses in the tensile region is neglected (Figure 2.121). With the latter assumption, the increase of the member stiffness from State I to State II is overestimated slightly (see Section 2.11.2). The equilibrium of the forces and moments results in:

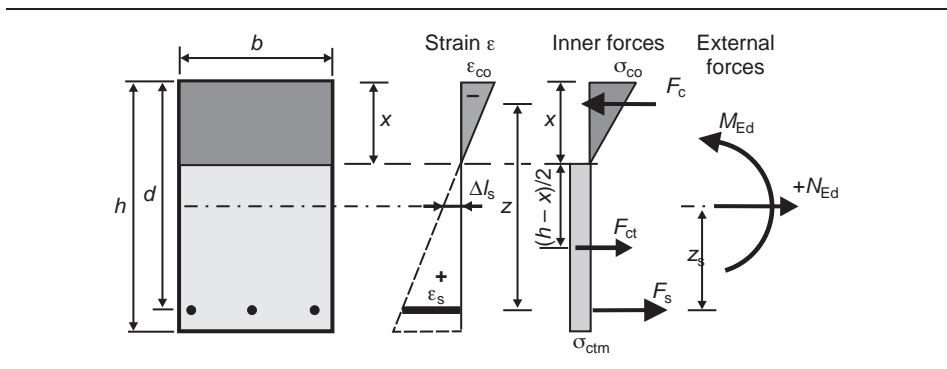
Force balance:

$$\begin{aligned} \Sigma F_h = 0 \quad F_s + F_{ct} - |F_c| &= N_{Ed} \implies \varepsilon_s \cdot E_s \cdot A_s + \sigma_{ctm} \cdot b \cdot (h - x) \\ &= -\varepsilon_{co} \cdot E_c \cdot b \cdot \frac{x}{2} + N_{Ed} \end{aligned}$$

Geometrical condition:

$$\frac{\varepsilon_s}{d - x} = \frac{-\varepsilon_{co}}{x} \rightarrow \varepsilon_s = \frac{-\varepsilon_{co}}{x} \cdot (d - x) \quad \text{or} \quad -\varepsilon_{co} = \varepsilon_s \frac{x}{(d - x)}$$

Figure 2.121 Cracked concrete cross-section – stresses and internal forces



Moment balance:

$$F_s \cdot z + F_{ct} \cdot \left(\frac{h-x}{2} + \frac{2 \cdot x}{3} \right) = M_{Eds}$$

Thus three equations are available to estimate the three unknowns, ε_s , ε_{co} and x . The mean concrete tensile strength σ_{cmt} depends on ε_s . The equations can easily be solved by means of mathematical programs. Alternatively, the height of the compression zone x and, with it, the curvature $1/r_{II}$, can be estimated iteratively. As a start value, one chooses the height x without tension-stiffening.

Concrete tensile strength

The concrete tensile strength f_{ct} plays a big role in all nonlinear structural analysis. It depends mainly on the same factors such as the concrete compressive strength, the gravel, the bond between concrete and gravel, the water-binder ratio, the hydration of concrete, the internal tensile stresses due to hydration, the unequal shrinkage over the height of the cross-section and the restraint of the shrinkage strains due to the reinforcement. Furthermore, the tensile strength decreases sharply with dynamic loading.

Hence, an exact determination of the concrete tensile strength is only possible by tests in the real structure. Any analytical estimation of f_{ctm} , for example, by means of the equations given in the codes, will have big uncertainties. Hence, boundary value considerations should be carried out if the concrete tensile strength has an essential role on the distribution of the member forces and the deformation.

In Eurocode 2 (2004: Part 1-1 Table 3.1), the following mean and quantile values are given:

$$\text{Mean value: } f_{ctm} = 0.30 \cdot f_{ck}^{(2/3)} \text{ for concrete } \leq C50/60$$

$$f_{ctm} = 2.12 \cdot \ln(1 + f_{cm}/10) \text{ for concrete } \geq C55/67$$

$$5\% \text{ fractile } f_{ctk;0.05} = 0.70 \cdot f_{ctm}$$

$$95\% \text{ fractile } f_{ctk;0.95} = 1.30 \cdot f_{ctm}$$

As can be seen from the values in Table 2.11, the mean concrete tensile strength f_{ctm} for normal concrete is approximately 10% of the typical concrete compressive strength f_{ck} .

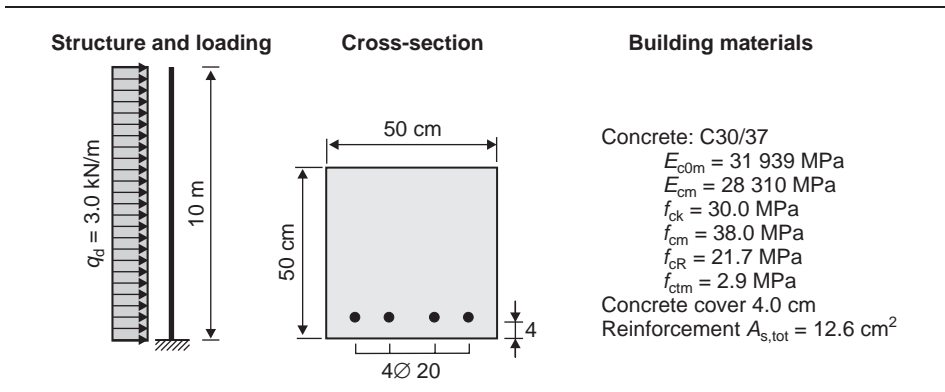
2.11.3.1 Example: Cantilever beam

In the following example, the deformations are estimated for a simple structure using the previously explained procedures. This is done to explain in greater detail the base of

Table 2.11 Concrete tensile strengths in MPa

f_{ck}	20	25	30	35	40	45	50	55
f_{ctm}	2.2	2.6	2.9	3.2	3.5	3.8	4.1	4.3
$f_{ctk;0.05}$	1.5	1.8	2.0	2.2	2.5	2.7	2.9	3.0
$f_{ctk;0.95}$	2.9	3.3	3.8	4.2	4.6	4.9	5.3	5.6

Figure 2.122 System and loading



the nonlinear analysis of reinforced concrete members that is absolutely necessary if one wants to interpret and understand the results of numerical analysis. Manual procedures, with which the deflections of a beam can be simply determined in the cracked state with sufficient accuracy, are explained.

A 10-m-high cantilever beam that is loaded by a uniform horizontal load $q_d = 3.0\text{ kN/m}$ (Figure 2.122) is treated. The self-weight of the concrete member and the time-dependent deflections due to creep of concrete are neglected. As the maximum concrete compressive stresses under the given load are considerably smaller than $0.4f_{ck}$, a linear stress–strain curve is used for the concrete (triangular-shaped concrete compression zone). With this simplification, manual calculations of the deflections are possible, and the arithmetic procedures are easier to understand.

First, the deformations are estimated.

1. Elastic analysis

Horizontal deflection of the cantilever tip:

$$f = \frac{q_d \cdot l^4}{8 \cdot E_{cm} \cdot I_c} = \frac{3.0 \cdot 10^4}{8 \cdot 28\,309 \cdot 0.5^4/12} = 25.4\text{ mm} \quad (f = 22.6\text{ mm with } E_{c0m})$$

2. Nonlinear analysis without tension-stiffening effect and with mean material parameters

For simplicity, the curvature ($1/r$) at the support section will be determined only in the following. The remaining values may be calculated accordingly.

$$\text{Height of the pressure zone: } x = d \left(\sqrt{[2 + \alpha_e \cdot \rho_1] \cdot \alpha_e \cdot \rho_1} - \alpha_e \cdot \rho_1 \right)$$

where:

$$\rho_1 = \frac{A_s}{b \cdot d} = \frac{12.6}{50 \cdot 46} = 0.0055$$

Secant modulus of concrete: $E_{cm} = 28\,310\text{ MPa}$

$$\alpha_e = \frac{E_s}{E_{cm}} = \frac{200\,000}{28\,310} = 7.07$$

$$x = 46 \left(\sqrt{[2 + 7.07 \cdot 0.0055] \cdot 7.07 \cdot 0.0055} - 7.07 \cdot 0.0055 \right) = 11.1\text{ cm}$$

$$z = d - x/3 = 46 - 11/3 = 42.3\text{ cm}$$

The curvature in the support section results in:

$$\frac{1}{r_{II}} = \frac{M_{Ed}}{z_{II} \cdot A_s \cdot E_s \cdot (d - x)} = \frac{0.150}{0.42 \cdot 12.6 \cdot 10^{-4} \cdot 200\,000 \cdot (0.46 - 0.11)} = 0.00405/\text{m}$$

Because the internal lever arm z is constant over the height of the beam, the curvature $1/r$ shows the same parabolic distribution as the bending moments.

$$\text{Steel strain: } \varepsilon_s = \frac{1}{r_{II}} \cdot (d - x) = 0.0040 \cdot (0.46 - 0.11) = 0.00141$$

$$\text{Steel stress: } \sigma_s = \varepsilon_s \cdot E_s = 0.00141 \cdot 200\,000 = 282\text{ N/mm}^2$$

$$\text{Concrete edge strains: } \varepsilon_{co} = -\varepsilon_s \cdot \frac{x}{(d - x)} = -0.00141 \cdot \frac{0.11}{0.46 - 0.11} = -0.00045$$

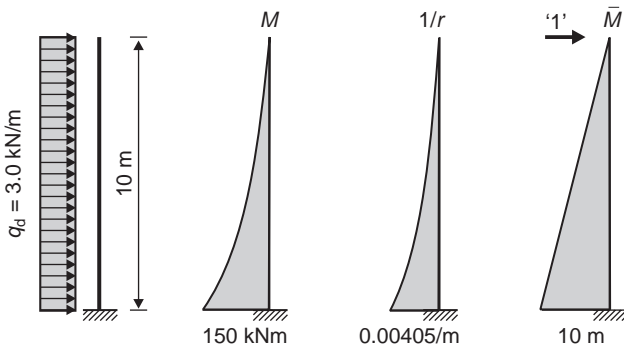
$$\text{Concrete compressive stress: } \sigma_{co} = \varepsilon_{co} \cdot E_{cm} = -0.00045 \cdot 28\,310 = -12.7\text{ N/mm}^2$$

With the known curvature, the maximum deflection of the beam can be easily calculated by means of the principle of virtual work (Figure 2.123).

$$f = \int_0^l \bar{M} \cdot \frac{1}{r} \cdot dx = \frac{1}{4} \cdot 10 \cdot 0.00405 \cdot 10 \cdot 10^3 = 101.3\text{ mm}$$

If one considers that the concrete tensile stresses from a height of approx. 3.60 m are smaller than the mean tensile strength ($\sigma_{ct} \leq f_{ctm}$), and thus the concrete is uncracked in this region in theory, the maximum deflection of the beam decreases to approx. $f = 88\text{ mm}$.

Figure 2.123 Structure, bending moments and curvature



2.11.4 Nonlinear, with tensile stiffening effect

2.11.4.1 Reduction of the steel strains

$$\text{Cracking moment: } M_{\text{cr}} = f_{\text{ctm}} \cdot \frac{b \cdot h^2}{6} = 2.90 \cdot \frac{0.5 \cdot 0.5^2}{6} = 0.0604 \text{ MNm}$$

$$\text{Steel force: } F_{\text{sr}} = \frac{M_{\text{cr}}}{z} = \frac{0.0604}{0.42} = 0.1438 \text{ MN}$$

The internal lever arm z_{II} of a cracked cross-section with a triangular-shaped concrete pressure distribution is independent of the loads.

Steel tensile stress and strain with the cracking moment M_{cr} in the State II (cracked):

$$\sigma_{\text{sr2}} = \frac{F_{\text{sr}}}{A_s} = \frac{0.1438}{12.6 \cdot 10^{-4}} = 113.5 \text{ MPa}$$

$$\varepsilon_{\text{sr2}} = \frac{\sigma_{\text{sr2}}}{E_s} = \frac{113.5}{200\,000} = 0.00057$$

Steel tensile stress and strains with the cracking moment M_{cr} in the State I (uncracked):

$$\sigma_{\text{sr1}} = \alpha_e \cdot \frac{M_{\text{cr}}}{I_c} \cdot z_s = 7.07 \cdot \frac{0.0604}{0.5^4/12} \cdot 0.21 = 17.2 \text{ MPa}$$

$$\varepsilon_{\text{sr1}} = \frac{\sigma_{\text{sr1}}}{E_s} = \frac{17.2}{200\,000} = 0.00009$$

$$\begin{aligned} \text{Strain difference: } \Delta\varepsilon_s &= \beta_t \cdot (\varepsilon_{\text{sr2}} - \varepsilon_{\text{sr1}}) = 0.25 \cdot (0.00057 - 0.00009) \\ &= 0.00012 \quad (\beta_t = 0.25 \text{ for a constant load}) \end{aligned}$$

The mean steel parameters are used.

$$f_{\text{yk}} = 500 \text{ MPa}$$

$$f_{\text{yR}} = 1.1 \cdot f_{\text{yk}} = 550 \text{ MPa}$$

$$\varepsilon_{\text{syR}} = f_{\text{yR}}/E_{\text{sm}} = 550/200\,000 = 0.00275$$

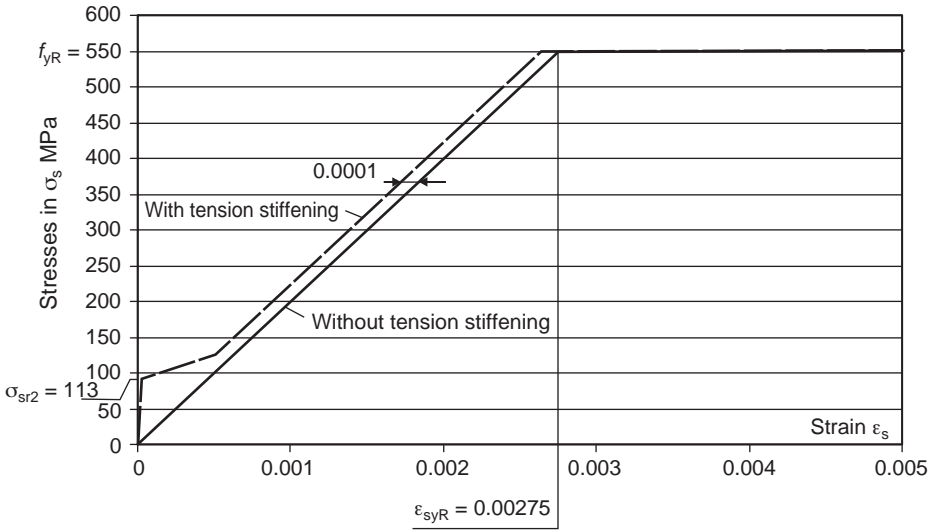
$$f_{\text{tR}} = 1.08 \cdot f_{\text{yR}} = 594 \text{ MPa (high ductility)} \quad \varepsilon_{\text{suk}} = 0.05$$

$$E_{\text{sm}} = 200\,000 \text{ MPa}$$

The maximum steel tensile stresses must be below $\sigma_s = 239 \text{ N/mm}^2$ when the tension-stiffening effect is neglected. Hence, it is unimportant whether the calculation is carried out with a yield stress of $f_{\text{yR}} = 550 \text{ MPa}$ or $f_{\text{yd}} = 435 \text{ MPa}$.

The resulting stress–strain curves in the reinforcement are shown in Figure 2.124. In this example, the reduction of the steel strain is low, about 0.1 mm/m, which results in a change of steel stresses of around $\Delta\sigma_s = 24 \text{ N/mm}^2$. Therefore, the tension-stiffening effect has little influence on the deformation of the beam.

Figure 2.124 Stress–strain curves of the steel



The numerical integration of the curvature over the length of the beam results in a maximum horizontal deflection of the cantilever beam of $f = 83$ mm.

2.11.4.2 Procedures according to Quast (1981)

The estimation of the curvature according to the procedure of Quast can only be done iteratively or by means of mathematical programs. With a concrete tensile strength of $f_{ct,R} = 1.9$ MN/m² and $\epsilon_{cr} = 0.10$ mm/m, the following values in the support region are obtained:

$$1/r_{max} = 0.0030 \quad x = 0.142 \text{ m}$$

$$\sigma_s = 190 \text{ MN/m}^2$$

$$\sigma_{co} = -12.0 \text{ MN/m}^2$$

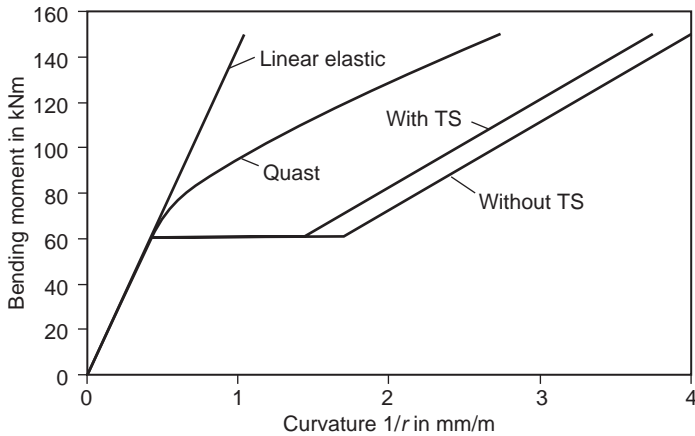
$$\sigma_{ct} = 0.56f_{ct,R} = 1.1 \text{ MN/m}^2$$

Within this method, a relatively high concrete tensile strength of $\sigma_{ct} = 1.1$ MN/m² is used in the support region. Hence, it is also not surprising that the maximum deflection of the cantilever is only $f = 48$ mm.

The considerably higher stiffness of the method of Quast compared with the procedure using the reduction of the mean steel strain also becomes clear with the moment-curvature curves (Figure 2.125).

Furthermore, the big change in curvature $1/r$ can be seen in Figure 2.125 when State I remains. The method of Quast avoids this discontinuity. A reduction of the mean steel

Figure 2.125 Moment-curvature diagram



strain has only a low influence on the deflections, and with it on the curvature. In Table 2.12, the main results of four models are listed.

2.11.4 Design values of the material parameters

In the preceding sections, a major problem of nonlinear analysis was not mentioned: the material parameters and the permissible tensile stresses for the concrete and the steel reinforcement.

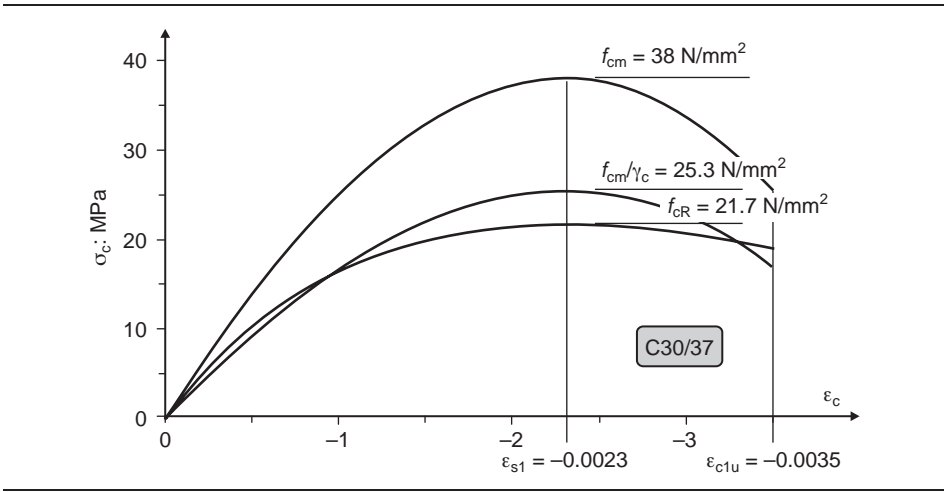
The deformations of a structure are usually estimated with the mean values of the material parameters f_{cm} , f_{ctm} and E_{cm} . Hereby, one assumes that local damage or a locally bad-quality material (e.g. by bad compaction of concrete) has little effect on the member forces and the deformations.

In contrast, the calculation of load-bearing capacity of a structure in the ultimate limit state is based on design fractile values of the material strength (e.g. $f_{cd} = \alpha \cdot f_{ck} / \gamma_c$) and loads ($E_d = \gamma \cdot E_k$).

Table 2.12 Results of four models

	f : mm	$1/r_{max}$	σ_s : MN/m	σ_{co} : MN/m
Elastic	25	0.0010	43	-7.2
Without TS	101	0.0040	282	-12.7
With TS – reduction of the steel strain	83	0.0037	258	-12.3
With TS – Quast	48	0.0030	190	-12.0

Figure 2.126 Stress–strain diagram for concrete grade C30/37



The required safety standards are reached through a decrease of the characteristic material parameters and an increase of the characteristic loads. An analysis with these design values would overestimate the deformations of a structure.

Hence, for a nonlinear analysis, the ‘real’ material parameters and stress–strain relations for the building materials are needed to estimate the member forces and to design the structure in the ultimate limit state with a sufficient safety margin. Two very different approaches are given in Eurocode 2, Part 2 (2005) and DIN 1045-1 (2008).

With the global safety factor method, the ultimate resistance of a section R_d and the member forces are estimated with the mean material parameters divided with a partial safety coefficient γ_R . The partial safety coefficient for permanent and frequent design situations and fatigue analysis is $\gamma_R = 1.27$ (EC2) and 1.3 (DIN). For exceptional situations, $\gamma_R = 1.1$ has to be used.

$$R_d = \frac{1}{\gamma_R} (f_{cR}; f_{yR}; f_{tR}; f_{p0,1R}; f_{pR})$$

The material values are defined in DIN 1045-1 (2008) as follows:

$$f_{yR} = 1.1 f_{yk} \text{ (DIN 1045-1, 2008: Equation 18)}$$

$$f_{tR} = 1.08 f_{yR} \text{ for reinforcement steel with high ductility (DIN 1045-1, 2008: Equation 19)}$$

$$f_{tR} = 1.05 f_{yR} \text{ for reinforcement steel with normal ductility (DIN 1045-1, 2008: Equation 20)}$$

$$f_{p0,1R} = 1.1 f_{p0,1k} \text{ (DIN 1045-1, 2008: Equation 21)}$$

Table 2.13 Concrete compressive strength in N/mm^2

f_{ck}	20.0	25.0	30.0	35.0	40.0	45.0	50.0
$f_{cm} = f_{ck} + 8 \text{ N}/\text{mm}^2$	28.0	33.0	38.0	43.0	48.0	53.0	58.0
$f_{cd} = \alpha \cdot f_{ck} / \gamma_c$	11.3	14.2	17.0	19.8	22.7	25.5	28.3
f_{cm} / γ_c	18.7	22.0	25.3	28.7	32.0	35.3	38.7
$f_{cR} = 0.85 \cdot \alpha \cdot f_{ck}$	14.5	18.1	21.7	25.3	28.9	32.5	36.1

$$f_{pR} = 1.1 f_{pk} \quad (\text{DIN 1045-1, 2008: Equation 22})$$

$$f_{cR} = 0.85 \cdot \alpha \cdot f_{ck} \quad \text{for concrete} \leq \text{C50/60} \quad (\text{DIN 1045-1, 2008: Equation 23})$$

$$f_{cR} = 0.85 \cdot \alpha \cdot f_{ck} / \gamma_c' \quad \text{for concrete} \geq \text{C55/67} \quad (\text{DIN 1045-1, 2008: Equation 24})$$

$$E_{cR} = 0.85 \cdot E_{c0m} / 1.1$$

The factor α is equal to 0.85 for normal concrete. It considers the lower fatigue strength of the concrete for dynamic loads as well as the difference between the cylinder and uni-axial compressive strength. Hence, with short-term loads, for example, in the ultimate limit state, bigger values of $0.85 \leq \alpha \leq 1.0$ can be used.

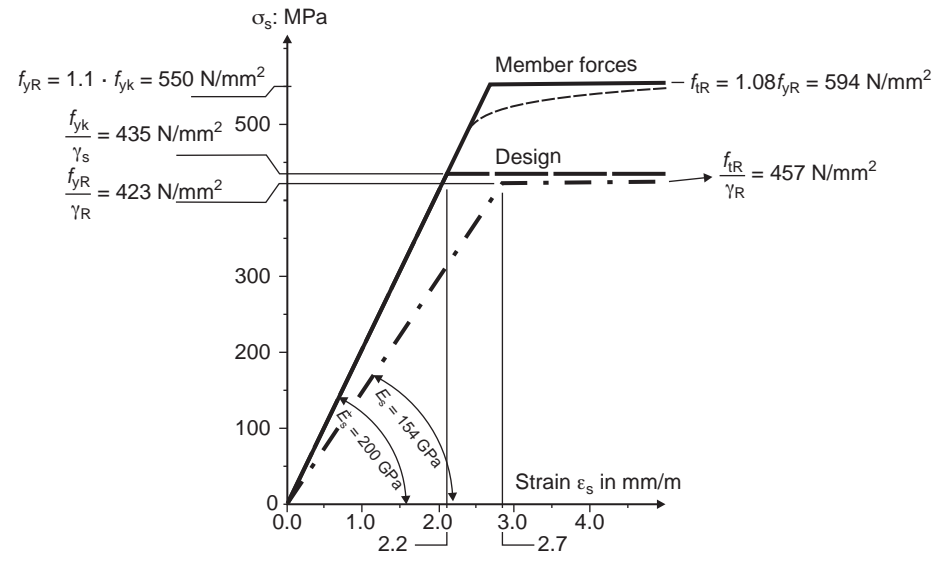
As can be seen from Table 2.13, the value of the concrete strength f_{cR} deviates from the mean value f_{cm} , divided by the safety coefficient $\gamma_c = 1.5$ by up to 30%. Figure 2.126 shows the stress–strain relations for the different approaches.

In contrast to the previously mentioned procedure, the deformations of slender beams and columns under bending and normal forces may be estimated by the partial safety method where the design values f_{cm}/γ_c or E_{cm}/γ_c are used (DIN 1045-1, 2008: §8.6.1). Nevertheless, after this estimation, the design of the critical sections must be conducted with the design values of the material strength, for example, $f_{cd} = \alpha \cdot f_{ck}/\gamma_c$, and the ultimate stress–strain curves. The estimation of the member forces is conducted with a different material behaviour than the design of a section. This is also known as ‘double accountancy’.

It should be noted that the modulus of elasticity of the reinforcing steel E_s should not be modified by a safety coefficient ($E_{sR} = E_{sm}/\gamma_R = 153.846 \text{ MPa}$; Figure 2.127). This would result in a considerable reduction of the structural stiffness and significantly higher deformations with regard to the mean values if the steel has not reached its yielding strength. The yielding stresses of the reinforcing steel of both methods are nearly identical, with $f_{yk}/\gamma_s = 435 \text{ N}/\text{mm}^2$ or $f_{yR}/\gamma_R = 423 \text{ N}/\text{mm}^2$.

With the reduction of the modulus of elasticity of the reinforcing steel E_s comes an increase in the deflection of the cantilever tip in the preceding example (with $q_d = \gamma_Q \cdot q_k = 1.5 \cdot 3 = 4.5 \text{ kN}/\text{m}$) by 24% to $f = 132 \text{ mm}$ and $f = 164 \text{ mm}$ (procedure with reduction of the steel strains). With Quast’s method, a maximum cantilever deflection is estimated as $f = 100 \text{ mm}$. The big increase in the deflection can lead to

Figure 2.127 Stress–strain diagram for reinforcing steel



uneconomical cross-section dimensions or uneconomical amounts of reinforcement. Hence, the E-modulus of steel should not be modified by a safety coefficient.

The question of which procedure gives more accurate, realistic results is still an issue of research. Nevertheless, for practical purposes, it is important to know that both methods can give very different results, even for simple systems. This clearly demonstrates that the nonlinear analysis of reinforced concrete structures is still very complicated, even with the software available today. In this respect, it is clear why nonlinear methods are not permitted for the design of the superstructures of concrete bridges in Germany.

Hence, if nonlinear procedures are used, it is advised to carry out boundary value analysis and to check the sensitivity of the results for different input parameters.

A complex probabilistic analysis is rarely justified for a real concrete structure due to the big effort and the missing statistical data. Thus, simple approaches for nonlinear analysis are still needed.

REFERENCES

- Beck H and Schäfer H (1969) Die Berechnung von Hochhäusern durch Zusammenfassung aller aussteifenden Bauteile zu einem Balken. *Der Bauingenieur* **44**: 80–87.
- Becker M (1994) Erneuerung der Theodor-Heuss-Brücke in Heidelberg. *Beton- und Stahlbetonbau* **89**: 154–156.
- Busjaeger D and Quast U (1990) *Programmgesteuerte Berechnung beliebiger Massivbauquerschnitte unter zweiachsiger Biegung mit Längskraft*. Deutscher Ausschuss für Stahlbeton, Heft 415, Berlin.

- CEB-FIP Model Code (1990) CEB-Bulletin 213/214, Lausanne.
- CEN (European Committee for Standardization) (2004) Eurocode 2, Part 1: Design of concrete structures – General rules and rules for buildings. December.
- CEN (2005) Eurocode 2, Part 2: Design of concrete structures – Concrete Bridges – Design and detailing rules. December.
- Czerny F (1999) *Tafeln für Rechteckplatten*. In *Betonkalender 1999*, (Eibl J (ed.)) Volume 1. Ernst & Sohn, Berlin.
- DAfStb (2003) Erläuterungen zu DIN 1045-1; Deutschen Ausschusses für Stahlbeton Heft 525. Berlin.
- DIN 1045-1 (2008) Concrete, reinforced and prestressed concrete structures – Part 1: Design. Deutsches Institut für Normung. Berlin, August.
- DIN 4014 (1990) Bohrpfähle: Herstellung, Bemessung und Tragverhalten, Deutsches Institut für Normung. Berlin, March.
- Grasser E *et al.* (1991) *Hilfsmittel zur Berechnung der Schnittgrößen und Formänderungen von Stahlbetonbauwerken*; Deutscher Ausschusses für Stahlbeton Heft 240, Berlin.
- Homberg H (1973) *Platten mit zwei Stegen*. Springer Verlag, Berlin.
- Homberg H and Ropers W (1965) *Fahrbahnplatten mit veränderlicher Dicke*, Band I, Springer Verlag, Berlin.
- Mühle R and Kroppen H (1997) Don Muang Tollway – Eine 14 km lange Hochstraße durchzieht Bangkok. In *Vorträge auf dem Deutschen Betontag* (Betonverein D (ed.)). Wiesbaden, pp. 510–529.
- Quast U (1981) Zur Mitwirkung des Betons in der Zugzone. *Beton- und Stahlbetonbau* **10**: 247–250.
- Rombach G and Specker A (2003) Segmentbrücken. In *Betonkalender 1/2004* (Bergmeister/Wörner (eds)) pp. 177–212. Verlag Ernst & Sohn, Berlin.
- Rombach G (1997) ‘New’ concepts for prestressed concrete bridges – Segmental box girder bridges with external prestressing. *Conference ‘Actual Problems in Civil Engineering’*. Proceedings, St. Petersburg, July.
- Rühl M (2000) Der Elastizitätsmodul von Beton. Forschungskolloquium des Deutschen Ausschusses für Stahlbeton. Darmstadt Oct: 135–148.
- Schlaich J and Schäfer K (1998) Konstruieren im Stahlbetonbau. In *Betonkalender* (Eibl J (ed.)), part II, Berlin.
- Schlaich J *et al.* (1987) Towards a consistent design of structural concrete. *PCI Journal*, May–June: 77–150.
- Schneider KH and Reeh H (1978) Tragwerk des Bürohochhauses Mainzer Landstraße in Frankfurt am Main. *Beton- und Stahlbetonbau* **73**: Heft 12: 285–293.
- Timm U and Baldauf H (1988) *Betonkonstruktionen im Tiefbau*. Ernst & Sohn, Berlin.
- Wong YC and Coull A (1980) Interaction between Floor Slabs and Shearwalls in Tall Buildings. In *Reinforced Concrete Structures Subjected to Wind and Earthquake Forces*. Publ. SP-63, Detroit.

Chapter 3

Shear walls and deep beams

Shear walls and deep beams are thin 2D flat spatial structures that are loaded by forces parallel to the midplane of the membrane (Figure 3.1). The stresses and strains are uniformly distributed over the thickness. However, one must make a distinction between shear walls and deep beams (Figure 3.2). Shear walls are continuously supported plane members loaded by normal forces, where the maximum width of the cross-section is greater than four times its minimum width. If this is not the case, a member is treated as a column. Deep beams are plane spatial members whose height is greater than half of their effective span width l_{eff} . Furthermore, these beams are not continuously supported. In contrast to ordinary beams, shear walls and deep beams usually have a nonlinear strain distribution over their depth (see Figure 3.3). Shear deformation cannot be neglected.

The distinction between deep and slender beams is not only necessary for the calculation of the internal forces, but also for the reinforcement arrangement. In ordinary beams, a minimum shear reinforcement (stirrups) is needed, whereas deep beams only need the minimum surface reinforcement.

This section only discusses the FE analysis of deep beams, as they are more often used in practice. Shear walls can be designed in the usual manner similar to a column.

In accordance with Section 5.1.1 of EC2 (Eurocode 2, 2004), the internal forces in the ultimate limit state can be calculated by using the following methods

- methods based on linear elastic material behaviour
- methods based on linear elastic material behaviour with limited redistribution
- methods based on plastic material behaviour including strut-and-tie models
- methods based on nonlinear material behaviour.

Of these methods, the one that uses FE models based on linear elastic material behaviour is most commonly used in practice. Comments on the evaluation of strut-and-tie models (plastic analysis) are given at the end of this chapter.

The member forces of calculations based on linear elastic material behaviour can be used for the design in the ultimate limit state and the serviceability limit state. The effects of the redistribution of internal forces due to cracking of concrete or its 'yielding' under

Figure 3.1 FE of a shear wall and stresses considered in the model

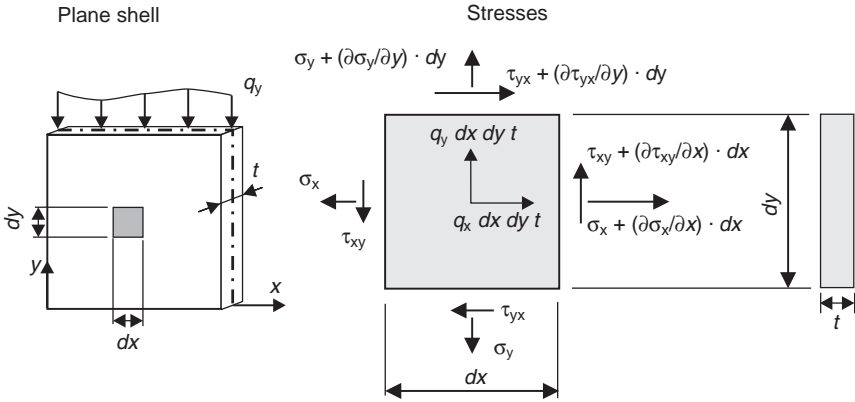


Figure 3.2 Shear wall and deep beam

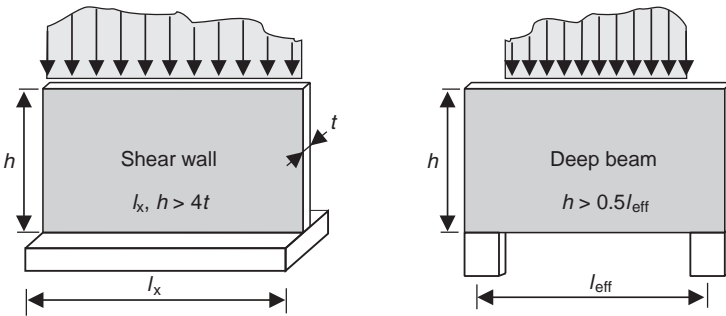
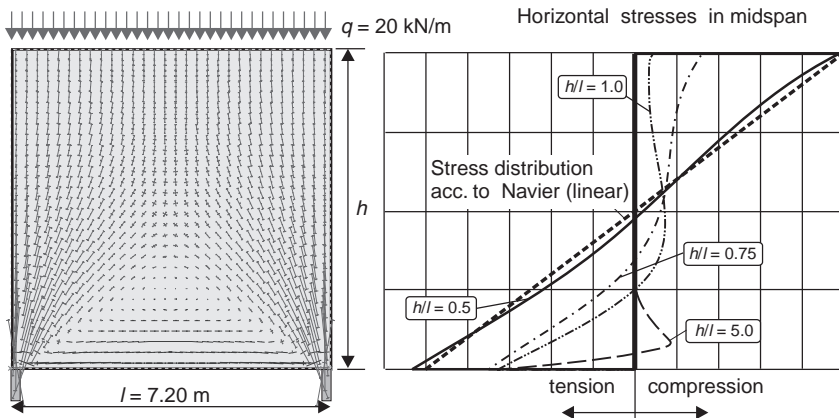


Figure 3.3 Single-span deep beam – main membrane forces (left) and horizontal stresses in midspan (right) for various heights h



high pressures are neglected. Nevertheless, the nonlinear behaviour should be considered in both the design and the detailing of the reinforcement. For example, the longitudinal reinforcement of a single-span deep beam should be located at the bottom face of the member, and should not be distributed according to the tensile stresses, which are estimated by linear elastic analysis (Section 3.3).

The next section will provide the principles of an FE calculation for deep beams by a very simple example of a single-span deep beam.

3.1. Estimation of stress resultants of deep beams

The beam in this example has a width-to-depth ratio of 1 : 1 ($l_x = l_y = 7.20$ m) (Figure 3.4). A uniform loading of $q = 20$ kN/m is acting on its upper free edge. The structure is modelled by $30 \times 30 = 900$ rectangular plane elements, which gives an element size of 0.24×0.24 m.

The results of the FE calculation are the node deflections v_x, v_y , the membrane forces n_x, n_y, n_{xy} and the stresses $\sigma_x, \sigma_y, \sigma_{xy}$ within the elements (see Figures 3.1 and 3.5). The membrane forces are obtained by multiplying the normal stress σ_x or σ_y by the thickness of the wall.

The objective of the design of a concrete member is to estimate its required reinforcement. For beams and slabs, this can be automatically produced by well-known algorithms that are implemented in structural software. In the case of walls, a computer program is usually unable to estimate these reinforcement requirements or its correct distribution, as it is based on an element per element design. This problem will be further discussed in Section 3.3. The reinforcement requirements of the single-span deep beam, therefore, should be estimated by numerical integration of the horizontal tensile forces n_x over the midspan depth. For the structure in this example (load case 1), this results in a tensile force of $F_s = 31$ kN (see Figure 3.5). The lever arm of the compressive and tensile

Figure 3.4 System and FE model

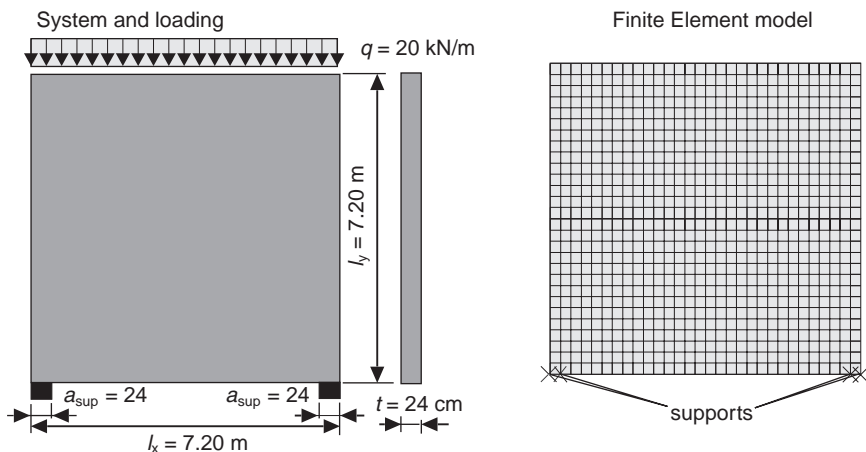
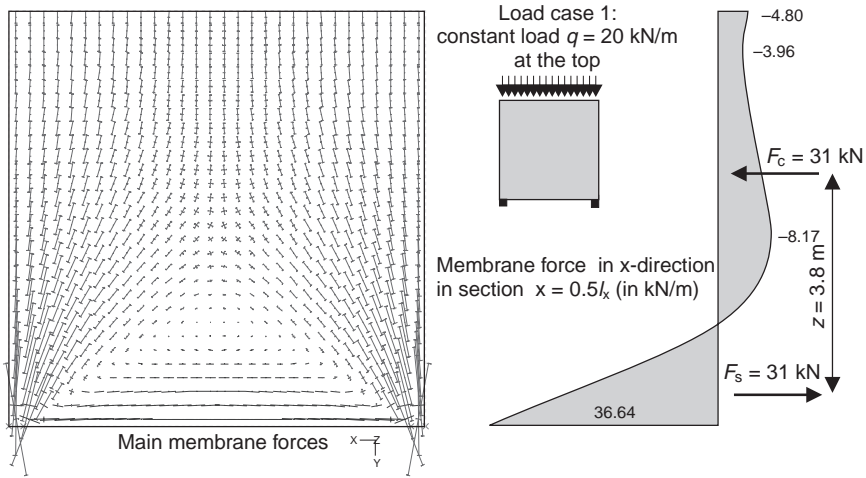


Figure 3.5 Main membrane forces – load case 1: uniform load $q = 20 \text{ kN/m}$ on the upper edge



force is equal to $z = 3.80 \text{ m}$. The reinforcement requirements are obtained from dividing the tensile force F_s by the permissible stresses of steel: $A_{s, \text{req.}} = F_s / \sigma_{\text{sd}}$. The stress in the reinforcement should be chosen to fulfil the crack width requirements ($\sigma_{\text{sd}} \leq f_{\text{yd}}$).

We will now compare the results of the FE calculation with the widely used manual design method given in CEB (Comité Européen du Béton, 1970) or ‘Heft 240’ of the German Association of Reinforced Concrete (DAfStb; see Grasser *et al.*, 1991). The example considers four different load cases.

- Load case 1: uniform load $q = 20 \text{ kN/m}$ on the upper edge of the deep beam.
- Load case 2: uniform load $q = 20 \text{ kN/m}$ on the lower edge of the deep beam.
- Load case 3: concentrated load $F = 96 \text{ kN}$ on the upper edge of the deep beam (loaded width: 0.96 m).
- Load case 4: concentrated load $F = 96 \text{ kN}$ on the lower edge of the deep beam (loaded width: 0.96 m).

The results of the FE analysis are shown in Figure 3.5 and Figures 3.7 to 3.9 for the various load cases. The resulting forces and the lever arms are obtained from numerical integration of the horizontal membrane forces at midspan.

CEB (Comité Européen du Béton, 1970) and ‘Heft 240’ of the German Association of Reinforced Concrete (Grasser *et al.*, 1991) offer two different design methods (see boxed text)

- beam theory: the resulting tensile force of a single-span deep beam:

$$F_s = M_F / z_F, \text{ with } z_F = 0.6l \text{ (for single-span deep beam with } h/l \geq 1.0)$$
- tables based on membrane theory.

Manual design methods (beam theory)

The horizontal tensile force is estimated from the bending moments of a beam at midspan (field) $M_{Ed,F}$ and at the supports $M_{Ed,S}$ (Figure 3.6).

Resulting tensile force in midspan:

$$F_{td,F} = M_{Ed,F}/z_F$$

Resulting tensile force over the supports of a multispans or cantilever beam:

$$F_{td,S} = M_{Ed,S}/z_S$$

where:

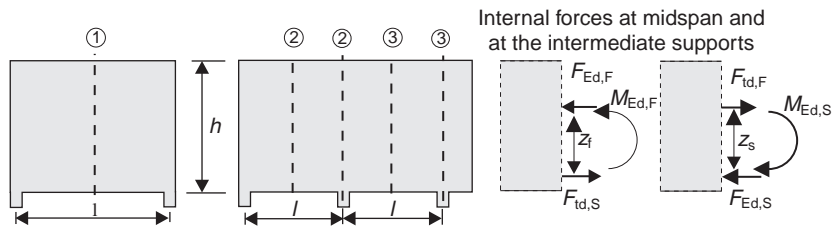
M_F is the midspan moment of a beam having the same span lengths as the deep beam

M_S is the moment over the supports of a beam having the same span lengths as the deep beam

z_F is the lever arm of the internal forces at midspan

z_S is the lever arm of the internal forces over the supports.

Figure 3.6 Internal forces according to the simplified design model



The lever arm of the internal forces z_F and z_S can be estimated as follows:

1. Single-span member

$$0.5 < h/l < 1.0 \quad z_F = 0.3h (3 - h/l) \quad (\text{Grasser } et al., 1991)$$

$$z_F = 0.2 (l + 2h) \quad (\text{Comité Européen du Béton, 1970})$$

$$h/l \geq 1.0 \quad z_F = 0.6l \quad (\text{Comité Européen du Béton, 1970; Grasser } et al., 1991)$$

2. Two-span member and end span of a multispans member

$$0.4 < h/l < 1.0 \quad z_F = z_S = 0.5h (1.9 - h/l) \quad (\text{Grasser } et al., 1991)$$

$$z_F = z_S = 0.2l (1 + 1.5h) \quad (\text{Comité Européen du Béton, 1970})$$

$$h/l \geq 1.0 \quad z_F = z_S = 0.45l \text{ resp. } 0.5l \quad (\text{Comité Européen du Béton, 1970})$$

3. Intermediate spans of a multispans member

$$0.3 < h/l < 1.0 \quad z_F = z_S = 0.5h (1.8 - h/l) \quad (\text{Grasser } et al., 1991)$$

$$h/l \geq 1.0 \quad z_F = z_S = 0.40l \quad (\text{Grasser } et al., 1991)$$

4. Cantilever member

$$1.0 < h/l_k < 2.0 \quad z_F = z_S = 0.65l_k + 0.10h \quad (\text{Grasser } et \text{ al.}, 1991)$$

$$h/l \geq 2.0 \quad z_F = z_S = 0.85l_k \quad (\text{Grasser } et \text{ al.}, 1991)$$

where:

h is the height of the deep beam

l is the span of the deep beam

l_k is the span of a cantilever member.

Table 3.1 summarises the main results of the FE analysis and the simplified method of ‘Heft 240’ (Grasser *et al.*, 1991).

A good agreement can be seen between the FE results and the manual calculation, except for load case 3 (beam theory), which is mainly due to the simple single-span system. However, greater differences may be estimated for other structures (for example, multi-span deep beams), as shown in the following example.

The internal forces for a two-span deep beam are calculated, carrying the loads from the facade columns of an 11-storey office building, above the entrance to the underground car park (Figure 3.10). The concentrated loads in the columns are simplified to an equivalent uniformly distributed load ($g_{Ed}/q_{Ed} = 400/200 \text{ kN/m}$). The deep beam is modelled by 52×15 plane shell elements (element size $0.25 \times 0.25 \text{ m}$). In the first analysis, an infinitely stiff vertical support is assumed. The stiffness of the supporting columns is neglected.

Figure 3.7 Main membrane forces – load case 2: uniform load $q = 20 \text{ kN/m}$ on the lower edge

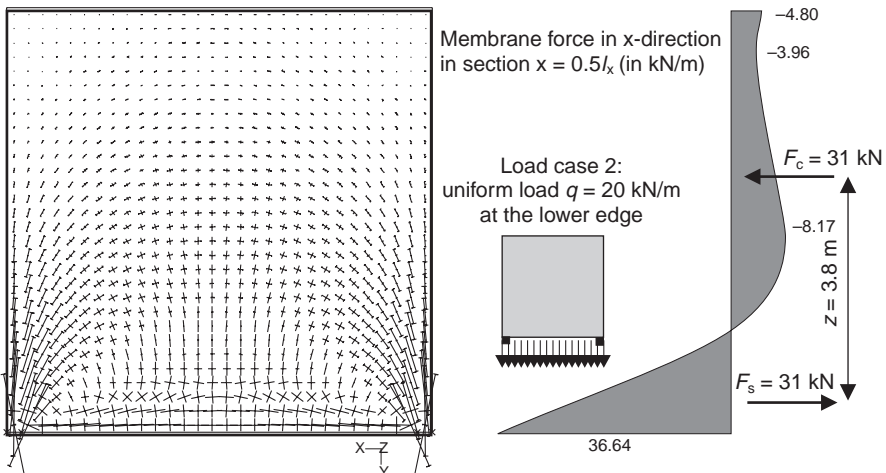


Figure 3.8 Main membrane forces – load case 3: Force $F = 96$ kN on the upper edge

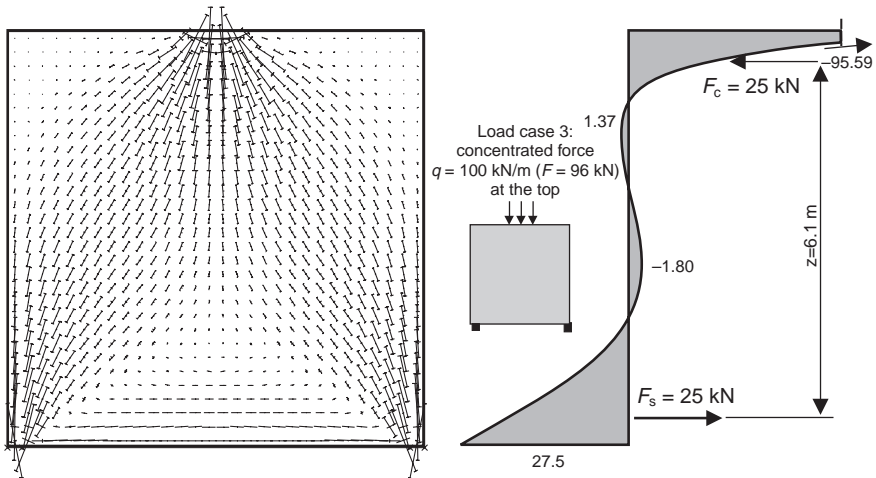


Table 3.2 shows the resulting tensile forces in midspan and at the intermediate support and the support reactions. The tensile forces obtained from the manual design method (in accordance with ‘Heft 240’; Grasser *et al.*, 1991) are greater than those from the FE analysis. In particular, the beam model results in much higher forces over the intermediate support (+172%). This is due to the small lever arm z_s with respect to the numerical analysis.

3.2. Modelling the support condition

In the case of statically indeterminate structures like multi-span deep beams, it is very important to model the existing support conditions as accurate as possible. In contrast

Figure 3.9 Main membrane forces – load case 3: Force $F = 96$ kN at the lower edge

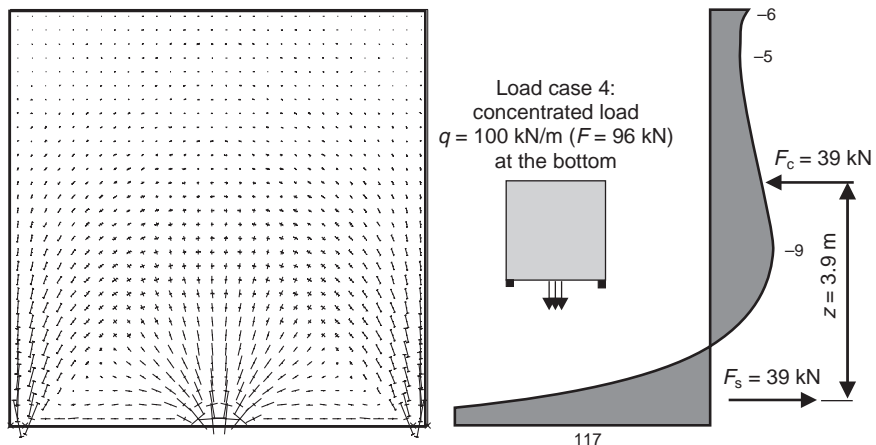


Table 3.1 Resulting forces and lever arms – single-span deep beam

	Load case 1		Load case 2		Load case 3		Load case 4	
	$F_s = -F_c$ (in kN)	z (in m)	$F_s = -F_c$ (in kN)	z (in m)	$F_s = -F_c$ (in kN)	z (in m)	$F_s = -F_c$ (in kN)	z (in m)
FE-analysis	31	3.8	31	3.8	25	6.1	39	3.9
DafStb								
beam	29	4.2	29	4.2	40	4.2	40	4.2
tables	29	–	29	–	26	–	38	–

to normal beam structures, the stiffness of the supports and the resulting deflections have a considerable effect on the stresses and resulting internal forces in deep beams, as will be demonstrated in the following section.

3.2.1 The influence of support settlements

The previously mentioned two-span deep beam (Figure 3.10) was fully restrained in the vertical direction at the supports. In general, the stiffness of the flexible supports should not be neglected. This is particularly true in the case of deep beams supported on slender columns or walls, or where differential settlements of the foundations or bearings are expected. It is a well-known fact that the internal forces and the reactions of multi-span deep beams are very sensitive to differential deflections of the supports. This will be discussed in the following example.

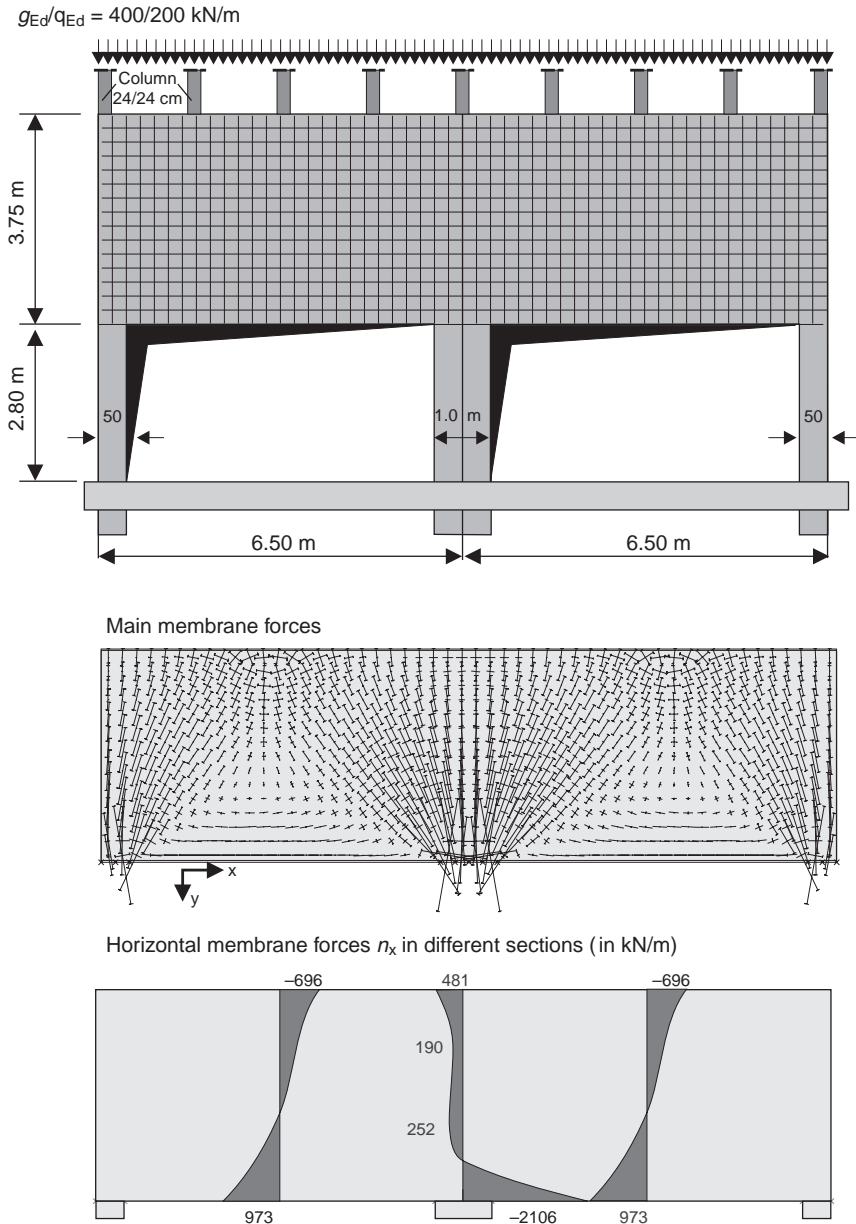
First, the influence of the deflection of the supports will be demonstrated for the slender ($h/l = 0.6$) double-span deep beam shown in Figure 3.10. The structure is loaded by a uniform vertical load of $q = 600 \text{ kN/m}$ at the top edge. Furthermore, it is assumed that there is a settlement of the intermediate support by up to 7 mm. Figures 3.11 and 3.12 show the results of the numerical analyses for different settlements.

The reactions and the resultant horizontal forces are very considerably influenced by the amount of settlement at the intermediate support. A deflection of only 2 mm is needed to increase the vertical forces at the end supports by 37% and reduce the reaction at the intermediate support by 38%. The resulting horizontal tensile force is increased by 200% in midspan and 33% at axis B. With increasing deflections, the stress distribution becomes similar to that of a single-span beam with a span length of $2 \times 6.25 = 12.50 \text{ m}$ (Figure 3.12). A deflection of only 7 mm ($= 0.001l$) is needed to reduce the reactions at the intermediate support to zero.

3.2.2 Modelling of flexible supports with springs

The preceding example clearly demonstrates that the stiffness of the supports of a statically indeterminate structure must be considered in the design model. Deep beams

Figure 3.10 Two-span deep beam: System, loading and membrane forces



are often supported by slender columns or walls. The simplest and often used approach to consider the stiffness of the bearing structure is to model them by using individual springs. For simplicity, the column itself is not modelled. This will be shown in the following section.

Table 3.2 Tensile forces and lever arms – double-span deep beam

	Midspan				Intermediate support				Support forces			
	$F_{s,F}$		Z_F		$F_{s,S}$		Z_S		$A = C$		B	
	kN	%	m	%	kN	%	m	%	kN	%	kN	%
FE analysis	650	100	2.6	100	700	100	3.6	100	1692	100	4417	100
'Heft 240'	675	104	2.4	94	1201	172	2.4	68	1609	95	4802	109
Grasser <i>et al.</i> (1991)	713	110	–	–	825	118	–	–	1609	95	4802	109

A column has a bending and a normal stiffness. Both should be modelled by individual springs. It should be noted that bending springs cannot be used in conjunction with plane membrane elements, as they have no degree of freedom for rotation (see the following section); hence, a different method of modelling the bending stiffness of columns has to be found.

In general, deep beams are loaded by large vertical forces that require large bearing areas. This continuous support can be modelled by using several spring elements or special boundary elements. The advantage of the latter model is that the elastic support stresses can easily be estimated. These have to be checked in the design.

The axial stiffness of springs C_N is obtained from the following expression (Table 3.3):

$$C_N = E \cdot A_c / l$$

where:

$E \cdot A_c$ is the axial stiffness of the column

l is the height of the column.

Figure 3.11 Support forces and tensile forces depending on the settlement Δs of the intermediate support

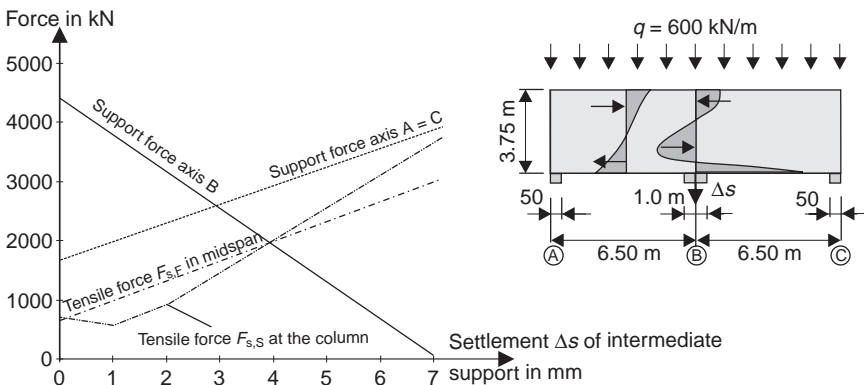
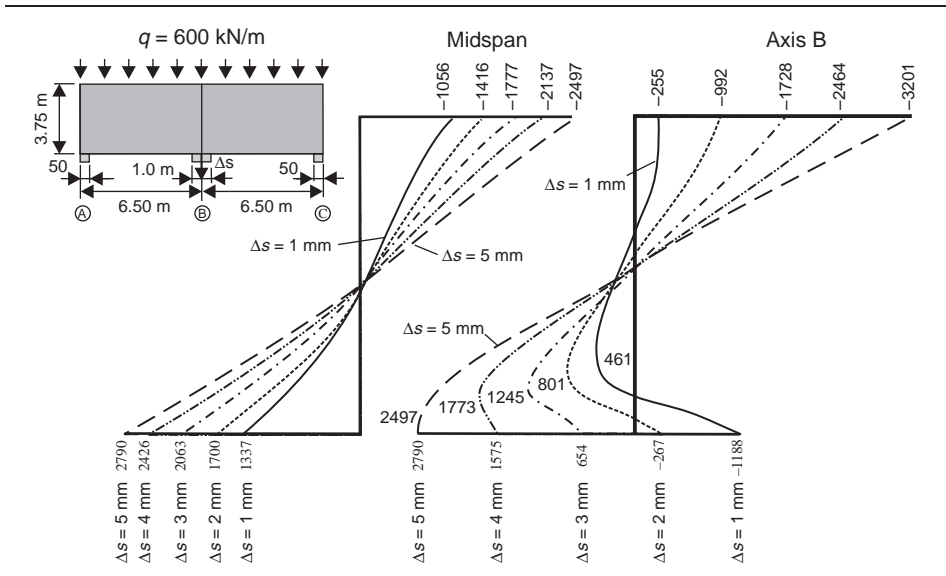


Figure 3.12 Horizontal membrane forces at the midspan and at the intermediate support B depending on the amount of vertical deflection Δs at axis B



As bending springs cannot be used in conjunction with plane shell elements, the rotational stiffness of the column is modelled by using multiple springs, having a given distance from each other (Figure 3.13).

The principles are demonstrated on a single-span deep beam (Figure 3.14). The structure is supported on two columns ($b/h = 0.24/0.48 \text{ m}$) that are clamped at their base. This

Table 3.3 Equivalent spring stiffness of a column

Normal stiffness

$$F = C_N \cdot v$$

where: $C_N = E_c \cdot A_c / l$

Rotational stiffness

$$M = C_\varphi \cdot \varphi$$

where: $C_\varphi = 3E_c \cdot I_c / l$

where: $C_\varphi = 4E_c \cdot I_c / l$

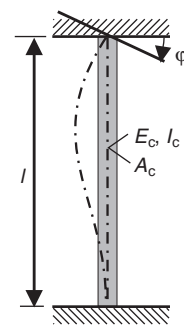
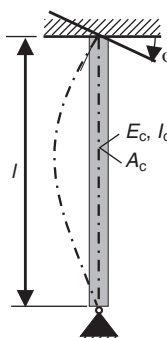
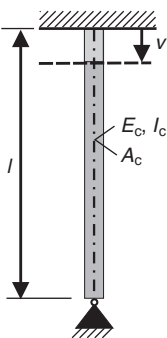
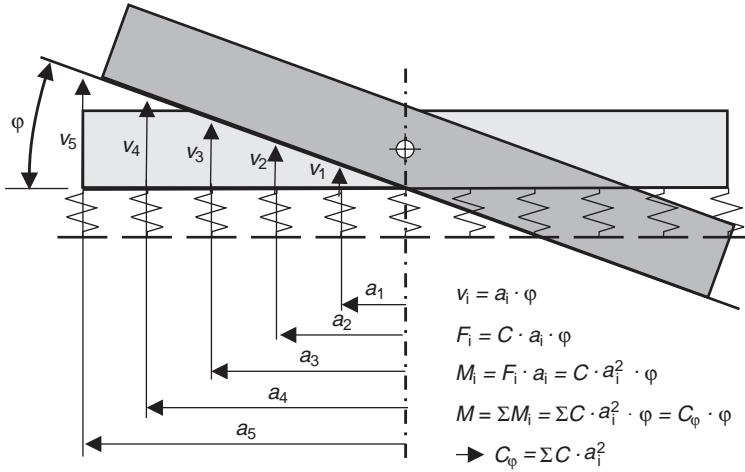


Figure 3.13 Rotational stiffness resulting from axial springs



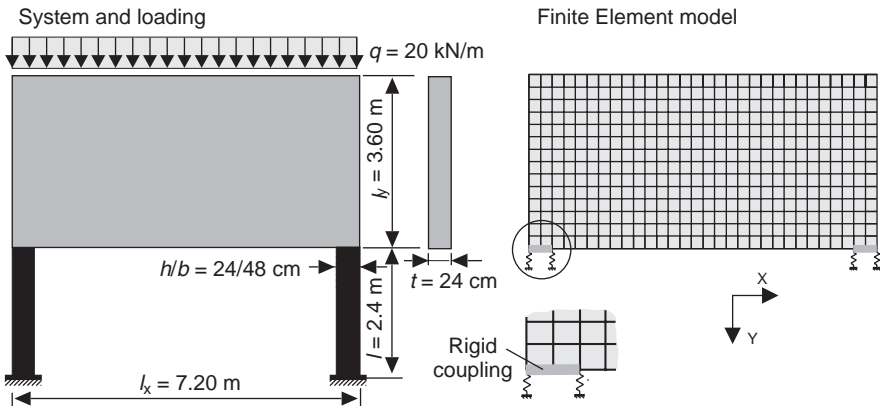
results in the following equivalent stiffness for the springs: (concrete grade C 25/30, $E_c = 30\,500$ MPa).

$$C_N = \frac{E_c \cdot A_c}{l} = \frac{30.5 \cdot 10^6 \cdot 0.24 \cdot 0.48}{2.4} = 1.464 \text{ MN/m}$$

$$C_\varphi = \frac{4 \cdot E_c \cdot I_c}{l} = \frac{4 \cdot 30.5 \cdot 10^6 \cdot 0.24 \cdot 0.48^3 / 12}{2.4} = 112.4 \text{ MNm/m}$$

Two springs are used for each support. The supported nodes are coupled with each other, and thus the supported area remains plane before and after loading in the numerical model. The distance of the normal springs has to be determined in order to get the correct

Figure 3.14 Structure and FE model



rotational stiffness C_φ :

$$C_\varphi = 2 \cdot C_N \cdot a_i^2 \Rightarrow a_i = \sqrt{\frac{C_\varphi}{2 \cdot C_N}} = \sqrt{\frac{112.4}{2 \cdot 1.464}} = 0.20 \text{ m}$$

where:

a_i is the distance of the spring from the centre of the supported area.

For the given structure, it is necessary to use a distance that is smaller than the actual supported width. As this is an exceptional case, the springs are located at the face of the supported area. This results in a distance of 0.48 m between the springs. The analysis gives a spring force of 31.6 kN and 40.4 kN at the outer spring and inner spring, respectively. The total vertical force is equal to 72 kN. The resulting bending moment at the top of the column is:

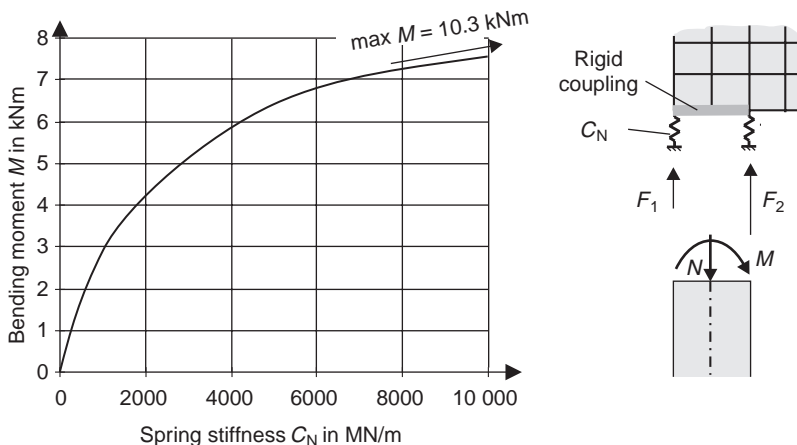
$$M = (40.44 - 31.6)/2 \cdot 0.48 = 2.12 \text{ kNm}$$

The influence of the spring stiffness on the bending moment is shown in Figure 3.15. It can be seen that, in the practical relevant region of $C_N \approx 1000 \text{ MN/m}$, the spring stiffness has a significant effect on the bending moment at the column head. An infinite stiff support results in a bending moment of $M = 10.3 \text{ kNm}$.

3.2.3 Modelling of the columns with beam elements

Instead of using springs, it may be easier to model the whole structure including the shear wall and the columns. The latter one is modelled by beam elements. This system has the big advantage with regard to springs that the member forces M , V , N and the reinforcement requirements of the column are calculated automatically by the computer program. It is also possible to model the columns using the same plane shell elements as the deep beam (Figure 3.17). However, this has the disadvantage that the member forces (i.e. the

Figure 3.15 Bending moment at the supports against normal spring stiffness C_N



bending moments, shear and normal forces) that are required for the design of the columns must be separately calculated by the integration of the stresses in various sections. Both of these models will be further discussed.

The connection of the beam elements with the plane shell elements should be handled with great care, as will be demonstrated in the following example, which uses a single-span deep beam. The columns are modelled with beam elements located on the axis of gravity of the column. The top beam node is rigid, connected to the node of the deep beam element at the same location.

The results of the FE analysis are shown in Figure 3.16. No bending moments are estimated at the column heads. This result is not expected, as a rotation of the supported area of the deep beam is likely to happen (note the deflected structure in Figure 3.17). Furthermore, considerable distortions can be seen for the elements in the vicinity of the column heads.

Figure 3.16 Deep beam supported on two columns (beam elements)

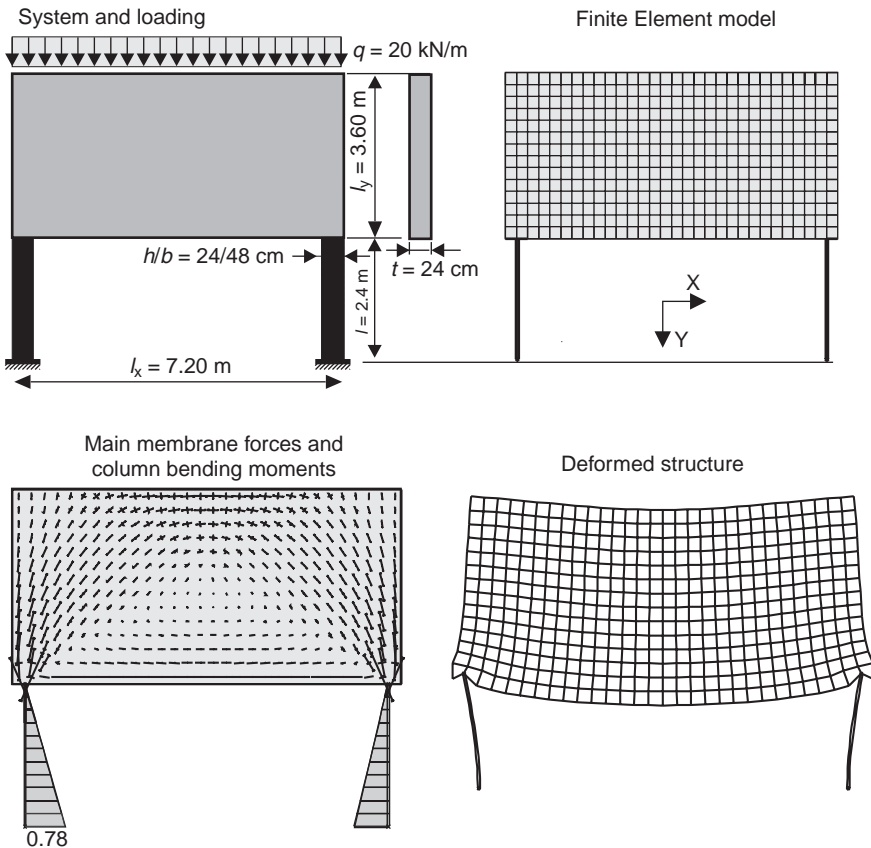
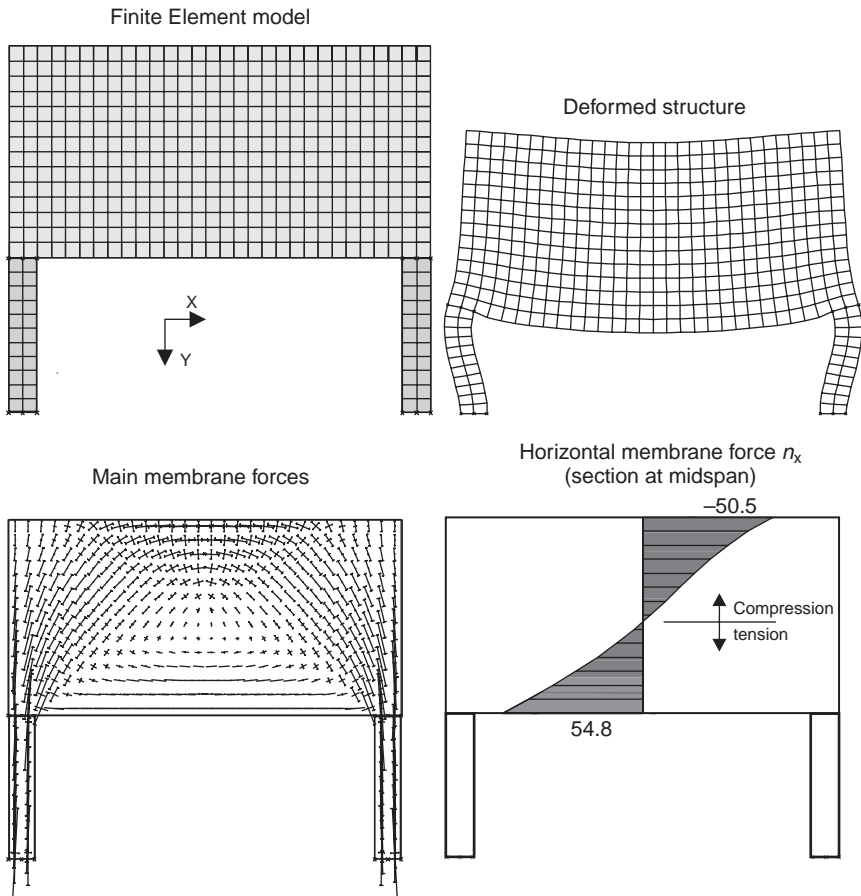


Figure 3.17 Deep beam supported on columns (plane shell elements)

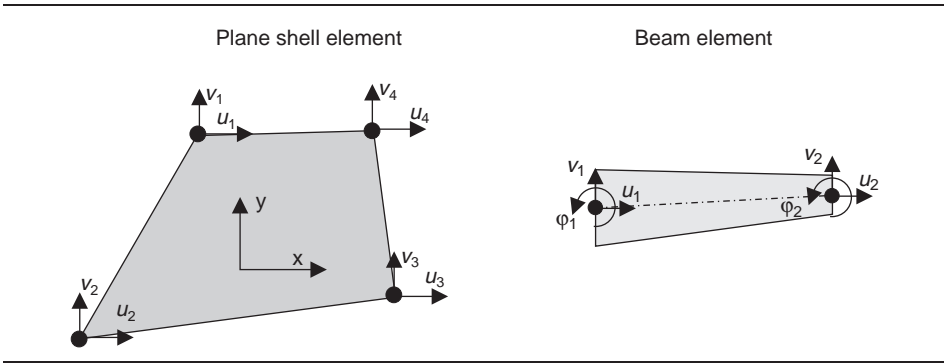


As zero bending moments are highly unexpected at the stiff joint between the column and the deep beam, the same structure is recalculated, using plane shell elements for the columns. Figure 3.17 shows the results of this analysis. A rotation of the upper end of the column can be seen that must result in bending moments in the column.

The error of the beam model can be traced back to the fact that plane shell elements have only two degrees of freedom for deflection, v_x and v_y , but no degree of freedom for rotation (Figure 3.18). Thus, coupling of beam and plane shell elements results in a so-called 'incompatible' element mesh. This means that there is a missing degree of freedom (rotation) between the two types of elements. Thus, a plane shell element can be used to only estimate membrane forces and not bending moments.

The rigid connection between the column and the deep beam must be modelled by stiff coupling of the top node of the beam element to some nodes of the deep beam

Figure 3.18 Degrees of freedom of a plane shell and a beam element (2D)



(Figure 3.19). The rotation of the supported nodes of the deep beam should be identical to the rotation of the upper end of the beam element. Distortions of the shell elements above the columns as shown in Figure 3.16 should be avoided.

A rigid connection can either be modelled with a special coupling of the nodes (Figure 3.19 left) or by extension of the beam elements into the deep beam (Figure 3.19 right). Both models only provide a rough approximation of the real structural behaviour. The number of coupled nodes can have a great effect on the bending moments in the column. This is demonstrated by the results shown in Figure 3.20, where considerable differences between both approaches in the calculated bending moments at the column head can be seen. For the case with horizontal coupling, a bending moment at the junction of $M = -3.7 \text{ kNm}$ is estimated, whereas for the other model the bending moment is only $M = -2.0 \text{ kNm}$. The ratio of the first moment with respect to the second one is $3.7/2.0 = 1.85!$

Figure 3.19 Connection of a beam element with a plane shell element

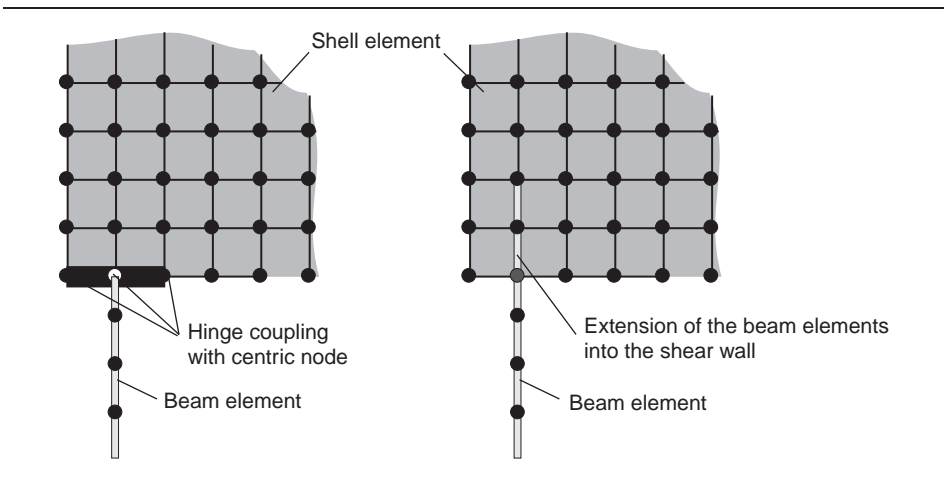
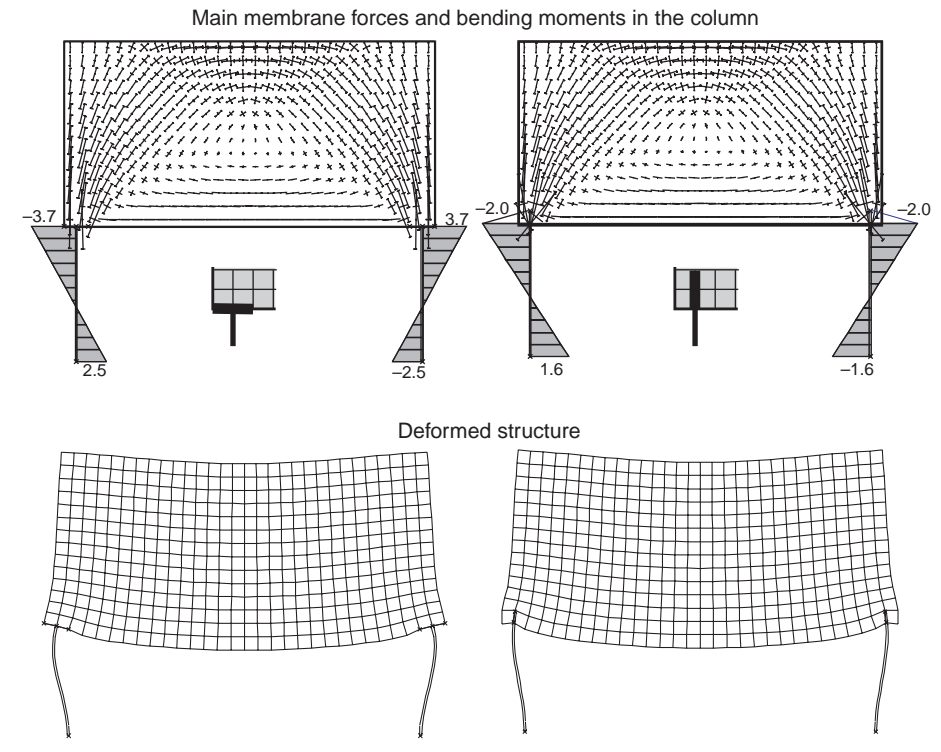


Figure 3.20 Membrane forces and the deformed structure for two different models – coupling with supported nodes (left) and extension of the beam elements (right)

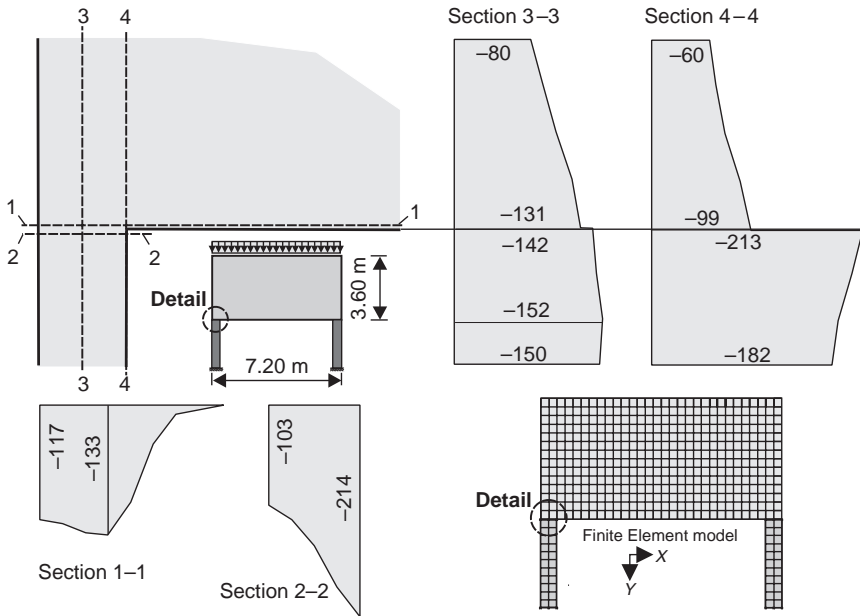


Here, it should be noted that there are also plane shell elements, which have a rotational degree of freedom (based on Cosserat continuum). However, these elements are rarely implemented in structural software used for the practical design of concrete structures.

A highly refined FE mesh has to be used to obtain a more accurate value for the bending moment at the column head. The results of this analysis are shown in Figure 3.21. The numerical integration of the vertical membrane forces at the top of the column (Section 2.2) results in a force of $F = 72 \text{ kN}$ ($F = 7.20 \text{ m} \times 20 \text{ kN/m} \times 0.5 = 72 \text{ kN}$) and a bending moment of $M = 2.6 \text{ kNm}$. This value is between the two results from the earlier-mentioned models.

An unbalanced distribution of the vertical membrane force n_y in Section 4-4 at the inner face of the corner can be seen in Figure 3.21. This is a result of the simplifications and assumptions of the used numerical model and does not occur in real structures. The corner causes a model problem. The unbalanced boundary condition results in high (infinite) stresses resp. membrane forces. If the element size is further reduced, the stresses at the inner face of the corner will become infinite. However, the resulting bending moment M is only slightly changed.

Figure 3.21 Vertical membrane force n_y in various sections near the corner of a deep beam



The stress distribution in any corner region of membranes can only be approximated when using plane elements with a linear elastic material behaviour. High tensile stresses would cause cracking of the concrete, thus resulting in a redistribution of the internal forces. The same effects occur in the case of large pressures at the inner edge of the corner. Therefore, a highly refined element mesh does not model reality any more precisely than a coarse element mesh.

3.2.4 Horizontal restraint

In deep beam analysis, great care should be taken with regard to horizontal restraints caused by incorrect modelling of the support conditions. They may result in an arching effect with considerable reduction in the design tensile forces, as will be illustrated in the following example.

The deep beam shown in Figure 3.22 is a very slender structure, having a width-to-depth ratio of 1:2. The member can, therefore, also be considered as a normal beam with the assumption of a linear strain distribution over its depth at midspan. The structure is modelled with 14×30 plane shell elements. It is loaded with a vertical uniformly distributed loading of $q = 20 \text{ kN/m}$ at its upper free edge.

Two ultimate support conditions are treated.

- System 1: both supports are fixed in the vertical direction, and only one support is fixed in the horizontal direction.
- System 2: both supports are fixed in both the horizontal and vertical directions.

Figure 3.22 Structure and element mesh

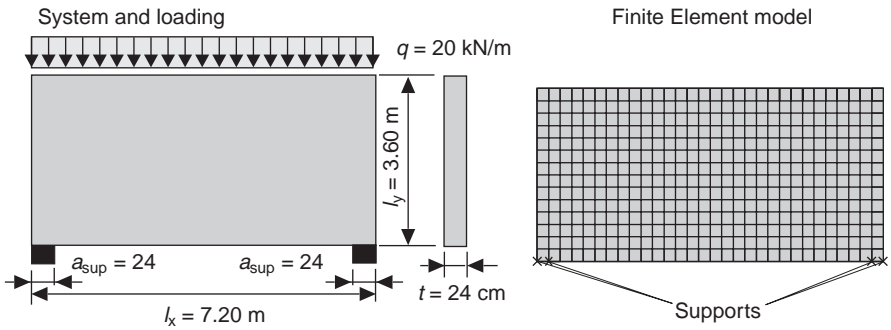
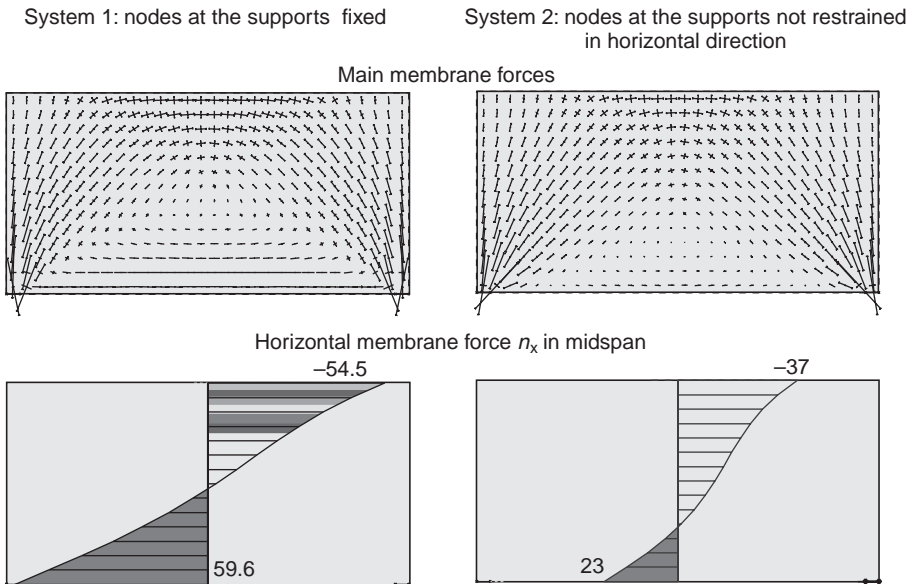


Figure 3.23 shows the distribution of the main membrane forces n_I and n_{II} and the horizontal membrane force n_x at midspan. Significant differences can be seen between the two models.

If one uses the manual design models provided in ‘Heft 240’ (Grasser *et al.*, 1991), the calculated tensile force is $F = 53$ kN. This is the same value as the resulting tensile force of System 1. If the structure is fully restrained in the horizontal direction (System 2), the resulting tensile force in midspan is only 1/5 of the value calculated of System 1, even for this very slender structure.

Figure 3.23 Membrane forces with and without horizontal restraints



3.3. Dimensioning of deep beams

The design of plane shell or membrane elements is based on the following assumptions.

- Concrete takes no tension ($\sigma_{1c} = 0$): This assumption is not true in the serviceability limit state, where one has to consider a reasonable tensile strength of concrete to get realistic results.
- Cracks are orientated orthogonal to the principal tensile stress: The orientation of the cracks depends not only on orientation of the stresses, but further on the rebar arrangement.
- Mohr's failure criterion is applied: Research is still ongoing to develop consistent models to describe the behaviour of reinforced concrete membranes. Mohr's failure criterion is an old model, but is still used quite often.
- Sufficient ductility: The capacity of concrete sections for redistribution of forces after cracking is limited. This is also called as ductility demand. Therefore, the assumed load path after cracking should be similar to the elastic flow of forces. The maximum compressive strength of a concrete element having compressive and tensile stresses is less than the uni-axial compressive strength. A reduction or 'disturbance' factor of at least $\beta = 0.85$ should be used to take this effect into account ($f_{cd} = 0.85 \cdot \beta \cdot f_{ck} / \gamma_c$).

The required reinforcement of a membrane element in both directions can be easily estimated based on equilibrium condition if the reinforcing bars are orientated along the principal axes. This is called a 'trajectory' reinforcement arrangement (Figure 3.24, element A).

$$\rho_1 \cdot f_{yd} = \sigma_1 \quad (\sigma_1 \text{ is the principal tensile stress})$$

This gives the minimum amount of reinforcement for a shear wall or deep beam. As the orientation of the principal axes changes in each point of a structure, and as various load cases have to be considered, the trajectory arrangement of reinforcing bars is mostly not possible.

In general cases, Mohr's failure criterion may be applied (Fédération Internationale du Béton, 2007). This results in the following equations, which must be fulfilled in each membrane element (Figure 3.25):

$$\rho_y \cdot f_{yd} \geq \sigma_y + |\tau_{xy}| \cdot \cot|\theta|$$

$$\rho_x \cdot f_{yd} \geq \sigma_x + |\tau_{xy}| \cdot \cot|\theta|$$

$$f_{cd} \geq \rho_x \cdot f_{yd} + \rho_y \cdot f_{yd} - \sigma_x - \sigma_y$$

The angle of the compression struts θ should be chosen with regard to the stress field based on a linear elastic analysis to minimise the required redistribution of forces.

The implementation of these equations in a software package is an easy task. However, this does not solve the main design problem of plane membranes as will be demonstrated by the following structure, a simple deep beam. The approach should only be used if the

Figure 3.24 Design of a membrane element

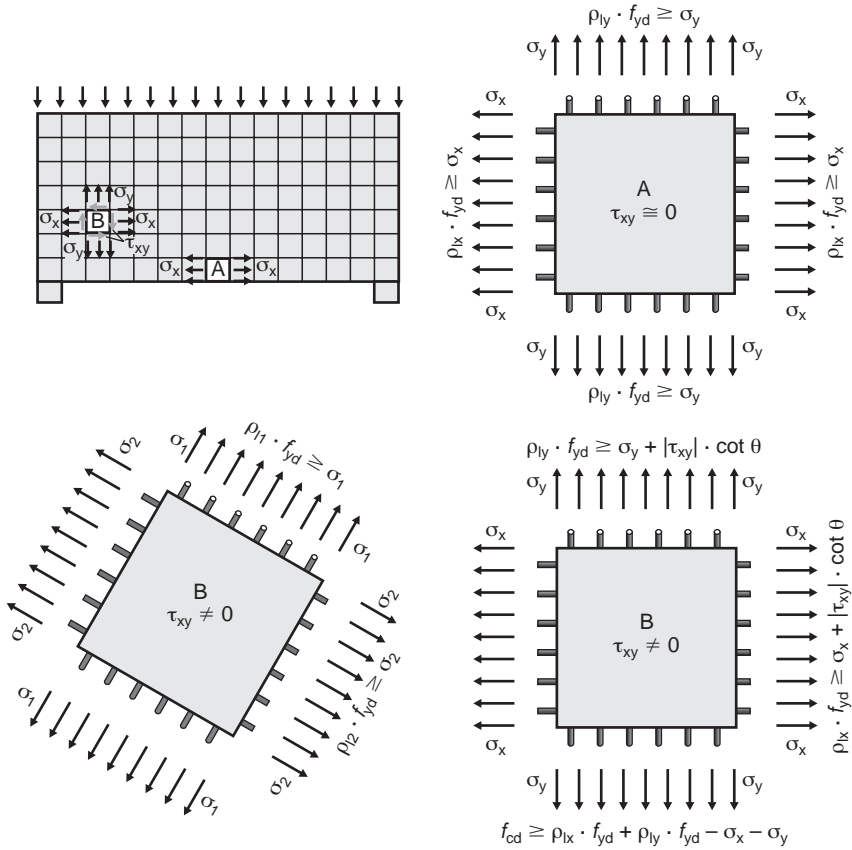


Figure 3.25 Design of a membrane element

Adapted from Fédération Internationale du Béton (2008) with permission of the International Federation for Structural Concrete (*fib*, www.fib-international.org)

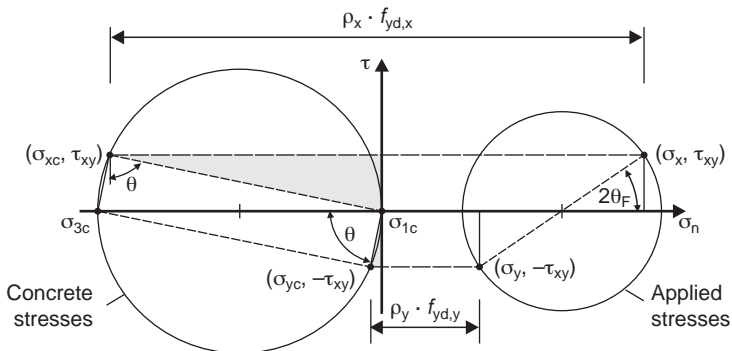
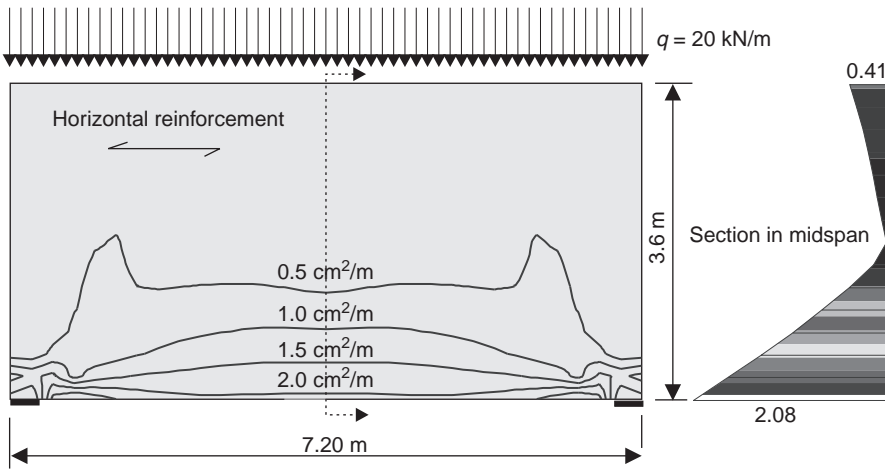


Figure 3.26 Horizontal reinforcement



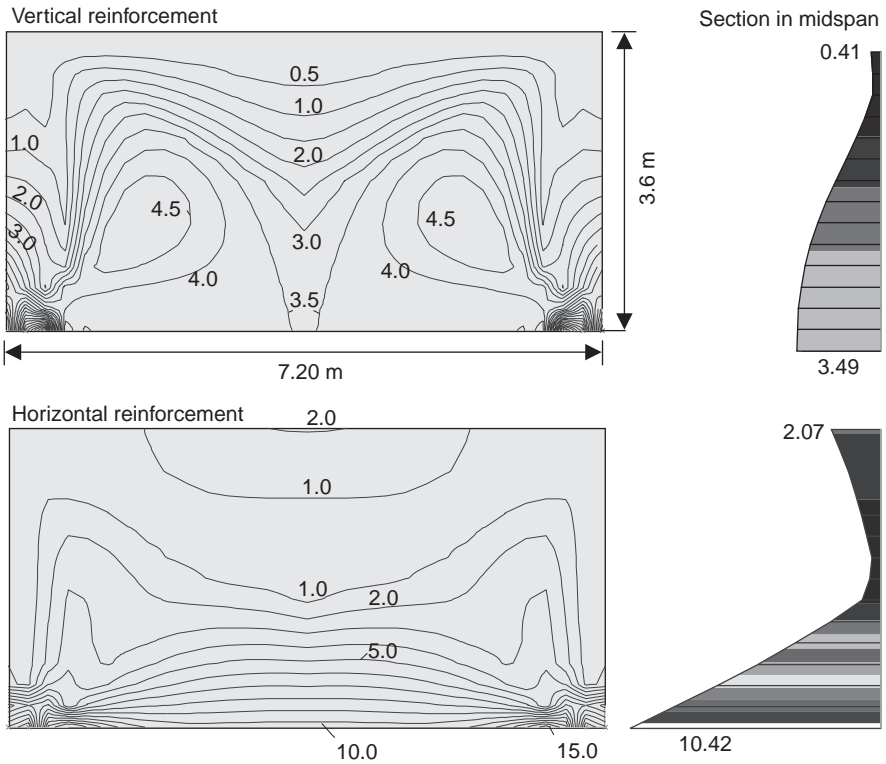
flow of forces in a cracked member does not differ much from that of an uncracked one. Membranes having significant shear forces should not be designed with this approach. Instead, strut-and-tie models can be used.

As already mentioned in Section 3.1, individual dimensioning of each membrane element of the whole structure does not result in a useful arrangement of the required reinforcement. This can be seen in Figure 3.26, where the distribution for the required reinforcement as calculated automatically by the computer program for the ultimate limit state is plotted. The reinforcement requirements are estimated by dividing the total membrane forces in each element by the design yield stress of steel f_{yd} separately for each element. Thus, the arrangement of the horizontal reinforcement over the depth of the deep beam is similar to the distribution of tensile membrane force. According to Figure 3.26, horizontal reinforcement is also required at the top of the wall in the compression zone. Here, the software assumes a uni-axial compressed member and calculates the required minimum reinforcement.

The same problem exists when the deep beam is loaded at the bottom edge. The amount of vertical reinforcement is calculated correctly (Figure 3.27). However, it must be kept in mind that the vertical reinforcement should not be staggered over the depth of the deep beam in accordance with the vertical tensile force distribution. The external vertical force has to be completely transferred to the top of the deep beam.

In general, an element-wise dimensioning of membranes or shells does not result in a useful arrangement of the required reinforcement. The reason for this is the assumption of linear elastic material behaviour of the concrete when estimating the internal forces. The distribution of the membrane forces in a cracked deep beam is different from an uncracked one. Reinforcing bars that are located in the region of the greatest tensile

Figure 3.27 Horizontal and vertical reinforcement (loading with $q = 152.3$ kN/m at the bottom edge)

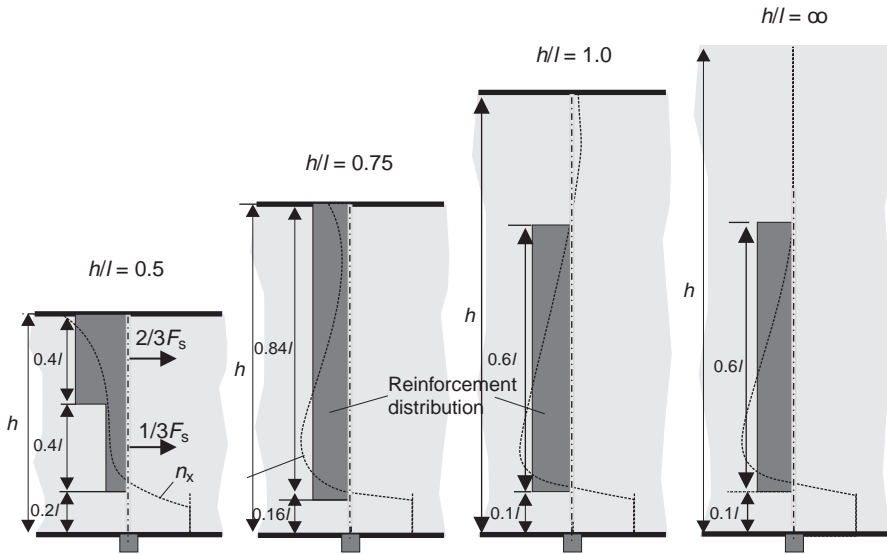


stresses are much more efficient than rebars in regions with less tensile stresses. Reinforcement in the upper part of the tensile zone will only yield under ultimate limit loads if very wide vertical cracks are formed. Thus, the tensile reinforcement of a single-span deep beam (as in an ordinary beam) has to be concentrated at the bottom of the beam and should not be staggered over the depth of the tensile zone, in accordance with the local tensile forces (Figures 3.26 and 3.27).

Furthermore, when detailing the reinforcement of deep beams from an examination of the numerical results, the following has to be considered.

- The horizontal reinforcement in the field should be concentrated at the bottom of the deep beam. The bars should be distributed over a height that is not greater than $0.1l$ or $0.1h$ (l = span length, h = depth of deep beam).
- The tensile reinforcement should not be staggered as per the tensile stresses. It must be anchored at the supports for a force of $0.8F_{t,\text{span}}$ (where $F_{t,\text{span}}$ is the maximum horizontal tensile force in the field).

Figure 3.28 Arrangement of the horizontal reinforcement for the tensile force F_t over the supports of multi-span deep beams
 Adapted from Grasser *et al.* (1991) with permission



- At the intermediate supports of multi-span deep beams, only straight horizontal bars should be used for horizontal reinforcement. These bars can overlap where necessary. The arrangement of the horizontal bars should follow Figure 3.28.
- Half of the required horizontal reinforcement over the intermediate supports should go from support to support without any staggering. The rest should have a length of $2 \times 1/3l$ from the end of the support (without further anchorage length).

Loads acting at the bottom of deep beams, that is, loads acting in the region of a half circle with a radius of $0.5l$ (where $l \leq h$), including the self-weight, should be carried by vertical reinforcement, which must have a length of $l \leq h$.

As can be seen from the preceding list, it is not sufficient to only determine the relevant design forces.

The internal forces of ordinary beams can be estimated by using beam and plane shell elements. This was already demonstrated through some examples in Chapter 2. FE calculations based on linear elastic material behaviour may be useful to determine the flow of forces in discontinuous regions, where the Bernoulli hypothesis is not valid. Examples for this are regions with highly concentrated forces, which occur when anchoring the tendons in prestressed structures, or where there are sudden changes in cross-sectional depths, such as halving joints.

In order to demonstrate the problems in the automatic calculation of the required horizontal reinforcement, the following considers a ‘simple’ single-span beam. The

advantage of this simple structure is that the required reinforcement for the ultimate limit state can be estimated manually by well-known formulae, whereas for the case of deep beams only approximate methods are available.

The single-span beam has a span length of $l=20$ m. A uniformly distributed load of $q_k=20$ kN/m is applied to the structure. The dead load of the structure is neglected. This system is symmetric, and therefore only one half of the structure is modelled in order to reduce the amount of required calculations.

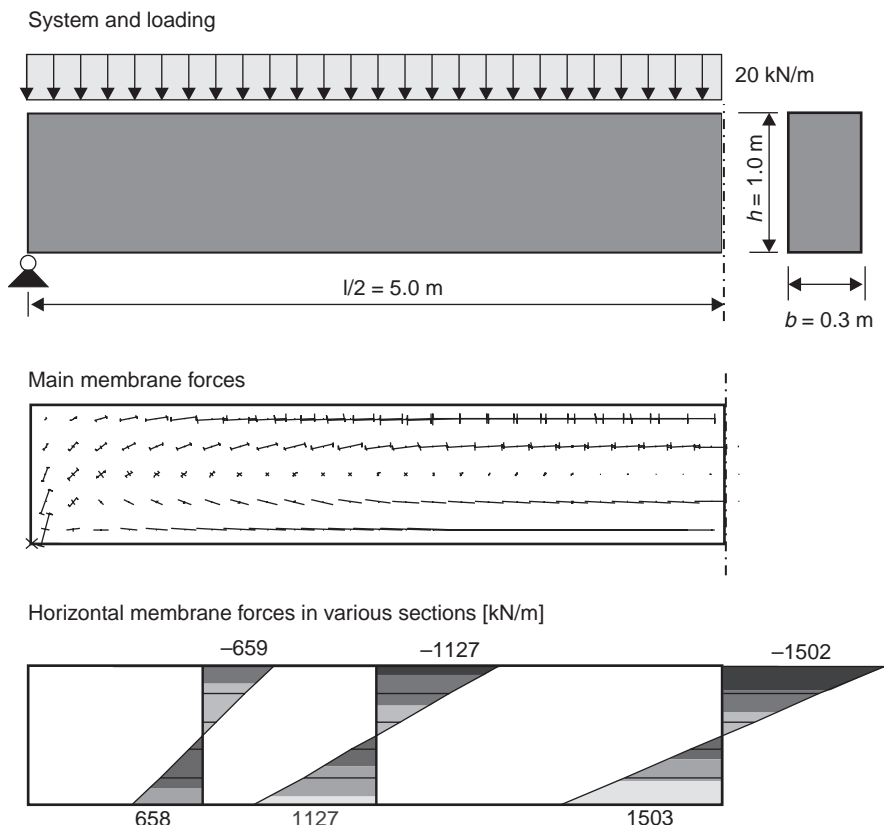
The member forces and the stresses can be simply estimated:

$$M_k = \frac{q_k \cdot l^2}{8} = \frac{20 \cdot 10^2}{8} = 250 \text{ kNm}; \quad \sigma_{\max} = \frac{M}{W} = \frac{0.250 \cdot 6}{0.3 \cdot 1.0^2} = 5.0 \text{ MN/m}^2$$

$$n_{x,\max} = \sigma \cdot b = 5.0 \cdot 0.3 = 1.5 \text{ MN/m}$$

The manually calculated values are in a very good agreement with the resulting forces of the FE analysis (Figure 3.29).

Figure 3.29 Single-span beam: system, loading and main membrane force distribution



A partial safety coefficient of $\gamma = 1.45$ is used for estimating the required bending reinforcement. This gives the required amount of horizontal reinforcement at the midspan (concrete grade C25/30, $f_{yk} = 500$ MPa, $b/d/h = 0.30/0.95/1.0$ m):

$$\text{moment coefficient } \mu_{Eds} = \frac{M_{Eds}}{b \cdot d^2 \cdot f_{cd}} = \frac{250 \cdot 1.45 \cdot 10^{-3}}{0.3 \cdot 0.95^2 \cdot (0.85 \cdot 25/1.5)} = 0.095$$

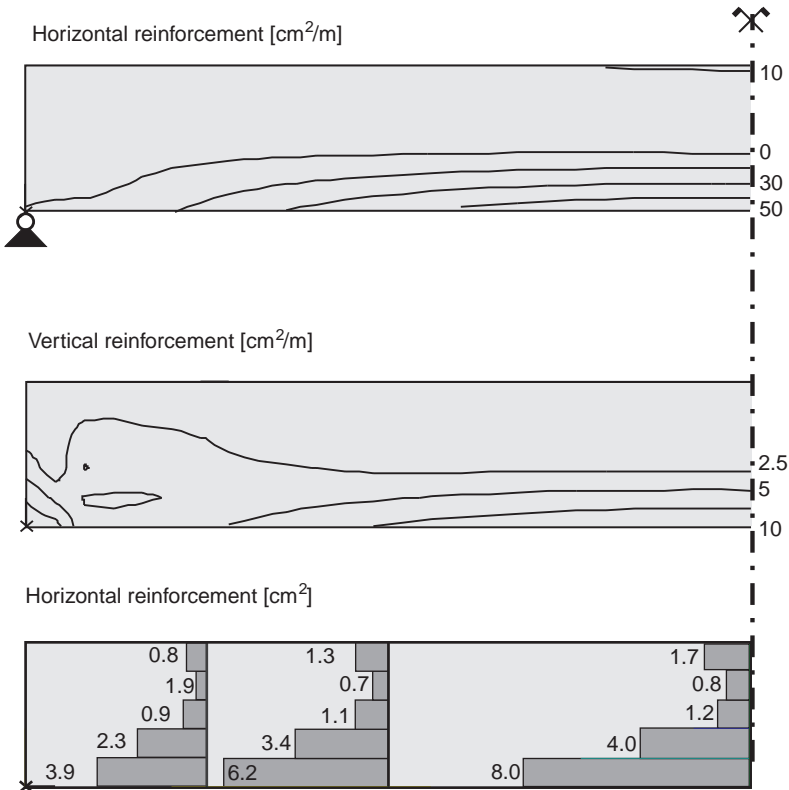
$$\text{inner lever arm } z = (1 - 0.6 \cdot \mu_{Eds}) \cdot d = (1 - 0.6 \cdot 0.095) \cdot 0.95 = 0.896 \text{ m}$$

$$\text{required reinforcement } req A_s = \frac{M_{Eds}}{z \cdot f_{yd}} = \frac{250 \cdot 1.45}{0.896 \cdot 43.5} = 9.3 \text{ cm}^2$$

The computer program estimates the reinforcement in each element separately. For the lowest element, this results in a required horizontal reinforcement of (Figure 3.29):

$$\begin{aligned} req A_s &= (n_{x1} + n_{x2})/2 \cdot (h/5) \cdot \gamma/f_{yd} \\ &= (1500 + 900)/2 \cdot (1.0/5) \cdot 1.45/43.5 \\ &= 8.0 \text{ cm}^2 \text{ (over a depth of 0.2 m!)} \end{aligned}$$

Figure 3.30 Simply supported beam with uniform loading – distribution of the reinforcement calculated by means of a membrane model



Reinforcement for the other elements is shown in Figure 3.30. If one extrapolates the results in the middle of the bottom elements to the lower boundary, the estimated maximum reinforcement $A_{s,required}$ would be greater than $50 \text{ cm}^2/\text{m}$ depth.

The numerical integration of the tensile zone results in a required total reinforcement of:

$$\begin{aligned} req A_s &= (n_{x1} + 0)/2 \cdot (h/2) \cdot \gamma/f_{yd} \\ &= (1500 + 0)/2 \cdot (1.0/5) \cdot 1.45/43.5 \\ &= 12.9 \text{ cm}^2 \end{aligned}$$

Such a numerical calculation not only results in a wrong distribution of the reinforcement, but it is also uneconomical: it overestimates the reinforcement requirements by 39%. This is due to the lever arm of the internal forces of a cracked member which is greater than the one of an uncracked structural element (see Figure 3.31).

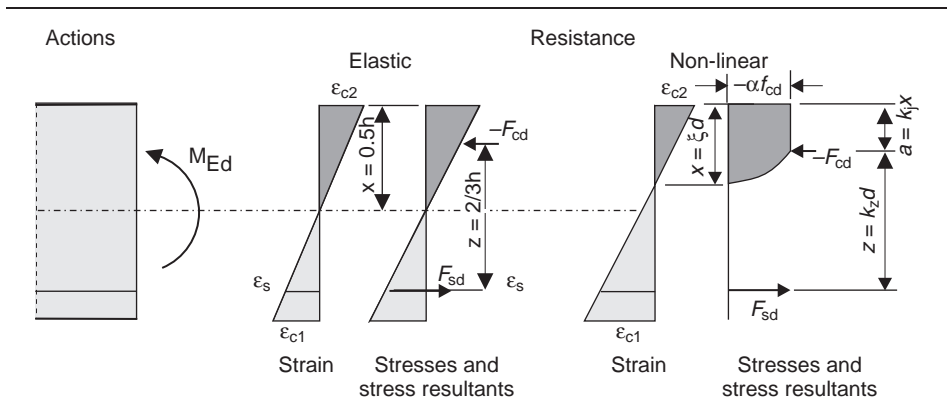
Uncracked member (Stage I): $z = 2/3 \cdot h = 2/3 \cdot 1.0 = 0.667 \text{ m}$

Cracked member (Stage II): $z = 0.896 \text{ m}$ (see preceding calculation)

This is also true for deep beams. The distribution of the vertical reinforcement is shown in Figure 3.30. The estimated area of stirrups in the critical section at a distance of $1.0d$ from the face of the supports is $a_{s,w} = 5 \text{ cm}^2/\text{m}$. This is much greater than the required value calculated by the manual design. According to EC2, stirrups of area $a_{s,w} = 0.9 \text{ cm}^2/\text{m}$ are sufficient to carry the loads in the ultimate limit state.

In addition, the distribution of the vertical reinforcement in the longitudinal direction is incorrect. According to the numerical analysis (Figure 3.30), the vertical reinforcement decreases from the midspan to the supports. This is in contrast to the normal beam theory. In the case of an ordinary single-span beam, the shear forces and, thus, the required shear reinforcement, increases from the midspan to the supports. The reason

Figure 3.31 Strain and stress distribution and internal forces of cracked (elastic) and uncracked members



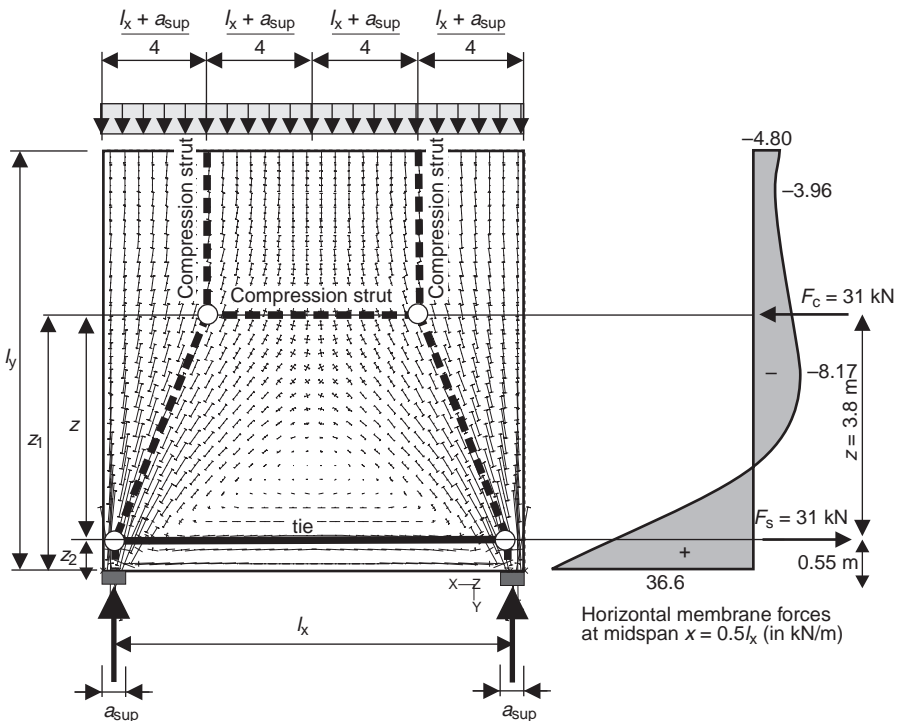
for this error in the shell model is the assumption of linear elastic uncracked material behaviour. The design for shear of a reinforced or prestressed beam is usually based on a strut-and-tie model, with a fully cracked member.

This very simple example of a simply supported beam should demonstrate that the nonlinear material behaviour of concrete, as well as the cracking of the composite material ‘reinforced concrete’, has to be considered in the design. Estimation of the reinforcement requirements by integrating the tensile forces of a linear elastic model may lead to incorrect and even sometimes unsafe values.

3.4. Strut-and-tie models

Even if the internal forces of a cracked member cannot be correctly estimated by means of a linear elastic shell model, as demonstrated by the before mentioned examples, it may be very useful to gain an understanding of the flow of forces in the structure. Linear elastic FE analysis may and should be used as a basis to develop strut-and-tie models. According to EC2, Part 1, the strut-and-tie model and, especially, the location and orientation of the main compression struts, should be similar to that of linear elastic FE analysis to avoid major redistribution of forces and cracking.

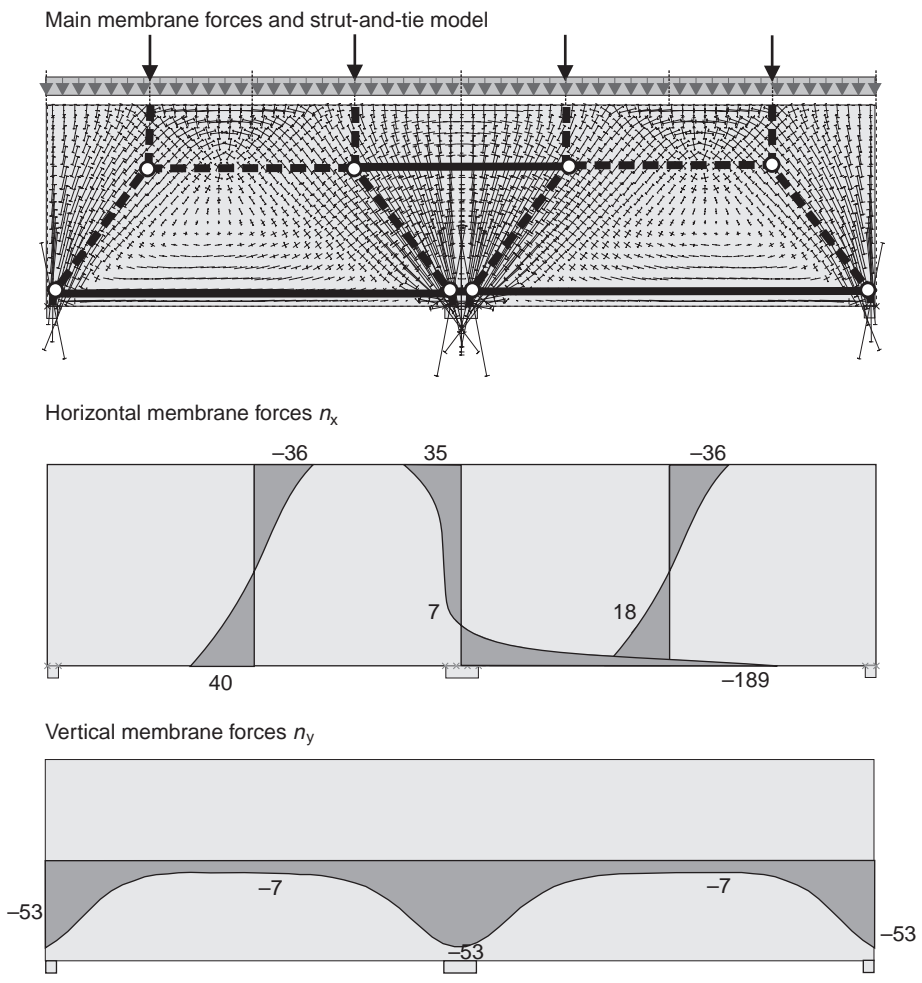
Figure 3.32 Strut-and-tie model for a single-span deep beam



Strut-and-tie models consist of straight compression and tension struts, which are connected by hinges. The truss model should be statically determined and should represent the main force distribution in the member. Schlaich and Schäfer provide further information regarding this design method (Schlaich *et al.*, 1987; Schlaich and Schäfer, 1998). The main principles are explained in the following for a simple single-span deep beam.

At first, one has to determine the force distribution in the member. This can be done by means of the force flow method or linear elastic FE analysis. The strut locations are similar to the main compression stresses. The only unknown in the manual analysis for the given single-span deep beam is the location of the horizontal compression strut and the distance z_1 and z_2 , respectively (see Figure 3.32). The horizontal compression

Figure 3.33 Two-span deep beam ($= 2 \times 7.5/3.65$ m)



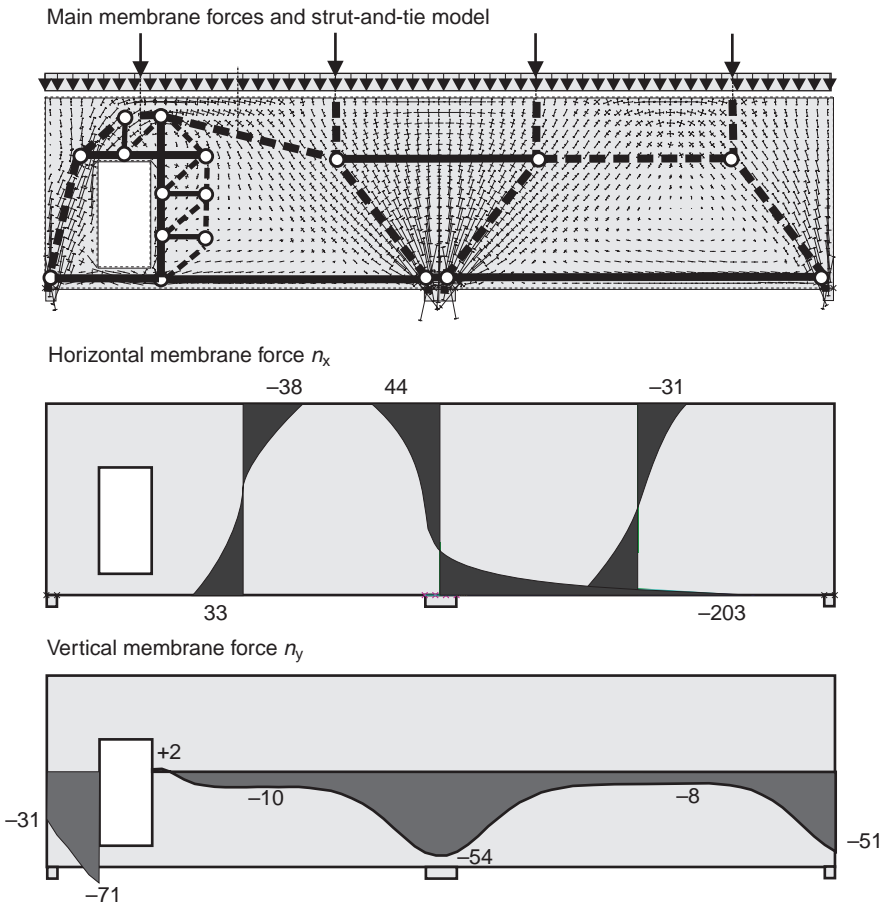
and tension struts are located in the centre of the stress field at the midspan. Thus, the increase of the lever arm of the cracked member under ultimate loads is neglected. The strut-and-tie model is a statically determined truss structure. Thus, all forces can be estimated based on the geometry of the truss system only. The resulting tensile force for the given structure ($l_x = l_y = 7.20$ m; $a = 0.24$ m; $q = 20$ kN/m) is:

$$F_t = \frac{l_x - a}{4} \cdot \frac{q \cdot l/2}{z} = \frac{7.20 - 0.48}{4} \cdot \frac{20 \cdot 7.2/2}{3.8} = 31.8 \text{ kN}$$

The calculated force is nearly identical to the value given in Grasser *et al.* (1991). There is a small difference of 3 kN only (see Table 3.1).

In the preceding example, the reinforcement requirements are estimated from the resulting tensile forces. However, as will be shown later, this reinforcement can be inadequate with respect to the serviceability of a structure. Figure 3.33 shows the

Figure 3.34 Two-span deep beam ($l_x/l_y = 2 \times 7.5/3.65$ m) with an opening



distribution of the main membrane forces and the resulting strut-and-tie model for a two-span deep beam ($l_x/l_y = 2 \times 7.5/3.65$ m). The model is nearly identical to that of a single-span deep beam. The tensile force at the intermediate support is the only addition to be considered. The tensile reinforcement at the midspan must not be concentrated at the centre axis of the tensile zone, but at the bottom of the deep beam.

Figure 3.34 shows the same system with a small opening near to the left support. Here, the reinforcement calculated from the resulting tensile forces is insufficient. A linear elastic calculation does not show any vertical tensile forces near the opening. This is in contrast to engineering practice and contradicts with the strut-and-tie model. Vertical reinforcement is required.

Therefore, the nonlinear behaviour of the material has to be considered when developing a strut-and-tie model.

3.5. Singularities

In shell systems, infinite stresses and deformations (singularities) may be calculated, which are caused by the assumptions of the numerical model. Examples of these singularities are (see Figure 3.35, Table 3.4)

- corners (free or fully restrained)
- concentrated loads or pin supports.

An FE analysis will always estimate finite results, whereby the maximum stress will increase considerably with any decrease in the element size. The ‘exact’ calculation of

Figure 3.35 Singularity regions in walls and deep beams

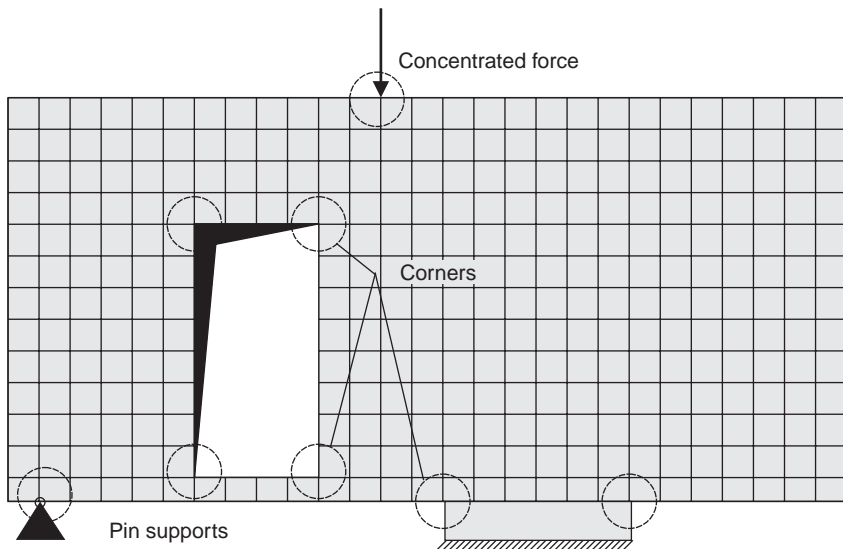
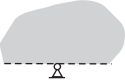
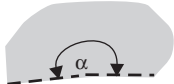

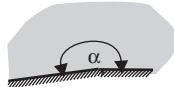
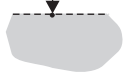

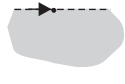
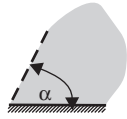






Table 3.4 Singularity regions in plane shell structures (walls and deep beams)

Reactions resp. forces	Displacements	Stresses	Support condition	Stresses infinite for
	Yes	Yes		$\alpha > 180^\circ$
	No	Yes		$\alpha > 180^\circ$
	Yes	Yes		$\alpha > 63^\circ$
	Yes	Yes		
	No	No		
	No	Yes		
	No	(σ_x)		
	No	No		
		No		

the maximum value of the stresses is generally not required, as the problems are caused by the simplifications of the numerical model, an inaccuracy of the boundary conditions. A real structure does not show any singularities. In the case of high stresses, the material will ‘yield’. In tensile regions, the concrete will crack. Furthermore, in discontinuity regions, the stress distribution is a complex 3D one that will not be modelled with plane shell elements. The main concern will be the good detailing of the reinforcement in the corner regions and in the area of concentrated loading.

Numerical problems with concentrated loads can be avoided if the width of the loaded area is considered. The same is true for pin supports. However, any refinement of the numerical model is generally not required, as the stress distribution in these regions is not needed for the design.

REFERENCES

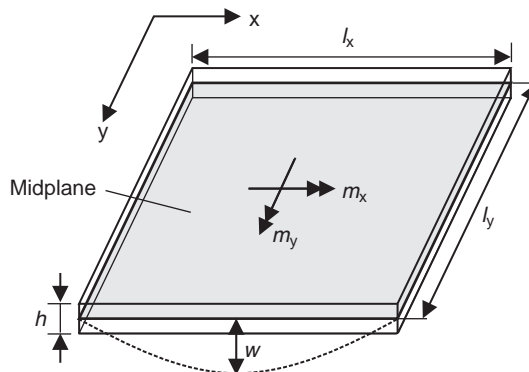
- CEN (European Committee for Standardization) (2004) Eurocode 2, Part 1: Design of concrete structures – General rules and rules for buildings. December.
- Comité Européen du Béton (1970) *Recommendations for design and construction of concrete structures, Appendix 3*, London, June.
- Fédération Internationale du Béton (fib) (2007) Practitioners' guide to finite element modelling of reinforced concrete structures. FIB-Bulletin No. 45, Lausanne, November.
- Grasser E *et al.* (1991) Hilfsmittel zur Berechnung der Schnittgrößen und Formänderungen von Stahlbetonbauwerken; Deutscher Ausschusses für Stahlbeton Heft 240. Berlin.
- Schlaich J and Schäfer K (1998) *Konstruieren im Stahlbetonbau*. In *Betonkalender* (Eibl J (ed.)), part II, Berlin.
- Schlaich J *et al.* (1987) Towards a consistent design of structural concrete. *PCI Journal*, May–June: 77–150.

Chapter 4

Slabs

4.1. General

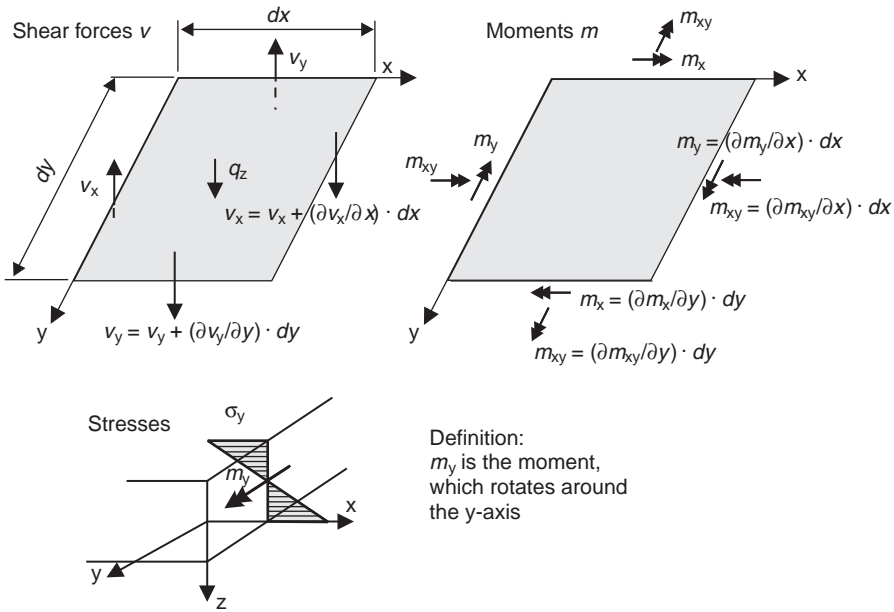
Slabs are thin plane spatial surface structures that are only loaded perpendicular to their middle plane and where the minimum panel dimension is greater than five times the overall slab thickness (Eurocode 2, 2004). The internal forces in slabs are the bending moments m_x and m_y , twisting moment m_{xy} and shear forces v_x and v_y per unit length (see Figure 4.1). Normal forces on the middle plane are not considered in this approach; however, they can be taken into account by an additional shell analysis (diaphragm). It should be noted that the linear combination of various load cases is only permissible if the structural behaviour is fully linear elastic (Stage I, tensile stresses in the concrete $\leq f_{ctk;0.05}/\gamma_c$). Owing to the mentioned basic model assumptions, normal forces are not even estimated if a slab is fully restrained: the middle plane is always stress-free. In addition, the following assumptions are generally used



- thin slab: $h \ll l$; vertical stresses $\sigma_z = \tau_{xz} = \tau_{yz} = 0$; h = depth of slab = constant
- small vertical displacements ($w \ll h$; first-order theory)
- linear strain distribution over the section depth (Navier)
- no strains at the middle plane (i.e. no normal or membrane forces)
- stresses in normal direction can be neglected
- plane sections remain plane before and after loading (Bernoulli-Euler).

The basics of a plate analysis are not mentioned any further in this book as extensive information on this topic has already been published (e.g. see Girkmann 1978; Timoshenko and Woinowsky-Krieger, 1959).

Figure 4.1 Internal forces and stresses of a finite plate element

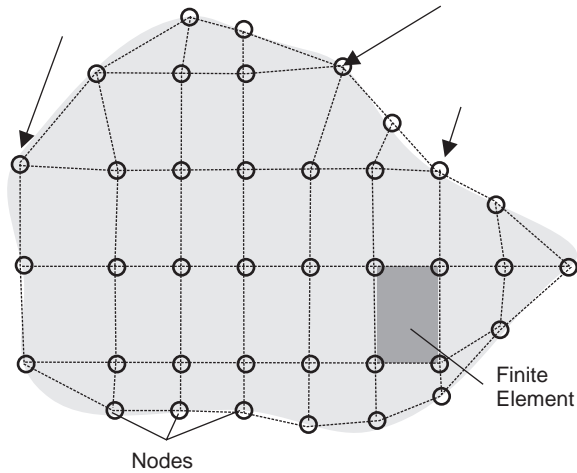


An analytical solution of the partial differential equation $\Delta w = q/K$ (Kirchhoff slab equation; where K is the flexural rigidity of the plate $K = [E_c h^3]/[12(1 - \nu^2)]$) is only possible for axisymmetric structures and loading, like circular slabs. The shear forces and moments of rectangular slabs can only be estimated by means of numerical methods. The Kirchhoff slab equation was solved by Fourier analysis or finite difference approximations (Girkmann, 1978; Stiglat and Wippel, 1983) and various weighted residual procedures before efficient computer hardware and software were available. Nowadays, FEM is generally used, as it is more flexible with regard to the boundary conditions and load arrangements as compared to the finite difference method.

Slabs can be analysed manually by means of the strip method. In this approach, the 2D load transfer is simplified to two ordinary beams or a grillage system. This simple method is still applied to this day, as has been shown in Section 2.8. Nevertheless, the 2D behaviour of slabs (dispersion of loads) is represented much more accurately by FE models using plate and shell elements.

In recent years, FEM has become a standard tool for the analysis of spatial structures. The practical applications have dramatically increased with the significant improvements of the software. The graphical pre- and post-processing makes it fast and easy to handle whole buildings, including all slabs, walls, columns, and foundations, within one big numerical model. Also, the hardware has become much faster. However, complex FE models include a big danger, as the collapse of the Sleipner platform has impressively

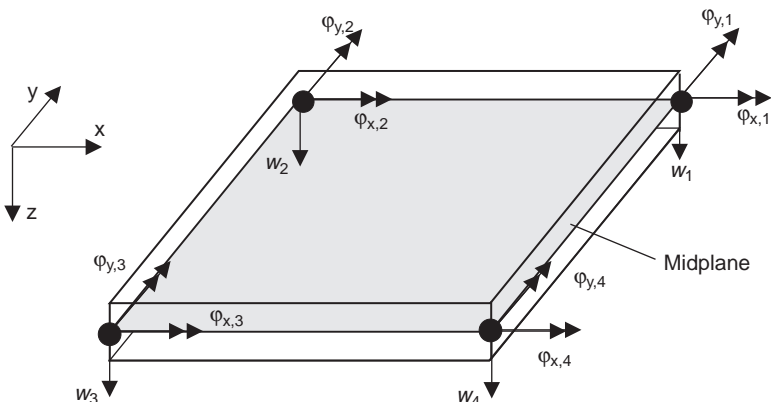
Figure 4.2 Discretisation of a slab



demonstrated (see Section 5.1.1). Therefore, only simple flat slabs will be mentioned in the following.

In FEM, the slab is divided into small FEs (discretisation of a continuum), which are connected to each other by their nodes (Figures 4.2 and 4.3). The deflections, strains and internal forces within an element are interpolated from the node displacements by means of so-called form functions, which are mostly polynomials. The form function may but must not fulfil the compatibility conditions at the boundaries between the elements. Therefore, the deformations, strains and stresses, as well as the internal forces, may be discontinuous between the elements. The difference of the stresses at the boundaries of the elements may be used to verify the quality of the FE model.

Figure 4.3 Degrees of freedom of a four-node plate element



A detailed description of the basis of FEM is explained in various literatures (for example, Bathe, 1982; Hughes, 1987; Zienkiewicz and Taylor, 1989). Therefore, no further theoretical information regarding the theory is provided here.

The required effort to generate an adequate FE model has decreased dramatically due to the availability of user-friendly graphical pre-processors. In the near future, it may even be possible to perform the analysis and design of the slab for a ‘simple’ one-storey residential building (such as the one shown in Figure 4.4) by means of the FE techniques instead of manual analysis. Therefore, one may worry that FE software will be more and more used by designers without a proper understanding of the method and experience in design of concrete structures. This problem becomes even worse as a main advantage of FEM is that the user does not have to simplify the load transfer of a structure as by manual analysis. Therefore, young engineers without structural experience tend to use the numerical method. This may lead to mistakes in the results that may even cause the collapse of a structure (see Section 5.1.1).

It should always be kept in mind that a numerical model is only a simplification of reality. It is only as accurate as its basic assumptions. Therefore, it must be especially understood that the usage of FEM requires experience in numerical modelling.

When using FEM, the following items should always be checked

- *correct modelling of the support conditions*
 - pin and simple line supports
 - girders (joists)
 - flush beam strips in slabs
 - support by masonry, concrete walls and columns, or elastomer bearings
 - slab monolithically fixed to the supports or free to uplift
 - discontinuous simple support (supporting walls which end within the slab)
 - continuously supported on ground
- *location and orientation of the fixed nodes*: relevant in the case of curved boundaries
- *singularities*: regions where the internal forces and deflections of a slab may become infinite
- *size of elements*: the element size should be checked in regions with high deformation and stress gradients
- *numerical – mechanical models*: form functions; polynomial functions of first or higher order – Kirchhoff or Reissner/Midlin models

It is not necessary to use complex structures to demonstrate the problems of FEM. Even the slab of a simple one-storey residential building (Figure 4.4) is sufficient. The manual design of this slab can be easily and quickly performed by means of the strip method. Therefore, this structure is only used here to demonstrate the problems of FEM.

The real system is simplified for an FE analysis. A simple line support is assumed underneath all supporting walls (breadth of support neglected), whereby small openings like

that of doors or windows are neglected. The slab thickness is $h=0.18$ m. Concrete grade C20/25 is assumed for the building material. The slab is discretised by 451 plane plate elements. Figures 4.4a–d show the internal forces and deflections for a uniformly distributed load of $g_d=5.0$ kN/m². For simplicity, the most unfavourable arrangements of live loads are not considered here. Very high bending moments and shear forces can be observed in axis B-2 and B-3. The slab cannot be designed for these high member forces. Even an inexperienced user can recognise this problem. The structural engineer has to know that the design for such high internal forces is not required. These peaks are caused by simplifications of the numerical model (singularities; see Section 4.12). In the following sections, such problems in the model for reinforced concrete slabs will be discussed with emphasis on the accurate representation of the support conditions.

Most engineers believe that a ‘complex’ numerical calculation saves reinforcement, where the structural system is modelled with greater accuracy than in a manual design. This is very often not the case. A comparison between the manual and the FE design of the slab shown in Figure 4.4 has resulted in a very small or negligible difference in the amount of reinforcement required. Thus, this simple example demonstrates that a more detailed design may not be economical, when considering the great effort required for a numerical analysis and the resulting labour cost of the designer.

Figure 4.4 Slab of a simple one-storey residential building

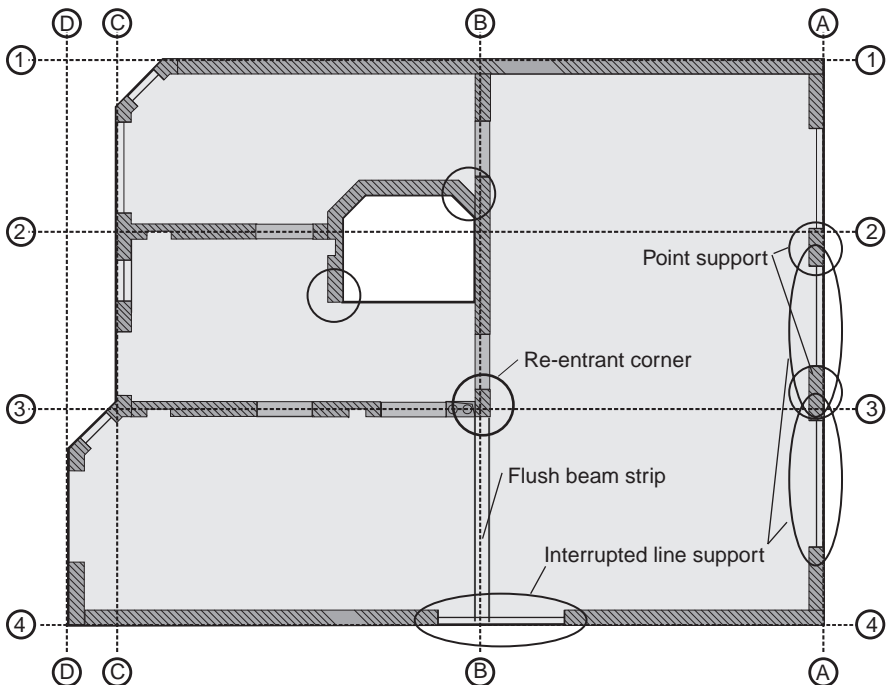


Figure 4.4a Deflections in mm (linear elastic material behaviour)

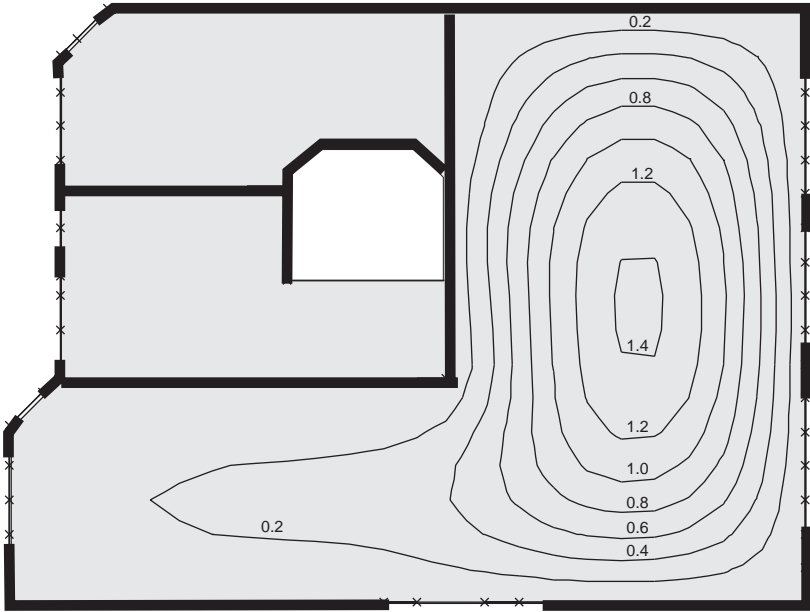


Figure 4.4b Tensor plot of the principal bending moments

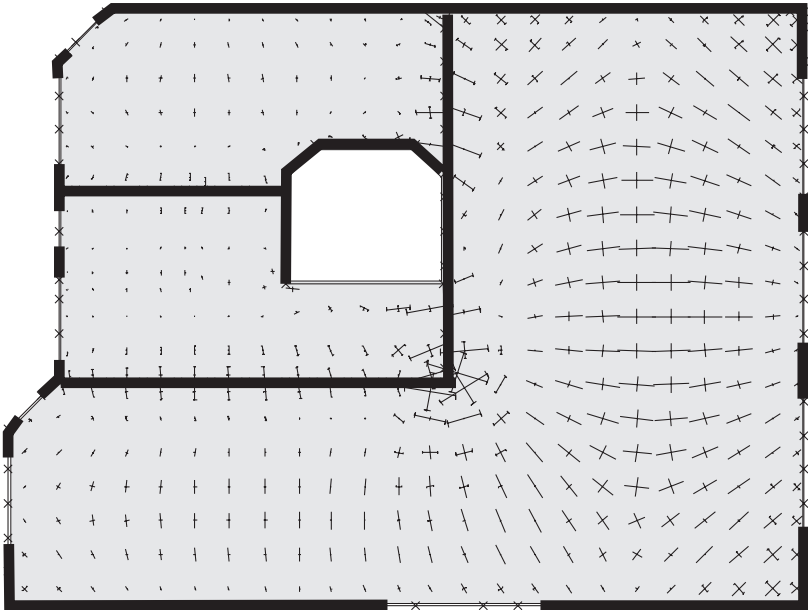


Figure 4.4c Contour plot of the principal bending moment m_l in kN/m

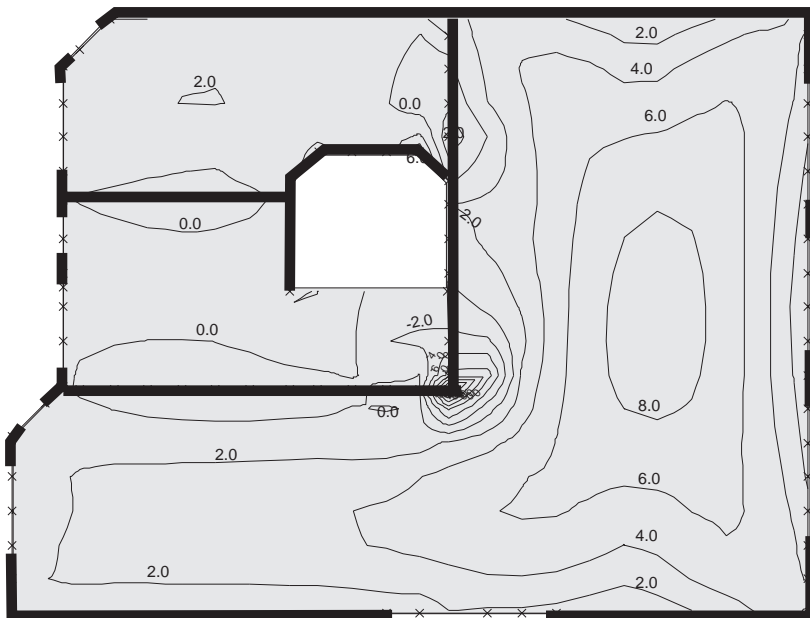
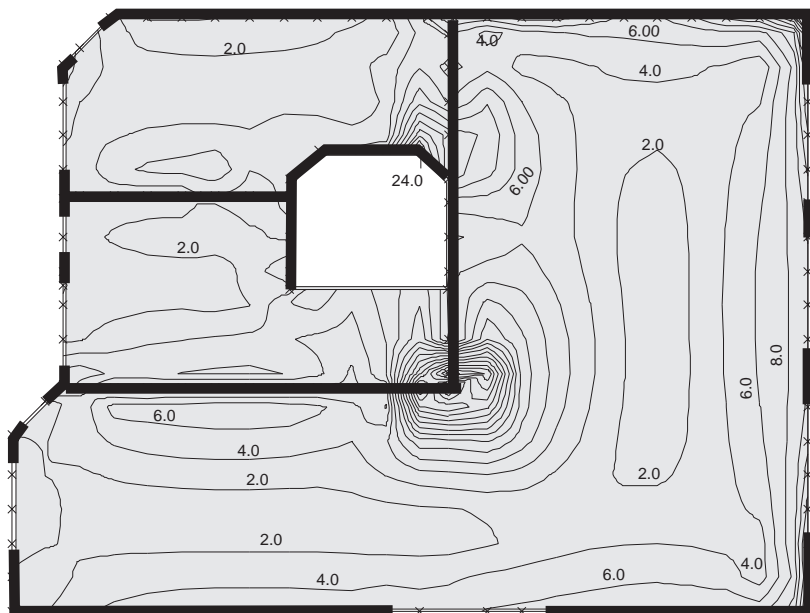


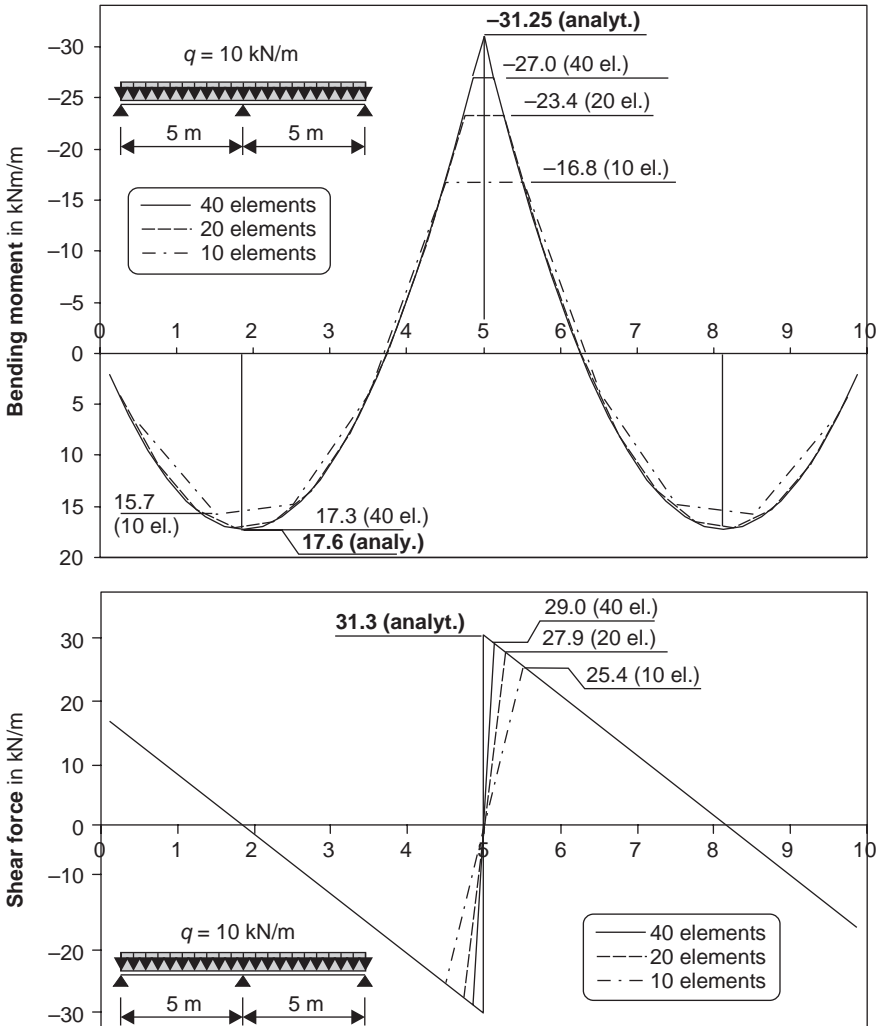
Figure 4.4d Principal shear force $v = \sqrt{v_x^2 + v_y^2}$ in kN/m



4.2. Meshing – size of elements

With the structural software available nowadays, the number of elements is almost unlimited. The size of the FE model is restricted mainly by the amount of time the computer needs to solve the global element stiffness matrix and to design the members for the various load cases. Hence, even nowadays, a structure will be modelled with the minimum number of elements. Nevertheless, a too coarse mesh can lead to significant errors. This problem will be illustrated by means of a one-way slab. The bending moments and the shear forces for 5–20 elements per span (four-noded elements, linear deflection) are shown in Figure 4.5. It can be seen that, in the case of constant loading, the member forces are nearly independent of the number of elements.

Figure 4.5 Member forces of a one-way slab for different numbers of FEs



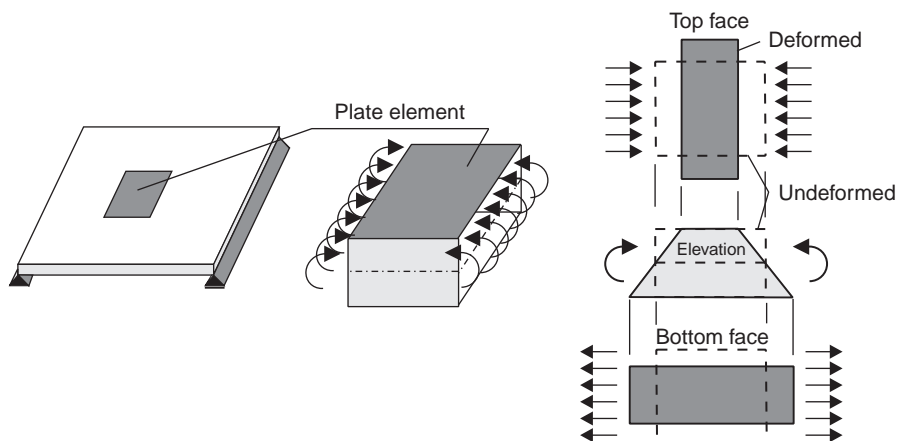
The greatest field moment with five elements is 11% less than the 'exact' analytical value only. Nevertheless, this small difference does not apply for support areas or near single forces and area loads. Here, very high gradients in the member forces appear, which cannot be modelled by a coarse mesh. Furthermore, it is to be noted that an FE program based on four-noded elements calculates the member forces and the reinforcement mostly in the centre of the elements only. Hence, with a coarse discretisation, the moment peak in midspan is cut off (Figure 4.5). This can result in a considerably unsafe design near the inner supports. Similar problems also appear with flat slabs.

4.3. Material parameters – Poisson's ratio

The analysis of a slab is usually based on a linear elastic isotropic behaviour of the building materials. The nonlinear behaviour of concrete and its reduction in stiffness in the case of crack formation are neglected. With this simplification, only two different material parameters, the modulus of elasticity E_c and Poisson's ratio ν , are needed in the design. The modulus of elasticity can be taken either from tests or from codes (Eurocode 2, 2004), whereby the creep effect has to be taken into account. Poisson's ratio ν is not an exact value for reinforced concrete. Values varying from $\nu = 0.0$ and $\nu = 0.2$ are generally used.

The Poisson's ratio ν is defined for an elastic member as the ratio between the lateral strain and the axial strain. According to EC2 (Eurocode 2, 2004: Section 3.1.3), the Poisson's ratio in an uncracked compression region of the cross-section may be taken as $\nu = 0.2$, which is the mean value of a 'homogeneous' uncracked concrete under compression. In the tension zone, ν may be assumed to be equal to zero. However, this information is not very helpful as a slab under pure bending always has a compression and a tension zone (Figure 4.6).

Figure 4.6 Strain in transverse direction of a linear elastic plate element under bending (one-way slab)



Bittner (1965) has conducted theoretical investigations to determine the correct value for Poisson’s ratio. He proposed that a value of $\nu=0.0$ should be used in the design of reinforced concrete slabs. With this value, the compressive stresses are underestimated. This is not mostly critical, as the compressive stresses are usually not relevant in the design.

So, the structural engineer can choose any value for ν between 0.0 and 0.2 for the design. The influence of the Poisson’s ratio on the internal forces will be discussed in the following box.

Internal forces according to the Kirchhoff theory

$$m_x = -K \cdot \left(\frac{\partial^2 w}{\partial x^2} + \nu \cdot \frac{\partial^2 w}{\partial y^2} \right) \approx m_x^{\nu=0} + \nu \cdot m_y^{\nu=0} \quad m_{xy} = -K \cdot (1 - \nu) \cdot \left(\frac{\partial^2 w}{\partial x \partial y^2} \right)$$

$$m_y = -K \cdot \left(\frac{\partial^2 w}{\partial y^2} + \nu \cdot \frac{\partial^2 w}{\partial x^2} \right) \approx m_y^{\nu=0} + \nu \cdot m_x^{\nu=0} \quad \nu_x = -K \cdot \left(\frac{\partial^3 w}{\partial x^3} + \nu \cdot \frac{\partial^3 w}{\partial x \cdot \partial y^2} \right)$$

$$F_e = 2 \cdot m_{xy} = 2 \cdot (1 - \nu) \cdot F_e^{\nu=0} \quad \nu_y = -K \cdot \left(\frac{\partial^3 w}{\partial y^3} + \nu \cdot \frac{\partial^3 w}{\partial x^2 \cdot \partial y} \right)$$

where:

$$K = \frac{E_c \cdot h^3}{12 \cdot (1 - \nu^2)} = \text{flexural rigidity of the slab} \quad w = \text{deflection of the slab}$$

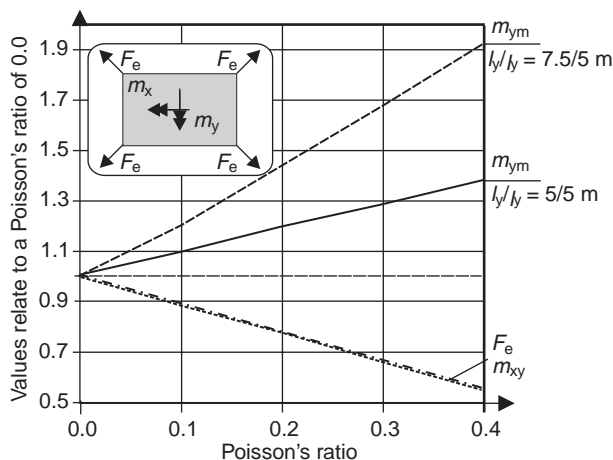
$$F_e = \text{corner tie-down force (uplifting)} \quad \nu = \text{Poisson’s ratio}$$

The Kirchhoff plate theory leads to the following expressions, which show the influence of the Poisson’s ratio on the bending moments, the shear forces and the corner tie-down force.

Based on these expressions, the bending moments m_x and m_y are proportional to Poisson’s ratio ν . When ν is decreased, the twisting moment m_{xy} and the corner tie-down force F_e are reduced.

The simplified expressions are verified by a parametric study on a rectangular simply supported slab ($l_x = 5.0$ m, $l_y = 5.0\text{--}7.5$ m and $h = 0.20$ m), as shown in Figure 4.7. The internal forces have been estimated for different Poisson’s ratios by means of FEM. The midspan bending moment m_{ym} is oriented along the longer panel dimension, and increases almost linearly with an increasing Poisson’s ratio. This agrees with the expressions listed earlier. With an increase in Poisson’s ratio, the twisting moment m_{xy} and the corner tie-down force F_e decrease linearly. The bending moment m_x and the shear forces are not shown in Figure 4.7, as they are only slightly affected by Poisson’s ratio. The maximum shear force at the support at midspan decreases by less than 10%, if Poisson’s ratio increases from $\nu=0.0$ to $\nu=0.4$. The maximum deflection at midspan is approximately reduced by 20%.

Figure 4.7 Bending moment m_y , twisting moment m_{xy} and corner tie-down force F_e for different Poisson's ratios ν ($l_x/l_y = 5.0/5.0$ m and $5.0/7.5$ m, and $h = 0.20$ m)



In slabs, the secondary transverse reinforcement should not be less than 20% of the principal reinforcement (Eurocode 2, 2004). Thus, the value of the Poisson's ratio is often not critical. However, this minimum transverse reinforcement has to be considered in the FE design of slabs.

4.4. Support conditions for slabs

Modelling of the support conditions of slabs should be done with great care, as they have a significant effect on the results.

The following support conditions may occur in practice

- continuous support of the whole slab or part of it by the ground
- knife-edge (line) support on walls – free to uplift or fully or partially restrained
- pin support on columns, for example, flat slabs.

Normal and shear forces, as well as bending moments, can be transferred if the slab is monolithically connected to the support. The stiffness of the support can be represented either by individual springs or by special boundary elements. In both cases, the rotational stiffness of the springs should be determined with regard to the nonlinear material behaviour of the concrete and the reduction of stiffness in the case of crack formation.

Where the supports have different vertical stiffness values, any possible deflection of the supports should be considered. This can be the case for flat slabs that are supported by columns with different cross-sections, normal forces or building materials. Slabs usually have only a small bending stiffness. Thus, the influence of the differential deformation on the internal and support forces can be mostly neglected.

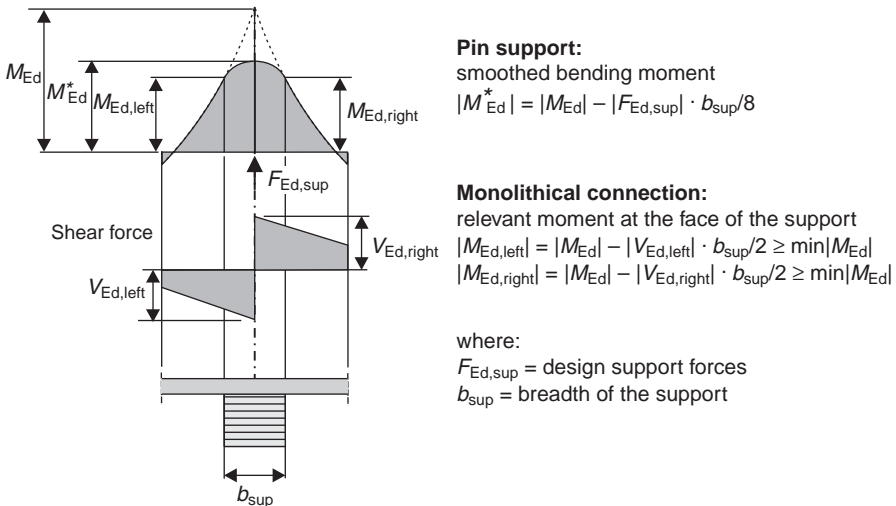
If the slabs are supported on different building materials, having different time-dependent properties, such as aerated concrete brick and clay brick walls, then the time-dependent deformations of the supports (e.g. due to creep or shrinkage) should be considered in the analysis. A wall made of gypsum blocks – or sand-lime concrete – may become shorter with time, whereas the height of a clay brick wall remains nearly constant. Differential settlements of the foundations should be considered if relevant.

Various numerical models are used in practice to describe the support conditions of slabs. These may result in rather different internal forces in the restrained regions. However, one should not compare the maximum peak values. Only the bending moments and shear forces in the sections, which are relevant for design of concrete slabs, should be used.

The peak bending moments and shear forces over the centreline of an intermediate support are generally not relevant in the design. In the case of a stiff monolithic connection between the slab and the supported columns or walls, the design in bending is carried out for the forces at the face of the support. If the slab is restrained in vertical direction only, for example, it is supported on block or brick walls, the maximum design bending moment is calculated from the values at the face of the supports and smoothed parabolically (see Figure 4.8).

The relevant section for shear design is either the face of the support, in the case of indirect supports, such as support on upstand beams, or at a distance of $0.5\text{--}1.0d$ from the face for direct supports (d =effective depth of the slab). The slab should be designed for punching in regions of concentrated single loads or pin supports by columns and not for the high resultant shear forces. To summarise, the maximum values and the

Figure 4.8 Relevant sections for design in the support region



distribution of the bending moments and shear forces over the supports are generally not required for the design of concrete slabs.

Therefore, in the following comparison calculations, only the values that are relevant for the design are considered.

First, the various possibilities of modelling a ‘hinge’ line support are examined for a simple one-way slab. This simple structure is used since the member forces from a beam system can be used to check the numerical results. The outcome of this investigation will then be used to determine the ‘accurate’ model of flat slabs, where analytical solutions are not available.

4.5. One-way slab

The following analysis will be carried out on a two-span, simply supported, one-way slab having equal span length of 2×5.0 m (Figure 4.9). The slab has a constant depth of $h = 0.20$ m. The intermediate support has a breadth of 25 cm. For this simple structure, the internal forces can easily be estimated by manual calculations (see Figure 4.10). These values will be used to verify the numerical results.

Two different load cases are considered in the analysis

- load case 1: uniform loading of $q = 10$ kN/m² on both spans
- load case 2: uniform loading of $q = 10$ kN/m² on the left span only

The different models for a support on walls that are used in practice are shown in Figure 4.11.

- (a) *3D model of the whole structure (column and walls) by volume elements:* If the whole structure behaves as linear elastic, then the load-bearing behaviour of the system is modelled with great accuracy by means of volume elements. The nonlinear strain distribution in the support region (discontinuity region) is considered in this model. However, the assumption of an uncracked section over the intermediate support is not valid, as it is very likely that the tensile stresses

Figure 4.9 System

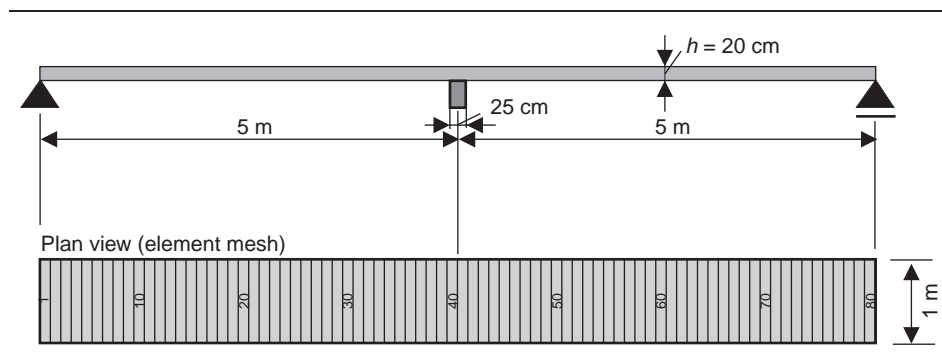
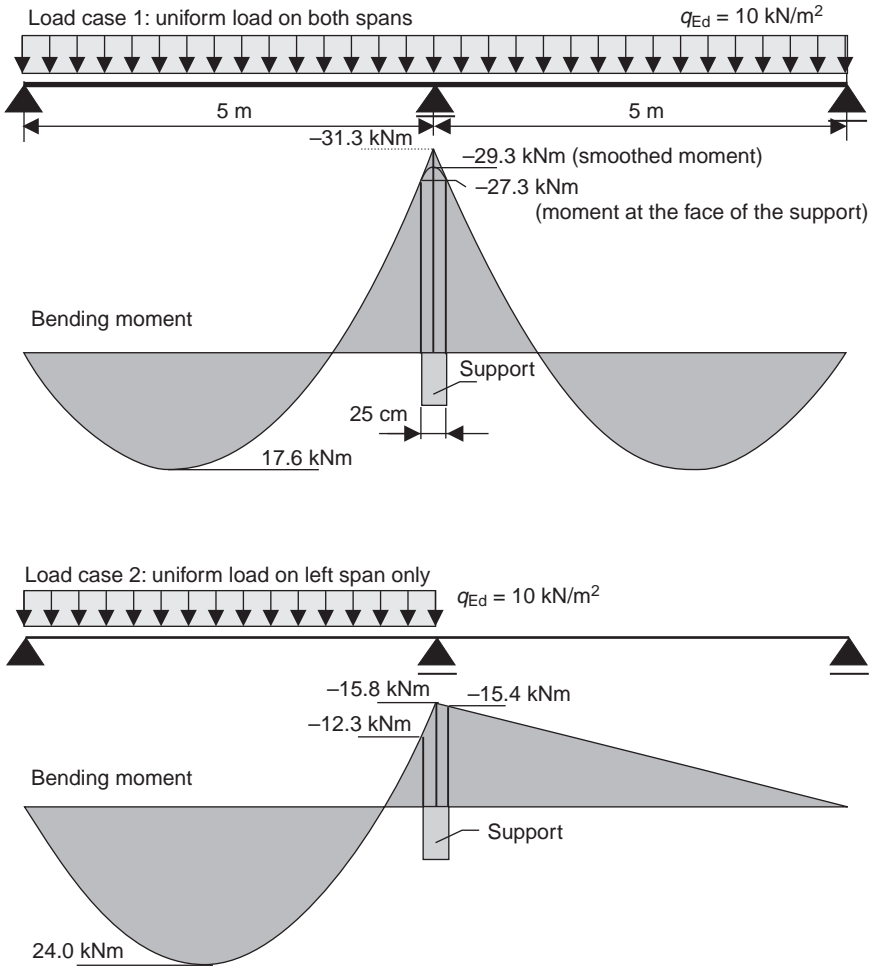


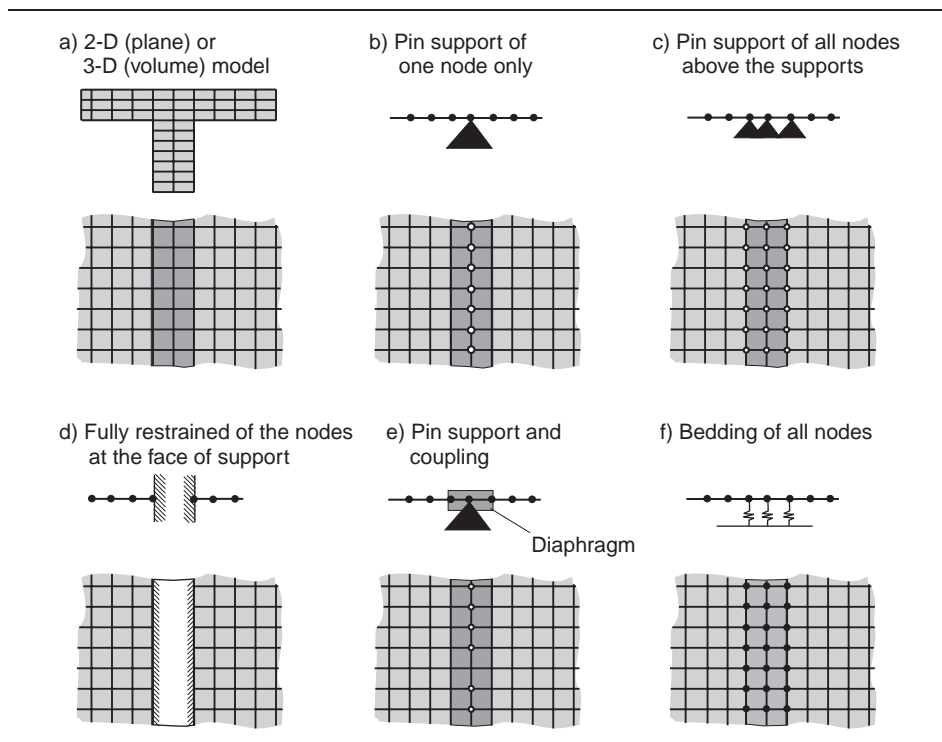
Figure 4.10 Loading and bending moments – manual beam analysis



exceed the tensile strength of the concrete. Moreover, great effort has to be taken to handle a 3D volume or even a 2D shell model, which is often not required. It should be noted that the problems arise when the reinforcement requirements are being estimated. Therefore, in practice, a 3D shell or volume model is very rarely used.

- (b) *Pin support of one node*: The node in the centre of the support is restrained in the vertical direction, as in a beam model.
- (c) *Pin support of all nodes at the support – restrained in vertical direction only*: This model is sometimes used to consider the breadth of a very rigid wall.
- (d) *Fully restrained of all nodes at the supports*: The vertical deformation as well as the rotation of all nodes at the support are completely restrained. The elements over the support are, therefore, free of stresses and show no internal forces.

Figure 4.11 Models for line support of slabs



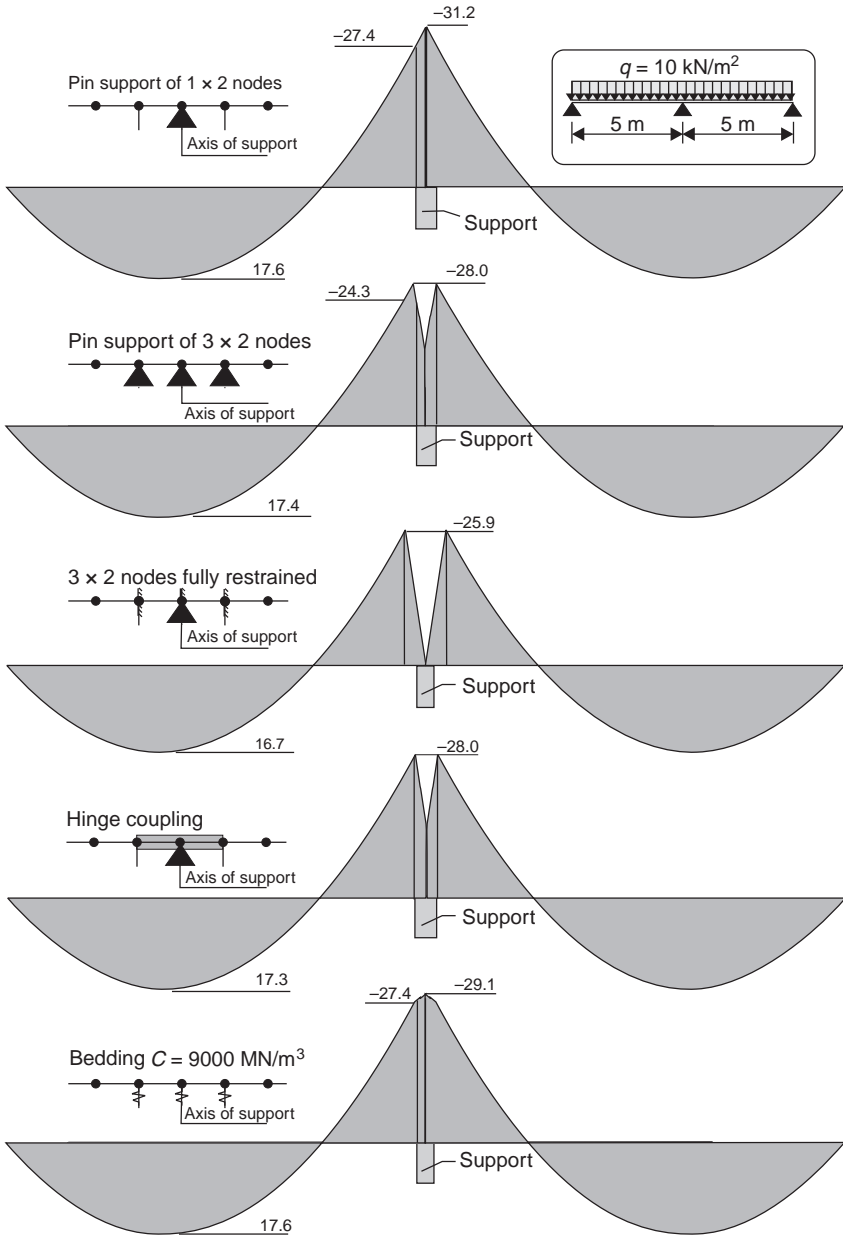
- (e) *Coupling of nodes*: The nodes at the support are coupled with the node in the centre of the support to simulate an infinite stiff element that can rotate around the centre node. This model has already been discussed in Section 2.6.3.
- (f) *Bedding of the supported elements*: The elements over the wall are elastic supported. A flexible, plane support is simulated.

The different bending moment distributions, resulting from the models described earlier, are shown in Figures 4.12 and 4.13. The relevant results are further summarised in Table 4.1.

Model B (pin support of one node only) gives a good correlation between the beam and the FE (plate element) results for both load cases. Any further refinement of the element mesh does not change the results. Knife-edge-supported one-way slabs do not show any singularities.

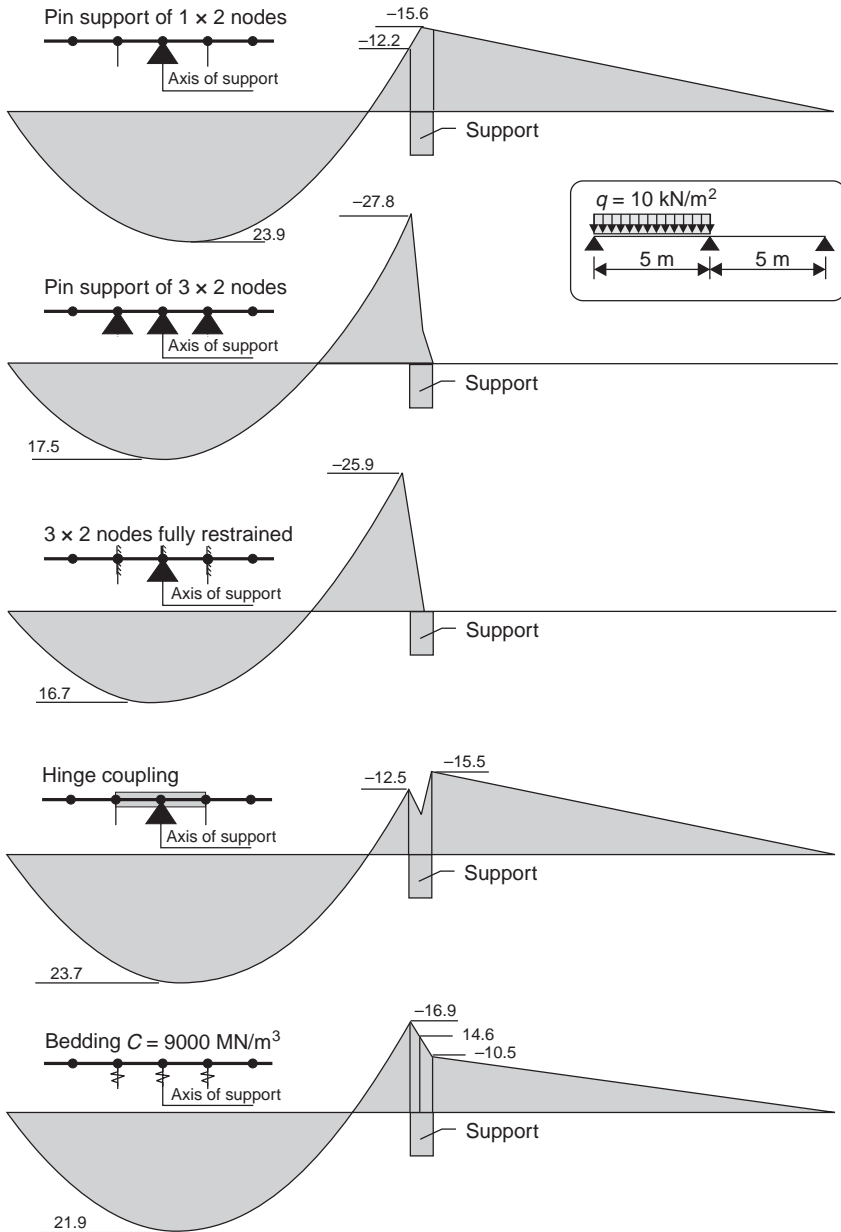
If three nodes are fixed in a vertical direction at the support (Model C), the resulting bending moments at the face and those at the centre of the support are underestimated for uniform loading over both spans by 89% and 47%, respectively. On the other hand, if only one span is loaded, the support bending moment is overestimated by 226%.

Figure 4.12 Bending moments – uniform load at both spans – plate elements



Therefore, this model should not be used. A further refinement of the element mesh would result in a fully restrained intermediate support. Doubling the number of elements increases the bending moments by 15% ($M_{\text{sup,face,max}} = -28.1 \text{ kNm/m}$). The influence of the element size decreases by 1%, when only one span is loaded.

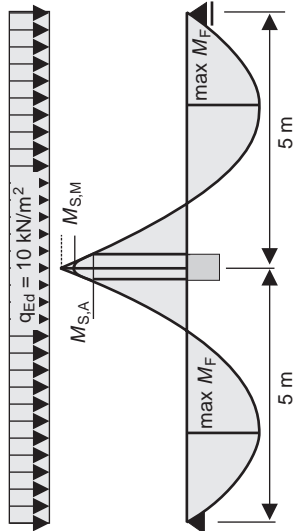
Figure 4.13 Bending moments – uniform load at left span only – plate elements



The results of Model D (all nodes at the supports are completely restrained) show little difference from those of Model C. The internal forces of the elements over the support become zero, as the nodes can neither move nor rotate. Furthermore, there are no bending moments or shear forces in the unloaded part of the structure. Therefore,

Table 4.1 Bending moments

Uniform loading on both spans



	Field moment max M_F : kNm/m	Moment at the edge of support $M_{S,A}$: kNm/m	Moment at the cl. of support $M_{S,M}$: kNm/m
(b) Pin support of one node	17.6 (100%)	-27.4 (100%)	-31.2 (100%)
(c) Pin support of three nodes above the wall	17.4 (99%)	-24.3 (89%)	-14.5 (47%)
(d) Fully restraint of the nodes at the face of the column	16.7 (95%)	-25.9 (95%)	0
(e) Hinge coupling	17.3 (98%)	-28.0 (102%)	-14.5 (47%)
(f) Bedding ($C = 9 \times 10^6$ kN/m ³)	17.6 (100%)	-27.4 (100%)	-29.1 (94%)
Beam analysis (manual)	17.6	-27.3	-29.3/-31.1*

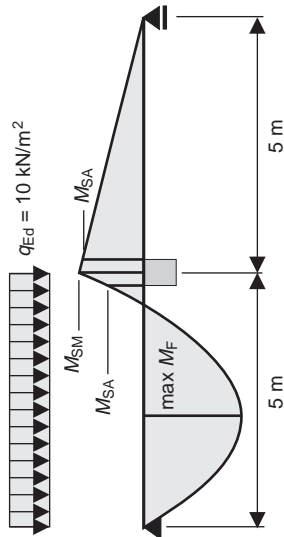
* Smoothed and not smoothed bending moment

Table 4.1 Bending moments (Continued)

Uniform loading on left span only

	Field moment max M_F : kNm/m	Moment at the edge of support M_{SA} : kNm/m	Moment at the cl. of support M_{SM} : kNm/m
(b) Pin support of one node	23.9 (100%)	-12.2/-15.2 (99/99%)	-15.6 (99%)
(c) Pin support of three nodes above the wall	17.5 (73%)	-27.8/0 (226/-%)	-7.5 (48%)
(d) Fully restraint of the nodes at the face of the column	16.7 (70%)	-25.9/0 (211/-%)	0
(e) Hinge coupling	23.7 (99%)	-12.5/-15.5 (101/101%)	-14.5 (92%)
(f) Bedding ($C = 9 \times 10^6$ kN/m ³)	21.9 (91%)	-16.9/-10.5 (137/68%)	-14.6 (92%)
Beam analysis (manual)	24.0	-12.3/-15.4*	-15.8

* Moment at left and right face of support



this model should not be used. Refining the element mesh results in a higher bending moment at the support (see Section 4.13.2).

The ‘hinge’ coupling (Model E) shows a good correlation with the beam model. Only the support moment M_{sup} in load case 1 shows greater deviations from the beam values. Further refinement of the element mesh only changes the moments at the centre of the support (from $M_{sup,max} = -17.9$ to -7.4 kNm/m) that are not relevant for design.

An elastic bedding of the supported elements at the wall (Model E) results in a sufficient correlation with the beam moments and shear forces for both load cases. When only one span is loaded, the bending moment at the face of the support is approximately 37% greater than the values that are manually calculated. However, it should be noted that the results are highly dependent on the bedding modulus C used in the analysis. High values may result in fully restrained nodes such as those in Model C.

When soft supported elements are used, the bedding modulus C has to be calculated first. In practice, C is often derived from the normal stiffness of the wall ($C = EA/l$) or the bearing (see Figure 4.14). It must be emphasised that this approach considers only the global deformation of the supporting structure and the resulting force redistribution. The local deformations, the stresses and strains in the slab in the vicinity of the wall with respect to the column head, which are required to determine the ‘exact’ internal forces, cannot be modelled with this simple approach either.

The main assumption of all plate elements, the linear strain distribution, is not valid in the region of the support (see Figure 4.15). Therefore, the bedding of the elements is an engineering tool, to get a smooth distribution of the bending moments over the support, in a manner similar to those in manual analysis.

Figure 4.14 Stiffness of an elastic bearing

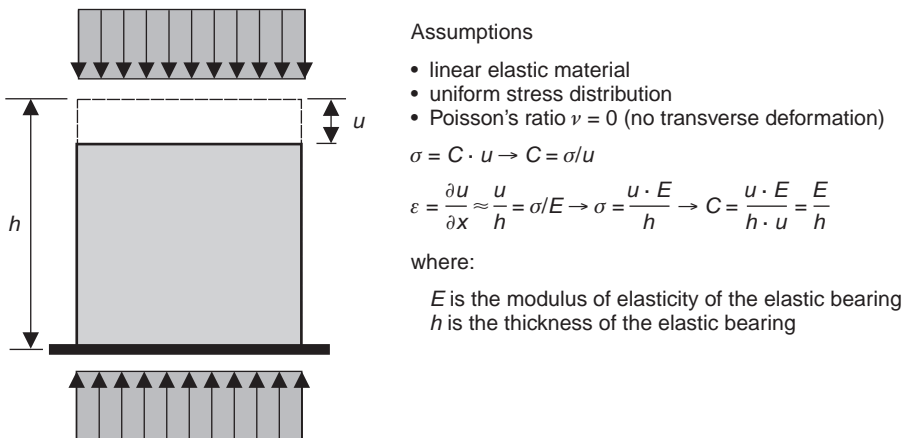


Figure 4.15 Stress distribution of a one-way slab at the supports

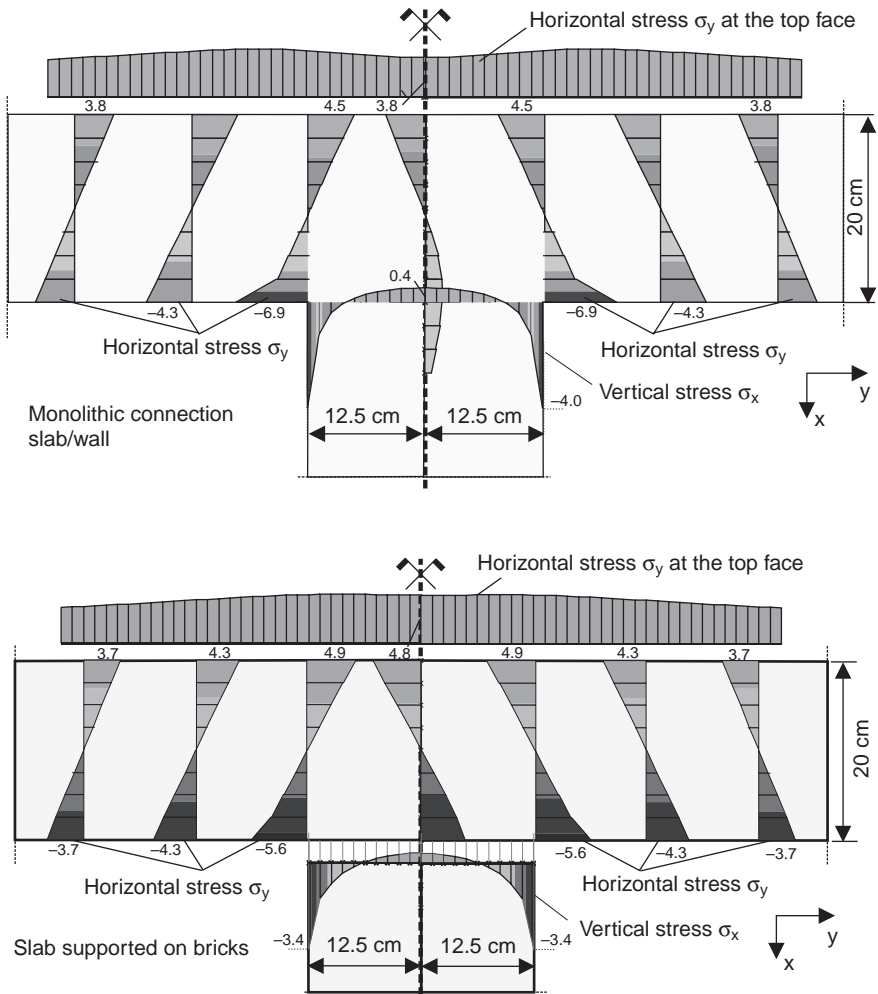


Table 4.2 shows the bending moments for different values of C from $C = 9 \times 10^5 \text{ kN/m}^3$ to $C = 9 \times 10^7 \text{ kN/m}^3$. The results are not sensitive to the bedding modulus C used for a uniform loading over both spans, as the deflection curve over the support show a horizontal tangent. On the other hand, when only one span is loaded, the bending moments are highly dependent on the value of C (see Table 4.2). A refinement of the element mesh in the support region does not change the internal forces significantly.

A slab has to be designed for both bending and shear. The section at a distance of $1.0d$ from the face of the support is relevant for the shear design for the given direct support of the structure. The shear forces are listed in Table 4.3 for different models. A constant static depth of $d = 20 - 2.5 \text{ cm} = 17.5 \text{ cm}$ is used for comparison.

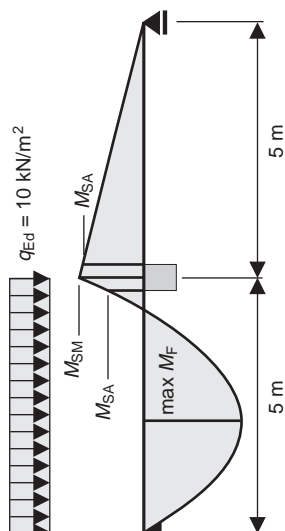
Table 4.2 Bending moments for different bedding modulus C

Uniform loading on both spans		Field moment max M_F : kNm/m	Moment at the edge of support M_{SA} : kNm/m	Moment at the cl. of support M_{SM} : kNm/m
$C = 9 \times 10^5$ kN/m ³	17.8 (101%)	-26.7 (98%)	-28.6 (92%)	
$C = 9 \times 10^6$ kN/m ³	17.6 (100%)	-27.4 (100%)	-29.1 (94%)	
$C = 9 \times 10^7$ kN/m ³	17.6 (100%)	-27.5 (101%)	-28.2 (91%)	
Beam analysis (manual)	17.6	-27.3	-29.3/-31.1*	

* Smoothed and not smoothed bending moment

Table 4.2 Bending moments for different bedding modulus C (Continued)

Uniform loading on left span only

		Field moment max M_F : kNm/m	Moment at the edge of support M_{SA} : kNm/m	Moment at the cl. of support M_{SM} : kNm/m
$C = 9 \times 10^5 \text{ kN/m}^3$		23.8 (99%)	-12.5/-14.2 (102/92%)	-14.3 (91%)
$C = 9 \times 10^6 \text{ kN/m}^3$		21.9 (91%)	-13.5/-14.6 (110/95%)	-16.9 (107%)
$C = 9 \times 10^7 \text{ kN/m}^3$		18.6 (77%)	-24.7/-2.7 (201/18%)	-14.1 (89%)
Beam analysis (manual)		24.0	-12.3/-15.4*	-15.8

* Moment at left and right face of support

Table 4.3 Shear forces at a distance of $d = 17.5$ cm from the face of the intermediate support

	Uniform loading		Uniform load on left span only shear force	
	shear force left/right: kN/m		Left: kN/m	Right: kN/m
(b) Pin support of one node	28.0 (99%)		24.9 (99%)	3.1 (97%)
(c) Pin support of three nodes above the wall	28.1 (100%)		28.4 (113%)	0.0
(d) Fully restraint of the nodes at the face of the column	28.5 (101%)		28.5 (114%)	0.0
(e) Hinge coupling	28.1 (100%)		24.9 (99%)	3.2 (100%)
(f) Bedding ($C = 9 \times 10^6$ kN/m ³)	28.0 (99%)		25.8 103%	2.2 (69%)
Beam analysis (manual)	28.3		25.1	3.2

The results of the various models are similar if both spans are loaded, whereas in load case 2, significant differences can be seen. A restraint of all nodes at the support (Models B and C) results in much higher shear forces in the supported elements (maximum +13%) of the loaded span. The shear forces are much smaller than the beam values in the unloaded span, and the forces are even zero in some models. This is also the case if the elements over the support are bedded by spring or contact elements.

In conclusion, in order to model a support on walls, only the centre node should be fixed to avoid numerical restraints.

In this section, the internal forces and moments calculated manually by a beam structure have been used to verify the numerical model. It should be noted that the major assumption of a beam model, a linear strain distribution over the supports, is not valid. This is illustrated in Figure 4.15 where the stresses of a plane shell model (diaphragm) of a one-way slab are shown near the intermediate support for a monolithic connection and a free, non-restrained support ($l = 2 \times 5.0$ m).

A nonlinear strain distribution can be seen at the inner face of the support. High compressive stresses are estimated for the fixed connection (singularity). In both cases, the tensile stresses do not increase over the supports. Therefore, it is generally sufficient to use the bending moments at the face of the support for obtaining the smoothed values for design.

Even complex shell models can only approximate the real load-bearing and deformation behaviour of a slab at the supports, as the basic assumption of a linear elastic material behaviour is not valid in this region. The concrete slab will show some cracks in reality.

4.6. Slabs that can lift from the supports

The design of slabs is usually based on the assumption that the slab cannot lift from the supports. It must be emphasised that even a rectangular simply supported slab under constant loading will partially lift from the supports at its edges if it is not fixed. Therefore, one has to consider this effect, if the slab is not fixed to the supports or if the vertical force, for example, due to walls above, is not sufficiently high to restrain the uplifting.

This support condition can easily be modelled by individual vertical springs or special boundary elements that have no tensile stiffness. An iterative solution is required due to this nonlinearity. Load superimposition is generally not valid in this analysis.

Figure 4.16 shows the bending moments, shear forces and deflections of a rectangular slab ($l_x/l_y = 5.0/7.5$ m) that is free to lift from the supports. It can be seen that approximately 20% of the supported length on both edges has been uplifted under uniform load.

The internal forces and midspan deflections of a rectangular, simply supported slab that is fixed to the supports and one that can uplift, are given in Table 4.4. If the deformation of the slab is not restrained in the vertical direction, the bending moments at midspan increase by approximately 13%. The support forces per unit length increase (due to

Figure 4.16 Internal forces and deflections of a rectangular slab free to uplift from the supports under uniform load

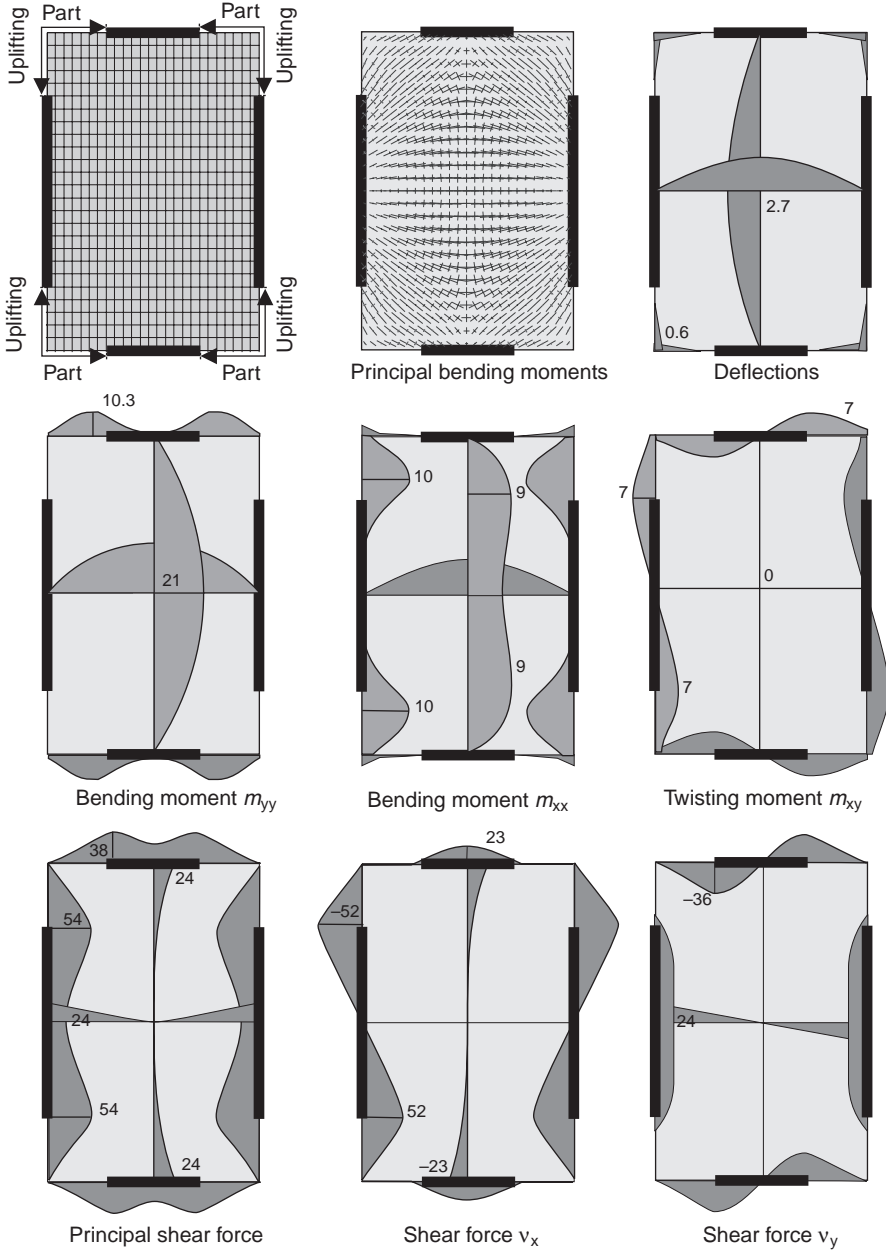
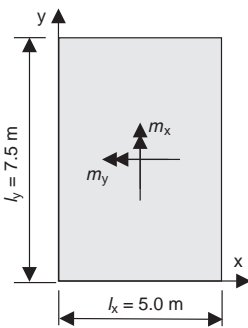


Table 4.4 Bending moments and deflections at midspan and shear forces at the supports of a rectangular slab with and without restraint in vertical direction at the supports

		Values from Czerny (1999) simply supported slab	Finite Element analysis simply supported slab (= 100%)	Finite Element analysis slab can uplift
m_{xye}	in kNm/m	15.3 (132%)	11.6	7.1 (61%)
m_{xm}	in kNm/m	18.3 (98%)	18.7	21.0 (113%)
m_{ym}	in kNm/m	7.0 (97%)	7.2	7.5 (104%)
$m_{y,max}$	in kNm/m	7.2 (96%)	7.5	9.1 (121%)
v_{yrm}	in kN/m	18.2 (102%)	17.9	23.9 (134%)
\bar{v}_{yrm}	in kN/m	26.5 (106%)	25.0	34.5 (138%)
v_{xrm}	in kN/m	21.2 (98%)	21.6	23.3 (108%)
\bar{v}_{xrm}	in kN/m	25.6 (97%)	26.5	28.0 (106%)
F_e	in kN	30.7 (124%)	24.8	– –
f	in mm	24.5 (105%)	23.4	27.3 (117%)

where:

m_{xye} is the twisting moment at the edges

m_{xm} , m_{ym} is the bending moments at midspan

$m_{y,max}$ is the greatest bending moment around x-axis

v_{yrm} , v_{xrm} is the greatest shear force per unit length at the supports

\bar{v}_{yrm} , \bar{v}_{xrm} is the greatest support force per unit length

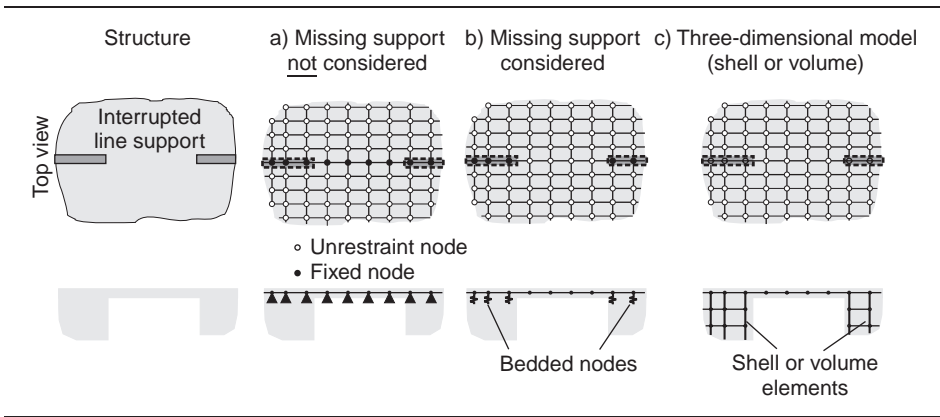
f is the greatest midspan deflection

the reduced supported length) by approximately 38% (shorter edge) and 6% (longer edge).

4.7. Discontinuous line support

The numerical modelling of discontinuous support of slabs or a wall support that ends in a slab can cause considerable problems. In both cases, infinite shear forces and bending moments are estimated at unsupported edges. This singularity problem is caused by the sudden change of the boundary conditions (see Figures 4.19 and 4.20). Dimensioning of the slab for these ‘theoretical’ peaks is not required, as they only result from a numerical problem. The basic assumption of a linear strain distribution does not hold near the end of a wall support. The large tensile stresses calculated are reduced due to the cracking of concrete. However, an analysis that considers the nonlinear material behaviour and the complicated 3D stress distribution is too difficult and extensive for any practical

Figure 4.17 Different models for a discontinuous line support



application. Hence, three different models may be used to overcome the numerical problem (Figure 4.17). First, one may neglect the discontinuity of the line support in the numerical model. The design of the opening region has to be done separately on a fully or partially restrained equivalent beam system ('flush beam strip', see Figure 4.18). This additional effort can be avoided when the opening is considered in the numerical model. The nodes at the end of the line support may be fully or partially restrained in the vertical direction. Another variation is to use a 3D volume model of the slab and the wall underneath. However, this model again requires a big effort and is not for practical use.

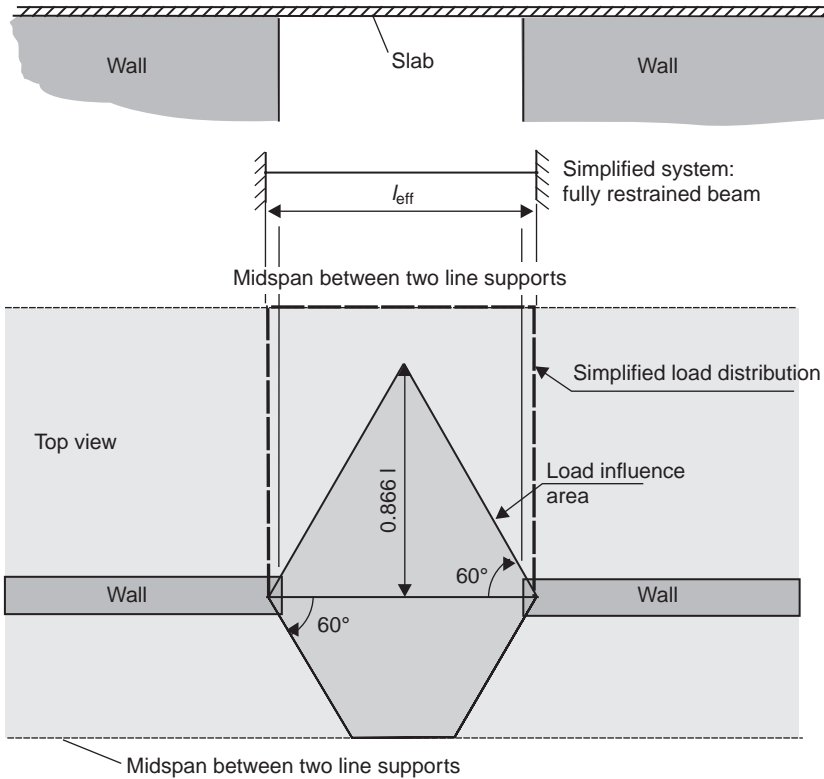
In the FE model, the missing line supports can be neglected if their length is smaller than 15 times the depth of the slab ($l_{\text{eff}}/h < 15$). The dimensioning of this region can be done manually using an equivalent beam system ('flush beam strip') in accordance to 'Heft 240' (Grasser *et al.*, 1991) (see Figure 4.18). More detailed investigations based on FEM are only necessary if the opening length exceeds 15 times the section depth h of the slab.

'Theoretical' singularities at the unsupported edge can be found if the wall opening is considered by the FE model. These load peaks can be reduced significantly by a soft, elastic support, by elastic bedding of the nodes or the elements, as the results of a comparison calculation demonstrates. Figure 4.19 shows the internal forces for a soft and a stiff support. A bedding modulus of $C = 2327 \text{ MN/m}^2$ is used, which corresponds to a concrete wall (grade C25/30) with a thickness of $h = 20 \text{ cm}$ and a height of $l = 2.75 \text{ m}$ ($C = E \cdot h/l = 32.000 \cdot 0.2/2.75 = 2.327 \text{ MN/m}^2$) (modulus of elasticity, see Table 4.5).

A large reduction in the moment peaks at the unsupported edges can be seen (Figure 4.19), if the stiffness of the support is considered.

Bending moments for fixed and elastic supports and the values of Stiglat (Stiglat and Wippel, 1983) are given in Table 4.6. Stiglat used the finite difference method and a

Figure 4.18 Beam system ('flush beam strip') and load influence areas for a discontinuous line support, according to Grasser *et al.* (1991)



Poisson's ratio of $\nu=0.0$ to estimate the internal forces in the region of the missing support. With this assumption, the bending moment becomes nearly twice as high as that of the fully restrained supported slab. This large difference may be caused by the influence of the element size. The bending moments at midspan of the FE analysis correspond well to Stiglat's values.

Figure 4.21 shows the bending moment distribution of a slab with a partition wall. For this structure, a singularity occurs at the face of the opening. To demonstrate the large influence of the vertical stiffness of the support on the internal forces, a very small bedding modulus was used ($C=50 \text{ MN/m}^2$), which correspond to a wall made of hollow or aerated concrete bricks.

As shown in Figure 4.21, the peak of the bending moment and the large concentrated shear force at the unsupported edge disappear. This load redistribution causes a considerable increase of the bending moments and the deflections of the slab.

Figure 4.19 Bending moments and shear forces for a slab with a discontinuous line support

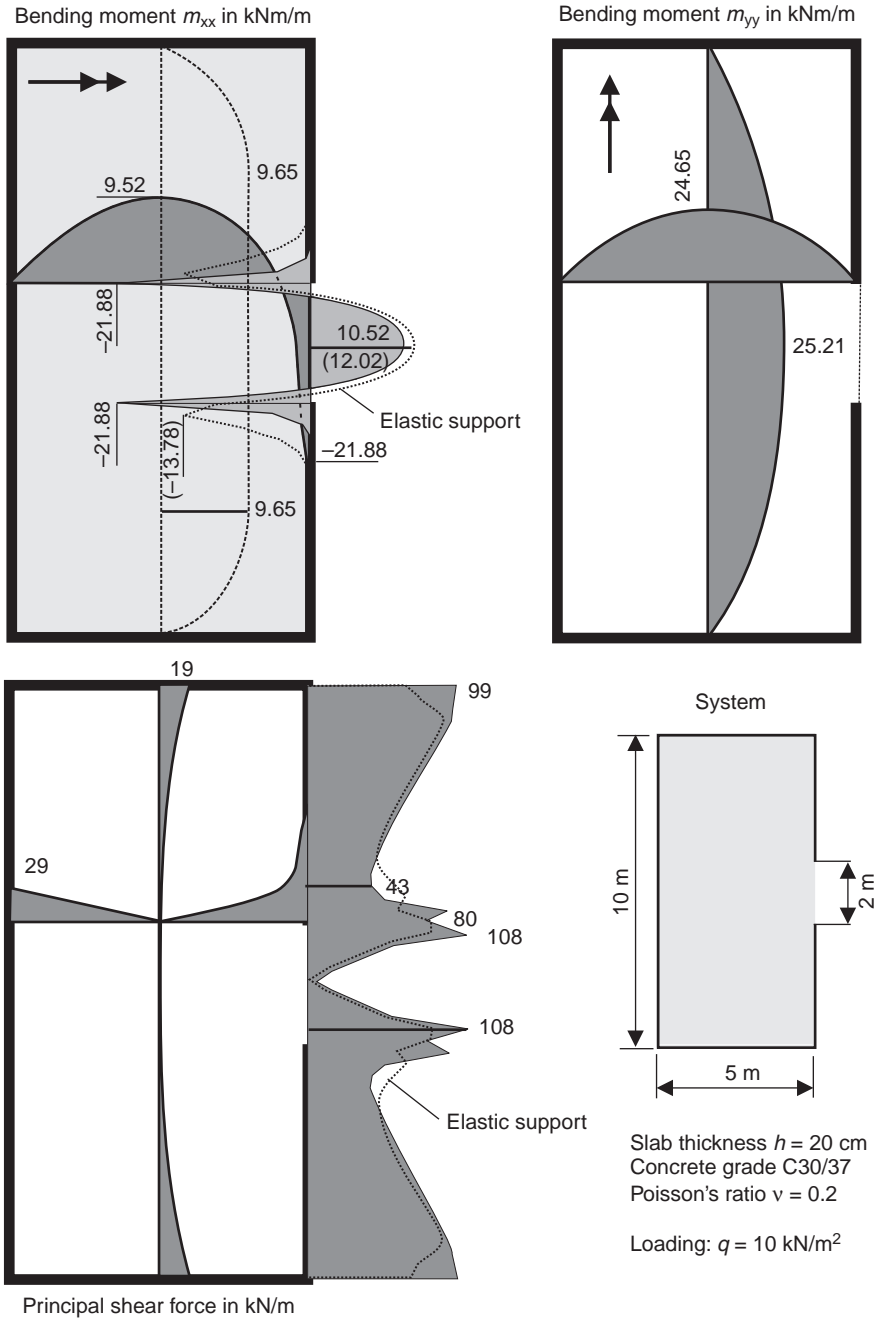


Figure 4.20 Support forces of the outer wall near the face of the opening (nodes fully restrained in the vertical direction)

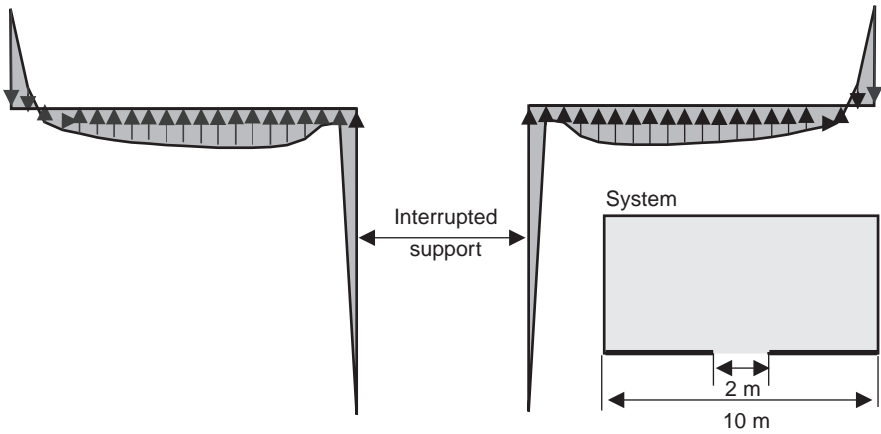


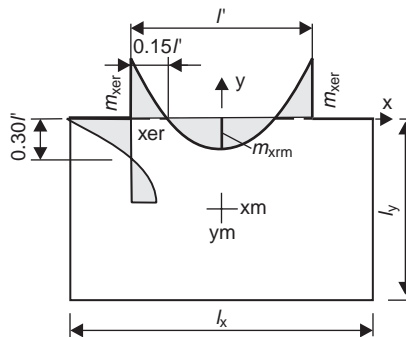
Table 4.5 Modulus of elasticity of different building materials

Concrete	$E_{cm} = 9.5 \cdot (f_{ck} + 8)^{1/3}$
Clay bricks	$E = 3000 \cdot \sigma_0$
Steel	$E_s = 210\,000 \text{ N/mm}^2$

where:

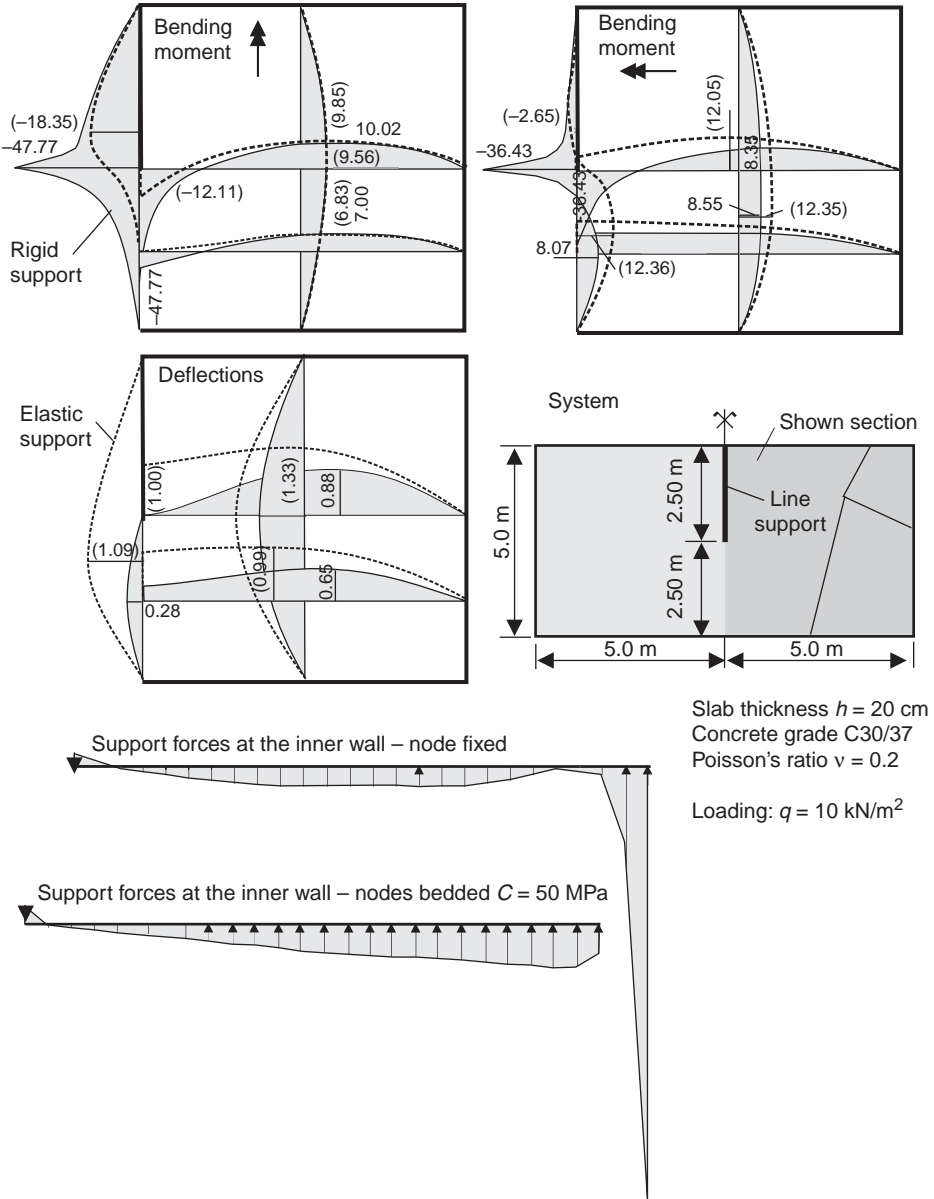
f_{ck} is the characteristic concrete compressive strength in N/mm^2 ;
 σ_0 is the permissible compressive strength of a brick wall.

Table 4.6 Bending moments in the opening region



	Rigid support	Soft support	Stiglat and Wippel (1983)
m_{xrm} : kNm/m	10.52	12.02	9.0
m_{xer} : kNm/m	-21.88	-13.78	-42.0

Figure 4.21 Slab with partition wall



The dimensioning of the slab can be done either with a stiff or elastic support. In the case of a stiff wall, it should be noted that a redistribution of the bending moment at the unsupported edge is only possible if the concrete slab cracks. Therefore, reinforcement to limit the crack width should be inserted in the top face of the slab.

It must be emphasised that a flexible support of the slab can only represent the overall deflection behaviour of the supporting wall. The complex 3D stress and strain distribution at the unsupported edges cannot be modelled with plain plate elements based on a linear strain distribution.

4.8. Concrete joist floors

Several variations exist to model joist floors. At first, one may consider the joist in the FE model as a stiff vertical continuous support. The resulting support forces are used as external loads for an equivalent T-beam, which may then be analysed manually. This model is based on the assumption of a rigid support, that is, the stiffness of the joist is much higher than the bending stiffness of the slab.

A more refined model has to be used if this assumption does not apply. The joist has to be discretised together with the slab in the same system. In this case, the real T-beam system is idealised as a slab of constant depth and with an additional separate beam or a plate element having a greater thickness, located at the midplane of the slab. In actual dimensioning, the depth of the equivalent beam element has to be greater as the eccentricity of the joist is neglected. The moment of inertia of the real T-beam should be identical to that of the idealised system. The effective width of the flanges of the joist b_{eff} has to be considered in this calculation. It may be estimated from EC2, Part 1 (Eurocode 2, 2004) as follows:

$$b_{\text{eff}} = \sum b_{\text{eff},i} + b_w$$

$$b_{\text{eff},i} = 0.2 \cdot b_i + 0.1 \cdot l_0 \leq \begin{cases} 0.2 \cdot l_0 \\ b_i \end{cases}$$

where:

l_0 is the distance between points of zero moments

b_w is the width of the web.

The flexural stiffness of the FE model of the beam-plate system has to be identical to that of the real structure. Thus, the depth of the equivalent beam h_w^{equiv} has to be greater than the sum of the depth of the web h_w and the flange h_f (see Figure 4.22). The width $b_{\text{eff},i}$,

Figure 4.22 Model for a concrete joist floor

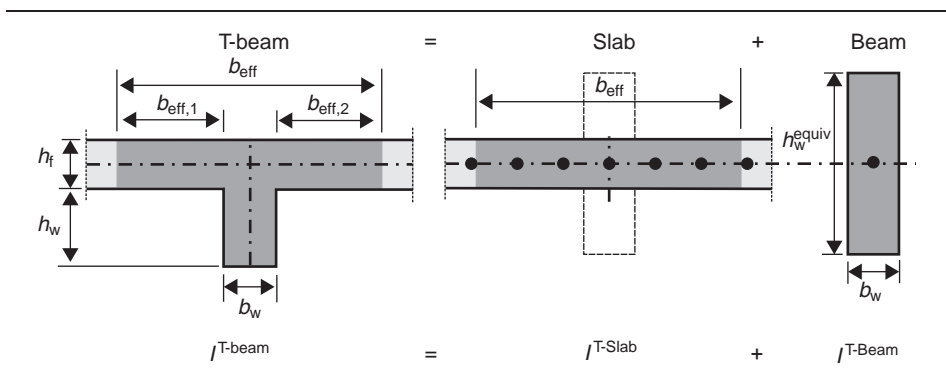
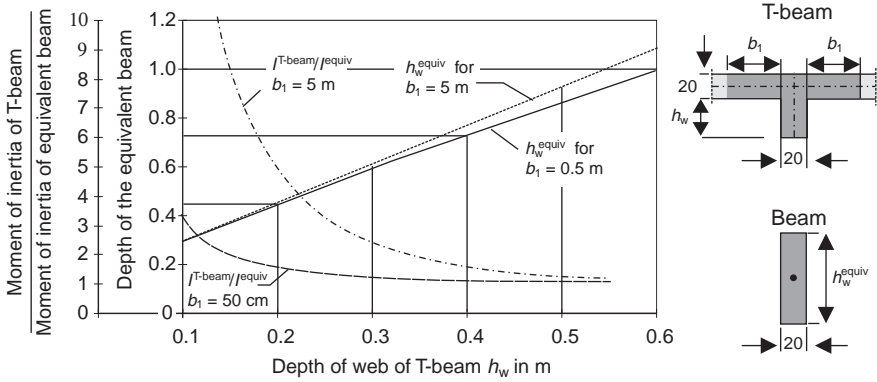


Figure 4.23 Depth of the equivalent beam h_w^{equiv} and relation of the moment of inertias



which is part of the effective width b_{eff} , depends on the structural system and the loading. However, it is not necessary to consider the change of b_{eff} in the longitudinal direction of the beam in detail. It can be seen from Figure 4.23 that the depth of the equivalent beam h_w^{equiv} is nearly independent to that of the effective width b_{eff} .

The dimensioning of the joist is made by using the resulting forces of the equivalent beam multiplied by the relation of the moment of inertia. This factor has to be considered, especially if the depth of the web h_w is small (see Figure 4.23).

Another approach for joist floors increases the height of the plate element instead of an extra beam element. The relevant member forces of the T-beam have to be calculated from the internal forces of the slab, as explained earlier, for the dimensioning of the joist.

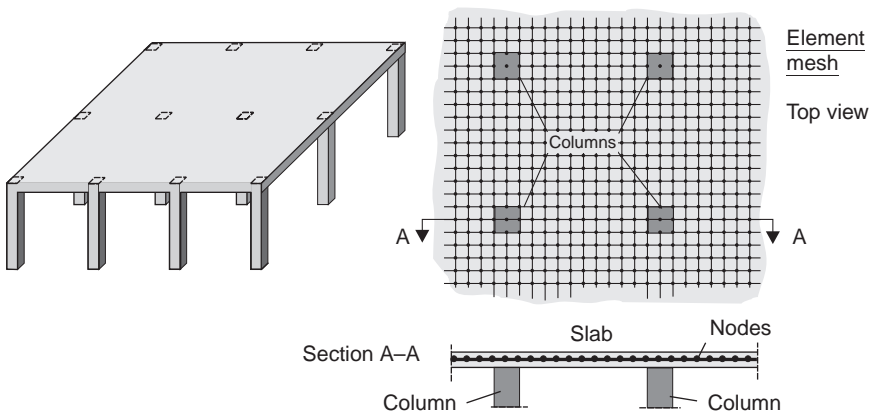
Furthermore, one can model the real load-bearing behaviour (folded plates) by means of a 3D FE model (plane shell elements + eccentric beam element). This alternative, much better method will be explained in Section 5.3.

4.9. Flat slabs

Flat slabs and flat plate floors are directly supported on columns and monolithically connected with them. There are no interior beams as supporting elements. They are widely used since flat slab construction is economical (Figure 4.24). A manual analysis can easily be carried out by the analytical methods given in EC2, Part 1 (Eurocode 2, 2004) or in ‘Heft 240’ (Grasser *et al.*, 1991) for regular systems with approximately equal span lengths. The bending moments and shear forces for irregular panels or loadings have to be estimated by means of FEM.

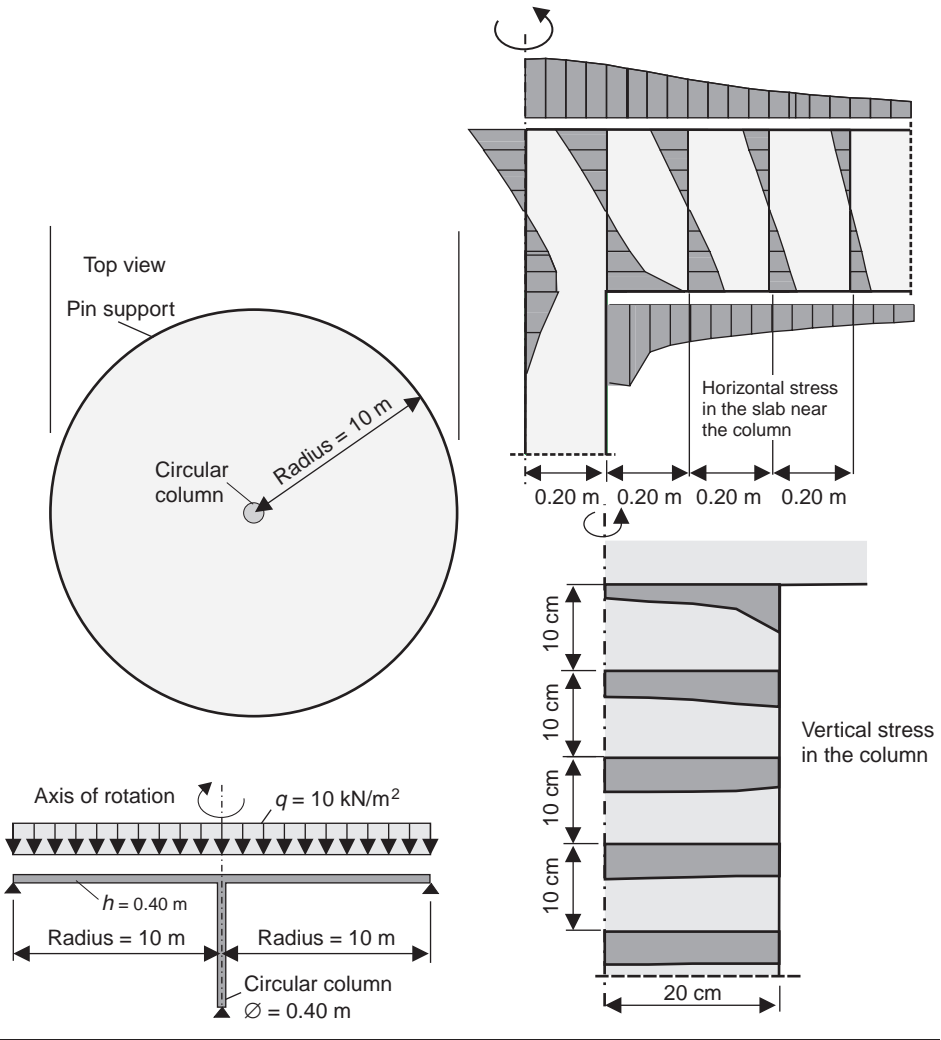
The numerical analysis has to model the actual behaviour of the pin support at the columns. Different approaches are available, which will be discussed in the following text.

Figure 4.24 Flat slab



It must be emphasised here that the behaviour of the structure in the region of the columns cannot be calculated exactly due to the underlying assumptions of the FE slab model. In the supported area, the strain distribution is very complex. This behaviour cannot be modelled by plate elements that are generally based on a linear strain distribution over their cross-section depth. In Figure 4.25, the stresses of a circular slab are shown near the supported area. The slab is simply supported at the outer edge and has a circular column at its centre. The slab is subjected to a uniformly distributed load of $q = 10 \text{ kN/m}^2$. The axisymmetric model represents very well the load-bearing behaviour of a flat slab for the region of the column. Even in the case of a rectangular arrangement of the supports, the force distribution around the columns is nearly axisymmetric.

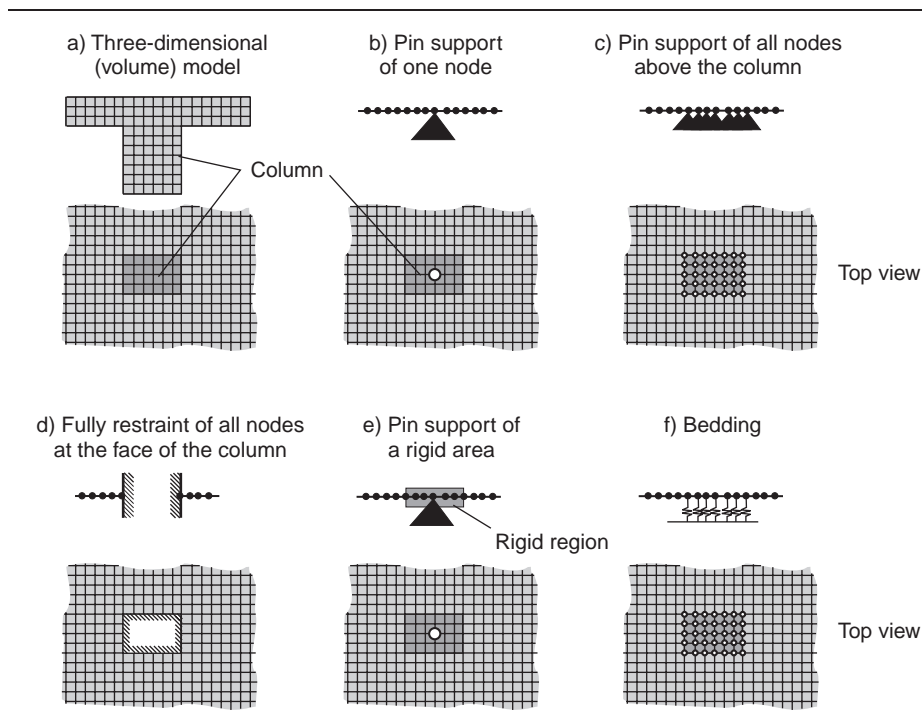
Figure 4.25 Normal stresses in a flat slab near the column (FE analysis)



An ‘exact’ determination of the internal forces and the stresses of a pin-supported slab is only possible by means of a 3D (volume) model. The nonlinear behaviour of the concrete due to cracking has to be considered. Such a complex model of a flat slab is too extensive for practical use. Furthermore, the dimensioning cannot be done automatically by the software.

Therefore, in practice, a 2D plane plate model is used, and the columns are modelled by special support conditions. Various models, as shown in Figure 4.26, can be used. These have already been explained in detail in Section 4.5 for a simply supported one-way slab.

Figure 4.26 Flat slab – various models for the column support

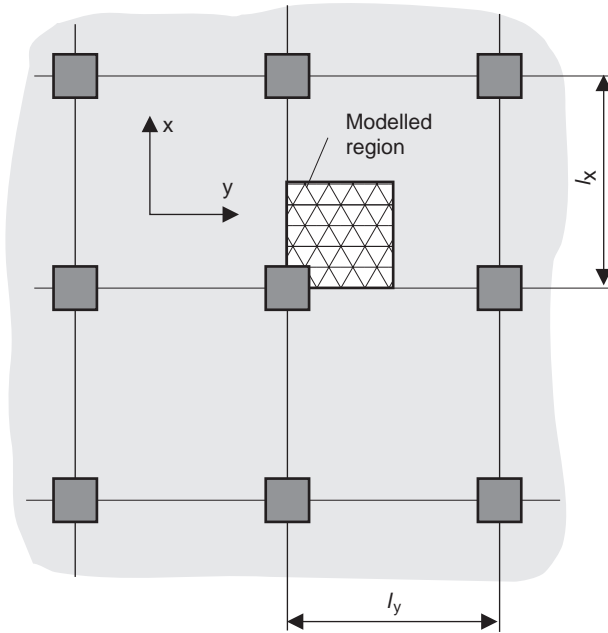


- (a) 3D model with volume elements.
- (b) Pin support of one node: A pin support in a plate theoretically results in infinite bending moments and shear forces, which however are smoothed by the limited size of the FEs. The size of the element has a significant influence on the distribution of the internal forces near the column.
- (c) Pin support of all nodes above the column.
- (d) All nodes at the face of the column are fixed.
- (e) Pin-supported stiff region above the column (coupling of nodes).
- (f) Bedding of the nodes or elements above the column.

The main structural differences between the various models for the line support discussed in Section 4.5 and that of a pin-supported flat slab is that the latter is a 2D spatial structure, carrying the loads in two dimensions.

The ‘correct’ bending moments, shear forces and stresses of a flat slab in the region of the column supports are unknown. Therefore, the results of the various models are examined in a simple structure, using an interior panel of a flat slab with regular panel dimensions of $l_x = l_y = 5.0$ m. For comparison purposes, the bending moment at the face of the column is used. This value is relevant for dimensioning the slab. A uniformly distributed load of $g = 10$ kN/m² is applied to the slab.

Figure 4.27 Modelled region of the slab



Owing to the symmetric structural system and the load arrangement, it is sufficient to only analyse one quarter of the slab and to consider the boundary conditions at the symmetry lines (Figure 4.27). Therefore, in the following figures, only a quarter of the whole slab is shown.

The results of the FE analysis are compared with the values estimated by the widely used equivalent frame (Eurocode 2, 2004, Tables 4.7 and 4.8) and beam method (Grasser *et al.*, 1991). Here, the bending moments of a flat slab are estimated by means of an equivalent frame or beam system and distributed in a transverse direction with factors given in the tables for a column width of $b/h = 0.25/0.25$ m and $0.5/0.5$ m (see Figures 4.28 to 4.30).

The method given in Grasser *et al.* (1991) results in the following bending moments for the inner slab:

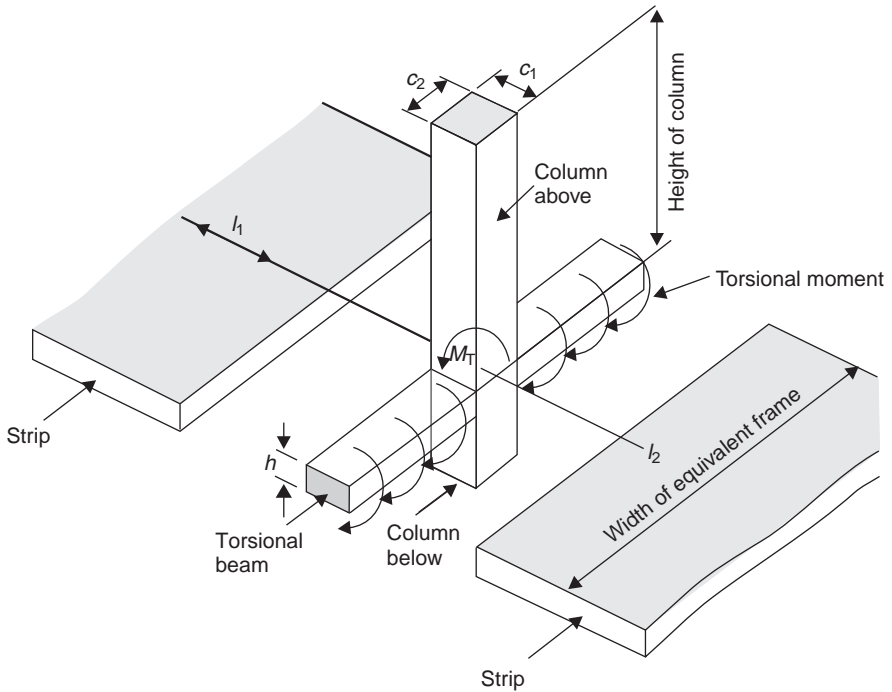
Input variables:

$$\begin{aligned} \varepsilon &= l_x/l_y = 5.0 \text{ m}/5.0 \text{ m} = 1.0 \\ b_{\text{sup}}/l &= 25/500 = 0.05 \text{ resp. } 50/500 = 0.1 \\ \text{uniform load } g &= 10 \text{ kN/m}^2 \end{aligned}$$

where:

b_{sup} is the width of column
 l is the span length.

Figure 4.28 Equivalent frame model of flat slabs



Support bending moments

In the inner strip above the column:

$$\begin{aligned}
 m_{SS} &= k_{SS}^g \cdot c \cdot g \cdot l_{m1}^2 + k_{SS}^q \cdot c \cdot q \cdot l_{m1}^2 \\
 &= \begin{cases} -0.224 \cdot 1.0 \cdot 5^2 = -56 \text{ kNm/m (column 25/25 cm)} \\ -0.160 \cdot 1.0 \cdot 5^2 = -40 \text{ kNm/m (column 50/50 cm)} \end{cases}
 \end{aligned}$$

in the other strip beside the column:

$$m_{SG} = 0.7m_{SS} = -39.2 \text{ kNm/m} \quad \text{resp.} \quad -28 \text{ kNm/m}$$

in the field strip:

$$m_{SF} = k_{SF}^g \cdot g \cdot l_1^2 + k_{SF}^q \cdot q \cdot l_1^2 = -0.03 \cdot 10 \cdot 5^2 = -7.5 \text{ kNm/m}$$

Span moments

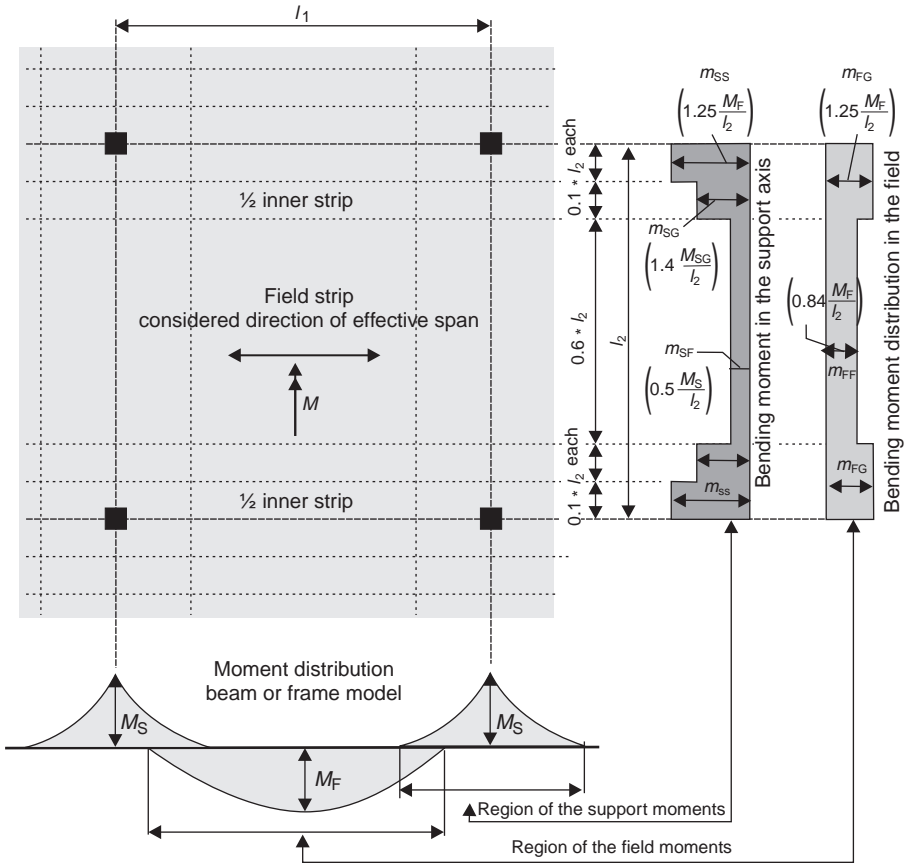
In the inner strip:

$$m_{FG} = k_{FG}^g \cdot g \cdot l_1^2 + k_{FG}^q \cdot q \cdot l_1^2 = 0.052 \cdot 10 \cdot 5^2 = 13.0 \text{ kNm/m}$$

in the field strip:

$$m_{FF} = k_{FF}^g \cdot g \cdot l_1^2 + k_{FF}^q \cdot q \cdot l_1^2 = 0.041 \cdot 10 \cdot 5^2 = 10.3 \text{ kNm/m}$$

Figure 4.29 Moment distribution of a flat slab according to Grasser *et al.* (1991)



where:

k represents the moment factors (see Grasser *et al.* (1991); Tables 3.1–3.5)

The equivalent frame analysis (Eurocode 2, 2004) gives the following bending moments:

Table 4.7 Simplified appointment of bending moment for a flat slab#Data taken from Eurocode 2 (2004)

	Negative moments	Positive moments
Column strip	60 to 80%	50 to 70%
Middle strip	40 to 20%	50 to 30%

Note: Total negative and positive moments to be resisted by the column and the middle strips together should always add up to 100%

Figure 4.30 Equivalent frame model of a flat slab according to Eurocode 2 (2004)

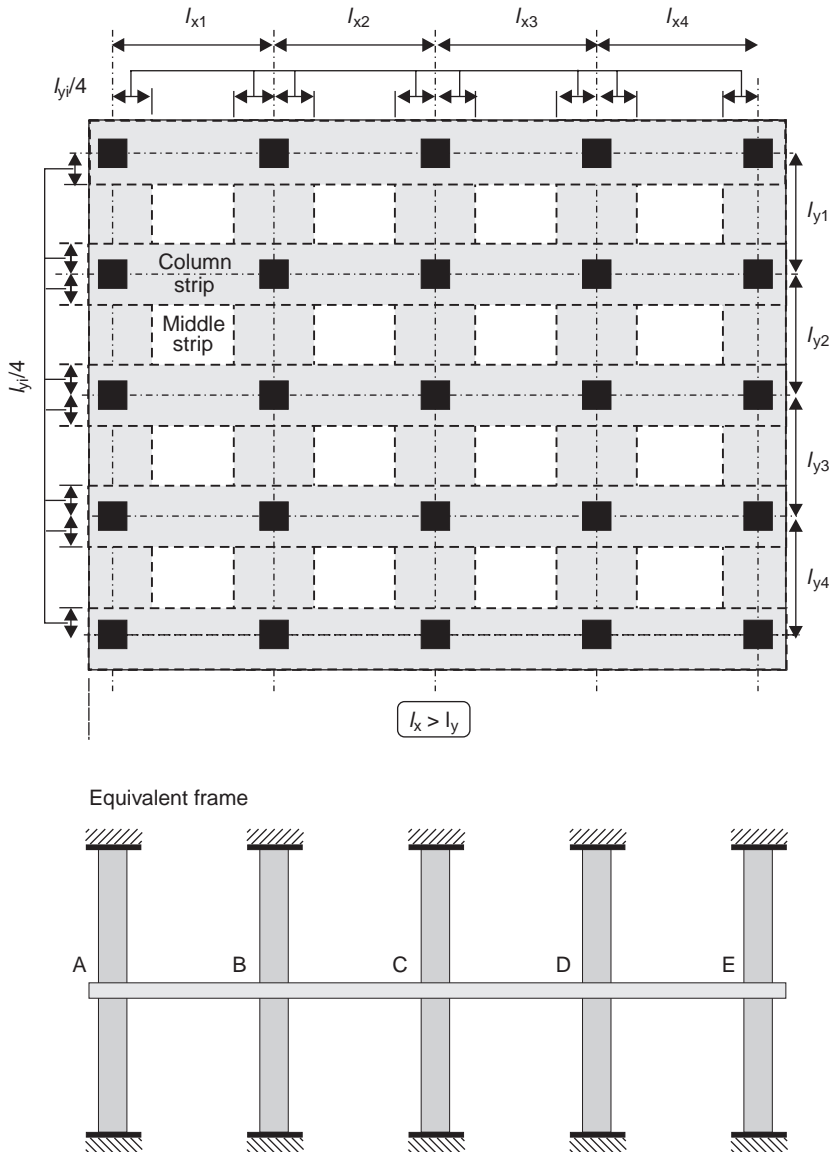


Table 4.8 Bending moment in strips

	Negative moments	Positive moments
Column strip	-25.0 to -33.3 kNm/m	+10.4 to 14.6 kNm/m
Middle strip	-16.7 to -8.3 kNm/m	+10.4 to 6.3 kNm/m

The calculated negative bending moment in the column strip $m_{\text{sup,max}} = -33.3 \text{ kNm/m}$ is significantly less than the value from the equivalent beam method $m_{\text{sup,max}} = -56.0 \text{ kNm/m}$.

The distribution of the bending moments in the direction of the main load bearing is treated first (see Figure 4.29 bottom). Next, we consider the distribution of the bending moments in transverse direction (see Figure 4.29 right).

4.9.1 Pin support of one node

The influence of the element size on the distribution of the bending moments is first examined at the section $y=0$. The quarter of the interior panel is divided into 4×4 , 8×8 and 16×16 elements. The size of the element is kept constant in each model for comparison. There is no refinement of the meshes in the region of the support. Figure 4.31 shows the dimensionless bending moment distribution in the column axis ($y=0$). It is obvious that a refinement of the element mesh results in a significant increase of the maximum support moment. This can be traced back to a singularity problem caused by the pin support and the concentrated support force. The bending moment in the span is nearly independent of the element size, except for the very coarse mesh of 4×4 elements.

The moment distribution of the models with 8×8 and 16×16 elements are well matched for the span and up to $x/l \approx 0.06$ from the centreline of the pin support. Consequently, a further refinement of the element mesh would only slightly affect the moments at $x > 0.06l$. Both curves meet in the region of $x/l \approx 0.02$.

The bending moment at the face of the column is needed in the design. Therefore, the considerable differences in the peak moment at the pin support ($m_S = -241/ -471 \text{ kNm/m}$) are of no practical importance. As illustrated in Figure 4.31, the results are highly dependent on the element size in the region of $x/l < 0.02$ and $b_c/l < 0.04$. Therefore, a pin-supported node should not be used for a column width of $b_c < 0.04l$. Such slender columns ($b_c < 20 \text{ cm}$ for $l_{\text{slab}} = 5 \text{ m}$) are rarely used in practice.

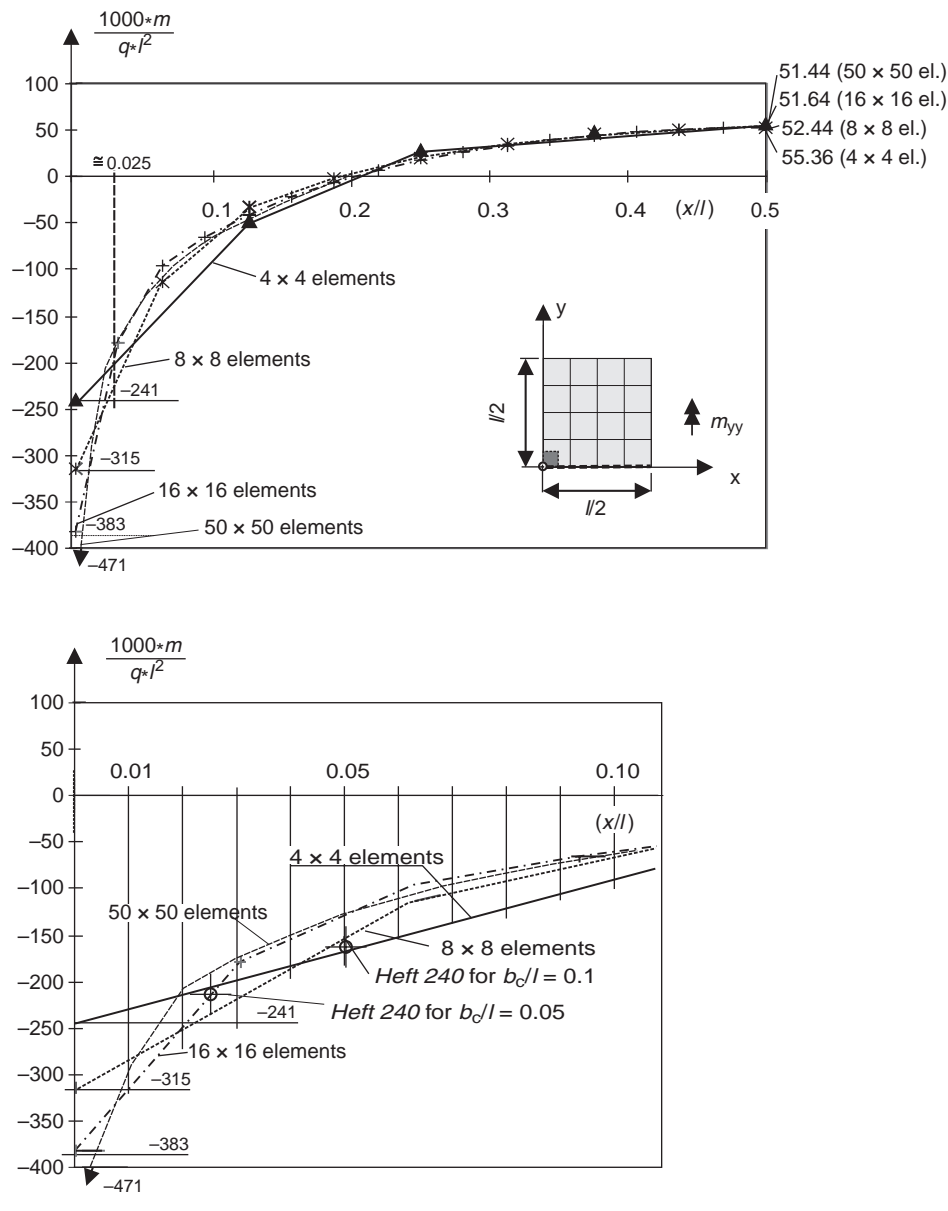
Furthermore, one can see that the greatest bending moments at the supports for all meshes correlate well with values calculated by the analytical method given in Grasser *et al.* (1991). This is not surprising, since the moment factor k had been estimated for a pin-supported plate.

4.9.2 Pin support of all nodes

The slab is fully restrained if all nodes at the column are fixed in the vertical direction. This mis-modelling is important for asymmetric loading, as has been shown for a one-way slab (see Section 4.5) (Figure 4.33).

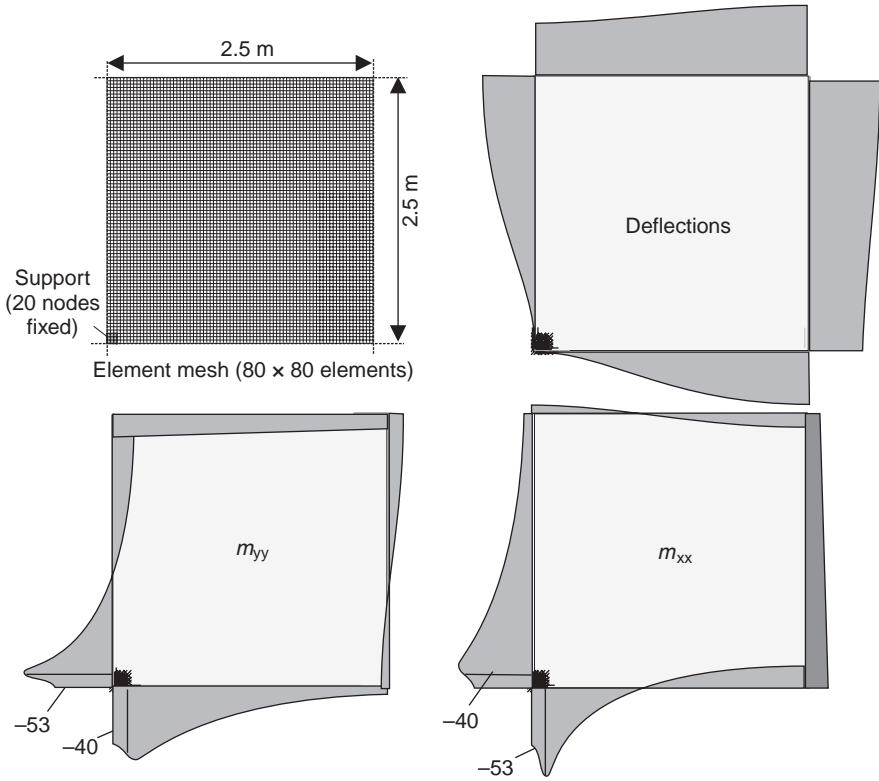
The distribution of the bending moments in the symmetry lines for two different cross-sections of the column ($b_c = 25 \text{ cm}$ and $b_c = 50 \text{ cm}$) is shown in Figures 4.32 and

Figure 4.31 Moment distribution m_{yy} for $y=0$ in the region of an interior column for different element meshes – pin-supported node



4.34. It can be seen that the bending moments in the span are only slightly dependent on the width of the column. In contrast, the internal forces at the face of the column increase considerably when the width of the column becomes smaller. This is caused by the concentration of the support reactions.

Figure 4.32 Element mesh, bending moments and deflections of a flat slab – all nodes above the column fixed in vertical direction



4.9.3 Fully restrained of all nodes

If, in addition to the previous example, the rotation of all supported nodes is restrained, then there is a high moment peak at the column (Figures 4.35 and 4.36). The maximum value is not located at the face of the column. The elements over the support are free of any internal forces as their nodes are fully restrained.

As illustrated in Figure 4.37, the size of the elements has a great influence on the maximum support bending moment. The bending moments near the face of the column (maximum value) are compared for various mesh refinements with the values calculated according to Grasser *et al.* (1991).

where:

- m_{SG} is the support bending moment in the inner strip
- m_{SF} is the support bending moment in the field strip
- m_{FF} is the span moment in the field strip
- m_{FE} are the moments from FE analysis
- m_{240} are the moments according to Grasser *et al.* (1991).

Figure 4.33 Numerical restraint caused by the pin support of all nodes above the column

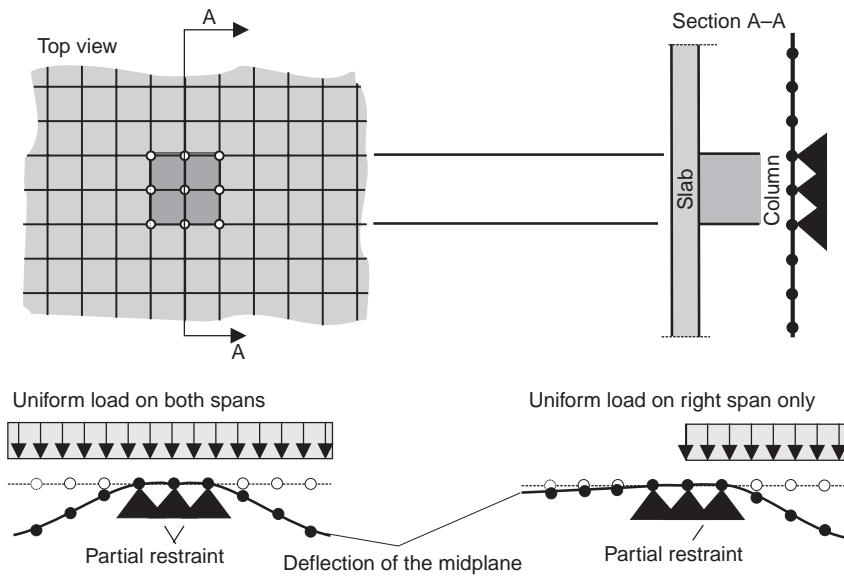


Figure 4.34 Bending moment m_{yy} and m_{xx} in the section $y = 0$ – pin support of all nodes above the column

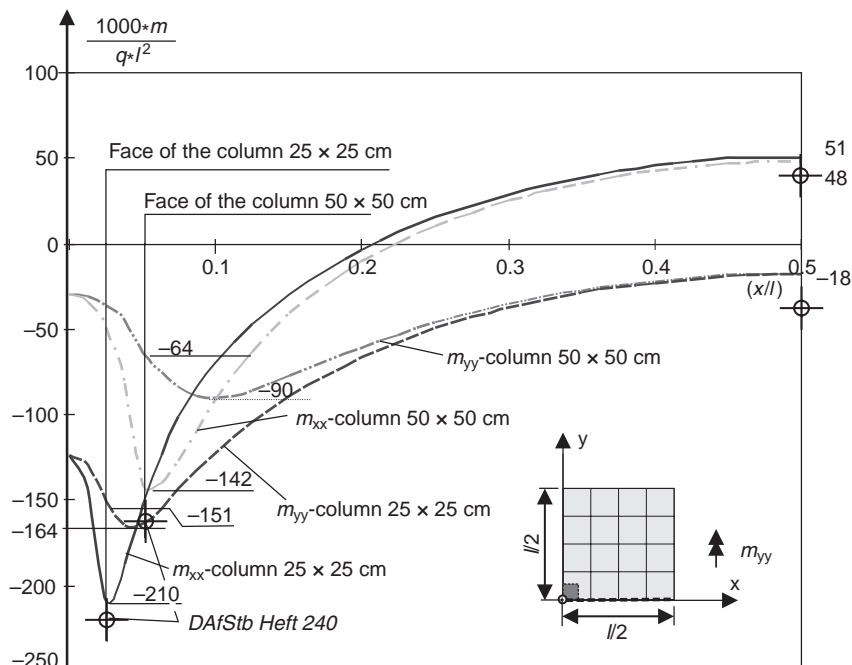
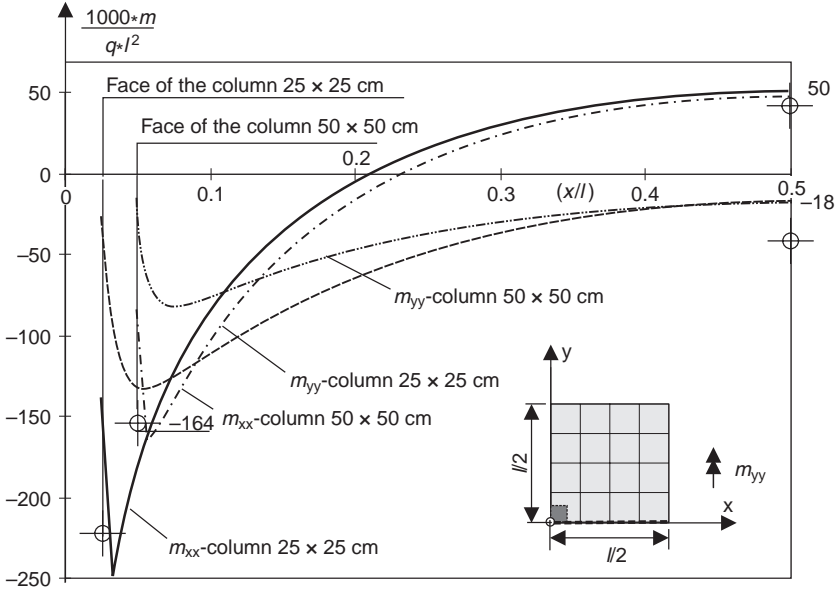


Figure 4.35 Bending moment m_{yy} and m_{xx} in the section $y=0$ – all nodes above the column are fully restrained



4.9.4 Elastic bedded elements

The problem of estimating the correct bedding modulus C has already been discussed in Section 4.5. It has to be noted that the bedding of the elements above the column results in a partial restraint of the slab, as is the case when all nodes are restrained in the vertical direction. For a very high bedding modulus C , the same effects occur as for fully restrained nodes.

Figure 4.36 Bending moment in the symmetry lines – all nodes above the column are fully restrained

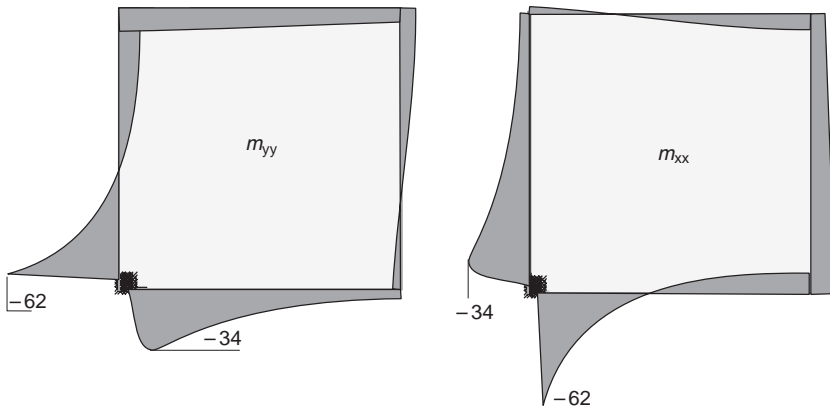
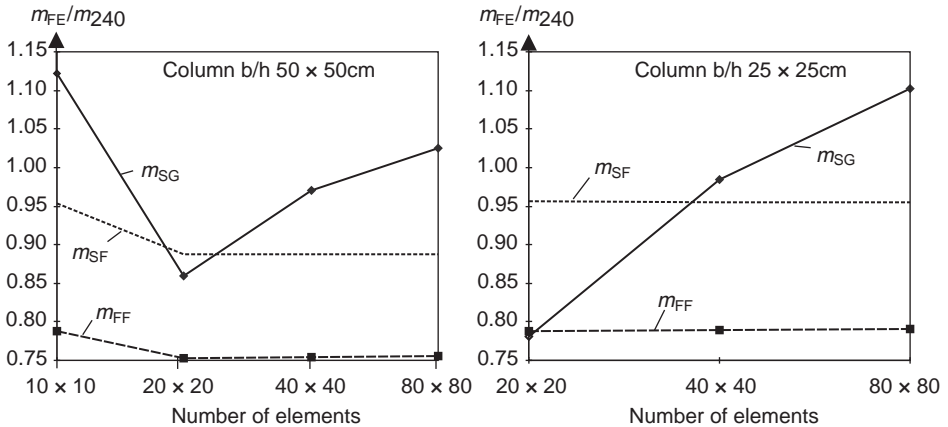


Figure 4.37 Bending moment near the face of the column for different refined element meshes; column size 25×25 cm and 50×50 cm – deflection of all supported nodes fixed



where:

- m_{SG} is the support bending moment in the inner strip
- m_{SF} is the support bending moment in the field strip
- m_{FF} is the span moment in the field strip
- m_{FE} are the moments from FE analysis
- m_{240} are the moments according to *Heft 240* (Grasser *et al.*, 1991)

Figure 4.38 shows the moment distribution in the column axis for a bedding modulus of $C = 9000 \text{ MN/m}^3$. 40×40 elements are used for a quarter of the slab. The column has a cross-section of 25×25 cm. Hence, 2×2 elements and 4×4 elements for a column of 50×50 cm are bedded. The results of the numerical analysis do not change much if the element mesh is further refined.

The desired smoothed distribution of the bending moment over the column can be seen in Figure 4.38. The maximum bending moment decreases with the size of the column. A good correlation of the results with the values provided by ‘Heft 240’ Grasser *et al.* (1991) is obtained.

As shown by the parametric study with different bedding modulus C , only the greatest bending moment at the support $m_{S,max}$ is effected by the stiffness of the support (see Figure 4.39). As C changes, the bending moment at the face of the support keeps nearly constant, whereas it decreases in the centre of the support with an increase in C . The distribution of the internal forces becomes similar to that for all nodes being fixed.

4.9.5 Coupling of nodes above the column

Another model for a column support that is often used in practice is the combination of the nodal degrees of freedom of the nodes above the column, the coupling of the nodes. The deflections of all nodes above the column are coupled with the master node in the centre of the supported area. Various coupling conditions were discussed

Hinge coupling of nodes

$$v_x = v_{x0} + \varphi_{y0} \cdot (z - z_0) - \varphi_{z0} \cdot (y - y_0)$$

$$v_y = v_{y0} + \varphi_{x0} \cdot (z - z_0) + \varphi_{z0} \cdot (x - x_0)$$

$$v_z = v_{z0} + \varphi_{x0} \cdot (y - y_0) - \varphi_{y0} \cdot (x - x_0)$$

$$\varphi_x = \varphi_{x0}$$

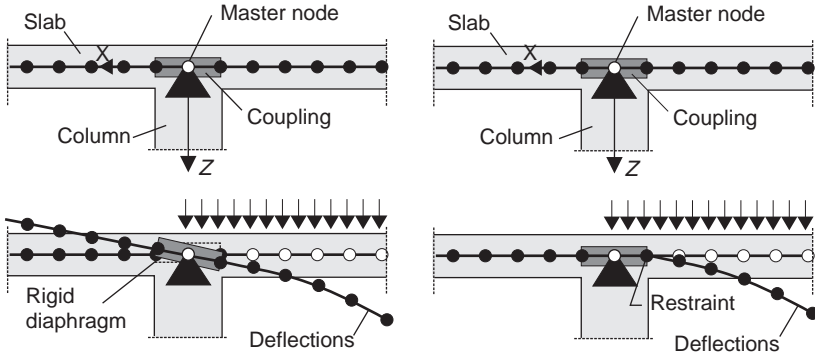
($v_{x0}, v_{y0}, v_{z0}, \varphi_{x0}, \varphi_{y0}, \varphi_{z0}$ = deflection/rotation of master node)

Rigid coupling of nodes

$$v_x = v_{x0}; \varphi_x = \varphi_{x0}$$

$$v_y = v_{y0}; \varphi_y = \varphi_{y0}$$

$$v_z = v_{z0}; \varphi_z = \varphi_{z0}$$



in Section 2.6.3. A stiff and hinge coupling can be used for flat slabs. In the case of fixed coupling, all nodes of the supported area are restrained in the vertical direction ($v_z = v_{z0} = 0$). Thus, the rotation of the elements is prevented. The slab is fully restrained for uniform loading.

Figure 4.38 Bending moment in section $y = 0$ – elastic bedded elements

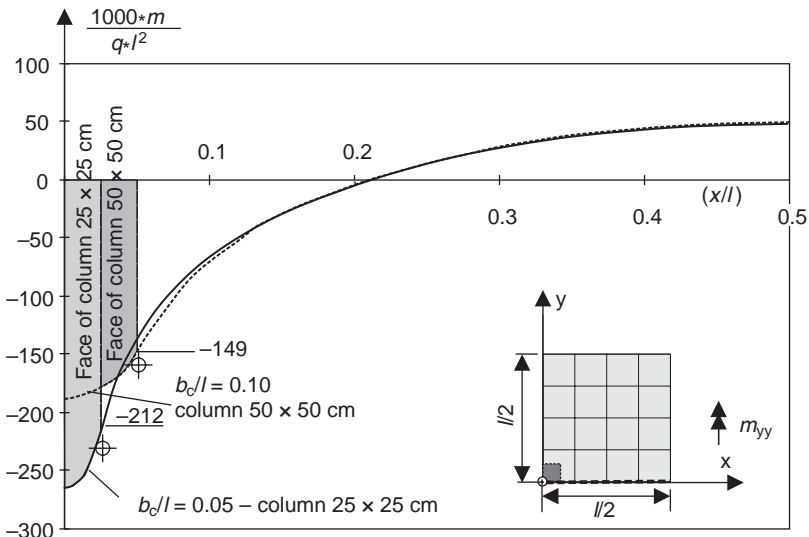
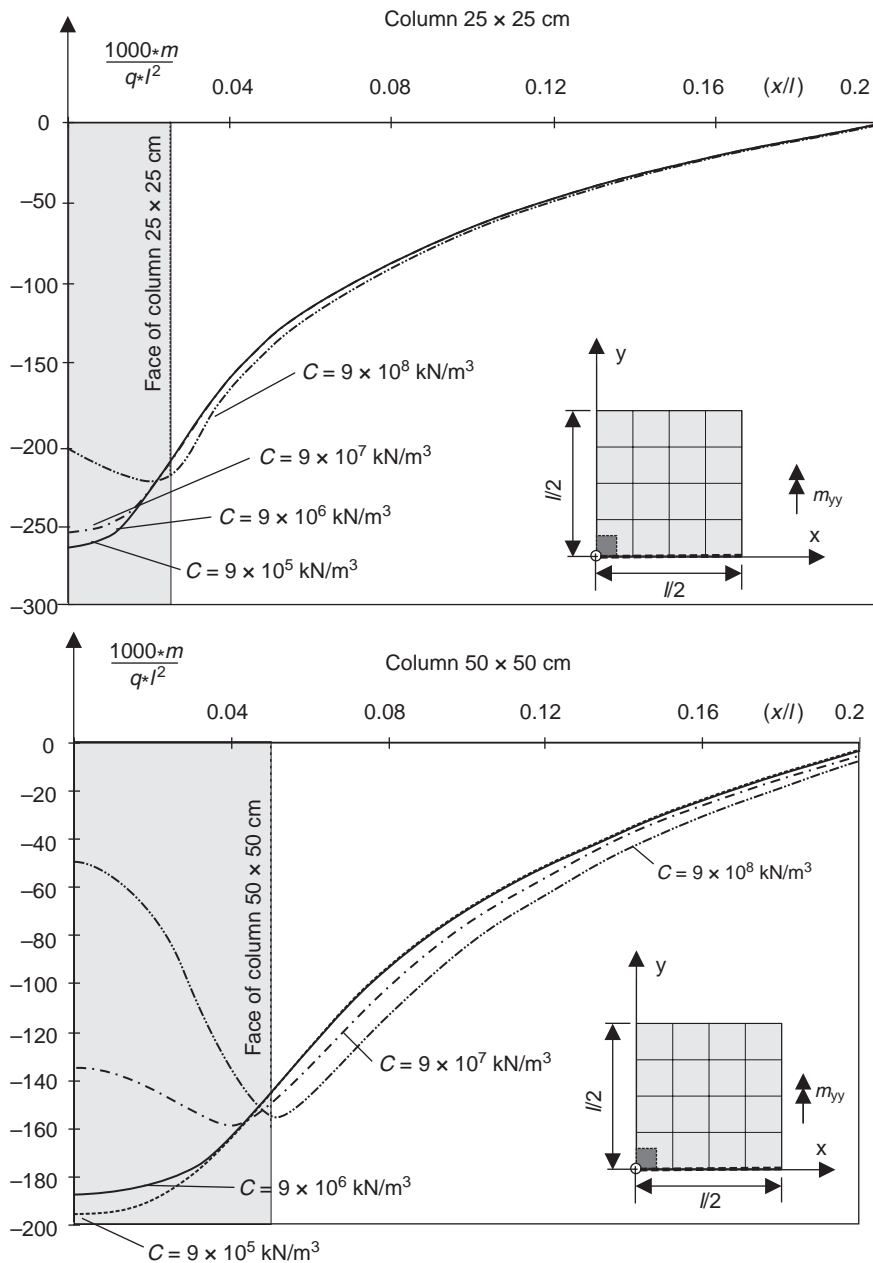


Figure 4.39 Bending moment in section $y=0$ – elastic bedded elements with different bedding modulus C



Therefore, a stiff coupling should not be used for asymmetric load arrangements, as has already been demonstrated in Section 4.5.

In contrast to the previously mentioned model, the rotation of the nodes ($\varphi_x, \varphi_y, \varphi_z$) are not combined for a hinged coupling. Only the deflections are coupled with the master node, according to the expressions listed earlier. This model is similar to a stiff coupling for a symmetric system and loading, since the rotation of the slab in the centre of the supported area with respect to the master node ($\varphi_{x0} = \varphi_{y0} = \varphi_{z0} = 0$) is equal to zero. This statement is confirmed by the results shown in Figure 4.40. There are no internal forces and no bending moments for the elements in the supported area. Hence, this model does not give a smooth bending moment distribution at the support. The results shown in Figure 4.40 demonstrate that the bending moment at the face of the column is nearly independent of the element size.

4.9.6 Comparison of the various models

In the previous sections, the distribution of the bending moment in the main direction of the load transfer has been discussed for the various models. Next, the moments of the different models in the transverse direction are compared. It should be pointed out that the bending moments calculated by the procedures given in ‘Heft 240’ (Grasser *et al.*, 1991) do not represent the ‘correct’ values. They are only used here for comparison purposes. The simple analytical method of the equivalent continuous girder or frame system has been used in practice for a long time without any major problems. The results are summarised in Table 4.9.

As expected, the model of the column support has only a minor influence on the field moments, as can be seen in Figure 4.41. The smallest bending moment in midspan calculated with FEM is 40% less than that of the simplified analytical model. It is only the values in the support strip that are different for the various models (see support strip, Figure 4.41 top). The support strip moments for the model with 3×3 fixed nodes and the stiff coupling are some 25% lower than the values provided by Grasser *et al.* (1991).

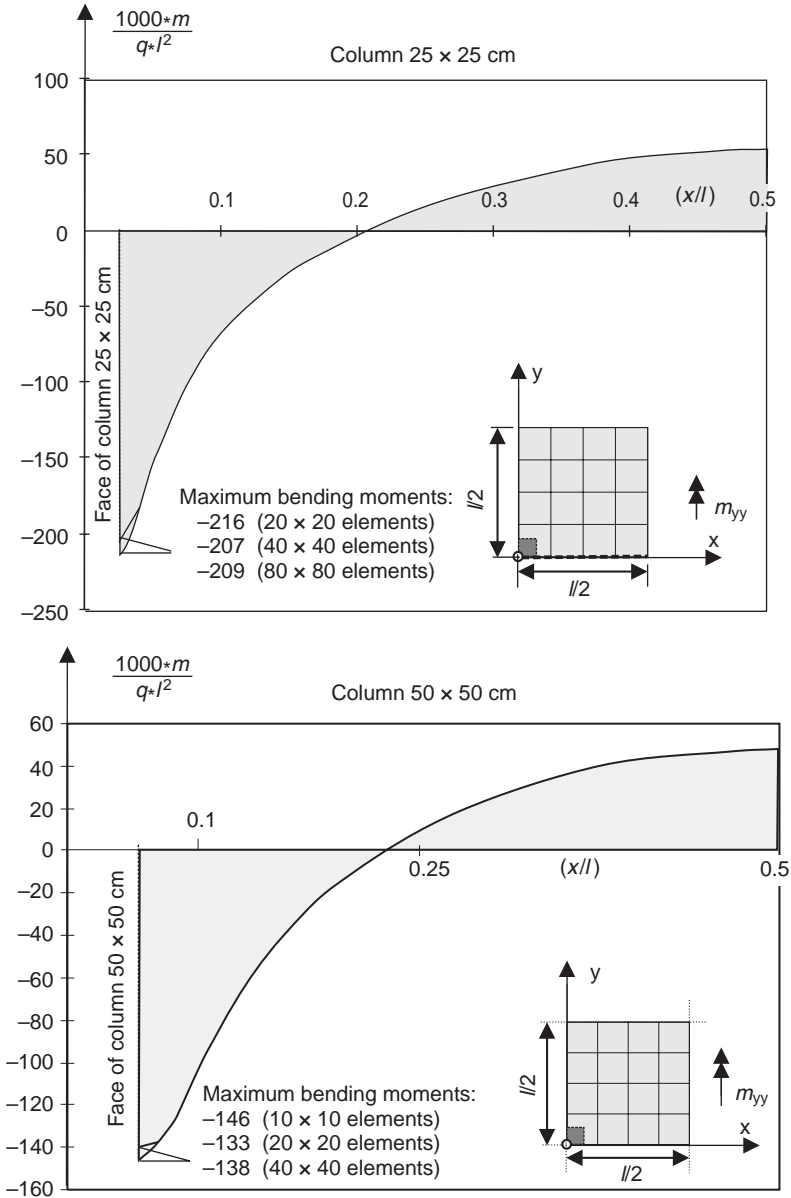
Overall, a very good correlation is found between the different models. This is because of the use of the simple system and uniform loading.

4.9.7 Results of the investigations

The previous investigations have shown that the support of a flat slab should be modelled by a pin support in the axis of the column. All other models may cause numerical restraints, as shown by the various analysis of a simply supported one-way slab. The bending moments at the face of the column have to be used in the design for bending. It should be noted that, in most cases, the design is done in the centre of the elements and not at the nodes. A parabolic smoothed bending moment distribution over the support should be used if there is no monolithic connection between the slab and the column.

4.9.8 Slab–edge column connection

In general, the bending stiffness of interior columns can be neglected, but this does not apply to edge or corner columns. The partial restraint of the slab can be modelled by

Figure 4.40 Bending moment in section $y=0$ – hinged coupling of the nodes

torsional springs or by bedding of the support elements. A spring stiffness of $C = 3EI/l$ and $C = 4EI/l$ may be used for a column that is pin ended on the base and a fully restrained column, respectively (Figure 4.42). The upper boundary value is gained if all nodes are fully restrained. The reduction of stiffness of a cracked member relative to the elastic value should be considered.

Table 4.9 Span and support bending moments for a flat slab according to different models ($b_c = 25 \times 25$ cm, $l_x = l_y = 5$ m, 40×40 elements)

Span moments	Grasser <i>et al.</i> (1991) (manual analysis)	Pin support of 1 node	Pin support of 3 nodes	Bedding	Hinged coupling
Inner strip 1 m_{FG}	13.0 (13.0)* (100%)	12.9 (99%)	12.7 (98%)	12.8 (99%)	12.7 (98%)
Field strip m_{FF}	10.3 (8.75)* (100%)	8.3 (81%)	8.2 (80%)	8.3 (81%)	8.2 (90%)
Support moments (at the face)	Grasser <i>et al.</i> (1991) (manual analysis)	Pin support of 1 node	Pin support of 3 nodes	Bedding	Hinged coupling
Inner strip 1 (face) m_{SS}	-56.0 (-44.8)* (100%)	-63.3 (113%)	-41.2 (74%)	-59.1 (106%)	-41.2 (74%)
Inner strip 2 m_{SG}	-39.2 (-29.2)* (100%)	-32.3 (82%)	-30.6 (78%)	-31.7 (81%)	-30.6 (78%)
Field strip m_{SF}	-7.5 (-10.4)* (100%)	-4.6 (61%)	-4.5 (60%)	-4.6 (61%)	-4.5 (60%)

* Values in parentheses: equivalent girder system according to Grasser *et al.* (1991)

The node in the centre of the supported area is fixed in the vertical direction. Thus, a small cantilever slab is created that shows bending moments perpendicular to the free edge.

The following calculations are carried out on a simple system, a rectangular flat slab with equal span length $l_x = l_y = 5.0$ m supported by four edge columns ($b/h = 25/25$ cm). Due to this being a symmetric system, only a quarter of the whole slab has to be modelled. A uniform load of $q = 10$ kN/m² is applied.

Bedding moduli between $C = 9 \times 10^6$ kN/m³ and 27×10^6 kN/m³ are used. The first value corresponds to the normal stiffness $C_N = E/l$ of a 3.55-m-high column with a Young's modulus of $E_c = 32\,000$ MN/m² (concrete grade C30/37). If the bending stiffness is considered, a value of $C_N = 3E/l = 27 \times 10^6$ kN/m³ has to be used.

Figure 4.43 shows the bending moment distribution m_{yy} at the edge of the slab ($y = 0$) for different models. The moment at the face of the column and at midspan is very sensitive to the numerical model of the support by the edge columns.

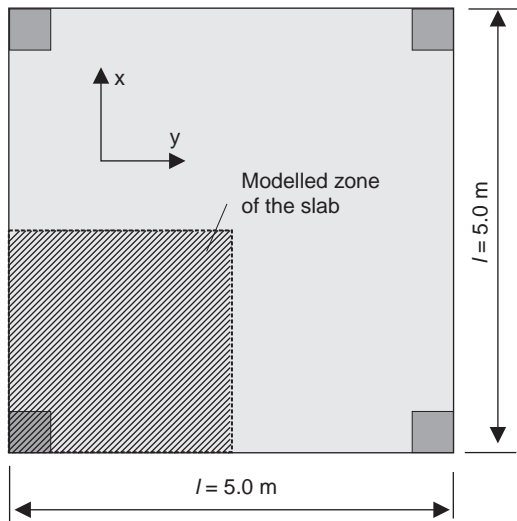


Figure 4.41 Transverse distribution of the bending moment perpendicular to the main load transfer direction according to Grasser et al. (1991) (shaded area) and FEM

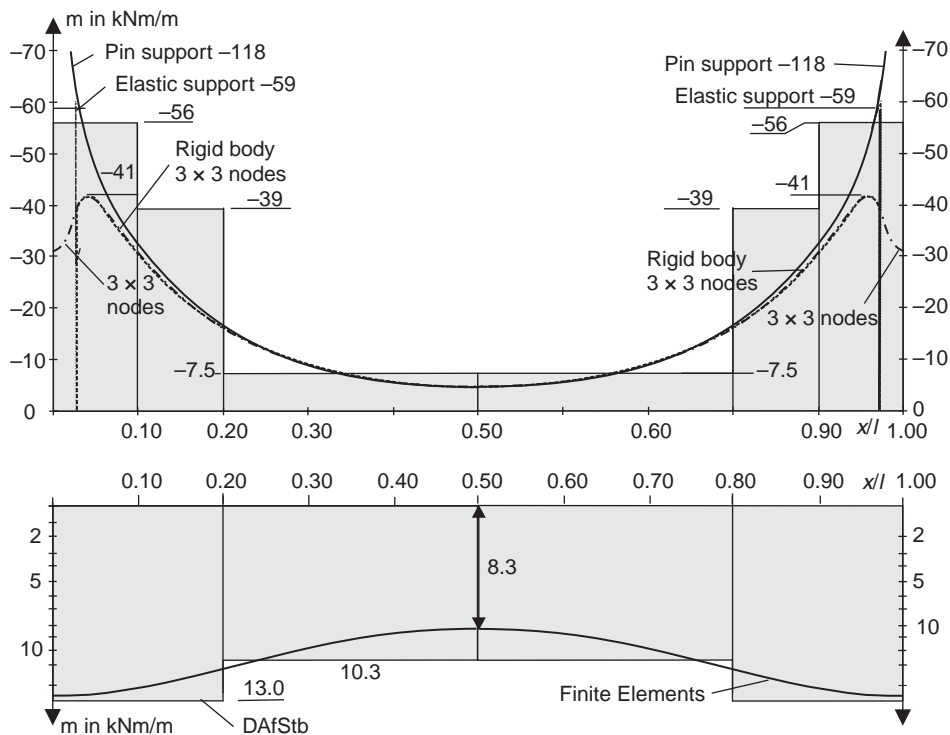


Figure 4.42 Bedding modulus C_N to model the bending stiffness of a column

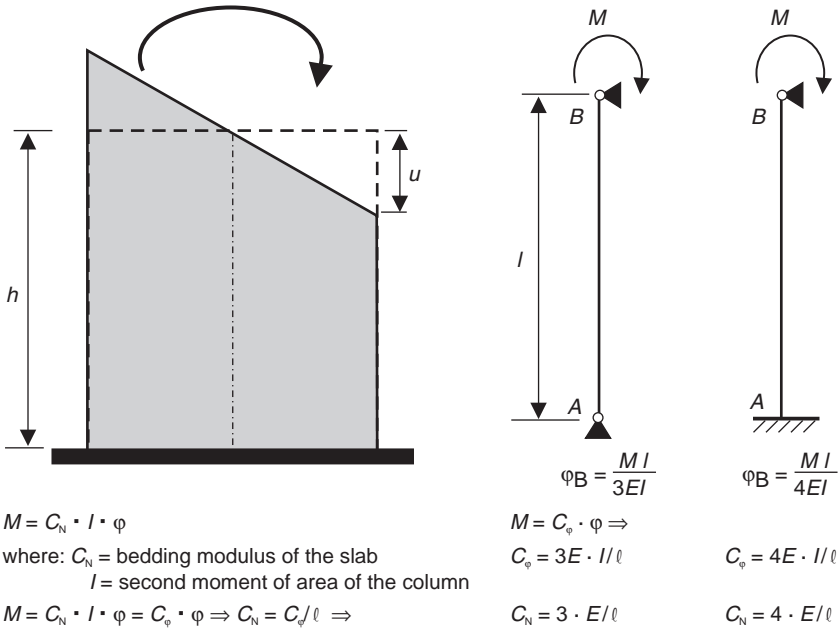
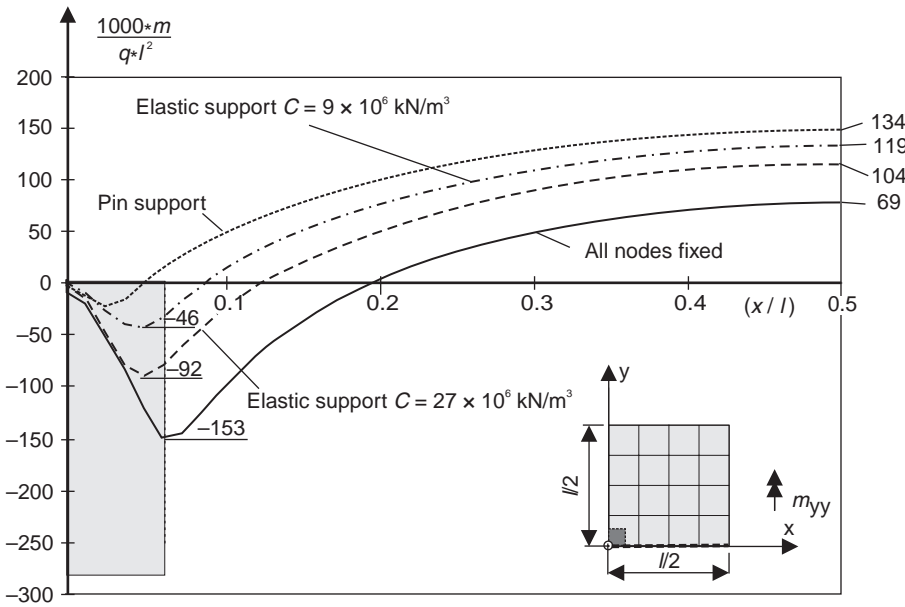


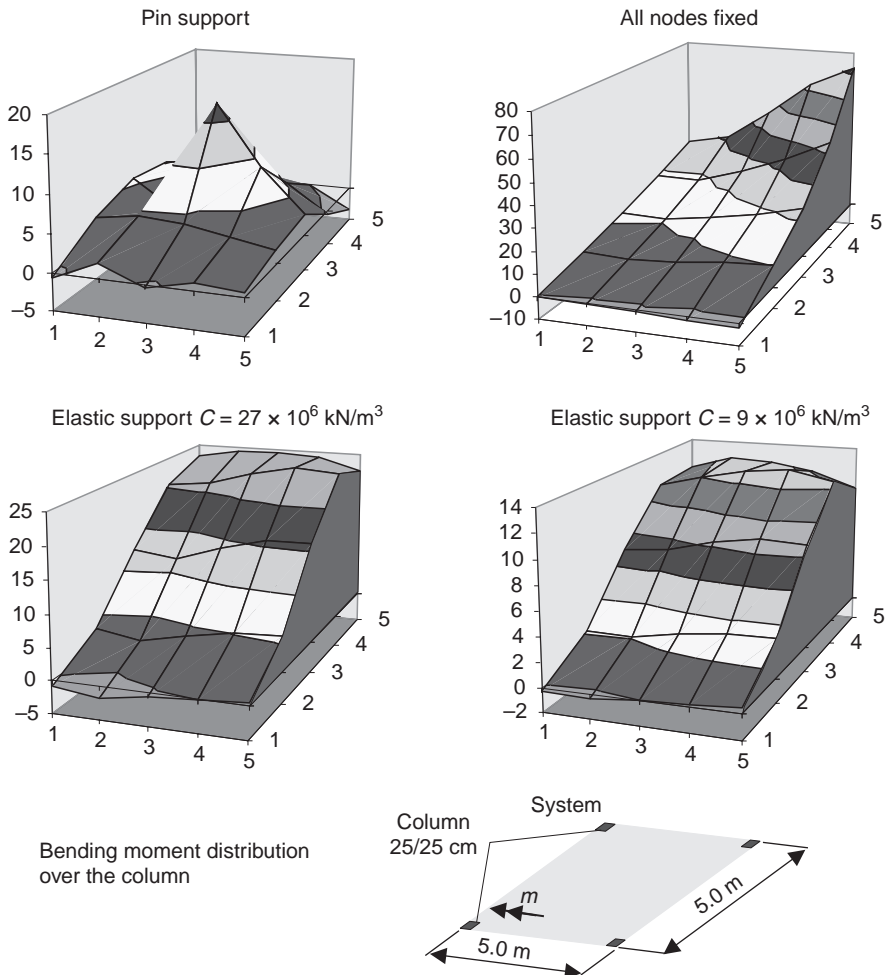
Figure 4.43 Bending moment m_{yy} in section $y = 0$ of an edge supported slab for different bedding moduli C



The span moment at the outer edge of the slab is 30% greater, if bedded elements are used instead of a pin support. Significant differences can be observed at the relevant sections for design at the face of the column. The extreme values are $m = 0$ kNm/m to $m = -38$ kNm/m.

These differences become clear when the 3D distribution of the bending moments above the column is checked (Figure 4.44). The peak values are not located on the symmetry axis. The largest bending moment is between $m = -14$ kNm/m for bedded elements with $C = 9000$ MN/m³ and $m = -73$ kNm/m for fixed nodes.

Figure 4.44 Bending moments at an edge column for different bedding moduli C (thin shell elements)



4.10. Foundation slabs

Foundation slabs are spatial concrete structures that distribute the load of the structure before transferring it into the ground. Thus, the ground pressure is mostly reduced in comparison to footings.

The following foundation types are used in practice

- (a) footings: used for high concentrated forces (e.g. those resulting from column loadings)
- (b) strip foundations: used underneath walls or series of columns
- (c) foundation slabs: used under buildings as load-bearing elements and for watertight structures.

The design of a strip foundation in the direction of the longitudinal axis can be done by means of a flexible supported beam model. The member forces in the transverse direction can be determined either analytically, if the deformation of the structure can be neglected, or by means of a 2D plate model (see Section 4.10.2).

The internal forces of a foundation slab are mostly estimated by means of the stiffness modulus method. The inaccuracies of this approach have already been discussed in Section 2.4.1. The main advantage of this model lies in the fact that the bedding behaviour can easily be implemented within the element functions. Thus, no contact or interface elements are required, which simplifies the mesh generation and the numerical analysis. Furthermore, a 2D plane FE model is sufficient, whereas the constraint modulus method requires a 3D model of the structure and the ground or an iterative solution. The following calculations are based on the stiffness modulus approach.

4.10.1 Footings

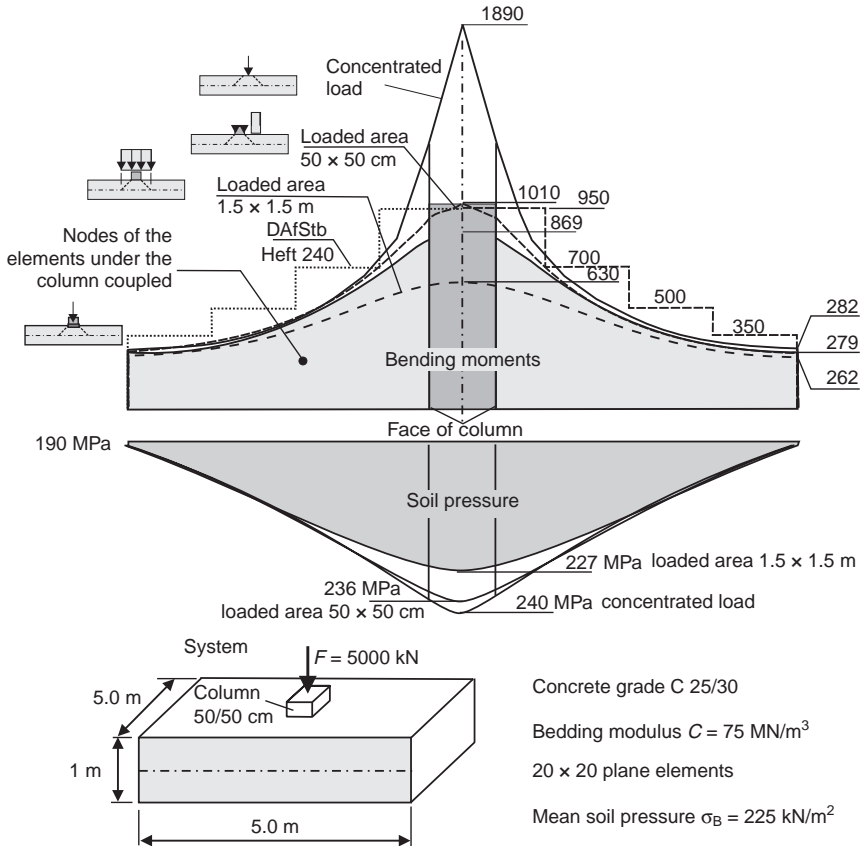
Footings are used under high concentrated loads, for example, those caused by columns. The panel dimensions necessary for these foundations are mostly determined by the permissible soil pressures. The slab depth is fixed by the design for bending or by shear (punching). For small loads, massive block foundations can be used that may be not reinforced. Such structures can be designed by means of strut-and-tie models. Numerical analysis is not required.

The following example focuses on the design of the foundation slabs. The internal forces can be calculated by means of an FE model or simplified analytical approaches, such as the equivalent strip method given in Grasser *et al.*, 1991. Hence, different models are available to verify the results of the numerical analysis.

The columns, which transfer the load to the foundation, can be modelled with different approaches such as those used for flat slabs. The variants are (Figure 4.45)

- a concentrated single loading
- uniform loading over the area of the column (50/50 cm)
- uniform loading, extension of the loaded area to the midplane of the slab (1.50/1.50 m)

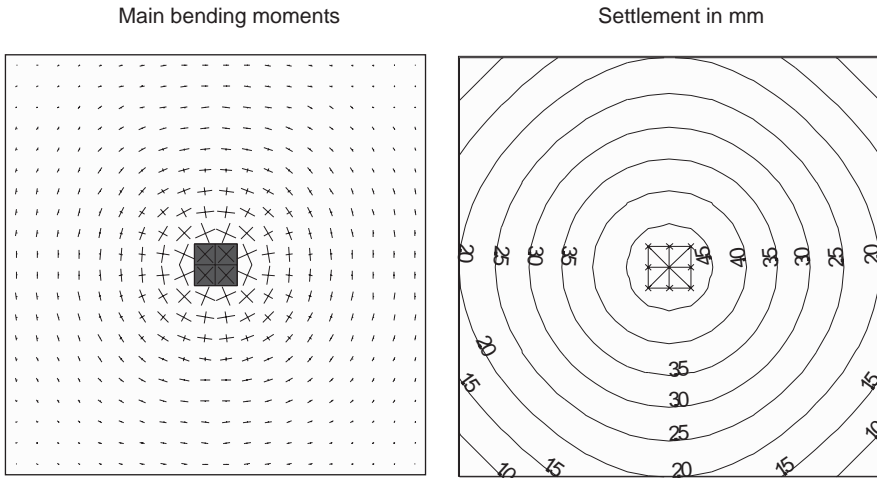
Figure 4.45 Moment distribution of a single slab foundation in the central axis



- hinge coupling of the elements in the column area with the node at the centre of the column (coupled area is equal to column dimensions, 50/50 cm).

The bending moment distribution in the symmetry axis calculated for the different models are presented in Figure 4.45. The rectangular slab with $l_x = l_y = 5.0 \text{ m}$ is loaded by a concentrated force of $F = 5000 \text{ kN}$. The stepped curve is calculated with the simple analytical approach given in Grasser *et al.*, 1991. With the given FE model, a single concentrated load results in a very high moment peak (singularity) of $m_{\max} = 1890 \text{ kNm/m}$. If the load is distributed over the area of the column ($m_{\max} = 1010 \text{ kNm/m} = 100\%$), it results in only half of this value. A coupling of the elements under the column results in a further decrease in the maximum moment by approximately 14%. A bending moment of $m_{\max} = 630 \text{ kNm/m} = 62\%$ is obtained when the column load is dispersed up to the midplane of the foundation slab at an angle of 45° , resulting in a loaded area of $1.50 \times 1.50 \text{ m}^2$. It can be observed that the size of the loaded area has a significant effect on the bending moment distribution. On the other hand, the soil pressure is not sensitive to the loaded area in this example.

Figure 4.46 Main bending moments and settlements



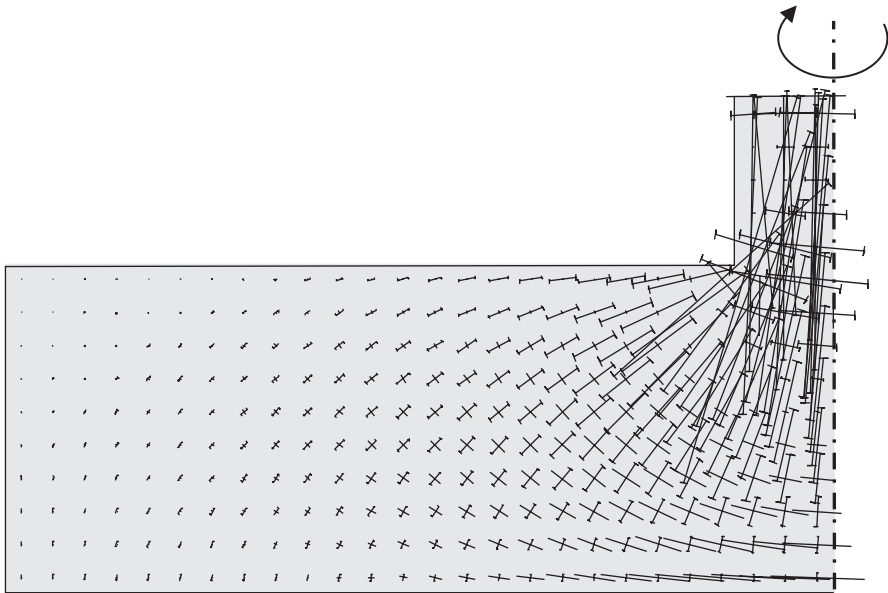
The correct model respectively the correct loaded area can only be found by verification of the used method with experimental results or by means of a 3D FE analysis. The main bending moments show an axisymmetric pattern in the column region, as can be seen in Figure 4.46. Thus, an axisymmetric model (diaphragm), and not a 3D model, is sufficient to determine the correct linear elastic values. Figure 4.47 shows the main membrane forces and Figure 4.48 the horizontal stresses in three sections of a circular foundation slab with a diameter of $d = 5$ m.

The numerical integration of the horizontal stresses at the face of the column results in a bending moment of $m_{\max} = 637$ kNm/m. This value is similar to that of the slab model with a loaded area of 1.5×1.5 m². However, such agreement seems to be only a coincidence, since the essential assumption of a plate model, a linear strain distribution over the width of the slab, does not apply to most parts of the structure (Figure 4.48). The external load is carried by bending and by inclined compression struts. Strut-and-tie models should be used for the design of such a structure. The compression struts form a truncated cone for the given axisymmetric foundation slab (Figure 4.49).

A horizontal tensile force of $n_x = 5000 / (2\pi \cdot 0.90) = 884$ kN/m is calculated under the assumption of an angle of load distribution of $\theta = 45^\circ$. The value is quite similar to the tensile force in the region of the column ($n_x = 710 + 999$ kN/m), with a mean value of $n_x = 855$ kN/m).

The previous analysis should demonstrate an essential problem in numerical models of slab foundations. The plate model is based on a linear strain distribution over the depth of the slab. This assumption does not apply to thick foundation slabs and in regions near the column.

Figure 4.47 Main membrane forces of a circular foundation slab



Test results are used in the following to verify the earlier-mentioned results. Figure 4.50 shows the measured and calculated steel tensions in the reinforcement and the soil pressure on the support and the field strip of a footing. The footing has a height of 0.32 m and a square base of 1.50 m \times 1.50 m. In the test, the footing was loaded by a uniform load on the slab bottom instead of a single force in the column. The measured

Figure 4.48 Horizontal stresses in kN/m^2

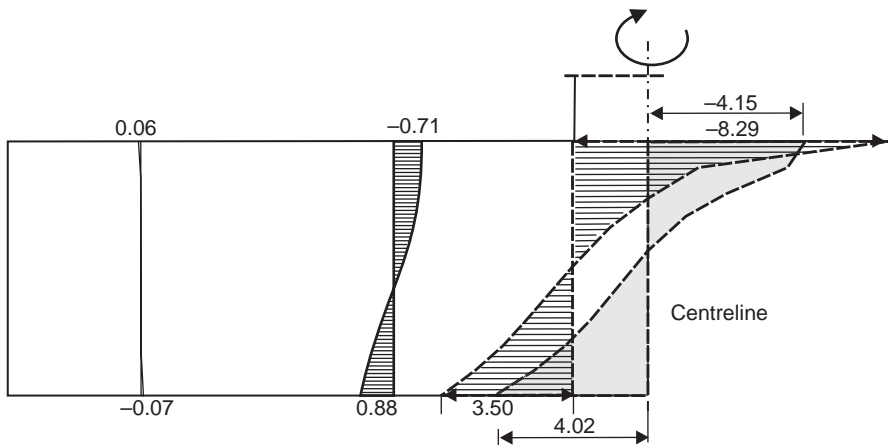
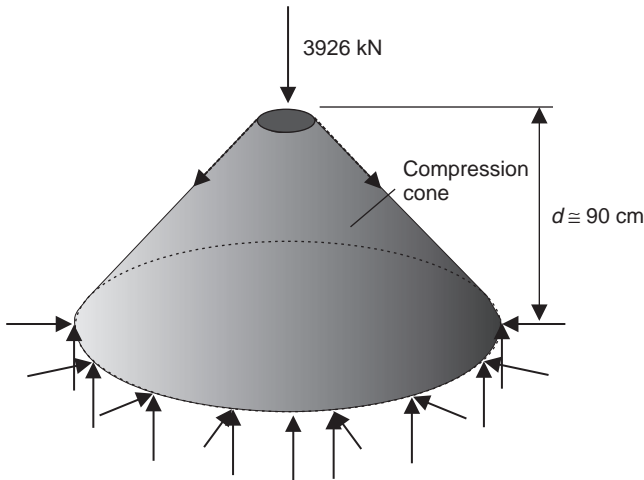


Figure 4.49 Equivalent strut-and-tie model – truncated cone



steel stresses are smaller in the supporting strip than at the face of the column (column strip). Therefore, the face of the column is relevant for the design of the footing and not the middle of the column.

In the right figures, the results of the FE analysis are given for different loaded areas. The footing was modelled with 20×20 plane elements. For the calculation of the steel tensions from the bending moments, a steady inner lever arm from $z = 0.9d = 0.27$ m was used. As one sees from the curves on the right in Figure 4.50, the relevant bending moment in the face of the column can be determined with sufficient accuracy within the scope of the measuring tolerance with all models. The point-load should not be used, however, because the maximum moment increases with a refinement of the element mesh and, at the same time, the relevant moment at the face of the column decreases. In the field region, slightly conservative values are determined with almost all FE models.

4.10.2 Strip foundations

A slab model can be used to design a strip foundation in the transverse direction. For the uniformly distributed loading of a beam or plate, a strip is sufficient to describe the behaviour of the whole structure (see Figure 4.51). The following calculations are carried out on a strip foundation with the same dimensions as the previous example (width $b = 5$ m, depth $h = 1$ m and bedding modulus $C = 75$ MN/m²).

The bending moment distribution for the various loaded areas is shown in Figure 4.52. It must be noted that a uniform continuous load does not cause a moment peak. The loaded area slightly changes the maximum bending moments. There is a difference of approximately $\pm 15\%$ in the mean value.

Figure 4.50 Stresses in the reinforcement and soil pressure of a footing – test results against FE analysis

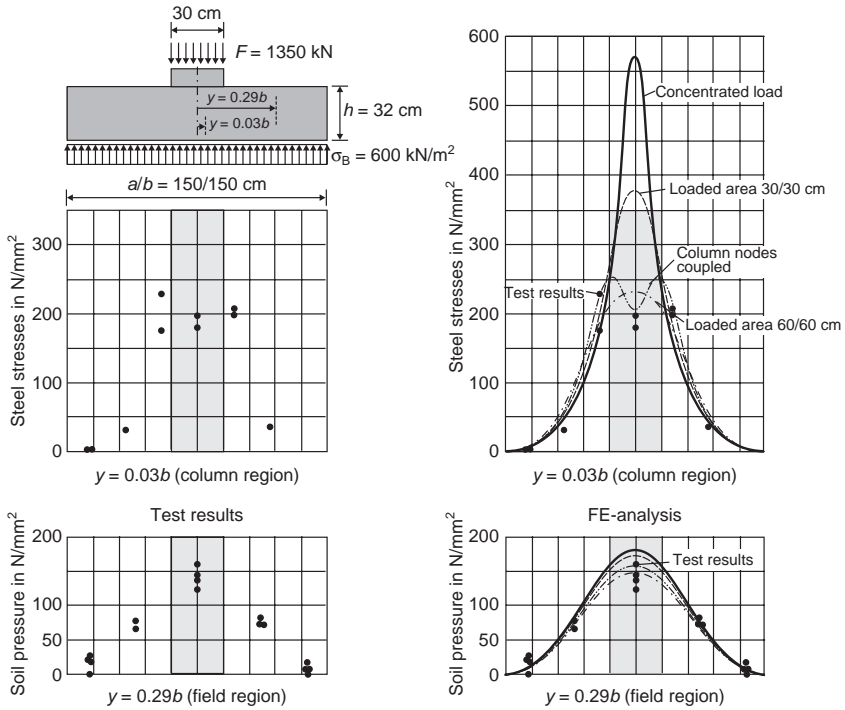


Figure 4.51 Strip foundation: structure and FE model

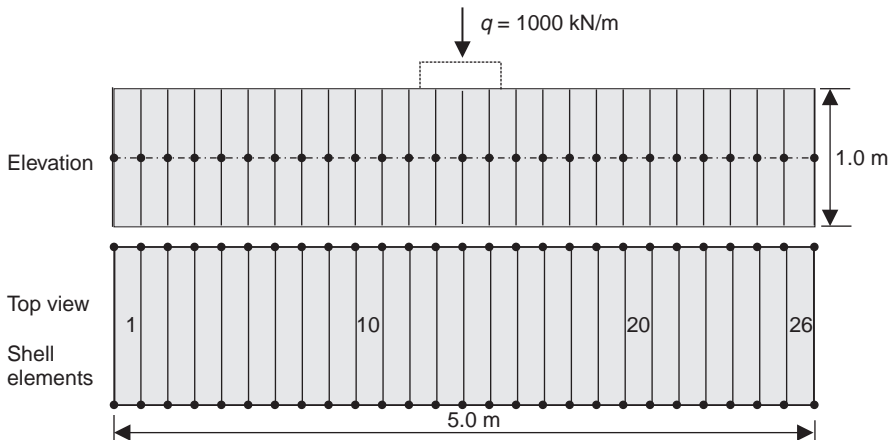
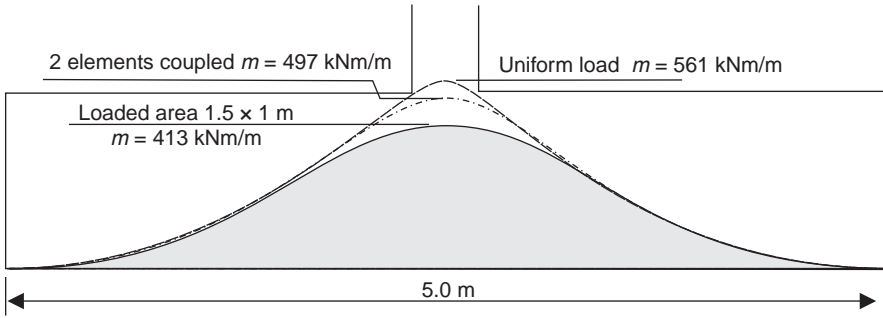


Figure 4.52 Bending moment distribution of a strip foundation (plane shell model)



The same system has been analysed with a shell model. The results are shown in Figure 4.54. It can be seen that the distribution of the horizontal stresses over the cross-section depth is almost linear. The numerical integration of the horizontal stresses results in a bending moment of $m_{max} = 449 \text{ kNm/m}$. This is similar to that of the shell model with coupled nodes. Thus, extending the loaded area up to the midplane of the slab at an angle of 45° results in unsafe bending moment distribution. This model should not be used.

A tensile force of $F = 500 \text{ kN}(125 - 12.5/90) = 625 \text{ kN/m}$ ($\theta = 39^\circ$) can be calculated from a simple strut-and-tie model (Figure 4.53). This force is greater than that of the plate model, as a uniform soil pressure distribution has been assumed for simplicity.

4.11. Skewed slabs

The previous sections only focus on rectangular slabs or flat slabs. These simple structures have been used to demonstrate the basic problem in adequate modelling of

Figure 4.53 Simple strut-and-tie model of a strip foundation in transverse direction

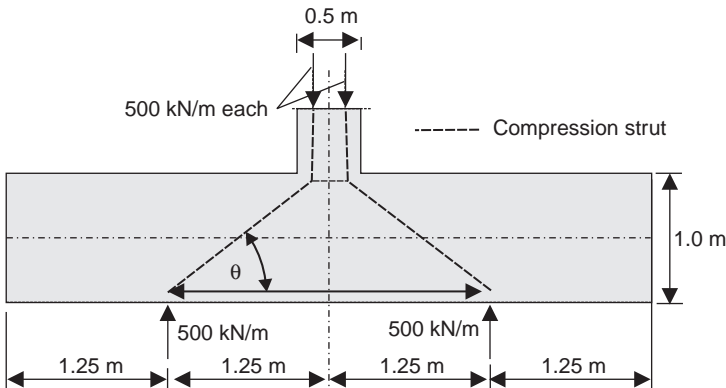
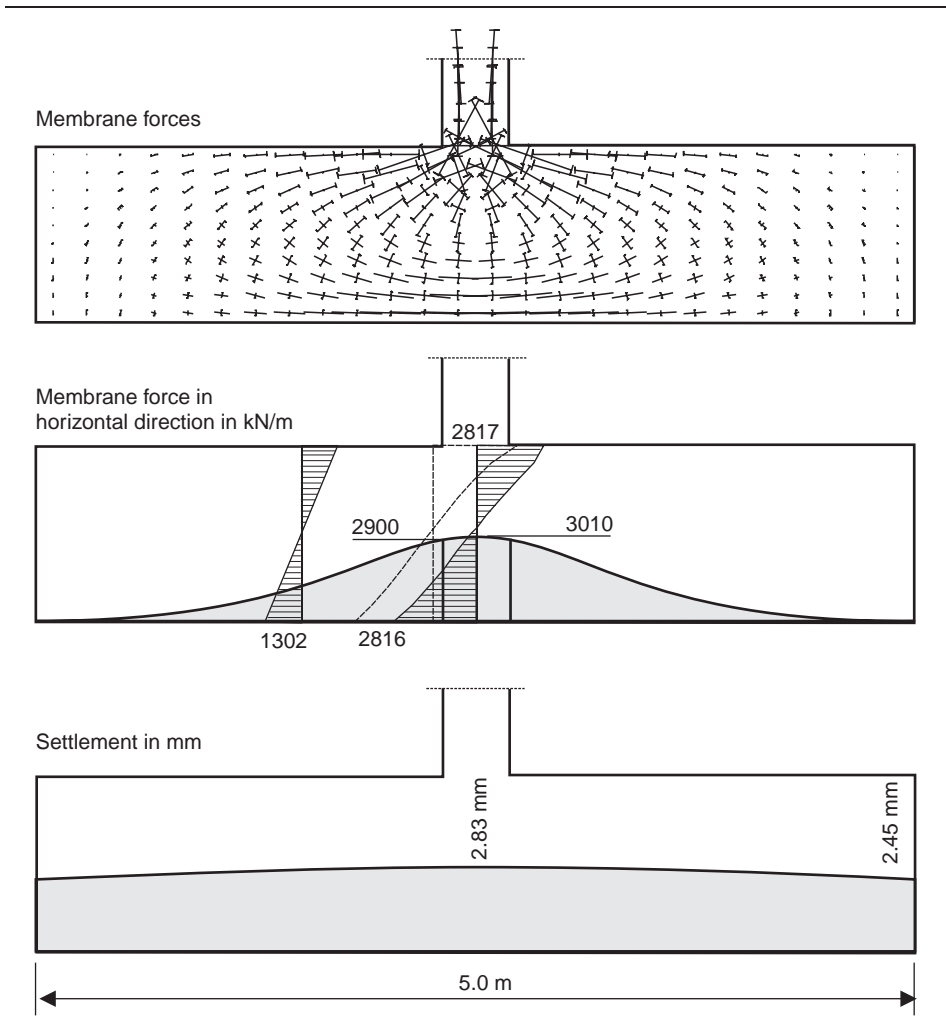


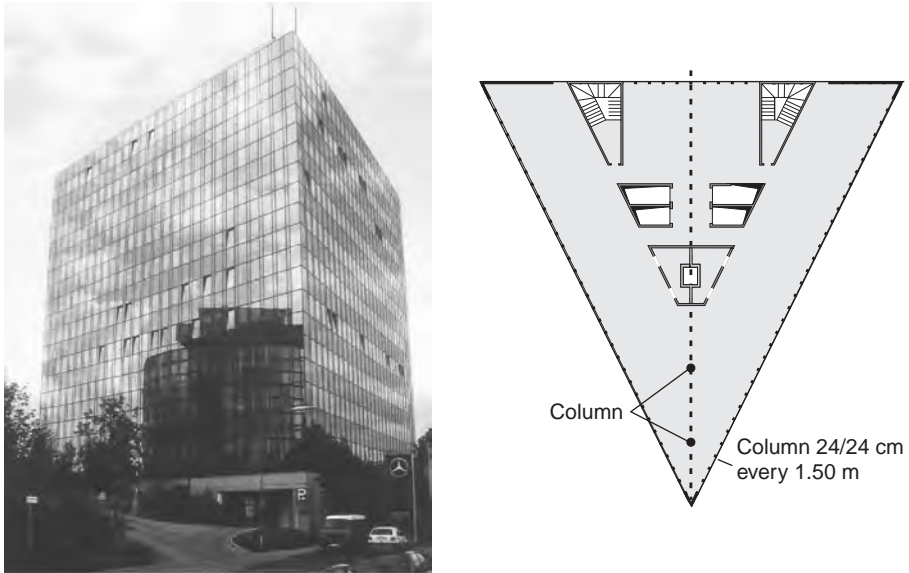
Figure 4.54 Strip foundation – membrane forces and settlements



the support condition and the loaded area. In practice, more complicated slab systems are built that have complex support conditions and irregular layout (Figure 4.55). It is one of the most important advantages of concrete that structures can be built in arbitrary shapes.

Skewed slabs, where two parallel edges are simply supported and the other edges are free, are often used for single-span bridges. A line support results in infinite shear forces and bending moments in the obtuse corner, as can be seen in Figure 4.56, where the distribution of the internal forces at a simply supported edge are presented. The slab has a width of 13 m and an angle of 45° to the supported axis. The singularity of the support forces can be seen clearly.

Figure 4.55 Triangular slab of an office building (details see Section 6.2)



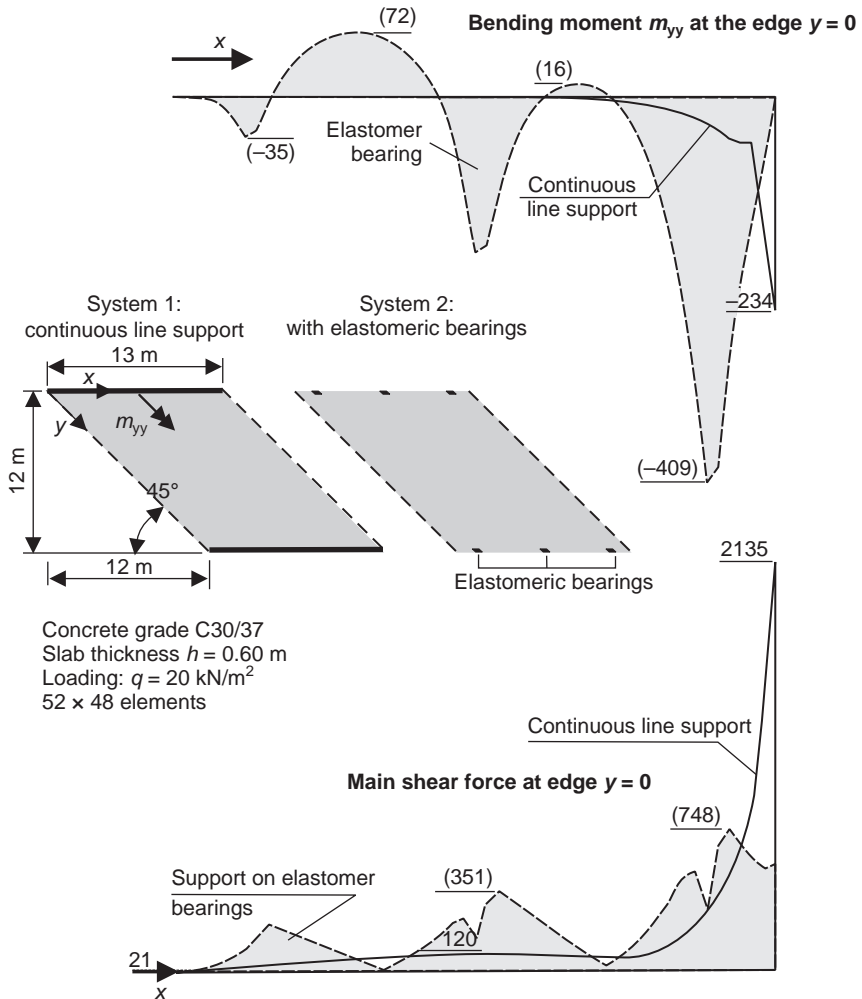
The peak moments can be reduced significantly if the stiffness of the individual bearings is considered. In Figure 4.56, the internal forces are plotted for a slab with three elastomeric bearings ($50 \times 25 \text{ cm}^2$, height $h = 10 \text{ cm}$) closed to two parallel edges. The main shear force in this system is one-third of that of the simple continuous supported slab. The bending moment m_{yy} in transverse direction is increased from -234 kNm/m to -409 kNm/m . The transverse bending moment can be reduced if the number or the size of the bearings is increased.

The internal forces at the midspan are almost independent of the support conditions, as shown by the figures given in Table 4.10.

Table 4.10 Internal forces and deflections at midspan ($y = 0.5l = 6 \text{ m}$)

	Rigid support		Elastomer bearings	
	Centre	End	Centre	End
Bending moment m_{yy} : kNm/m	0	131	-29	121
Bending moment m_{xx} : kNm/m	397	195	414	196
Shear force v : kN/m	0	331	0	406
Deflection w : mm	11.5	14.7	18.6	20.6

Figure 4.56 Bending moment and main shear force at the supported edge of a skewed slab

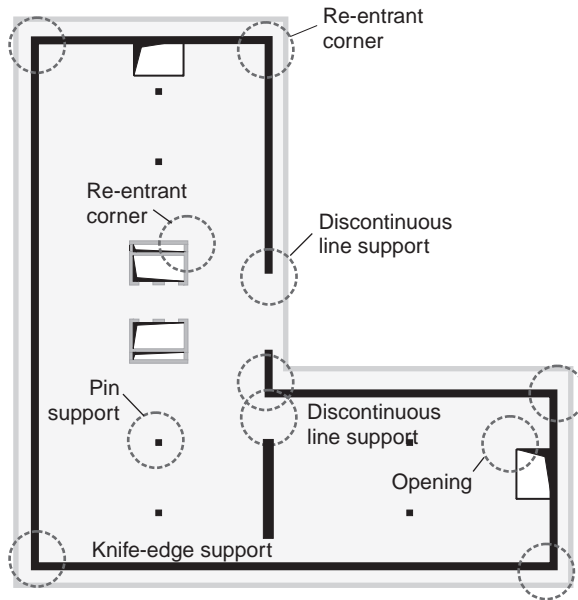


4.12. Singularities

Singularity problems may arise in linear elastic slab calculations, as has been previously shown. Some problems can be avoided by a flexible support or an extension of the loaded area. Singularities may occur in the regions of (Figure 4.57 and Table 4.11)

- walls that end within a slab (Section 4.7)
- discontinuous line supports (Section 4.7)
- pin support (Section 4.9)
- obtuse corners (Section 4.11).

Figure 4.57 Singularities



Two more singularity regions that are relevant in practice are treated next

- openings
- re-entrant corner ($\alpha \geq 90^\circ$)
- concentrated loads.

Singularities are caused by simplifications of numerical models (Burton and Sinclair, 1956). The assumption of a linear strain distribution over the section depth does not apply close to the supports. Moreover, infinite stresses do not occur in reality. The building material 'concrete' may yield under high compressive stresses or show some cracking if the tensile strength is exceeded. Therefore, the aim of a numerical calculation is not to determine the 'correct' value of the action effects by highly refined element meshes. For the dimensioning of the structure, only realistic safe values are required.

4.12.1 Opening with re-entrant corners

If linear elastic material behaviour is assumed, then the bending moments and shear forces will reach infinite values in the region of re-entrant corners. However, these highly concentrated forces are reduced in the real structure due to cracking of concrete. Hence, it is not required to design the slab for these high values or to refine the element mesh.

The singularity is caused by a sudden change of the boundary conditions at the corners of the unsupported edges. There are no bending moments in the direction of the free

Table 4.11 Singularities of FE-models based on Kirchhoff plate elements

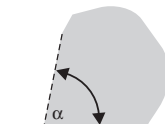
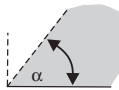
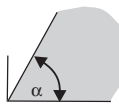
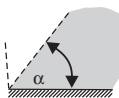
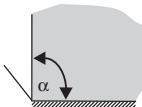
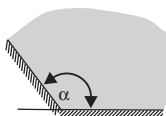
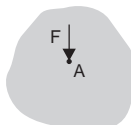
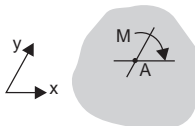
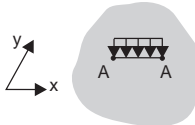
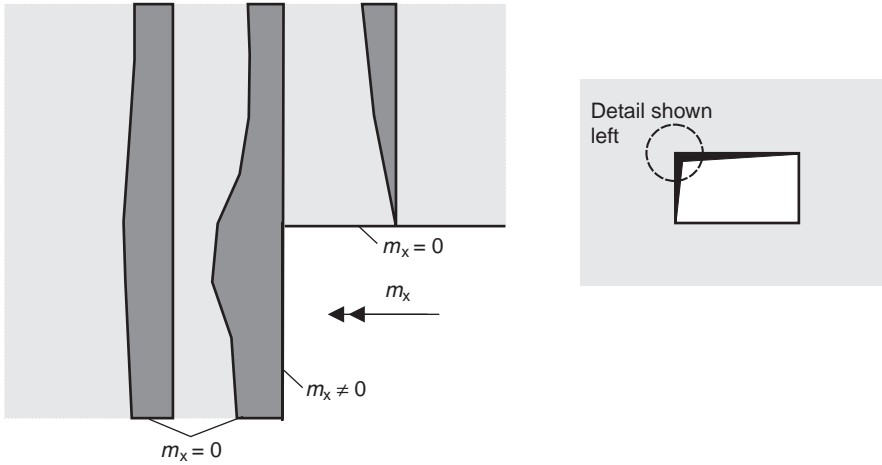
Support condition	Moments	Shear forces
	$\alpha > 180^\circ$	$\alpha > 78^\circ$
	$\alpha > 90^\circ$	$\alpha > 51^\circ$
	$\alpha > 90^\circ$	$\alpha > 60^\circ$
	$\alpha > 95^\circ$	$\alpha > 52^\circ$
	$\alpha > 129^\circ$	$\alpha > 90^\circ$
	$\alpha > 180^\circ$	$\alpha > 126^\circ$
<p>----- free edge</p> <p>———— hinge support</p> <p>////// fully restraint</p>		
Loading	Displacement, rotation	Internal forces
	No	Yes (m_x, m_y, v_x, v_y)
	Yes ($\varphi_y = \frac{dw}{dx}$)	Yes (m_{xy}, v_y)
	No	Yes (v_x)

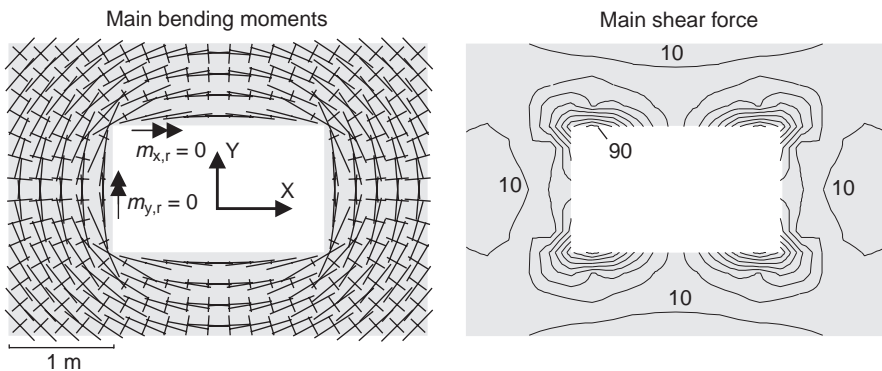
Figure 4.58 Moment distribution near the corner of an opening (FE results)



boundary, whereas bending moments perpendicular to the boundary may occur. This can be seen in Figure 4.58. The bending moment m_{xx} is not equal to zero at the left side of the corner, whereas it has to be equal to zero at the upper and lower side of the opening. This inconsistency leads to infinite internal forces and moments. An FE model always gives finite results. The maximum peak value depends on the size of the relevant elements. Only a small region near the corner is influenced by the singularity (Figure 4.58).

The distribution of the principal bending moments and shear forces in the region of an opening is presented in Figure 4.59. The high increase of the shear force in the corner indicates a singularity problem. The shear design of the slab is not possible (and not required) for these peak values.

Figure 4.59 Main bending moments and shear forces in the region of an opening



Singularity problems can be avoided by smoothing the edges, by rounding the corners in the FE model. However, this effort is not required in practice, as shown by the previous analyses.

4.12.2 Re-entrant corners ($\alpha \geq 90^\circ$)

Figure 4.60 shows the distribution of the main bending moments in the region of a cantilever slab, where two supporting walls meet at right angles. The singularity can be clearly seen. This problem can be solved if the vertical stiffness of the walls is considered in the numerical model (see Figure 4.60). The bedding modulus at the supports is chosen though the vertical deflection of the slab under the wall is less than 0.8 mm in this example. Even with this small value, the shear forces and the bending

Figure 4.60 Internal forces of a slab that is supported by two perpendicular walls – no supports at the outer edges

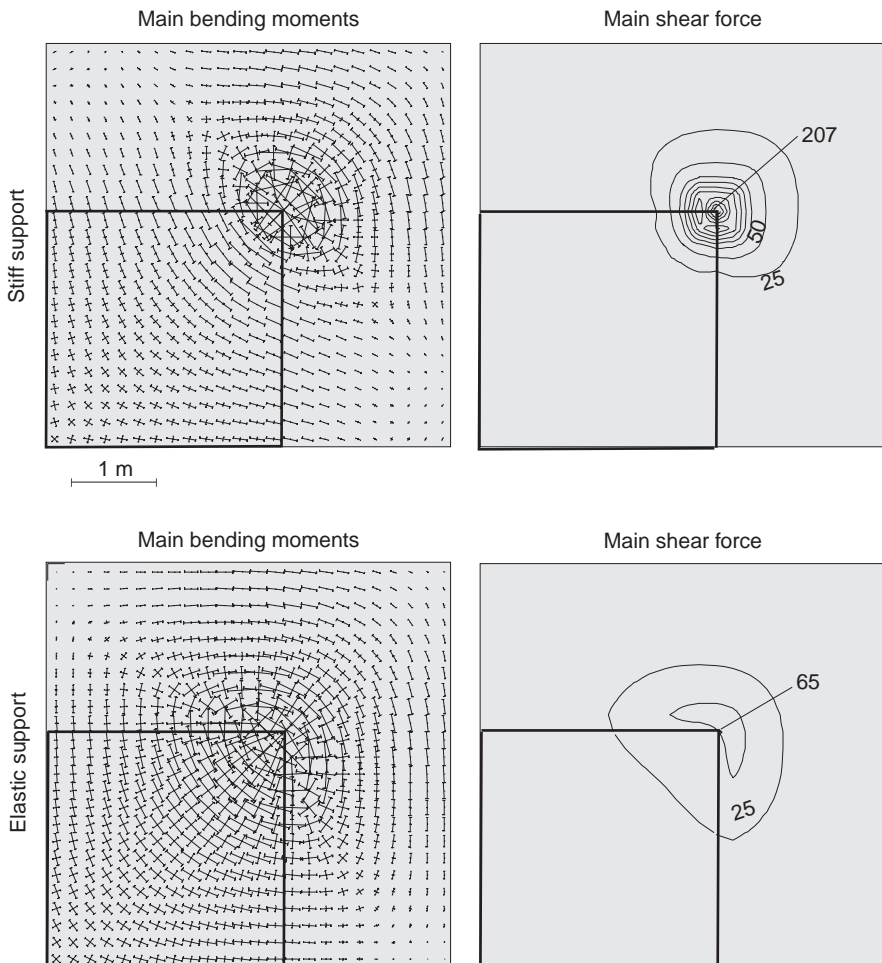
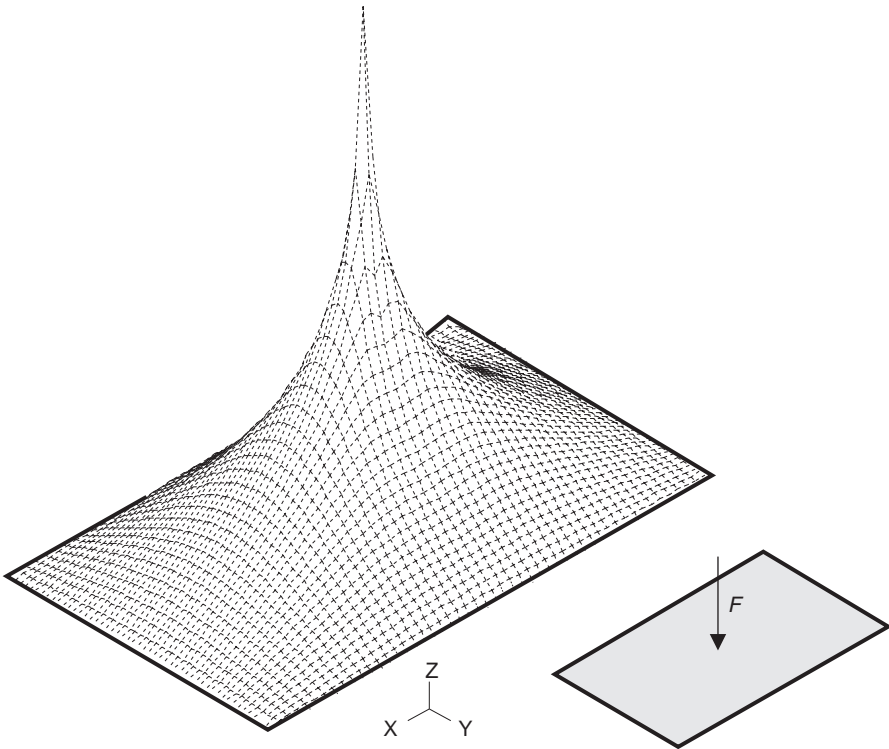


Figure 4.61 Moment distribution of a rectangular slab loaded by a point-load at the midspan



moments are reduced by a factor of 3 and 2, respectively, relative to those of a slab with rigid supports.

4.12.3 Concentrated loads

In the linear elastic Kirchhoff slab theory, infinite internal forces are calculated under a point-load (see Figure 4.61), whereas the deflections are limited. This singularity problem can easily be solved by extending the loaded area, as will be demonstrated in the following text.

Concentrated loads may occur, for example, on deck slabs of hollow box or T-beam bridges. The internal forces due to truck loading are calculated in the following example using a simplified system of a partially restrained equivalent slab (Figure 4.62), as in practice a 3D FE model of the whole structure is too extensive. A detailed estimation of the effective span length is not required with regard to the assumptions of the model. The rotational stiffness of the webs may be estimated by separate manual analysis, for example, using an equivalent beam model. It depends not only on the structural system, but also on the type of the loading.

The point-load has to be dispersed up to the midplane to avoid singularities (Figure 4.63).

Figure 4.62 Equivalent slab model for the deck of a hollow box girder bridge

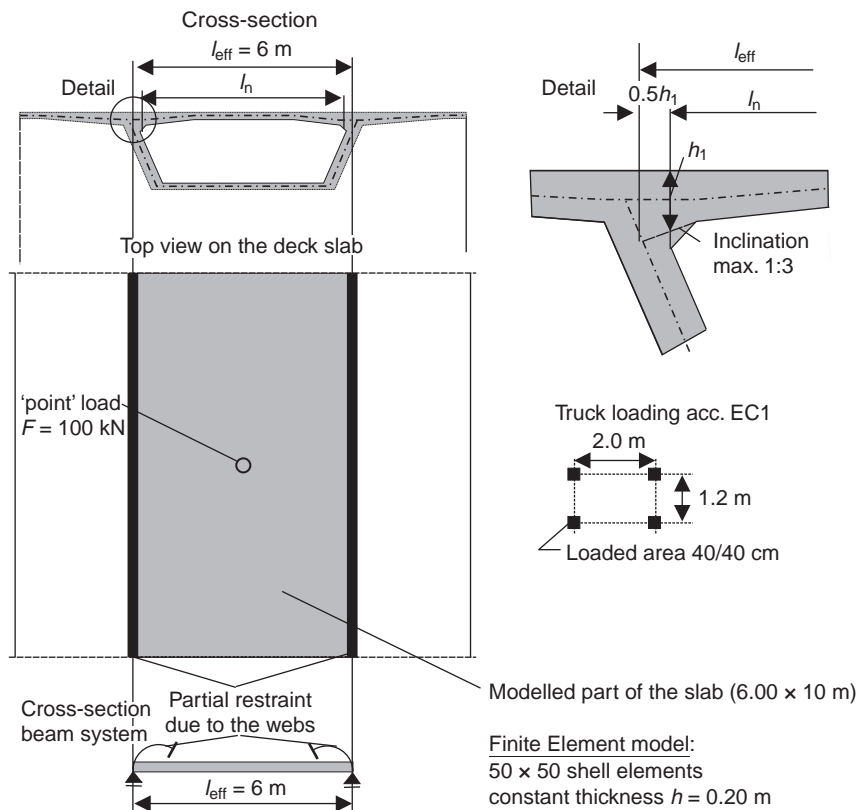


Figure 4.63 Dispersion of concentrated loads up to the midplane

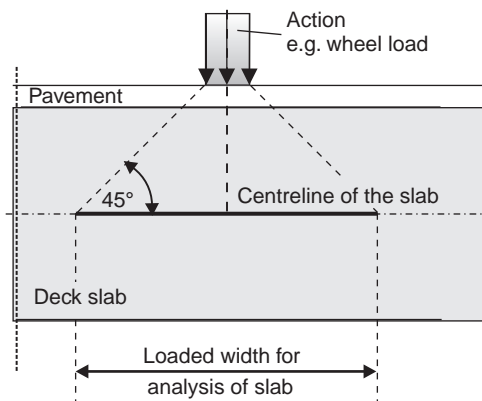
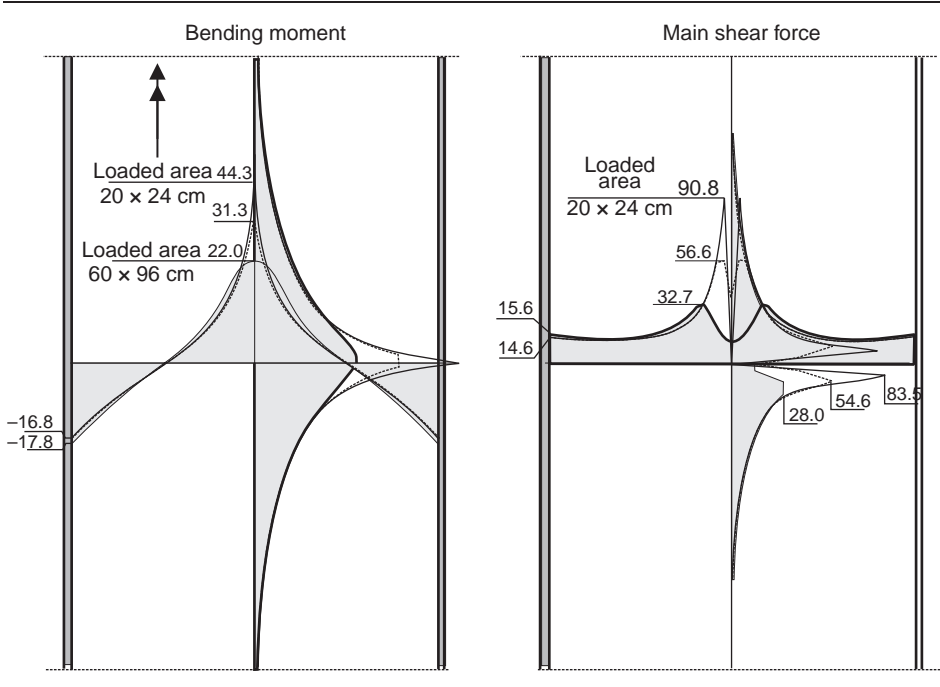


Figure 4.64 Moment and shear force distribution of a plate strip loaded by a force of $F = 100$ kN at midspan – different loaded areas



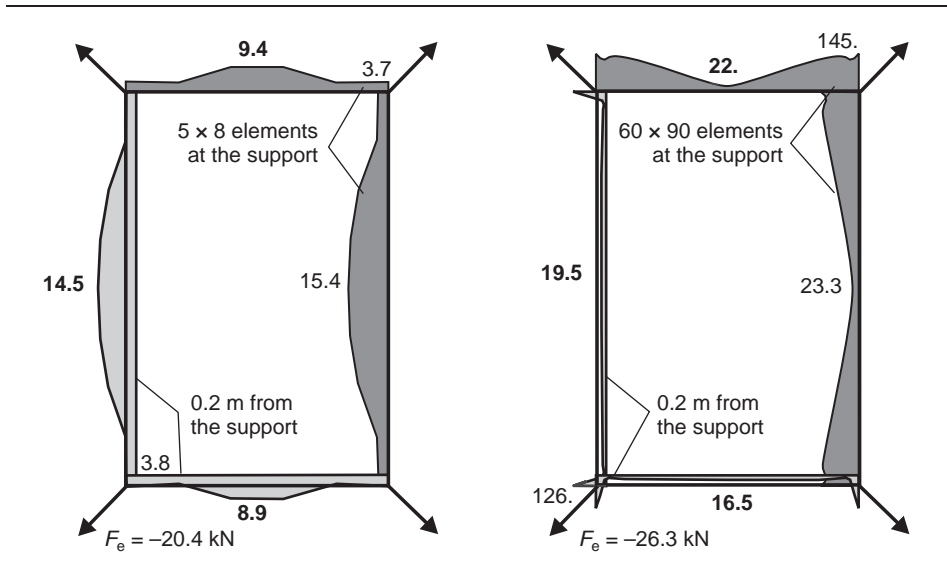
The significant influence of the loaded area on the bending moments can be seen in Figure 4.64. Here, the bending moments for a total force of $F = 100$ kN and a loaded area of 0×0 cm², 24×20 cm² and 60×96 cm² are plotted. The slab has an effective span length of $l_{\text{eff}} = 6.0$ m and a constant thickness of $h = 20$ cm. The inclined haunches near the webs are neglected.

An FE analysis of the deck slab is required if more accurate internal forces are needed for design or in the case of special load arrangements. Tables published in literature and influence lines provided by Homberg and Ropers (Homberg, 1973; Homberg and Ropers, 1965) can be used for normal conditions. The determination of the internal forces by means of tables may be time-consuming, as various values have to be interpolated; thus, an FE analysis may be economical.

4.12.4 Forces in the corners of simply supported rectangular slabs

The principal shear forces of a rectangular slab for different element meshes ($l_y/l_x = 5.0/7.5$ m, $h = 0.20$ m) are shown in Figure 4.65. The values are plotted in two sections, at the centreline of the support and at a distance of $1.0d \approx 0.20$ m from the support. The latter section is relevant for shear design. The slab is modelled by 5×8 and 60×90 plane shell elements. A uniform load of $q = 10$ kN/m² is applied. The principal shear force increases significantly with the number of elements, even for the section of $1.0d$. A big difference in

Figure 4.65 Principal shear forces at the centreline of the support and at a distance of 0.2 m from the support for 5×8 and 60×90 elements



the shear force distribution along the supports can be recognised. The high values in the corners result from a model problem. A sharp corner of a simple supported rectangular slab is a singularity region, as can be seen in Figure 4.65. Hence, one does not need to design the slab for such high shear forces.

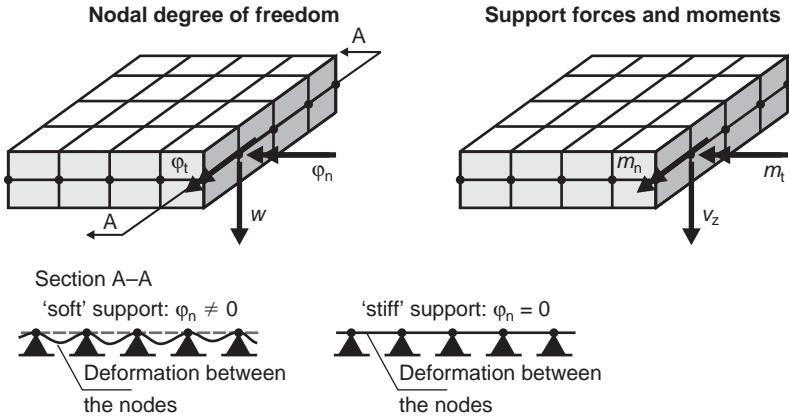
In Table 4.12, the principal shear forces, as well as the concentrated edge force F_e , are listed for both element meshes. It can be seen that the shear forces cannot be calculated with a broad mesh of 5×8 elements. Furthermore, it becomes clear that the maximum values in the middle of the support at $1.0d$ as well as the edge force are not sensitive to this discretisation.

Table 4.12 Principal shear forces and concentrated edge force for different element meshes in kN/m or kN

Discretisation	Support		At 0.20 m		F_e
	Midspan*	Corner	Midspan*	Corner	
5×8 elements	9.4/14.5	3.7	8.9/14.5	3.8	20.4
10×15 elements	16.0/19.2	29.8	15.1/18.2	26.9	23.7
20×30 elements	18.5/21.0	72.5	16.9/19.6	60.9	25.3
40×60 elements	20.9/22.5	120.4	16.9/19.8	101.5	26.4
60×90 elements	22.2/23.3	145.1	16.7/19.8	126.3	26.3

* Short/long span

Figure 4.66 Fixation of support nodes



Up to now, the nodes at the supports were fixed only in the vertical direction. This model is called ‘soft’ support (Figure 4.66). The rotation (torsion) at the support φ_n is not equal to zero as it should be with a stiff simple support. In contrast, φ_n is fixed at a ‘stiff’ support. The differences of both models are mostly negligible, but not in the area of the corners, as will be illustrated in the following.

‘Stiff’ support	$w = 0$	$\varphi_n = 0$	$\varphi_t \neq 0$	$v_z \neq 0$	$m_t \neq 0$	$m_n = 0$
‘Soft’ support	$w = 0$	$\varphi_n \neq 0$	$\varphi_t \neq 0$	$v_z \neq 0$	$m_t = 0$	$m_n = 0$

The shear forces at the support and at a distance of $0.2d$ for a ‘soft’ and a ‘stiff’ support are plotted in Figure 4.67. The big differences in the corners are easy to recognise. With the ‘stiff’ support, no shear peaks are estimated, and the edge force is close to zero. The fixation of the rotation φ_n at the edges leads to a fully clamped support in this region, which will rarely be the case in reality. Also, with this support condition, the real behaviour of a slab near the corners cannot be modelled. Better results can be achieved with a 3D model with volume elements. Due to symmetry of the slab and the loading, only a quarter of the slab must be discretised. Approximately 100 000 elements were used. Figure 4.68 shows that the support forces of the volume FE model are identical to the shear forces in the slab.

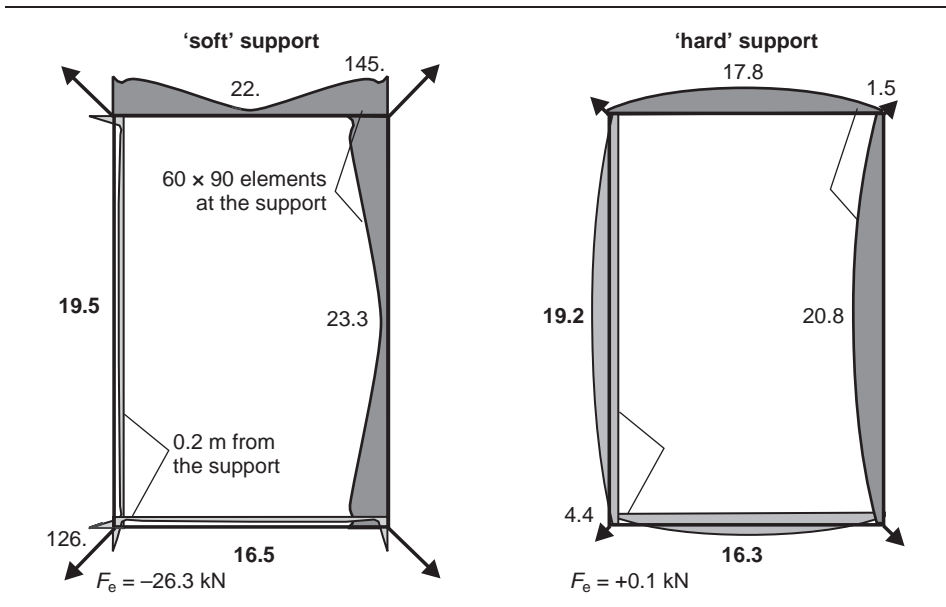
In middle of the span, a good agreement can be seen (Figure 4.67), whereas the concentrated edge force $F_c = 8.4 \text{ kN}$ is considerably lower than for a simple supported slab.

4.13. Discretisation – generation of the element mesh

Nowadays, the element mesh is generated by means of graphical pre-processors. The effort is considerably less than manual input. Also, input errors caused by incorrect coordinates of the nodes or restraints are mostly avoided by the visual control.

An automatic mesh generation can only consider the main geometrical boundaries. Refinements are required in regions of great stress gradients and high concentrated

Figure 4.67 Shear forces for 'soft' and 'hard' support



loads, and have to be done manually by the user, if no adaptive mesh-refinement tools are available. Hence, the mesh generation requires sufficient experience and skills in use of FEM and knowledge of the material properties too.

The problems of mesh generation are demonstrated by the following two real examples, where the author was involved as a designer and a checking engineer.

4.13.1 Location of the nodes at a line support

The nodes at the supports of simply supported circular slabs should be located exactly on the outer circumference. Even small differences may result in a partial restraint of

Figure 4.68 Support forces – 3D model

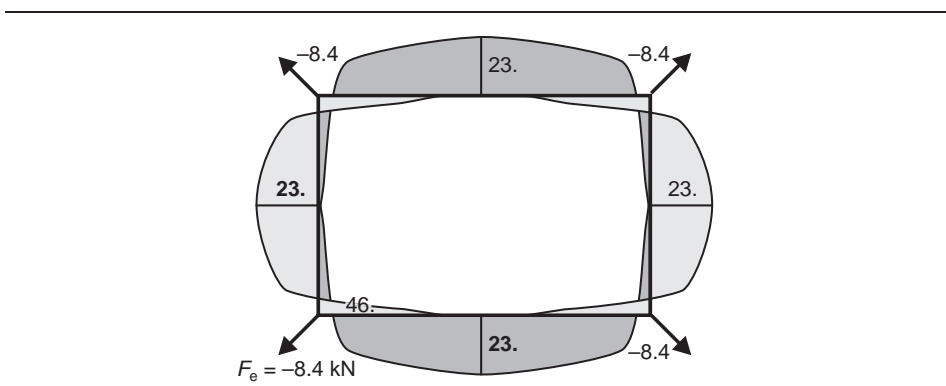
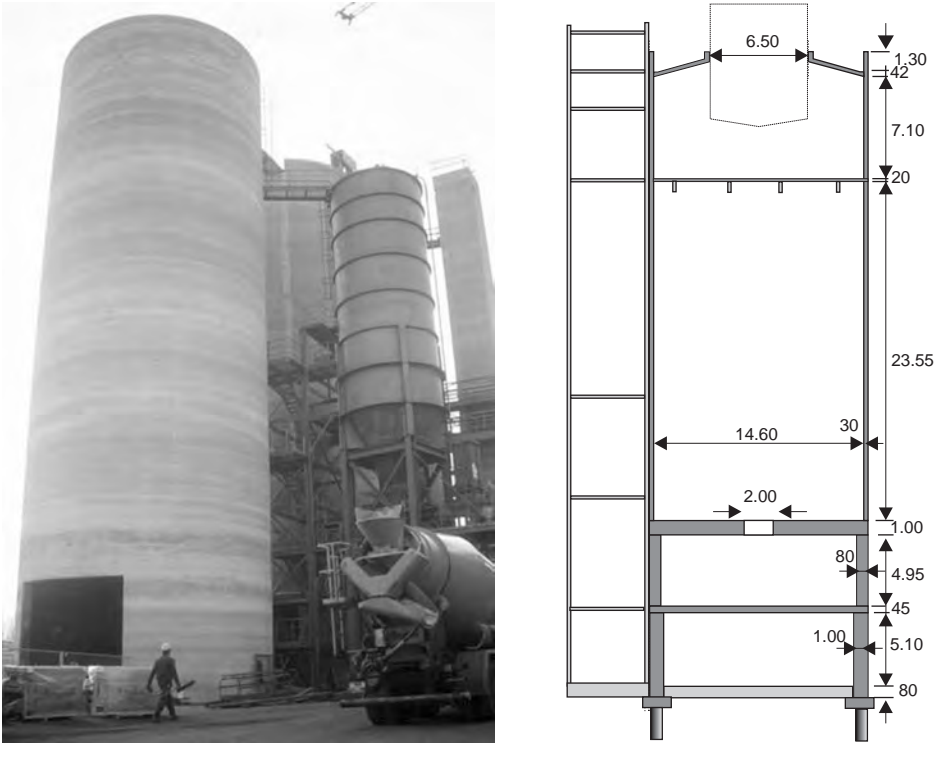


Figure 4.69 Silo structure



the slab even in the case of hinge support. This problem is demonstrated in a simple example.

Circular slabs are often used in tanks or bins, like the 48-m-high silo structure shown in Figure 4.69, which is used for storing fly ash. Large openings are necessary in the lower circular slabs to install discharge devices. In addition, high dynamic point-loads may occur due to the machines. The manual analysis of such a slab becomes very difficult. FEM can help us design these slabs.

The problem of mesh generation is not demonstrated for a real complex structure, but using a simplified system, for example, a circular slab (radius $r = 7.50$ m) which is simply supported at the outer edge. A uniform load of $q = 10$ kN/m² is applied on this structure (Figure 4.70). The internal forces and deflections can be estimated analytically. These values are used to verify the results of the FE analysis. The bending moment in the centre of the slab is:

$$m_1 = \frac{q \cdot r^2}{16} (3 + \nu) = \frac{10 \cdot 7.5^2}{16} (3 + 0.2) = 112.5 \text{ kNm}$$

Figure 4.70 Circular slab – boundary nodes not accurately placed on the outer circumference

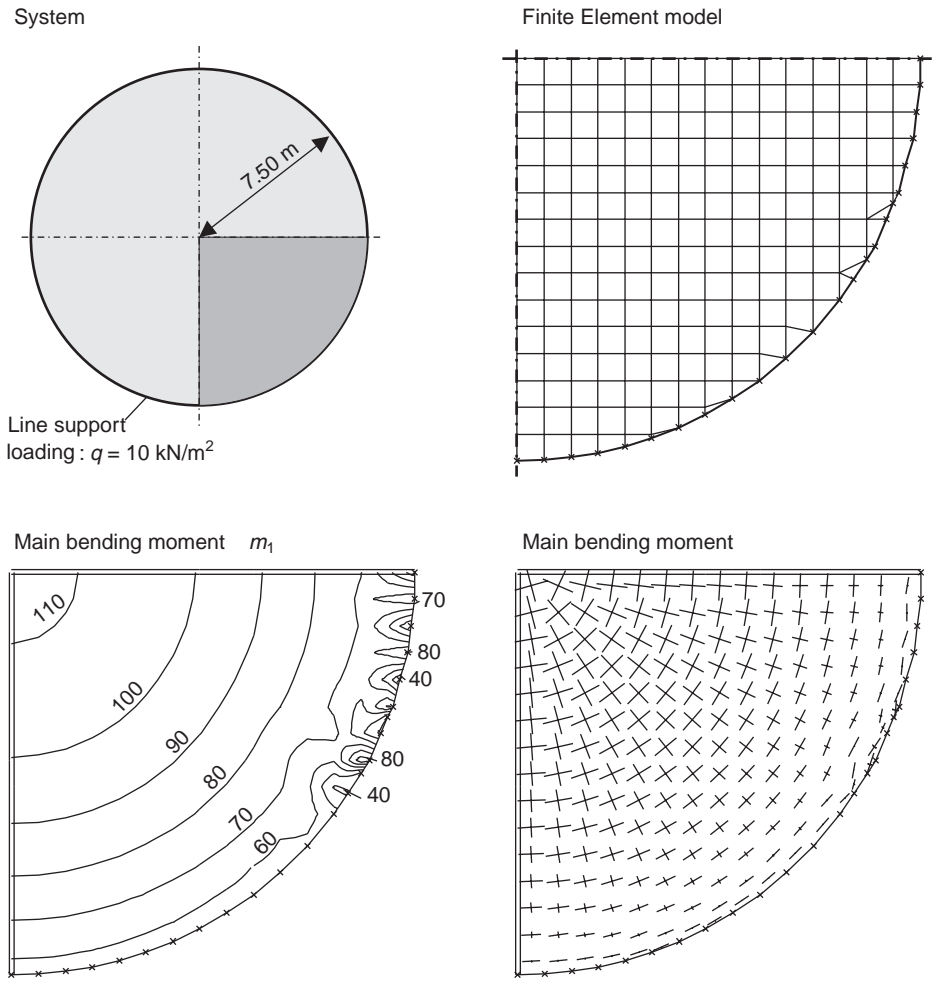


Figure 4.70 shows the FE mesh and the resulting main bending moments. Due to the symmetry conditions, it is sufficient to only model a quarter of the whole slab.

The orientation of the main bending moments at the upper edge of the slab is surprising. A support moment of $m_1 = 80 \text{ kNm/m}$ has been calculated. This moment is 70% of the maximum bending moment in the centre, even for a structure that is simply supported.

This error is caused by the faulty location of the nodes at the support. The fixed nodes at the upper right of the slab are located in a sawtooth manner, 1 mm away from the exact circle. Even this small value, equivalent to 1/1500 of the diameter, has a significant influence on the bending moments. The same problem arises in rectangular slabs, for cases where the fixed nodes are not located accurately on a straight line.

This example has impressively shown that the fixed nodes should be precisely located at the curved boundary.

Very often, only the graphical output of an FE analysis is checked. Errors in node coordinates, like those referred to earlier, can then hardly be noticed. Therefore, the checking of an FE analysis should not be restricted only to the graphical output of the software.

4.13.2 Size of the elements

A sufficient number of elements have to be used in order to model the real deformation characteristics and the load-bearing behaviour of a structure. This has to be considered particularly for curved boundaries, as will be demonstrated on the simply supported circular slab under uniform load of $q = 10 \text{ kN/m}^2$, mentioned previously.

Figure 4.71 shows the bending moment distribution and the deflection in the centre of the slab for different numbers of elements. The correct values can be estimated analytically.

bending moment in the centre

$$m_1 = \frac{q \cdot r^2}{16} (3 + \nu) = \frac{10 \cdot 7.5^2}{16} (3 + 0.2) = 112.5 \text{ kNm}$$

deflection in the centre

$$w = \frac{(5 + \nu) \cdot q \cdot r^4}{64 \cdot (1 + \nu) \cdot \frac{E \cdot h^3}{12 \cdot (1 - \nu^2)}} = \frac{(5 + 0.2) \cdot 10 \cdot 7.5^4}{64 \cdot (1 + 0.2) \cdot \frac{34 \cdot 10^6 \cdot 0.5^3}{12 \cdot (1 - 0.2^2)}} \cdot 10^3 = 5.8 \text{ mm}$$

Figure 4.71 FE meshes for a circular slab – various numbers of elements

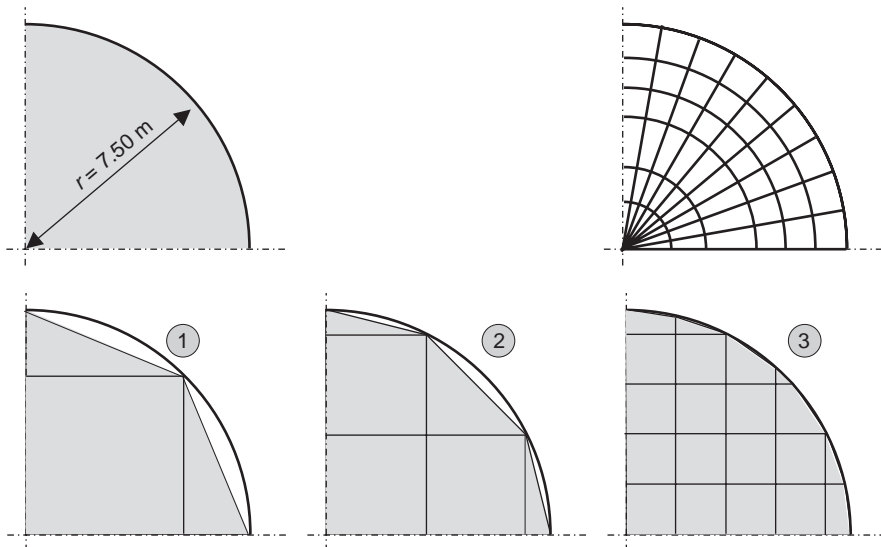
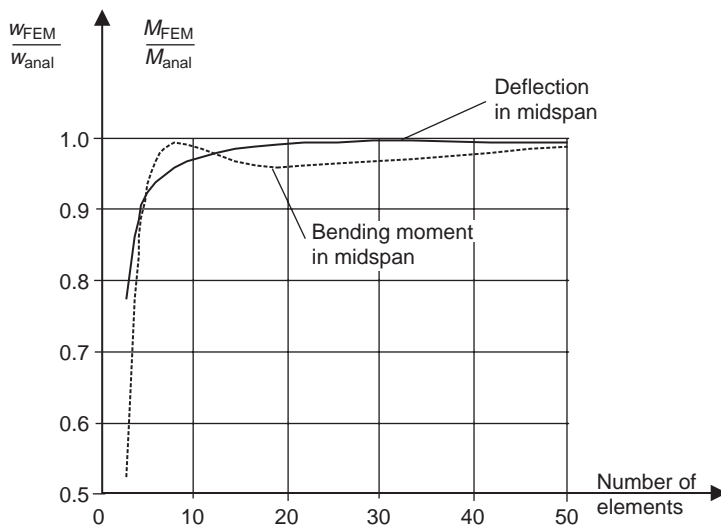


Figure 4.72 Deflections and bending moment in the centre of a circular simply supported slab for different number of elements



The results summarised in Figure 4.72 demonstrate that only $4 \times 6 = 24$ elements are required for the whole slab in order to get satisfactory results at the centre.

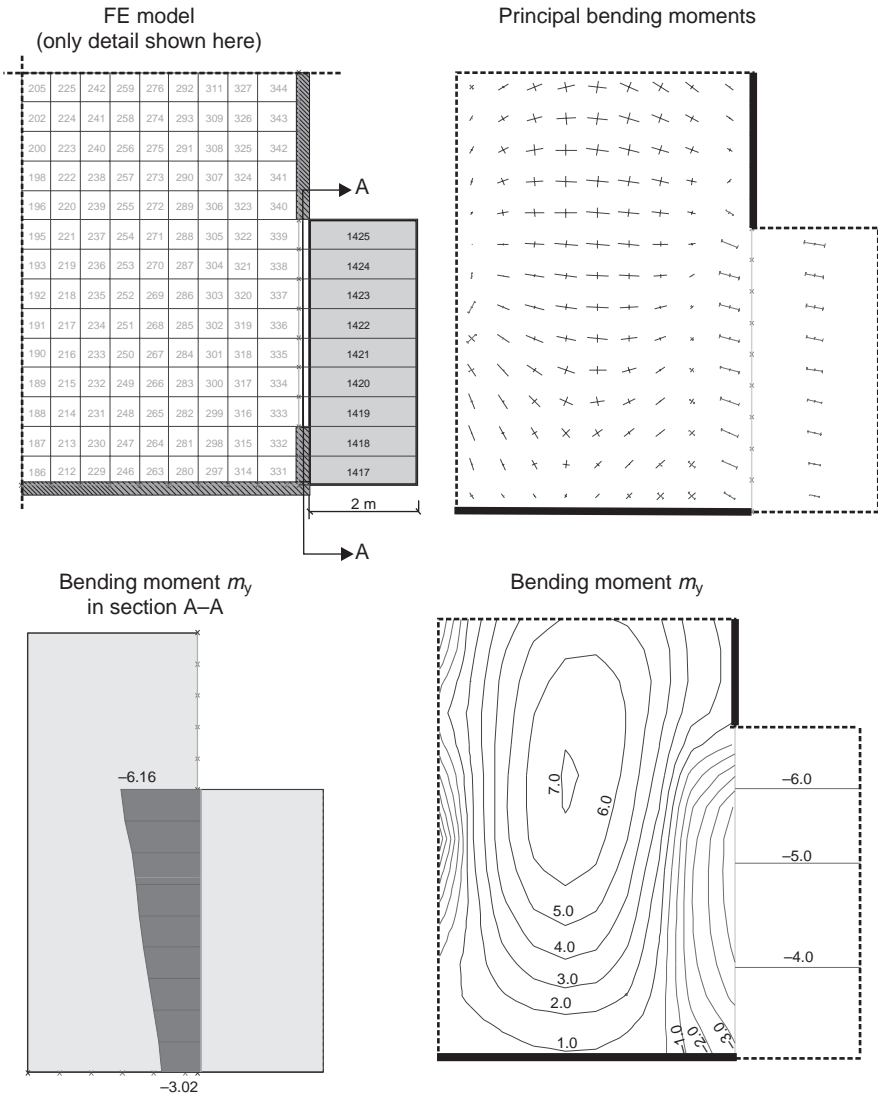
Nowadays, due to the increasing capacities of computers, the size of the numerical model or the number of elements does not usually play an important role. Therefore, modelling is often done quickly, without sufficient attention being paid to the relevant details. What may be considered as unimportant details, such as a one-way cantilever slab or a small opening in a flat slab near a column support, are not noticed. However, these are the regions where high gradients of the internal forces may occur and which are relevant for design.

The problems that occur due to neglecting such ‘unimportant’ details are demonstrated by a simple cantilever slab. This is not a theoretical example. Such a problem had occurred in a real big slab, where, unfortunately, the errors in the FE analysis were noticed only after the slab had been poured already with insufficient reinforcement. Excessive retro fitting was required. The system and the element model are shown in Figure 4.73 (full system shown in Figure 4.4). The balcony had been modelled with only one element layer, as it has a simple one-way load-bearing behaviour. A uniform load of $q = 5 \text{ kN/m}^2$ is applied on the whole slab. This results in a support bending moment of the equivalent cantilever beam of $m_s = 5 \times 2 \times 1 = -10 \text{ kNm/m}$. Values between $m_s = -3$ and $m_s = -6 \text{ kNm/m}$, which are much smaller than the analytical ones, are calculated by FE analysis. The differences are caused by the linear form functions of the four-noded elements used, which results in constant internal forces within an element. Thus, only the values in the centre of the element are calculated, and not the values required for design at the boundaries. The dimensioning of the slab, based on

the element values, would result in a considerable lack of reinforcement. Thus, an insufficient mesh refinement could cause an unsafe design, since, in contrast to multi-span slabs, a redistribution of the support bending moment is not possible for cantilever slabs.

The mesh problems may be noticed by the contour plots of the bending moment m_y (Figure 4.73). A large discontinuity between the elements can be seen. However, these obvious differences only occur in this example since the size of the elements in the

Figure 4.73 Bending moments in the region of the balcony

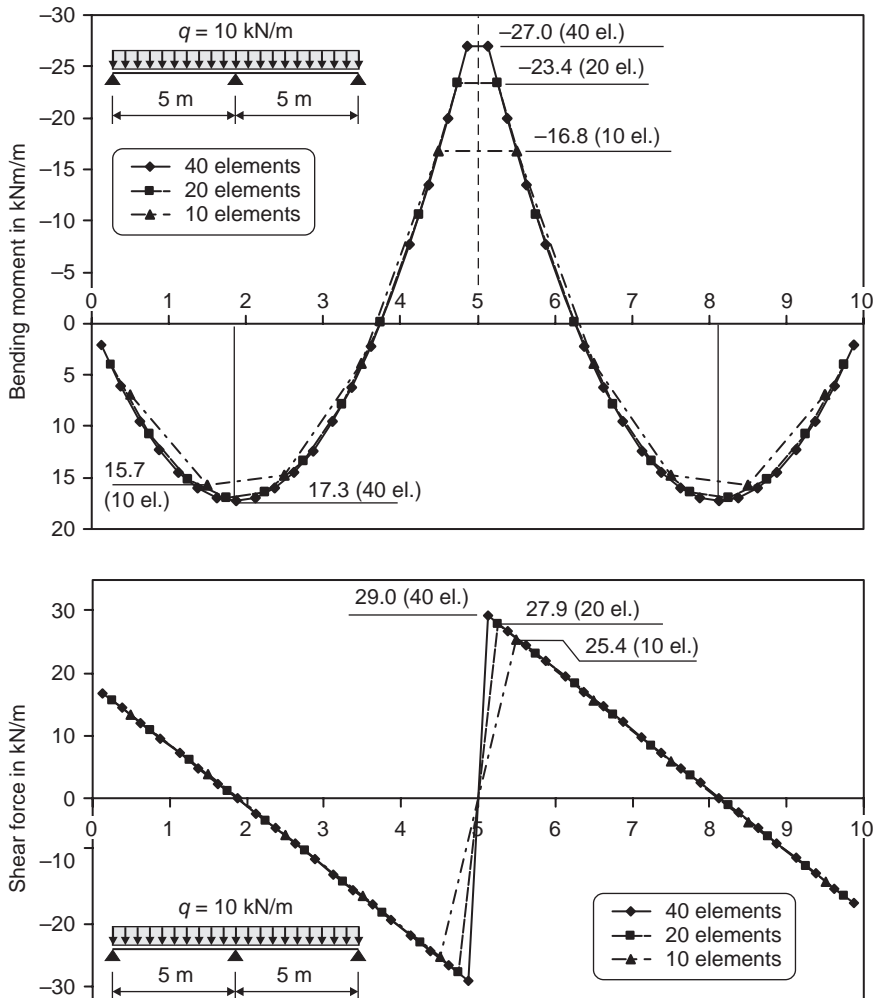


inner slab is much smaller than in the cantilever slab. The discontinuity would not occur if the size of the elements were similar.

The size of the elements is relevant in regions with big gradients in the inner forces or deflections. These problems are demonstrated with an easy example, a one-way slab with uniform loading ($l = 2 \times 5$ m). Figure 4.74 shows the bending moments and shear forces for a different number of elements.

With ten elements per field, a maximum support moment of $m_s = -16.8$ kNm/m is calculated, which nearly corresponds to the analytical value in the distance from $x = 0.25$ m of

Figure 4.74 Bending moments and shear forces for a one-way slab for different elements



the intermediate midsupport. The maximum moment increases by about 40% with 20 elements ($m_s = -23.4$ kNm/m) and by about 61% with 40 elements ($m_s = -27.0$ kNm/m). Hence, the number of elements is important in the case of small support widths. Please note that the face of the supports is relevant for the design and not the centreline. The curves of the member forces are quite similar for all element meshes except at the intermediate support.

In the field, a maximum bending moment of $m_F = 15.7$ kNm/m is determined with 10 elements, which is 12% less than the analytical value of $m_F = 17.6$ kNm/m. Therefore, in this case, the design in the field area gives a slightly unsafe result.

The amount of elements is not so significant if the shear force is regarded, owing to the lower gradient in the support regions. Furthermore, the relevant section for shear design is in the case of a direct support in a distance of $0.5-1.0d$ from the supported edge. It should be pointed out that some programs estimate the nodal values by an interpolation of the inner forces in the adjacent elements. In this case, a shear of $v = 0$ kN/m would be estimated, whereas the beam theory will give a maximum value of $v = 31.25$ kN/m.

4.14. Dimensioning of spatial structures

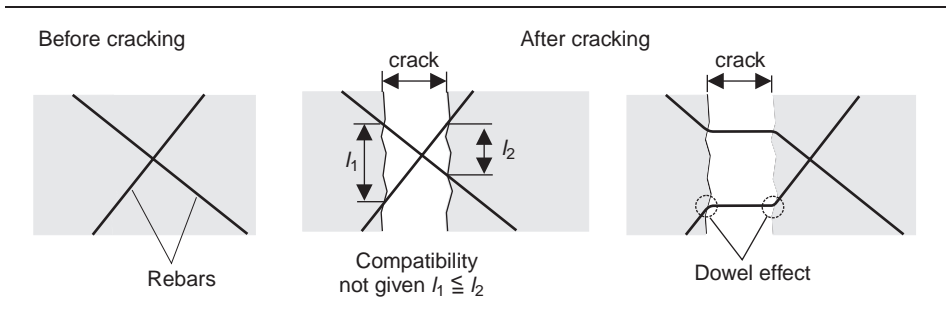
Dimensioning is done for the relevant sections of the structure. For beams, the longitudinal reinforcing bars for bending are always oriented perpendicular to bending cracks. This is usually not the case in real slabs, except for one-way slabs or ‘trajectory’ arrangement of the reinforcement (see Section 3.3). Due to practical constraints and various load arrangements, the orientation of the reinforcement mostly does not follow the orientation of the main bending moments or main membrane forces. In such cases, it is not possible to calculate the reinforcement separately for the two main directions, as it is in beams.

The dimensioning of spatial structures is based on the internal forces, which are estimated using the linear elastic behaviour of the concrete, in a similar manner to that in beams. In addition, the orientation and the area of reinforcing bars have to be chosen with respect to practical constraints and forces. Hence, two main input parameters – orientation of the reinforcing bars in the x - and y -directions – are mostly fixed for dimensioning.

Two unknowns remain: the internal forces and the orientation of the cracks from bending. The latter does not usually coincide with the orientation of the main compression forces. Among other things, the crack pattern depends on the level of the loading, the ratio of the main bending moments m_I/m_{II} and the ratio of the reinforcement in both directions. The compatibility conditions and the complicated stresses can only be estimated approximately if the reinforcement bars do not cross the crack in a right angle (Figure 4.75).

Hence, the design of a slab must be based on various simplifications and assumptions, such as, for example

Figure 4.75 Deformation of reinforcement bars at cracks



- neglecting the tensile strength of concrete
- estimating the internal forces based on linear elastic material behaviour
- neglecting the deflections and distortions of the reinforcement bars in a crack and the resulting forces (see Figure 4.75 right)
- neglecting the dowel effect of the bars and material interlock in the crack
- neglecting the shear forces in the compression zone
- assuming an identical strain of the reinforcement in both directions.

4.14.1 Model of Stiglat

First, the main bending moments have to be rotated to the orientation of the reinforcement by means of the following well-known expressions (Stiglat and Wippel, 1983) (Figure 4.76).

$$m_1 = m_x \cdot \cos^2 \alpha + m_y \cdot \sin^2 \alpha$$

$$m_2 = m_x \cdot \sin^2 \alpha + m_y \cdot \cos^2 \alpha$$

where:

α is the angle between m_1 and y-axis (orientation of rebar).

$$|m_1| > |m_2|; m_1 > 0; m_2 = k \cdot m_1$$

The resulting bending moments are distributed into the (orthogonal) directions of the reinforcement according to the ratio a_{sx}/a_{sy} .

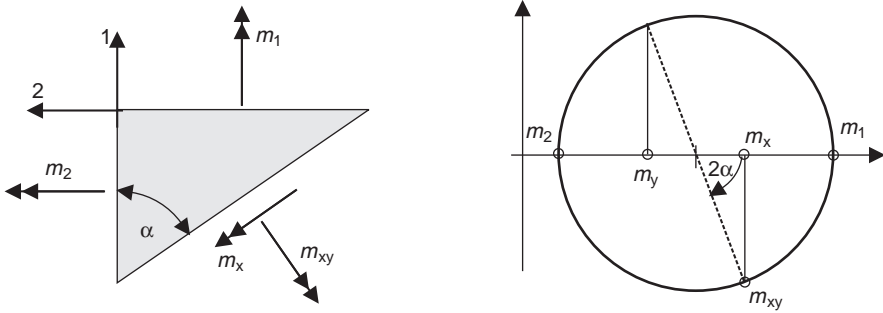
$$k_t = \frac{m_y}{m_x} = \frac{a_{sy} \cdot d_y}{a_{sx} \cdot d_x}$$

where $0 \leq k_t \leq 1$; d is the lever arm.

The parameter k_t is fixed by the second equation of equilibrium. The main bending moment m_2 (resistance) should be greater than the bending moment caused by the actions. This condition gives the lower limit of k_t :

$$k_t \geq \frac{k - \tan^2 \alpha}{1 - k \cdot \tan^2 \alpha}$$

Figure 4.76 Transformation of the bending moments

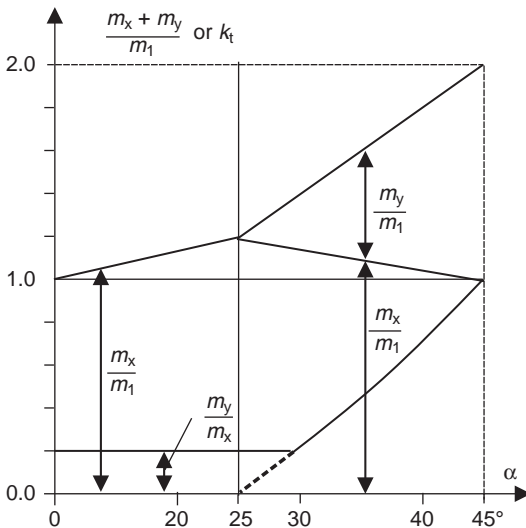


It should be noted that the codes specify a minimum transverse reinforcement (20% of the maximum reinforcement in the main load-bearing direction). Thus, the value k_t should always be greater than 0.2. Furthermore, for $\alpha \geq 25^\circ$, the reinforcement should be distributed in the orthogonal directions, as illustrated in Figure 4.77. In this figure, the bending moment m_2 is always greater than that caused by the external actions. The design bending moments in the direction of the reinforcing bars can be estimated by using the following expressions.

$$m_y = k \cdot m_1 = \frac{1}{\cos^2 \alpha + k_t \cdot \sin^2 \alpha} \cdot m_1$$

$$m_x = k_t \cdot m_y$$

Figure 4.77 Distribution of the main bending moment in the direction of the reinforcing bars



4.14.2 Model of Baumann

The design for the bending of a slab is transferred to the design of a plane slab (disk) for normal forces (Figure 4.78) (Baumann, 1972).

The forces in the reinforcement results from the equilibrium conditions on a flat plate element (see Figure 4.80). The angle of the cracks φ is determined by the principle of the minimum energy. A linear elastic material behaviour is assumed.

$$\cot^4 \varphi_1 + \cot^3 \varphi_1 \cdot \frac{\tan \alpha + k \cdot \cot \alpha}{1 - k} - \cot \varphi_1 \frac{\cot \alpha + k \cdot \tan \alpha}{\lambda \cdot (1 - k)} - \frac{1}{\lambda} = \frac{\nu}{\lambda} (1 - \cot^4 \varphi_1)$$

where:

$$\lambda = \frac{a_{sx}}{a_{sy}}; \nu = \frac{a_{sx}}{h} \cdot \frac{E_s}{E_c}$$

$$k = m_2/m_1 = n_2/n_1$$

m_1 and m_2 are the principal bending moments

α is the angle between direction of rebar (y) and main tensile force n_1 ($\alpha \leq 45^\circ$)

Figure 4.78 Transformation of bending moments into normal forces in an equivalent disc

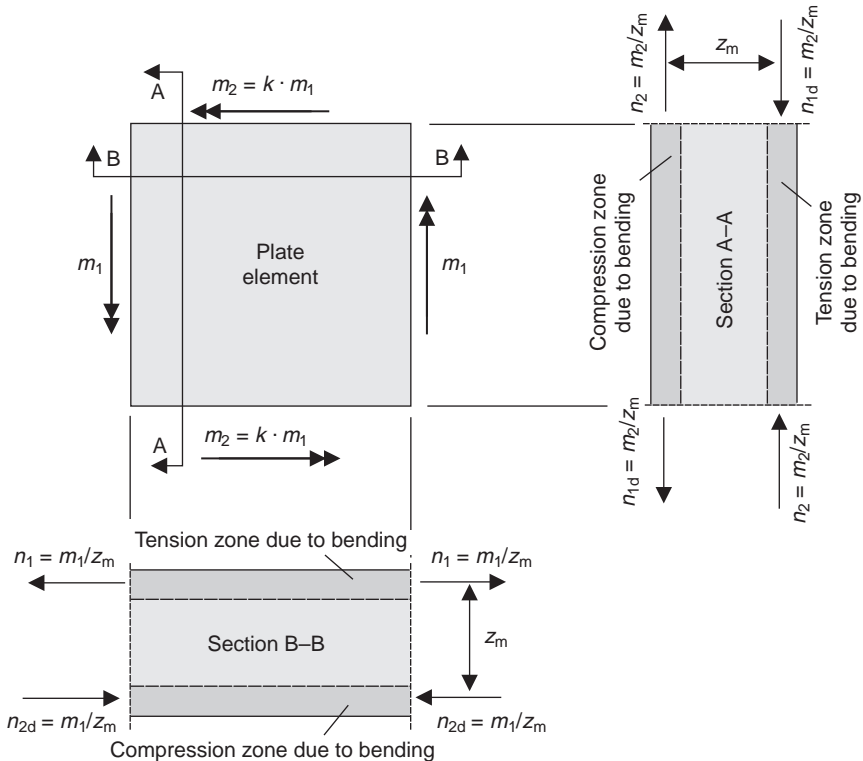
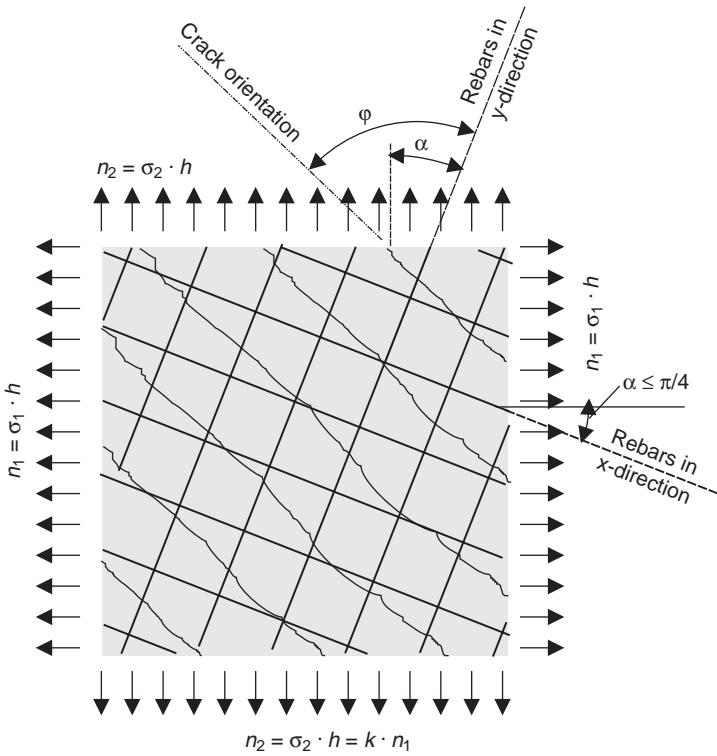


Figure 4.79 Definition of angles α and φ



- φ is the angle between direction of rebar (y) and cracks
- φ_1 is the angle between direction of rebar (y) and cracks, if the shear forces are neglected
- φ_2 is the angle between direction of rebar (y) and cracks, if the steel is yielding.

If the reinforcement in both directions reaches the yielding point, the angle of the crack φ_2 is given by the following expression.

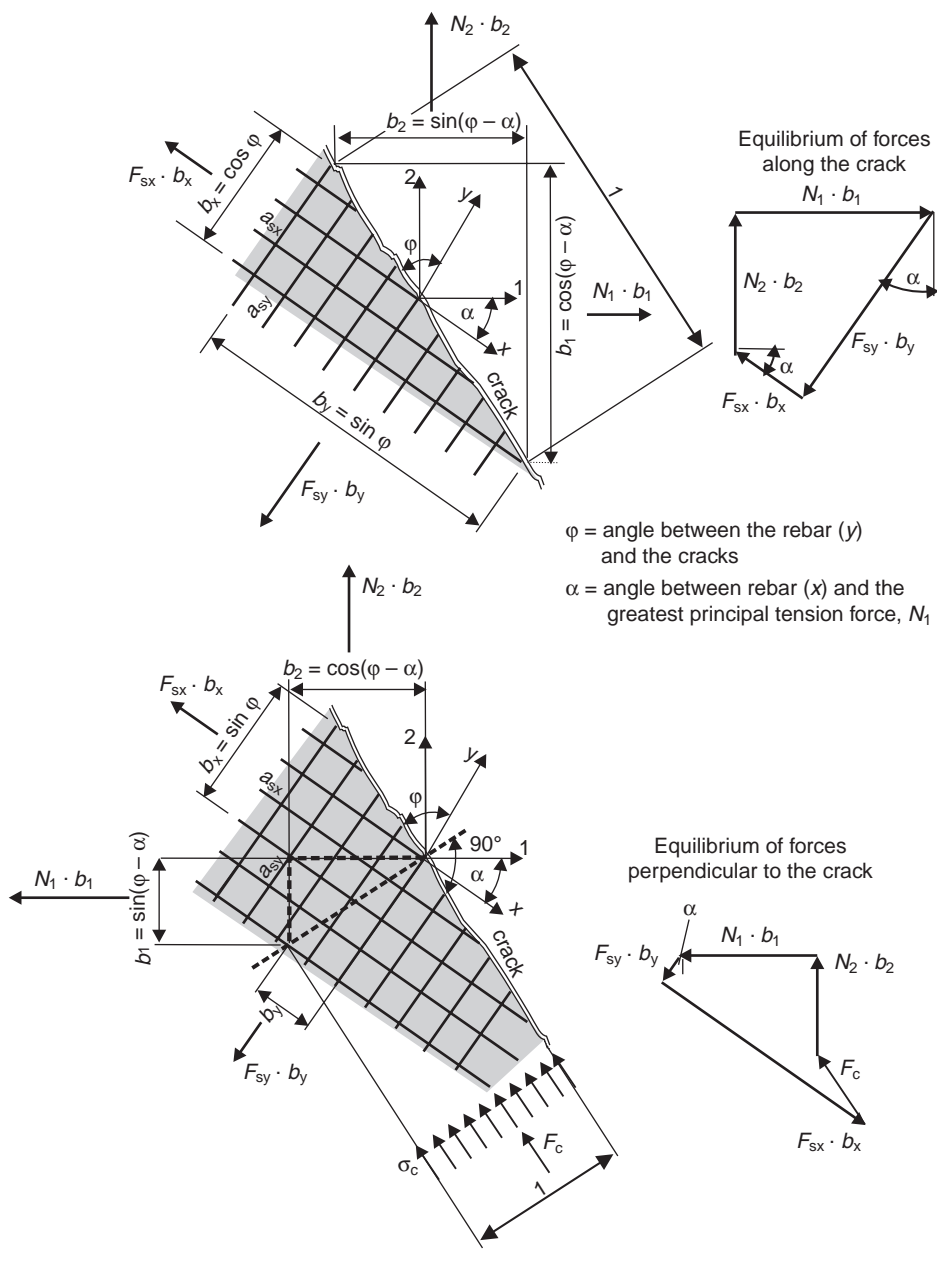
$$\tan \varphi_2 = -C + \sqrt{C^2 + \lambda}$$

where:

$$C = \frac{1 + \tan^2 \alpha \cdot (k - \lambda) - k \cdot \lambda}{2 \cdot \tan \alpha \cdot (1 - k)}$$

Further simplifications are justified under the assumption that both reinforcement directions are stressed equally, resulting in the most economical solution. However, this case will not always be possible. Based on this assumption, the angle φ is constant: $\varphi = \varphi_1 = \pi/4$.

Figure 4.80 Equilibrium between internal forces and actions for an orthogonal arrangement of rebars



The following expressions are used to determine the forces in the reinforcement F_{sx} and F_{sy} and the compressive force F_c :

k	$k = n_2/n_1 \geq \tan(\alpha + \pi/4) \cdot \tan \alpha$	$k = n_2/n_1 < \tan(\alpha + \pi/4) \cdot \tan \alpha$
$\varphi =$	$\pi/4$	$\varphi = a \tan \left[\frac{k - 1}{\tan \alpha + k \cdot \cotan \alpha} \right]$
$F_{sx} =$	$n_1 + \frac{n_1 - n_2}{2} \cdot \sin 2\alpha \cdot (1 - \tan \alpha)$	$\frac{n_2}{\sin^2 \alpha + k \cdot \cos^2 \alpha}$
$F_{sy} =$	$n_2 + \frac{n_1 - n_2}{2} \cdot \sin 2\alpha \cdot (1 + \tan \alpha)$	$= 0$
$F_c =$	$(n_1 - n_2) \cdot \sin 2\alpha$	$(n_1 - n_2) \cdot \sin 2\alpha / \sin 2\varphi_{0y}$

4.14.3 Model of Eurocode 2

The design model of EC2, Part 1, from June 1992 was also based on a transformation of the bending moments into the direction of the reinforcement (Figure 4.81). The results agree with the Baumann model if the bending moment m_x is equal or greater than the twisting moment m_{xy} ($m_x \geq |m_{xy}|$).

A more refined design model is given in appendix LL of EC2, Part 2 (Eurocode 2, 2005). This approach is suitable for numerical analysis only.

4.14.4 Comparison of the different models

Figure 4.82 shows a comparison of the reinforcement required for the ultimate limit state design, according to the earlier-mentioned models for $k = m_1/m_2 = 0.0$ and $k = 0.6$.

Figure 4.81 Dimensioning of slabs according to EC2, Part 1, 1992

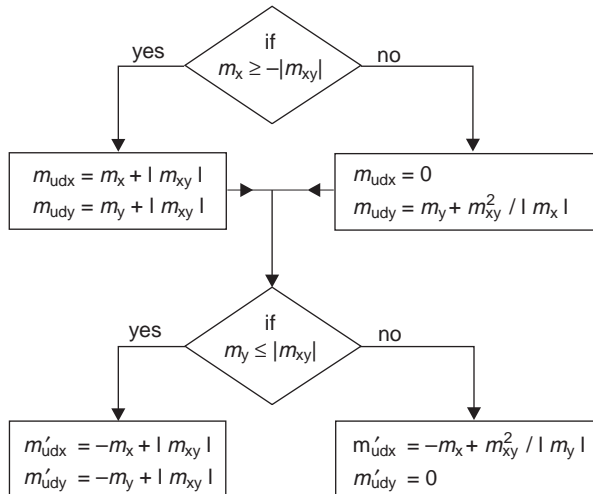
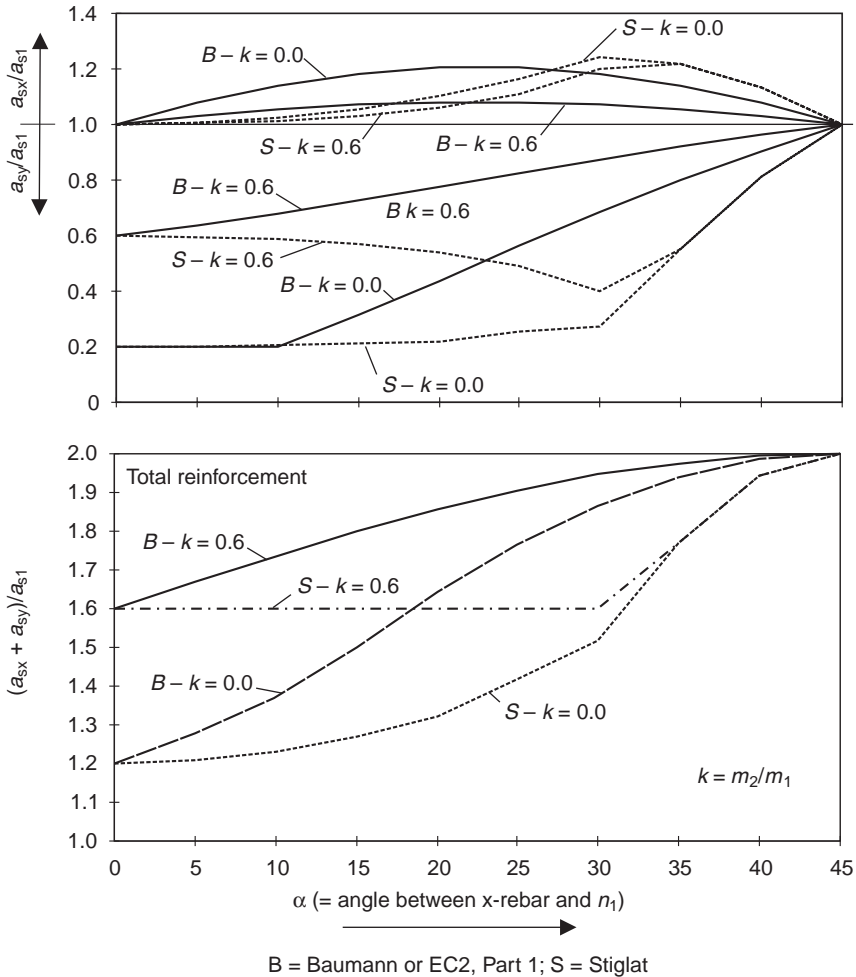


Figure 4.82 Reinforcement ratio a_{sx}/a_{s1} , a_{sy}/a_{s1} and $(a_{sy} + a_{sx})/a_{s1}$ in relation to the angle α between direction of rebar and main tensile force



The EC2 values are not shown, since they match with the approach of Baumann. The results of both models match for an angle between direction of rebar (γ) and main tensile force n_1 of $\alpha=0^\circ$ and 45° . Significant differences can be seen in the region in between these boundary values ($0^\circ < \alpha < 45^\circ$).

4.15. Comparison with analytical methods and tables

4.15.1 Comparison with table values

Various tables are available for determining the relevant internal forces and deflections for various standard cases such as simply supported rectangular slabs under uniform load. These values can be used to verify an FE analysis. However, the differences in the numerical models, assumptions and simplifications have to be considered: While

most tables have been calculated in accordance with the Kirchhoff theory, the FE software is generally based on the more consistent model of Reissner/Midlin. The main difference between the two approaches is in the shear deformation. The Kirchhoff model neglects shear deformations, while these are taken into account in the Reissner/Midlin model. This may result in significant differences with regard to shear forces. This is illustrated in the following example, a simply supported rectangular slab with a panel dimension of $l_y / l_x = 7.50/5.0$ m.

Figure 4.83 and Table 4.13 show the result of this comparison ($q = 10 \text{ kN/m}^2$). A very good agreement in the bending moments can be seen. However, the twisting moment m_{xy} of the FE model is 50% less than that calculated by Czerny (1999).

Figure 4.83 Bending moments and shear forces of a simply supported rectangular slab under uniform load calculated by FEM and with Czerny tables (Czerny, 1999)

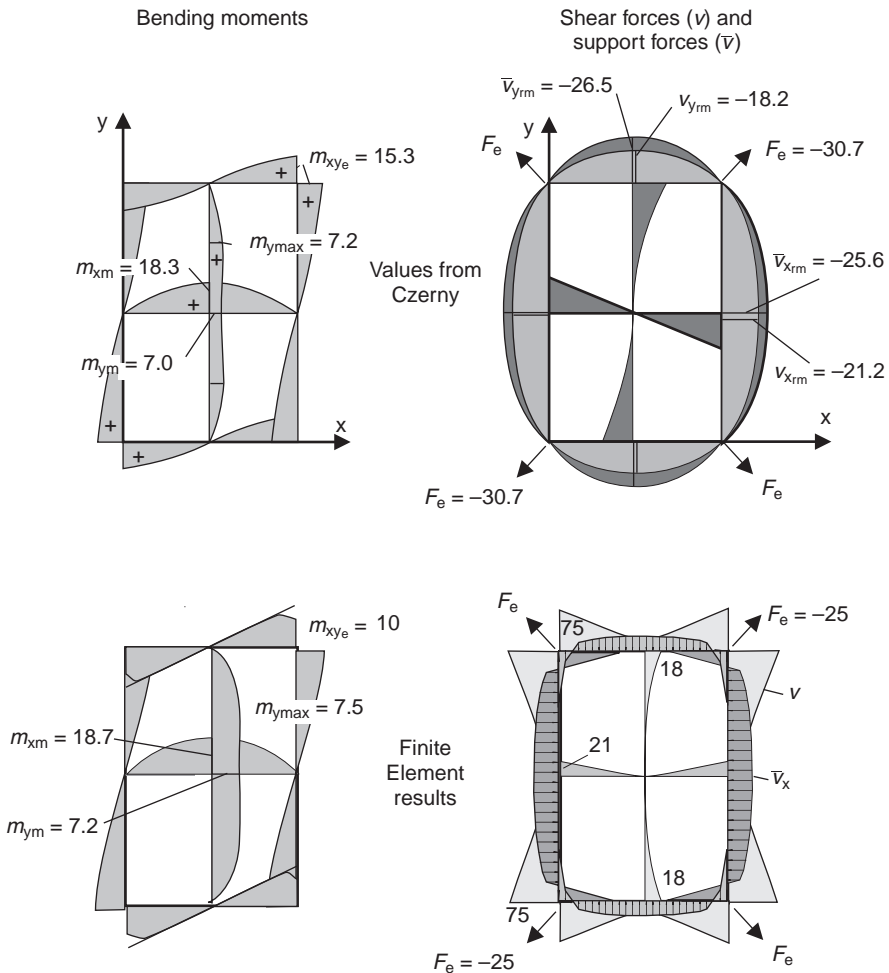
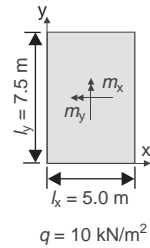


Table 4.13 Comparison of the internal force, support forces and deflection

		Czerny (1999)	FE $\nu = 0.2$	FE $\nu = 0.0$
m_{xye}	in kNm/m	15.3	13.5 (88%)	11.6 (76%)
$m_{x\text{m}}$	in kNm/m	18.3	20.0 (109%)	18.7 (102%)
$m_{y\text{m}}$	in kNm/m	7.0	10.9 (156%)	7.2 (103%)
$m_{y,\text{max}}$	in kNm/m	7.2	10.9 (151%)	7.5 (104%)
$v_{y\text{rm}}$	in kN/m	18.2	17.7 (97%)	17.9 (98%)
$\bar{v}_{y\text{rm}}$	in kN/m	26.5	25.0 (94%)	25.0 (94%)
$v_{x\text{rm}}$	in kN/m	21.2	21.2 (100%)	21.6 (102%)
$\bar{v}_{x\text{rm}}$	in kN/m	25.6	25.0 (98%)	26.5 (104%)
F_e	in kN	30.7	22.5 (73%)	24.8 (81%)
f	in mm	24.5	22.4 (91%)	23.4 (105%)



Large differences can be seen in the shear force distribution. According to Czerny, the distribution of the shear force at the supported edges is almost parabolic. The shear force at the corners of the slab is zero. On the other hand, the FE calculation gives maximum shear forces in the corners of the slab. This peak value is more than three times greater than the maximum shear force calculated with Czerny's tables. This may cause some design problems, because usually one wants to omit any shear reinforcement in a slab.

4.15.2 Partial restraint method of Pieper and Martens

The approach of Pieper and Martens (1966) is widely used in practice for the design of multi-span rectangular slabs. The midspan bending moments are estimated as the mean value of a simply supported and a clamped slab. Additionally, a full restraint is assumed for calculation of the intermediate support bending moments.

The internal forces for the slab shown in Figure 4.84 are estimated by FEM and the Pieper-Martens model. This structure has been used in the original publication (Pieper and Martens, 1966), but the loads and the thickness of the slab have been increased to represent up-to-date conditions.

The bending moment distributions calculated by FEM in both axes for various sections are plotted in Figures 4.85 and 4.86. Figure 4.87 shows the comparison of the bending moments in the relevant sections. A good agreement in the field bending moments can be seen for both calculations using the simple manual method and FEM. The support bending moments are generally greater due to the assumption of high flexural restraints (between 50% and 100%).

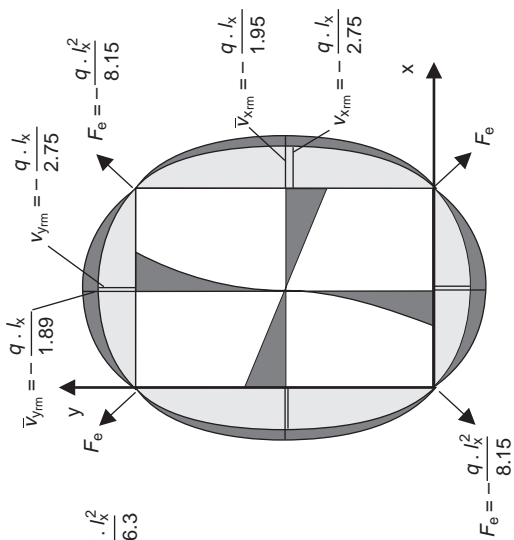
It should be noted that the minimum bending moments given in EC2, Part 1, are relevant in the small slabs – numbers 4 and 5 – and not the values from the linear elastic FE model. The minimum internal forces always have to be considered in addition to an FE analysis.

Table 4.14 Internal forces of a simply supported rectangular slab under uniform load#Czerny, 1999 © Wiley – VCH Verlag GmbH & Co. KGaA. Reproduced with permission.

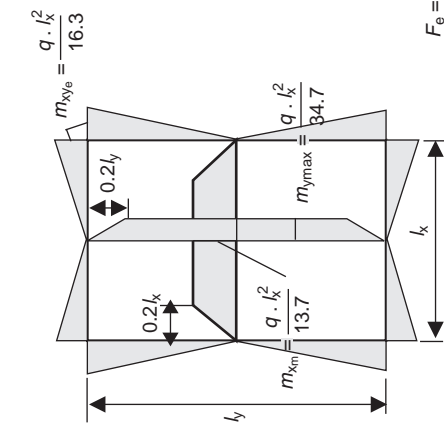
	$l_y/l_x = 1.0$	1.05	1.1	1.15	1.20	1.25	1.30	1.35	1.40	1.45	1.50
$m_{xm} = q \cdot l_x^2:$	27.2	24.5	22.4	20.7	19.1	17.8	16.8	15.8	15.0	14.3	13.7
$m_{y,max} = q \cdot l_x^2:$	27.2	27.5	27.9	28.4	29.1	29.9	30.9	31.8	32.8	33.8	34.7
$m_{xye} = q \cdot l_x^2:$	21.6	20.6	19.7	19.0	18.4	17.9	17.5	17.1	16.8	16.5	16.3
$F_e = q \cdot l_x^2:$	10.8	10.3	9.85	9.5	9.2	8.95	8.75	8.55	8.4	8.25	8.15
$V_{xrm} = q \cdot l_x:$	2.96	2.87	2.78	2.71	2.64	2.58	2.52	2.47	2.43	2.39	2.36
$\bar{V}_{xrm} = q \cdot l_x:$	2.19	2.15	2.11	2.07	2.04	2.02	2.00	1.98	1.97	1.96	1.95
$V_{yrm} = q \cdot l_x:$	2.96	2.92	2.89	2.86	2.84	2.82	2.80	2.78	2.76	2.75	2.75
$\bar{V}_{yrm} = q \cdot l_x:$	2.19	2.14	2.09	2.05	2.02	1.99	1.96	1.94	1.92	1.90	1.89
$f_m = \frac{q \cdot l_x^4}{E \cdot h^3}:$	0.0487	0.0536	0.0584	0.0631	0.0678	0.0728	0.0767	0.0809	0.0850	0.0890	0.0927

	$l_y/l_x = 1.50$	1.55	1.60	1.65	1.70	1.75	1.80	1.85	1.90	1.95	2.00
$m_{xm} = q \cdot l_x^2:$	13.7	13.2	12.7	12.3	11.9	11.5	11.3	11.0	10.8	10.6	10.4
$m_{y,max} = q \cdot l_x^2:$	34.7	35.4	36.1	36.7	37.3	37.9	38.5	38.9	39.4	39.8	40.3
$m_{xye} = q \cdot l_x^2:$	16.3	16.1	15.9	15.7	15.6	15.5	15.4	15.3	15.3	15.2	15.1
$F_e = q \cdot l_x^2:$	8.15	8.05	7.95	7.85	7.80	7.75	7.70	7.65	7.65	7.6	7.55
$V_{xrm} = q \cdot l_x:$	2.36	2.33	2.30	2.27	2.25	2.23	2.21	2.19	2.18	2.16	2.15
$\bar{V}_{xrm} = q \cdot l_x:$	1.95	1.94	1.93	1.92	1.92	1.92	1.92	1.92	1.92	1.92	1.92
$V_{yrm} = q \cdot l_x:$	2.75	2.74	2.73	2.73	2.73	2.72	2.72	2.71	2.71	2.70	2.70
$\bar{V}_{yrm} = q \cdot l_x:$	1.89	1.88	1.87	1.86	1.85	1.84	1.83	1.82	1.82	1.82	1.82
$f_m = \frac{q \cdot l_x^4}{E \cdot h^3}:$	0.0927	0.0963	0.0997	0.1029	0.1060	0.1093	0.1118	0.1145	0.1169	0.1195	0.1215

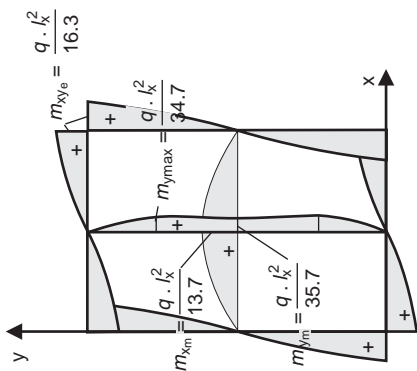
Note: h is the slab thickness; \bar{V}_{xrm} , \bar{V}_{yrm} is the vertical support force in the middle of the supported edge; V_{xrm} , V_{yrm} is the shear force at the line support in the middle of the supported edge.



Shear forces (v) and support forces (\bar{v})



Bending moments (simplified distribution)



Bending moments

Figure 4.84 Structure and loading

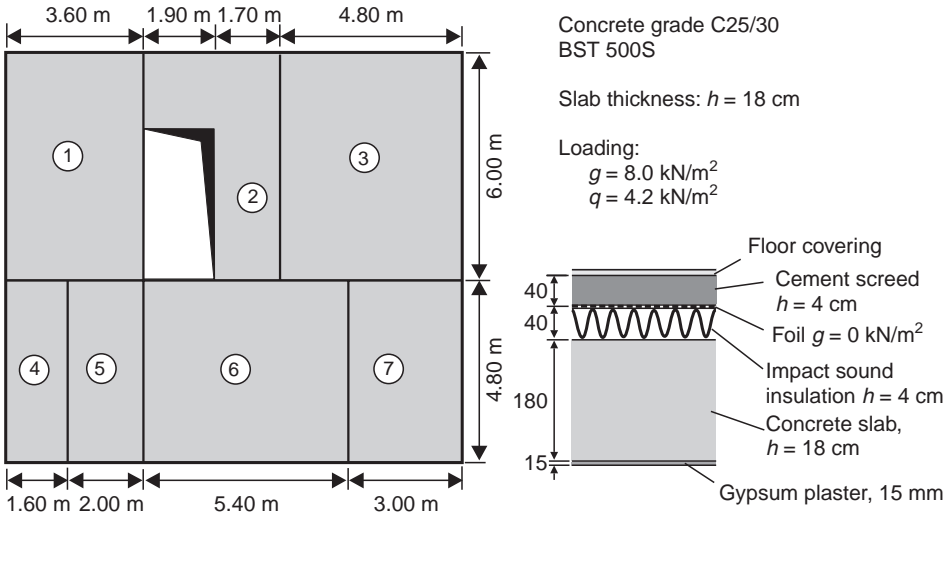


Figure 4.85 Bending moment distribution in various sections (FE analysis)

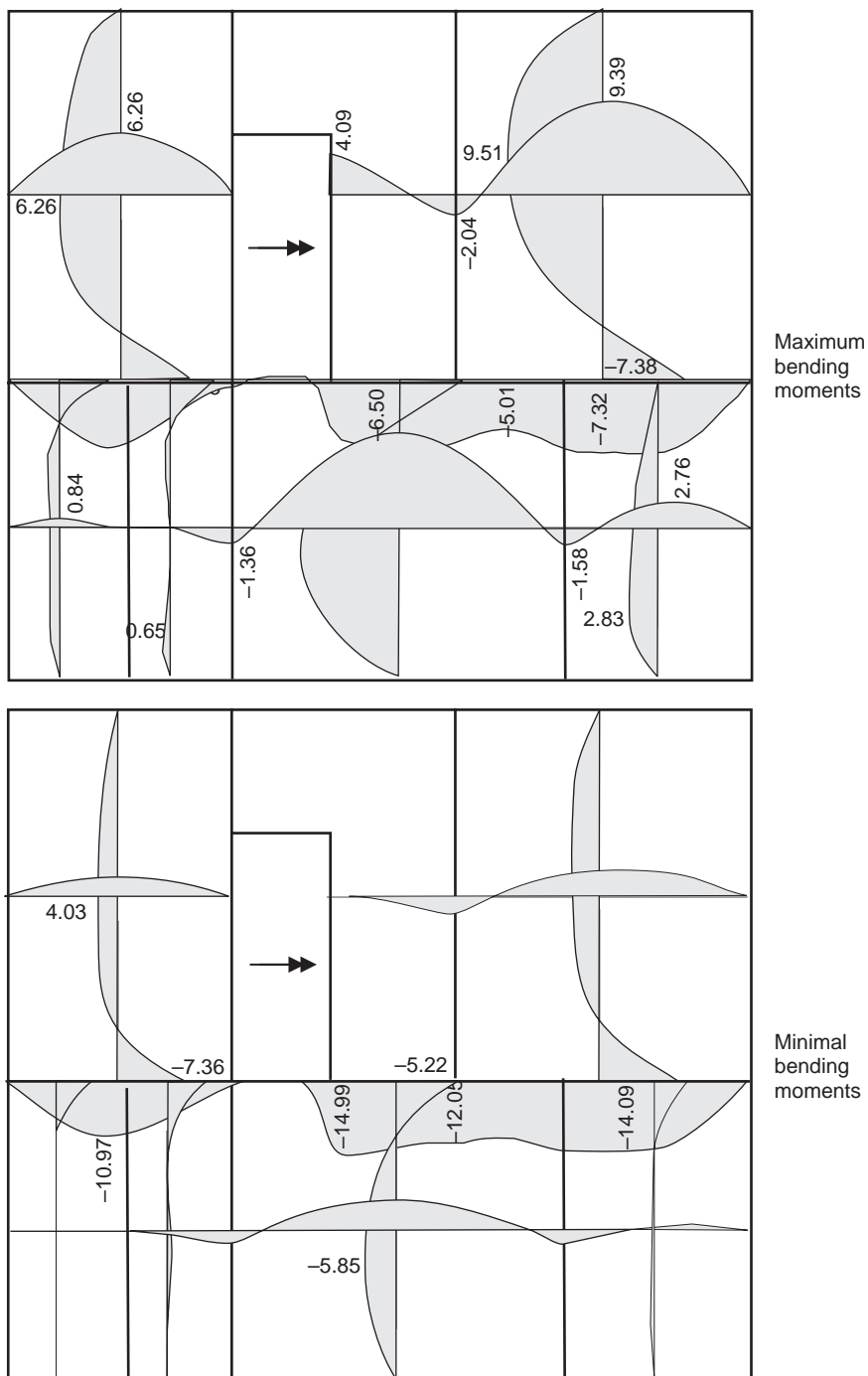


Figure 4.86 Bending moment distribution in various sections (FE analysis)

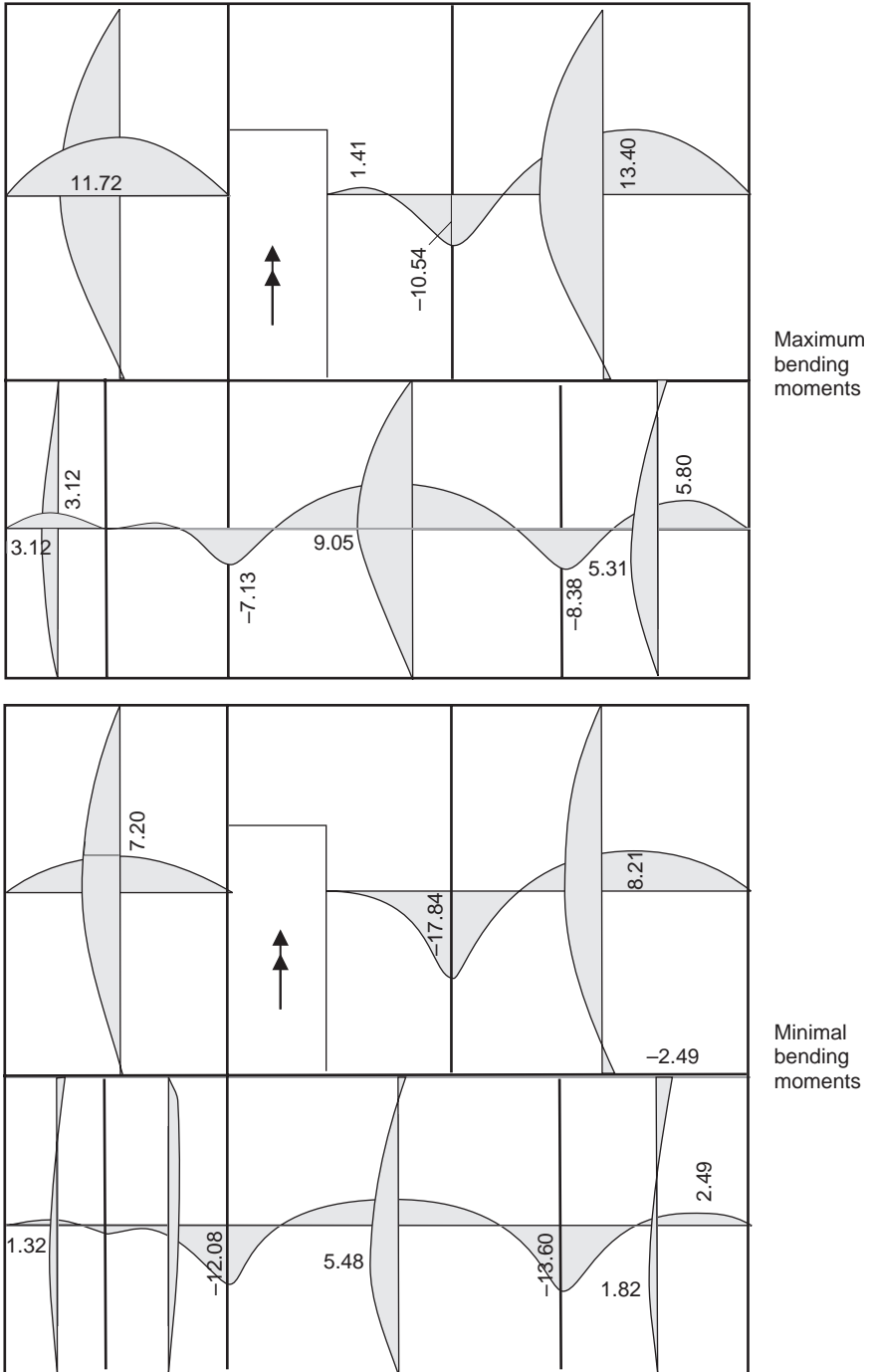
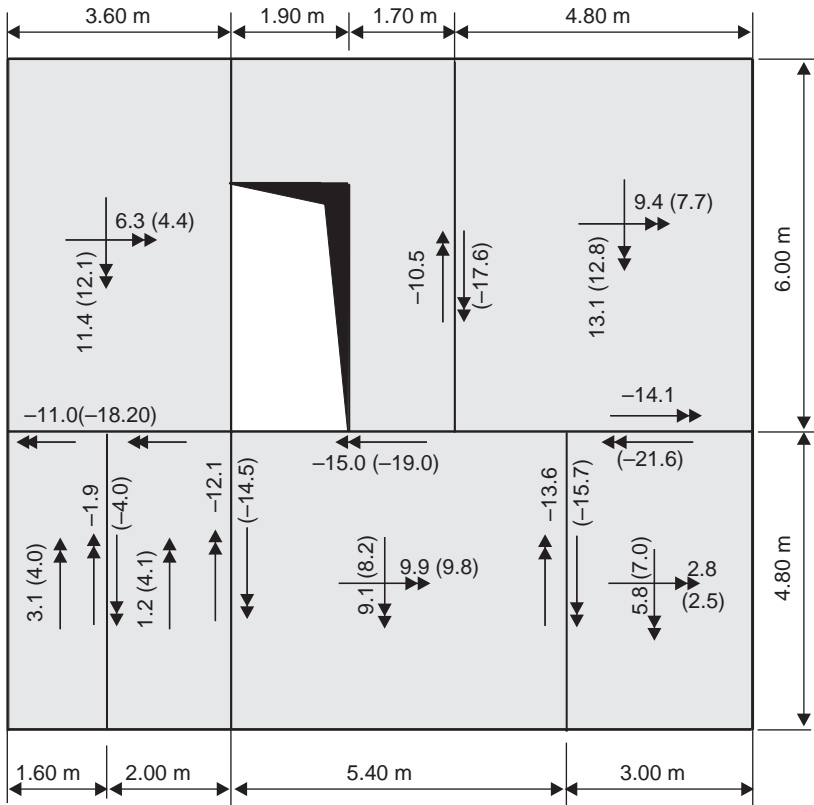


Figure 4.87 Bending moments in the relevant sections – comparison between FE analysis and Pieper-Martens analytical method (values in brackets)



REFERENCES

- Bathe K-J (1982) *Finite Element Procedures in Engineering Analysis*. Prentice Hall, Englewood Cliffs.
- Baumann Th (1972) Zur Frage der Netzbewehrung von Flächentragwerken. *Der Bauingenieur* **47(10)**: 367–377.
- Bittner E (1965) *Platten und Behälter*. Springer Verlag, Wien.
- Burton WS and Sinclair GB (1956) On the Singularities of the Reissner's Theory for Bending of Elastic Plates. *Journal of Applied Mechanics*, **53**(March): 220–222.
- CEN (European Committee for Standardization) (2004) *Eurocode 2, Part 1: Design of concrete structures – General rules and rules for buildings*. December.
- CEN (2005) *Eurocode 2, Part 2: Design of concrete structures – Concrete Bridges – Design and detailing rules*. December.
- Czerny F (1999) *Tafeln für Rechteckplatten*. In *Betonkalender 1999* (Eibl J (ed.)), Volume 1. Ernst & Sohn, Berlin.
- DIN 1045-1 (2008) *Concrete, reinforced and prestressed concrete structures – Part 1: Design*. Deutsches Institut für Normung. Berlin, August.

- Girkmann K (1978) *Flächentragwerke*. Springer Verlag, Wien.
- Grasser E *et al.* (1991) *Hilfsmittel zur Berechnung der Schnittgrößen und Formänderungen von Stahlbetonbauwerken*; Deutscher Ausschusses für Stahlbeton Heft 240, Berlin.
- Homberg H and Ropers W (1965) *Fahrbahnplatten mit veränderlicher Dicke*, Band I, Springer Verlag, Berlin.
- Homberg H (1973) *Platten mit zwei Stegen*. Springer Verlag, Berlin.
- Hughes TJR (1987) *The Finite Element Method*. Prentice Hall, Englewood Cliffs.
- Pieper K and Martens P (1966) Durchlaufende vierseitig gestützte Platten im Hochbau. *Beton- und Stahlbetonbau* **6**: 158–162.
- Stiglat K and Wippel H (1983) *Platten*, 3rd edn. Ernst & Sohn, Berlin.
- Timoshenko SP and Woinowsky-Krieger S (1959) *Theory of Plates and Shells*. McGraw-Hill, New York.
- Zienkiewicz OC and Taylor RL (1989) *The Finite Element Method*. London.

Chapter 5

Shell structures

Shells are spatially curved surface structures that exhibit the behaviour of both plates (Chapter 4) and shear walls (Chapter 3). They can be loaded perpendicular (as a plate) and normally (as a shear wall) at their middle surfaces. Thus, they can develop bending moments, membrane forces and shear forces. Each element node has six degrees of freedom: three for deflection and three for rotation (see Figure 5.1).

FEM allows the calculation of the internal forces for shells of arbitrary shapes. This chapter only deals with thin shells, where the shell thickness is much smaller than the main radius of curvature. With this assumption, the FE model can be reduced to the midplane of a shell. Brick or volume elements can be used for thick shells or massive structures.

The accuracy of an FE shell analysis is dependent on the numerical model, the shape functions of the elements used and the order of the numerical integration. The following calculations use a four-node flat shell element (quadratic displacement approach), where the bending and membrane-load-bearing behaviour is not coupled (Hughes, 1987).

5.1. Mesh generation

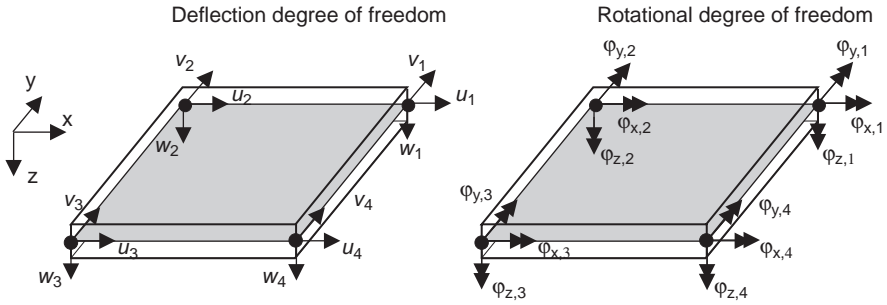
Plane shell structures, such as plates and disks, can usually be modelled with a sufficient number of elements without reaching the limits of computer capacity. However, in case of 3D curved shell structures, the element mesh has to be chosen keeping in mind the limits of the computer hardware and software. The element mesh has to be refined in regions with high stress gradients or high local loads. Otherwise, as demonstrated in the following example, the calculated internal forces will be too low, leading to an unsafe design.

5.1.1 Collapse of the Sleipner platform

The problems of FE calculations can be well demonstrated with respect to damage or failures of structures due to errors in the numerical analyses. Unfortunately, due to a lack of interest in demonstrating such design errors, only a few of such cases have actually been published so far.

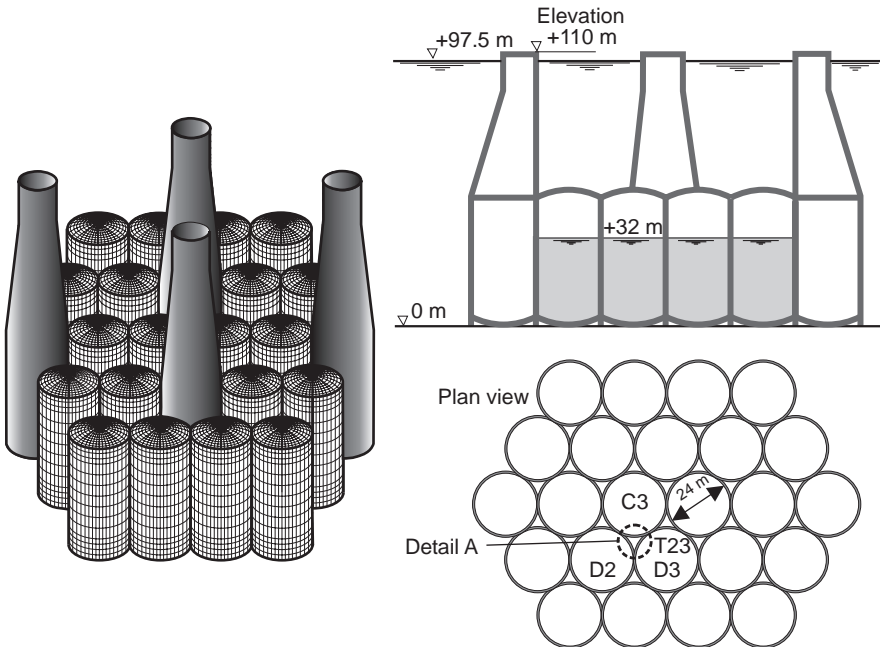
A good example of the failure of a concrete structure, caused by erroneous numerical analysis, is the collapse of the offshore platform 'Sleipner A'. Further detailed data is available in the literature (see Gudmestad and Coker, 1988; Holand, 1997; Jakobsen

Figure 5.1 Nodal degrees of freedom of a flat thin shell element



and Rosendahl, 1994). This so-called Condeep-type platform consists of 24 cylindrical caisson cells, each with an internal diameter of 24 m, which are closed at top and bottom by a dome (see Figure 5.2). These cells were used for buoyancy during the construction and shipping of the platform to its final location. The steel deck (total weight 40 000 tons) rested on four shafts, each having a minimum internal diameter of 12 m. The structure had a total height of 110 m. It was designed to operate at a location with a mean water depth of 82 m. The ‘Sleipner A’ platform was the twelfth in a series of gravity-based structures built for use in the exploitation of hydrocarbons in the North

Figure 5.2 Platform ‘Sleipner A’



Sea. There was no significant difference between this platform and the earlier-constructed structures of the Condeep type.

The structure collapsed during installation. The construction of this type of platform is carried out in three phases. In the first phase, the lower part of the foundation structure is built in a dry dock. Then, the dry dock is flooded and the structure is shipped to a deep-water construction berth, where the rest of the cylindrical caisson cells and the four shafts are erected. Finally, the whole platform is lowered to nearly the seawater level by partially flooding the cylindrical caisson cells, and the steel deck is lifted on the shafts and fixed in place.

The 'Sleipner A' platform collapsed on 23 August, 1991, when it was undergoing a controlled ballast test to check for minor leakage. At first, a loud noise was heard in the D3 shaft. At that time, the draft was 97.5 m. After 18 minutes, the structure disappeared from the surface of the sea.

Detailed experimental and numerical investigations were carried out after the accident. It was found that the collapse was initiated by the failure of a wall in the so-called tricell T23 (see Figures 5.2, 5.3 and 5.4). This failure allowed flooding of the buoyancy caissons, and the whole structure sank to the seabed. The financial loss from this accident was estimated at US\$250 million.

The failure was caused by the large differential pressure in the tricells. As noted earlier, the caisson cells are partly filled with seawater during the sinking operation. The area between these cells is open to the sea, and the high differential water pressure between the caissons and the tricells results in very high pressures on the walls (Figure 5.3). Investigations that were carried out after the collapse showed that the failure of the walls must have occurred under a water pressure of 670 kPa, equal to 67 m water depth.

Figure 5.3 Detail 'A' – tricell

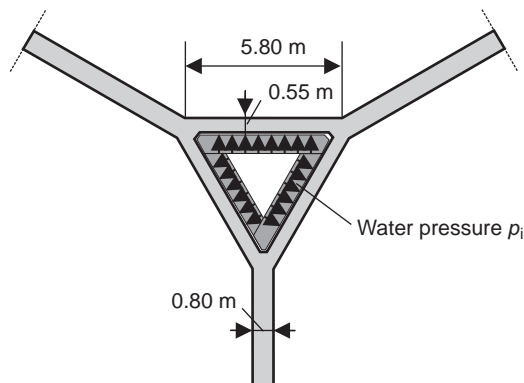
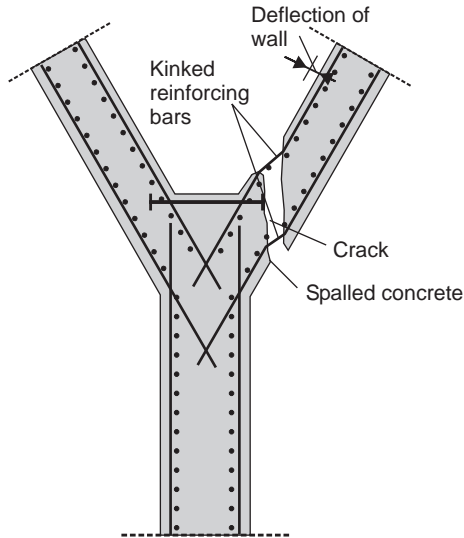


Figure 5.4 Failure mode



The subsequent, very extensive numerical and experimental investigations identified two main causes of the collapse

- erroneous FE analysis
- insufficient reinforcement and bad detailing of the tricell walls.

The bad detailing of the intersection between the cell walls can be seen in Figure 5.5. The T-headed bar of diameter $d_s = 25$ mm was not anchored in the compression region of the walls. More information about this problem is given in the available literature (e.g. Holand, 1997; Jakobsen and Rosendahl, 1994).

The errors in the FE analysis of the platform lay in insufficient discretisation, and in the poor geometrical shaping of some elements in the tricells (Figure 5.6). Simplifications had been made with regard to the number and shape of the elements, due to the size and complexity of the structure, and the limited computing capacity. This resulted in the incorrect modelling of the load-bearing behaviour of the tricells. The walls of the cells were modelled using only two element layers.

Using a coarse FE mesh, the internal tensile forces (i.e. the shear forces at the wall supports) are underestimated by nearly 50%. Due to the large amount of input and output data of the 3D model used, this mistake was not recognised by the design engineers.

The basic model problem is demonstrated by the following parametric study. For simplicity, a membrane model is used.

Figure 5.5 Arrangement of the reinforcement in the intersection of the caisson cells (tricells)

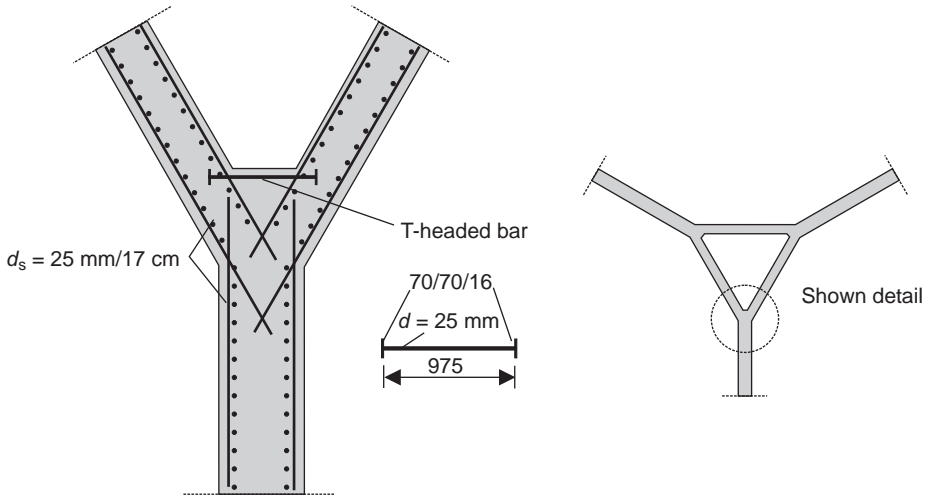


Figure 5.7 shows the distribution of the main membrane forces in the region of the wall intersections. The inclination of the compression struts result in a high tensile force, which should be carried by the T-headed bars. However, the size of this force is highly dependent on the size of the elements, as can easily be demonstrated by calculations with different FE meshes. Figure 5.8 shows the distribution of the horizontal tensile force in the walls for different mesh refinements (see Figure 5.9).

With a very coarse mesh, there appears to be no tensile force in the intersection region (mesh number 1). Refinements result in a large increase in the horizontal force resultants

Figure 5.6 Element mesh of the tricells

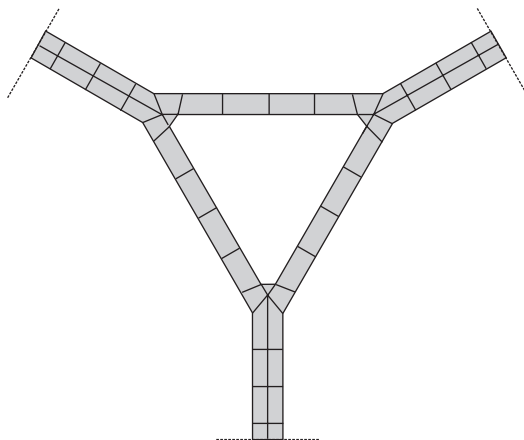
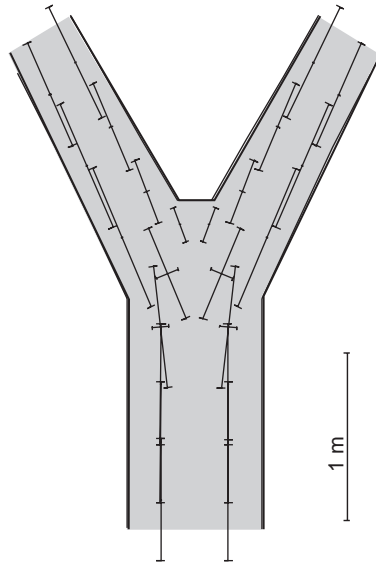


Figure 5.7 Main membrane forces



(see Table 5.1). It should be noted that the results are highly dependent on the element type and size used.

The resultant forces in the walls of the tricells loaded with water pressure of $w = 0.67 \text{ MN/m}^2$ can be easily determined with the truss model shown in Figure 5.10.

Figure 5.8 Distribution of the horizontal membrane force in the wall

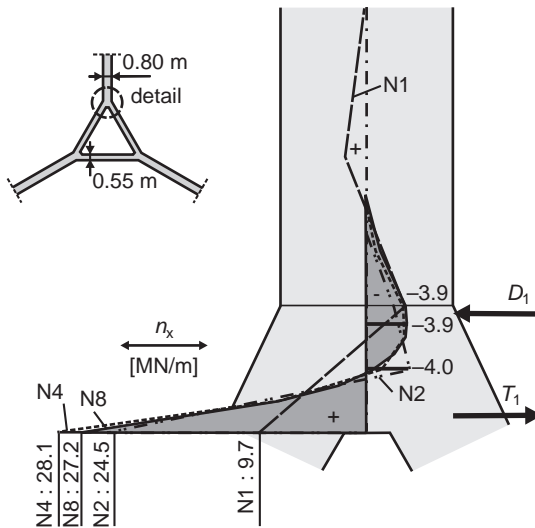
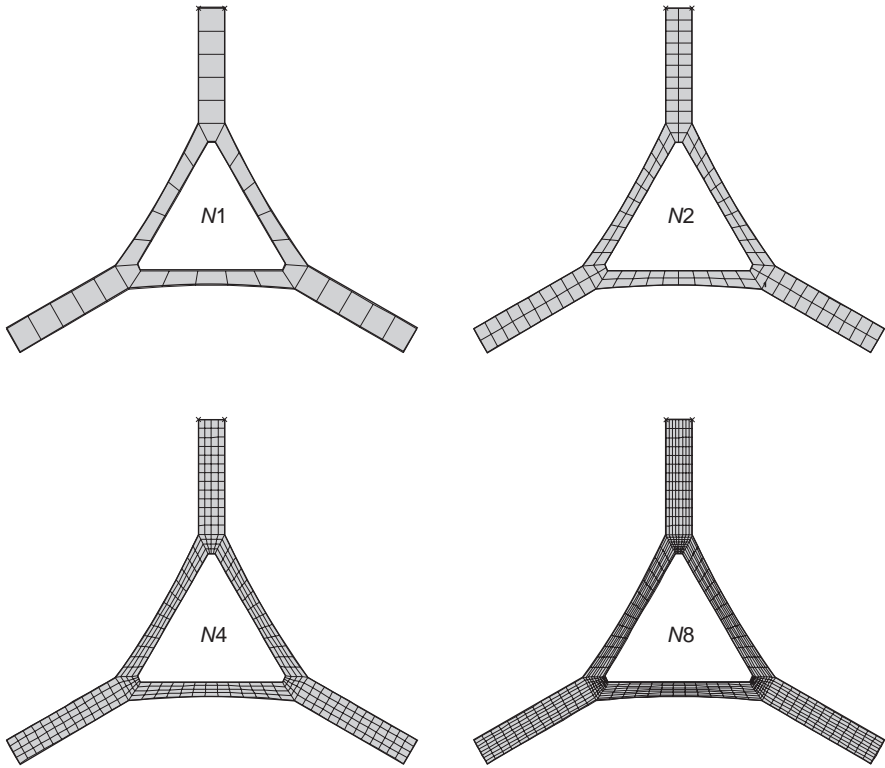


Figure 5.9 Element meshes for the tricells



The normal forces $N = 1.69$ MN/m are in good agreement with the FE results of mesh N4 to N8 ($T_1 - D_1 = 1.66$ MN/m, see Table 5.1). The resultant tensile force from the bending moment is difficult to estimate, as the internal lever arm is not known. For the following manual analysis, the inner lever arm is taken from the FE calculations as $z = 0.50$ m.

$$T_1^M = \frac{m}{z} = \frac{q \cdot l^2}{12 \cdot z} \approx \frac{0.67 \cdot 4.38^2}{12 \cdot 0.5} = 2.14 \text{ MN/m}$$

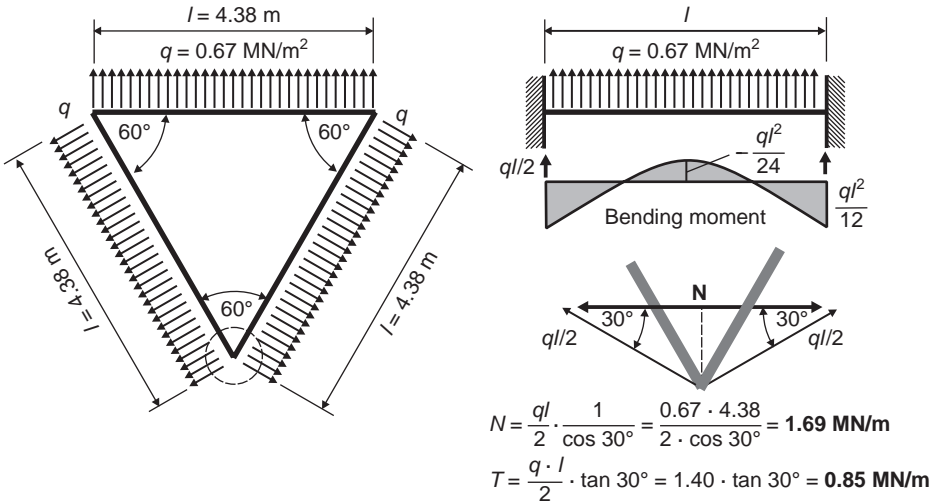
The FE analysis gives a value of (see Table 5.1):

$$T_1^M = 3.45 - 1.66 = 1.79 \text{ MN/m}$$

Table 5.1 Resultant tensile force for various FE meshes

Mesh number	N1	N2	N4	N8
Resultant tensile force $T_1 - D_1$ in MN/m	0.95	1.35	1.67	1.66
Resultant tensile force T_1 in MN/m	2.32	3.25	3.41	3.45

Figure 5.10 Truss model of a tricell



What are the conclusions we can draw from analysing this failure (Bergan, 1998)? Complicated shell models with various arbitrary loadings can hardly be checked by manual analysis of simplified equivalent structures, whereas this is possible for flat plates and shear walls. Furthermore, the checking of the equilibrium condition of the external loads and the support forces is not sufficient to guarantee the correctness of the analysis. Other checks have to be performed for shells with complicated shapes.

The essential problem in the numerical analysis of the platform was that the element mesh used was not able to model the real deformation characteristics and load-bearing behaviour of the structure. The element mesh used was too coarse; furthermore, the assumption of linear elastic behaviour did not hold for all sections of the structure.

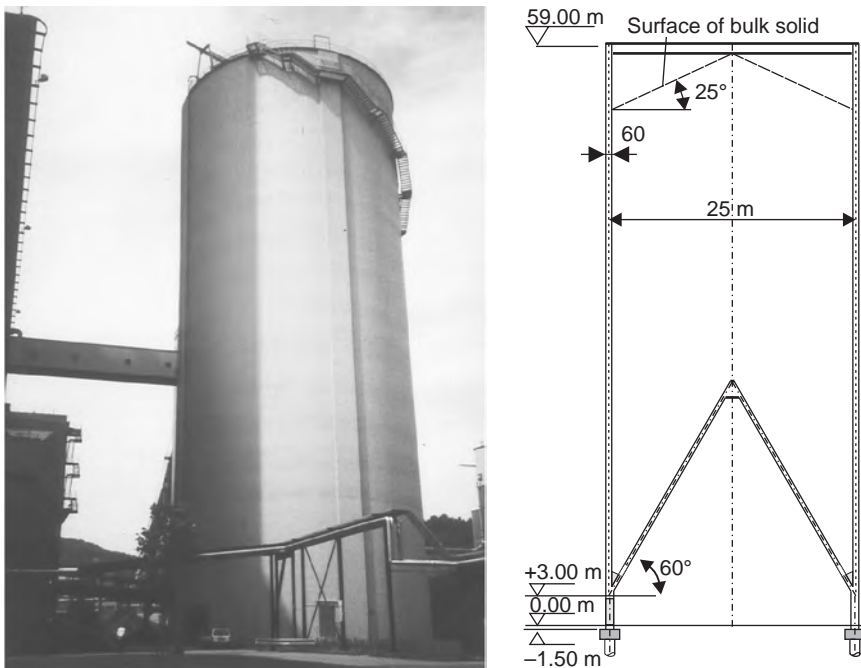
Thus, each structure has to be checked for regions where the assumptions of the numerical model do not apply. Detailed knowledge of both FEM and the material behaviour are required for this task. Numerical algorithms such as automatic mesh refinement cannot compensate for the knowledge of the user. When the element mesh used is too coarse, they are often not able to detect critical sections.

Critical regions of the structure can be analysed separately from the whole structure by means of, for example, strut-and-tie models or refined FE models (substructure method). The resultant forces at the outer surface of the substructure can then be applied to a global model, and vice versa.

5.1.2 Patch loads on shells

The design of a huge offshore platform is very specialised and not a routine task. However, model problems can appear even on simple cylindrical shells. The following demonstrates this on a cylindrical silo.

Figure 5.11 Silo

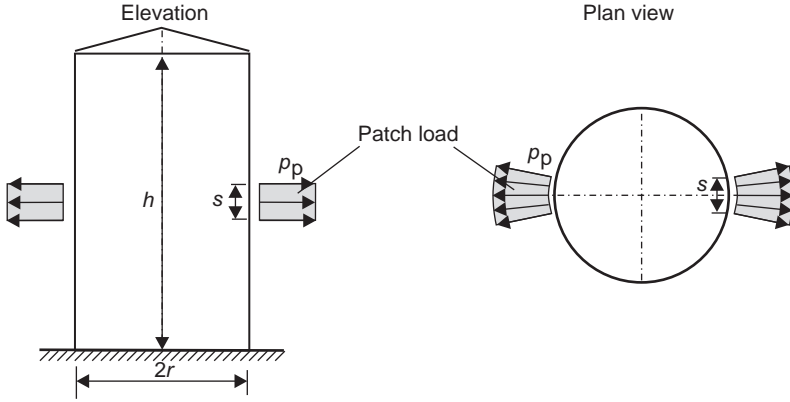


The cylindrical bin, which is used for storage of fly ash, has a height of 59 m and an inner diameter of 24.4 m (see Figure 5.11). The following analysis is carried out on a simplified model. Only the cylindrical shaft is modelled. The inverted cone and the partial restraint of the walls in the pile foundation are neglected.

For axisymmetric structures, 3D models are only required if unsymmetric loads have to be applied. This is the case for most silo structures. The main loading of a silo results from the pressure due to the bulk material inside the bin, which can be estimated from various codes (e.g. EC1, Part 4; see Eurocode 1, 1997). A uniform pressure distribution around the perimeter of the bin is generally assumed. In addition, a horizontal partial overpressure, a so-called ‘patch load’, has to be applied to the structure (Figure 5.12). The size of the square loaded area, s , is equal to $s = 0.2d_c = 0.4r$ (where r = internal diameter) for cylindrical concrete shells. For the structure shown in Figure 5.11, this results in $s = 4.88$ m. Generally, it is sufficient to apply this load at mid-height of the cell.

The patch load causes bending moments in the cylindrical walls. Charts to calculate the resulting internal forces for thin shells have been published by Hennig (1971). These tables can only be applied to infinite long cylindrical shells. The restraint on the walls by the foundation or the roof is neglected. More accurate values of the internal forces can be determined by a 3D FE analysis. Here, a sufficient fine element mesh in the region of the patch load has to be used, as shown in the following calculations.

Figure 5.12 Patch load according to EC1 Part 4 (Eurocode 1, 1997)



The FE analysis is carried out with three different meshes (Figure 5.13). For simplicity, the sizes of all elements are kept constant within each model, whereas the element size is only relevant in the region of the patch load. The element size is chosen so that the loaded area covers one element in mesh number 1, 2×2 elements in mesh number 2 and 4×4

Figure 5.13 Element meshes

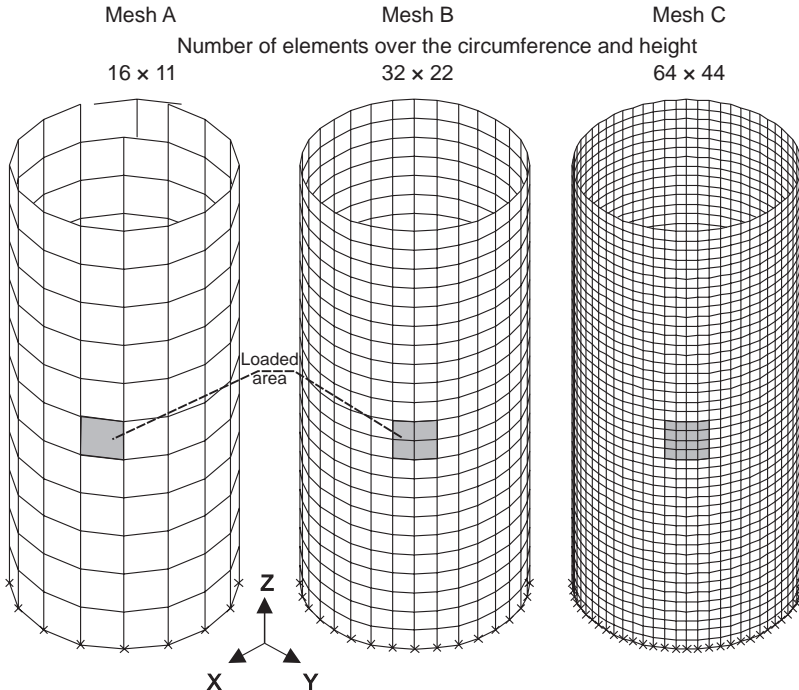
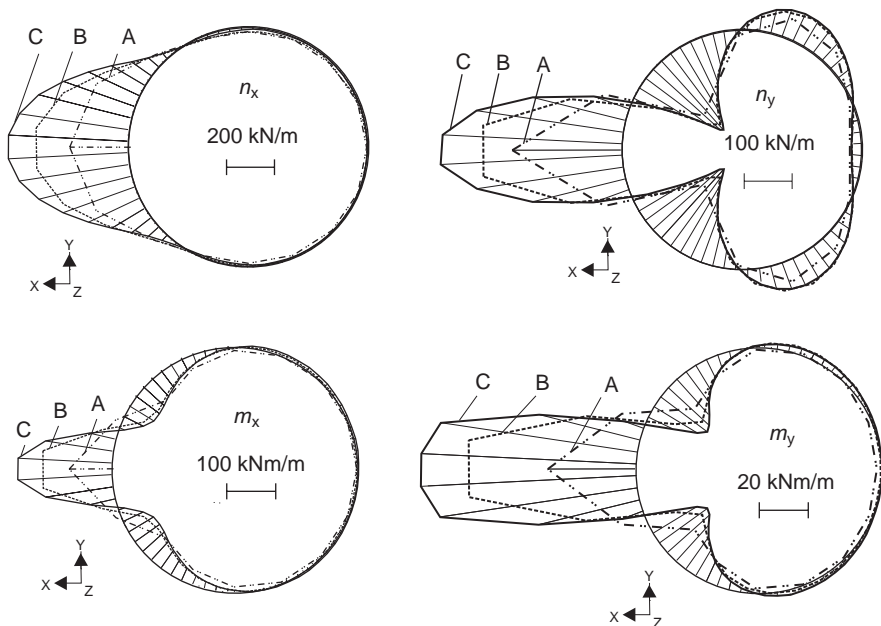


Figure 5.14 Internal forces in a horizontal section at $z = h/2 = 28$ m (element values)



elements in mesh number 3. A uniform horizontal patch load of $q = 100 \text{ kN/m}^2$ is applied to the walls.

The internal forces under the patch load increase considerably with an increase in the number of the elements, as can be seen in Figure 5.14. Table 5.2 gives the maximum values of the internal forces. The maximum bending moment, calculated with the coarse element mesh A, is only one-third of that of mesh C. Calculating the reinforcement

Table 5.2 Maximum internal forces (nodal value)

		Mesh A	Mesh B	Mesh C	Hennig (1971)	
n_x in kN/m	Min	-97 (86%)	-106 (94%)	-113 (100%)	-	-
	Max	244 (39%)	492 (79%)	627 (100%)	424	(68%)
n_y in kN/m	Min	-487 (85%)	-556 (97%)	-571 (100%)	-540	(95%)
	Max	273 (71%)	356 (92%)	387 (100%)	-	-
m_x in kNm/m	Min	-50 (78%)	-68 (106%)	-64 (100%)	-	-
	Max	93 (44%)	202 (97%)	209 (100%)	188	(90%)
m_y in kNm/m	Min	-15 (63%)	-22 (92%)	-24 (100%)	-	-
	Max	36 (31%)	114 (98%)	116 (100%)	120	(103%)

n_x, m_x = internal forces in circumferential direction

Figure 5.15 Contour plot of the bending moment m_x in circumferential direction (mesh C)

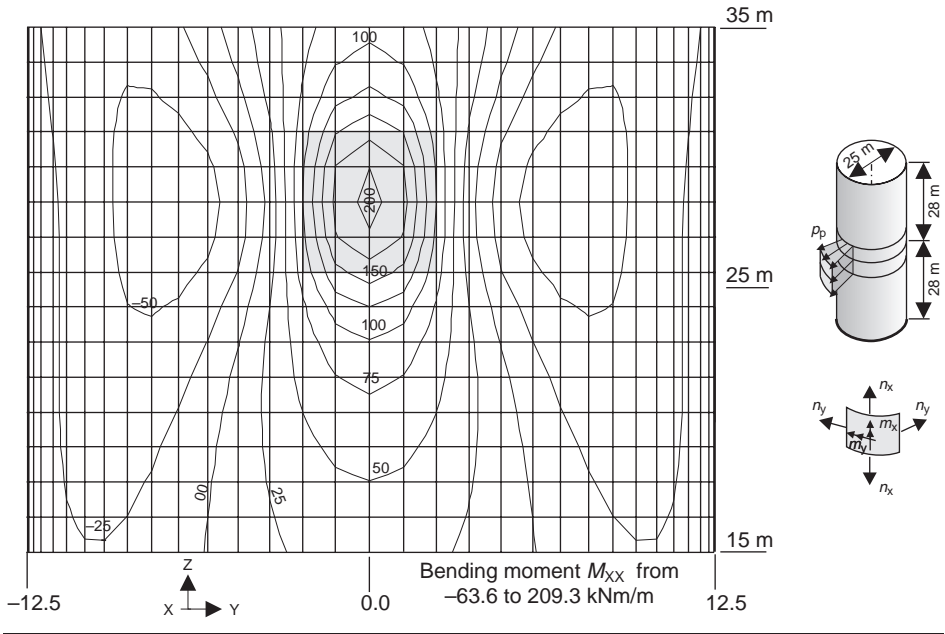
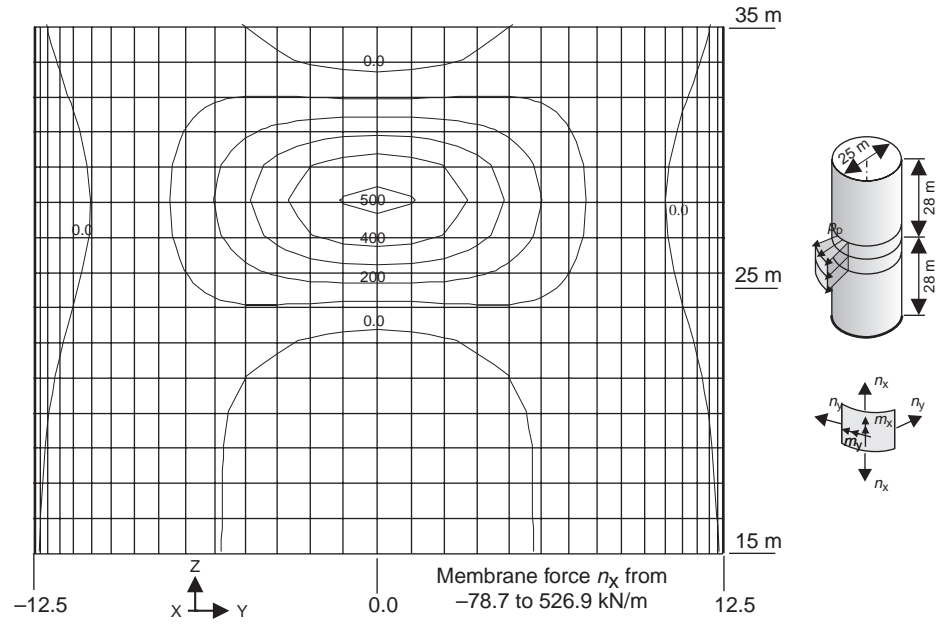


Figure 5.16 Contour plot of the membrane force n_x in circumferential direction (mesh C)



requirements using such considerably lower value for the bending moments would result in a lack of safety. A contour plot of the bending moment and the normal forces in circumferential direction calculated with mesh C are shown in Figures 5.15 and 5.16 respectively.

Due to the large uncertainty in the actual loading conditions, a high accuracy in the analysis is not required. The patch load represents only a rough idealisation of the non-uniform pressure distribution in a silo bin in the circumferential direction caused by the granular bulk material. In this respect, an extensive 3D FE shell analysis is only useful in special cases. Table 5.2 shows that a simple manual analysis of the maximum bending moments, using the parameters published by Hennig (1971), gives a good agreement with the FE analysis.

As previously mentioned, the patch load represents a rough simplification of the real pressure distribution. Therefore, material nonlinear calculations are not permissible, as the theoretical bending moments in the walls would be considerably reduced.

5.2. T-beams

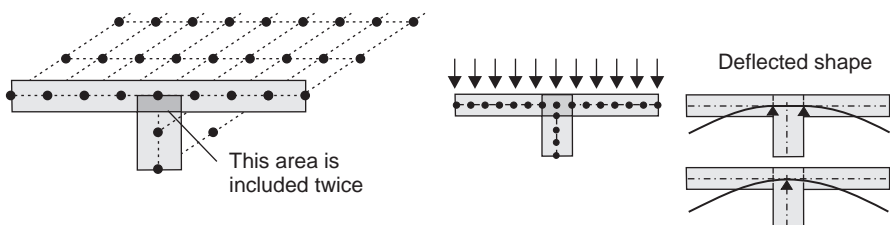
T-beams are widely used in concrete structures, whether as a main longitudinal girder in bridges or as the support (joist) of slabs (see Sections 2.8.2 and 2.8.3). An analysis can easily be carried out manually on equivalent girder systems. However, the use of 3D FE calculations is reasonable and would be required if the load-bearing behaviour of the structure has to be modelled to greater accuracy. In these calculations, one does not depend on simplifications such as the effective width of the flange b_{eff} . In contrast to grillages, a 2D spatial load distribution is modelled. However, the increase in accuracy requires a much greater workload.

5.2.1 Models for T-beams

T-beams can be idealised by different models (Rombach, 2007) (see Figure 5.18)

- (a) knife-edge support of a slab (simply supported)
- (b) 3D model with flat shell elements
- (c) additional beam elements on the midplane of the plate
- (d) shell elements with eccentric coupled beam elements
- (e) shell with different section depths but with common upper edge.

Figure 5.17 Web/flange junction



Model A: Knife-edge support

For the analysis of a slab, the T-beam may be treated as an infinite stiff member, resulting in a rigid vertical support condition for the slab. The support forces in the plate analysis can then be used as loading for the T-beam girder to calculate the internal forces and dimensioning of the T-beam. This simplified model is only permissible for very stiff T-beams, as the deflections of the girder and the redistribution of the resulting forces are neglected. The main advantage of this method in comparison to other approaches is that the internal forces of the slab can be calculated by means of a simple 2D FE model with flat plate elements or table values in the case of simple boundary conditions. The loads for the T-beam can be easily determined by influence surfaces such as those given in Grasser *et al.* (1991). The main disadvantage of this model is the additional effort needed for the separate analysis of the girder. Nevertheless, this extra work required is generally minimal.

Model B: Shell elements

The entire structure is modelled using flat thin shell elements (folded slabs). The FE analysis has to be done with shell elements, as plate elements have (per definition) only bending moments and no normal forces in their midplane.

In this model, the behaviour of the T-beam is given with a high degree of accuracy. However, this is only the case when the assumption of a linear elastic material behaviour holds true and the flange and the webs are not too thick. Massive structures must be analysed with volume elements.

The elements of the web are mostly arranged up to the midplane of the plate. This approach results in a greater cross-section area due to the intersection of the flange (plate) and the web (beam) elements (see Figure 5.17). In general, this inaccuracy can be neglected, due to the relatively small influence of the bending stiffness on the internal forces. As an alternative, the nodes in the web and the flange elements may be coupled. The main disadvantage of a shell model is the considerable effort needed in the generation of the 3D mesh. Furthermore, an automatic dimensioning of the girder by the computer program is not possible (see Section 3.3).

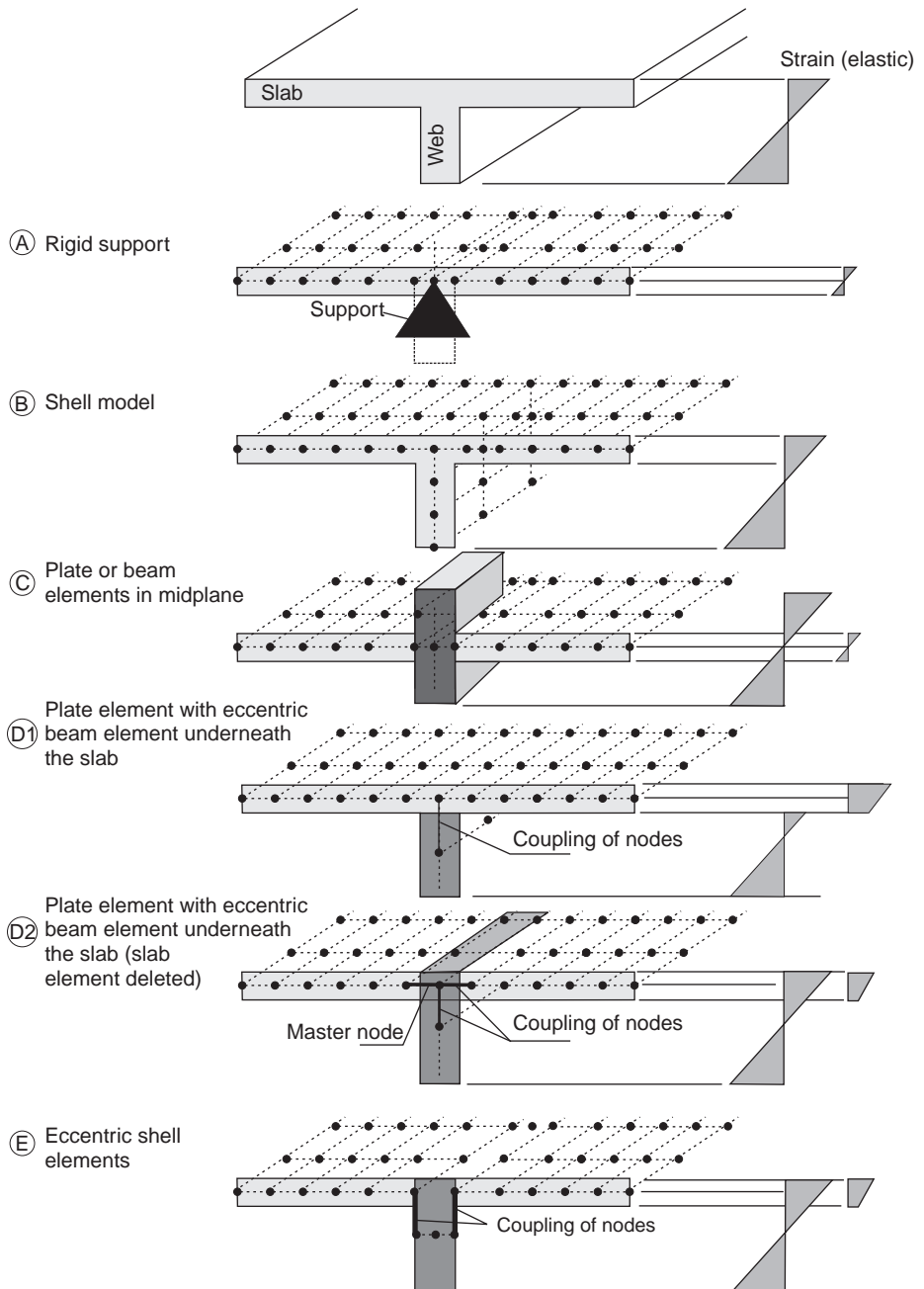
Model C: Replacement of the web by additional beam elements at the midplane of the slab

This numerical model has already been discussed in Section 4.8. The advantage of this approach lies in the fact that a simple 2D analysis is sufficient in comparison with the 3D model used in other approaches.

Model D: Shell elements with eccentric coupled beam elements

This model is similar to Model C; however, the beam is located eccentrically to the plate elements. Owing to the correct representation of the load-bearing behaviour of the system in this model, a modification of the depth of the beam elements is not required. The beam elements can be as deep as the web h_w (Model D1) or the total depth ($h_w + h_f$) (Model D2). The main difference between these two approaches is that Model D2 requires the plate elements to be deleted in the web area. Furthermore, Model D1

Figure 5.18 Models for a T-beam



does not need an additional coupling node at the midplane of the slab. Thus, the element mesh generation for Model D1 is easier and faster than D2.

The local connection of the beam and plate elements results in a non-uniform distribution of the bending moments and shear forces in the beam (web), which may be smoothed for design purposes.

Both models require additional work in the dimensioning of the T-beam. The internal forces in the flange must be integrated for the calculation of the bending moment M_y and shear force V in the beams (member forces). The T-beam must then be dimensioned for both group forces and not for the internal forces of the beam element only.

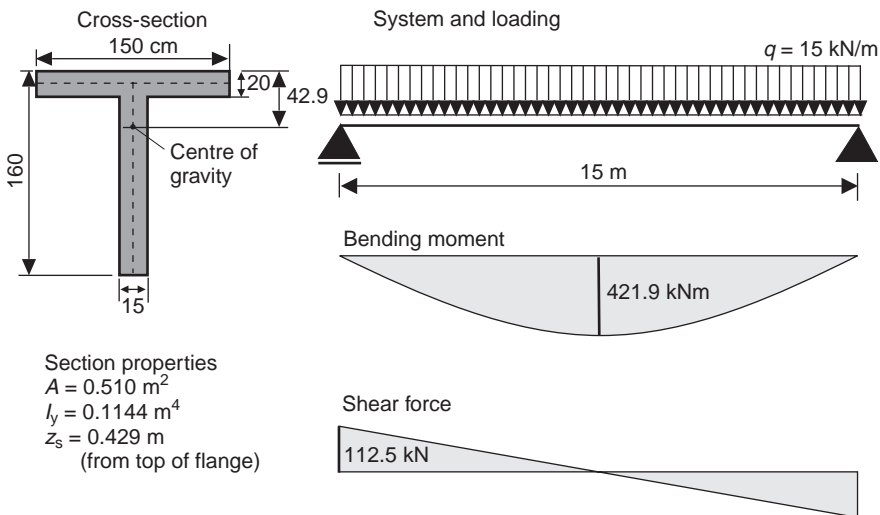
Model E: Flat shell elements with varying thickness

In contrast to Model C, the shell elements in this model have different thicknesses in accordance with the real system. The elements are arranged in such a way that the common upper surface is flat. Due to the eccentric arrangement of the shell elements, both bending moments and normal forces are calculated in the web and plate elements. In contrast to the other approaches, in this model, the load-bearing behaviour is represented correctly, and no additional analysis is required. However, this approach may give uneconomical results for large section depths, as the dimensioning has to be carried out separately for each element.

5.2.2 Comparison calculations with the different models

The results of the different approaches will be compared on a very simple structure, a simply supported single-span T-beam (span width of $l = 15$ m) under a uniform load of $q = 15$ kN/m (see Figure 5.19). The internal forces can easily be calculated manually

Figure 5.19 T-beam: system, loads, internal forces (beam model)



by means of a girder system, as the whole flange is under constant compression ($b_{\text{eff}} = b_{\text{fl}}$). This manual analysis results in the following maximum stresses in midspan of the structure.

$$\sigma_c = \frac{M}{I} \cdot z = \frac{421.9}{0.1144} \cdot \begin{Bmatrix} -0.429 \\ -0.229 \\ 1.171 \end{Bmatrix} = \begin{cases} -1582 \text{ kN/m}^2 & \text{(top)} \\ -845 \text{ kN/m}^2 & \text{(lower face of flange)} \\ +4310 \text{ kN/m}^2 & \text{(bottom)} \end{cases}$$

These values serve as a reference for the other models.

The results of the shell model are shown in Figures 5.20–5.22. The structure and the loading are symmetric. Therefore, it is sufficient to model only half of the whole structure

Figure 5.20 Shell model

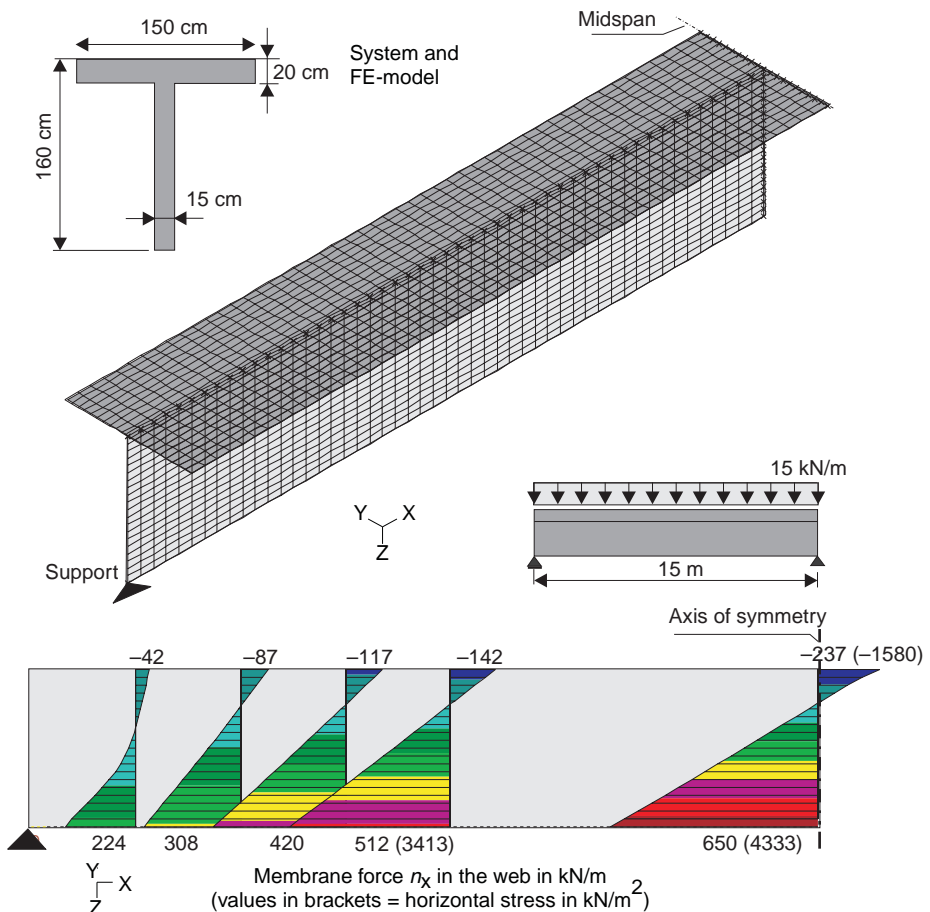
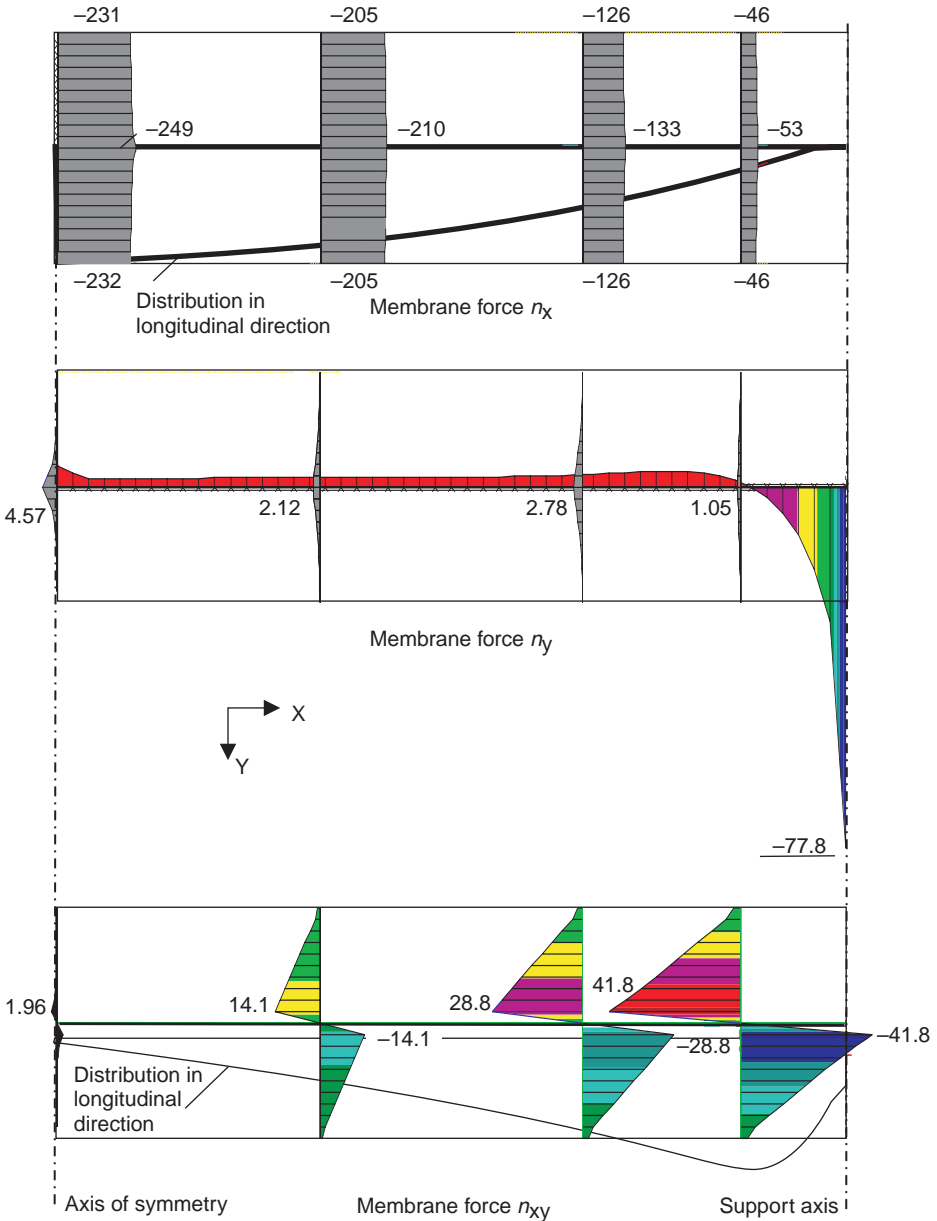
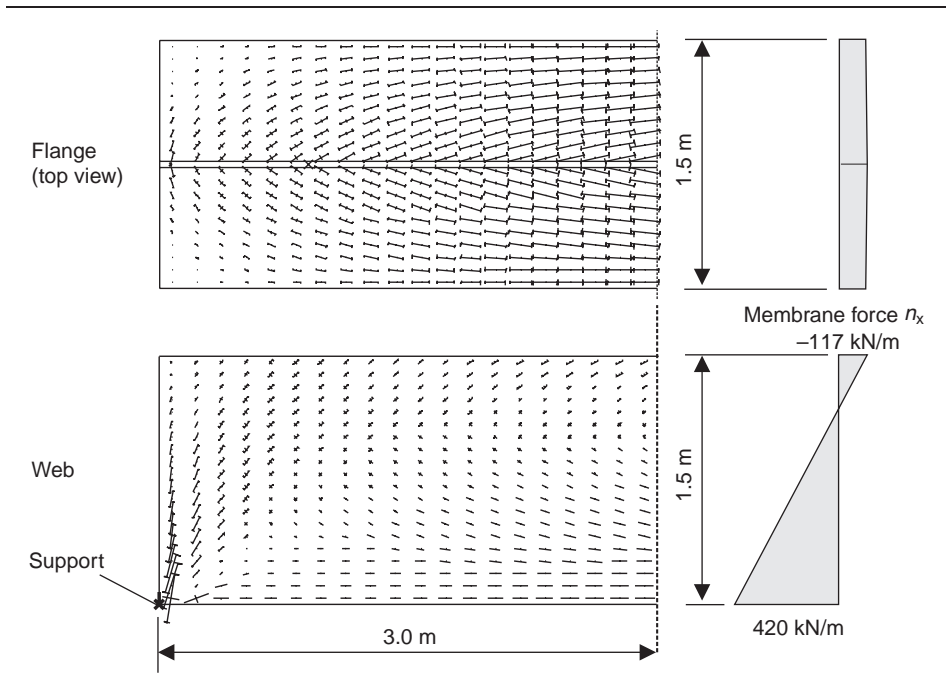


Figure 5.21 Membrane forces n_x , n_y , n_{xy} in the flange in different sections



and to consider the special boundary conditions at midspan. The web and the flange of the T-beam are each modelled by 20×50 elements. A pin support is used, since the internal forces near the supports are of no further interest. A uniform load of $q = 10 \text{ kN/m}^2$ is applied to the flange.

Figure 5.22 Main membrane forces in the support regions



The distribution of the horizontal membrane forces and the horizontal strains across the section depth are linear except near the supports (Figure 5.20). The main assumption of any beam analysis, the linear strain distribution over the depth of the cross-section, is valid for almost the whole structure. Therefore, it is not surprising that the normal stresses of the FE model correspond well with the results of the beam analysis (stresses at the upper and lower edges of the section at midspan ($\sigma^{\text{top}} = -1580 \text{ kN/mm}^2$; $\sigma^{\text{bottom}} = +4333 \text{ kN/mm}^2$; see Figure 5.20).

The compressive stresses $\sigma_x = n_x/h_f$ in the flange increase parabolically from the support axis to midspan in agreement to the bending moment distribution (Figure 5.21). The support force causes high transverse compressive stresses $\sigma_y = n_y/h_f$ in the flange, at the end of the beam (Figure 5.21 middle). The membrane shear forces n_{xy} in the flange are greatest at the intersection with the web. They decrease in a longitudinal direction to zero at midspan. Consequently, the shear force is not constant as assumed in most models for shear design of a flange in the transverse direction (e.g. see Eurocode 2, 2004, Section 6.2.4).

A 3D folded slab model of a T-beam is, in general, too extensive for most practical cases, especially as the dimensioning task is difficult (see, e.g. shear walls, Section 3.3). However, shell models are very helpful in determining the flow of forces in a structure and to evaluate an accurate strut-and-tie model (see Section 5.2.3).

Figure 5.23 Model C: Plate elements (flange) with central equivalent beam elements (web)

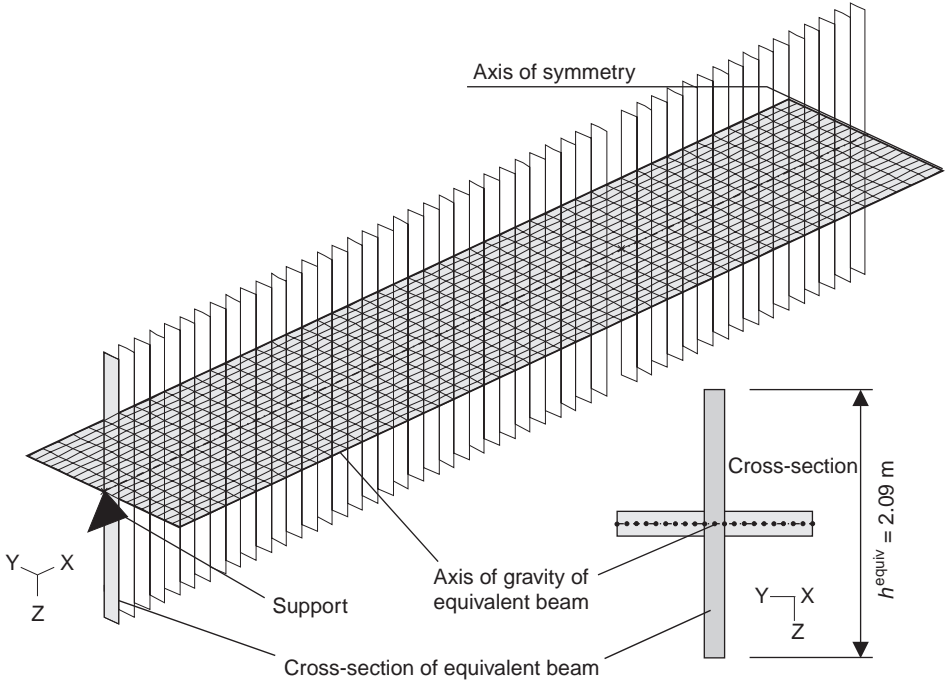


Figure 5.23 shows a model with beam elements located in the midplane of the plate. An equivalent depth of $h^{equiv} = 2.09$ m and a width of $b_w = 0.15$ m (same as a real web) can be calculated for the given dimensions of the T-beam. The models with an eccentric beam element are shown in Figures 5.24 and 5.25.

The total internal forces of the T-beam are calculated by summation of the beam forces N_{beam} , M_{beam} and the membrane forces in the shell n_x , m_x . The latter values are gained by numerical integration.

$$\text{Edge stresses of a beam: } \sigma_c = N/A \pm M/W$$

$$\text{Edge stresses of a slab: } \sigma_c = \frac{n_x \cdot b_F}{A} \pm \frac{m_{xx} \cdot b_F}{W} = \frac{n_x}{h_f} \pm \frac{m_{xx} \cdot 6}{h_f^2}$$

$$\text{Total normal force of T-beam: } N_{tot} = N_{beam} + N_{slab} = N_{beam} + n_{slab} \cdot b_{flange}$$

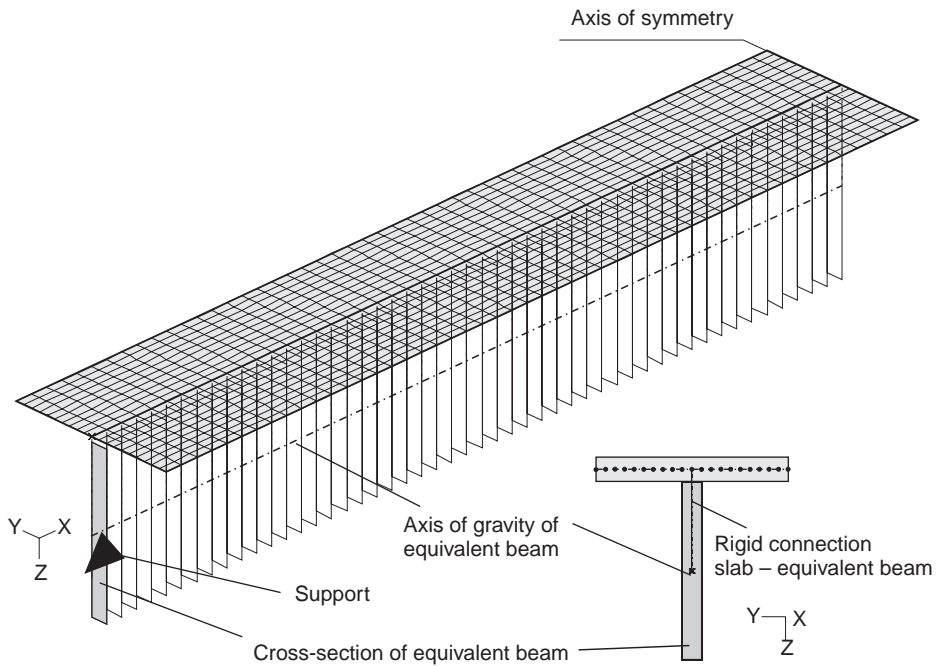
Total bending moment of T-beam:

$$M_{tot} = M_{beam} + N_{beam} \cdot z_{beam} + m_{slab} \cdot b_{flange} + n_{slab} \cdot b_{flange} \cdot z_{slab}$$

where:

- b, b_F are the widths of web and flange
- h, h_F are the depths of web and flange

Figure 5.24 Model D1: Shell elements (flange) with eccentric beam elements (web)



z is the distance between the centre of gravity of the flange or the web to that of the T-beam.

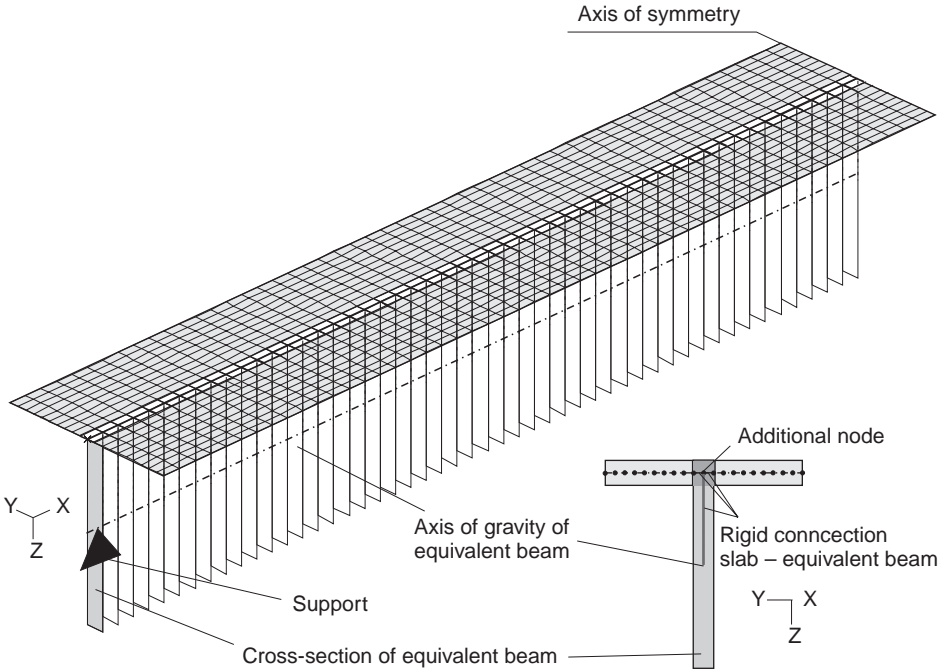
The results of the various approaches are summarised in Table 5.3. A very good agreement can be observed between all three different numerical models and the values of the manual analysis. The small differences between the results are caused by rounding errors. The distributions of the edge stresses are shown in Figure 5.26.

The bending behaviour of the T-beam is well represented in all the models. No differences in the deflection of the girder can be observed.

As was expected, the stress distributions in the slab and in the equivalent girder of Model C are completely different from the other cases (see Figure 5.26). These values cannot be used in design (e.g. checking the edge tensile stresses in the serviceability limit state for partial prestressed structures). In contrast, the stresses of Model D agree well with that of the T-beam girder, both in the web and the flange.

In Model D, single forces and single bending moments are introduced in the nodes due to the local coupling of the beam and shell elements. This results in an unsteady sawtooth distribution of the internal forces (Figure 5.27). For the purpose of the dimensioning of the T-beam, the distribution of the internal forces may be smoothed.

Figure 5.25 Model D2: Shell elements (flange) with eccentric beam elements (web)

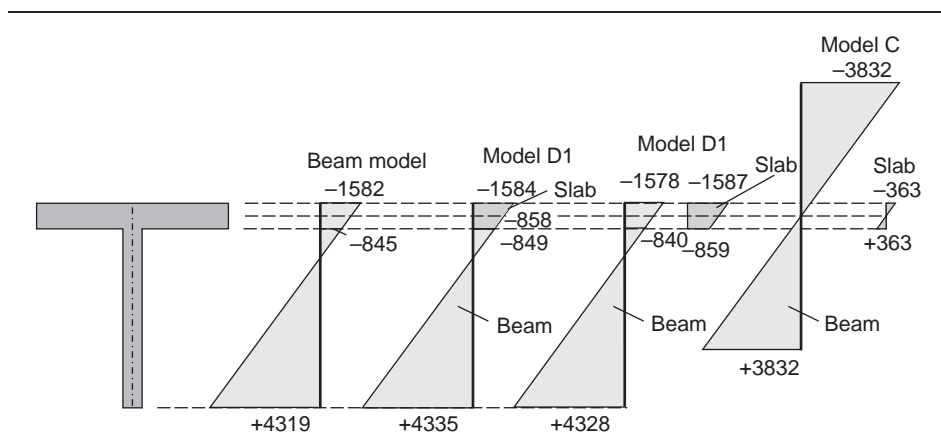


In case of automatic computational design for shear, there are significant differences between the various models. These are caused by the difference in the inner lever arm z . Therefore, the dimensioning should be done for the resultant internal shear forces acting on the T-beam.

Table 5.3 Member forces at midspan over the section depth of different models (dimensions kN and m)

Model	N_{slab}^{beam}	M_{slab}^{beam}	b_{slab}^{beam}	h_{slab}^{beam}	z_{slab}^{beam}	σ_{top} kN/m ²	σ_{bottom} kN/m ²	N_{slab}^{beam}	M_{slab}^{beam}
C	0.0	418.5	0.15	2.09	0	-3832	+3832	0.0	418.5
	0.0	2.42	1.5	0.2	0	-363	+363	0.0	3.63
	Total					0.0		422.1	
D1	366.1	126.0	0.15	1.40	1.171	-0.7	-849	+4335	366.1 126.0 + 172.4
	-244.0	2.42	1.5	0.2	0.429	-0.1	-1584	-856	-366.0 3.6 + 120.4
	Total					0.1		422.0	
D2	330.0	189.0	0.15	1.60	0.8	-0.429	-1578	+4328	330.0 189.0 + 122.4
	-245.0	2.43	1.5	0.2	0.429	-0.1	-1587	-859	-366.0 3.3 + 108.8
	Total					-0.8		423.0	

Figure 5.26 Stress distribution in midspan over the section depth of different models [kN/m²]



To summarise, it should be noted that in addition to an FE analysis, effort is separately required for the various approaches to design a T-beam. The resultant internal forces and the deflections of the girder in Models B and D agree well with the manual T-beam girder analysis. Consequently, the choice of the model is dependent on the required results. If edge stresses are needed, for example, in the design of T-beam bridges, only Model B (folded shell) and Model D (shell with eccentric beam) should be used.

5.2.3 Flow of forces in the anchorage region of tendons

Transverse tensile stresses occur in the web and in the flange close to the anchorage region of prestressing tendons. The design of this discontinuity region can be based on the strut-and-tie approach. The main unknown parameter in such a model is the orientation of the compression strut or the location of the tensile strut in the flange. The geometry of the model used has a great influence on the calculated transverse tensile

Figure 5.27 Internal forces in the beam elements (Model D1)

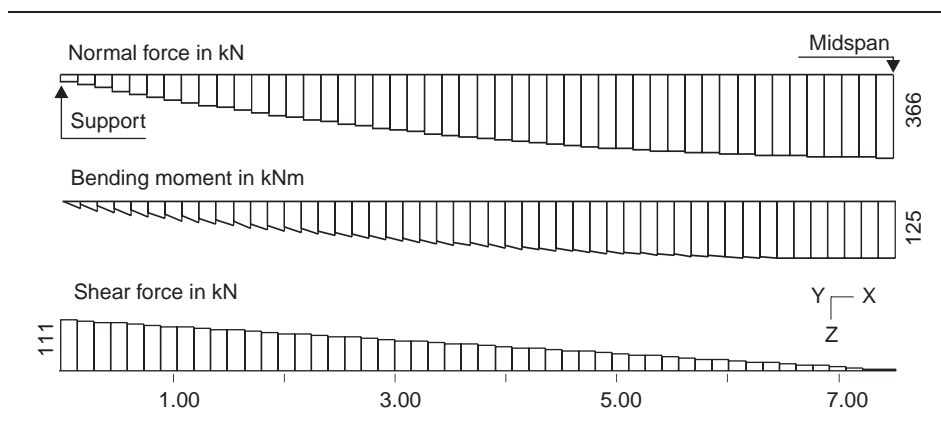
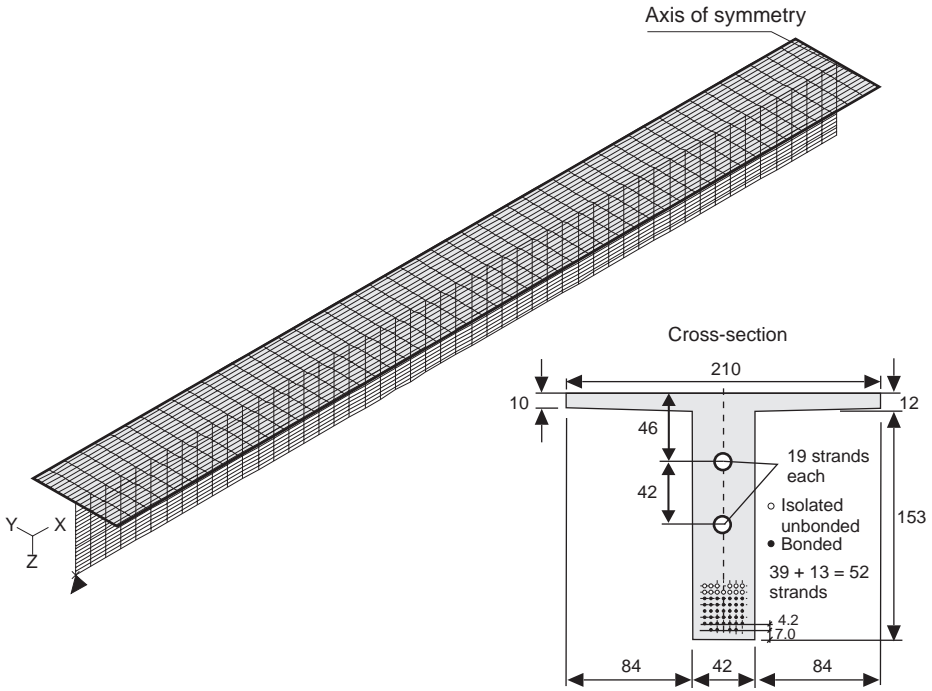


Figure 5.28 Structure and FE model



stresses and the required reinforcing steel in the support region. Therefore, accurate information on the flow of forces is useful. A 3D FE shell analysis can be helpful in this task.

The strut-and-tie modelling based on an elastic FE analysis will be illustrated for a precast T-beam of the single-span concrete bridge shown in Figure 5.28 (see also Figure 2.98). This structural system has already been explained in Section 2.8.3. The beam has a span length of $l = 38$ m. The following calculation only considers the prestressing forces. The T-beam girder was stressed by 52 straight tendons of grade ST 1570/1770.

The analysis can be restricted to half of the system, as the structure and the uniform loading are symmetrical to midspan. 20×50 shell elements are used to model the web and the flange.

The results of the shell analysis are shown in Figures 5.29 and 5.30. The strut-and-tie model was adapted to the orientation of the main membrane forces. The large transverse tensile stresses in the flange at the support region are clearly shown in Figure 5.30.

The preceding analysis was based on linear elastic material behaviour. This applies mostly to the web, as almost no tensile stresses occur under prestressing; nevertheless, force redistributions may happen in the flange due to cracking.

Figure 5.29 Main membrane forces at the end of the girder ($l = 3.0$ m) and membrane forces in longitudinal direction in various sections – strut-and-tie model

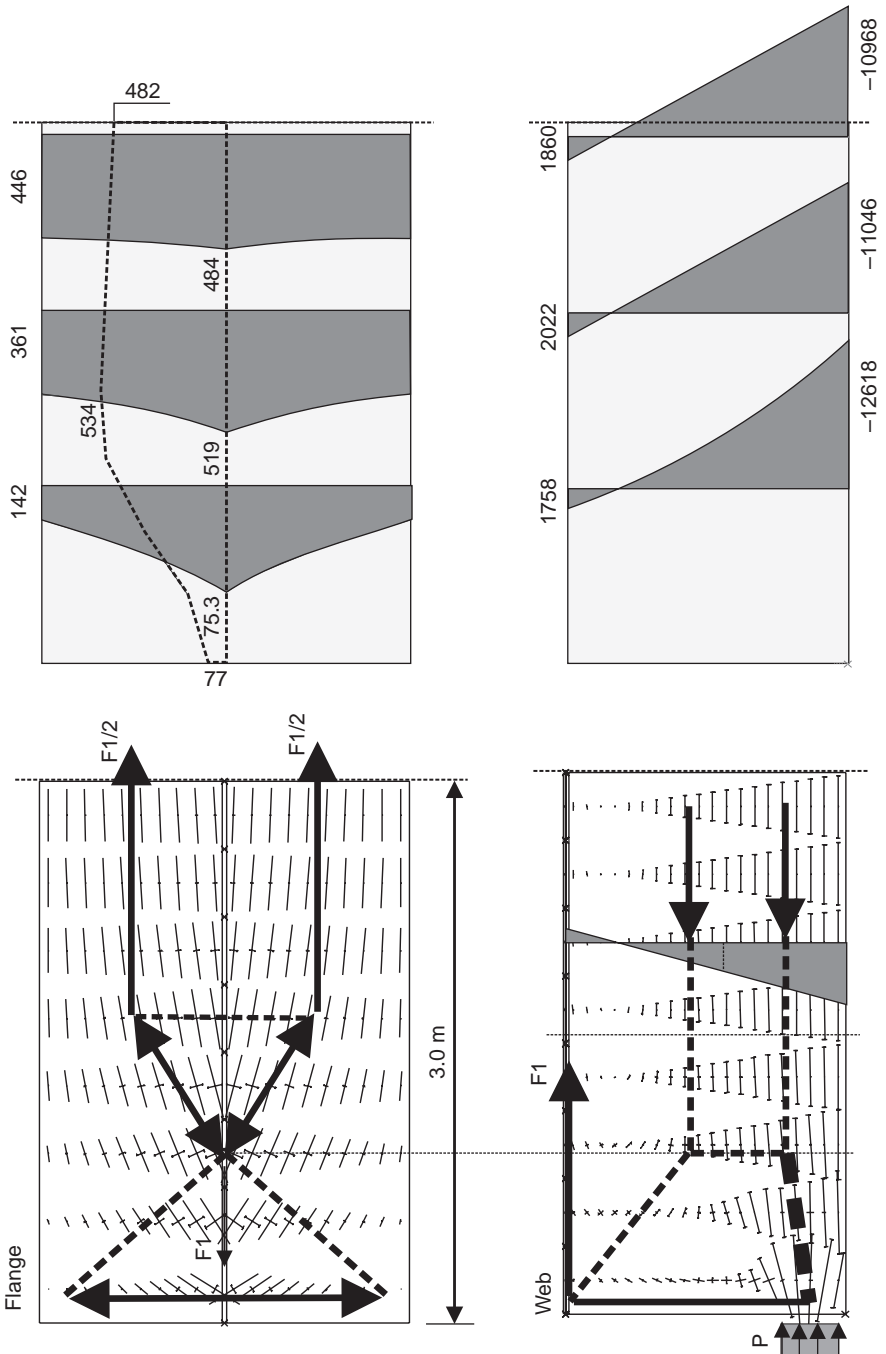
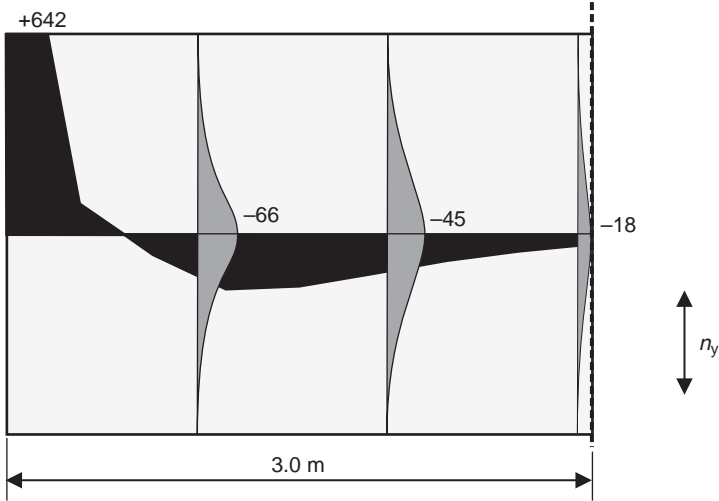


Figure 5.30 Distribution of the membrane forces in transverse direction in the flange near the end of the beam (top view)



5.3. Slab-on-beam structure

Section 5.2 explored the modelling of T-beams, where the compressive stress is nearly constant over the width of the flange (see Figure 5.21). The effective width b_{eff} is equal to the whole width of the flange over the whole span. The member forces can be estimated through the summation of the flange and web forces.

With a slab supported on beams, the available ‘flange’ width of the downstand beam is often considerably bigger than the real one, b_{eff} . This raises the questions: which part of the member forces in the slab should be used, and which b_{eff} should be applied for design of the downstand beam? Complex, time-consuming analyses does not make much sense for this kind of common structure. An automatic design by a computer program is required.

In the following, the member forces and the required amount of reinforcement are estimated for a regular slab supported by beams with different model variations. The folded plate model is regarded as the most realistic solution, and is used to verify the other models. The analysis is done with a web height of $h_w = 3h_f$ and $h_w = h_f$ (where h_f is the thickness of the slab), as the relation h_w/h_f has a large influence on the member forces. The span of the slab in both directions is chosen so that a design of both structures is possible with a reasonable amount of reinforcing steel.

The slab is clamped on one side to simulate a multi-span structure. Furthermore, a statically indeterminate system is chosen, because here the member forces depend on the distribution of the stiffness in the structure (width of the compression flange).

5.3.1 Slab supported by a high downstand beam

Figure 5.31 shows the structural system. The slab has a thickness of $h_F = 20$ cm. A slab with a span of $l_{\text{eff}} = 10$ m is not possible with regard to the design in the serviceability and ultimate limit state. Thus, every 6.2 m, a downstand beam is arranged. The web height of the downstand beam is $h_w = 60$ cm only, in order to get a soft support. Detailed investigations are not required in the case of a large downstand beam or a rigid support. In the upper end (axis A), the slab is supported by a wall and is free to rotate. The slab is clamped in axis B to simulate a continuous structure. A uniform load of $(g + q)_d = 16 \text{ kN/m}^2$ is applied.

First, the member forces and the required reinforcement in the slab and the T-beam are estimated manually. These values are compared to the results of the numerical calculation.

5.3.1.1 Manual analysis

For a manual calculation, the structure is divided into two equivalent systems, a rectangular slab and a T-beam. The latter is regarded as a stiff support for the slab. The plate is clamped on three edges (axis B and over the downstand beams due to the uniform loading) and simply supported in axis A ($l_x/l_y = 10.0/6.20$ m).

The bending moments and shear forces for the rectangular slab are as follows (Czerny, 1999; see Figure 5.32):

$$\begin{aligned}
 m_{x_{\text{ermin,d}}} &= -50.2 \text{ kNm/m} \quad (-46.7) & m_{x_{\text{m,d}}} &= 23.2 \text{ kNm/m} \quad (24.3) \\
 m_{y_{\text{erm,d}}} &= -35.2 \text{ kNm/m} \quad (-32.4) & m_{y_{\text{max,d}}} &= 7.8 \text{ kNm/m} \quad (11.4) \\
 v_{x_{\text{erm,d}}} &= 51.1 \text{ kNm/m} \quad (50.2) & v_{y_{\text{erm,d}}} &= 45.3 \text{ kNm/m} \quad (41.6) \\
 v_{y_{\text{rm,d}}} &= 23.9 \text{ kNm/m} \quad (23.0) & \bar{v}_{y_{\text{rm,d}}} &= 35.7 \text{ kNm/m} \quad (31.2) \\
 f &= 3.4 \text{ mm} \quad (3.4 \text{ mm}) \quad (\text{concrete grade C 20/25, } E_c = 24\,914 \text{ MPa})
 \end{aligned}$$

Figure 5.31 Slab supported on beams

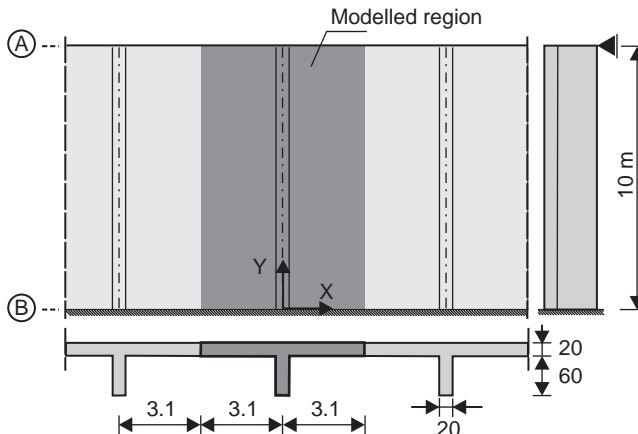
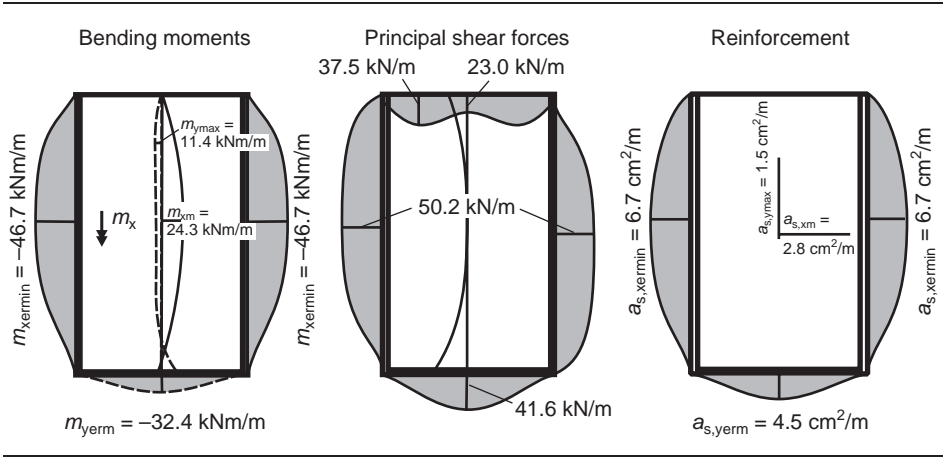


Figure 5.32 Member forces and required reinforcement for the slab (FE analysis)



The values in brackets are gained from an FE analysis of the slab with Poisson’s ratio of $\nu = 0.2$. The other figures are from Czerny (1999), where $\nu = 0$ is assumed.

The manual design is done with a constant internal lever arm of $d_m = 0.17$ m in both directions. This analysis results in the following amount of reinforcing steel (Figure 5.32):

$$\begin{aligned}
 x \text{ direction: } a_{s,x,ermin} &= 6.6 \text{ cm}^2/\text{m} \quad (6.7) & a_{s,xm} &= 2.8 \text{ cm}^2/\text{m} \quad (2.8) \\
 y \text{ direction: } a_{s,y,erm} &= 4.0 \text{ cm}^2/\text{m} \quad (4.5) & a_{s,y,max} &= 0.9 \text{ cm}^2/\text{m} \quad (1.5)
 \end{aligned}$$

This concludes the manual design for the bending of the slab.

The vertical loads on the downstand beam can be estimated very easily, for example, by means of influence surfaces according to Grasser *et al.* (1991). The effective widths b_{eff} for the design of the downstand beams are given in EC2, Part 1 §5.3.2.1 (Eurocode 2, 2004):

Distance between the point of zero moment of the clamped edge:

$$l_o = 0.25l = 2.50 \text{ m}$$

Prop: $b_{eff,axis B} = 0.2 \cdot b_{av.} + 0.1 \cdot l_o = 0.2 \cdot 3.1 + 0.1 \cdot 2.50 = 0.87 \text{ m}$

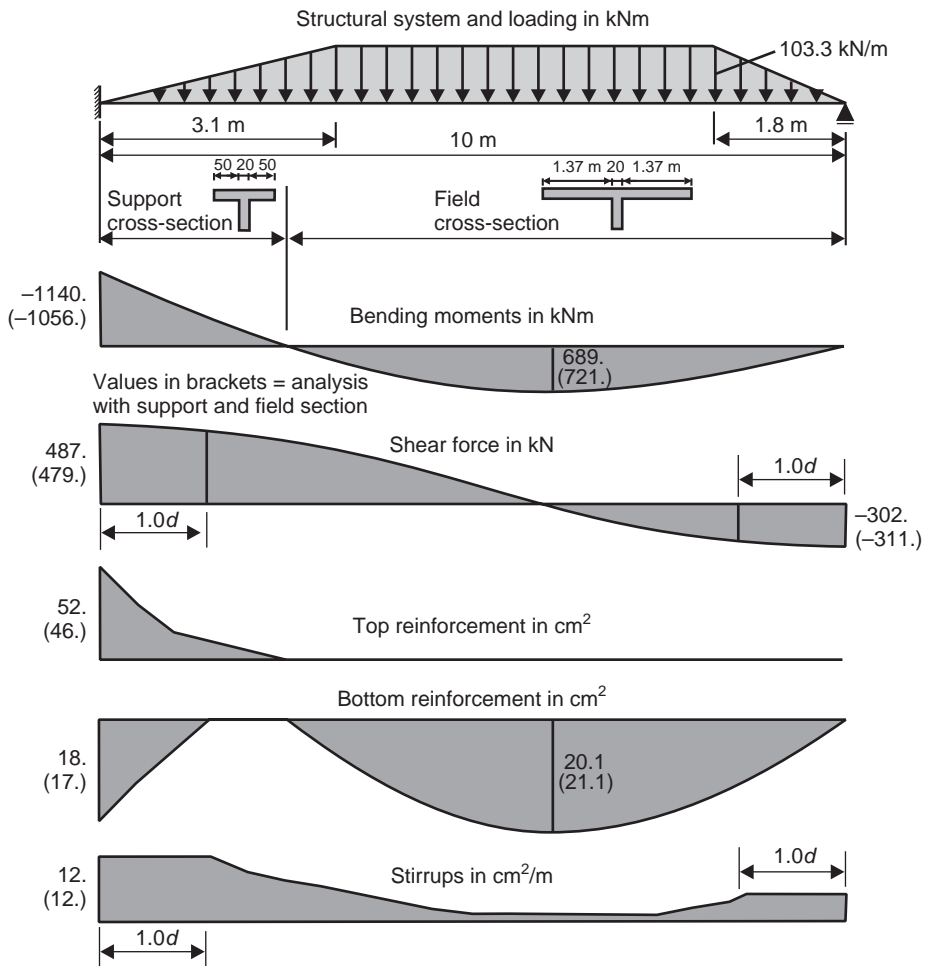
$$\leq \begin{cases} 0.2 \cdot l_o = 0.50 \text{ m} \\ b_{av.} = 3.10 \text{ m} \end{cases} \Rightarrow b_{eff,axis B} = 0.50 \text{ m}$$

Field: $b_{eff,field} = 0.2 \cdot b_{av.} + 0.1 \cdot l_o = 0.2 \cdot 3.1 + 0.1 \cdot 7.50 = 1.37 \text{ m}$

$$\leq \begin{cases} 0.2 \cdot l_o = 1.50 \text{ m} \\ b_{av.} = 3.10 \text{ m} \end{cases} \Rightarrow b_{eff,field} = 1.37 \text{ m}$$

Figure 5.33 shows the loads, member forces and required reinforcement for the T-beam with and without consideration of the effective width $b_{eff,axis B}$ in the region of the

Figure 5.33 Member forces and reinforcement for the T-beam

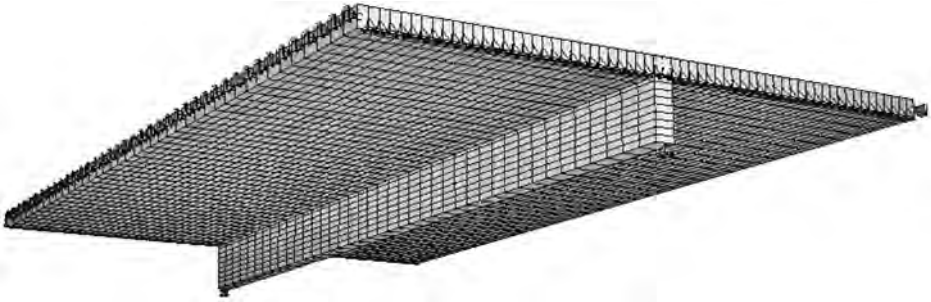


clamped support. The value of b_{eff} has an insignificant effect on the member forces. The bending moment in axis B is 8% larger if a constant effective width of $b_{\text{eff,field}}$ is used. The influence of the different stiffness at the support and in the field can be neglected, in particular because of the inaccuracy of b_{eff} .

It should be noted that the whole analysis is based on linear elastic material behaviour. An effective width in the support region, where the slab is under tension, does not make sense. The preceding equations are only valid for flanges under compression.

The previously shown manual analysis of the structure is an easy and quick task. Therefore, complex and time-consuming FE calculations do not seem to be necessary. Nevertheless, a disadvantage of the manual design lies in the fact that the real behaviour

Figure 5.34 Shell model (folded slab)



of the system is rather simplified. Usually, the downstand beam is not a rigid support for the slab, as has been assumed. Its deformation causes force redistributions and an increase of the member forces in the slab. The real behaviour of the system can be studied by means of a folded plate model with a higher accuracy. In the following, a pure folded slab system (FW) and a shell with a downstand beam (FB) is analysed. The first system serves as a reference.

5.3.1.2 Shell and folded slab system

Due to the regular system and the uniform load of $(g + q)_d = 16 \text{ kN/m}^2$, only one section of the whole structure must be modelled (see Figure 5.34). The symmetry conditions are considered with suitable restraints at the nodes in midspan.

Figure 5.35 shows the member forces of both models (FW and FB). One recognises a very good agreement of the results in the slab. The structural behaviour can be modelled, therefore, also with the shell/beam system (FB) very well. Different shear forces are obtained only in the region close to the clamped edge. However, these are not relevant for the design of the slab, as the relevant section is located in the distance $1.0d = 0.17 \text{ m}$ or 0.77 m from the edge of the support. The computer program makes a design for punching due to the high concentrated forces, which does not make much sense.

If one compares the member forces of FW or FB models with the manual calculation, large differences in the bending moments of the slab m_y in the direction of the downstand beam can be observed. The deformation of the beam leads to doubling of the bending moment at the clamped support from $m_{y,erm} = -32.4 \text{ kNm/m}$ (see Figure 5.32) to $m_{II,erm} = -68 \text{ kNm/m}$ and to a three-times-greater bending moment in the field $m_{y,max}$ ($m_{y,max} = 11.4$ and $m_{I,field} = 29 \text{ kNm/m}$).

For both models, the resultant bending moments were calculated in different sections by numerical integration of the member forces in the elements (Figure 5.36). It turns out that the distribution of the bending moments corresponds to a single-span beam, clamped on one side, with a uniform load of $6.2 \text{ m} \times 16 \text{ kN/m}^2 = 99.2 \text{ kN/m}$

Figure 5.35 Deflections and member forces of the folded slab (FW) and shell/beam (FB) model

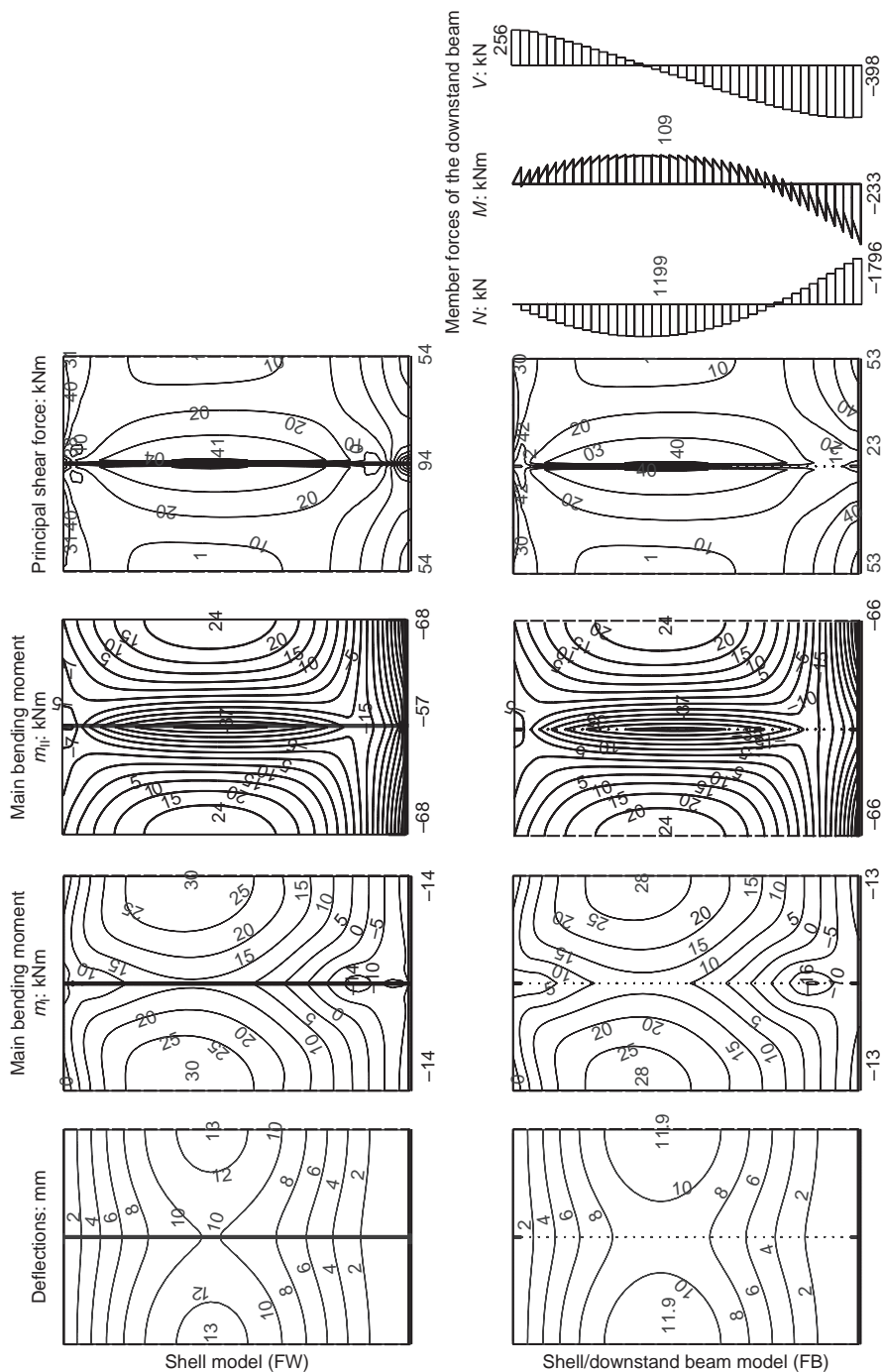
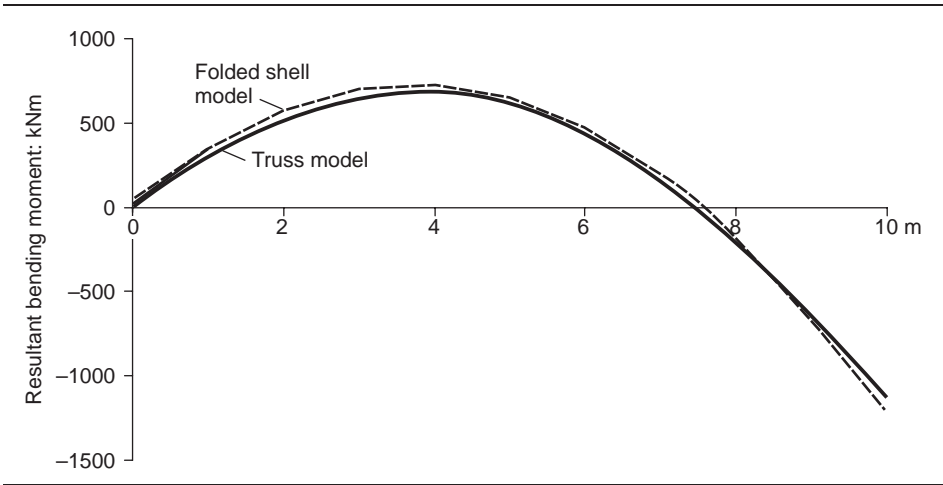


Figure 5.36 Bending moment for the pure shell and shell/beam models



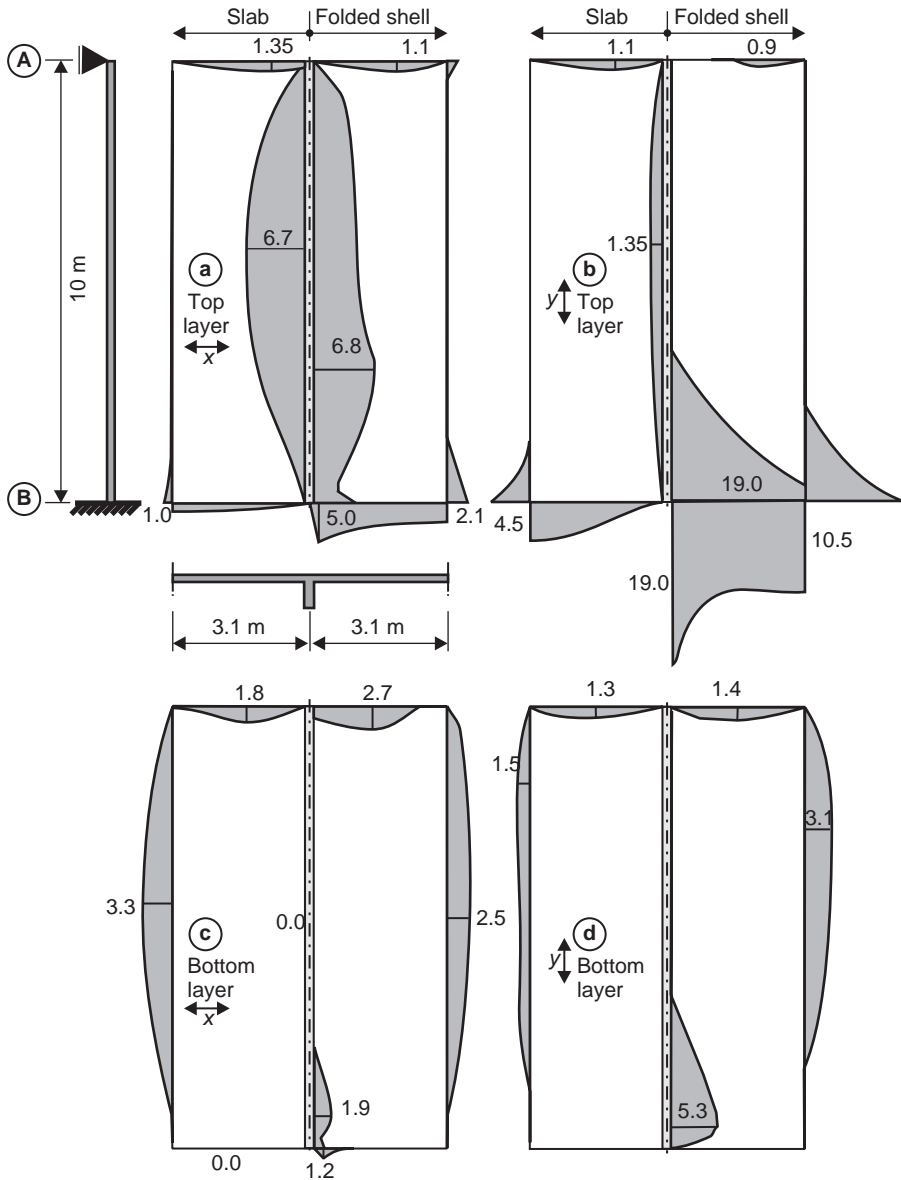
($M_{\text{Field}} = 698 \text{ kNm}$, $M_{\text{Supp}} = -1240 \text{ kNm}$). The same also applies for the shear forces. This is not surprising, because, regardless of the structure, equilibrium condition must be fulfilled. An integration of the shell forces over the whole width of 6.2m results in the same forces, as if the whole load is carried by the T-beam only. This corresponds to the manual analysis where the downstand beam is regarded as a stiff support. A safe design of the T-beam is achieved if the whole width of the ‘flange’ is applied. More realistic results for the member forces of the T-beam can be obtained if the integration of the shell forces is limited to a certain width. This will be explained in Section 5.3.1.3.

To illustrate the differences between a stiff and a soft support by means of a downstand beam, the required reinforcement of the rectangular slab (see manual analysis) and the folded shell system is plotted in the relevant sections (see Figure 5.37).

Only minor differences between both models are experienced with regard to the amount of reinforcement in the x-direction at the top of the slab over the downstand beam (Figure 5.37a). Here, the deflection curve shows a horizontal tangent due to the uniform load. Big differences are obtained at the clamped support (Figure 5.37a,b). With a stiff support, a reinforcement of approximately $a_{\text{sy}} = 5 \text{ cm}^2/\text{m}$ is required, whereas the shell model gives a four-times-higher value of $a_{\text{sy}} = 19 \text{ cm}^2/\text{m}$. The manual design deviates in this section considerably from the ‘exact’ FE analysis.

The big reinforcement at the clamped support a_{sy} with the pure folded plate model is caused by the large support bending moments in the slab. In addition, big tensile membrane forces of almost $n_y = 980 \text{ kN/m}$ are calculated in the shell in axis B. Due to the assumption of a linearly elastic material behaviour, the computer program cannot realise that it should design a T-beam. It calculates the member forces and the reinforcement for the flange and the downstand beam separately from each other. This example shows again that an automatic design by software is not possible in some areas of a structure.

Figure 5.37 Reinforcement in the slab: left: stiff support; right shell/beam system in cm^2/m



Furthermore, the deformation of the T-beam results in load redistributions from the transverse to the longitudinal direction. Therefore, the transverse reinforcement decreases in the folded plate model with regard to the three-sided clamped slab by approximately 25% (Figure 5.37c) and the longitudinal reinforcement in the y -direction increases by about approximately 100% (Figure 5.37d).

The computer program estimates, at the clamped support on the lower side of the slab, a reinforcement of at most $a_{sy} = 5.3 \text{ cm}^2/\text{m}$ (Figure 5.37d). This results from the big tensile force in the flange. This reinforcement should be arranged on the top of the slab in addition to the calculated value there.

Therefore, it can be concluded that the flexible support of the slab due to the downstand beam results in a significant redistribution of the forces. A computer program is not able to design such a structure.

5.3.1.3 Effective width

It is sometimes recommended to integrate the normal forces and bending moments in the slab over the effective width b_{eff} to estimate the member forces for the design of the T-beam. Nevertheless, this is not correct, as will be shown in the following.

The effective width b_{eff} is a simple approach to determining the resultant force F_{cd} in the concrete compression zone, the location of the centre axis and the stiffness of the jointed cross-section. The compressive stresses are not uniform in the flange of a T-beam. They decrease with increasing distance from the web (see Figures 5.38 and 5.39).

Nevertheless, the distributions of the compressive stresses or the membrane forces in the flange are not known in general. Therefore, for easy manual analysis of T-beams, the effective width has been introduced. The distribution of the compressive membrane force n in the flange was analysed by FE models for various structural systems, cross-sections and loadings and in different sections. The effective width results from the resultant compressive force in the flange $F_c = \int n \, ds$ divided by the maximum membrane force $\max n$.

$$F_c = \int n \, ds = b_{\text{eff}} \cdot \max n \quad b_{\text{eff}} = \frac{\int n \, ds}{\max n}$$

The effective widths from the FE analysis are shown in Figure 5.39, together with the values of EC2 (Eurocode 2, 2004). Good agreement is achieved in the field, whereas

Figure 5.38 Membrane force n in various sections

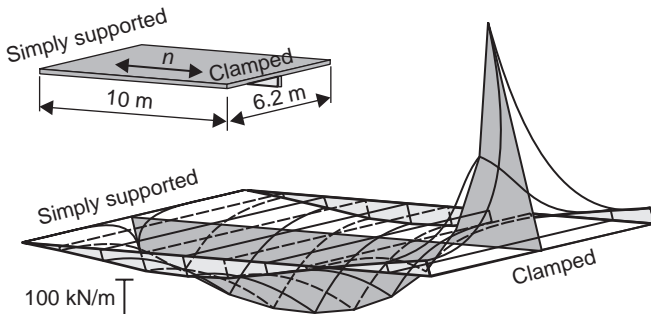
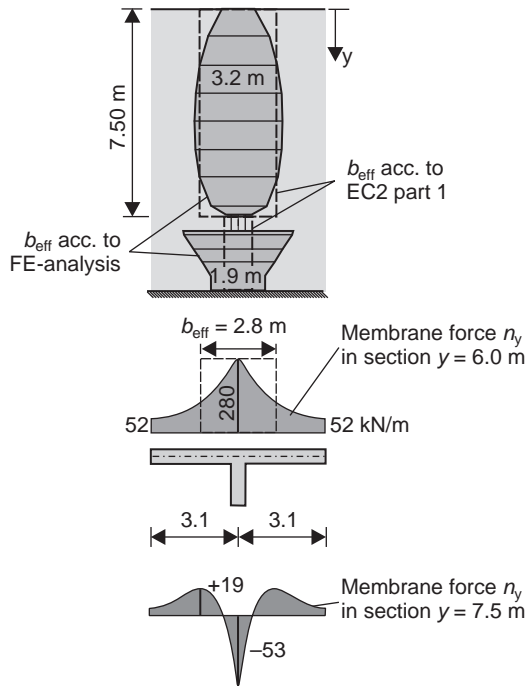


Figure 5.39 Effective width b_{eff} according to EC2 Part 1 (Eurocode 2, 2004) and FE analysis



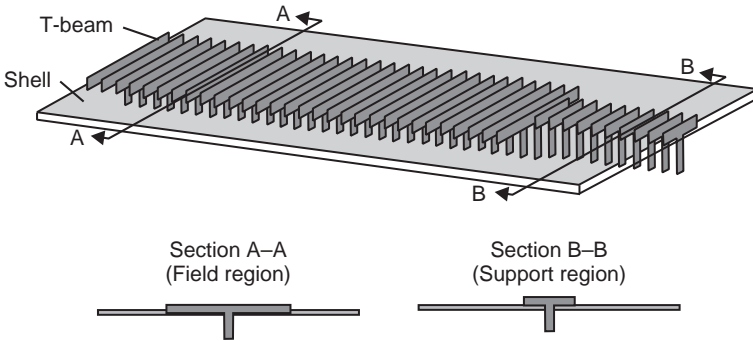
big differences can be observed in the support region. In the region of zero moments, negative and positive membrane forces occur in the flange. The estimation of the stresses in this section based on b_{eff} is incorrect.

The regions in which the existing b_{eff} is smaller than the code value are relatively small and have, hence, only a low influence on the member forces of the structure. Calculations with a constant effective width over the whole span will generally give good results.

The effective width depends on the span length, the support conditions, the transverse reinforcement and also particularly on the type of loading. The equations from the codes are valid only for uniformly distributed loads on the flange. Concentrated forces result in significantly smaller values of b_{eff} . Furthermore, an elastic material behaviour is assumed. This only applies for uncracked concrete regions in the serviceability state. In the ultimate limit state, the concrete in the compression zone will show a nonlinear behaviour in the plastic regime by which the width b_{eff} will increase. In a tension zone, the effective width is useful only as long as the concrete has not cracked yet.

If the compression stresses are integrated over the effective width only to estimate the member forces M and V of the girder, a part of the actual load is neglected. This load portion can be assigned to the slab in the case of a suitable support. The required reinforcement necessary for this is determined by the FE program.

Figure 5.40 Modelling of a slab on girder structure by shell and truss elements



5.3.1.4 Estimation of the design forces

The design of the T-beam can be done with the integrated member forces M and V . This analysis results in a safe design, as explained earlier. The slab carries only 20% of the bending moments in the longitudinal direction of the demonstrated example. This portion can be neglected with regard to the inaccuracies of the numerical model.

The integration of the membrane forces and bending moments in the slab and in the girder is very time consuming if it is not automatically done by the FE program. To avoid this effort, the T-beam can be viewed as a separate truss in the numerical model (Figure 5.40). The centre axis of the beam is located in the midplane of the slab to avoid additional normal forces. This T-beam can be designed by the program automatically. If necessary, one can delete the stiffness of the shell elements in the longitudinal direction in the width b_{eff} . For the given system, the influence of this measure is not significant.

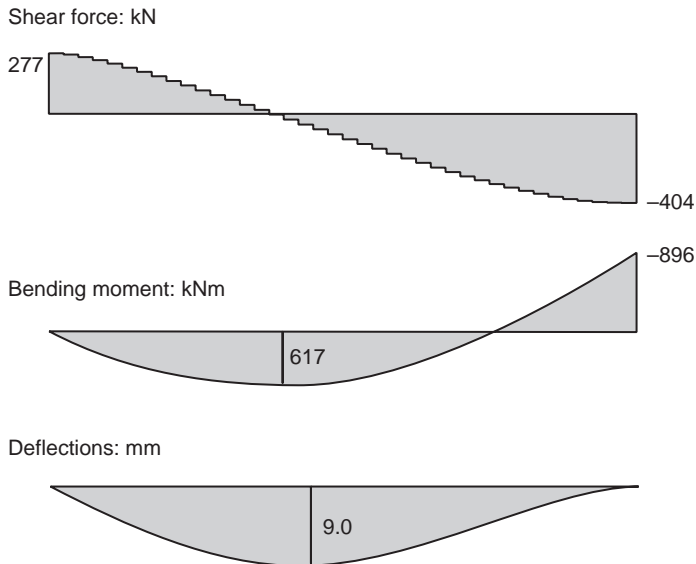
In Figure 5.41, the calculated member forces and the deflections of the T-beam are shown. The deformations are in agreement with the pure folded shell analysis. The load-deformation behaviour is therefore properly modelled.

In Table 5.4, the results of the FE analysis and the manual analysis are listed (see Figures 5.41 and 5.33). The differences between both models are relatively small. The ‘accurate’ FE model gives approximately 15% lower member forces. Hence, the greater effort of a numerical calculation does not seem to be justified for this structure.

5.3.2 Slab supported by a small downstand beam

In the previously mentioned structural system, the downstand beam was very stiff in relation to the slab, and the beam could therefore be regarded as a stiff support. In the following, a ‘soft’ support and a small downstand beam are examined. The slab shown in Figure 5.42 is supported on a beam with a height of only 20 cm ($h_F = h_w$). The structural system and the loading are the same as in the previously mentioned example. The span length has to be reduced to adapt to the smaller bearing capacity of the T-beam.

Figure 5.41 Member forces and deflection of the T-beam



The system is analysed again with a pure folded plate (FW) and a shell/T-beam (FB) model. The flange width of the T-beam is equal to the effective width, according to Eurocode 2 (2004).

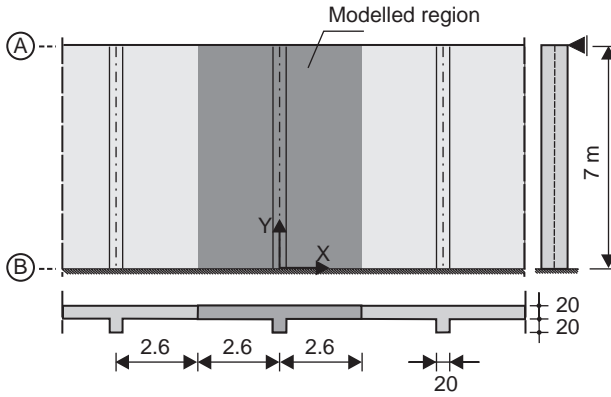
The bending moments of both models are shown in Figure 5.43. Both approaches are in good agreement. This demonstrates that the FB model can be used for this system too. The bending moments in the transverse direction (m_x) correspond very well in the field area. Significant differences can only be observed over the web of the girder. The bending moment m_y in the direction of the T-beam differs by approximately 15%. Bigger values are obtained with the shell/T-beam model.

Because the flange of the T-beam exists twice in the slab and in the beam, the stiffness of the system is overestimated. This affects the deformation. The maximum deflection of the

Table 5.4 Member forces of the manual analysis against the FE model

	Max M_{field} : kNm	M_{support} : kNm	V_A : kN	V_B : kN
1 Manual analysis (see Figure 5.33)	689	-1140	302	487
2 FE model (see Figure 5.41)	617	-896	277	404
3 (2)/(1)	90%	77%	92%	83%

Figure 5.42 Slab supported on a small downstand beam – system and FE model



folded slab model is 8.75 mm, whereas the FB model gives 7.81 mm only ($\Delta = 12\%$). The results can be improved if the normal stiffness of the shell elements in the effective width of the flange and in the direction of the girder is set to zero. Nevertheless, the effect of this measure is relatively low.

The computer program estimates longitudinal reinforcement on the upper side of the slab in the region of the downstand beam due to positive bending moments. Due to

Figure 5.43 Bending moments in the plane shell – (FW) against FB model

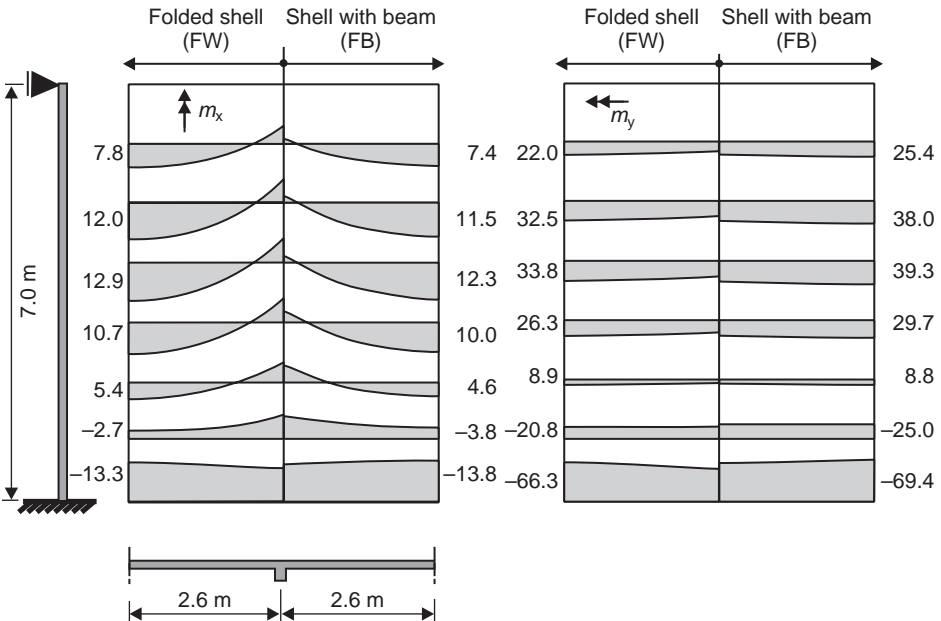
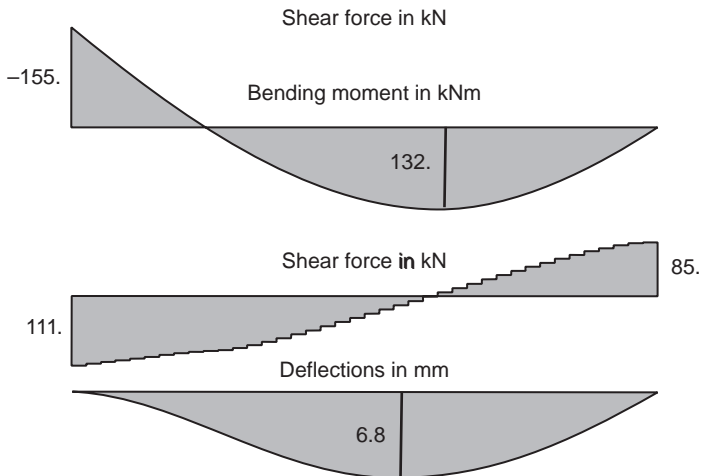


Figure 5.44 Member forces and deflections of the downstand beam



the linear elastic analysis, the numerical approach cannot realise that the reinforcement is more effective, if it is put in the upper layer of the downstand beam.

The member forces of the T-beam are shown in Figure 5.44.

The manual analysis, which is based on a stiff support of the slab by the downstand beams, should not be used for this flexible structure. The equivalent forces on the

Figure 5.45 Member forces of the girder

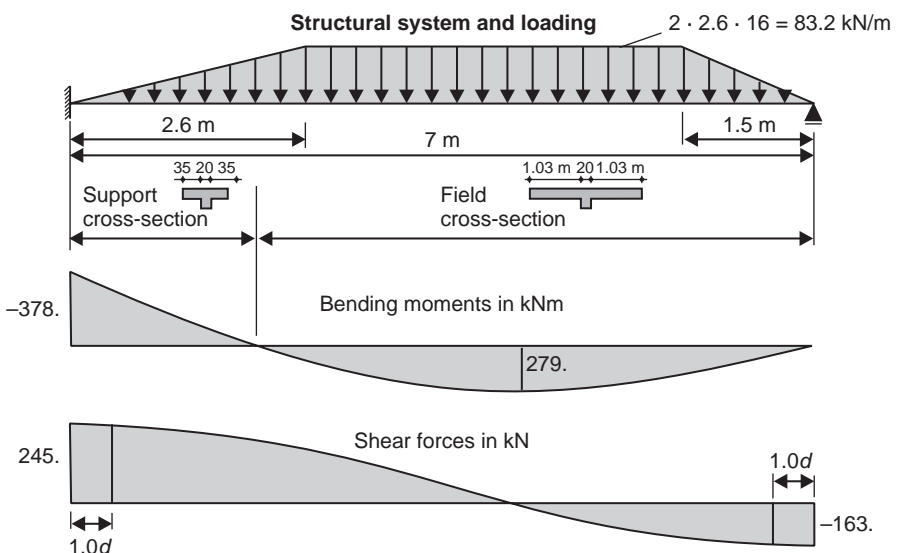
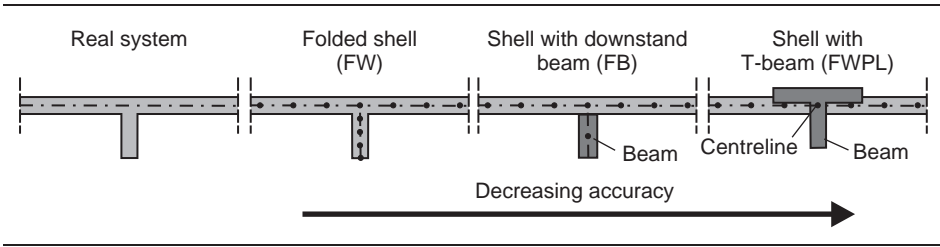


Figure 5.46 Different models for a slab supported on beams



T-beams are overestimated, as the results shown in Figure 5.44 illustrate. The member forces of the T-beam in the manual analysis are 2.5-times bigger than the real value of the FW analysis.

5.3.3 Summary

The member forces of a slab supported on beams can be estimated very well with a rather easy shell/T-beam model. A difference of only 15% with regard to the folded shell model is estimated in the aforementioned examples.

In the case of complicated systems or loads, it is recommended to conduct limit value analysis with different models (Figure 5.46). The best results are gained with the folded shell model (FW). This approach is useful to study the flow of forces in the discontinuity regions (e.g. point-loads, openings). Nevertheless, the estimation of the required member forces for design of the T-beam is very time consuming. The folded shell/beam model (FB) shows good results, but an automatic design of the T-beam is not possible. A numerical integration of the shell and beam forces is very time consuming if it is not done automatically by the computer program.

If a T-beam is arranged in the centreline of the shell (model FWPL), the automatic design of the shell and the downstand T-beam is possible. Nevertheless, the stiffness of the T-beam is overestimated, which may result in an unsafe design of the slab. In both models, the amount and arrangement of the reinforcement has to be checked carefully.

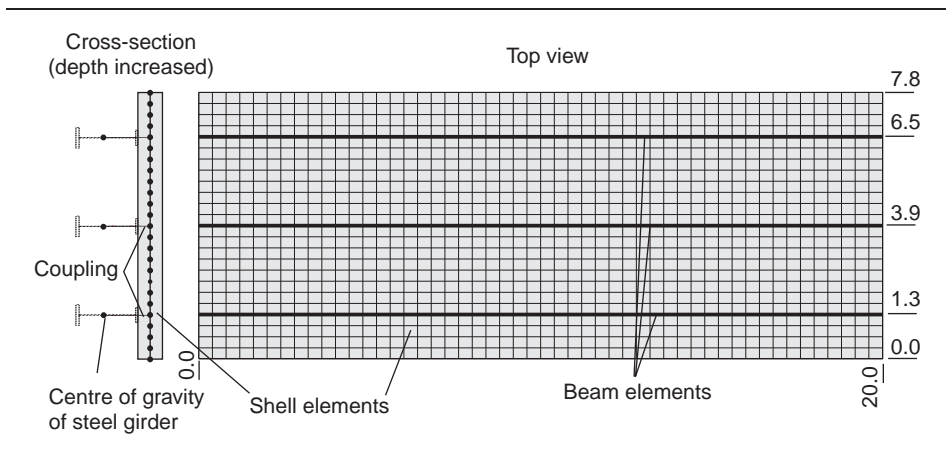
5.4. Composite structures

The model – flat shell with eccentric beam – can be used for the analysis of composite structures (Figure 5.47). Construction stages can be considered by activating the relevant load-bearing parts of the structures, that is, the elements. The shear forces in the joint are obtained directly from the coupling forces in the nodes. Time-dependent characteristics of the concrete can be considered in the analysis.

5.5. Singularities

Singularities of the internal forces can be observed in shell structures as well as in plate systems. They are caused by the same numerical errors. Therefore, only one practical problem – single forces on shell structures – is discussed in the following example.

Figure 5.47 Composite structure – FE model



As explained already for plate structures, single forces should only be applied to an FE shell model if the internal forces close to the loaded area are not needed for design. Otherwise, the estimation of high bending moments and membrane forces close to the concentrated load may result in an uneconomical design. This will be demonstrated on the silo structure (height $h = 56$ m and diameter $d = 25$ m), which was already mentioned in Section 5.1.2 (Figure 5.48).

Figure 5.49 shows the distribution of the bending moments and normal forces in circumferential direction for a single force of $F = 5 \text{ m} \times 5 \text{ m} \times 100 \text{ kN/m}^2 = 2500 \text{ kN}$. A comparison of this result with that of a distributed uniform load over an area of $5 \times 5 \text{ m}$ shows that the internal forces are higher but on the safe side (see Table 5.5). The greatest bending moment in circumferential direction m_x under a concentrated load is three times higher than if a distributed load is applied.

Figure 5.48 Cylindrical shell with patch and single load

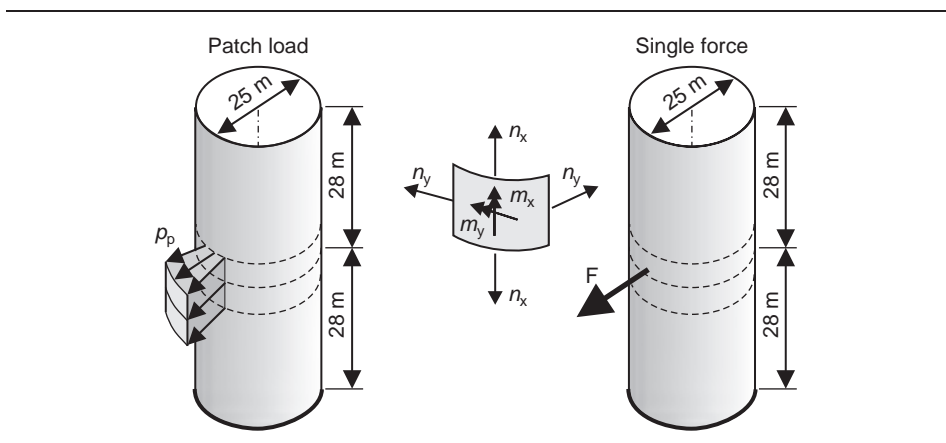
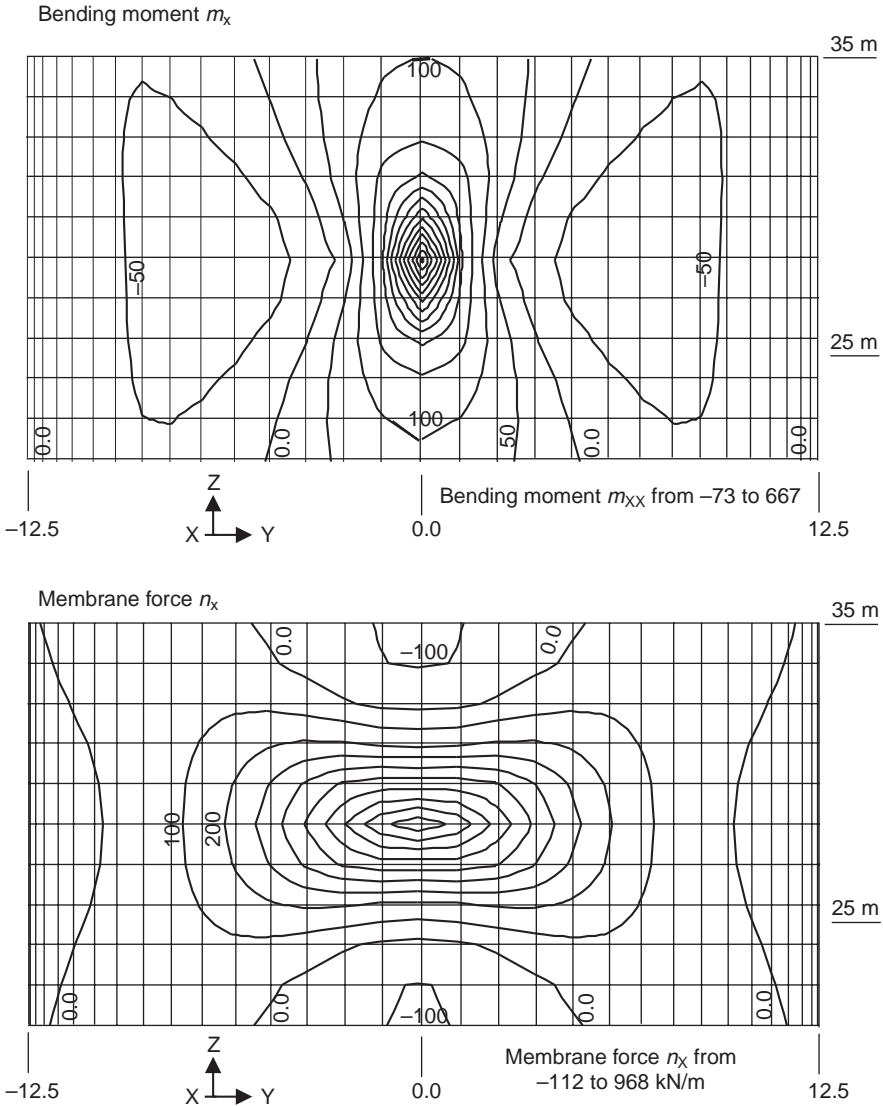


Figure 5.49 Bending moment m_x and membrane force n_x in the loaded area (point-load)



It should be noted that the maximum values will greatly increase with the number of elements in the loaded area.

5.6. Material nonlinear analysis of shells and massive members

In the recent past, material nonlinear FE calculations have gained popularity for shell structures, whereas they have been used for several decades for columns and beams.

Table 5.5 Internal forces (mesh: 64×44 elements) loaded area – single force

	n_x in kN/m		n_y in kN/m		m_x in kN/m		m_y in kN/m	
	Min.	Max.	Min.	Max.	Min.	Max.	Min.	Max.
Loaded area 5×5 m: $q = 100$ kN/m	-113	627	-571	387	-64	209	-24	116
Point-load: $Q = 2500$ kN	-117	968	-590	576	-73	667	-31	541

n_x, m_x membrane force and bending moment in circumferential direction

The main purpose of such an analysis is to get results that are closer to the real behaviour of a structure and to get a more economic design and construction.

In Section 2.11, it was demonstrated that significant problems already appear in the nonlinear analysis of columns and beams. The materially nonlinear calculation of shells and massive concrete sections is considerably more complicated.

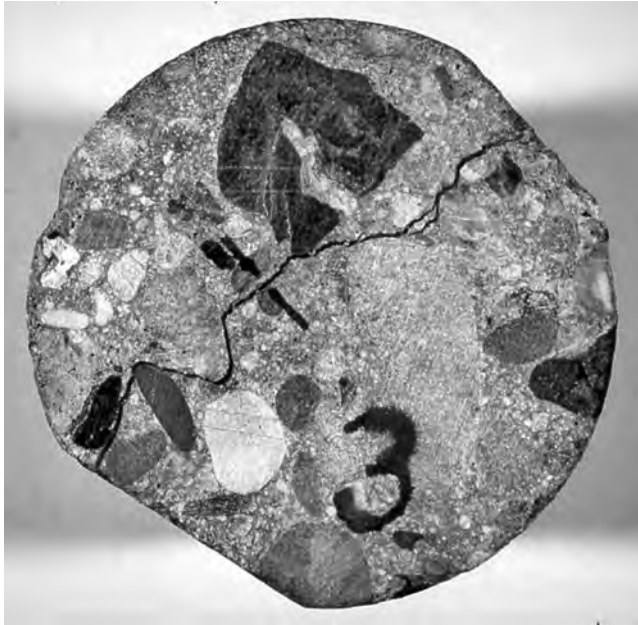
In the following, the state of the art in the field of nonlinear analysis of concrete structures and the software development in this field cannot be mentioned in detail. This complicated field of research can only be understood by experts. Therefore, only the fundamental problems of material nonlinear FE calculations are illustrated. Solutions for the following problems are needed.

(A) Description of the complex material behaviour

■ *Realistic description of the nonlinear material behaviour for concrete and reinforcing steel:* Figure 5.50 should make it clear that reinforced concrete is a very inhomogeneous material that mainly consists of cement paste, gravel of different forms and hardness, aerial pores and reinforcement. Furthermore, it often has cracks even in the unloaded state. Nevertheless, most FE calculations are based on a homogeneous material.

First, one has to formulate a material model for pure, unreinforced concrete under tension and compression strains and stresses for arbitrary uni- or multi-axial load paths (Figure 5.52). Figures given in codes (see Figure 2.110) are valid only for uni-axial compressive stresses. It is obvious that concrete under different load paths shows different $\sigma_c - \varepsilon_c$ behaviour as compared to a cylindrical test specimen under uni-axial compression (Figure 5.51). Furthermore, long-time effects (creep and shrinkage, dynamic loading, fatigue) have to be taken into account if necessary. Any damage in the concrete before loading, for example, by restraints during the hydration of cement paste, as a result of temperature effects, by shrinkage and creep or by a previous load, must be considered in the numerical analysis. As one can notice from these items, the boundary conditions at the beginning of a numerical analysis are not known in real structures, in contrast to post-calculations of beam-tests in laboratories after they have been conducted.

Figure 5.50 Composite material reinforced concrete



Nevertheless, the essential problem in construction practice mostly entails the correct modelling of the concrete behaviour under tensile strains and stresses. Although the characteristic tensile strength f_{ctk} can be measured in the laboratory in a standardised test, in a real building, the actual value may be significantly different. If the concrete tensile strength is estimated on the safe side, then this will generally lead to uneconomical construction requirements, or to instabilities in the numerical analysis. It should be noted that according to EC2, Part 1, §6.1(2) (Eurocode 2, 2004), the tensile strength of concrete should be ignored in the design of the ultimate limit state.

Figure 5.51 Stress–strain diagram for concrete under uni-axial compression (on the left) and uni-axial tension (on the right)

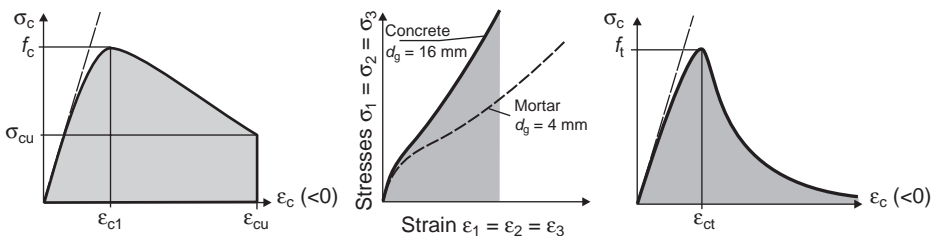
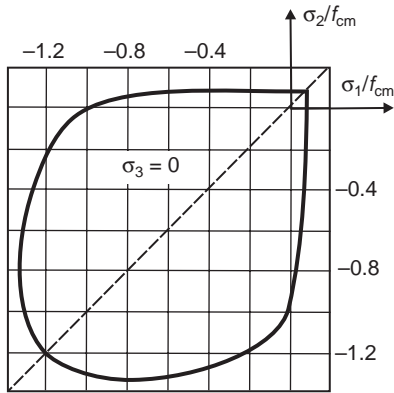
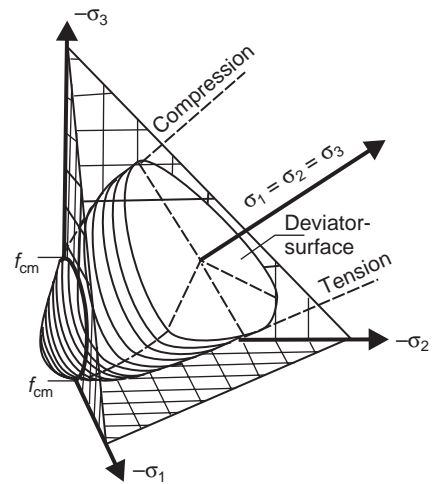


Figure 5.52 Yield surfaces for concrete

2-axial yield surfaces acc. to Ottosen



Yield surfaces for 3d



- *Description of the bond between concrete and reinforcement:* Most FE programs assume a stiff bond between the concrete and reinforcement. This does not apply, for example, in the anchorage region, at lap splices of reinforcing bars and in cracks. Modelling of a soft bond as well as the distinct reinforcing bars is connected with a very big expenditure. Moreover, special bond elements and realistic shear-slip models are required.
- *Description of the force transfer in the cracks:* An exact calculation of the location and orientation of cracks as well as the consideration of crack behaviour is very important for the results of any nonlinear analysis. The forces in a crack are transferred through the roughness of the crack surfaces (gravel) as well as through dowel effects of the reinforcing bars (Figure 5.53). Both effects must be correctly modelled.

(B) Numerical modelling

- *Numerical modelling:* Reinforcing bars can be modelled discretely, by means of truss elements, or smeared in the FE shell or volume element. Local effects cannot

Figure 5.53 Force transfer in cracks

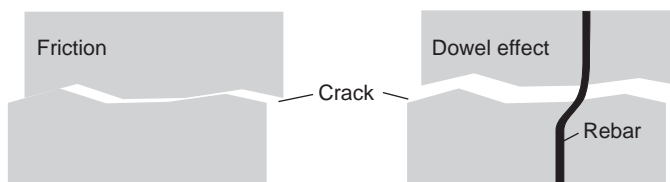
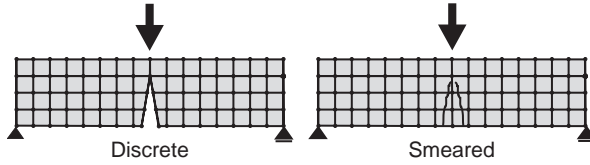


Figure 5.54 Modelling of cracks



be analysed with the last-mentioned model. The same is valid for the numerical modelling of cracks. The discrete consideration of the cracks generally requires a modification of the element mesh during the calculation (Figure 5.54). In general cases, this is connected to a big expenditure, which is why most FE programs use a smeared crack model.

- *Numerical procedures:* Robust numerical integration algorithms that guarantee the exactness of the solution are necessary for a nonlinear calculation.

The analysis of shear walls and beams with plane shell elements under high shear forces presents big problems.

In the field of research, nonlinear FE analyses are used mainly to study the behaviour of a test specimen *after* the test has been conducted. Within such calculations, the material parameters, the structural system and the arrangement and amount of the reinforcement as well as the actions are most exactly known. Furthermore, enough time exists to verify the numerical model thoroughly. These conditions are generally not given in the construction practice.

5.6.1 Analysis of a cantilever column

The following example should demonstrate the principal problems of a material nonlinear analysis in practice. Figure 5.55 shows a cantilever column that supports a single-span segmental bridge with a span length of approximately 45 m. This exceptional construction was necessary, as the maximum span of the segmental bridge was smaller than the required clearance for the road underneath.

The reinforcement arrangement is outlined in Figure 5.56. It becomes clear that the lapping of the horizontal cantilever reinforcing bars ($d_s = 28 + 16/10$ cm) with the very massive vertical reinforcement in the column ($d_s = 2 \times 28/10$ cm) is absolutely insufficient by the loops $d_s = 16/10$ cm. More than 50% of the required reinforcement is missing in this region.

Unfortunately, this mistake was noticed after the construction of the column and after the left span of the bridge superstructure was already erected. The load-bearing capacity could not be proved by means of strut-and-tie models. Therefore, the engineer in charge for the design of the structure conducted a complicated 3D material nonlinear FE analysis (volume elements, discrete reinforcing bars). This analysis proved that the load-bearing capacity of the construction is sufficient.

Figure 5.55 Cantilever column

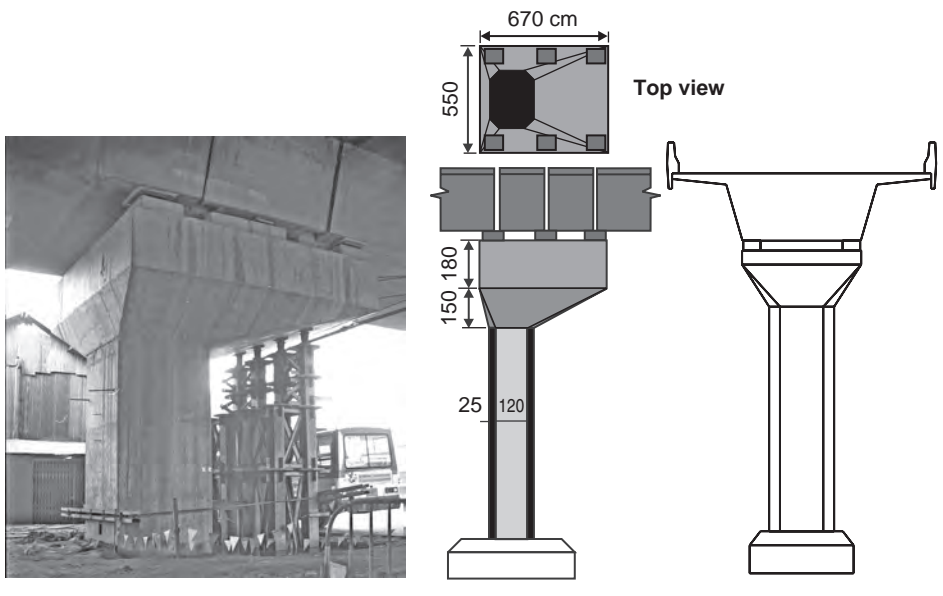
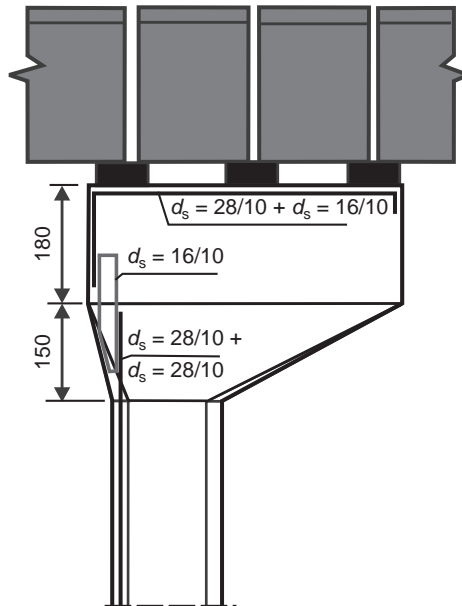


Figure 5.56 Reinforcement layout



Nevertheless, the responsible checking engineer still had doubts about the results of the FE analysis. Even by means of the complicated FE analysis, a simple strut-and-tie model or a reasonable force transfer mechanism could not be formulated that could prove the stability of the special column head. Furthermore, the bridge is a statically determined single-span structure without any redistribution of loads in the ultimate limit state. Thus, the stability of the special column is needed for the safety of the whole structure.

With the used commercial, well-known FE program, principal software mistakes are not likely to occur. The graphics of deflections, stresses and crack patterns were reasonable, but the exact values could not be verified. Nevertheless, the checking of the assumptions used in the numerical analysis, in this case of the material parameters, uncovered a serious mistake. In the FE model of the cantilever column, the tensile strength $f_{ctk;0.05}$ according to EC2, Part 1 (Eurocode 2, 2004), had been used. With this value, no horizontal cantilever reinforcing bars are needed at all due to the massive cross-section of the cantilever section, as can be easily demonstrated by manual checks. In the real structure, the available tensile strength of concrete might be significantly lower due to the hydration restraints of the massive sections and the dynamic loads on the bridge. The design checker requested a second FE analysis with half the concrete tensile strength ($0.5f_{ctk;0.05}$), which showed instabilities. The structural safety was insufficient and, consequently, the cantilever column had to be retrofitted.

This example clearly demonstrates that with complex, nonlinear FE calculations, a large amount of scepticism is warranted with regard to the results. In particular, detailed engineering experience is necessary and not just theoretical knowledge of the FE method. Hence, a complicated materially nonlinear FE analysis should only serve to reduce the available safety margin of an easy and clear simplified model, and not as a substitute for the design engineer lacking in knowledge about the force transfer and behaviour of the system. The design engineer who is in charge must be convinced of the plausibility of the inputs and results by detailed checking.

REFERENCES

- Bergan PG (1998) *Computational Challenges for the Finite Element Method in Offshore Engineering*. Conference Finite Elemente in der Baupraxis, Darmstadt, 1998.
- CEN (European Committee for Standardization) (1997) *Eurocode 1, Part 4: Basis of Design and Actions on Structures – Actions on Silos and Tanks*. December, 1996. Brussel.
- CEN (2004) *Eurocode 2, Part 1: Design of concrete structures – General rules and rules for buildings*. December.
- Czerny F (1999) *Tafeln für Rechteckplatten*. In *Betonkalender* (Eibl J (ed.)) 1999, Volume 1. Ernst & Sohn, Berlin.
- Grasser E *et al.* (1991) *Hilfsmittel zur Berechnung der Schnittgrößen und Formänderungen von Stahlbetonbauwerken*; Deutscher Ausschusses für Stahlbeton Heft 240. Berlin.
- Gudmestad OTG and Coker JWA (1988) *The Sleipner Platform*. SPE 18344: 111–126.
- Hennig E (1971) *Experimentelle und analytische Untersuchung der Spannungsverteilung in örtlich belasteten dünnwandigen zylindrischen Schalen*. Fortschrittsberichte der VDI-Zeitschriften, Reihe 1, Nr.: 33, Düsseldorf.

- Holand I (1997) SINTEF Report No. 17: *Sleipner A GBS Loss, Main Report*. Trondheim.
- Hughes TJR (1987) *The Finite Element Method*. Prentice Hall, Englewood Cliffs.
- Jakobsen B and Rosendahl F (1994) The Sleipner Accident. *Structural Engineering International* **3**: 190–193.

Chapter 6

Three-dimensional building models

6.1. General problems

A few years ago, a 3D model of a complex building as a whole could not be analysed due to lack of computer processing power and adequate software. The structure had to be disassembled into its different structural elements, such as beams, columns, plates, shear walls, etc. Each of these members had to be designed separately. This analysis was based on significant simplifications. Sometimes, the architectural plans for a structure had to be modified, as it could not be designed at that time. The opera house in Sydney is a good example (see Section 6.6) of such an engineering challenge. The complicated form of the single shells could not be designed at that time (construction period: 1959–1973). Hence, the spatial structures of the shells were substituted with arches made of single pre-tensioned segmental T- and V-beams.

The days of structural simplifications seem to be over. Nowadays, the FE modelling of whole buildings, including the foundations and taking into account material and geometrical nonlinear effects, is an easy and quick task. With the help of special programs, complicated slab systems can be easily discretised by graphical pre-processors based on the general layout drawings of the building. Afterwards, the single slabs are jointed by columns and shear wall elements to get a building model.

The future points to more and more complex FE models, as one can notice from the numerous contributions in technical periodicals and conferences of the past years. Why should one disassemble a building into its different structural components, into simple equivalent structures, when the analysis and the design of the whole building by means of a 3D FE model is faster and also more accurate? Next, the numerous load combinations according to the codes can hardly be handled manually.

Daily experience shows that results from computer analyses are often trusted with blind faith. The required checking of the model as well as a clear documentation of the main results are often lacking, because of time constraints. This development raises concerns regarding the safety of structures in the future.

The collapse of the platform ‘Sleipner A’ (see Section 5.1.1) has demonstrated the consequences of blind trust in FE analysis. The more complicated the numerical model, the more difficult it is to maintain a global overview of the structure and to check the accuracy of the results. The latter is the responsibility of the structural designer,

not the checking engineer, as is often assumed. In addition, a software company will rarely be responsible for errors in their code. The structural engineer must be convinced that his or her numerical analysis is correct. He or she should always be aware that a faulty analysis may endanger human lives, for which the designer is responsible.

Not to be misunderstood; the author does not express himself against complicated FE calculations. He would like to merely point out to the software user the dangers which can result from insufficient checking of his FE analysis and a lack of experience in this field. In special cases one will always try to model the structural behaviour of a building as accurate as possible with nonlinear 3D models. Nevertheless, for normal buildings the big expenditure is not justified in most cases in relation to the expected reduction in required building materials.

Besides, it is often overlooked that the FE method is a numerical approach only, and is based on numerous assumptions and simplifications (Bathe, 1982; Hughes, 1987; Zienkiewicz and Taylor, 1989). Hence, the accuracy of FE analysis is limited. The results could even be wrong and unsafe. Also, the nonlinear material behaviour of reinforced concrete can have significant influence on the force distribution in a structure. Therefore, the results of FE design are not automatically correct even if the input is error-free.

The essential problem of big FE models does not exist in the element mesh generation, but in the control of the input and output of the analysis. Much effort and experience in the field of concrete engineering and numerical modelling is needed to check a complex FE analysis, because no easy, program-controlled procedures are available up to now. The behaviour of a building must be modelled by simple equivalent members. This is the only method that gives certainty to the correctness of results from FE calculations. Experienced engineers are needed for this task (fortunately).

All principal problems of truss, beam, plate and shell elements have been discussed in Chapters 1–5. It should be remembered that a slab element has no normal forces in its midplane (pure bending). Discontinuity regions of beams and singularity regions of spatial structures are common problems of FE models. In the following, the problems and limits of complex FE building models are illustrated by two real structures, an office building (Figure 6.1) and an arch bridge (Figure 6.13), in which the author was engaged as a designer and a checking engineer, respectively. It will be demonstrated that no software is able to design these structures, at least in some areas. A careful, independent checking of the numerical results is always required.

Checking the safety and serviceability of FE building models basically does not differ from simple structures. However, there are some basic differences between manual and FE design.

1. *Documentation of the analysis:* With manual calculation, one limits the output to the essentials because of time limitations. In contrast, the printing of all results of a complicated FE analysis is quicker than summarising the relevant outcome to a minimum, to the relevant results only (Section 6.5).

2. *Model accuracy*: During the decomposition of a structure into simple members, the structural behaviour is easily overlooked. By contrast, it is rather difficult to ensure that a complex FE model reflects the behaviour of a real structure and whether the member forces and deflections are correct. These problems are discussed in detail in Section 6.3.
3. *Safety*: In a building model, all members are used as a load-bearing element. Thus, such analysis shows smaller global safety compared to manual analysis, where several assumptions on the safe side have to be drawn and the analysis is limited to the relevant members only. The optimisation of a structure may be more economical with regard to the required amount of building material. However, it should be noted that any change of the structure either during construction or during the lifetime of the building may require a complex, extensive retrofitting of certain members.

6.2. FE modelling of a building

The accurate modelling of the load-bearing behaviour and the deformation characteristics of a building are essential for the results. The difficulty of 3D FE calculations is that one big numerical model is given, rather than single structurally equivalent systems. In the discretisation of a real structure, numerous mistakes can be made. The errors can hardly be noticed when checking the analysis by means of a 3D plot of the FE mesh (see Figure 6.1).

6.2.1 Soil parameters

The member forces and the deflections in a building depend on the interaction between the ground and the structure. This aspect is of great importance in building models where the effect of the soil stiffness on the member forces is difficult to foresee. In reality, the

Figure 6.1 Real building and FE building models



soil parameters show a big scatter. Therefore, upper and lower bound values should be considered in the FE analysis. This limit analysis has to be conducted in general, whether it is an easy arch bridge (Section 6.4) or a complex building (Section 6.2).

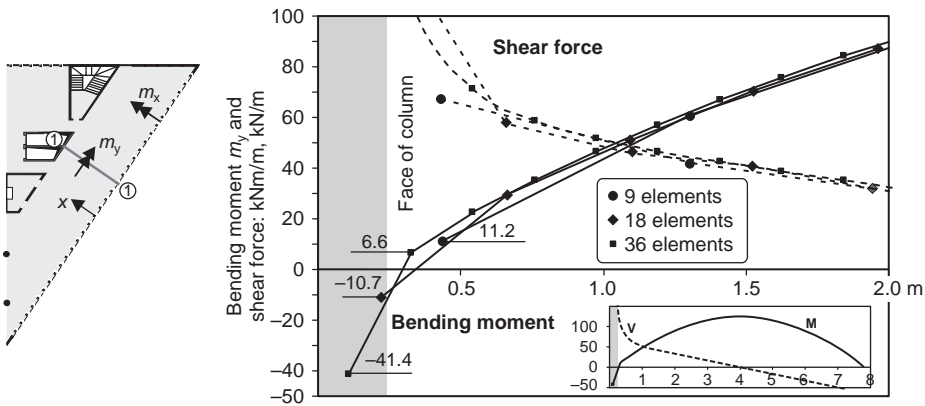
6.2.2 Discretisation – size of FEs

Even with the common hardware and software, the number of elements for a big building model is still limited by the time the computer needs for the estimation of the deformations, the member forces and the design of the structure. For this reason, taking the smallest number of elements is always preferred. However, as has been discussed in Sections 4.13.2 and 5.1.2, using too big elements could result in significant errors.

For an office building, the size of the elements must be mainly checked in the support regions (columns, walls), where a big strain gradient appears. This will be illustrated by a simple one-way slab. Figure 6.2 shows the distribution of the bending moment m_y parallel to the boundaries and the shear forces v_x in the region of the facade as a function of the number of the elements in the outer span. The analysis is based on a simplified equivalent system, a one-way slab that is clamped on one edge. The slab has a span length of $l = 7.8$ m. The distribution of the member forces close to the columns is not influenced by the number of elements. Nevertheless, with a coarse discretisation, the member forces are not estimated in the relevant section at the face of the columns, but in the centre of the nearest big element, far away from the correct location. This may lead to an unsafe design. For the accurate estimation of the transverse bending moment m_x , the region between the façade columns has to be discretised with a sufficient number of elements. With only four elements, half of the correct field moment $m_{x,f}$ is estimated. The bending moments at the column heads are nearly independent of the size and number of the elements.

The elements should be so small that the member forces are independent of any further decrease of their size. Exceptions are singularity regions. Here, the member forces increase with the number of elements to ‘infinity’. To check whether the high member

Figure 6.2 Member forces of a one-way slab (column strip) for different numbers of elements



forces of an FE analysis are real or only caused by a numerical problem, one can analyse the structure with different element meshes. This is not done, since a big effort is needed to create a different FE mesh. As shown before, local problems can also be examined by equivalent substructures.

6.2.3 Size of the loaded area

The FE programs common in practice are based on nodal loads, nodal deflections and nodal rotations. A real block load acting on a small area is always substituted with equivalent nodal forces. With a coarse discretisation, this can lead to the fact that an FE model cannot make a distinction between a single force and a uniform load (Figures 1.5, 4.74). Furthermore, single forces and block loads are distributed to the nearest nodes, by which the loaded area is increased. This may result in smaller member forces of slabs.

6.2.4 Discontinuity regions in truss models

Beam and plane shell elements are more or less simplified numerical models of a real beam or a slab. Most beam elements are thus, such as in the manual analysis, based on a linear strain distribution over the height of the cross-section (see Chapter 2). This simplification is not valid in the so-called discontinuity regions, which are common in real structures (Figure 2.18). Hence, an FE beam model cannot, in principle, properly determine the deflections, member forces and, in particular, the required amount and arrangement of reinforcement in these D-regions. Here, detailed analysis by means of strut-and-tie models is required. Nevertheless, it is important that the stiffness in the D-regions be modelled appropriately, as this can have a big influence on the member forces in a statically indeterminate system.

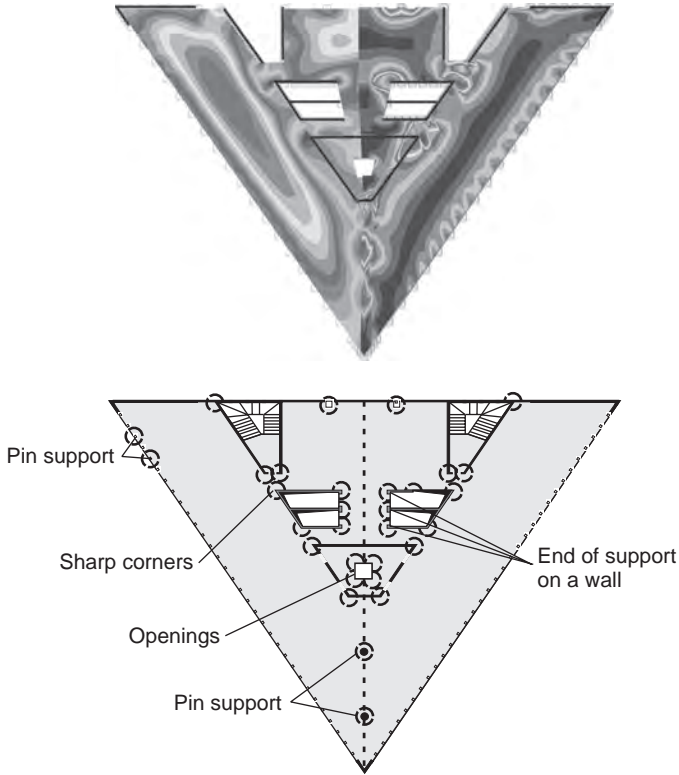
6.2.5 Singularity regions in slab models

Plate elements are usually based on the simplification of a linear strain distribution over their thickness and zero normal stresses in their midplane (see Section 4.1). This fundamental assumption leads to numerous singularities in slab models. Figure 6.3 illustrates this problem. The high moments and shear forces on the corners of the simply supported edges, in the area of columns and not continuous simple supports are clear to recognise. The high member forces at the face of intermediate wall supports or at the corners of walls can be considerably reduced by a soft support (springs). However, the real behaviour of the slab is also not modelled with higher accuracy because the model – plate or shell element with linear strain and stress distribution – does not apply in these areas. Hence, the soft support serves only as an engineering approach to reduce the high member forces. Singularity regions sometimes need a detailed investigation by means of a strut-and-tie model. In rare cases, a detailed nonlinear FE analysis that considers the reduction of the concrete stiffness due to cracking may be required. However, a good detailing of singularity regions is often sufficient and is more justified than a complex numerical analysis.

6.2.6 Incompatible element meshes

Common software includes numerous structural elements such as beams, slabs, shear walls, shells, etc. These elements may not be simply jointed with each other. For example,

Figure 6.3 Principal moment m_1 (on the left) and main shear force v_1 (on the right) in the slab as well as singularity regions

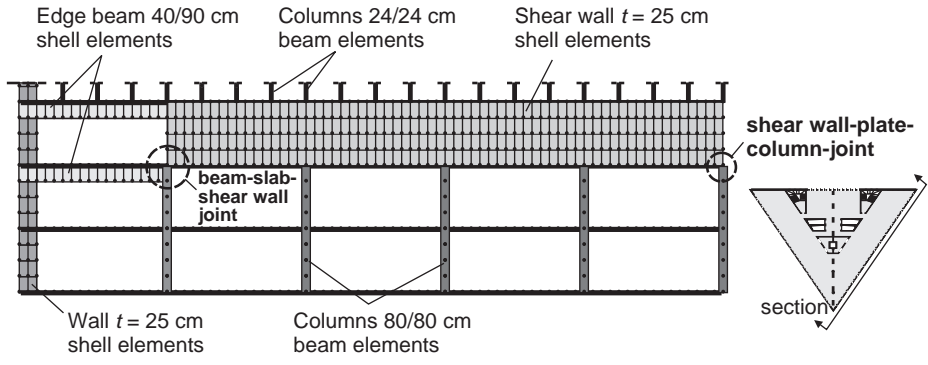


a beam element should not be connected to a plane shell element (see Section 3.2.3), as the latter has no rotational degrees of freedom. Therefore, the rotation of a node is not restrained, and the bending moment in the beam at the joint becomes zero. This problem can be solved with special nodal coupling or by the extending of the truss into the shell elements. The type of coupling should be checked carefully to avoid unintentional constraints. The office building has, in this respect, a very complex region. In the outside façade, a column is jointed with a spandrel beam, a slab and a shear wall (see Figure 6.4).

6.2.7 Minimum reinforcement – nonlinear analysis

The horizontal deformation of a slab due to shrinkage, heat of hydration of concrete or temperature changes is restrained between stiff structural elements, such as shear walls (Figure 6.5). This restraint results in high tensile stresses in these regions that will likely exceed the existing tensile strength of concrete. Thus, the slab will crack, which reduces the restraint. A minimum reinforcement is required to limit the crack width.

Figure 6.4 FE model of the outer shear wall junction



The minimum reinforcement $A_{s,min}$ of a fully tensioned section can easily be estimated from the equilibrium condition before and after the cracking. In the crack, the reinforcing steel has to take the whole tensile force.

$$F_{sd} = \sum A_{s,min} \cdot \sigma_{sd} = F_{ct} = A_c \cdot f_{ct,eff}$$

where:

σ_{sd} is the permissible tensile stress in the reinforcing steel, depending, for example, on ρ_l , d_s and w_k

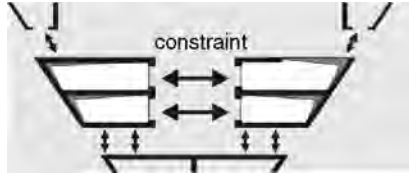
$f_{ct,eff}$ is the actual tensile strength of concrete at time of cracking.

In Eurocode 2 (2004), some parameters (k_c , k) are added to the preceding equation to consider special effects, such as the thickness of a member ($A_{s,min} \cdot \sigma_s = k_c \cdot k \cdot f_{ct,eff} \cdot A_{ct}$ EC2 eq. 7.1).

The design of the fully restrained slab between the elevator shafts (see Figure 6.5), according to EC2, Part 1, §7.3.2, with $f_{ctm} = 3.2$ MPa (C35/45), gives a reinforcement requirement of $a_s = 9$ cm²/m (top and bottom), which is much more than is needed to carry the external loads. Inexperienced engineers who do not know the background of the minimum reinforcement will just load the structure by the temperature change and shrinkage effect, respectively. This procedure results in a very high, uneconomical reinforcement rate of $a_s = 100$ cm²/m, as linear elastic material behaviour is assumed. Thus, it is not recommended in an FE analysis to apply thermal or shrinkage effects to the concrete structure if the big decrease in stiffness due to cracking of concrete is not considered. On the other hand, if the nonlinear behaviour of concrete is applied in the analysis, one must assume a high tension-stiffening effect (TS) to get realistic results. The restraint diminishes if the stiffness of concrete between the cracks is neglected (TS = 0). A nonlinear FE analysis, which is based on this assumption, gives $a_s \sim 0$ cm²/m. The lack of minimum reinforcement may cause a sudden collapse of the slab.

$$t = 0.26 \text{ m}, f_{ctm} = 3.2 \text{ MPa}, \quad \varepsilon_{cc,\infty} = -0.0005 \text{ (C35/45)}$$

Figure 6.5 Restrained slab between the elevator shaft



External load	$a_s = 2 \text{ cm}^2/\text{m}$ (bottom, top)
EC 2 (minimum reinforcement)	$a_s = 18 \text{ cm}^2/\text{m}$
Shrinkage (elastic)	$a_s = 100 \text{ cm}^2/\text{m}$
Shrinkage (cracked, TS = 0)	$a_s \sim 0 \text{ cm}^2/\text{m}$

6.2.8 Slab supported on beams and T-beams

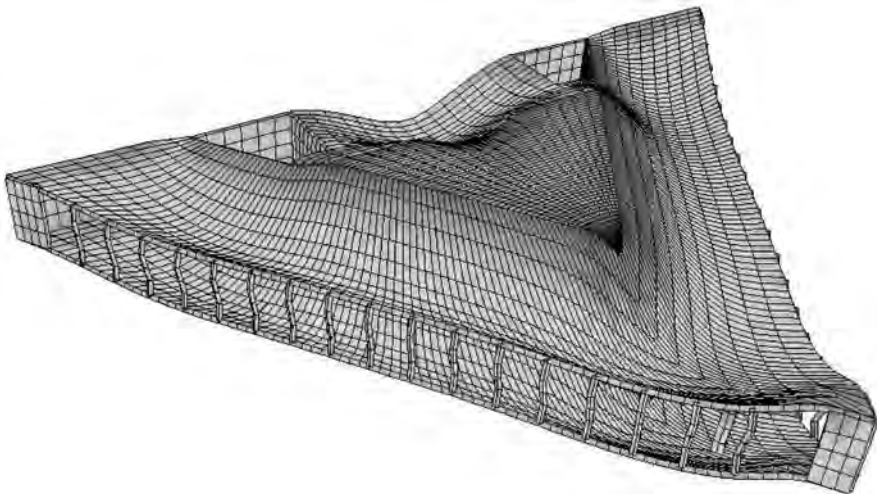
If the slab-on-beam structure is modelled by shell elements only, such as in the building model, a program-internal design is not possible (see Chapter 4). The downstand beam should be modelled by a T-beam located in the midplane of the slab to avoid the integration of the member forces.

6.2.9 Construction sequences

The FE analysis is mostly based on the final structure. The construction of a building is not considered, as this is a difficult and time-consuming task. In some cases, this simplification is not justified.

Figure 6.6 shows the deformation of the columns and the slabs in the most upper floors of the building. Unexpected, big deflections of the slab close to the inner columns can be

Figure 6.6 Deflections of uppermost floors



seen. First, one may assume that these unexpected results are caused by errors in the FE model, incorrect support of the system or an insufficient cross-section of both columns. However, this is not the case. Neglecting the construction sequences result in such unrealistic deformations of the slab. In a usual FE analysis, the final structure is loaded by the dead load of the members in one step. This leads to big deflections of the columns as compared to the stiff inner walls. In reality, the various floors are built one after the other, and the previous deflections are compensated. The uppermost slab shows no deformations due to the dead load of the floors underneath. The big deflections point out the fact that the creep and shrinkage effects of the columns are to be followed in the design of the building.

The effect of the construction sequences is illustrated by a simplified structure of the building. The one-way slab ($h = 0.26$ m, $l_s = 7.8$ m) is clamped in an infinitely stiff wall on one side and supported by façade columns ($b/h = 24/24$ cm, spacing $a = 1.5$ m) on the other (Figure 6.7). Only the dead load of the structure is applied.

In reality, each floor is built one after another. This results in the deflections shown in Figure 6.7. Total different deflections in the edge columns are obtained if the final structure is loaded in one step only (Figure 6.8). Thus, different member forces are obtained in the slab. As the slab has a small bending stiffness with regard to the span length, the deflections result in small differences in the bending moments (see Table 6.1). This is not the case if the span length is to be reduced, for example, to 1.95 m.

where:

F is the support force ($= 0.375(g + q) \cdot l$)

l is the height of a column in each storey

E is the modulus of elasticity of concrete

A is the area of the column.

6.3. Design of a building

6.3.1 Design of membrane elements

The aim of a design is not the most accurate estimation of the member forces and the deflections of the structure but the amount and arrangement of the required reinforcement in each section. Unfortunately, automatic, program-internal design is not possible in many regions of a structure (see Section 3.3). The fundamental problem of any FE analysis lies in the fact that every element is designed separately, with the help of the locally available stresses or member forces. The global structural system cannot be considered. This approach gives incorrect results if the flow of forces of a linear elastic structural analysis is significantly different from that of a cracked member (ultimate limit state).

6.3.2 Design of shell elements

The program-internal design for bending and shear forces of shells (shear walls) and massive sections after the algorithms listed in the national codes gives mostly incorrect values. The design for shear of a concrete section is based on a truss or stress-field

Figure 6.7 Deflections of the structure during construction (after hardening of concrete)

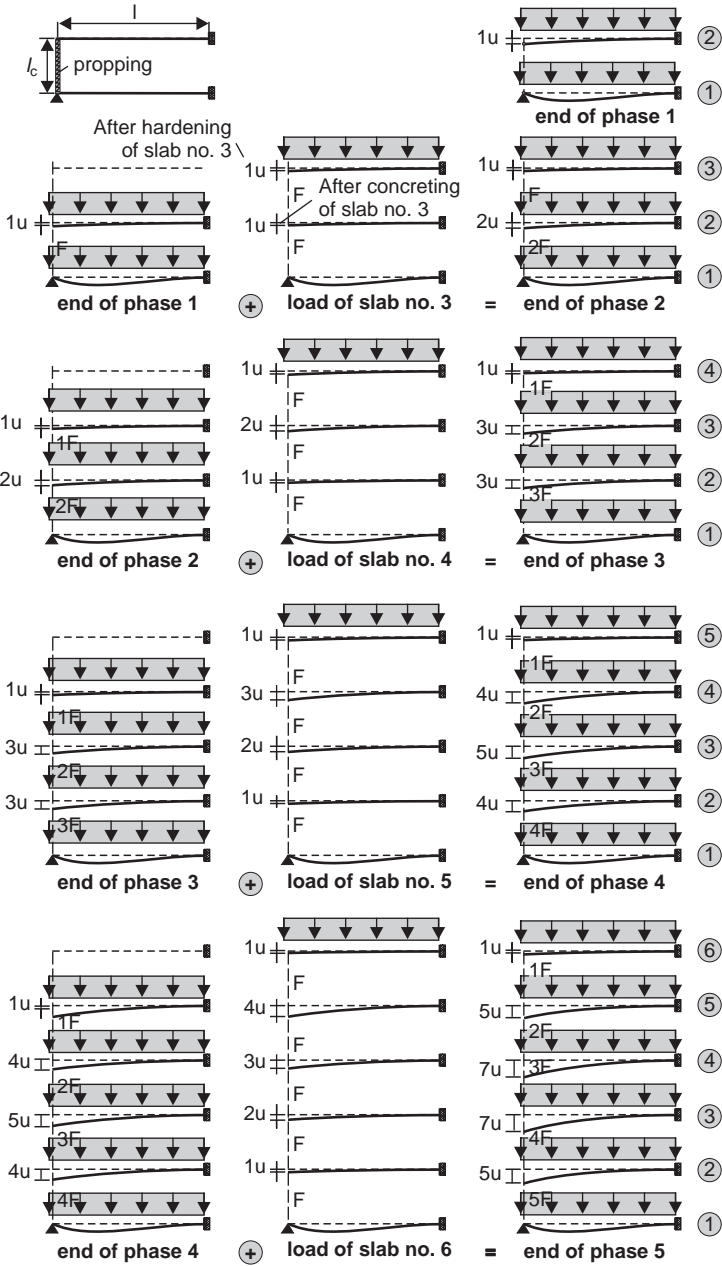
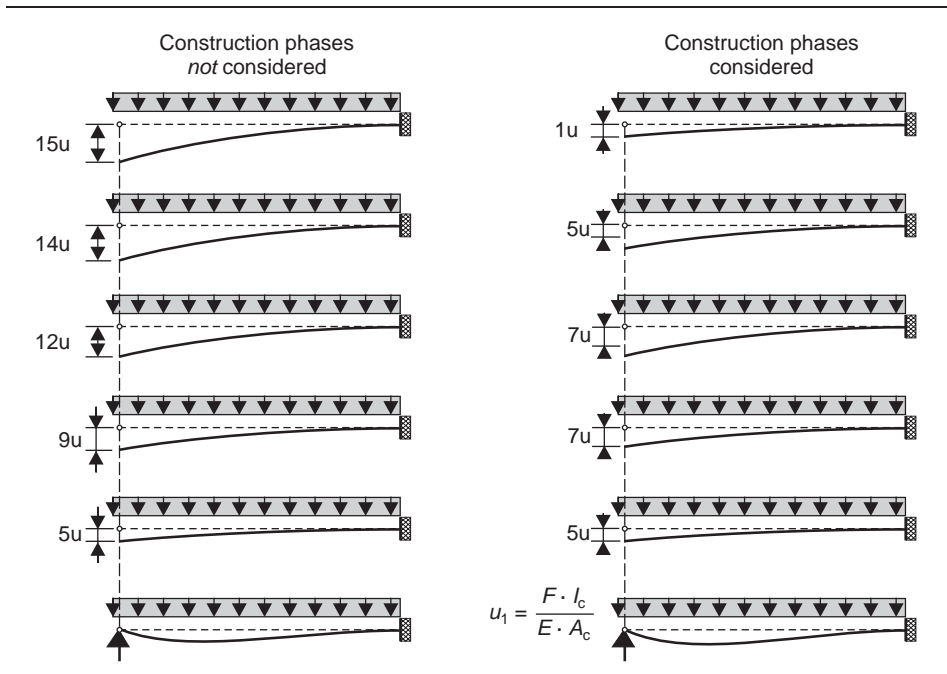


Figure 6.8 Deflections of the structure with and without construction phases


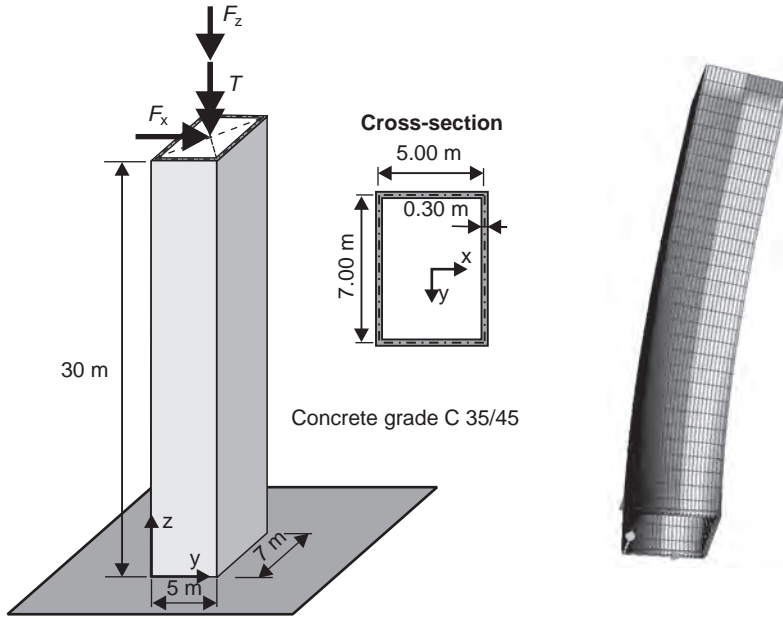
models. This structural behaviour in the ultimate limit state cannot be modelled with an FE analysis, based on a linear material behaviour.

This problem will be demonstrated in the following analysis by means of a simplified structure, a bracing element, of a real office building (Figure 6.9). For reasons of simplicity, the cantilever beam is loaded by forces and moments at its upper end only.

Table 6.1 Maximum hogging moment of slab

Loads:	Construction	$g_k = 0.26 \cdot 25 = 6.5 \text{ kN/m}^2$	
	Final structure	$(g + q)_d = 16 \text{ kN/m}^2$	
System:	Column: height	$l_c = 3.6 \text{ m}$, $b/h = 24/24 \text{ cm}$, $a = 1.50 \text{ m}$	
	Slab: height	$h = 0.26 \text{ m}$, span length $l_s = 7.8\text{--}1.95 \text{ m}$	
Concrete grade:	C35/45		
Support moment	$l_s = 7.8 \text{ m}$	$l_s = 3.9 \text{ m}$	$l_s = 1.95 \text{ m}$
$m_{s,(g+q)d} =$	-121.7 kNm/m	-30.4 kNm/m	-7.6 kNm/m
$m_{s,15u} =$	-1.9 kNm/m	-3.9 kNm/m	-7.7 kNm/m
$m_{s,1u} =$	-0.1 kNm/m	-0.3 kNm/m	-0.5 kNm/m

Figure 6.9 Structure and deformed mesh



This simple structure is used to verify the shell model as the deflections, member forces (M, V, T) and required reinforcement can be easily estimated by manual analysis.

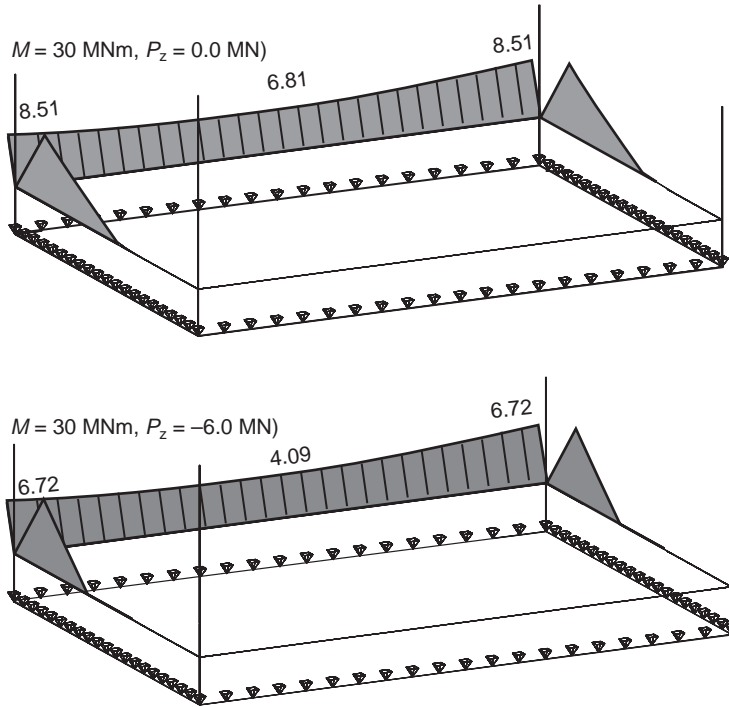
First, only a horizontal force of $F_{Ed,x} = 1 \text{ MN}$ is applied at the top of the cantilever beam. This load requires a total vertical reinforcement of $\Sigma A_s = 129 \text{ cm}^2$ at the support. The FE program estimates a slightly higher value of $\Sigma A_s = 141 \text{ cm}^2$ ($\Delta = 10\%$) due to the smaller internal lever arm of the linear elastic analysis (Figure 6.10 top).

The difference between manual and FE analysis increases if, in addition to the horizontal force, a normal force is applied. With $F_{Ed,x} = 1 \text{ MN}$ and $F_{Ed,z} = -6 \text{ MN}$ ($\sigma_{cd,N} = -0.84 \text{ MPa}$), a total bending reinforcement $\Sigma A_s = 62 \text{ cm}^2$ is required due to the manual analysis. The FE calculation gives a 64% bigger value ($\Sigma A_s = 102 \text{ cm}^2$). This result makes it clear that a complex shell analysis must not always result in a more economical design, as is believed quite often.

An FE program designs an element on the basis of elastic material behaviour and the resulting member forces. Nevertheless, in the cracked state, external compressive forces (F_z) are not equally dispersed over the whole cross-section, as is assumed in the FE model. It directly reduces the required tensile reinforcement. This becomes clear from the generally known design equation:

$$req A_s = \frac{1}{f_{yd}} \cdot \left(\frac{M_{Eds}}{z} + N_{Ed} \right)$$

Figure 6.10 Vertical reinforcement at the support for two load cases (shell analysis)

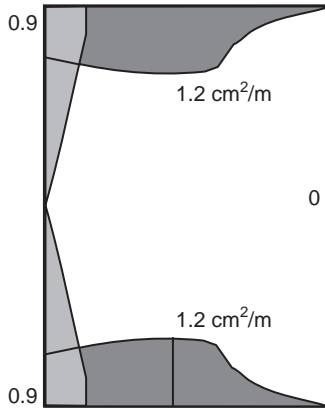


An FE analysis always gives member forces and reinforcement values on the safe side in the case of bending. Nevertheless, this does not apply to the design for shear and torsion, as will be shown in the following. Stirrups of $a_{s,w} = 6.1 \text{ cm}^2/\text{m}$ are needed to carry a horizontal force of $F_{\text{Ed},x} = 1 \text{ MN}$ according to manual design for shear. The FE analysis gives a maximum value of only $1.23 \cdot 2 = 2.5 \text{ cm}^2/\text{m}$ (Figure 6.11). Furthermore, the arrangement of the estimated horizontal reinforcement has nothing in common with stirrups. *The FE analysis is unsafe.* Furthermore, only a surface reinforcement for every FE separately is given. Hence, it is not evident for the present hollow box cross-section that stirrups are required, which should tie the compression zone and the tension reinforcement together. The design problem of shell models can only be solved by integrating the stresses in various sections numerically to get member forces (N , V , M), which can then be used to design the beam manually.

For a torsional moment of $T_{\text{Ed}} = 10 \text{ MNm}$, the FE design as well as the manual design gives a horizontal reinforcement, or stirrups, of $a_{sw} = 3.3 \text{ cm}^2/\text{m}$, for each wall (Figure 6.12).

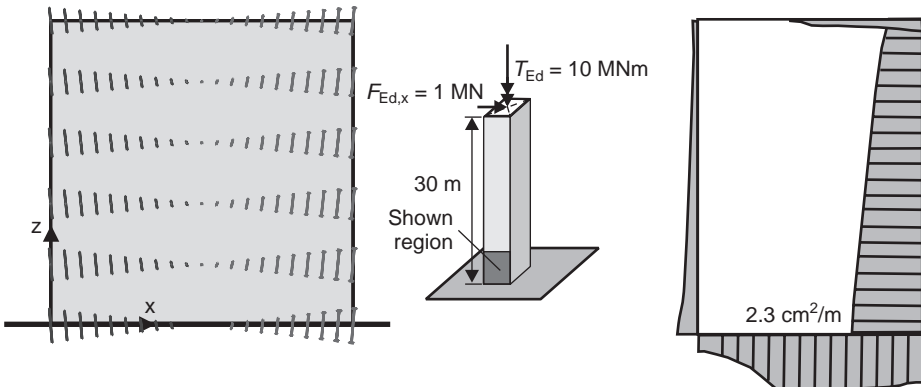
$$\frac{A_{sw}}{s_w} = \frac{T_{\text{Ed}}}{2 \cdot A_k \cdot f_{yd} \cdot \cot \theta} = \frac{10.0}{2 \cdot (7.0 \cdot 5.0) \cdot 435 \cdot \cot 45^\circ} \cdot 10^4 = 3.3 \text{ cm}^2/\text{m}$$

Figure 6.11 Horizontal reinforcement at the support of the beam, load $F_{Ed,x} = 1 \text{ MN}$



Nevertheless, this full correspondence between FE and manual analyses arises only if one assumes an inclination of compression stresses to the vertical beam axis by an angle of $\theta = 45^\circ$, the same as in the linear elastic analysis. Nevertheless, smaller values for θ ($18^\circ \leq \theta \leq 60^\circ$), which result in considerably lower reinforcement, can be used. If the section is loaded by a bending moment and normal forces, in addition to a torsional moment, the main tensile stresses in the compression area are almost vertical. This is illustrated in Figure 6.12, where the orientation of the main membrane forces as well as the horizontal reinforcement in the support region due to a load of $T_{Ed} = 10 \text{ MNm}$ and $F_{Ed,x} = 1 \text{ MN}$ is shown. The results of the FE design correspond neither to the amount nor to the arrangement of the reinforcement for a cantilever beam with a hollow box cross-section under bending and torsional loads.

Figure 6.12 Main membrane forces in the wall (left) and the horizontal reinforcement at the support (right)



6.4. Portal frame bridge

In the following, a skewed portal frame bridge founded on bored piles with a clear span of approximately 28 m is examined. The massive reinforced concrete arch has a variable thickness of 1.18 m close to the abutment beam and 0.40 m in the centre of the span. The structure as well as the numerical model used for the following calculations is shown in Figure 6.13.

Due to the screwed superstructure and the soft foundation of the arch bridge, it seems reasonable to use a 3D FE model of the whole structure to design the bridge, including the foundations. Plane shell elements are used for the arch, the side and wing walls as well as for the abutment beams. The piles are modelled by truss elements that were horizontally supported by distinct elastic springs.

The structure is mainly loaded with the dead load, the ground surcharge of the bridge, traffic loads and temperature effects. Furthermore, time-dependant concrete deformations such as creep and shrinkage have to be considered in the design of the ‘integral’ bridge without bearings. The traffic loads are not significant due to the high load by the ground on top of the arch. Hence, it does not seem necessary to consider numerous load arrangements.

6.4.1 FE modelling problems

6.4.1.1 Support condition

The arch bridge is supported by vertical bored piles that are fixed by the ground. The soil parameters and, with it, the vertical and horizontal soft support of the piles, always show a big scatter in practice. Thus, a parametric study with upper and lower bound values has to be conducted. It should be noted that, for the given ‘integral’ structure, not only mean values of the soil parameters are needed but also lower and upper bound values. The foundation modulus is estimated by means of an oedometric test, where the horizontal deflections of the cylindrical soil sample are completely restrained by a stiff steel ring.

Figure 6.13 Portal frame bridge: Structure and FE model

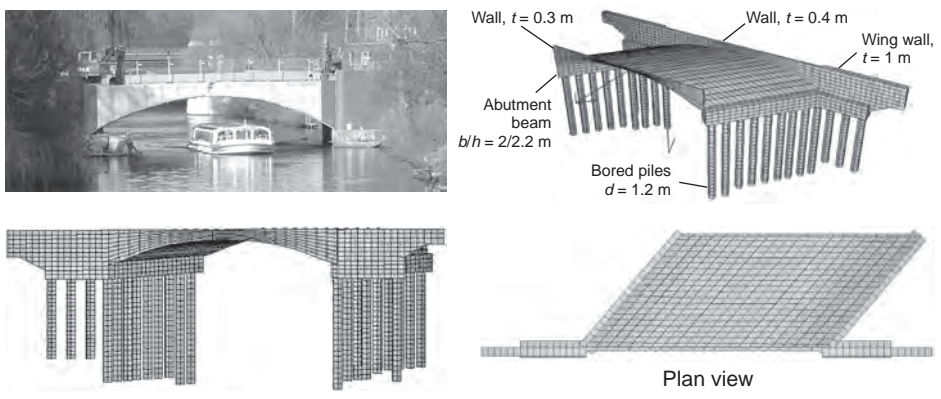
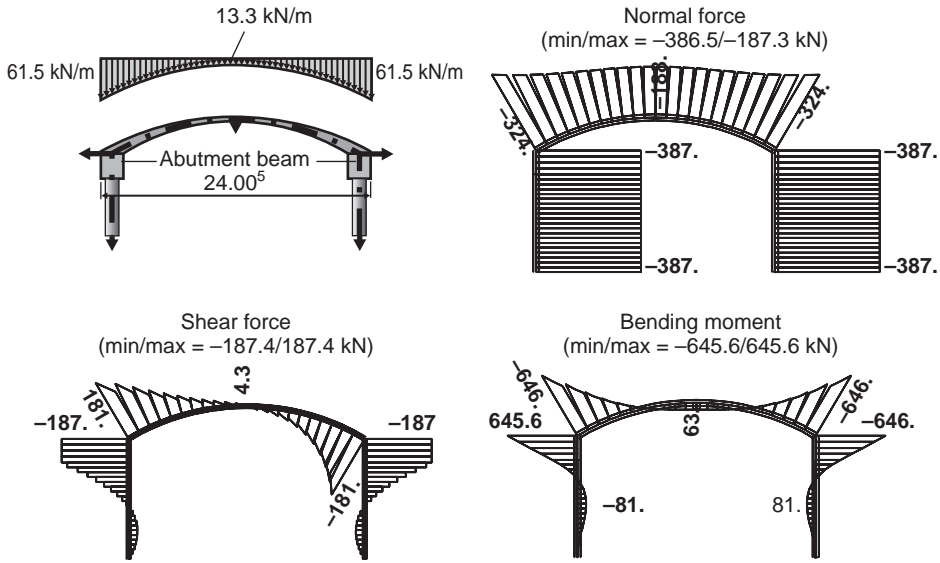


Figure 6.14 Portal frame bridge: structure, loading and member forces (truss model) due to ground surcharge



These conditions rarely apply in reality. Thus, the experimental value has to be adjusted to the real structure.

The influence of the foundation coefficient should be examined by means of a simple equivalent system (Figure 6.14) and not by the complex FE model of the whole structure. This analysis can further serve for the checking of the 3D model. In the following, only the ground surcharge on the arch is considered. Figure 6.15 shows the influence of the foundation coefficient on the member forces of the frame and the pile head. It becomes clear that the bending moment at the pile heads is highly affected by the stiffness of the soil.

The reinforced concrete arch is supported by the abutment beams and the piles. The latter are modelled by beam elements, whereas shell elements are used for the rest of the structure. Because the plane shell (membrane) elements have no rotational degrees of freedom, the joint of the piles with the abutment beam must be considered by coupling the element nodes together or by extending the beam elements of the pile into the shell elements of the abutment beam (see Chapter 3, Figure 6.16). No artificial restraints should be generated in the case of nodal coupling. If the upper node of the pile is fixed with two nodes of the shell elements, temperature loads may cause infinite stresses in this region.

6.4.1.2 Singularities – massive regions

A beam element generally shows, by definition, a linear strain distribution over the height of the cross-section. This simplification does not apply, for example, in the area of openings, on the edges of simply supported slabs or in massive regions. Here, an

Figure 6.15 Member forces in the pile head in relation to the oedometric modulus of the soil (truss model)

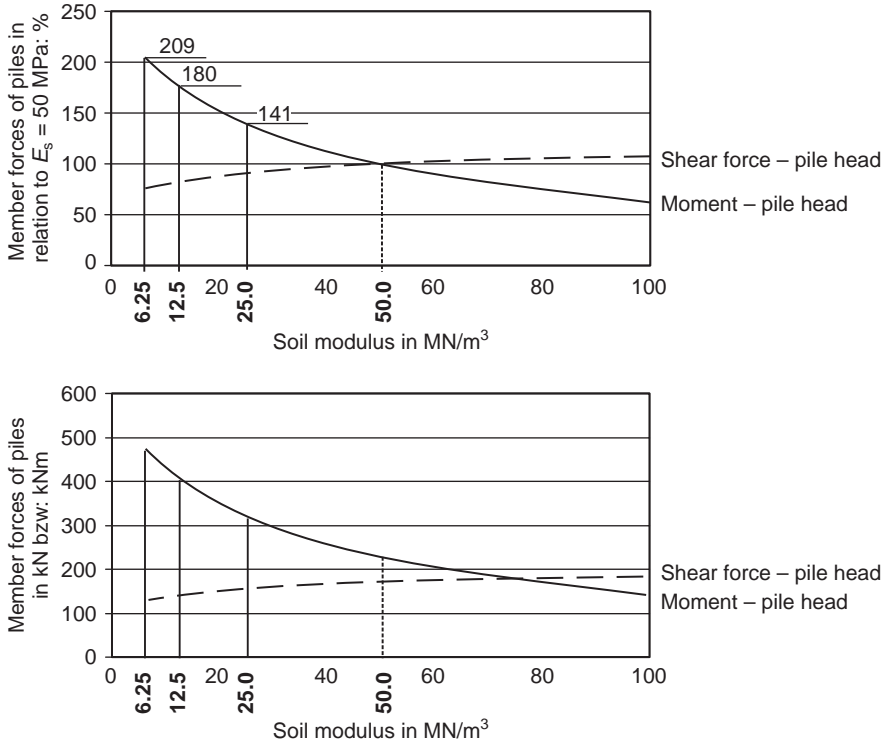
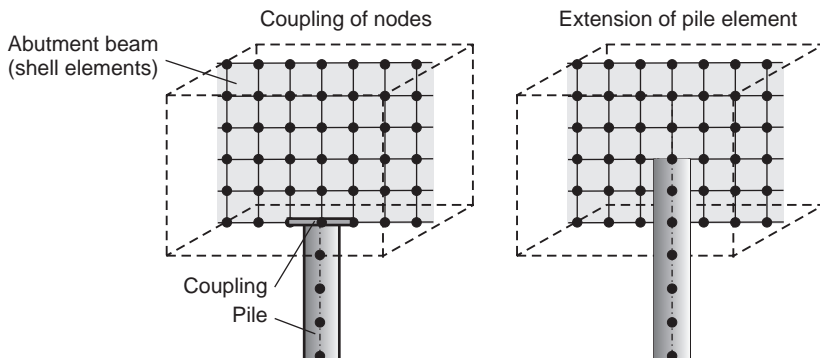


Figure 6.16 Connection between the piles and the abutment beam



FE analysis cannot give appropriate member forces. The abutment beam has a massive cross-section of 2.0×2.21 m, and thus a nonlinear strain and stress distribution is likely to occur. This will be examined further in the next section.

6.4.1.3 Loading and member forces

The loading on a structure can be taken from the National Standards. For the arch bridge, the most relevant load cases are: dead weight of the concrete structure, ground surcharge and change of temperature ΔT_N .

It should be noted that an FE analysis is based on nodal forces and displacements. Therefore, arbitrarily distributed patch loads, such as, for example, wheel loads on bridge decks, are automatically converted by the used program into equivalent nodal forces. Hence, the size of the elements has a significant influence on the member forces in the area of patch loads (see Section 5.1.2).

A temperature difference of $\Delta T_N = 16$ K was applied between the superstructure and the substructure (abutment beam and the piles). This value is much smaller than the values given in the codes as the whole substructure is under water and the arch is covered by the ground. About 40% of the elastic stiffness is used in sections where the concrete is under tension, in order to take into account the nonlinear material behaviour.

If the temperature of the screwed reinforced concrete arch increases with regard to the substructure, big tensile forces are generated in the abutment beam in the horizontal direction. The membrane force due to $\Delta T_N = 16$ K is approximately six times greater than for the other loads (Figure 6.17). A design for this high tensile force would result in a large amount of rebar, which in some sections cannot be arranged. A design based on an elastic material behaviour seems not to be required anyhow. A minimum reinforcement should be arranged in the beam rather than designing it for high-restraint forces. The abutment beam should be designed for fully tensioned sections and a crack width of $w_k = 0.2$ mm. This measure results, even for this massive cross-section, in a significant reduction of the required reinforcement. It should be noted that linear elastic analysis of a structure under restraint actions (temperature, shrinkage, etc) is, in most cases, not useful.

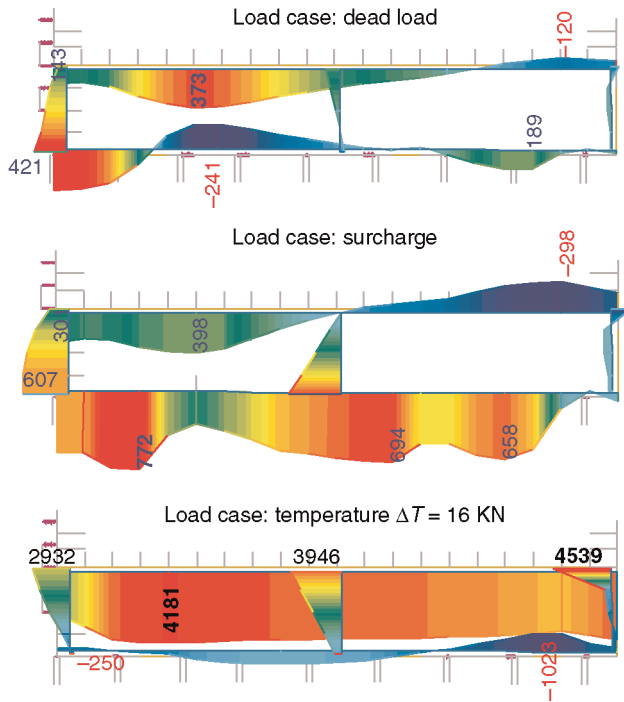
6.4.2 Dimensioning and detailing

6.4.2.1 Frame corners

In the FE model, the massive frame corner between the 2-m-wide abutment beam and the arch is neglected. All FEs are arranged in the centreline of the structure. The arch should be designed for the bending moments at the face of the massive section and not for the high member forces at the centre of the frame corner. To avoid a complex modelling of the stiff corner region by a coupling of the nodes, the estimated reinforcement at the face of the support is often used for design. This approach is not correct, as can easily be demonstrated.

Figure 6.18 shows the member forces of a rather simplified equivalent structure of the arch, a single-span girder clamped on both ends into a massive beam. Analysis is

Figure 6.17 Horizontal membranes force n_x of the abutment beam above the piles for various loads



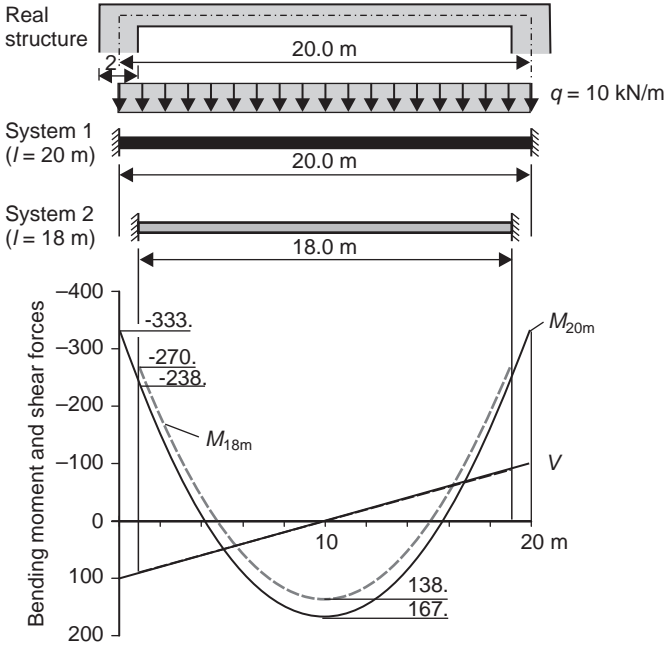
conducted with a span width of 20 m (system 1: fixed in the centre axis) and 18 m (system 2: fixed at the inner face of the support). The bending moment of model 1 at the face of the support ($x = 1.0$ m) is $M_s = -238$ kNm, while model 2 gives a 13% higher value of $M_s = -270$ kNm. The differences between both models increase when the span length decreases. A span length of $l_n = 10$ m, for example, results in a 28% difference between both approaches. The fixed end moment of the 20-m-long beam is 40% bigger, with $M_s = -333$ kNm than the value at $x = 1.0$ m. A design for the maximum value is uneconomical.

6.4.2.2 Detailing of plane shells

An FE software will always design each shell element independent of the existing structural system. This approach is not permitted for plane shells and shear walls (see Chapter 3). The reinforcement of a deep beam under uniform loading on the top edge, for example, must be concentrated at the bottom of the wall and not distributed over the tensile zone, as will be done by the FE program. A design of a deep beam or a shear wall must be based on the member forces rather than on an element-wise integration of the local stresses. Thus, an automatic design of the shear walls is not possible.

For the given structure, the arrangement of the reinforcement in the parapet walls should be examined. The wall shows very big tensile membrane forces (Figure 6.19). Hence, it

Figure 6.18 Member forces of a fully restrained beam with span lengths of 20 m and 18 m, respectively



has to be clarified whether the tensile stresses are caused by tensile action effects (e.g. temperature) or by bending of an upstand unsymmetrical T-beam (Figure 6.19). In the first case, the reinforcement has to be arranged over the whole height of the beam, whereas in the latter case it has been concentrated at the top edge (bending). From the

Figure 6.19 Horizontal membranes force and required reinforcement of the parapet wall

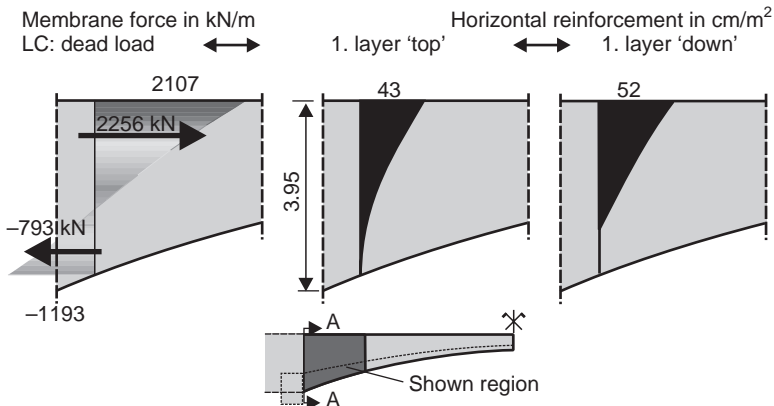
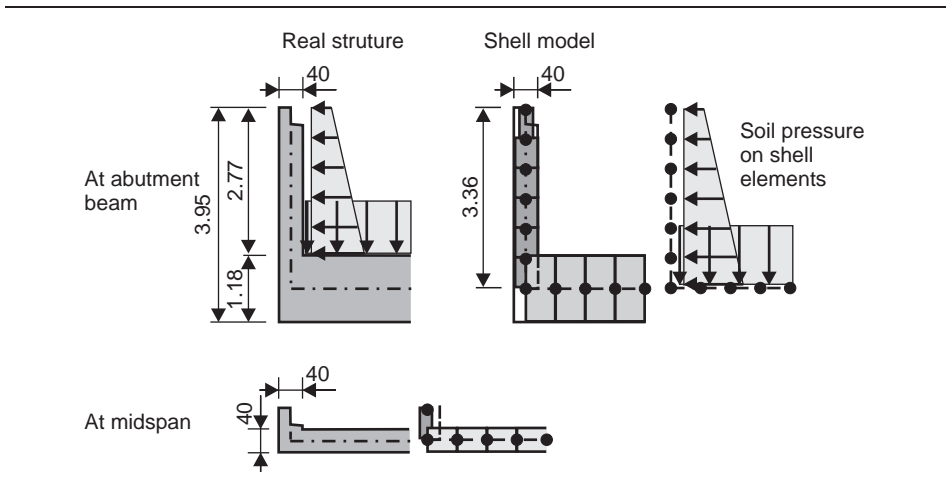


Figure 6.20 FE models of the parapet wall



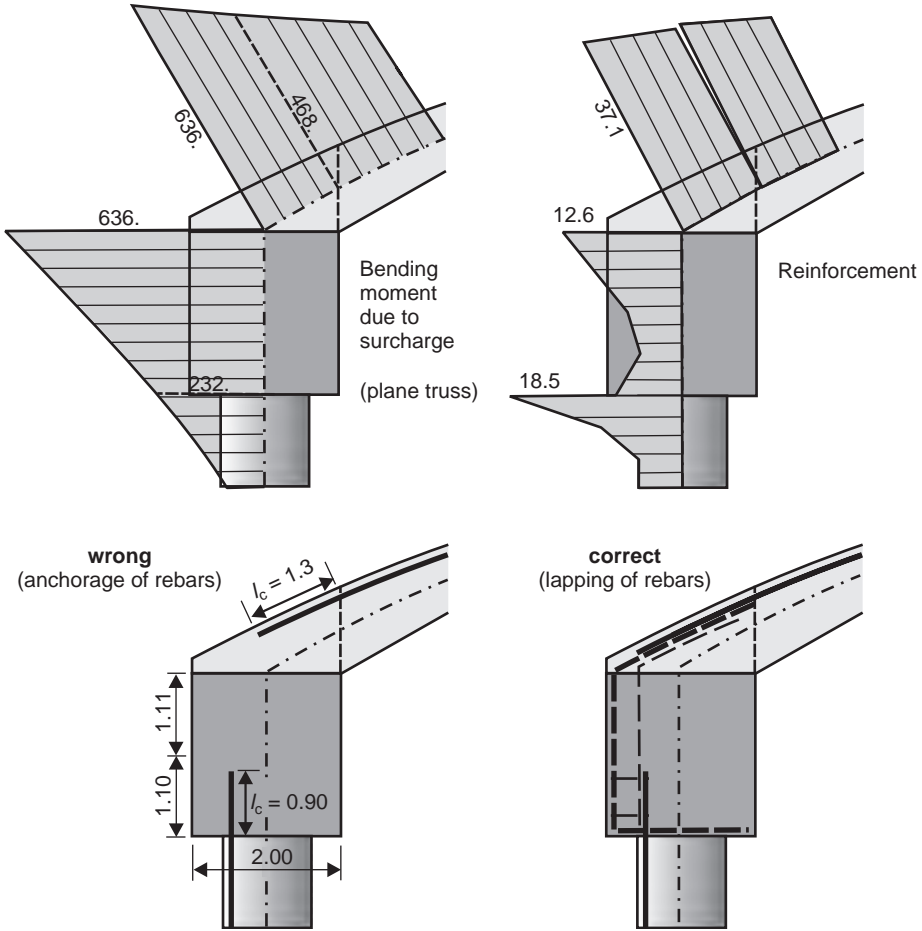
distribution of the membrane forces (Figure 6.19), it becomes clear that the parapet wall shows a bending behaviour and, therefore, the required reinforcement has to be concentrated at the top edge. The parapet wall acts as a web of an unsymmetrical upstand beam and has to be designed like a girder. Therefore, the local shear forces have to be supported by stirrups that must tie the compression zone and the tensile reinforcement together. The distribution of the shear forces should be examined carefully.

6.4.2.3 Flow of forces

As already mentioned, an FE design is based on an element-wise estimation of the required reinforcement, independent of the existing structure. Hence, the designer and the draftsman have to transfer the enormous amount of data from the numerical analysis into practical reinforcement arrangements. This concerns not only a reasonable staggering of the required reinforcement, but also requires the flow of forces to be considered in detail. Here, as an example, the flow of the forces from the superstructure (arch) into the abutment beam and, finally, into the piles is discussed. The required reinforcement is very different in the various structural elements due to the big change of the cross-sections. This raises the question as to where the high amount of reinforcement in the arch and in the pile heads should end. Some designers just anchor the required rebar of the arch and the pile in the abutment beam. This can be easily done due to the massive section. However, the flow of forces is not considered in this approach, and thus the design is unsafe (Figure 6.21 left). The rebar for the tensile force at the clamped edge of the arch has to be lapped with the rebar of the piles.

The FE program cannot estimate the tensile forces that result from the dispersion of the high pile forces into the abutment beam. For such massive structural elements as abutment beams, strut-and-tie models are needed for design. Linear elastic FE analysis may be used to develop a realistic stress-field model (Figure 6.22).

Figure 6.21 Arrangement of reinforcing bars between pile and superstructure



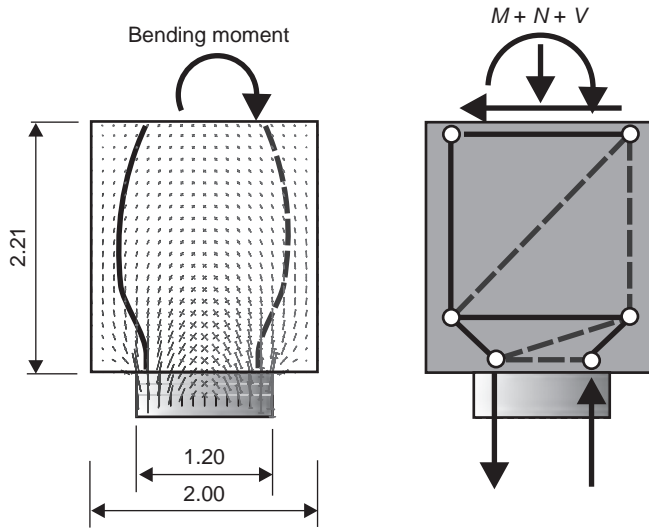
6.4.2.4 Minimum reinforcement

In addition to the required reinforcement for the external actions, a reasonable minimum reinforcement has to be arranged. The arch of the bridge is concreted on top of the already existing massive abutment beam. The heat of hydration of concrete causes high tensile forces in the arch. The crack width has to be limited to a certain value by choosing a reasonable amount of rebar and a suitable arrangement, rather than by designing the section for the high restraint.

6.4.2.5 Design for shear

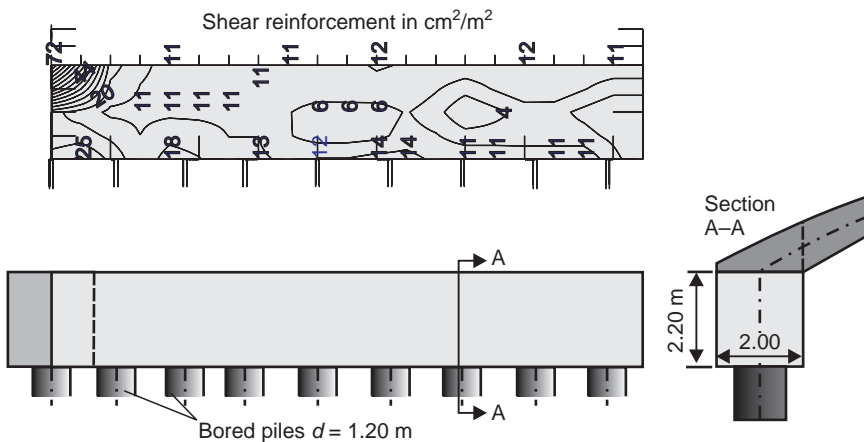
The existing models for shear design of reinforced concrete components have been developed extensively only for beams under pure bending. The used truss model does not apply to massive regions, such as the abutment beam. Thus, it is not reasonable to use this design approach here. An FE program estimates the required vertical reinforcement

Figure 6.22 Strut-and-tie model of the abutment beam



based on the integration of the local vertical stresses in each element. Figure 6.23 shows the result of such an analysis for the abutment beam. This approach is not correct here. According to the numerical design, stirrups of approximately $12 \text{ cm}^2/\text{m}^2$ are needed in the upper region of the beam. The arrangement of such stirrups would require a big effort. By means of a strut-and-tie model (Figure 6.22), one can demonstrate that no shear reinforcement is required.

Figure 6.23 Required shear reinforcement according to EC2 (Eurocode 2, 2004)



The high shear forces in the upper left part of the abutment beam are not relevant for design because of the massive region.

The example makes it clear that the shear design of massive components must be questioned.

6.5. Checking and documentation of FE analyses

The main problem of big FE models is not in the discretisation, in the generation of the huge element mesh. The checking of the input and output of the numerical analysis is rather difficult and requires much more effort. It must be pointed out again that the structural engineer in charge and not someone else, such as the checking engineer, must be convinced of the correctness of his or her design, as he or she bears the sole and final responsibility. If a designer does not check his or her analysis, he or she acts highly irresponsibly.

The checks require an entire and clear documentation of the structural data, the actions and the essential results of the FE analysis as well. Although this should be quite normal, the quality and quantity of the documentation of an FE calculation is a permanent matter of discussion between the design and the checking engineers. Hence, in addition to the general remarks in Section 6.1, some further explanations are given in the following for complex building models.

6.5.1 Checking of FE analyses

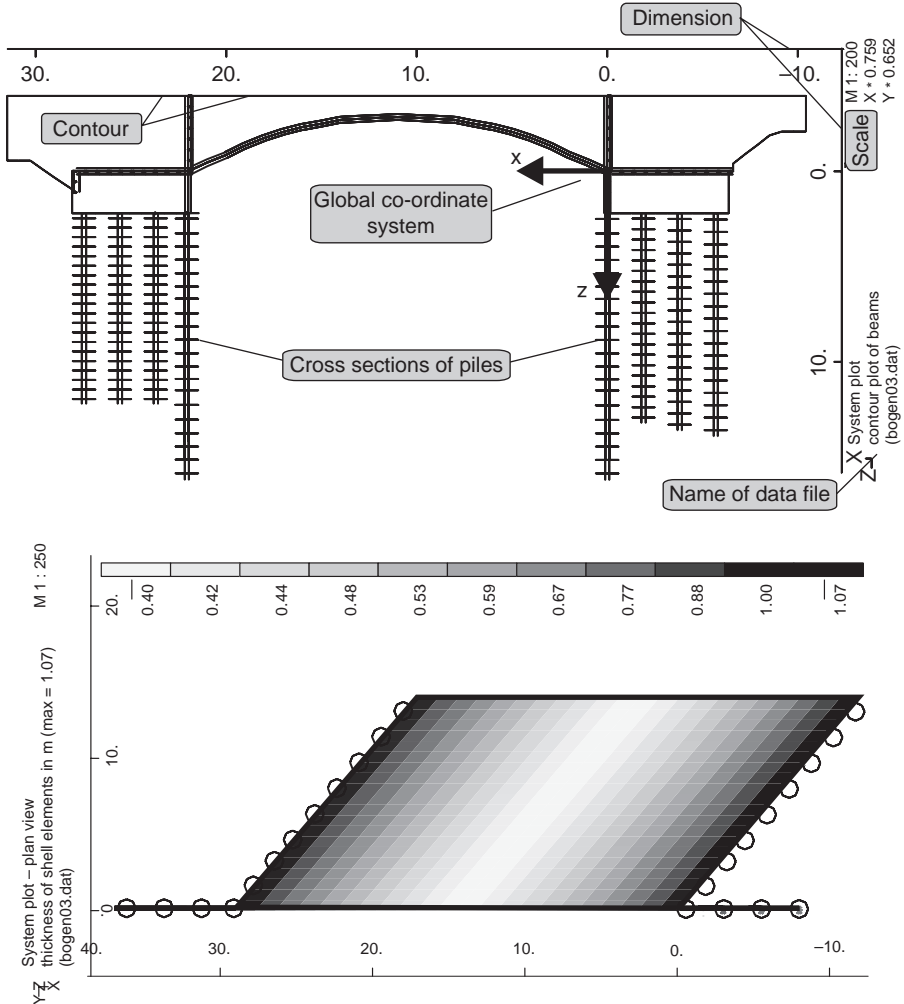
First, the FE model has to be checked primarily by means of graphical output. This includes scaled section plots of the system on which, among other items, the geometry, the dimensions (cross-sections), the support conditions, the orientation of the local and global coordinate systems, all coupled nodes and rigid regions and the joints and hinges as well as the cross-sections of the beams and columns can clearly be seen (Figure 6.24). 3D plots of a structure (Figure 6.13) are generally not of great use.

Numerous *material parameters* are needed for the design of a structure, like the modulus of elasticity (see Section 2.11.1) and the Poisson's ratio (Section 4.3). All parameters show a significant scatter in practice, which may influence the results of the analysis. Thus, all material parameters and the used material model, as well as the allocation to the various structural elements, have to be checked.

Furthermore, the *assumptions of the FE model* have to be checked. Is the strain over the height of the cross-section linear in all relevant regions of a beam and a plate, or do the discontinuity or singularity regions need further attention? Does the reduction of stiffness in a cracked concrete region due to tensile stresses or torsional moments have a significant influence on the distribution of the member forces in the structure? The FE mesh is to be checked for possible incompatibilities if different types of elements, for example, beam and plane shell elements, are jointed together. Massive sections should be designed with strut-and-tie models.

The control of the level and the arrangement of all relevant *load cases* (including imperfections) are difficult and time consuming. The partial safety concept has led to

Figure 6.24 Plan and top view of structure



an enormous number of load combinations that can hardly be overseen. The arrangement of the loads may be checked graphically. The total support force of a load case given by the program can be used as a quick check, whether the actions are considered in the correct integral size. Loads on fixed nodes are not considered and printed out by some programs, because they give no contribution to the deflection energy of the system. In such a case, one must add the missing nodal forces to get the correct load for the supporting structures. Constraint effects are to be controlled with regard to the cracking of concrete.

The distribution of the strains, deflections, and member forces must be plotted in the relevant sections for the relevant load cases.

Tensor plots of the main moments or main membrane forces serve for the view of the flow of forces in a structure.

Furthermore, the *deformation of the structure* has to be checked. Is the deformation of the structure reasonable under the relevant actions? Nodes that are fixed or released unintentionally may cause an incorrect structural behaviour, as has been demonstrated by deep beams and truss structures (see Sections 3.2.4 and 2.2).

The *delicacy of the structure* on slight changes of the input parameters, for example, the soil parameters or the stiffness of supports and members, should be checked by means of *parametric studies* with lower and upper bound values.

Construction sequences may have a significant influence on the member forces.

The effect of geometrical imperfections given in the codes (Eurocode 2, 2004) should be checked.

The *amount of reinforcing* estimated by the FE program and its *arrangement* is to be questioned. A program-controlled design of deep beams does not give a reasonable arrangement of the rebar. Furthermore, the flow of forces is to be followed between the different structural components. With complicated 3D FE models, the direction of the reinforcement as well as the location ('upper' or 'lower' side of a slab) should be shown unambiguously on the plots.

The preceding (incomplete) listed items demonstrate that the checking of big FE analysis requires a large effort, which must be considered in the financial budget of the project.

Nevertheless, all these controls cannot give absolute certainty about the correctness of numerical analysis. This is possible only by means of *independent comparative calculations* with *simple equivalent structural models* (e.g. simple beams).

One problem of big FE models should still be pointed out here. During the planning and construction phases of a building, numerous changes of the original draft are often necessary. In the case of the arch bridge, one pile was drilled at a slightly wrong location. As the structural behaviour of the bridge couldn't be simplified by the design engineer as he believed in his 3D FE model, the whole structural system had to be calculated again. Moving a pile in the numerical model is a very easy task. Nevertheless, the clear documentation of the new results as well as the comparison with the original calculations was connected with a large expenditure.

6.5.2 Documentation of FE analyses

Not only the amount of checking but also the expenditure for a clear, understandable output of the important results of a numerical calculation increases with the complexity of the FE model. As day-by-day practice shows, the output and the documentation of a structural analysis is often not paid much attention.

The formal demands for a numerical analysis are given in, for example, the regulation for the conducting and checking of computer-supported structural analysis (RI-EDV-AP-2001) (Verein Deutscher Prüfengeure, 2001). This or similar regulations should generally be fixed in the contract documents of any structural design. If this directive is postponed, the designer must convince himself or herself of the plausibility of the inputs and results by various checks. In the following, the essential items of this directive are listed.

The numerical output should be reduced as much as possible in favour of clear, graphical outputs.

Among other things, the documentation of a structural analysis must contain the following items:

Information of the used software

- program name (version, date of release)
- description of the structural system to be analysed with the program
- short description of the structure, for example, by means of sketches
- used methods (theories used and arithmetic procedures)
- regulations (codes, regulations) that are considered by the program
- notations, symbols, units (if different to the existing technical building regulations)
- specific features
- documents (if necessary, essential parts of the user manual, program documentation, etc).

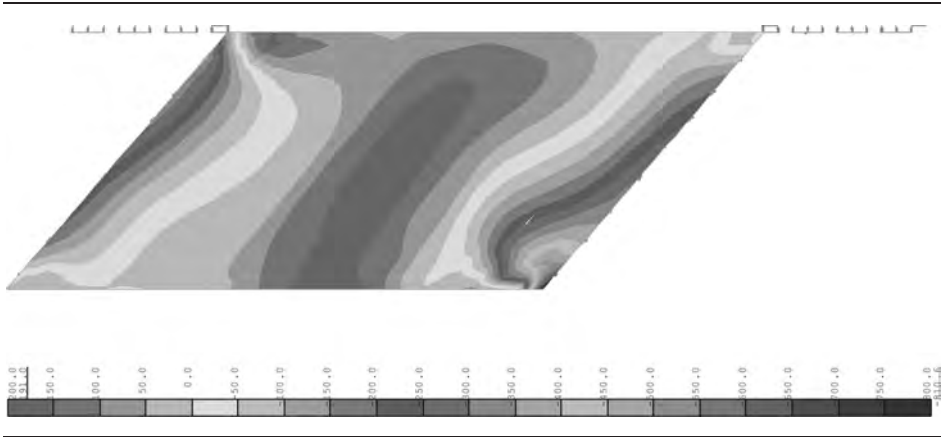
Formal demands

- table of contents to come at first
- page numbers (including exchange and supplementary pages)
- cross-references (*with page numbers*)
- notations, symbols and units according to the existing technical building regulations
- conventions
 - coordinate systems
 - portent definitions (member forces, deflection, stresses and loads)
 - allocations (structural members to numbers, node element numbering)
 - load cases, combinations of load cases.

Input

- general demands: completeness, necessary allocations, special conditions and simplifications to be given
- mechanical structural model: *graphical* representation of the structural model. including geometry, dimensions, support conditions, joints, cross-section allocation, boundary conditions (see Figure 6.24)

Figure 6.25 Shading plot of principal bending moment due to uniform loading



- material parameters, cross-section dimensions, stiffness
- loads, generally graphical output, including all relevant load combinations
- additional information, for example, moment redistributions, construction phases.

Output of the results

The following decisive results are required for checking the safety and serviceability of the structure, as for example:

- member forces and deflections for the *relevant* load cases and load combinations
- design member forces and estimated reinforcement with cross-section distortions and cross-section dimensions (for relevant load cases and sections only)
- material grades
- construction sequences, if considered
- restrictions for the use of the structure
- necessary intermediate results (e.g. support forces including the used safety coefficients)

Please note that coloured plots should only be made if all copies of the design document are coloured. This may cause significant costs in bigger projects. Black-and-white copies of coloured drawings are useless, as can be seen in Figure 6.25. The grey shadings cannot be assigned to the level of the main bending moment m_1 in the superstructure.

As in every structural analysis, the documentation of the design should be clear and easy to be verified. Sketches are very helpful.

6.6. The power of FE analysis

Despite the previously described problems, one should also not forget that FEM offers big advantages. It gives us a tool with the ability to design almost any arbitrary structure. To illustrate this, two buildings, the Sydney Opera House (Figure 6.26) and

Figure 6.26 Opera house in Sydney, Australia



the 'Auditorio de Tenerife' (Figure 6.27), are compared. The famous building in Australia required a construction time of 14 years (1959–1973). The building cost that was originally estimated at £3.5 million increased in this time period by a factor of more than 14, to approximately £50 million. The dream of the architect could only be

Figure 6.27 Auditorio de Tenerife



realised when the complex shells of the roof were substituted by a frame structure made of prestressed T- and V-beams. In contrast, the impressive ‘Auditorio de Tenerife’, which opened in 2003, is a shell structure that could not have been built without FE analysis. During the construction (1998–2003), the original estimated building cost of €30 million increased to approximately €80 million.

6.7. Summary and conclusions

The essential problems of 3D building models were discussed in this chapter. The presented examples make it clear that no software can substitute the expertise of a structural engineer. If the current trend in using the FE method continues, it is to be feared that big FE models will be applied increasingly by people who have little or no knowledge in the field of numerical analysis and have no practical experience. To prevent this, it is necessary to establish accepted regulations for the FE design of structures. The *written* documentation of all the major controls by the design engineer should be compulsory. We should give the practicing engineers enough time to verify their FE models. Furthermore, we need better software that supports the engineer in the checking of his or her complex numerical models. Benchmark tests of the software are useful but cannot prevent errors caused by the ignorant use of the program.

Development in the field of numerical analysis continues. After the 3D building models, where the engineer controls the meshing, even more complex ‘building information models’ (BIM) will be used. These models contain *all* the data of a building, including the structural elements and the required reinforcement for any member, the construction sequences, quantity and qualities of building materials etc. The whole FE mesh is generated automatically with the available data from a general database. Any changes during design and construction of the building are automatically considered in all elements of the building. This raises the following questions: Who is controlling the flood of information? Do we still need experienced structural engineers if the design of a complex building can be done automatically by software in a very short time?

REFERENCES

- Bathe K-J (1982) *Finite Element Procedures in Engineering Analysis*. Prentice Hall, Englewood Cliffs.
- CEN (European Committee for Standardization) (2004) *Eurocode 2, Part 1 Design of concrete structures – General rules and rules for buildings*. December.
- Hughes TJR (1987) *The Finite Element Method*. Prentice Hall, Englewood Cliffs.
- VPI (Verein Deutscher Prüfingenieure) (2001) *Richtlinie für das Aufstellen und Prüfen EDV-unterstützter Standsicherheitsnachweise (RI-EDV-AP-2001)*. Der Prüfingenieur 18.
- Zienkiewicz OC and Taylor RL (1989) *The Finite Element Method*. London.

Index

Page numbers in *italic* refer to diagrams or illustrations

- anchorage of tendons 293–296, *295*, *296*
- Auditorio de Tenerife *349*
- Bangkok (Thailand)
 - Don Muang Tollway *96*
 - Expressway System *17*, *19*
- Baumann model, spatial structure
 - dimensioning *257–260*, *257*, *258*, *259*, *261*
- beams
 - see also* concrete joist floors; deep beams; foundation beams; reinforced beams; T-beams
 - bending moment distributions *31–33*, *32*
 - characteristic length *41–42*
 - column intersections *14*, *14*, *16*, *29*
 - loading *17*
 - shear walls *56*, *38*, *58*
 - curvature *121–122*, *122*
 - deformation
 - creep *119*
 - cracked, with TS *123–128*
 - cracked, w.t. TS *120–123*, *120*
 - uncracked *117–120*
 - dimensioning *110–114*, *111*, *112*
 - halving joints *29–30*, *30*
 - stress distribution *30*
 - strut-and-tie models *34*
 - membrane model *162–166*, *163*, *164*
 - nonlinear analysis *114–136*
 - openings in *29–37*, *29*, *31*, *36*, *37*
 - deformation *37*
 - stress distribution *31–33*, *33*, *34*, *35*
 - strut-and-tie models *36*
 - restrained, member forces *26–29*, *27*
 - support conditions *105–110*, *108*, *110*
 - torsional moments *67*, *68*
 - variable depth, inclined haunches *23–29*, *24*, *25*, *27*, *28*
- bending moments
 - beams
 - distributions *31–33*, *32*
 - restrained *26–29*, *27*
 - circumferential, shell, silos *281*, *312*
 - column supports *151*, *151*
 - column head *151–152*, *151*, *152*, *155*
 - Finite Element mesh *155*, *152*, *155*
 - distribution, high-rise buildings *62*, *63*, *72–76*, *72*
 - footings, distribution *229–232*, *229*, *230*, *231*
 - foundation beams *39–43*, *40*, *41*, *42*, *44*, *45*
 - concentrated loads *43*
 - hollow box girder bridges *19–23*, *21*, *22*
 - top slab *84*, *85*
 - inclined bored pile foundations *54–56*, *55*
 - Kirchhoff plate theory
 - equation *174*, *182*
 - singularities *239*
 - uses *262*
 - portal frame bridges *15*, *15*, *16*
 - residential building slabs *177*, *178*, *179*
 - shell structures *311–312*, *312*
- slabs
 - Baumann model *257–260*, *257*, *258*, *259*, *261*
 - cantilever *251–253*, *252*
 - circular *249*, *249*
 - discontinuous line support *201–205*, *202*, *204*
 - Eurocode 2 (EC2) model *260*, *260*
 - Finite Element Method *262–263*, *262*, *265*, *267*, *268*
 - flat *209–214*, *212*

- bending moments (*continued*)
 - one-way 186, 187–193, 188, 189
 - partially lifting 197–199, 198
 - Pieper-Martens model 263, 267, 268
 - pin supports 214–215, 215, 216
 - skewed 235–236, 237
 - Stiglat model 255–256, 256, 261
 - at support points 183–185, 184
 - strip foundations 232–234, 233, 234
 - T-beam bridges 89, 89, 90
- Bernoulli hypothesis 13, 29, 33, 111, 162, 173
- bored pile foundations
 - bedding modulus 46–47, 46
 - bridge columns 47, 48, 49
 - forces carried 46, 46
 - horizontal deformation 53–54, 53
 - inclined, bending moments 54–56, 55
 - manual analysis 47, 50
 - rigs 50
 - truss system 47–48, 51
 - vertical spring stiffness 48–53, 52
- bond of rebars 315
- box girder bridges *see* hollow box girder bridges
- bracing systems
 - high-rise buildings 58–80, 65
 - bending moment distribution 63, 72–75, 72
 - coupling of nodes 67–70, 68, 69, 70
 - equivalent cross-section 63
 - fictitious bar method 61–62, 64, 66–67
 - location of beam elements 67, 68
 - modelling 70, 71
 - shear walls 56–61, 57, 58, 60, 61
 - shell models 74, 75
 - stability 76, 81
 - structural deformations 74–76, 76
 - torsional moments 73–74, 72, 73
- bridges
 - see also* hollow box girder bridges; portal frame bridges; T-beam bridges
 - bored pile foundations 49, 49, 50
 - columns, loadings 49, 51
 - Don Muang Tollway 96
 - Expressway System 17, 19
- Building Information models 350
- building materials
 - see also* material parameters, concrete
 - material behaviour, concrete 8, 111, 111, 203
 - material parameters, concrete 128
 - modulus of elasticity 118, 118
 - nonlinear behaviour 43–45, 44, 45
 - steel, stress–strain relationship 111, 111, 116
 - stress–strain relationship 112–113, 113, 114, 116–117, 116, 117, 314, 315
 - torsional stiffness, concrete 63
 - yield surfaces, concrete 315
- building models
 - checking 322–323, 344–346
 - construction 328–331, 328, 330, 331
 - design 329–334, 333, 334
 - FE-modelling 324–325, 324
 - incompatible element mesh 325–326, 327
 - minimum reinforcement, slab 326, 327
 - problems 322
 - soil parameters 323
 - singularities 325, 326
- calculators, first programmable 3
- cantilever column 316, 317
 - reinforcement layout 317
- cantilever slabs
 - bending moments 251–253, 252
 - inadequate modelling 251–252, 252
- characteristic length, calculation of 41–42
- checking of FE-analysis 322–323, 344–346
- column supports
 - bending moments 151, 151
 - column head 151–156, 152, 155
 - Finite Element mesh 155, 154, 155
 - bending stiffness 148–149, 149
 - deep beams, stiff connections 154, 154
 - deformations, time-dependant 184
 - modelling
 - with beam elements 151–156, 152, 153
 - equivalent spring stiffness 146–151, 149
 - normal stiffness 148–149, 149
 - rotational stiffness 149, 150
- composite shell structures 310, 311
- concentrated loads, singularities 242–244, 242, 243, 244
- concrete
 - cracked members
 - considerations 3
 - torsional stiffness 63
 - cracking considerations 3
 - material behaviour 8, 111, 111
 - material parameters 128

- Modulus of Elasticity 118, *118*
- nonlinear behaviour 43–45, *44, 45*
- steel, stress–strain relationship 111, *111, 116*
- stress–strain relationship 112–113, *113, 114, 116–117, 116, 117, 314, 315*
- yield surfaces *315*
- concrete floor joists
 - dimensioning 206
 - models 205–206, *205*
- Condeep-type platform 3
 - see also* Sleipner A platform
- constraint modulus method 39, *39*
- cracked members
 - considerations 3
 - cracks
 - modelling 316, *316*
 - force transfer 315, *315*
 - torsional stiffness 63
- Czerny tables, slabs 262–263, *262, 263*
- deep beams
 - column supports
 - beam element modelling 151–156, *152, 153*
 - spring equivalent modelling 146–151, *149, 150, 151*
 - corner region, stress distribution 155–156, *156*
 - definition 139, *140*
 - degree of freedom 153, *154*
 - dimensioning 158–166, *159, 160, 161, 162*
 - detailing 160–162, *162*
 - internal forces, linear-elastic calculations 139
 - membrane force distribution 157, *157*
 - membrane model *153*
 - multi-span
 - loading forces 147, *147*
 - stress distribution 147, *149*
 - strut-and-tie model *167, 168*
 - support settlement 146, *148, 149*
 - reinforcement
 - horizontal distribution 158–162, *160, 161, 162*
 - vertical distribution 160, *161, 165–166*
 - single span
 - membrane forces *142, 143–145, 144, 145*
 - reinforcement requirements 141, *162–1662, 163, 164*
 - stress resultants 141–145, *142, 144, 145*
 - strut-and-tie models 166–169, *166*
 - tensile forces 142, *146*
 - singularities 169–170, *169*
 - shear design 342–343, *343*
 - and slender beams 162–166, *164*
 - stress/strain distribution
 - cracked members 165, *165*
 - uncracked members 165, *165*
 - strut-and-tie models 166–169, *166, 167, 168*
 - support
 - modelling of 145–157
 - horizontal restraint 156–157, *157*
 - springs 146–151, *149, 150, 151*
 - beam elements 151–156, *152, 153*
 - incompatible 153, *154, 325–326, 327*
 - two-span, strut-and-tie models 167–169, *167, 168*
- deformation, beam
 - creep 119
 - cracked, with TS 123–128
 - cracked, w.t. TS 120–123, *120*
 - uncracked 117–120
- dimensioning
 - beams 110–114, *114*
 - concrete joist floors 206
 - shear walls 158–162, *159, 160, 161, 162*
 - spatial structures
 - Baumann model 231–234, *231, 232, 233*
 - cracking 254, *255*
 - internal forces 254
 - simplifications 254–255
 - Stiglat model 255–256, *256, 261*
- discontinuity regions 13
 - definition 13
 - truss systems 14, 22, 22, 29, 29, 30, *325*
- discretization
 - definition 2, 5, 5
 - modelling errors in 8–12
- displacements, T-beam bridges 88, *89, 90*
- documentation of FE-analysis 346–348
- double T-beam bridges *91*
 - beams
 - locations 92–93, *93, 94*
 - numbers, transverse beams 95
 - stiffness 95–98, *97*
 - deformation 93, 95, *101*
 - design 91

- double T-beam bridges (*continued*)
 - girder model 91, 92, 93
 - inclined haunches 97, 98, 102
 - longitudinal girders, bending moments 99, 100, 101, 103
 - member forces
 - three-dimensional truss system 98, 99, 101
 - two-dimensional truss system 98, 100, 101
 - moment distributions 101, 102
 - numerical models 92
 - torsional moments 93, 95
 - transverse beams 93–98, 102, 93, 94, 95, 97, 102, 103
 - downstand beam 296
 - effective slab widths, high-rise buildings 60
 - effective span length, frame 338–339, 340
 - elastic structure analysis, membrane models 21–22, 22, 31, 35, 37
 - elastic support
 - foundations
 - modelling 38, 38
 - settlement forces 44–46, 44, 45
 - fictitious bar method 61–62, 64, 66–67
 - Finite Element analysis
 - building models 324–325, 324
 - errors, Sleipner A platform 271–278, 274, 275, 277
 - shell structures, silos 279, 279, 280, 281
 - Finite Element design
 - introduction 5–7, 5, 6, 7
 - principles of 1–2
 - software
 - availability 1–2
 - uncritical use of 3–4
 - Finite Element Method
 - bending moments, rectangular slabs 262–263, 262, 264, 265, 267, 268
 - principles 5–7, 5, 7
 - nodal loading versus real loading 8–10, 9, 10
 - problems 7–12
 - shell structures, mesh generation 271
 - slab analysis 172, 172, 262–263, 263
 - flat slabs 206, 207
 - see also* foundation slabs
 - bending moments 212–214, 212
 - bedding modulus variations 218–219, 219
 - columns 218–219, 220
 - deflections 216, 217
 - hinge coupling of nodes 219–220, 220, 223
 - nodes restrained 216, 217, 218
 - pin supports 214–215, 215, 216
 - circular 207, 208
 - coupling of nodes
 - hinge 219–220, 220
 - rigid 219–220, 220
 - equivalent frame models 210, 211, 213
 - manual analysis 210–212, 211, 212, 213, 224, 225
 - moment distribution 212
 - nodes restrained 214, 216, 217, 218
 - plane plate models 208–209, 209
 - span moments 211
 - support
 - all nodes restrained 216, 218
 - coupling of nodes
 - hinge 219–220, 220, 223
 - rigid 219–220, 220
 - elastic bedded 218–219
 - models 209, 209
 - pin supports
 - all nodes 214, 216
 - single nodes 214, 215
- footings
 - bending moment distribution 229–230, 229, 230
 - definitions 228
 - uses 228
- form functions 6
- foundation beams
 - bending moments 39–43, 40, 41, 42
 - concentrated loads 43, 41, 42
 - concrete, nonlinear behaviour 43–46, 44, 45
 - elastic bedded 37–43, 38
 - settlement forces 44–46, 44, 45
 - number of elements 39–43, 40, 41, 42
 - shear forces 40, 40, 41, 42
 - soil model 38, 38
- foundation slabs
 - circular
 - membrane forces 229–232, 231
 - strut-and-tie models 230, 232
 - definitions 226

- footings
 - bending moment distribution 229–230, 229, 230
 - definitions 228
 - uses 228
- internal forces, determination 228
- stresses 230, 231
- strip foundations
 - bending moment distribution 232–234, 233, 234
 - definition 226
 - membrane force 235, 231
 - modelling 232, 233
 - tensile force 234, 234
 - test results 233
- foundations
 - see also* pile foundations
 - portal frame bridges 16–17, 16
 - soil deformation 38–39, 39, 40
- frame models, straight truss elements 56
- frame structures, rigid regions 14, 14
- grillage structure, slab 84–90, 87, 88, 89
- halving joints 29–30, 30
 - stress distribution 30
 - strut-and-tie models 34
- haunches
 - inclined
 - double T-beam bridges 97, 98
 - internal forces 24–26, 25, 27
 - bending moments 28
 - shear design 24, 25, 26
 - strutted frame 26
 - truss model 25
- Heidelberg (Germany) Theodor-Heuss
Brigde 104, 105
- high-rise buildings
 - see also* shear walls, building models
 - bracing systems 58–80, 65
 - bending moment distribution 63, 72–75, 72
 - coupling of nodes 67–70, 68, 69, 70
 - fictitious bar method 61–62, 64, 66–67
 - modelling 70, 71
 - shear walls 56–61, 57, 58, 60, 61
 - structural deformations 74–76, 76
 - torsional moments 73–74, 72, 73
 - slab width, effective 60
 - stability
 - support forces 77–79
 - sway system 76
 - parameters 80
- hollow box girder bridges 19
 - bending moments
 - distribution 18–23, 21
 - top slab 84, 85
 - decks, equivalent slab model 242, 243
 - distortions 83, 83, 84
 - longitudinal design 80–82, 81, 82
 - numerical model 81, 82
 - reinforcement
 - frame corners 20, 22, 24
 - layout 20
 - shear forces, top slab 84
 - shell models 83
 - torsional moments 80–82
 - transverse design 17–23, 20
 - truss model 17, 20
- inclined haunches
 - double T-beam bridges 97, 98
 - internal forces 24–26, 25, 27
- incompatible element mesh 153, 154, 325–326, 327
- industrial buildings, T-beam girders 23–24, 25
- Kirchhoff plate theory
 - equation 174, 182
 - singularities 239
 - uses 262
- material parameters
 - see also* building materials
 - constraints 3
 - design values 133–135
 - modulus of elasticity 118, 118, 119, 119, 203
 - shear modulus 64
 - Poisson's ratio 181–183, 181
- meshing
 - cantilever slab 251–253, 252
 - circular slab 248–251, 249, 250
 - foundation beam 39–43, 40, 41, 42
 - one-way slab 180, 180, 181, 253–254, 253
 - rectangular slab 246–247, 247, 249
 - shell structures 277, 280
- modelling errors
 - discretization 10–12
 - Finite Element nodal loading versus real loading 8–10, 9, 10

- modelling errors (*continued*)
 - nonlinear materials 8
 - reinforcement determination 10
- modulus of elasticity, building materials 118, 118, 119, 119, 203
- Mohr's failure criteria 159, 159
- nodal displacements, and nodal reactions 5–6, 5, 6
- nonlinear behaviour, concrete
 - foundation beams 43–46, 44, 45
 - beams 114–136
 - material parameters 133–136
 - tension stiffening effect 123–126, 124, 125, 126
 - use 115
 - yield surfaces 315
- numerical analysis
 - problems
 - modelling errors 8–12, 9
 - program errors 8
- openings
 - singularities, slab 238–242, 238, 240, 241
 - beam
 - deformation 61, 61, 63
 - modelling 56–59, 58, 59
- patch loadings, silos 250–252, 253
- Pieper-Martens model, rectangular slabs 263, 269
- pile foundations
 - bored
 - bedding modulus 46–47, 46
 - bridge columns 47, 48, 49
 - forces carried 46, 46
 - horizontal deformation 53–54, 53
 - inclined, bending moments 54–56, 55
 - load-settlement curves 52
 - manual analysis 47, 50
 - numerical model 46, 46, 51
 - rigs 50
 - soil stiffness modulus 46–47
 - truss model 47–48, 51
 - vertical spring stiffness 48–53, 52
 - caps, horizontal restraints 54, 54
 - uses 46
- plates, nodal forces 9, 10
- Poisson's ratio 181–183, 181
- portal frame bridges 15, 15, 16, 335
 - abutment beam 337
 - beam model 16
 - bending moments 17, 18
 - dimensioning 338–344
 - frame corner 338–339
 - detailing 339
 - effective span length 338–339, 340
 - FE-modell
 - support conditions 335–336, 337
 - singularities 336–338
 - output data 345, 346
 - flow of forces 341, 342
 - foundations 16–17, 16
 - loadings 15–17, 338, 341
 - shear design 342, 343, 344
 - shell model 325
 - strut-and-tie model 343
- re-entrant corners, singularities 238–242, 238, 240, 241
- real loading versus Finite Element nodal loading 8–10, 9, 10
- rectangular slabs
 - bending moments 262–263, 262, 264, 265, 267, 268
 - shear forces 262–263, 263
- reinforced beams
 - see also* deep beams
 - resistance 111, 111
 - dimensioning 110–114, 114
 - nonlinear analysis 114–135
 - shear/torsion design 113–114, 114
 - strain distributions 112, 112
 - stress-strain relationship 111, 111
 - tension stiffening effect 112, 113
- reinforcement
 - deep beams
 - horizontal distribution 158–162, 160, 161, 162
 - vertical distribution 160, 161, 165–166
 - determination, by modelling 10
 - hollow box girder bridges 20
 - slabs 183, 254–261, 255, 256, 261
- Reissner/Midlin plate theory 262
- residential buildings
 - slabs 176–177, 177
 - bending moments 177, 178, 179
 - deflections 178
 - shear forces 179

- shear design
 - abutment beam 342, 343, 344
 - beams 113, 114
 - haunches, inclined 24, 25, 26
- shear forces
 - foundation beams 40, 40, 41, 42
 - grillage 88, 89
 - hollow box girder bridges, top slab 84
 - rectangular slabs 262–263, 262
 - slabs
 - Czerny tables 262–263, 262, 263
 - discontinuous line support 201, 202
 - one-way 193, 196
 - partially lifting 197, 198
 - residential buildings 179
 - skewed 235–236, 237
- shear modulus 64
- shear walls
 - beam/column junctions 56, 58
 - definition 139, 140
 - design 139
 - finite element stresses 139, 140
 - high-rise buildings 56–63, 57, 58, 59, 60, 61, 63
 - large openings
 - deformation 61, 61, 63
 - modelling 56–59, 58, 59
 - singularities 169–170, 169
 - as truss systems 56–59, 58, 59
- shell models
 - see also* Sleipner A Platform, building models
 - elastic structure analysis 20–21, 22
 - truss model verification 74–75, 75, 76
- shell structures
 - composite 310, 311
 - definition 271
 - mesh generation
 - coarseness 274, 277
 - Finite Element method 271
 - nodal degree of freedom 271, 272
- silos
 - bending moments 281, 281, 282
 - Finite Element analysis 279–281, 280
 - internal forces 281–283
 - patch loadings 278–280, 280
- erroneous Finite Element analysis
 - 271–278, 274, 275, 277
- reinforcement layout 275
- tensile force distribution 275, 276
- tricells 273, 273
- truss model 276–277, 278
- T-beams
 - additional beam elements 284–286, 285
 - eccentric beam elements 284–286, 285, 291, 292, 293
 - knife-edge supports 284, 285
 - shell elements 284, 285
 - shell models 287–288, 287, 288
 - support region forces 289
 - uses 283
- silos
 - bending moments 281, 281, 282
 - circular slabs
 - bending moments 249, 249
 - boundary nodes 249–250, 249
 - circumferential bending moments, shell 282, 283
 - Finite Element analysis 279–281, 280
 - internal forces 281–283
 - patch loadings 278–280, 280
- singularities
 - concentrated loads 242–244, 242, 243, 244
 - deep beams 169–170, 169
 - Kirchhoff plate elements 239
 - openings, re-entrant corners 238–242, 238, 240, 241
 - portal frame bridge 336, 338
 - re-entrant corners 238–242, 238, 240, 241
 - shear walls 169–170, 169
 - shell structures, internal forces 310–313, 312
 - slab 237–238, 238, 239, 325, 325
- skewed slabs 234–235, 236
 - bending moments 235–236, 237
 - shear forces 235–236, 237
- slabs
 - see also* foundation slabs, slab-on beam structure
 - analysis
 - Finite Element Method 174–175, 175
 - strip method 174
 - bending moments
 - Finite Element Method 262–263, 262, 265, 267, 268
 - Pieper-Martens model 263, 267, 268

- slabs (*continued*)
 - bending stiffness 183
 - cantilever
 - bending moments 251–253, 252
 - inadequate modelling 251–253, 252
 - checking 176
 - circular
 - bending moments 249, 249
 - boundary nodes 249–250, 249
 - element sizes 250, 250
 - Finite Element meshes 249, 249, 250
 - concrete floor joists
 - dimensioning 206
 - models 205–206, 205
 - definition 173, 173
 - degree of freedom, 4-node plate element 175
 - dimensioning
 - Baumann model 257–260, 257, 258, 259, 261
 - comparison of different models 260, 260, 261, 261
 - Eurocode 2 (EC2) model 260, 260
 - general problems 254–263, 255
 - Stiglat model 255–256, 256, 261
 - discontinuous line support
 - bending moments 201–205, 202, 204
 - models 199–200, 200, 201
 - opening regions 203
 - outer wall support forces 203
 - shear forces 202
 - discretization
 - element mesh generation 246–247
 - restrained node location 247–250, 249
 - edge force 244–245, 245
 - edge supported
 - bedding modulus 224–227, 225
 - bending moments 226
 - column connections 222, 226, 227
 - effective widths, high-rise buildings 60
 - flat 184, 185
 - bending moments 212–214, 212
 - bedding modulus variations 218–219, 219
 - column bending moment 218–219, 220
 - deflections 216, 217
 - hinge coupling of nodes 223, 219–220, 220
 - nodes restrained 216, 217, 218
 - pin supports 214–215, 215, 216
 - circular 207, 208
 - equivalent frame models 210, 211, 213
 - manual analysis 210–212, 211, 212, 213, 224, 225
 - moment distribution 212
 - nodes restrained 214, 216, 217, 218
 - plane plate models 208–209, 209
 - span moments 211
 - support
 - all nodes restrained 216, 218
 - coupling of nodes
 - hinge 219–220, 220
 - rigid 219–220, 220
 - elastic bedded 218–219
 - models 209, 209
 - pin supports
 - all nodes 214, 216
 - single nodes 214, 215
 - internal forces 173, 174
 - joist floors 205, 205
 - Kirchhoff equation 174, 182
 - loads, concentrated 242–244, 242
 - material parameters, Poisson's ratio 181–183, 181
 - meshing
 - cantilever slab 251–253, 252
 - circular slab 248–251, 249, 250
 - one-way slab 253–254, 253
 - rectangular slabs 246–247, 247, 249
 - minimum reinforcement 326–328, 328
 - one-way 185, 185
 - bending moments 186, 187–193, 188, 189
 - line support models 185–186, 187
 - meshing 180, 180, 181
 - modelling 162–164, 164
 - shear forces 193, 196
 - stress distribution 192, 193
 - partially lifting
 - bending moments 197–199, 198
 - deflections 197–199, 198
 - shear forces 198, 199
 - partition walls, bending moments 201, 204
 - point loads, moment distribution 242–244, 242, 243, 244
 - rectangular
 - bending moments 236–237, 236
 - shear forces 236–237, 236
 - reinforcement 183, 254–261, 255, 256, 261

- residential buildings 176–177, 177
 - bending moments 177, 178, 179
 - deflections 178
 - shear forces 179
- shear forces, Czerny tables 262–263, 262
- shear forces, support 244–246, 245
- skewed 234–235, 236
 - shear forces 235–236, 237
- singularities
 - corners 238–240, 240
 - openings 238–242, 238, 240, 241
 - regions 237–238, 238, 239
- skewed 234–235, 236
 - bending moments 235–236, 237
 - shear forces 235–236, 237
- stiff, bending displacement 72–73, 73
- supports
 - bending moments at 183–185, 184
 - circular slab 248–251, 249, 250
 - discontinuous line support 199–205, 200
 - elastic bearing 192, 192
 - line support 183–186, 187, 241–242, 241
 - partially lifting 197–199, 198
 - soft support 246, 246
 - stiff support 246, 246
 - time-dependant deformations 184
- slab-on beam structure
 - downstand beam 296
 - effective width 298, 304–305, 304, 305
 - manual analysis 297–299, 298, 299, 307
 - member forces 301, 306, 309, 309
 - nonlinear analysis 313–316
 - reinforcement 302–304, 303
 - shell model 300, 300
- Sleipner A Platform 3, 4, 272
 - collapse 3–4, 271–278
 - erroneous Finite Element analysis 271–278, 274, 275, 277
 - reinforcement layout 275
 - tensile force distribution 275, 276
 - tricells 273, 273
 - truss model 276–277, 278
- slender beams, and deep beams 162–166, 164
- software
 - bugs 9
 - Finite Element design
 - availability 1–2
 - uncritical use of 3–4
 - program errors 8
- soil
 - deformation, foundations 38–39, 39, 40
 - parameters 323–324
 - stiffness modulus 47
- spatial shell structures, simplification by
 - simple beams 13
- spatial structures
 - dimensioning
 - Baumann model 231–234, 231, 232, 233
 - cracking 254, 255
 - internal forces 254
 - simplifications 254–255
 - Stiglat model 255–256, 256, 261
- stability
 - high-rise buildings
 - support forces 77–79
 - sway systems 76
 - parameter, high-rise buildings 76, 80
- steel
 - stress–strain relationship 111–113, 111, 113, 116, 125
- Stiglat model, slab dimensioning 255–256, 256, 261
- stress distribution
 - beams with openings 31–33, 33, 34, 35
 - one-way slabs 192, 193
- strip foundations
 - bending moment distribution 232–234, 233, 234
 - definition 226
 - membrane force 235
 - modelling 232, 233
 - tensile force 234, 234
 - test results 233
- structural deformation, high-rise buildings 74–76, 76
- strut-and-tie models,
 - abutment beam 341, 343
 - anchorage region 293–294, 295, 296
 - deep beams 166–169, 166, 167, 168
 - footings 230, 232, 234, 234
 - frame corner 24
 - halving joints 34
 - openings 36
- support settlement, multi-span deep beams 146, 147, 148, 149
- sway systems, high-rise buildings 76

Sydney (Australia), Opera House 349–350, 349

T-beam bridges 86, 91, 104

see also double T-beam bridges, T-beams

bending moments 99, 101, 106, 107

deck slab 84, 85

design 84

eccentric loads, torsional moments 99, 100, 102–103

longitudinal girders

eccentric line load forces 106–107

placement 105, 105

torsional stiffness 89–90, 90

T-beams

additional beam elements 284–286, 285

bridges 84–105, 86, 104, 105

eccentric beam elements 284–286, 285, 291, 292, 293

effective width 298, 304, 304, 305, 305

knife-edge supports 284, 285

member forces 290–292

modelling 283, 285

shell elements 284, 285

shell models 287–288, 287, 288

web/flange junctions 283

shell structures, uses 283, 294

stress distribution 293

structure 294, 294

support region forces 289

tensile stresses, anchorage region

293–294, 295, 296

tensile force, strip foundations 211, 212, 233
tension stiffening effect 123–126, 124, 125, 126

torsional moments

beams 67, 68

bracing systems, high-rise buildings 73–74, 72, 74

double T-beam bridges 93, 95

hollow box girder bridges 80–82

T-beam bridges, eccentric loads, 99, 100, 102–103

torsional stiffness, T-beam bridges 89–90, 90

tricells, Sleipner A platform 273, 273

truss model verification, shell models 74–75, 75

truss systems

bored pile foundations 47–48, 51

discontinuity regions 22, 22, 29, 29, 30

equivalent cross-sections 63–64

hollow box girder bridge 17, 20

portal frame bridges 15

bending moments 17, 18

foundations 16–17, 16

loadings 15–16

uses of 13

shear walls with openings 56–61, 57, 58, 59

wrapping torsion 67, 76–79

Zuse, Konrad 2